

GAIA-CLIM Report/Deliverable D2.8

Final report on the measurement uncertainty gap analysis from each subtask under Task 2.1 of WP2



A Horizon 2020 project; Grant agreement: 640276

Date: 02/02/2018

Beneficiary: BKS

Nature: R

Dissemination level: PU



Work Package	WP 2 (Measurement uncertainty quantification)
Deliverable	D 2.8
Title	Final report on the measurement uncertainty gap analysis from each subtask under Task 2.1 of WP2
Nature	R
Dissemination	PU
Beneficiary	BK Scientific GmbH
Date	02/02/2018
Status	Template Version 1.0, final
Authors	Karin Kreher (BKS), Arnoud Apituley, Anne van Gijssel (KNMI), Domenico Cimini, Fabio Madonna, Marco Rosoldi (CNR), Francois Hendrick, Michel Van Roozendaal, Martine DeMaziere, Bavo Langerock (BIRA), Kalev Rannat (TUT), Matthias Schneider (KIT), Justus Notholt, Matthias Buschmann (Uni Bremen), Jonathan Jones (Met Office), Johanna Tamminen (FMI), Tom Gardiner, Paul Green (NPL).
Reviewers	Peter Thorne (NUIM), Anna Mikalsen (NERSC)
Contacts	karin.kreher@bkscientific.eu
URL	http://www.gaia-clim.eu/

This document has been produced in the context of the GAIA-CLIM project. The research leading to these results has received funding from the European Union's Horizon 2020 Programme under grant agreement n° 640276. All information in this document is provided "as is" and no guarantee or warranty is given that the information is fit for any particular purpose. The user thereof uses the information at its sole risk and liability. For the avoidance of all doubts, the European Commission has no liability in respect of this document, which is merely representing the authors' view.

Executive Summary

This deliverable presents the results of the work within GAIA-CLIM aiming to metrologically qualify measurements from a range of non-satellite instrument techniques as “reference quality”. The techniques that have been considered, in order of the progress achieved, are:

- Microwave Radiometer to measure temperature and water vapour profiles;
- Lidar to measure aerosol, ozone, and temperature profiles;
- UV-visible spectroscopy to measure ozone total columns;
- GNSS to measure total column water vapour;
- FTIR to measure CH₄, CO₂, ozone, and water vapour columns and profiles;
- MAX-DOAS to measure tropospheric ozone.

The main text of this deliverable provides a brief summary of the overall progress for each technique in turn. It is complemented by a series of Annexes, one or more per technique, which describe in detail the traceability and uncertainty work on a per product basis. These “Product Traceability and Uncertainty” documents in the Annex have been produced following the guidance provided by NPL as described in deliverable D2.6¹.

While considerable process has been achieved, in most cases, further work should be undertaken, e.g. to quantify effects that have been assumed minor and to use our improved understanding of the uncertainties and their sources to further reduce these contributions to the total uncertainty budget. Finally, it should be stressed that the work within GAIA-CLIM considered solely a subset of the range of potential techniques that would benefit from such an analysis in future.

¹ http://www.gaia-clim.eu/sites/www.gaia-clim.eu/files/document/d2_6_final.pdf

Table of Contents

Executive Summary.....	3
1. Introduction	6
2. Summary of the reference quality measurement capabilities and uncertainty quantification for the instrument techniques investigated within Task 2.1	8
2.1. Temperature and H ₂ O profiles measured by microwave radiometer	8
2.1.1. Measurement technique basics.....	8
2.1.2. Understanding the metrological processing chain	8
2.1.3. Quantified uncertainties	9
2.1.4. Identification and description of the remaining challenges	10
2.1.5. MWR PTU documents.....	10
2.2. Aerosol extinction coefficient profile measured by Raman lidar	11
2.2.1. Measurement technique basics.....	11
2.2.2. Understanding the metrological processing chain	11
2.2.3. Quantified uncertainties	12
2.2.4. Identification and description of the remaining challenges	13
2.2.5. Lidar Aerosol PTU document	14
2.3. Ozone concentration profiles measured by differential absorption lidar	15
2.3.1. Measurement technique basics.....	15
2.3.2. Understanding the metrological processing chain	15
2.3.3. Quantified uncertainties	16
2.3.4. Identification and description of the remaining challenges	17
2.3.5. Lidar Ozone PTU document	18
2.4. Temperature profiles measured by lidar	19
2.4.1. Measurement technique basics.....	19
2.4.2. Understanding the metrological processing chain	19
2.4.3. Quantified uncertainties	20
2.4.4. Identification and description of the remaining challenges	22
2.4.5. Lidar Temperature PTU document	22
2.5. Total column O ₃ measured by UV-visible spectroscopy	23
2.5.1. Measurement technique basics.....	23
2.5.2. Understanding the metrological processing chain	23
2.5.3. Quantified uncertainties	23
2.5.4. Identification and description of the remaining challenges	24
2.5.5. UV-vis PTU document	25
2.6. Total column water vapour measured by GNSS.....	26

2.6.1.	Measurement technique basics	26
2.6.2.	Understanding the metrological processing chain	26
2.6.3.	Quantified uncertainties	26
2.6.4.	Identification and description of the remaining challenges	27
2.6.5.	GNSS-IPW PTU document	28
2.7.	CH ₄ , CO ₂ , O ₃ , and H ₂ O columns and profiles measured by FTIR	29
2.7.1.	Measurement technique basics	29
2.7.2.	Understanding the metrological processing chain	29
2.7.3.	Quantified uncertainties	31
2.7.4.	Identification and description of the remaining challenges	32
2.7.5.	FTIR PTU documents	34
2.8.	Tropospheric O ₃ measured by MAX-DOAS and Pandora	35
2.8.1.	Measurement technique basics	35
2.8.2.	Understanding the metrological processing chain	35
2.8.3.	Quantified uncertainties	36
2.8.4.	Identification and description of the remaining challenges	36
3.	Conclusions	38
4.	References	43
5.	Annex I - XI	44

1. Introduction

The GAIA-CLIM project aims to assess and improve global capabilities to use ground-based, balloon-borne, and aircraft measurements (termed non-satellite measurements henceforth) to characterize space-borne satellite measurement systems. Work within GAIA-CLIM covers:

- Improving discovery metadata and quantifying geographical aspects of the non-satellite observations segment.
- Quantification of non-satellite measurement uncertainties.
- Techniques to account for the effects arising from non-coincidence of measurements on resulting comparisons.
- The potential utility of data assimilation techniques as integrators.
- Presentation of match-up information to users via a “Virtual Observatory facility”.
- Identification of gaps in capabilities and production of a set of ensuing recommendations for subsequent work.

In this context, the goal of WP2 is to improve the metrological characterisation of a subset of high-quality non-satellite observational techniques, which were chosen because the technique and data analysis were deemed to be mature enough for these Essential Climate Variable (ECV)/technique combinations to be likely candidates for data products of “reference quality”. Here, reference quality has a specific meaning around traceability, uncertainty quantification, comparability, and representativeness as discussed in Thorne et al., 2017.

A reference-quality measurement is sufficiently well metrologically understood that the data user can have confidence that the true value of the reported measurand falls within the reported measurement uncertainty range with a specified probability. This probability depends upon the coverage factor, k , with typical reports given at $k=2$, which provides 95% probability that the true value lies within the interval. Well behaved and understood measurement techniques, for which systematic effects can be uniquely identified and removed and random effects minimized, typically have small uncertainty. Such a state should be strived for. However, reference quality in first instance means that the uncertainty is well quantified, comprehensive, and traceable. It does not imply that a certain method or instrument type is the best available or provides the best possible solution for a specific application. Traceability is a prerequisite for making such informed decision. Reported uncertainties that do not have traceability should not, generally, be trusted. Hence, it is equally important that users consider whether the measurements are useful for their application. In cases where target ECVs are measured by multiple techniques, users should consider a range of measurement properties, such as altitude range and frequency of measurements, for example, as well as uncertainty quantification, in making an informed decision.

The work described herein on the development of such reference-quality measurement capabilities and their uncertainty quantification builds upon prior efforts of groups and networks such as the Global Climate Observing System (GCOS) Reference Upper-air Network (GRUAN) and the Network for Detection of Atmospheric Composition Change (NDACC) and

related FP7 and H2020 projects such as QA4ECV² and FIDUCEO³. Several data products measured under the umbrella of these high quality global networks were considered at project outset to require only relatively minor effort to ensure traceability and robust uncertainty estimation. Our aim within WP2 was to expand and deepen the understanding of the fundamental measurement uncertainties of these selected ECV-instrument combinations and to further develop some of the existing data products so they can be of reference quality. This work was undertaken by the respective instrument experts within the GAIA-CLIM consortium in consultation with the wider scientific community.

The purpose of this deliverable is to describe and document in each case progress toward the complete traceability chain from raw measurement to final product, and to summarize the uncertainty characterization for these final data products. This has been done in close collaboration with NPL and follows the guidelines that they developed within Task 2.3⁴. For each of the instruments and selected ECVs, specific data products have been characterized in a set of Product Traceability and Uncertainty (PTU) documents (given as a series of Annexes). Each PTU document includes a product overview, instrument description, product traceability chain, detailed traceability chain element contributions with an uncertainty summary table, and finally a traceability uncertainty analysis.

The PTU documents represent the final synthesis of our current metrological understanding and provide the background and uncertainty information for the data sets included in the Virtual Observatory (VO) facility, which has been developed within WP5. The VO facility provides users with access to satellite and non-satellite data for comparison studies and most of the non-satellite data sets used within the VO have been selected and investigated as part of Task 2.1.

Within Section 2, progress within GAIA-CLIM for each measurement technique is summarized in turn. To aid readability these sub-sections have been structured identically such that they describe in turn:

1. The measurement technique basics
2. Understanding of the metrological processing chain
3. A summary of the quantification of uncertainties
4. Discussion of outstanding issues and challenges
5. Summary of the PTU documents and what observational sites they refer to

Section 3 then summarises.

² Quality Assurance for Essential Climate Variables (QA4ECV): <http://www.ga4ecv.eu/>

³ Fidelity and uncertainty in climate data records from Earth Observations (FIDUCEO): <http://www.fiduceo.eu/>

⁴ Cf. The Guide to Uncertainty in Measurement & its Nomenclature (D2.6): http://www.gaia-clim.eu/sites/www.gaia-clim.eu/files/document/d2_6_final.pdf

2. Summary of the reference quality measurement capabilities and uncertainty quantification for the instrument techniques investigated within Task 2.1

2.1. Temperature and H₂O profiles measured by microwave radiometer

2.1.1. Measurement technique basics

Atmospheric temperature and humidity profiles can be inferred by ground-based microwave radiometer (MWR) observations. Ground-based MWR measures the natural down-welling thermal radiation from the atmosphere. The quantity measured is expressed as brightness temperature T_B [K]. The received down-welling radiation is converted into voltage and then related to T_B through the radiometer calibration. The calibrated T_B is processed to obtain atmospheric variables (temperature and humidity profiles, as well as total column water vapour and liquid water) through the application of a retrieval method. Common MWR commercial units operate in the 20-60 GHz frequency range. These represent the large part of the operational MWR deployed worldwide.

2.1.2. Understanding the metrological processing chain

Commercial MWR instruments provide T_B and atmospheric retrievals with no estimate of the associated uncertainty. Uncertainties in MWR derived products are usually estimated *ex-ante* through simulated analysis and/or *ex-post* through validation against collocated radiosonde profiles. As part of GAIA-CLIM WP2 activities, a traceability chain for the MWR T_B observations and atmospheric retrievals was designed. The main chain is pictured in Figure 1, while further details are given in the attached MWR PTU documents (see Annex I-IV).

MWR measurement: Main Chain

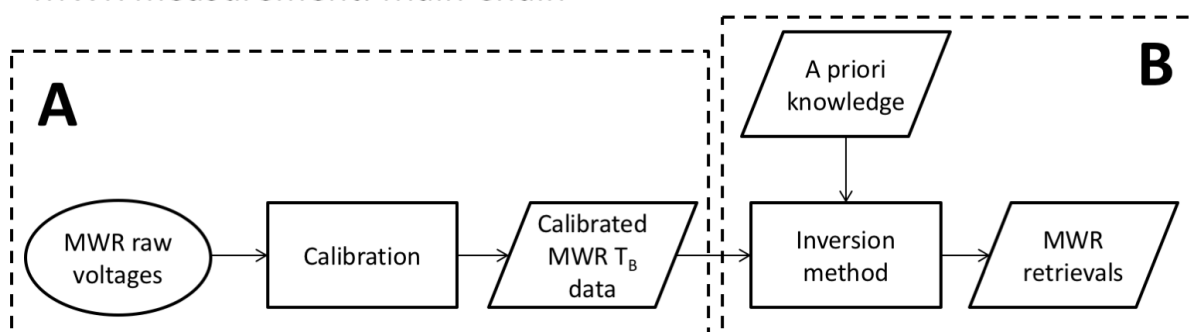


Figure 1. Main chain of the MWR instrument model diagram. The main chain displays the process of producing a geophysical product from MWR measurements. Process A leads from raw voltages to calibrated brightness temperature T_B . Process B leads from calibrated T_B to atmospheric temperature and humidity retrievals.

2.1.3. Quantified uncertainties

The estimation of the uncertainty associated with MWR calibration and retrieval processes has been reviewed and documented in the annexed PTU documents. An example of typical uncertainty for temperature and humidity retrievals is shown in Figure 2. Five specific gaps, documented in the Gap Assessment and Impacts Document (GAID; G2.13-G2.17), were identified as relevant for the full uncertainty budget and SI-traceability assessment of MWR products. Four of these gaps (G2.14-G2.17) were later combined into one higher-level gap (G2.36)⁵. WP2, in cooperation with the European COST Action TOPROF⁶ has designed and developed a unified network data processing to process MWR level 1 (calibrated T_B) into level 2 (atmospheric retrievals) data products, partially covering G2.36. The developed software, Network 1DVAR retrieval (Net1D), is based on the optimal estimation method and provides temperature and humidity profile retrievals with the associated uncertainty vertical profiles. Two open literature papers describe specific parts of Net1D (De Angelis et al., 2016; De Angelis et al., 2017), and another paper describing the whole network data processing is in preparation. WP2 also addressed the lack of a clear reference for microwave absorption model uncertainties, identified in G2.36, by reviewing the open literature for information on oxygen and water vapour microwave absorption model uncertainties. The collected information is used to investigate the sensitivity of the absorption model to the reported uncertainty. The uncertainties are also propagated through a radiative transfer model to estimate the impact on simulated T_B and the retrieved products. This work is being finalized (Cimini et al., 2017) and shall be completed by the end of GAIA-CLIM.

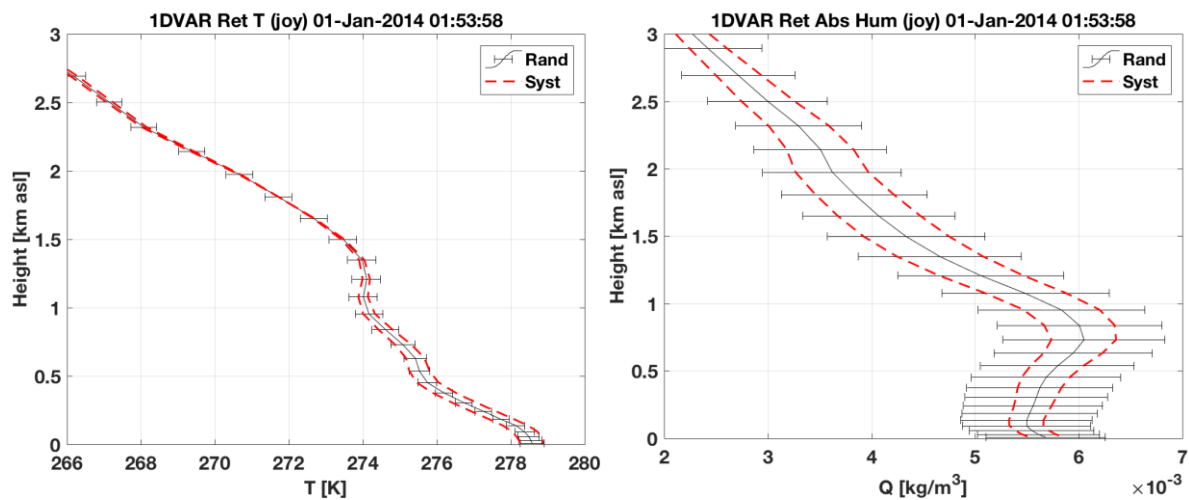


Figure 2. An example of temperature (left) and absolute humidity (right) profile retrievals at the Joyce site (Jülich, Germany) on January 1st 2014, 01:53 UTC. The associated estimates for random (error bars) and systematic (red dashed lines) uncertainties are also shown.

⁵ The current fourth version of the GAID is available under: <http://www.gaia-clim.eu/page/gaid>

⁶ www.toprof.eu

2.1.4. Identification and description of the remaining challenges

The achievements above partially cover the identified G2.36 gap. For a full coverage, level 0 (raw voltages) data should also be processed uniformly to produce level 1 data. This shall be implemented in the future, while currently the instrument-specific processing is used. The remaining identified gap (G2.13) currently precludes full SI traceability of MWR observations and retrievals, due to the lack of SI standards for microwave radiances maintained by any metrological institute. WP2 has been following and reporting on the activities at the US National Institute of Standards and Technology (NIST) to develop the metrology applicable to microwave radiometry. It is expected that SI-traceable calibration targets and transfer standards will become available at NIST in the next few years (Houtz et al, 2017).

2.1.5. MWR PTU documents

The following PTU documents are attached as Annex I – IV:

- Product Traceability and Uncertainty for the Microwave Radiometer (MWR) brightness temperature product
- Product Traceability and Uncertainty for the Microwave Radiometer (MWR) temperature profile product
- Product Traceability and Uncertainty for the Microwave Radiometer (MWR) total water vapour content product
- Product Traceability and Uncertainty for the Microwave Radiometer (MWR) humidity profile product

All 4 PTU documents apply to the following subset of existing MWR sites:

- Juelich, Germany, 50.91 °N, 6.41 °E, 111 m
- Leipzig, Germany, 51.35 °N, 12.43 °E, 125 m
- Payerne, Switzerland, 46.82 °N, 6.95 °E, 491 m
- Paris, France, 48.80 °N, 2.36 °E, 156 m
- Cabauw, the Netherlands, 51.97 °N, 4.93 °E, -0.7 m
- Lindenberg, Germany, 52.21 °N, 14.12 °E, 125 m

2.2. Aerosol extinction coefficient profile measured by Raman lidar

2.2.1. Measurement technique basics

The lidar technique, acronym for ‘light detection and ranging’, is based on the transmission into the atmosphere of short light pulses, with duration ranging from a few to several hundreds of nanoseconds, by a laser transmitter by means of transmission optics. At every point of the atmospheric volume crossed by the laser beam, the incident light interacts with the atmospheric constituents by various scattering and absorption processes. A small fraction of the incident light is backscattered by atmospheric constituents and it is collected by a receiving telescope. The light received from the atmosphere, including any background sky light, passes through an optical system, consisting of various elements (lenses, mirrors, filters, etc.), which filters out one or more specific wavelengths related to the emission wavelength of the laser transmitter from the light collected by the telescope. The light from the optical system is forwarded to detectors, which convert it into electrical signals. The resulting signals, acquired as a function of the distance from the lidar system, can then be converted into vertical profiles of the parameters of interest.

2.2.2. Understanding the metrological processing chain

Figure 3 shows the traceability chain for atmospheric profiles of aerosol extinction coefficient $\alpha(z)$ retrieved with the Raman lidar technique within the EARLINET⁷ network. These profiles are retrieved using the lidar signals due to the Raman inelastic backscattering by atmospheric nitrogen molecules. Raman signals produced by single laser pulses are integrated over a fixed time interval, typically ranging from 10 to 60 seconds. This integration produces the raw Raman signals, with a vertical resolution typically from a few meters up to a few tens of meters. The raw Raman signals are pre-processed to apply instrumental corrections and, optionally, a vertical smoothing and/or a temporal averaging. This stage is commonly known as “pre-processing” of raw Raman signals. The pre-processed Raman signals have a time and vertical resolution which depends on a temporal and vertical integration performed by the pre-processing module. Typically, time and vertical resolutions range from a few tens of minutes to a few hours and from 30 to 60 meters, respectively. The pre-processed Raman signals are the input of the second part of the processing algorithm, known as “processing” of the pre-processed Raman signals, providing the aerosol extinction coefficient profile. This profile has a time sampling, which is the integration time used in pre-processing stage and effective vertical resolution ranging from a few hundreds of meters to many hundreds of meters, depending on the vertical integration performed in pre-processing and processing modules. Further details can be found in the lidar aerosol PTU (see Annex V).

⁷ https://www.earlinet.org/index.php?id=earlinet_homepage

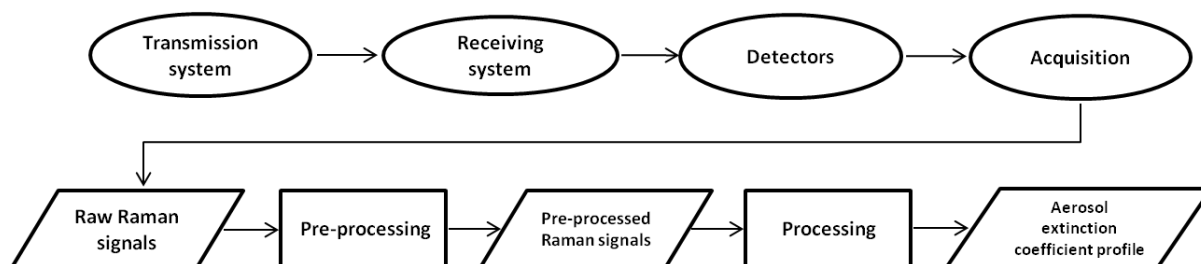


Figure 3. Traceability chain for atmospheric profiles of the aerosol extinction coefficient retrieved with the Raman lidar technique within the EARLINET network

2.2.3. Quantified uncertainties

Two main uncertainty contributions have been identified and quantified:

- Random uncertainty due to the detection noise of lidar signals, which is calculated starting from random uncertainties of raw lidar signals, by using the uncertainty propagation rules or Monte Carlo simulation for all applied signal handling procedures both in pre-processing and processing stages. Random uncertainty is typically less than 10% for $\alpha(z) > 2 \times 10^{-5} \text{ m}^{-1}$ and greater for lower values of $\alpha(z)$.
- Systematic uncertainty due to the estimation of molecular density/extinction profile and the assumption of the Ångström exponent, which is a dimensionless parameter describing the wavelength dependence of aerosol extinction coefficient. Systematic uncertainty is typically less than 15% for $\alpha(z) > 2 \times 10^{-5} \text{ m}^{-1}$ and greater for lower values of $\alpha(z)$.

As an example, Figure 4 shows the aerosol extinction coefficient profile at 532 nm, retrieved from measurements made at the EARLINET station of Potenza (Italy) on 10 June 2010, with an integration time from 20:29 to 21:56 UT and an effective vertical resolution of 540 m. The station is 760 m above sea level (a.s.l.). The horizontal bars show the random uncertainty, which is less than 10% for most of the extinction values. The systematic uncertainty due to the assumptions of the retrieval algorithm is typically less than 15% and should also be considered.

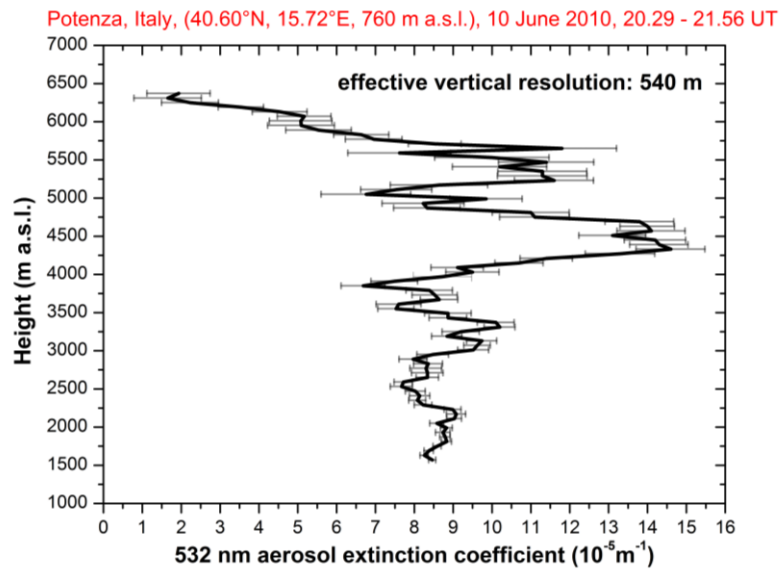


Figure 4. Example of aerosol extinction coefficient profile retrieved using Raman lidar technique and EARLINET processing algorithm

2.2.4. Identification and description of the remaining challenges

In order to improve the uncertainty characterization of the EARLINET aerosol extinction coefficient profile, the following recommendations should be followed:

- ✓ The systematic uncertainty due to the estimation of molecular density/extinction profile can be reduced by using pressure and temperature profiles measured with co-located and simultaneous radio-soundings, if available, or provided by Numerical Weather Prediction (NWP) re-analysis.
- ✓ The estimate of systematic uncertainty, based on sensitivity studies performed on specific measurement sessions and lidar systems, could be improved by extending the above studies to multiple measurements and lidar systems and by standardizing the methodologies to estimate the molecular density profile and the Ångström exponent.
- ✓ An assessment of the uncertainty of the detector efficiency should be evaluated.
- ✓ The experimental characterization of optical and geometrical properties of all the systems in the network can improve the estimate of extinction coefficient at low altitudes, typically below 250-500 m above the ground, depending on the instrument.
- ✓ The statistical uncertainty could be improved by standardizing all applied signal handling procedures both in pre-processing and processing stages.
- ✓ Finally, eight not quantified uncertainty contributions have been identified that are considered negligible. Some analysis to determine the magnitude of these potential contributions would better constrain the uncertainty budget.

2.2.5. Lidar Aerosol PTU document

The following PTU document is attached as Annex V:

- Product Traceability and Uncertainty for the EARLINET LIDAR aerosol extinction coefficient product

This PTU document applies specifically to lidar measurements taken at the following sites:

- Evora, Portugal, 38.568 °N, 7.912 °W, 293 m
- Granada, Spain, 37.164 °N, 3.605 °W, 680 m
- Leipzig, Germany, 51.353 °N, 12.435 °E, 90 m
- Napoli, Italy, 40.8380 °N, 14.1830 °E, 118 m
- Potenza, Italy, 40.601 °N, 15.724 °E, 760 m

2.3. Ozone concentration profiles measured by differential absorption lidar

2.3.1. Measurement technique basics

The lidar technique, acronym for ‘light detection and ranging’, is based on the transmission into the atmosphere of short light pulses, with a duration ranging from a few to several hundreds of nanoseconds, by a laser transmitter by means of transmission optics. At every point of the atmospheric volume crossed by the laser beam, a small fraction of the incident light is backscattered and/or absorbed by atmospheric constituents. The backscattered light is collected by a receiving telescope. The light received from the atmosphere, including any background sky light, passes through an optical system, consisting of various elements (lenses, mirrors, filters, etc.), which filters out one or more specific wavelengths related to the emission wavelength of the laser transmitter from the light collected by the telescope. The resulting lidar signal(s) can then be converted into a vertical profile of the parameter of interest.

For the Differential absorption lidar (DIAL) technique, at least two lidar signals at different detection wavelengths are needed. One wavelength is absorbed more strongly by the target species, in this case ozone, while the second wavelength is less absorbed. The ozone concentration profile is derived by differentiating the ratio of the two lidar signals.

2.3.2. Understanding the metrological processing chain

Figure 5 shows the traceability chain for atmospheric profiles of ozone retrieved with the differential absorption lidar technique in the NDACC network. Lidar signals produced by single laser pulses are integrated over a fixed time interval, typically several minutes. Further averaging of signals over periods up to one or more hours may be needed. This integration produces the raw lidar signals, with a vertical resolution typically from a few meters up to a few tens of meters. The raw lidar signals are pre-processed to apply instrumental corrections and, optionally, a vertical smoothing and/or a temporal averaging. This stage is commonly known as “pre-processing”. The pre-processed lidar signals have time and vertical resolutions depending, respectively, on temporal and vertical integration performed by the pre-processing. The pre-processed lidar signals are the input of the second part of the processing algorithm, known as “processing”, providing the ozone concentration profile. This profile has a time sampling which is the integration time used in pre-processing stage and effective vertical resolution ranging from a few hundreds of meters up to a kilometer or more, depending upon the required level of smoothing out of random uncertainty.

The “processing” of pre-processed signals to retrieve the ozone concentration profile comprises several steps indicated in Figure 5. The processing steps described contribute to the uncertainty of the final product N_{O_3} (number density) or q_{O_3} (mixing ratio): the ozone differential absorption cross section, the Rayleigh scattering differential cross section, the differential absorption cross section of several interfering gases NO_2 , SO_2 , O_2 , the assumed vertical distribution of the interfering gases, the uncertainty resulting from external input of air density and temperature and finally that of the spatio- temporal integration.

Further details can be found in the ozone profile differential absorption lidar PTU (see Annex VI).

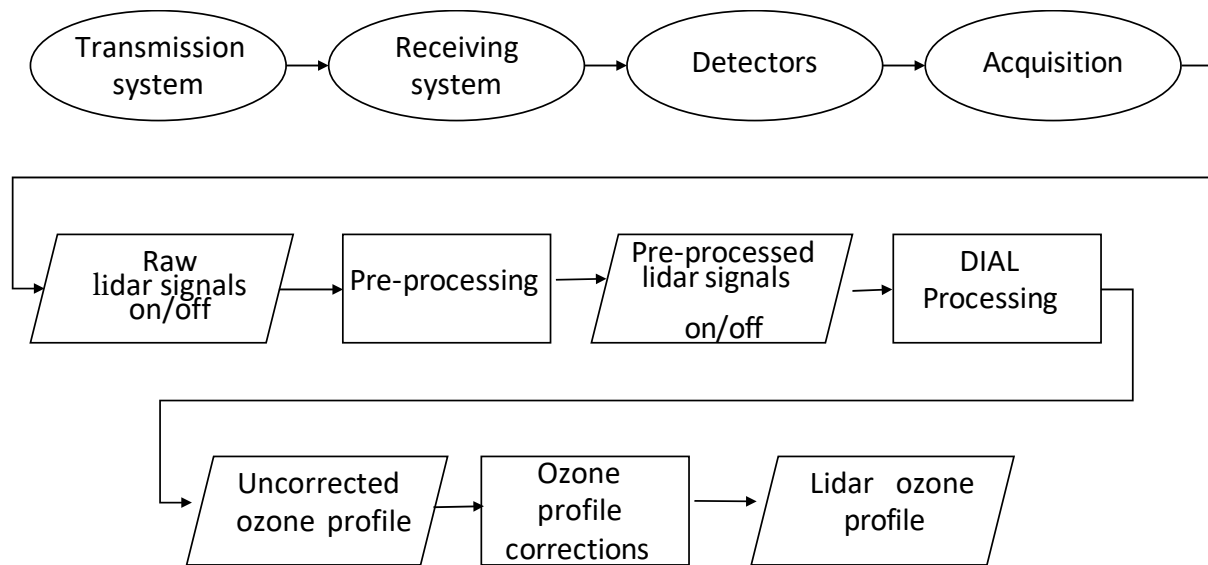


Figure 5. Traceability chain for ozone differential absorption profiles.

2.3.3. Quantified uncertainties

For stratospheric ozone lidar observations with the lidar located above the boundary layer, the ozone number density standard uncertainty results mainly from three components: i) Rayleigh extinction cross section differential at the bottom of the profile; ii) ozone absorption cross section differential in the middle of the profile; and iii) detection noise at the top of the profile. For the derived ozone mixing ratio, the uncertainty component associated with the *a priori* use of ancillary air pressure is largely dependent on the uncertainty of the used source profile, which when combining for instance a radio sounding with a reanalysis product, may introduce a large change in uncertainty at the switch between sources. For both ozone number density and ozone mixing ratio uncertainty, the dominant source above 40-45 km is detection noise, depending on the site altitude and laser strength. For lidars located at lower altitudes, local air pollution may play a role and interfering gases should be considered when pollution conditions occur.

The combined ozone number density standard uncertainty results mainly from the ozone absorption cross section differential uncertainty. Below 12 km, the uncertainty owing to Rayleigh extinction cross section differential and detection noise are the other important components. Uncertainty owing to detection noise dominates in the upper part of the profile (above 22 km). For lidars located at lower altitudes inside the boundary layer, interfering gases may play a substantial role, depending on local circumstances and the time of observation. The total uncertainty will thus depend on location (altitude and air composition) and the chosen lidar setup (laser strength, wavelengths, etc.).

Figure 6 gives an example of a stratospheric ozone DIAL uncertainty after optimal combination of three DIAL wavelength pairs, the ozone number density standard uncertainty results mainly from those three key sources of uncertainty described earlier. For the derived

ozone mixing ratio, the uncertainty component associated with the a priori use of ancillary air pressure became abruptly important above 30 km as a result of the transition between the a priori use of radiosonde measurement ($z < 30$ km) and the a priori use of the NCEP analysis ($z > 30$ km). The dominant source of ozone mixing ratio uncertainty above 45 km is detection noise.

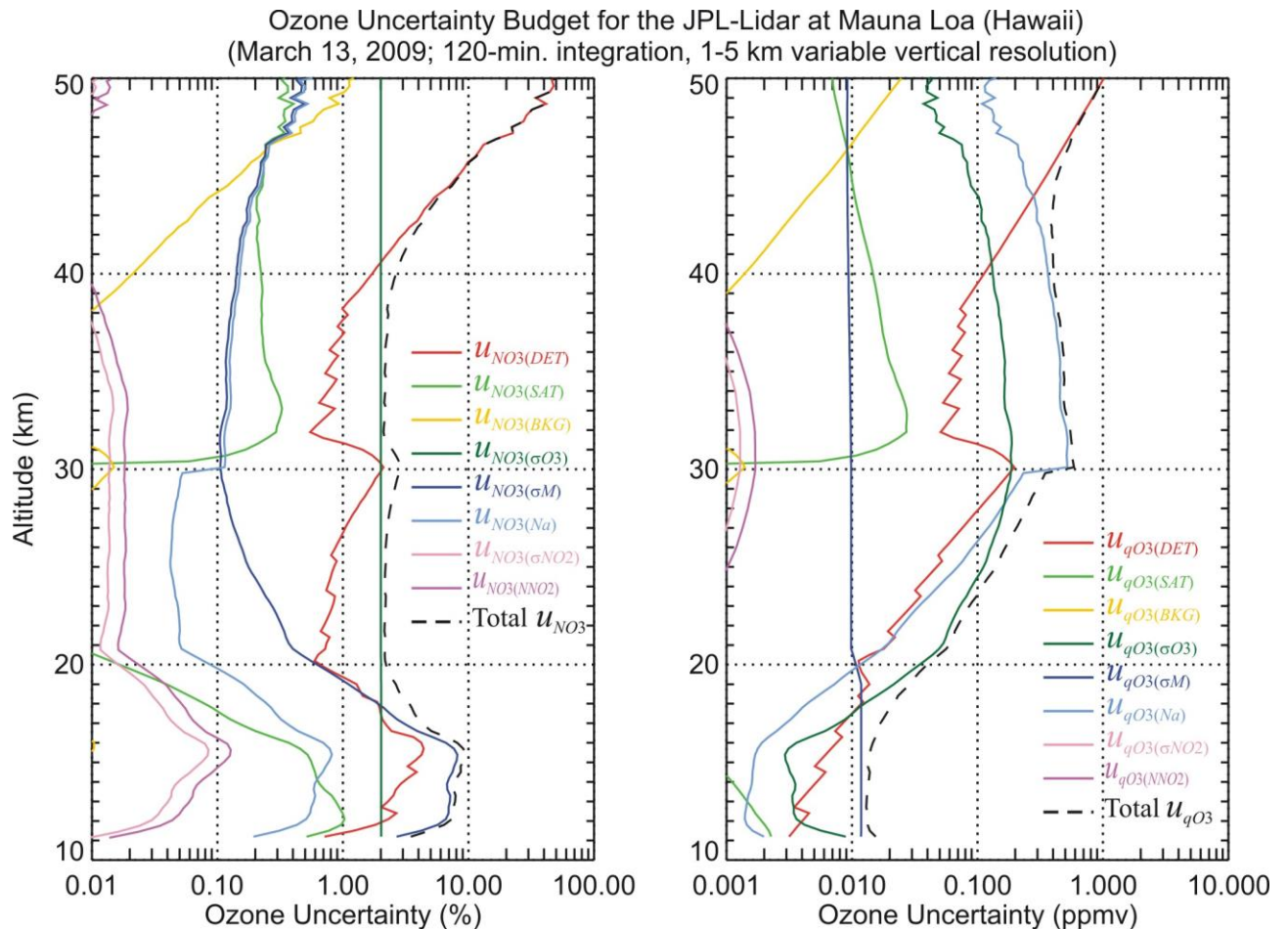


Figure 6. Example of ozone relative uncertainty (left) and mixing ratio uncertainty (right) budgets computed for the JPL stratospheric ozone DIAL located at Mauna Loa Observatory (Hawaii) for a night time observation. Uncertainty (u) components: DET=Detection noise; SAT=Saturation correction; BKG=Background correction; σO_3 =Ozone cross-sections; σM =Rayleigh scattering cross-sections; Na=Ancillary air number density; σNO_2 =NO₂ absorption cross-sections; NNO2=Ancillary NO₂ number density. From Leblanc et al. (AMT, 2016a, their Figure 16).

2.3.4. Identification and description of the remaining challenges

Additional work on improving information on the vertical distribution of interfering gases could be of importance in special cases, such as observations during specific events (high SO₂ from fires and volcanic eruptions) or enhanced air pollution (NO₂) for measurement of tropospheric ozone. Furthermore, improved information on the external input of pressure and temperature would have a mitigating effect on the uncertainty in the top of the concentration profile above 30 km.

It is recommended to set up a centralized data processing facility for the differential absorption lidars for ozone.

Various variable uncertainty sources have been identified that are hard to quantify or highly variable in space/time or instrument-specific. Further research into these items, and consideration of these items for individual systems when building their PTU, is recommended.

2.3.5. Lidar Ozone PTU document

The following PTU document is attached as Annex VI:

- Product Traceability and Uncertainty for the Ozone Profile Differential Absorption Lidar Product

This PTU document pertains to lidar measurements undertaken at the following sites:

- Table Mountain, USA, 34.4 °N, 117.7 °W, 2300 m
- Mauna Loa, Hawaii/USA, 19.54 °N, 155.58 °W, 3397 m
- Lauder, New Zealand, 45.038 °S, 169.684 °E, 370 m

2.4. Temperature profiles measured by lidar

2.4.1. Measurement technique basics

The lidar technique, acronym for ‘light detection and ranging’, is based on the transmission into the atmosphere of short light pulses, with duration ranging from a few to several hundreds of nanoseconds, by a laser transmitter by means of transmission optics. At every point of the atmospheric volume crossed by the laser beam, a small fraction of the incident light is backscattered and/or absorbed by atmospheric constituents. The backscattered light is collected by a receiving telescope. The light received from the atmosphere, including any background sky light, passes through an optical system, consisting of various elements (lenses, mirrors, filters, etc.), which filters out one or more specific wavelengths related to the emission wavelength of the laser transmitter from the light collected by the telescope. The resulting lidar signal(s) can then be converted into a vertical profile of the parameter of interest.

For the temperature lidar technique, at least one lidar signal is used. Multiple receiver channels with different intensities or different wavelengths can be used to cover different altitude regions.

2.4.2. Understanding the metrological processing chain

To retrieve a lidar temperature profile in the stratosphere or mesosphere, the density integration technique is used. The traceability chain is shown in the accompanying Figure 7. In the absence of aerosols, the lidar signal is proportional to the air number density. Temperature can then be computed by vertically integrating the air number density under the assumptions that there is a hydrostatic balance and that the air is an ideal gas. This inversion technique works for both elastic scattering (Rayleigh backscatter by the air molecules) and inelastic scattering (vibrational Raman backscatter by the nitrogen molecules). A temperature tie-on at the top of the profile is needed from external sources.

Further details can be found in the lidar temperature profile PTU (see Annex VII).

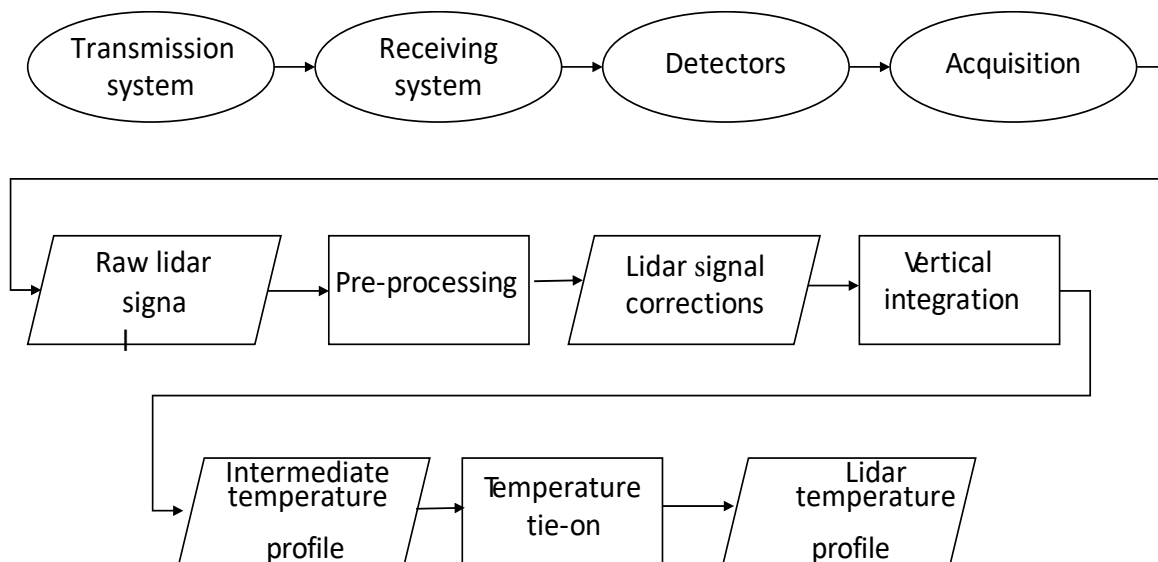


Figure 7. Traceability chain for lidar temperature profiles.

2.4.3. Quantified uncertainties

Quantitatively, the most significant uncertainty components are typically detection noise and temperature tie-on at the top of the profile; and saturation correction and molecular extinction at the bottom of the profile. The interfering gases to consider in practice are ozone and NO₂. Because of either very low concentrations or very low values of their absorption cross-sections, no other atmospheric gases or molecules are known to interfere with the temperature retrieval. The impact of absorption by ozone on the temperature retrieval is very small (<0.1 K) if working at wavelengths near the ozone minimum absorption region (e.g., 355 nm, 387 nm), but can account for up to 1 K systematic uncertainty if neglected when working in the Chappuis band (e.g., 532 nm and 607 nm). Conversely, absorption by NO₂ is very small for temperature retrievals in the Chappuis band, but can account for up to a 0.2 K systematic uncertainty if neglected at 355 nm and 387 nm.

The uncertainty contribution of the acceleration of gravity is very small (<0.1 K) provided an adequate altitude-dependent formulation of gravity. In the upper mesosphere, the change in the air major species' mixing ratio induces a change with altitude of the air molecular mass and Rayleigh scattering cross-sections. However, the induced changes remain below 0.1 K below 90 km, which is much less than the expected uncertainty due to remaining sources, such as detection noise and tie-on temperature uncertainty. For temperature profiles reaching 100 km or higher, the change of the molecular mass of air with altitude should be taken into account. See Figure 8 for an example of the full uncertainty budget.

Temperature uncertainty budget for the JPL-Lidar at Mauna Loa (Hawaii)
(13 March 2009; 120 min. integration, 0.3–5 km variable vertical resolution)

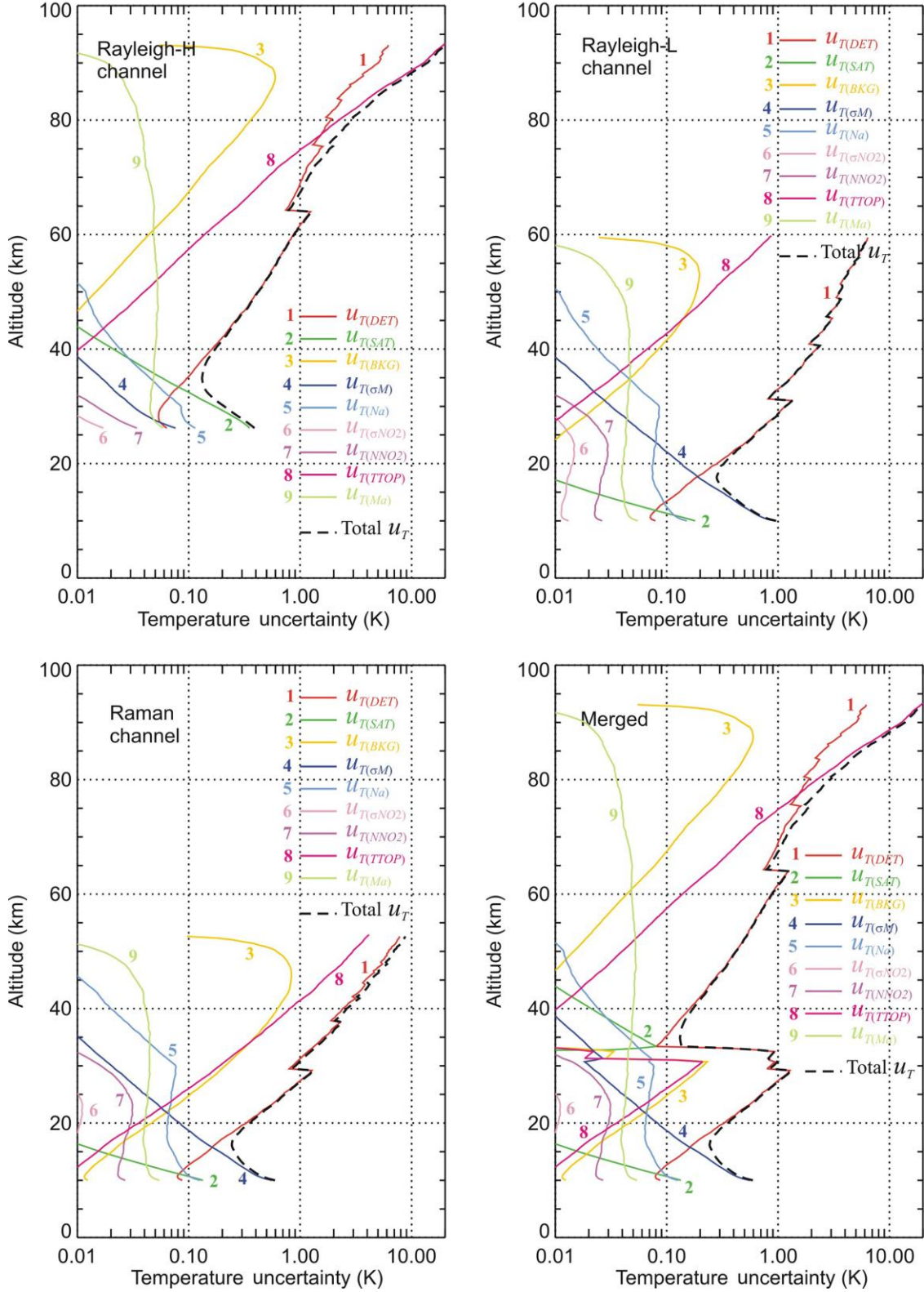


Figure 8. Example of uncertainty budget for the temperature retrievals done with the lidar at Mauna Loa for the high intensity Rayleigh channel (upper left), low intensity Rayleigh channel (upper right), the Raman channel (lower left), and the final profile combining these three channels. Individual uncertainty components: 1=Detection noise; 2=Saturation correction; 3=Background correction;

4=Rayleigh scattering cross-sections; 5=Ancillary air number density; 6=NO₂ absorption cross-sections; 7=Ancillary NO₂ number density; 8=Temperature tie-on; 9=Molecular mass of air. Figure reproduced from Leblanc et al., AMT, 2016b, their Figure 10.

2.4.4. Identification and description of the remaining challenges

Additional work on improving information on the vertical distribution of interfering gases could be of importance in special cases. Furthermore, improved information on the external input of pressure and temperature would have a mitigating effect on the uncertainty in the bottom of the temperature profile. Improvement of the external temperature tie-on is also recommended.

Various variable uncertainty sources have been identified that are hard to quantify or highly variable in space and time or are instrument-specific. Further research into these items, and consideration of these items for individual systems when building their PTU, is recommended.

2.4.5. Lidar Temperature PTU document

The following PTU document is attached as Annex VII:

- Product Traceability and Uncertainty for the temperature profile lidar product

This PTU document describes quantified uncertainties for the following lidar sites:

- Table Mountain, USA, 34.4 °N, 117.7 °W, 2300 m
- Mauna Loa, Hawaii/USA, 19.54 °N, 155.58 °W, 3397 m
- Purple Crow Lidar, Ontario, Canada, 43.07°N, 81.34 °W., 275 m

2.5. Total column O₃ measured by UV-visible spectroscopy

2.5.1. Measurement technique basics

UV-visible spectroscopy (also referred to as DOAS, Differential Optical Absorption Spectroscopy) is a measurement technique used to determine the amount of atmospheric trace gas species, such as O₃, by analysing zenith-sky spectra at large solar zenith angles (SZAs). For the analysis of total column O₃, the absorption features of O₃ and other relevant trace gases are fitted in a wavelength window of 450-550 nm using a nonlinear least-squares fitting algorithm. Because the light source is the sun, which is low on the horizon at large SZA, this allows for a long light path through the atmosphere and the depth of the absorption of the trace gas of interest is used to determine the amount of trace gas measured along the slant path. Primary products of the spectral analysis are the slant column densities (SCDs), which are then converted into vertical column densities (VCDs), using air-mass factors (AMFs) derived by radiative transfer (RT) calculations from locally measured or climatological ozone and air-density profiles.

2.5.2. Understanding the metrological processing chain

As part of GAIA-CLIM WP2 activities, a traceability chain for the UV-visible O₃ observations and atmospheric retrievals was completed and this is discussed in detail in the annexed PTU (Annex VIII). The high-level chain is shown in Figure 9 providing a brief, high-level summary of the analysis process. As indicated in Figure 9, the data analysis is divided into two parts with the first part dealing with mostly instrumentally induced corrections and the spectral fitting routine, i.e. the conversion of the measured spectrum into the SCDs, while the second part deals with the AMF calculation and conversion of the SCDs into the VCDs and, in turn, the final O₃ data product in Dobson units.

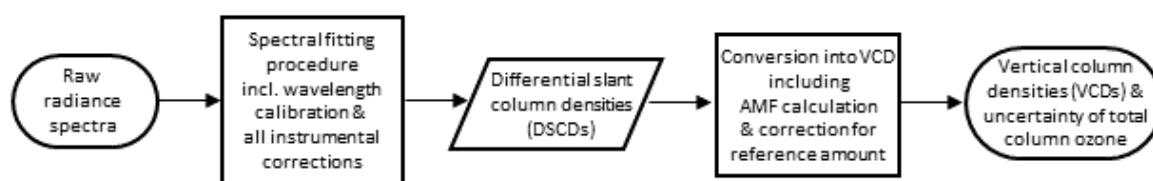


Figure 9. Main chain for total column O₃ measured with UV-visible spectroscopy. This chain displays a high-level overview of the analysis process producing the final O₃ data product.

2.5.3. Quantified uncertainties

Guided by the traceability chain introduced above, the assessment of the uncertainties associated with the UV-visible zenith-sky measurement and analysis process has been thoroughly reviewed and documented. This uncertainty assessment is expected to flow on

into other projects, such as the ESA project FRM₄DOAS⁸ and it will be further reviewed and discussed within the NDACC UV-vis working group so it can be included within the recommendations document provided by the NDACC UV-vis working group.

The “UV-vis” PTU (see Annex VIII) describes and assesses in particular the uncertainties for two selected NDACC stations, Jungfraujoch (Switzerland) and Harestua (Norway). These two time series are well characterized and representative for NDACC total column O₃ time series and have been included into the VO together with their uncertainties. Figure 10 shows as an example the daily values with their total uncertainties for 2017 measured at Harestua. The precision in the total column ozone measurements is 4.7% at 1 σ level to which the largest contribution is coming from the AMF and from the uncertainty in the SCD estimated to be 3% (1 σ) at twilight (including the impact of unknown instrumental and systematic misfit effects). The total accuracy, important for comparison with other instruments, is 5.9 % (Hendrick et al., 2011).

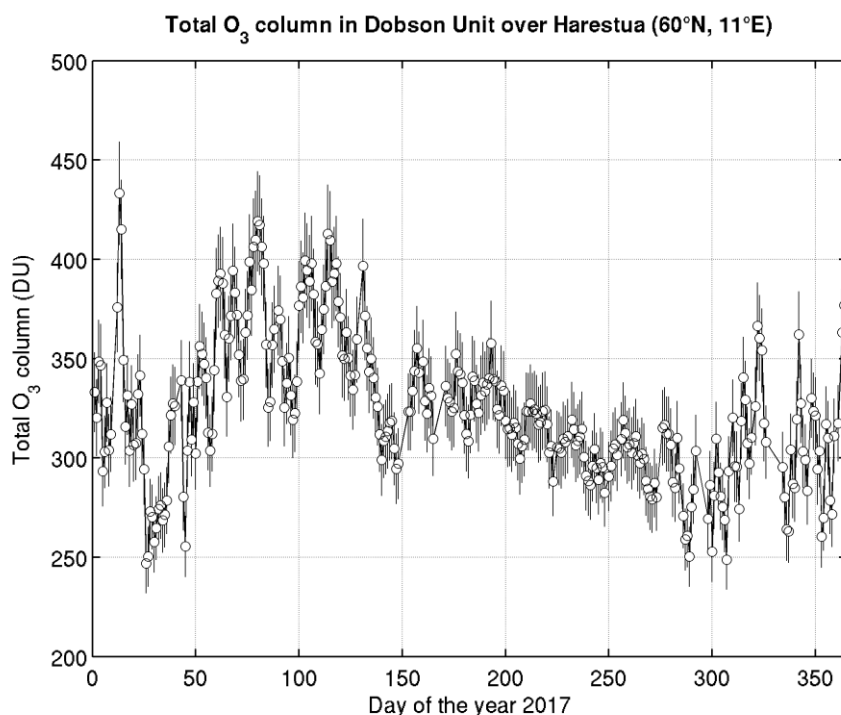


Figure 10. Daily total column O₃ values and their uncertainties for 2017. The measured values are given by the dots and the quantified uncertainties by the whiskers. Here all uncertainties have been combined so the total assessed uncertainty is being shown rather than its components.

2.5.4. Identification and description of the remaining challenges

Four specific gaps (G2.26 - G2.29) were identified within the Task 2.1 work as relevant for improving our understanding of the uncertainty budget and SI-traceability assessment of the UV-visible data products. Three of these four gaps (G2.27 - G2.29) were collapsed into one

⁸ Fiducial Reference Measurements for Ground-Based DOAS Air-Quality Observations (FRM₄DOA): <http://frm4doas.aeronomie.be>

comprehensive gap within the GAID highlighting the different aspects in the lack of our understanding of random uncertainties, air mass factor calculations, and vertical averaging kernels in the total ozone column retrieval. The fourth gap (G2.26) was kept separate, because it addresses the uncertainty in O₃ absorption cross-sections, which is one of the main sources of systematic bias in the remote sensing of O₃ using a range of different UV-visible absorption spectroscopy techniques and applies also to MAX-DOAS and Pandora instruments, as well as to Brewer and Dobson instruments. All four gaps were addressed to some extent within GAIA-CLIM, often in association with other projects such as FRM4DOAS and the CINDI-2 intercomparison campaign, but they remain open. However, suggestions on how to remedy each of these gaps are provided within the GAID.

2.5.5. UV-vis PTU document

The following PTU document is attached as Annex VIII:

- Product Traceability and Uncertainty for the NDACC UV-visible spectroscopy total column ozone product

This PTU document describes the uncertainty characterization for the following sites:

- Harestua, Norway, 60.2 °N, 10.8 °E, 596 m
- Jungfraujoch, Switzerland, 46.55 °N, 7.98 °E, 3580 m

2.6. Total column water vapour measured by GNSS

2.6.1. Measurement technique basics

Measuring Global Navigation Satellite System (GNSS) Integrated Precipitable Water (IPW), also referred to as Total Column Water Vapour (TCWV), reported in mm or in kg/m^2 , is based on an inverse method where the GNSS signal path delays in the atmosphere are mapped into Zenith Total Delays (ZTDs) and converted into IPW via an inversion method using a forward model and either standard meteorological observations made at or near the site or NWP/reanalysis based estimates.

2.6.2. Understanding the metrological processing chain

The processing chain of GNSS IPW observations is schematically shown in Figure 11 and a more detailed traceability chain can be found in the corresponding PTU document (Annex IX). Observational data from GNSS receivers are processed by the forward modelling GNSS data processing software to obtain the corresponding ZTDs and uncertainties. These values, accompanied by additional atmospheric data (ground surface pressure and temperature with their uncertainties), physical constants and their uncertainties used in conversion formulas ($\text{ZTD}, \sigma_{\text{ZTD}} \rightarrow \text{IPW}, \sigma_{\text{IPW}}$), are used in a second phase of data processing to derive GNSS IPW and its uncertainty.

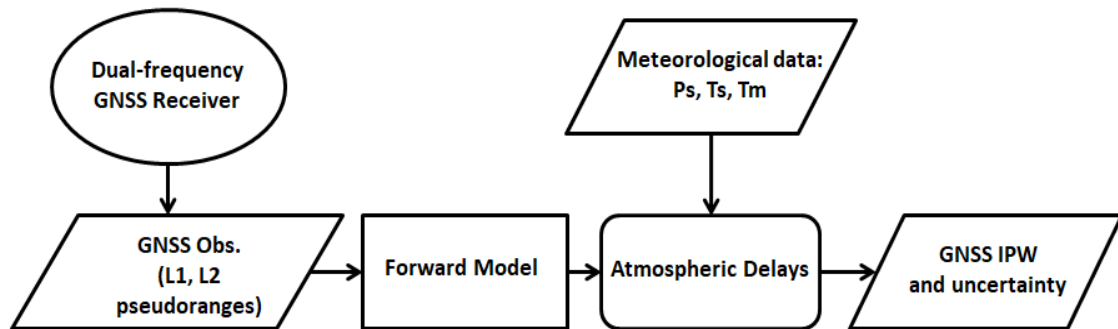


Figure 11. GNSS IPW measurements main traceability chain, where P_s denotes surface pressure, T_s the surface temperature, and T_m the mean temperature of the atmosphere.

2.6.3. Quantified uncertainties

As part of the GAIA-CLIM WP2 activities, a goal has been to clarify the sources of software-dependent differences in ZTD uncertainties. For deriving GNSS IPW and its uncertainty, the limiting factors in any GNSS-data processing software are the ZTD and its attendant uncertainty, which typically contributes more than 75% to the GNSS IPW total uncertainty budget. The ZTD is estimated using commercial software packages that are not fully open.

This makes it of paramount importance to understand the software-package dependencies, which often cause significant differences in reported ZTD uncertainty estimates for the same observational data. If we fully understand the systematic software-dependent differences, we

can rescale the ZTD uncertainty before calculating the IPW total uncertainty and thus reduce the uncertainty.

For the two most common software packages GAMIT and Bernese, the main differences originate from *a priori* uncertainties assigned to the L1-phase observables which differ by an order of magnitude: 1 mm for Bernese and 10 mm for GAMIT. These differences have an effect on the reported uncertainties in ZTD solutions. There are also differences in using *a priori* values of the Zenith Hydrostatic Delay (ZHD), the hydrostatic component of the ZTD, and in methods and criteria for evaluating the “goodness of fit”⁹ of the numerical solution. Hence, to compare how these two software algorithms (used as black-box solutions for the end-user) work, knowing the documented differences, systematic comparisons were required.

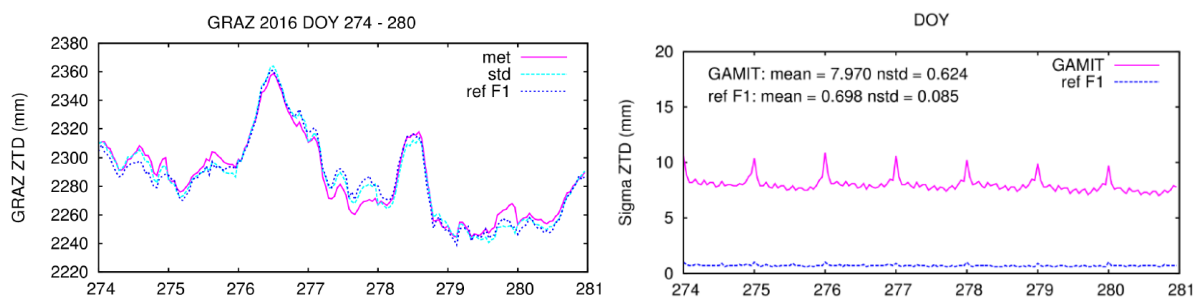


Figure 12 Left: GRAZ ZTD from GAMIT non-optimized solution with standard atmosphere model (light-blue) and with real meteorological data (violet) and Bernese reanalysis (blue). Right: 1σ ZTD from GAMIT and Bernese reanalysis. The horizontal axes display the day of the year (DOY).

Figure 12 shows an example where for similar ZTD values, the 1σ for both software packages do not agree. Based on an analysis of existing documentation, a comparison using different software packages (Bernese, GAMIT, and GIPSY) was run at E-GVAP benchmark sites, and a comparison undertaken with reanalysis (ERA5).

It can be concluded that the numeric values of uncertainties, originating from different software, without knowing software-specific constraints set for these uncertainties, may not be a reliable criterion for evaluating GNSS tropospheric products (ZTD and its 1σ uncertainty). For getting realistic GNSS IPW estimates for cal/val procedures the data analyst must rely on additional calibration of the observables (ZTD and IPW) based on results from intercomparison experiments. There is no concern about the software-dependences of ZTD 1σ uncertainties, but the data analyst needs to use these values responsibly.

2.6.4. Identification and description of the remaining challenges

As a recommendation, the full GNSS data processing should be transparent (which is mostly not the case across the global GNSS networks currently), and it would be helpful to continuously monitor what the main contributors to the total GNSS IPW uncertainty are (basically while any singularities noticed in ZTD or IPW uncertainty time series). High-quality

⁹ https://en.wikipedia.org/wiki/Goodness_of_fit

and systematically calibrated instrumentation should be used to avoid biases (even in solutions with “acceptable” uncertainties).

2.6.5. GNSS-IPW PTU document

The following PTU document is annexed as Annex IX:

- Product Traceability and Uncertainty for the GNSS IPW product

This PTU document is covering the following sites:

- Beltsville, USA, 39.05° N, 76.88° W, 53 m
- Boulder, USA, 39.95° N, 105.20° W, 1743 m
- Cabauw, Netherlands, 51.97° N, 4.92° E, 1 m
- Lauder, New Zealand, 45.05° S, 169.68° E, 370 m
- Lindenberg, Germany, 52.21° N, 14.12° E, 98 m
- Ny-Ålesund, Norway, 78.92° N, 11.92° E, 5 m
- Payerne, Switzerland, 46.81° N, 6.95° E, 491 m
- Potenza, Italy, 40.60° N, 15.72° E, 720 m
- Sodankylä, Finland, 67.37° N, 26.63° E, 179 m

These are all certified GRUAN sites (<https://www.gruan.org/network/sites/>).

2.7. CH₄, CO₂, O₃, and H₂O columns and profiles measured by FTIR

2.7.1. Measurement technique basics

Most atmospheric molecules interact with electromagnetic radiation in the infrared spectral region, which makes infrared remote-sensing an important tool for atmospheric research. The two main components of the ground-based instrumentation measuring these infrared spectra are a precise solar tracker and a high-resolution Fourier Transform Spectrometer (FTS). An FTS is based on a Michelson Interferometer, consisting of a beamsplitter that divides the incoming radiance into two beams. One of the beams is reflected by a fixed mirror or retroreflector, while the other one is sent to a moving mirror, causing a variable optical path. At the beamsplitter, they recombine and interfere according to their wavelength and optical path difference. The optical path difference is measured with a monochromatic laser. The observed intensity fluctuations are an interferogram, which is converted by a Fourier Transformation into a spectrum. These high quality solar absorption spectra are measured in the framework of the international networks NDACC¹⁰ (Network for the Detection of Atmospheric Composition Change) and TCCON¹¹ (Total Carbon Column Observing Network). NDACC covers the middle infrared spectral range 700 - 4200 cm⁻¹ and TCCON the near infrared spectral range 3900 - 14000 cm⁻¹.

2.7.2. Understanding the metrological processing chain

The physical model chain of the FTIR measurement (see FTIR PTUs for H₂O and O₃ in Annex X and Annex XI) displays the physical processes associated with the Fourier Transform Infrared Spectroscopy (FTIR) for atmospheric solar absorption measurements. As discussed above, the primary measurand is the interferogram, which is the detected (solar) light intensity against the optical path difference of the moving mirror of a Michelson interferometer setup. After applying a fast Fourier transform (FFT), the interferogram is then transformed into an (uncalibrated) transmittance spectrum. This is then processed via the following steps discussed in detail in the FTIR PTUs (see Annex X and Annex XI) and summarized in the main chain shown in Figure 13. Finalisation of the uncertainty quantification in the manner required for GAIA-CLIM WP2 was only possible for NDACC FTIR measurements covering two of the four target species.

¹⁰ <https://www2.acom.ucar.edu/irwg>

¹¹ <http://www.tccon.caltech.edu>

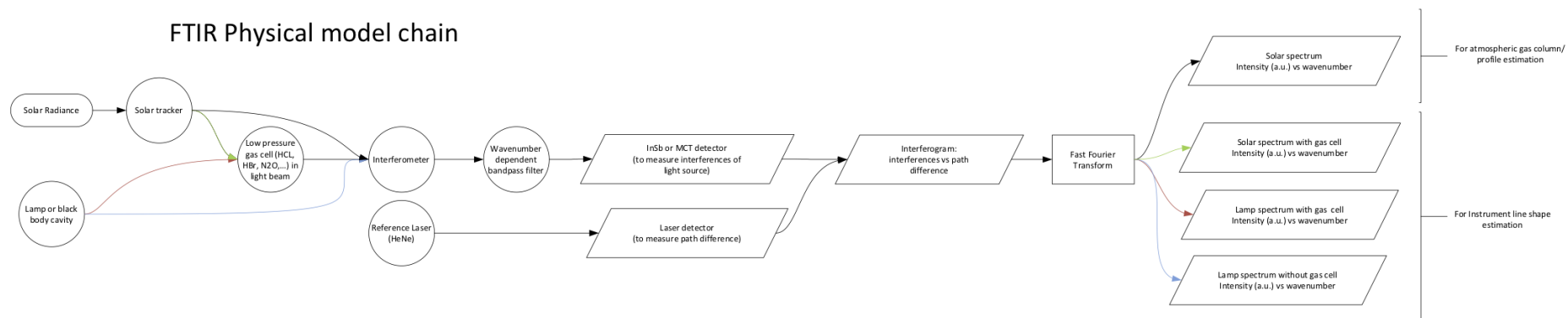


Figure 13. FTIR physical model chain applicable for NDACC measurements.

2.7.3. Quantified uncertainties

The retrieval software applied by the NDACC infrared working group uses optimal estimation or Tikhonov regularization for deriving information about the vertical distribution of the target gas in the atmosphere. The retrieval process requires *a priori* information of the state of the atmosphere and other input parameters necessary to determine a retrieval of the abundance of a target gas out of an FTIR spectrum. Spectroscopic parameters, solar position at the time of the measurement, pressure and temperature profile data are examples of such input parameters (see also the processing chain <http://www.gaia-clim.eu/page/ftir-traceability-diagram>).

All input parameters are provided with an uncertainty estimate and the retrieval software will propagate all the individual uncertainty contributions towards the uncertainty on the retrieved concentrations of the target gas using the formulas from Rodgers, 2000. The uncertainty budget reported in the NDACC GEOMS data files is representative for all uncertainty contributions of the input parameters for the retrieval software, except of the smoothing uncertainty. The data user has at its disposal the averaging kernel matrix (per measurement) to estimate or eliminate the smoothing uncertainty when using the data. The GEOMS data files distinguish the random and systematic uncertainty estimates. As an example, the CH₄ profile and uncertainty estimates are shown in Figure 14.

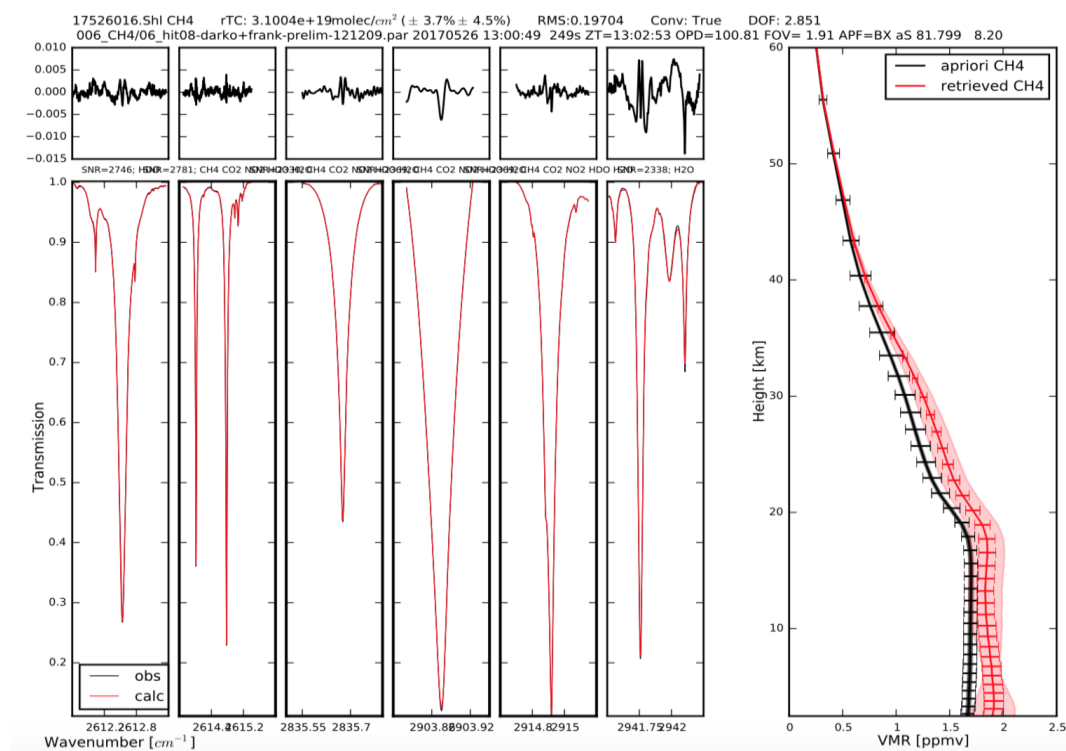


Figure 14. Example of a retrieved CH₄ profile (right, in red) from an absorption spectrum (selected retrieval microwindows, left). The retrieved profile shows the random uncertainty as error bars and the systematic uncertainty as the shaded area. The random and systematic uncertainty on the retrieved column is written in the title.

During the QA4ECV¹² and GAIA-CLIM projects, the uncertainty routines of the retrieval software packages (PROFFIT and SFIT) employed within the NDACC infrared working group were aligned. As part of GAIA-CLIM WP2, the uncertainty budget for the CH₄-retrieval setup was tuned and implemented in PROFFIT and SFIT. The CH₄ systematic uncertainty budget is dominated by the uncertainty on the spectroscopic CH₄ -line intensities, estimated at 3%. This is implemented across the NDACC infrared working group.

2.7.4. Identification and description of the remaining challenges

For TCCON data analysis, a least-squares fitting algorithm is used to scale an *a priori* profile to retrieve the column averaged dry-air mole fraction of the target gas. The official uncertainty estimation for the TCCON products was presented for the first time in detail in Wunch et al., 2011. An update was provided recently in the standard TCCON data archive documentation (Wunch et al., 2015), which accounts for changes in the current version (GGG2014) of the networks common processing software.

A quantification of the individual uncertainty contributions is often not possible for TCCON measurements. However, the retrieved averaged CO₂ and CH₄ data have been validated using vertically resolved in-situ observations by aircraft (validated against WMO standards) or AirCore (Wunch et al., 2015), covering the altitude range from 500 m to 12 km (aircraft) and up to 30 km for the AirCore. The correction factor derived from the vertically resolved in-situ data was found to be constant for all sites, and did not change with time. In view of this, the TCCON PTU format would deviate clearly from the NDACC PTU.

A processing chain has been developed and is shown in Figure 15. For a discussion of the official TCCON uncertainty budget we refer to the TCCON documentation in Wunch et al. (2015). An additional representation of this uncertainty quantification, as a PTU added to this document, would introduce ambiguities for the data users.

¹² <http://www.qa4ecv.eu/>

FTIR Processing chain - TCCON

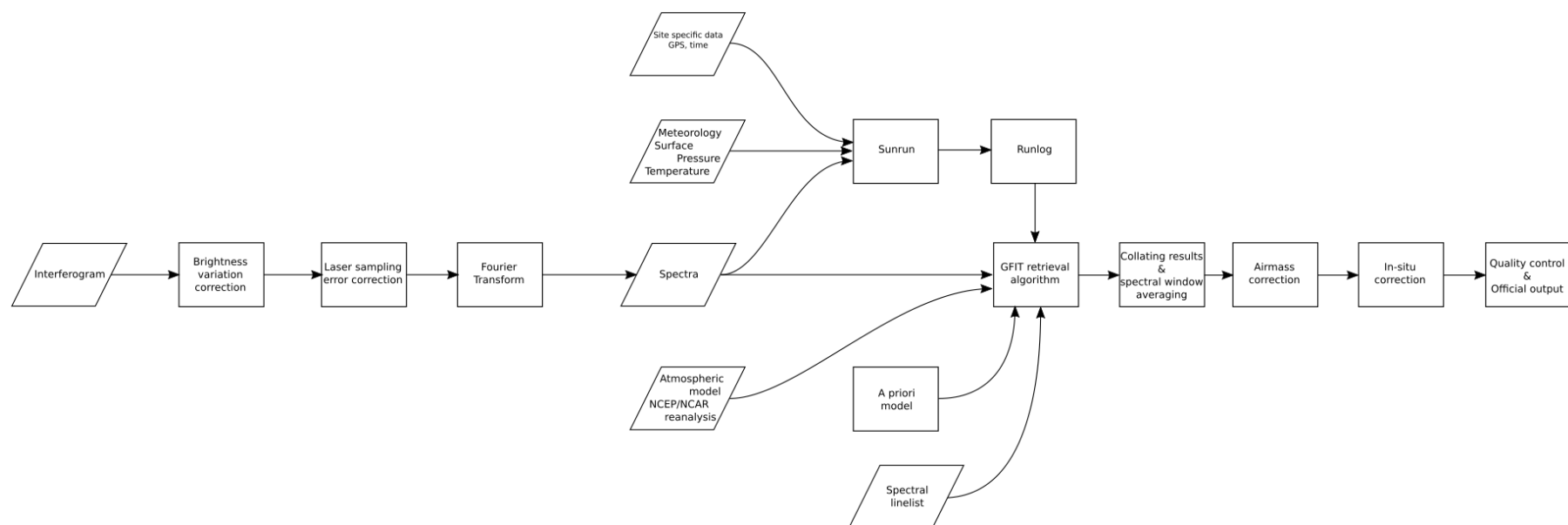


Figure 15. TCCON processing chain

2.7.5. FTIR PTU documents

Production of PTU documents for FTIR was possible only for two of the four target ECVs and solely for the NDACC network. The following two PTU documents are annexed as Annex X and Annex XI:

- Product Traceability and Uncertainty for the MUSICA ground-based NDACC/FTIR tropospheric H₂O profile product

This PTU document is covering the following sites:

- Eureka, Canada, 80.1° N, 86.4° W, 610 m
 - Ny-Ålesund, Norway, 78.9° N, 11.9° E, 21 m
 - Kiruna, Sweden, 67.8° N, 20.4° E, 419 m
 - Bremen, Germany, 53.1° N, 8.9° E, 27 m
 - Karlsruhe, Germany, 49.1° N, 8.4° E, 110 m
 - Jungfrauoch, Switzerland, 46.6° N, 8.0° E, 3580 m
 - Izaña, Tenerife, Spain, 28.3° N, 16.5° W, 2367 m
 - Altzomoni, Mexico, 19.1° N, 98.7° W, 3985 m
 - Addis Ababa, Ethiopia, 9.0° N, 38.8° E, 2443 m
 - Wollongong, Australia, 34.5° S, 150.9° E, 30 m
 - Lauder, New Zealand, 45.1° S, 169.7° E, 370 m
 - Arrival Heights, Antarctica, 77.8° S, 166.7° E, 250 m
-
- Product Traceability and Uncertainty for the ground-based NDACC/FTIR O₃ profile product.

This PTU document is covering the following sites:

- Kiruna, Sweden, 67.84 °N, 20.41 °E, 419 m
- Izaña, Tenerife/Spain, 28.30 °N, 16.48 °W, 2367 m.

2.8. Tropospheric O₃ measured by MAX-DOAS and Pandora

2.8.1. Measurement technique basics

MAX-DOAS is an extension of the UV-visible spectroscopy technique described in Section 2.4 using several different elevation angles to scan the sky and determine a vertical resolution. The MAX-DOAS tropospheric O₃ retrieval is based on a two-step approach: (1) a spectral inversion step using the Differential Optical Absorption Spectroscopy (DOAS) method and providing the O₃ slant column densities (SCDs), which is the O₃ concentration integrated along the effective light path, and (2) a subsequent conversion step, which ultimately provides the end products (tropospheric vertical columns and/or profiles). Regarding step 2, experimental retrieval methods, which are based on Optimal Estimation (OE) schemes (Liu et al., 2006; Irie et al., 2011) or on more simple approaches, such as the modified geometrical approximation (Gomez et al., 2014), have been applied so far to infer profile information on tropospheric O₃.

2.8.2. Understanding the metrological processing chain

A better characterisation of the tropospheric O₃ retrieval from MAX-DOAS measurements was also one of the main topics of the second Cabauw Intercomparison of Nitrogen Dioxide measuring Instruments (CINDI-2) campaign, which took place in September 2016 in Cabauw, the Netherlands. At this occasion, 36 MAX-DOAS systems, including 6 Pandora spectrometers, were operated side-by-side with a suite of ancillary instrumentation over a period of 3-4 weeks¹³. Preliminary investigations led by the Max Planck Institute for Chemistry (MPIC-Mainz) showed that (1) the temperature dependence of O₃ cross-sections can be used to explicitly separate tropospheric and stratospheric O₃, and (2) the elevation angle dependence of the warm O₃ SCDs (corresponding to effective lower tropospheric O₃ cross-sections) is well suited for the O₃ profile retrieval using the classic OE method. As part of CINDI-2, tests and developments towards a first tropospheric O₃ MAX-DOAS profiling algorithm are under progress. It should be noted that this activity is also important in the context of the ESA project FRM₄DOAS¹⁴, aiming at further harmonization and characterization of MAX-DOAS systems and data sets, through the development of a dedicated centralized processing system.

As envisaged, GAIA-CLIM has been collaborating closely with these activities and has been working towards developing a metrological traceability chain for tropospheric O₃. Although our efforts as part of GAIA-CLIM have clearly advanced the progress towards traceability and a thorough understanding of the uncertainties, currently such a fully traceable uncertainty chain is not yet available. When the WP2 subtask addressing this issue was originally planned, the expectation then was that the processing algorithm for tropospheric O₃ would have been further developed before the end of the GAIA-CLIM project to allow an in-depth investigation of the uncertainties, but due to delays in other projects which were expected to feed into the studies envisaged for GAIA-CLIM, as well as due to the more complicated nature of the data retrieval, the technique was not developed as far as expected within the GAIA-CLIM timeframe and it is currently not yet at a stage where it was possible to develop a fully traceable and well characterized processing chain. However, since a range of elements

¹³ <http://www.tropomi.eu/data-products/cindi-2>

¹⁴ <http://frm4doas.aeronomie.be>

discussed as part of the UV-visible traceability chain in the attached PTU (see Annex VIII) are also fully applicable to the MAX-DOAS analysis, clear progress has been made with regard to those elements, as well as in our understanding of what needs to be concentrated on next to reach the goal of a fully characterized uncertainty budget for tropospheric O₃.

2.8.3. Quantified uncertainties

In the OE method, the total retrieval uncertainty is given by the sum of three terms (see Rodgers et al., 2000): the smoothing uncertainty (uncertainty related to the smoothing of the true profile by the retrieval), the retrieval noise (noise on the measurements), and the forward model parameter uncertainty (uncertainty in the retrieval due to errors in the forward model parameters). The first two uncertainty sources are random, while the forward model parameter uncertainty may contain both random and systematic components. Another significant source of systematic uncertainty is the uncertainty on the absorption cross-sections used in the DOAS spectral inversion.

In the publication by Irie et al. (2011), the random uncertainty is assumed to be given by the sum of the smoothing and retrieval noise uncertainties, while the systematic uncertainty is assumed to be dominated by the uncertainty on the aerosol retrieval. Both random and systematic uncertainty estimates on the retrieved planetary boundary layer O₃ volume mixing ratio are of 2% and 26%, respectively.

Liu et al. (2006) have carried out sensitivity studies of their approach to reference normalization, spectral resolution, wavelength range, measurement uncertainty, surface albedo, and viewing geometry and they estimated the total uncertainty as the sum of the smoothing and measurement noise uncertainties. On average, they found a total uncertainty on the retrieved O₃ volume mixing ratio in Umkehr layers 1-5 and on tropospheric O₃ column of 11% and 25%, respectively.

In Gomez et al. (2014), the total relative uncertainty on the O₃ concentration at the altitude of the MAX-DOAS instrument retrieved by the modified geometrical approximation method is of about 7% for SZA lower than 70°. It takes into account the uncertainties of the DOAS fit, air density, and absorption cross-sections. At larger SZA, the uncertainty on the estimated light-path length becomes dominant and the total uncertainty reaches 45% at 80° SZA. This means that for higher SZA, this more simplified method leads to substantially greater uncertainties.

Given that some of these uncertainties are currently still rather large for a data set to be developed into a reference status data stream, either strict limitations need to be applied to the existing techniques (e.g. restriction of SZA range) or new and/or extended techniques need to be developed.

2.8.4. Identification and description of the remaining challenges

Although retrieving tropospheric O₃ from passive remote sensing observations is difficult, because almost 90% of the total column ozone resides in the stratosphere, the pioneering studies of Liu et al. (2006), Irie et al. (2011), and Gomez et al. (2014) have demonstrated that profile information on tropospheric O₃ can be extracted from multi-angular scattered-sunlight

observations using the MAX-DOAS technique (see also 2.5.3 above). The gap analysis undertaken within GAIA-CLIM was thus based on these studies and focused on the following gap types: better understanding of different MAX-DOAS tropospheric O₃ retrieval methods, their random and systematic uncertainties, and the associated information content. More specifically, the current lack of a full uncertainty characterization for the different retrieval methods and MAX-DOAS/Pandora tropospheric O₃ measurements validation using ozonesondes and/or in-situ surface O₃ data, limits the potential of a meaningful assessment of MAX-DOAS tropospheric O₃ network capabilities.

Further studies are needed to investigate these issues and should be preferably conducted in a coordinated way, e.g. as part of an instrument intercomparison experiment, such as CINDI and CINDI-2, and need to include exercises specifically targeted at measuring tropospheric O₃. Furthermore, new retrieval approaches should also be tested on MAX-DOAS/Pandora measurements. For instance, to efficiently use the available information content (which is usually low for MAX-DOAS and Pandora systems), the so-called “dimension reduction scheme” could be exploited; it transforms a large retrieval problem into a smaller sized one, depending only on few parameters and still achieving almost the same solution (e.g. Tukiainen et al. 2016).

In particular in the case of Pandora systems, studies published so far describe measurement uncertainties on total O₃ columns only (see e.g. Herman et al., 2015; Tzortziou et al., 2012). For example, systematic uncertainty in Pandora direct-sun measurements are limited by temperature effects not corrected in current operational baselines. The neglect of temperature effects (related to the ozone spectroscopy in the Huggins bands) leads to seasonally dependent systematic biases, of various amplitudes depending on the latitude of the site. In order to obtain information on tropospheric ozone, further algorithm development and uncertainty characterization is needed. In general, similar methods that are applied to MAX-DOAS instruments need to be considered.

3. Conclusions

Significant progress has been made in the traceable uncertainty analysis of the techniques investigated within WP2 of the GAIA-CLIM project. In-depth uncertainty assessments in form of the GAIA-CLIM PTU documents have been made for several ECVs. Each of these PTUs provides a comprehensive uncertainty evaluation for each of the steps of the traceability chains which were designed for selected ECV data products and measurement techniques. For temperature profiles, PTUs for two different techniques, i.e. MWR and lidar, have been produced. For water vapour, PTUs using three different techniques, i.e. MWR, FTIR and GNSS, have been generated. For ozone, two PTUs address the retrieval of profiles (lidar and FTIR) while a third PTU addresses the uncertainty assessment for total column ozone measurements using the UV-visible spectroscopy technique. Finally, for aerosol profiles, a PTU describing the uncertainty assessment of lidar measurements was also created.

However, given the limited time and resources available within the project, issues persist. In some cases, like for the lidar (task 2.1.1) and FTIR (task 2.1.3) subtasks, a rather ambitious target of 4 species was originally set and this was clearly envisaged in collaboration with other GAIA-CLIM external projects. And although in all cases discernible progress was achieved, neither the water vapour PTU for lidar nor the methane and CO₂ PTUs for FTIR could be fully realised. Also for the MAX-DOAS technique, progress towards a more complete understanding of the uncertainty budget was achieved but a complete uncertainty analysis as required for a PTU document could not be fully realised within the GAIA-CLIM timeframe. It should also be noted here that the work done within GAIA-CLIM considered just a specific subset of measurement techniques and ECVs, and that other ECV/technique combinations would benefit from such an analysis in future.

In summary, the PTU documents provided as annexes contain the current status of the uncertainty understanding as determined by the technique experts. The PTU documents each contain also a recommendations section, addressing the key issues still requiring some more attention to progress the technique uncertainty analysis towards reference grade. These are summarized in the “Identification and description of the remaining challenges” sections in this document. Table 1 highlights a summary of the principle recommendations from the PTU traceable uncertainty and gap analysis, together with the recommended remedy.

Table 1. PTU recommendation summary

ID#	Technique	Challenge	Recommended remedy
2.1-1	MWR	The lack of MW radiometry standards is currently hampering the SI traceability of MWR observations.	NIST is working towards addressing this challenge and currently developing such standards for MW radiometry. They plan to provide SI-traceability for calibration targets and transfer standards in the next few years.

2.2-1	Aerosol Raman lidar	Use of a representative pressure & temperature profile would reduce the systematic uncertainty in the density/ extinction coefficient profile.	Use pressure & temperature profiles either measured with co-located instrumentation (if available) or provided by NWP fields.
2.2-2	Aerosol Raman lidar	Non-standardised molecular density profile methodology across the network.	The molecular density profile methodology needs to be standardized across the network.
2.2-3	Aerosol Raman lidar	Insufficient information about the detector efficiency inflates uncertainties.	Additional analysis and in-depth assessment of the detector efficiency needs to be undertaken.
2.2-4	Aerosol Raman lidar	Poor low altitude estimation of the extinction coefficient.	An experimental characterisation of the optical & geometric properties of all the systems in the network is needed.
2.2-5	Aerosol Raman lidar	Non-standardised signal handling procedures.	The statistical uncertainty could be improved via standardisation of the signal handling procedures of both in pre-processing and processing stages.
2.3-1 2.4-1	Ozone abs lidar Temp lidar	Insufficient vertical distribution of interfering gases knowledge in specific scenarios.	Improved vertical distribution of interfering gases knowledge in specific scenarios necessary.
2.3-2	Ozone abs lidar	No representative pressure & temperature profile above 30 km available.	Effort needs to be spent on sourcing representative pressure & temperature profiles above 30 km.
2.3-3	Ozone abs lidar	Site-to-site variation in the processing of differential absorption lidar and, in turn, in uncertainty estimates.	A centralised data processing facility for differential absorption lidar should be setup to provide more homogeneous data processing.
2.4-2	Temp lidar	Low confidence in representative pressure & temperature profile in the lowest part/top of the profile.	More representative pressure & temperature profiles in the lowest part of the profile need to be sourced and used, and the 'tie-on' to the measured profile needs to be improved.
2.5-1	Ozone column UV-vis DOAS	Insufficient knowledge of the effects of random uncertainties on the ozone column retrievals.	Sensitivity studies to improve our understanding of the impact of a variety of random uncertainties on ozone column retrievals and final output data sets.
2.5-2	Ozone column UV-vis DOAS	Insufficient knowledge of the air mass factor calculation uncertainty contributors.	Sensitivity studies to improve our understanding of the impact of each of the air mass factor calculation uncertainties, review existing recommendations and standardize calculation inputs and settings

			where possible & review existing look-up tables.
2.5-3	Ozone column UV-vis DOAS	Insufficient knowledge of the vertical averaging kernel calculation uncertainty.	Studies to improve our knowledge of the vertical averaging kernel calculation uncertainty, e.g. by selecting specific retrieval algorithms coupled with chemistry-transport model output to run an in-depth comparison with the averaging kernels retrieved based on the airmass factor look-up tables.
2.5-4	Ozone column UV-vis DOAS	Insufficient knowledge of the ozone cross section uncertainty.	Sensitivity studies needed to understand the uncertainties caused by different sets of ozone cross-sections used within the data analysis and how this impacts on the overall measurement uncertainty.
2.6-1	GNSS	Black-box processing of the ZTD and its uncertainty does not allow transparency in the method or the resulting uncertainty.	Further studies are necessary to elucidate the methods & uncertainties within the proprietary data processing software.
2.7-1	FTIR	A quantification of a variety of individual uncertainty contributions was not possible within the available timeframe for TCCON measurements.	Community effort to further quantify all individual uncertainty contributions for TCCON based on the partially developed traceability diagrams.
2.7-2	FTIR	Only two of the four NDACC species (ozone and water vapour) were quantifiable within the GAIA-CLIM project timeframe.	Quantification of all uncertainty contributions for the remaining two NDACC species (methane and CO ₂).
2.8-1	Ozone profile UV-vis MAX-DOAS	The additional processing steps (and associated uncertainties) required to retrieve profile information beyond the total column ozone measurements need further attention.	An in-depth quantification of the additional steps beyond the total column ozone measurement needs to be undertaken, a complete traceability chain needs to be drafted and the individual elements in that chain need to be investigated and assessed.
2.2-6 2.3-4 2.4-3 2.5-5	Aerosol Raman lidar Ozone abs lidar Temp lidar Ozone column UV-vis DOAS	Identified unquantified uncertainty contributions.	Efforts towards investigating and assessing any of these unquantified uncertainty contributions.

N/A	Water vapour lidar	A complete quantification of the individual uncertainty contributions was not possible within the GAIA-CLIM timeframe.	Further effort is needed to provide the complete quantification of all individual uncertainty contributions for the water vapour lidar.
-----	--------------------	--	---

In terms of the meteorological assessment of the traceability for the techniques covered in WP2, a set of criteria were created as an independent measure of whether the data is reference quality. The metric, is one or a number of possible variations, but highlights the critical points necessary. The essential elements of this assessment are:

- A clear definition of the product dataset being assessed, including its temporal and spatial extend. Primarily to indicate to the user what is or is not covered by the assessment.
- Who undertook the assessment, together with their contact details.
- Is there a peer-reviewed document available to the user community describing the contributing uncertainties for the data product?
- Is there a peer-reviewed document available to the user community describing the specific measurement technique for the data product?
- Was a traceability diagram produced, showing the detailed measurement & processing steps according to the GAIA CLIM guidance (D2.6)?
- Was a PTU document produced according to the GAIA CLIM guidance (D2.6)?
- Has the impact of traceability confidence assessment been undertaken, according to the GAIA CLIM guidance (D2.6)?

The last three points provide the evidence base for the reference-quality assessment, with the PTU providing the current state of the uncertainty knowledge, and the traceability confidence assessment as a mechanism to assess whether any missing information is critical to the overall uncertainty knowledge.

Considering the products for which PTUs have been constructed within WP2:

The microwave radiometer temperature and humidity profile product measurement technique has been published in Westwater [2004] & [2005]. The data has been used in multiple published analyses. Construction of the PTU document showed a good level of overall uncertainty assessment, with a clear understanding of the technique uncertainty. The highlighted issues are reflected in the known gaps for this technique, in the temperature SI traceability of the calibration targets and underlying microwave spectroscopy uncertainties. With that caveat applied it is valid to serve the data from a metrological viewpoint as constituting a reference quality measurement series. The microwave radiometer community is urged to consider the stated gaps in any subsequent versions.

The LIDAR aerosol extinction coefficient product is derived from measurements using Raman lidar methods within the EARLINET network. The PTU assessment for this product identified some key areas of the uncertainty budget that would need to be addressed before the product could be considered to be fully metrologically traceable – these included more standardized methodologies, evaluation of the system-specific properties at low elevations, and assessment of the contribution of a number of

potential uncertainty sources that are currently assumed to be negligible. The EARLINET network is encouraged to address these issues.

The ozone profile differential absorption Lidar (DIAL) product is described for those measurements undertaken within the NDACC network. The PTU assessment is based primarily on the work described in a pair of papers by LeBlanc et al [2016 a & b], which provide an overview of the various sources of uncertainty within the ozone DIAL measurement process and how they are combined, with specific examples focused on two of the NDACC sites (Mauna Loa and Table Mountain). Since many of the uncertainty sources are system specific, it is recommended that consideration of these contributions are conducted for the individual sites across the network together with establishment of a centralized data processing facility. Implementation of these steps would result in the generation of a reference source of ozone profile data.

The conclusions for the traceability and uncertainty of the temperature profile LIDAR product have many similarities to those for the ozone DIAL product, with a common set of issues to be resolved in order to generate a fully traceable data source. One specific area of relevance to the temperature profile product is the influence of the external ancillary data (pressure, temperature, and other gases) on the final product. The relevant networks (NDACC and GRUAN) are encouraged to implement the recommended steps in order to provide a reference source of temperature and ozone profile data.

The UV-VIS DOAS product measurement technique and uncertainty budget has been published in Hendrik et al [2011], which also describes inter-comparison campaign results. Construction of the PTU document highlighted a number of effects that had not been considered and others that, although estimated in their native units, have not been propagated through the fitting and retrieval processes to the geophysical product. A fully traceable assessment of the overall uncertainty would require element uncertainties on a common (geophysical product) unit base. It is difficult to assess the relative magnitude or make a robust assessment of the overall uncertainty at a range of temporal and spatial averaging requirements. The UV-VIS DOAS community is urged to consider additional studies to allow a unified assessment in any subsequent versions.

The GNSS IPW product measurement technique and uncertainty budget has been published in Ning et al [2016]. Construction of the PTU document highlighted a number of issues, reflected in the known gaps for this technique; specifically, the 'black-box' nature of the ZTD processing that does not allow a traceable propagation of uncertainty contributors through the processing software; and also non-transparent variation in processing by different GNSS analysis centres. The GNSS community is urged to consider additional studies to allow a more transparent and traceable uncertainty propagation in any subsequent versions.

The ground-based FTIR tropospheric H₂O profile product is based on the MUSICA measurements of water vapour within the NDACC network, which use optimal estimation analysis methods [Rogers et al. 2000]. In addition to minor issues with regards to local temperature uncertainties and system-specific baseline distortions, the primary issue that would need to be resolved before a reference-data product was available, is improved knowledge of the uncertainties of the spectroscopic parameters, and the propagation of these uncertainties through the lineshape model and optimal estimation procedures. It is therefore strongly encouraged that further research into spectroscopic uncertainties is undertaken.

The ground-based FTIR O₃ profile product, again from NDACC network measurements, has similar uncertainty and traceability issues to the H₂O profile measurements, with the spectroscopic uncertainties being the primary recommendation for further research. In both cases, there are also some uncertainty components that are currently assumed to be negligible that would need to be checked in order to provide a set of fully traceable reference FTIR data products.

Implementation of reference FTIR data for O₃ and H₂O could be extended to CH₄ and CO₂ total column measurements within the TCCON network once a PTU assessment has been undertaken for these additional gases. Work on the uncertainties of the TCCON measurements has already been reported by Wunch et al [2011 & 2015] and this could form the basis of such an assessment.

4. References

- Cimini D., P. W. Rosenkranz, M. Tratyakov, and F. Romano, Sensitivity of microwave downwelling brightness temperatures to spectroscopic parameter uncertainty, ITSC21, Darmstadt, Germany, 29 November - 5 December, 2017
- De Angelis, F., Cimini, D., Hocking, J., Martinet, P., and Kneifel, S.: RTTOV-gb – adapting the fast radiative transfer model RTTOV for the assimilation of ground-based microwave radiometer observations, *Geosci. Model Dev.*, 9, 2721-2739, doi:10.5194/gmd-9-2721-2016, Online: <http://www.geosci-model-dev.net/9/2721/2016/>, 2016
- De Angelis, F., Cimini, D., Löhnert, U., Caumont, O., Haefele, A., Pospichal, B., Martinet, P., Navas-Guzmán, F., Klein-Baltink, H., Dupont, J.-C., and Hocking, J.: Long-term observations minus background monitoring of ground-based brightness temperatures from a microwave radiometer network, *Atmos. Meas. Tech.*, 10, 3947-3961, <https://doi.org/10.5194/amt-10-3947-2017>, 2017.
- Gomez, L., M. Navarro-Comas, O. Puertedura, Y. Gonzalez, E. Cuevas, and M. Gil-Ojeda (2014), Long-path averaged mixing ratios of O₃ and NO₂ in the free troposphere from mountain MAX-DOAS, *Atmos. Meas. Tech.*, 7(10), 3373–3386, doi:10.5194/amt-7-3373-2014. 2014.
- Hendrick, F., Pommereau, J.-P., Goutail, F., Evans, R., Ionov, D., Pazmino, A., Kyrö, E., Held, G., Eriksen, P., Dorokhov, V., Gil, M., Van Roozendael, M., NDACC/SAOZ UV-visible total ozone measurements: improved retrieval and comparison with correlative ground-based and satellite observations. *Atmospheric Chemistry and Physics* 11. 10.5194/acp-11-5975-2011, 2011.
- Herman, J., R. Evans, A. Cede, N. Abuhassan, I. Petropavlovskikh, and G. McConville, Comparison of ozone retrievals from the Pandora spectrometer system and Dobson spectrophotometer in Boulder, Colorado, *Atmos. Meas. Tech.*, 8, 3407–3418, www.atmos-meas-tech.net/8/3407/2015/doi:10.5194/amt-8-3407-2015, 2015.
- Houtz D. A., W. Emery, D. Gu, K. Jacob, A. Murk, D. K. Walker, and R. J. Wylde, Electromagnetic Design and Performance of a Conical Microwave Blackbody Target for Radiometer Calibration, *IEEE Transactions on Geoscience and Remote Sensing*, vol. 55, no. 8, pp. 4586-4596, doi: 10.1109/TGRS.2017.2694319, 2017.
- Irie, H., H. Takashima, Y. Kanaya, K. F. Boersma, L. Gast, F. Wittrock, D. Brunner, Y. Zhou, and M. Van Roozendael, Eight-component retrievals from ground-based MAX-DOAS observations, *Atmos. Meas. Tech.*, 4, 1027–1044, 2011.

- Leblanc, T., R.J. Sica, J.A.E. van Gijsel, S. Godin-Beekmann, A. Haefele, T. Trickl, G. Payen and G. Liberti, Proposed standardized definitions for vertical resolution and uncertainty in the NDACC lidar ozone and temperature algorithms – Part 2: Ozone DIAL uncertainty budget, *Atmos. Meas. Tech.*, 9, 4051-4078, <https://doi.org/10.5194/amt-9-4051-2016>, 2016a.
- Leblanc, T., R.J. Sica, J.A.E. van Gijsel, A. Haefele, G. Payen, and G. Liberti, Proposed standardized definitions for vertical resolution and uncertainty in the NDACC lidar ozone and temperature algorithms – Part 3: Temperature uncertainty budget, *Atmos. Meas. Tech.*, 9, 4079–4101, doi:10.5194/amt-9-4079-2016, 2016b.
- Liu, X. K. Chance, C. E. Sioris, M. J. Newchurch, and T. P. Kurosu, Tropospheric ozone profiles from a ground- based ultraviolet spectrometer: a new retrieval method, *Applied Optics*, 45 (No. 10), 2006.
- Rodgers, C. D.: *Inverse Methods for Atmospheric Sounding, Theory and Practice*, World Scientific Publishing, Singapore – New-Jersey – London – Hong Kong, 2000.
- Thorne, P. W., Madonna, F., Schulz, J., Oakley, T., Ingleby, B., Rosoldi, M., Tramutola, E., Arola, A., Buschmann, M., Mikalsen, A. C., Davy, R., Voces, C., Kreher, K., De Maziere, M., and Pappalardo, G.: Making better sense of the mosaic of environmental measurement networks: a system-of-systems approach and quantitative assessment, *Geosci. Instrum. Method. Data Syst.*, 6, 453-472, <https://doi.org/10.5194/gi-6-453-2017>, 2017.
- Tukiainen, S., J. Railo, M. Laine, J. Hakkarainen, R. Kivi, P. Heikkinen, H. Chen, and J. Tamminen (2016), Retrieval of Atmospheric CH₄ Profiles from Fourier transform Infrared Data Using Dimension Reduction and MCMC, *J. Geophys. Res. Atmospheric.*, 121, doi:10.1002/2015JD024657, 2016.
- Tzortziou, M., J. R. Herman, A. Cede, and N. Abuhassan, High precision, absolute total column ozone measurements from the Pandora spectrometer system: Comparisons with data from a Brewer double monochromator and Aura OMI, *J. Geophys. Res.*, 117, D16303, doi:10.1029/2012JD017814, 2012.
- Wunch, D., Toon, G. C., Blavier, J.-F. L., Washenfelder, R. A., Notholt, J., Connor, B. J., Griffith, D. W. T., Sherlock, V., and Wennberg, P. O.: The total carbon column observing network, *Philos. T. R. Soc. A*, 369, 2087–2112, doi:10.1098/rsta.2010.0240, 2011.
- Wunch, D., Toon, G. C., Sherlock, V., Deutsch, N. M., Liu, X., Feist, D. G., and Wennberg, P. O.: The Total Carbon Column Observing Network’s GGG2014 Data Version, Carbon Dioxide Information Analysis Center, Oak Ridge National Laboratory, Oak Ridge, Tennessee, USA, 43 pp., doi:10.14291/tccon.ggg2014.documentation.R0/1221662, 2015.

5. Annex I - XI

The eleven individual PTU documents are included here, entitled as Annex I to Annex XI.



Product Traceability and Uncertainty for the Microwave Radiometer (MWR) brightness temperature product

Version 1.0

*GAIA-CLIM
Gap Analysis for Integrated
Atmospheric ECV Climate Monitoring
Mar 2015 - Feb 2018*

A Horizon 2020 project; Grant agreement: 640276

Date: 30 November 2017

Dissemination level: PU

Work Package 2; Task 2.1.2; Compiled by Domenico Cimini (CNR)

Table of Contents

1	Product overview	4
1.1	Guidance notes	4
2	Introduction.....	6
3	Instrument description.....	7
4	Product Traceability Chain	8
5	Element contributions	9
5.1	Temperature sensor (A1).....	9
5.2	Target emissivity (A2).....	10
5.3	LN2 refractive index (A3).....	11
5.4	Resonance (A4)	12
5.5	Detector non-linearity (A5)	13
5.6	Noise diode temperature (A6)	14
5.7	Antenna beam efficiency (A7)	15
5.8	Mean radiating temperature (A8)	16
5.9	Antenna pointing (A9).....	17
5.10	Atmospheric inhomogeneity (A10)	18
5.11	Finite beam width (A11).....	19
6	Uncertainty Summary	20
7	Traceability uncertainty analysis	22
7.1	Recommendations	22
8	Conclusion	23
	References.....	24

Version history

Version	Principal updates	Owner	Date
0.1 draft	First draft	CNR	28.03.2017
0.2 draft	Second draft	CNR	31.03.2017
0.3 draft	Third draft - sent for initial external comments	CNR	16.06.2017
0.4 draft	Forth draft – adapted to format provided by NPL	CNR	28.06.2017
0.5 draft	Fifth draft – after comments from Paul Green (NPL)	CNR	27.07.2017
0.6 draft	Sixth draft – after Webex meeting on Oct 9 th 2017	CNR	31.10.2017
1.0	First issue as annex E of D2.6	CNR	30.11.2017

1 Product overview

Product name: MWR brightness temperature product

Product technique: Measurement of downwelling brightness temperature at multiple frequency channels

Product measurand: Brightness temperature

Product form/range: Multiple channels in the 20-60 GHz spectrum

Product dataset: TOPROF data set

Site/Sites/Network location:

SITE	LAT	LON	HEIGHT(m)	MWR	LOCATION	COUNTRY
JOYCE	50.91	6.41	111	HATPRO G2	Juelich	DE
LACROS	51.35	12.43	125	HATPRO G2	Liepzig	DE
Payerne	46.82	6.95	491	HATPRO G1	Payerne	CH
SIRTA	48.80	2.36	156	HATPRO G2	Paris	FR
CESAR	51.97	4.93	-0.7	HATPRO G1	Cabauw	NL
RAO	52.21	14.12	125	MP3000A	Lindenberg	DE

Product time period: Jan 1, 2015 – Feb 27, 2016

Data provider: TOPROF

Instrument provider: Site management

Product assessor: Domenico Cimini, CNR

Assessor contact email: domenico.cimini@imaa.cnr.it

1.1 Guidance notes

For general guidance see the Guide to Uncertainty in Measurement & its Nomenclature, published as part of the GAIA-CLIM project.

This document is a measurement product technical document which should be stand-alone i.e. intelligible in isolation. Reference to external sources (preferably peer-reviewed) and documentation from previous studies is clearly expected and welcomed, but with sufficient explanatory content in the GAIA CLIM document not to necessitate the reading of all these reference documents to gain a clear understanding of the GAIA CLIM product and associated uncertainties entered into the Virtual Observatory (VO).

In developing this guidance, we adopted the convention proposed by the QA4ECV project (<http://www.qa4ecv.eu/>) through the Traceability and Uncertainty Propagation Tool (TUPT). This convention is summarized in Figure 1.

QA4ECV TUPT convention

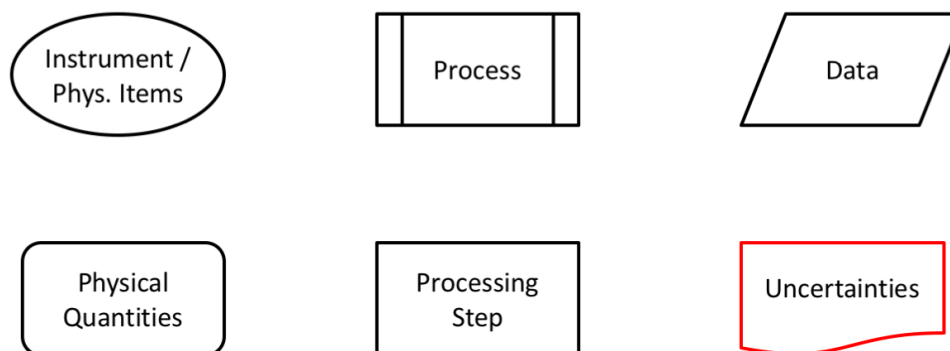


Figure 1. The convention proposed by the QA4ECV project (<http://www.qa4ecv.eu/>) through the Traceability and Uncertainty Propagation Tool (TUPT). This convention is adopted hereafter to draw the MWR model diagram.

The contribution table to be filled for each traceability contributor has the form seen in Table 1.

Table 1. The contributor table.

Information / data	Type / value / equation	Notes / description
Name of effect		
Contribution identifier		
Measurement equation parameter(s) subject to effect		
Contribution subject to effect (final product or sub-tree intermediate product)		
Time correlation extent & form		
Other (non-time) correlation extent & form		
Uncertainty PDF shape		
Uncertainty & units		
Sensitivity coefficient		
Correlation(s) between affected parameters		
Element/step common for all sites/users?		
Traceable to ...		
Validation		

Name of effect – The name of the contribution. Should be clear, unique and match the description in the traceability diagram.

Contribution identifier - Unique identifier to allow reference in the traceability chains.

Measurement equation parameter(s) subject to effect – The part of the measurement equation influenced by this contribution. Ideally, the equation into which the element contributes.

Contribution subject to effect – The top level measurement contribution affected by this contribution. This can be the main product (if on the main chain), or potentially the root of a side branch contribution. It will depend on how the chain has been sub-divided.

Time correlation extent & form – The form & extent of any correlation this contribution has in time.

Other (non-time) correlation extent & form – The form & extent of any correlation this contribution has in a non-time domain. For example, spatial or spectral.

Uncertainty PDF shape – The probability distribution shape of the contribution, Gaussian/Normal Rectangular, U-shaped, log-normal or other. If the form is not known, a written description is sufficient.

Uncertainty & units – The uncertainty value, including units and confidence interval. This can be a simple equation, but should contain typical values.

Sensitivity coefficient – Coefficient multiplied by the uncertainty when applied to the measurement equation.

Correlation(s) between affected parameters – Any correlation between the parameters affected by this specific contribution. If this element links to the main chain by multiple paths within the traceability chain, it should be described here. For instance, SZA or surface pressure may be used separately in a number of models & correction terms that are applied to the product at different points in the processing.

Element/step common for all sites/users – Is there any site-to-site/user-to-user variation in the application of this contribution?

Traceable to – Describe any traceability back towards a primary/community reference.

Validation – Any validation activities that have been performed for this element?

2 Introduction

This document presents the Product Traceability and Uncertainty (PTU) information for the Microwave Radiometer (MWR) brightness temperature product. The aim of this document is to provide supporting information for the users of this product within the GAIA-CLIM VO.

Using the convention in Figure 1, the main chain of the MWR instrument is pictured in Figure 2. The red boxes indicate the two main processes:

A) Calibration: the conversion from raw voltages corresponding to the received atmospheric radiance into calibrated brightness temperature (T_B);

B) Inversion: the inversion of calibrated T_B with the combination of some a priori knowledge to estimate the atmospheric products (retrievals).

Thus, MWR uncertainties are here divided in two groups: those affecting the MWR calibration (i.e. from atmospheric radiance to calibrated T_B) and those affecting the retrieval method (from calibrated T_B to MWR retrievals).

As T_B is the primary product of MWR instruments, the process A is treated in this document, while the process B is treated in three child documents (one for each product).

MWR measurement: Main Chain

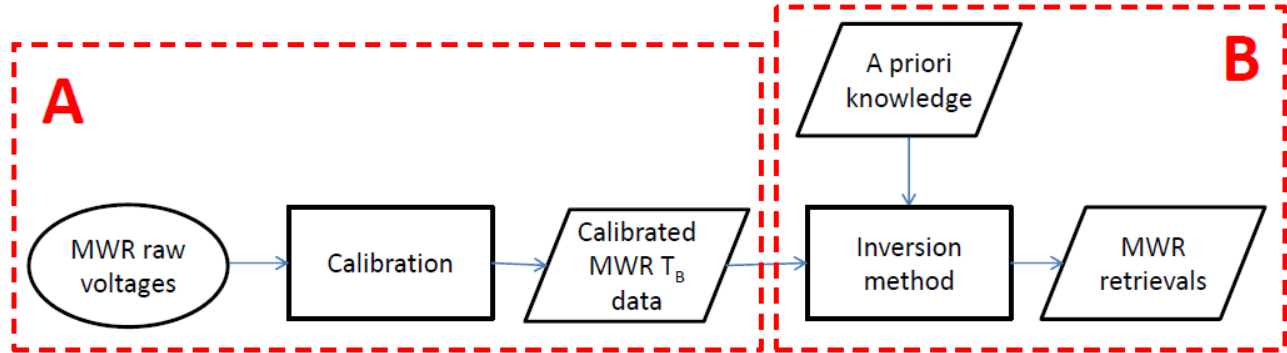


Figure 2. The main chain of the MWR instrument model diagram. The main chain displays the process of producing a geophysical product from the MWR instrument measurements. The process A (from raw voltages to calibrated brightness temperature T_B) is treated in this document. The process B is treated in children documents.

3 Instrument description

Ground-based microwave radiometers (MWR) are instruments calibrated to measure the natural down-welling thermal emission from the atmosphere. The quantity measured by a MWR is atmospheric radiance [$\text{W}/(\text{m}^2 \cdot \text{sr} \cdot \text{Hz})$], which is typically converted into brightness temperature (T_B , [K]) to adopt more familiar units.

Atmospheric temperature and humidity profiles, as well as column-integrated Total Water Vapour Content (TWVC) and Total Liquid Water Content (TLWC), can be inferred from ground-based MWR T_B observations.

Review articles on MWR measurements are given by Westwater et al., 2004 & 2005. Common MWR commercial units operate several channels in the 20-60 GHz frequency range. The 20-30 GHz range is sometimes referred to as K-band, while the 50-60 GHz range is called V-band.

A typical MWR calibration equation is given by:

$$T_B = \left(\frac{U_S}{g} \right)^{\frac{1}{\alpha}} - T_R$$

where:

T_B is the calibrated brightness temperature;

α is the detector non-linearity parameter;

U_S is the measured scene voltage;

g is the gain;

T_R is the system noise temperature.

The calibration parameters g , α , and T_R are determined through the MWR calibration.

MWRs are generally calibrated by so-called hot-cold calibration. Ideally, assuming the detector behaves linearly ($\alpha=1$), two reference points spanning the full atmospheric measurement range are

sufficient. The hot-cold method exploits two targets, one at hot or ambient temperature (T_H) and the other at cold cryogenic temperature (T_C), usually obtained by a liquid nitrogen (LN2) bath. To consider the detector non-linearity additional calibration points are needed, which are obtained by adding noise from a noise diode source while observing the two calibration targets. This method provides four reference points (4-point calibration) that are needed to solve for the four parameters g , α , and T_R and the noise diode equivalent temperature (T_N). Another calibration method, the so-called tipping curve calibration, exploits the relationship between atmospheric opacity and elevation angle at relatively transparent frequencies to refine one calibration factor. Details on these calibration methods may be found in Han and Westwater (2000), Hewison and Gaffard (2003), Maschwitz et al. (2013), and K  chler et al. (2015). For estimating the uncertainties affecting the MWR calibration, the uncertainties of the calibration parameters are propagated through these two common calibration procedures, i.e. the hot-cold and the tipping curve methods.

Figure 3 provides details of the MWR measurement metrological model chain for the calibration process (A). It describes the flow diagram of the T_B measurement, including uncertainty sources (highlighted in red) and linkages to reference standards (dashed lines, meaning the traceability to SI is not established yet).

4 Product Traceability Chain

MWR brightness temperature (T_B) product

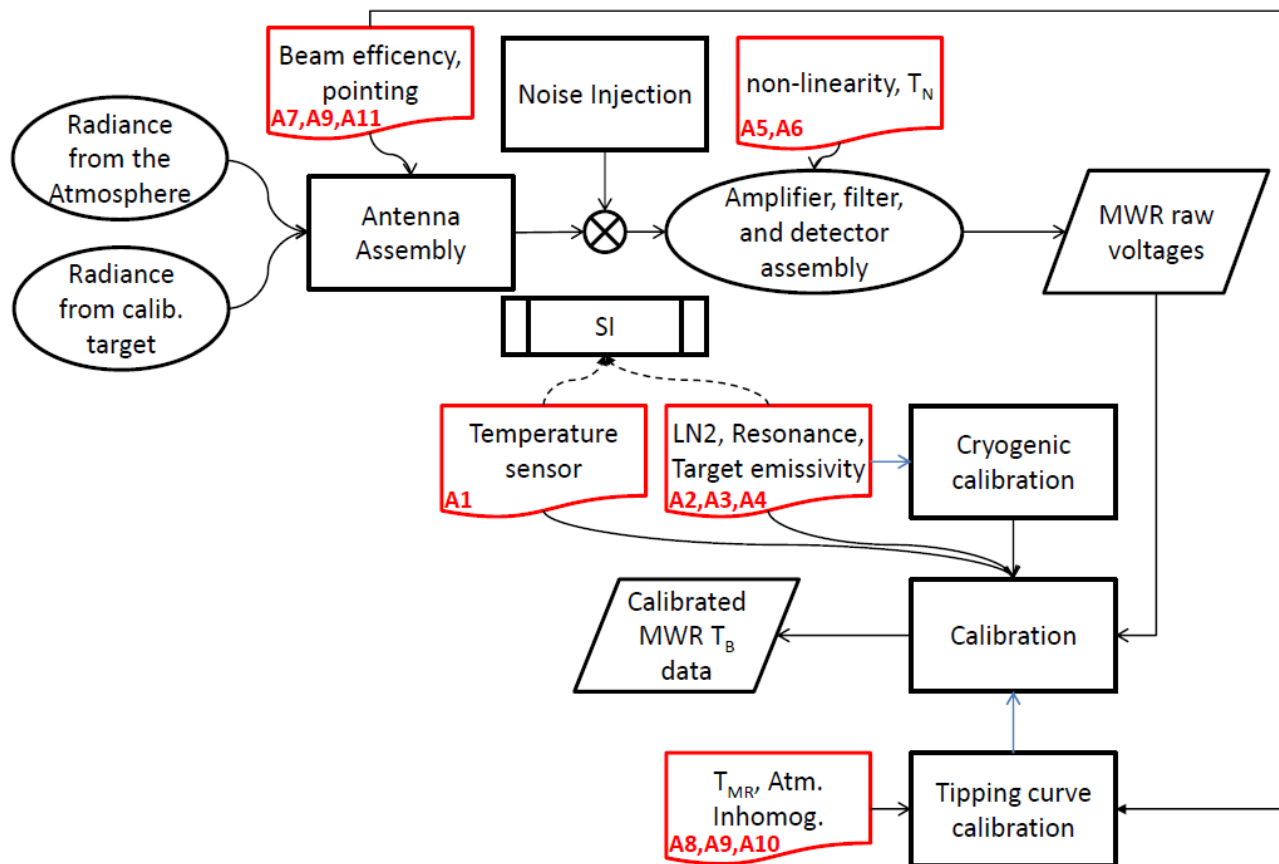


Figure 3. The metrological model chain of the MWR measurement. It describes the flow diagram of the measurement, including uncertainty sources and linkages to reference standards. The dashed lines indicate that the traceability to SI is not established yet.

5 Element contributions

5.1 Temperature sensor (A1)

Calibration uses an internal target at ambient temperature as a hot reference. The main source of uncertainty is the in-situ temperature measurement of the target. An uncertainty of ± 0.2 K is considered for the in-situ temperature measurement, which corresponds to the maximum difference typically found between two temperature sensors within the ambient target. The resulting T_B uncertainty is approximately ± 0.2 K for V-band opaque channels. All other channels are affected by approximately ± 0.1 K (Maschwitz et al., 2013). Certified temperature sensors must be deployed to establish traceability to SI. To our our knowledge, certified temperature sensors are not currently deployed on commercial MWR.

Information / data	Type / value / equation	Notes / description
Name of effect	Temperature sensor	
Contribution identifier	A1	
Measurement equation parameter(s) subject to effect	T_H	
Contribution subject to effect (final product or sub-tree intermediate product)	Calibrated T_B	
Time correlation extent & form	None	Random
Other (non-time) correlation extent & form	None	Random
Uncertainty PDF shape	Normal	
Uncertainty & units	± 0.1 K (1σ) – K-band ± 0.1 - 0.2 K (1σ) – V-band	Maschwitz et al., 2013
Sensitivity coefficient	1	
Correlation(s) between affected parameters	None	
Element/step common for all sites/users?	Yes	
Traceable to ...	Reference temperature sensor	Calibration in manufacturer's facility
Validation	Sensitivity study	Maschwitz et al., 2013

5.2 Target emissivity (A2)

Calibration targets are assumed to be ideal black bodies, while their emissivity ε and reflectivity r slightly differ respectively from 1 and 0. Manufacturers specifications give target reflectivity levels lower than -40 dB for frequencies higher than 8 GHz (i.e. $r < 0.0001$ and $\varepsilon > 0.9999$). The effective T_B is within 0.01 K if the ambient temperature varies from -30 to 40 °C. Therefore, the impact is assumed negligible. However, specifications in the spectral range of the observed MWR channels are not available to our knowledge.

Information / data	Type / value / equation	Notes / description
Name of effect	Non-ideal target emissivity	
Contribution identifier	A2	
Measurement equation parameter(s) subject to effect	T_C, T_H	$T_{Heff} = \varepsilon T_H + (1-\varepsilon) T_{Bamb}$ $T_{Ceff} = \varepsilon T_C + (1-\varepsilon) T_{Bamb}$
Contribution subject to effect (final product or sub-tree intermediate product)	Calibrated T_B	
Time correlation extent & form	None	Systematic
Other (non-time) correlation extent & form	None	
Uncertainty PDF shape	Rectangular	Assumed
Uncertainty & units (1σ)	± 0.02 K (1σ)	
Sensitivity coefficient	1	
Correlation(s) between affected parameters	None	
Element/step common for all sites/users?	Yes	
Traceable to ...	Manufacturer specifications	NIST is working on MW standards that shall be able to serve as primary and secondary standards
Validation	None	NIST secondary standards may be used in the future

5.3 LN2 refractive index (A3)

The refractive index of liquid nitrogen (n_{LN2}) determines the reflectivity of the cold target's surface. The value for $n_{LN2} = 1.2$ is derived from laboratory measurements with an uncertainty of ± 0.03 (Benson et al., 1983). The resulting T_B uncertainty is 0.7K at K-band channels, and it decreases linearly with higher T_B values. For the opaque channels in the V-band the uncertainty reduces to 0.1 K, and it disappears at the hot calibration point (Maschwitz et al., 2013).

Information / data	Type / value / equation	Notes / description
Name of effect	LN2 refractive index	
Contribution identifier	A3	
Measurement equation parameter(s) subject to effect	$r_{LN2} = (n_{LN2} - 1)^2 / (n_{LN2} + 1)^2$ $T_C = (1 - r_{LN2})T_{LN2} + r_{LN2}T_{rec}$	Maschwitz, 2012
Contribution subject to effect (final product or sub-tree intermediate product)	Calibrated T_B	
Time correlation extent & form	None	Systematic
Other (non-time) correlation extent & form	None	
Uncertainty PDF shape	Normal	Benson et al., 1983
Uncertainty & units (1σ)	± 0.7 K (1σ) – K-band ± 0.1 -0.6 K (1σ) – V-band	Maschwitz et al., 2013
Sensitivity coefficient	1	
Correlation(s) between affected parameters	None	
Element/step common for all sites/users?	Yes	
Traceable to ...	Laboratory measurements	Benson et al., 1983
Validation	Intercomparison study	Maschwitz, 2012

5.4 Resonance (A4)

During the cryogenic calibration, LN2 evaporates and its level diminishes, changing its distance to the receiver and the resonance conditions. This affects the uncertainty of the calibration point. The maximum uncertainty is estimated to be twice the amplitude of the oscillation observed at each channel, because the integration time within the LN2 calibration is small compared to the oscillation periods (~2-6 min depending on wavelength; Pospichal et al., 2012). K-band channels show oscillation amplitudes of 0.1 to 0.6 K. In the V-band the amplitudes are 0.1 to 0.3 K (Maschwitz et al., 2013). This effect is suppressed in new generation cryogenic targets, thanks to the employment of polarised anti-reflection coating, though these targets only became commercially available since 2016.

Information / data	Type / value / equation	Notes / description
Name of effect	Resonance	
Contribution identifier	A4	
Measurement equation parameter(s) subject to effect	T_C	
Contribution subject to effect (final product or sub-tree intermediate product)	Calibrated T_B	
Time correlation extent & form	Sinusoidal	Pospichal et al., 2012 Küchler et al., 2015 Paine et al., 2014
Other (non-time) correlation extent & form	None	
Uncertainty PDF shape	U-shaped	
Uncertainty & units (1σ)	$\pm 0.1\text{-}0.8\text{ K}$ (1σ) – K-band $\pm 0.1\text{-}0.3\text{ K}$ (1σ) – V-band	Maschwitz et al., 2013
Sensitivity coefficient	1	
Correlation(s) between affected parameters	None	
Element/step common for all sites/users?	Yes	
Traceable to ...	N/A	
Validation	Laboratory experiments	Pospichal et al., 2012 Küchler et al., 2015 Paine et al., 2014

5.5 Detector non-linearity (A5)

The relationship between input power (radiance) and detector output voltage slightly deviates from the ideal linear relationship. If the non-linearity is not accounted for in the calibration equation (e.g. through the two-point calibration) this effect leads to substantial systematic uncertainty, of the order of 0.5-0.6 K in the K-band, 0.01-0.40 K in the V-band (Hewison and Gaffard, 2003). However, the detector non-linearity impact can be accounted for through the non-linearity parameter α , whose value is estimated through the four-point calibration. The uncertainty in determining α is 0.1–0.2 % of the mean α value of each frequency channel. At K-band channels the effect ranges between ± 0.02 K and ± 0.04 K. In the V-band, the effect is below ± 0.02 K. Thus, in general the effect of uncertainties on detector non-linearity does not exceed ± 0.04 K and it is therefore deemed as negligible (Maschwitz et al. 2013).

Information / data	Type / value / equation	Notes / description
Name of effect	Detector non-linearity	
Contribution identifier	A5	
Measurement equation parameter(s) subject to effect	A	
Contribution subject to effect (final product or sub-tree intermediate product)	Calibrated T_B	
Time correlation extent & form	None	Quasi-systematic
Other (non-time) correlation extent & form	None	
Uncertainty PDF shape	Normal	
Uncertainty & units (1σ)	± 0.04 K (1σ)	Maschwitz et al., 2013
Sensitivity coefficient	1	
Correlation(s) between affected parameters	A6	Detector non-linearity and noise diode temperature are determined through calibration at the same time
Element/step common for all sites/users?	Yes	
Traceable to ...	None	
Validation	Sensitivity study	Maschwitz et al., 2013

5.6 Noise diode temperature (A6)

The noise diode temperature T_N is calibrated through the LN2 calibration. The impact of T_N uncertainty is estimated to be negligible for opaque channels, whose calibration is dominated by the ambient target temperature, and ranging between 0.2 and 0.4 K for the non-opaque channels. After the initial LN2 calibration, the measurement accuracy depends on the stability of the injected noise, which is characterized by T_N .

As the LN2 calibration is impractical to perform frequently, the stability is rather important for V-band channels which cannot be calibrated by the tipping curve calibration. A trend analysis of T_N showed +0.006 to +0.010 K/day and +0.054 to +0.072 K/day in the K- and V-band respectively. The uncertainty on the trend is 0.002-0.01 K/day depending on channel. The impact on calibrated T_B is estimated to be less than 0.01 K/day at all channels. Most affected channels are the relative transparent channels, with an estimated drift of ~0.3 K per month. When the effect of the drift is accounted for, the remaining uncertainty (due to the uncertainty on the trend) is ~0.1 K per month.

Information / data	Type / value / equation	Notes / description
Name of effect	Noise diode temperature	
Contribution identifier	A6	
Measurement equation parameter(s) subject to effect	T_N	
Contribution subject to effect (final product or sub-tree intermediate product)	Calibrated T_B	
Time correlation extent & form	Drift	Quasi-systematic
Other (non-time) correlation extent & form	None	
Uncertainty PDF shape	Normal	PDF peak value increases with time
Uncertainty & units (1σ)	± 0.01 K/day	Maschwitz et al., 2013
Sensitivity coefficient	1	
Correlation(s) between affected parameters	A5	Detector non-linearity and noise diode temperature are determined through calibration at the same time
Element/step common for all sites/users?	Yes	
Traceable to ...	None	
Validation	Sensitivity study	Maschwitz et al., 2013

5.7 Antenna beam efficiency (A7)

The antenna receiving the scene radiation is characterized by a finite beam and antenna pattern. The power fraction in the sidelobes is estimated by model simulations within 0.1%. Thus, the main beam efficiency η (the ratio of power in the main beam to the total received power) is estimated to be higher than 99.9%. Hewison and Gaffard (2003) estimated η indirectly by comparing calibrations derived from different sets of tip curve angles, and found η increasing from 99.0 to 99.9% with increasing frequency (22 to 30 GHz). The effect of η is accounted for in the calibration. However, there remains an uncertainty affecting the spurious internal radiation entering in the sidelobes, which is estimated within 10% with a resulting T_B effect of less than 0.02 K.

Information / data	Type / value / equation	Notes / description
Name of effect	Antenna beam efficiency	
Contribution identifier	A7	
Measurement equation parameter(s) subject to effect	T_C, T_H	$T_{Heff} = \eta T_H + (1-\eta) T_{Bamb}$ $T_{Ceff} = \eta T_C + (1-\eta) T_{Bamb}$
Contribution subject to effect (final product or sub-tree intermediate product)	Calibrated T_B	
Time correlation extent & form	None	Systematic
Other (non-time) correlation extent & form	None	
Uncertainty PDF shape	Normal	
Uncertainty & units (1σ)	± 0.02 K	Maschwitz et al., 2013
Sensitivity coefficient	1	
Correlation(s) between affected parameters	A11	The antenna beam efficiency is related to the finite beamwidth
Element/step common for all sites/users?	Yes	
Traceable to ...	None	
Validation	None	

5.8 Mean radiating temperature (A8)

The atmospheric mean radiative temperature (T_{mr}) is a frequency-dependent parameter entering in the tipping curve calibration method. The tipping curve calibration method requires relatively low opacity and thus it is usually applicable to K-band channels only, though in high-altitude low-pressure conditions may also be applied to lower V-band channels (Maschwitz et al., 2013). T_{mr} is usually estimated from either a climatological mean or a linear regression based on ambient surface temperature (T_{srf}), both derived from prior atmospheric profiles processed with radiative transfer calculations. Regression on T_{srf} is more accurate, with rms ranging from 3.4 to 1.1 K from K- to V-band channels in dry and low pressure conditions (Maschwitz et al., 2013) and up to 3.9 K for K-band channels at standard pressure conditions (Han and Westwater, 2000). For air mass lower than 3 (i.e. elevation angles higher than 19.5° , as usually observed by ground-based MWR), T_{mr} uncertainty impacts for up to 0.3 K on K-band calibration. In the V-band, T_{mr} uncertainty impacts for 1-3 K (Hewison and Gaffard, 2003), though the tipping curve method is usually not used for these channels. For conditions described by Maschwitz et al. (2013), T_{mr} uncertainty impact negligibly the K-band and by ≈ 0.1 K the V-band channels.

Information / data	Type / value / equation	Notes / description
Name of effect	Mean radiative temperature	
Contribution identifier	A8	
Measurement equation parameter(s) subject to effect	T_{mr}	Han and Westwater, 2000
Contribution subject to effect (final product or sub-tree intermediate product)	Calibrated T_B	
Time correlation extent & form	None	Random. The error in estimating T_{MR} depends on atmospheric conditions, thus some correlation with diurnal cycle and season may exist
Other (non-time) correlation extent & form	None	
Uncertainty PDF shape	Normal	
Uncertainty & units (1σ)	± 0.3 K (1σ)	Han and Westwater, 2000
Sensitivity coefficient	1	
Correlation(s) between affected parameters	None	
Element/step common for all sites/users?	Yes	
Traceable to ...	N/A	
Validation	Sensitivity study	Han and Westwater, 2000

5.9 Antenna pointing (A9)

The uncertainty in antenna pointing affects the T_B measurements in two aspects: calibration and slant path observations. Calibration through the tipping curve method relies on the knowledge of the elevation angle at which the antenna is pointing. A 1-degree mispointing, due to installation accuracy of zenith direction with respect to the surface normal, can lead to a calibration error of several K. This systematic error is explained by a tilt and can be balanced by averaging measurements of symmetric elevation angle prior to the tipping curve procedure. The correction results in a residual pointing uncertainty of 0.05° . This uncertainty has no effect on the K-band, and results in a ± 0.1 K T_B uncertainty in the V-band.

The effect on slant path observations is frequency, elevation angle, and scene dependent. Assuming manufacturers' pointing angle accuracy specifications (0.15°), the effect in the 20-60 GHz range has been quantified through perturbations of radiative transfer simulations for six different atmospheric conditions (from tropical to polar winter) and elevation angle from 5° to 90° . At zenith, the impact is negligible (<0.1 K) at all channels. For opaque V-band channels, the impact is negligible (<0.1 K) at all elevation angles. The impact becomes significant (>0.5 K) for elevation angles lower than 25° and frequency lower than 52 GHz. These channel/angle combinations are normally not used for the atmospheric retrievals.

Information / data	Type / value / equation	Notes / description
Name of effect	Antenna pointing angle	
Contribution identifier	A9	
Measurement equation parameter(s) subject to effect	θ	Observing elevation angle (0.15° pointing uncertainty) Han and Westwater, 2010
Contribution subject to effect (final product or sub-tree intermediate product)	Calibrated T_B	
Time correlation extent & form	None	Random
Other (non-time) correlation extent & form	None	
Uncertainty PDF shape	Normal	
Uncertainty & units (1σ)	$\pm 0.0-0.1$ K	Maximum values for typical channel/angle combinations used in retrievals
Sensitivity coefficient	1	
Correlation(s) between affected parameters	None	
Element/step common for all sites/users?	Yes	
Traceable to ...	None	
Validation	Perturbation analysis	

5.10 Atmospheric inhomogeneity (A10)

Atmospheric inhomogeneity affects the quality of the tipping curve calibration method. Thus, uncertainty of T_B calibrated with tipping curve method increases with increasing atmospheric inhomogeneity. Methods are usually used to reduce this effect, based on quality control screenings and averaging in time and azimuth angle (Han and Westwater, 2000). The remaining effect has been estimated as the standard deviation of T_B over a set of scans, resulting in 0.1–0.2 K for the K-band and 0.3–0.4 K in the V-band (Maschwitz et al., 2013), although this probably overestimates the contribution as it potentially captures other short term random effects. Note that this contribution should not be confused with the impact of atmospheric inhomogeneity on the comparison among different measurement techniques (i.e. contribution to colocation uncertainty, which is treated within GAIA-CLIM Work Package 3). Conversely, here we only refer to the impact of atmospheric inhomogeneity to the quality of the tipping curve calibration method.

Information / data	Type / value / equation	Notes / description
Name of effect	Atmospheric inhomogeneity	
Contribution identifier	A10	
Measurement equation parameter(s) subject to effect	G	Detector gain Maschwitz et al., 2013
Contribution subject to effect (final product or sub-tree intermediate product)	Calibrated T_B	
Time correlation extent & form	None	Random. Since it depends on atmospheric conditions, some correlation with diurnal cycle and season may exist
Other (non-time) correlation extent & form	None	
Uncertainty PDF shape	Normal	
Uncertainty & units (1σ)	$\pm 0.1\text{--}0.2$ K (1σ) – K-band $\pm 0.3\text{--}0.4$ K (1σ) – V-band	Han and Westwater, 2010 Maschwitz et al., 2013
Sensitivity coefficient	1	
Correlation(s) between affected parameters	None	
Element/step common for all sites/users?	Yes	
Traceable to ...	None	
Validation	Sensitivity study	Maschwitz et al., 2013

5.11 Finite beam width (A11)

The MWR antenna is characterized by a finite beam width. As described in A1, the contribution from outside the angular range of two antenna half-power beam widths (HPBW) is negligible. However, the finite beam width affects the effective air mass that the antenna is looking at. This effect can be modeled using a Gaussian-shaped lobe with a width matching twice the HPBW. For typical MWR antenna beam widths ($<6^\circ$), the impact on calibrated T_B depends on the pointing angle, but it is less than 0.1 K at three air masses ($\sim 19.5^\circ$ elevation) for all channels (Han and Westwater, 2000).

Information / data	Type / value / equation	Notes / description
Name of effect	Atmospheric inhomogeneity	
Contribution identifier	A11	
Measurement equation parameter(s) subject to effect	T_B	Brightness temperature of the effective air mass within the antenna finite beam width
Contribution subject to effect (final product or sub-tree intermediate product)	Calibrated T_B	
Time correlation extent & form	None	Systematic
Other (non-time) correlation extent & form	None	
Uncertainty PDF shape	Normal	
Uncertainty & units (1σ)	± 0.1 K (1σ)	Han and Westwater, 2010
Sensitivity coefficient	1	
Correlation(s) between affected parameters	A7	The antenna beam efficiency is related to the finite beamwidth
Element/step common for all sites/users?	Yes	
Traceable to ...	None	
Validation	Sensitivity study	Han and Westwater, 2010

6 Uncertainty Summary

Element identifier	Contribution name	Uncertainty contribution form	Typical value	Traceability level (L/M/H)	random, structured random, quasi-systematic or systematic?	Correlated to? (Use element identifier)
A1	Temperature sensor	Normal	K-band ± 0.1 K V-band ± 0.2 K	H	random	none
A2	Non-ideal target emissivity	Rectangular	± 0.02 K	H	systematic	none
A3	LN2 refractive index	Normal	K-band ± 0.7 K V-band ± 0.6 K	H	systematic	none
A4	Resonance	Normal	K-band ± 0.8 K V-band ± 0.3 K	M	quasi-systematic	none
A5	Detector non-linearity	Normal	± 0.04 K	M	quasi-systematic	A6
A6	Noise diode temperature	Normal PDF peak value increases with time	± 0.01 K/day	L	quasi-systematic	A5
A7	Antenna beam efficiency	Normal	± 0.02 K	M	systematic	A11
A8	Mean radiative temperature	Normal	± 0.3 K	M	random	none
A9	Antenna pointing angle	Normal	± 0.1 K	M	random	none
A10	Atmospheric inhomogeneity	Normal	K-band ± 0.2 K V-band ± 0.4 K	M	random	none
A11	Finite beam width	Normal	± 0.1 K	M	systematic	A7

The contribution of the major uncertainty sources is summarised in the Table above. These contributions are obtained following Han and Westwater (2000), Hewison and Gaffard (2003), Hewison (2006), Maschwitz (2012), and Maschwitz et al. (2013). The two calibration methods (LN2 and tip curve) can be applied in series, the tip curve resulting in a correction to the LN2 coefficients (e.g. the noise diode T_N). Typical atmospheric conditions do not allow the tip curve method to be applicable for V-band channels, so the combination only concerns K-band channels. However, keeping the two methods independent gives the opportunity to detect possible calibration problems (Maschwitz et al. 2013). For the GAIA-CLIM dataset, settings were such that only the LN2 calibration was adopted for all MWR instruments but the one in Lindenberg, for which the tipping curve was used for K-band channels.

Maschwitz et al. 2013 report the total calibration uncertainties of tipping curve and LN2 methods for one particular MWR instrument type (RPG HATPRO). The total calibration uncertainties is given as the sum of the systematic contributions in absolute value:

$$\begin{aligned}
 \text{Tipping curve:} \quad u_{TB(TIP)} &= |u_{TMR}| + |u_p| + |u_{atm}| \\
 \text{LN2:} \quad u_{TB(LN2)} &= |u_{LN2}| + |u_{res}| + |u_{hot}| + |u_{\alpha}|
 \end{aligned}$$

where the following uncertainties result from:

$u_{T_{MR}}$	derivation of the mean radiative temperature T_{mr}
u_p	beam pointing
u_{atm}	atmospheric inhomogeneities
u_{LN_2}	refractive index of the LN_2 surface
u_{res}	resonances between the receiver and the LN_2 target
u_{hot}	in-situ hot load measurement
u_α	detector non-linearity

Similar results were obtained by Hewison (2006) considering another MWR type (Radiometrics MP3000). However, it must be noted that these contributions are systematic on a single calibration realization, but result in random uncertainty when considering long-term time series with multiple repeated calibrations.

Hewison (2006) also report the random uncertainty of typical T_B when using tipping curve or LN_2 calibration methods:

$$\text{Tipping curve: } u_{T_B(TIP)} = \sqrt{u_{BB}^2 + u_{atm}^2 + u_{T_{ND}}^2 + u_{rec}^2 + u_{T_{MR}}^2}$$

$$\text{LN2: } u_{T_B(LN2)} = \sqrt{u_{BB}^2 + u_{LN2}^2 + u_{T_{ND}}^2 + u_{rec}^2}$$

where the following uncertainties result from:

u_{BB}	black-body noise
u_{atm}	atmospheric noise
$u_{T_{ND}}$	T_{ND} noise and drift
u_{rec}	receiver noise
$u_{T_{MR}}$	T_{MR} noise
u_{LN_2}	LN_2 noise

The resulting T_B uncertainties depend on the channel frequency and the atmospheric conditions through T_B itself. Typical systematic and random uncertainties for K- and V-band channels as derived from Hewison (2006) and Maschwitz et al. (2013) (considering two different types of MWR) are summarized in the table below. All values are in Kelvin. Note that the given uncertainties depend upon atmospheric conditions, e.g. tipping curve uncertainties may increase with increasing atmospheric opacity.

Reference	MWR type	TIP (K)		LN2 (K)		
		K-band	V-band	K-band	V-band	
Maschwitz et al. 2013	HATPRO	±0.1-0.2	±0.6-0.7	±0.9-1.6	±0.2-1.0	systematic
Hewison 2006	MP3000	±0.2-0.5	±0.4-0.8	±0.8-1.0	±0.2-1.0	systematic
Hewison 2006	MP3000	±0.3-0.5	±1.5-4.1	±0.6-1.1	±0.1-0.6	random

7 Traceability uncertainty analysis

Traceability level definition is given in Table 2.

Table 2. Traceability level definition table

Traceability Level	Descriptor	Multiplier
High	SI traceable or globally recognised community standard	1
Medium	Developmental community standard or peer-reviewed uncertainty assessment	3
Low	Approximate estimation	10

Analysis of the summary table would suggest the following contributions, shown in Table 3, should be considered further to improve the overall uncertainty of the MWR brightness temperature product. The entries are given in an estimated priority order.

Table 3. Traceability level definition further action table.

Element identifier	Contribution name	Uncertainty contribution form	Typical value	Traceability level (L/M/H)	random, structured random, quasi-systematic or systematic?	Correlated to? (Use element identifier)
A4	Resonance	Normal	K-band ± 0.8 K V-band ± 0.3 K	M	quasi-systematic	none
A6	Noise diode temperature	Normal PDF peak value increases with time	± 0.01 K/day	L	quasi-systematic	A5
A3	LN2 refractive index	Normal	K-band ± 0.7 K V-band ± 0.6 K	H	systematic	none

7.1 Recommendations

The top priority is to reduce the resonance contribution (A4). This requires technological improvements (e.g. anti-reflection coating of cold calibration target) which have been already developed and exploited on newer generation commercial MWR instruments.

The second priority is to better characterise the noise diode temperature drift (A6). This has been only estimated for one instrument during one field experiment. Ideally it should be characterized for each instrument periodically to account for drifts within two LN2 calibrations.

The third priority requires new and more accurate laboratory measurement of LN2 refractive index (A3), in order to update the uncertainty achievable by Benson et al., 1983.

In addition, although the contribution from the non-ideal target emissivity (A2) is deemed to be

small, the lack of MW radiometry standards is currently hampering the SI traceability of MWR observations. The U.S. National Institute of Standard and Technologies (NIST) is currently developing such standards for MW radiometry (Houtz et al., 2016). NIST plans to be able to provide SI-traceability for calibration targets and transfer standards in the next few years.

8 Conclusion

The MWR brightness temperature product has been assessed against the GAIA CLIM traceability and uncertainty criteria.

References

- Benson J., Fischer J. and Boyd D. A.: Submillimeter and Millimeter Optical Constants of Liquid Nitrogen, *Int. J. Infrared Milli.*, 4, 145–152, doi:10.1007/BF01008973, 1983.
- Boukabara S. A., S. A. Clough, J.-L. Moncet, A. F. Krupnov, M. Yu. Tretyakov, and V. V. Parshin (2005), Uncertainties in the Temperature Dependence of the Line-Coupling Parameters of the Microwave Oxygen Band: Impact Study, *IEEE Trans. Geosci. Rem. Sens.*, 43, 5, doi: 10.1109/TGRS.2004.839654.
- Cimini, D., T. J. Hewison, L. Martin (2006), Comparison of brightness temperatures observed from ground-based microwave radiometers during TUC, *Meteorologische Zeitschrift*, Vol.15, No.1, 2006, pp.19-25.
- Cimini, D., T. J. Hewison, L. Martin, J. Güldner, C. Gaffard and F. S. Marzano (2006), Temperature and humidity profile retrievals from ground-based microwave radiometers during TUC, *Met. Zeitschrift*, Vol. 15, No. 1, 45-56.
- Cimini D., E. R. Westwater, and A. J. Gasiewski (2010), Temperature and humidity profiling in the Arctic using millimeter-wave radiometry and 1DVAR, *IEEE Transactions on Geoscience and Remote Sensing*, Vol. 48, 3, 1381-1388, 10.1109/TGRS.2009.2030500.
- Han Y. and E. R. Westwater: Analysis and Improvement of Tipping Calibration for Ground based Microwave Radiometers. *IEEE Trans. Geosci. Remote Sens.*, 38(3), 1260–127, 2000.
- Hewison T.J. and C. Gaffard (2003), “Radiometrics MP3000 Microwave Radiometer Performance Assessment”, *Obs. Development Technical Report TR29*, Met Office, National Meteorological Library, Exeter, UK.
- Hewison T. (2006), *Profiling Temperature and Humidity by Ground-based Microwave Radiometers*, PhD Thesis, Department of Meteorology, University of Reading.
- Houtz D. A., D. K. Walker, D. Gu (2016), Cryogenic Design and Uncertainty Analysis of the NIST Microwave Blackbody, 14th Specialist Meeting on Microwave Radiometry and Remote Sensing of the Environment (MicroRad), Espoo, Finland, April 11-14, 2016.
- Küchler, N., D. D. Turner, U. Löhnert, and S. Crewell (2016), Calibrating ground-based microwave radiometers: Uncertainty and drifts, *Radio Sci.*, 51, 311–327, doi:10.1002/2015RS005826.
- Löhnert, U. and Maier, O. (2012), Operational profiling of temperature using ground-based microwave radiometry at Payerne: prospects and challenges, *Atmos. Meas. Tech.*, 5, 1121-1134, doi:10.5194/amt-5-1121-2012.
- Martinet, P., Dabas, A., Donier, J. M., Douffet, T., Garrouste, O., and Guillot, R. (2015), 1D-Var temperature retrievals from microwave radiometer and convective scale model, *Tellus A*, 67, 2015. Doi: 10.3402/tellusa.v67.27925.
- Maschwitz, G. (2012), *Assessment of Ground-Based Microwave Radiometer Calibration to Enable Investigation of Gas Absorption Models*. PhD thesis, Universität zu Köln. Online: <http://kups.ub.uni-koeln.de/5390/1/DissertationGerritMaschwitz.pdf>
- Maschwitz G., U. Löhnert, S. Crewell, T. Rose, and D.D. Turner (2013), Investigation of Ground-Based Microwave Radiometer Calibration Techniques at 530 hPa, *Atmos. Meas. Tech.*, 6, 2641–2658, doi:10.5194/amt-6-2641-2013
- Paine, S., D. Turner, and N. Küchler (2014), Understanding thermal drift in liquid nitrogen loads used for radiometric calibration in the field, *J. Atmos. Ocean. Tech.*, 31, 647–655, doi:10.1175/JTECH-D-13-00171.1.
- Pospichal B., Maschwitz G., and Rose T., Standing Wave Patterns at Liquid Nitrogen Calibration of Microwave Radiometers, *Proc. 9th Intern. Symp. Troposph. Prof. (ISTP)*, Cimini D., Di

Girolamo P., Marzano F. S., and Rizi V. (Eds.), ISBN: 978-90-815839-4-7, doi:10.12898/ISTP9prc, L'Aquila, Italy, September 2012. Online: http://cetemps.aquila.infn.it/istp/proceedings/Session_P_Posters/P35_Pospichal.pdf

Solheim F., J. Godwin, E. Westwater, Y. Han, S. Keihm, K. Marsh, R. Ware (1998), Radiometric Profiling of Temperature, Water Vapor, and Liquid Water using Various Inversion Methods, *Radio Science*, 33, pp. 393-404, DOI: 10.1029/97RS03656.

Stähli, O., Murk, A., Kämpfer, N., Mätzler, C., and Eriksson, P. (2013), Microwave radiometer to retrieve temperature profiles from the surface to the stratopause, *Atmos. Meas. Tech.*, 6, 2477-2494, doi:10.5194/amt-6-2477-2013.

Westwater E.R., S. Crewell, C. Mätzler: A Review of Surface-Based Microwave and Millimeter Wave Radiometric Remote Sensing of the Troposphere, *URSI Radio Science Bulletin*, No. 310, 59-80, 2004. Online:

<https://pdfs.semanticscholar.org/09ae/6c38f5d28fdd6c62703327c01a36d0d8af16.pdf>

Westwater E. R., S. Crewell, C. Mätzler, D. Cimini: Principles of surface-based microwave and millimeter wave radiometric remote sensing of the troposphere *Quaderni della Società Italiana di Elettromagnetismo* Vol.: 1, No.3, 50-90, 2005. Online:

http://radiometrics.com/data/uploads/2012/12/Westwater_QSIE_2005.pdf



Product Traceability and Uncertainty for the Microwave Radiometer (MWR) temperature profile product

Version 1.1

*GAIA-CLIM
Gap Analysis for Integrated
Atmospheric ECV Climate Monitoring
Mar 2015 - Feb 2018*

A Horizon 2020 project; Grant agreement: 640276

Date: 19 December 2017

Dissemination level: PU

Work Package 2; Task 2.1.2; Compiled by Domenico Cimini (CNR)



Consiglio Nazionale delle Ricerche

Table of Contents

1	Product overview	4
1.1	Guidance notes	4
2	Introduction.....	6
3	Instrument description.....	7
4	Product Traceability Chain	9
5	Element contributions	10
5.1	Brightness temperature uncertainty (B1)	10
5.2	A priori uncertainty (B2).....	12
5.3	Forward Model (B3).....	13
5.4	Spectroscopic parameters (B3a).....	14
5.5	Spectral Response Function (B3b).....	15
5.6	Fast Absorption Predictor (B3c).....	16
5.7	Discretization (B3d)	17
5.8	Representativeness (B4).....	18
5.9	Smoothing error (B5)	19
6	Uncertainty Summary	20
7	Traceability uncertainty analysis	22
7.1	Recommendations	22
8	Conclusion	23
	References	24

Version history

Version	Principal updates	Owner	Date
0.1 draft	First draft – adapted existing text to the template provided by NPL	CNR	28.06.2017
0.2 draft	Second draft – Sent for initial external comments	CNR	30.06.2017
0.3 draft	Third draft – after external comments from Paul Green (NPL)	CNR	27.07.2017
0.4 draft	Fourth draft – after Webex meeting on Oct 9 th 2017	CNR	8.11.2017
1.0	First issue as annex F of D2.6	CNR	30.11.2017
1.1	Second issue after comments on humidity profile PTU	CNR	19.12.2017

1 Product overview

Product name: MWR temperature profile product

Product technique: Temperature profile retrieval from multichannel brightness temperature measurements and a priori knowledge

Product measurand: Temperature [K]

Product form/range: Profile

Product dataset: TOPROF data set

Site/Sites/Network location:

SITE	LAT	LON	HEIGHT(m)	MWR	LOCATION	COUNTRY
JOYCE	50.91	6.41	111	HATPRO G2	Juelich	DE
LACROS	51.35	12.43	125	HATPRO G2	Liepzig	DE
Payerne	46.82	6.95	491	HATPRO G1	Payerne	CH
SIRTA	48.80	2.36	156	HATPRO G2	Paris	FR
CESAR	51.97	4.93	-0.7	HATPRO G1	Cabauw	NL
RAO	52.21	14.12	125	MP3000A	Lindenberg	DE

Product time period: Jan 1, 2015 – Feb 27, 2016

Data provider: TOPROF

Instrument provider: Site management

Product assessor: Domenico Cimini, CNR

Assessor contact email: domenico.cimini@imaa.cnr.it

1.1 Guidance notes

For general guidance see the Guide to Uncertainty in Measurement & its Nomenclature, published as part of the GAIA-CLIM project.

This document is a measurement product technical document which should be stand-alone i.e. intelligible in isolation. Reference to external sources (mostly peer-reviewed) and documentation from previous studies is given, but the content provided here shall not require the reading of all these reference documents to gain a clear understanding of the GAIA CLIM product and associated uncertainties entered into the Virtual Observatory (VO).

In developing this guidance, we adopted the convention proposed by the QA4ECV project (<http://www.qa4ecv.eu/>) through the Traceability and Uncertainty Propagation Tool (TUPT). This convention is summarized in Figure 1.

QA4ECV TUPT convention

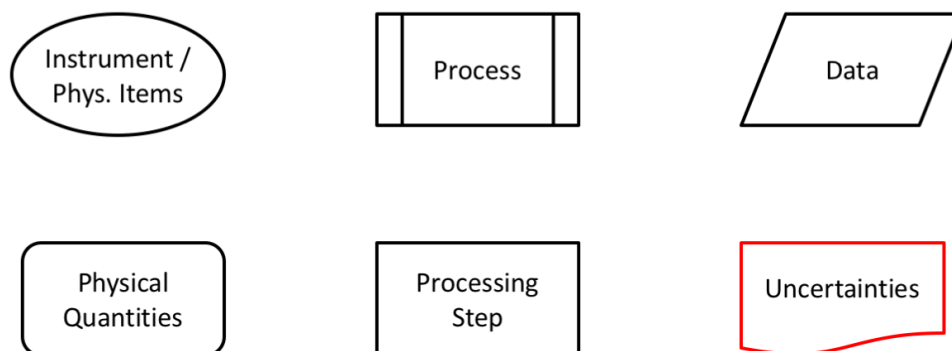


Figure 1. The convention proposed by the QA4ECV project (<http://www.qa4ecv.eu/>) through the Traceability and Uncertainty Propagation Tool (TUPT). This convention is adopted hereafter to draw the MWR model diagram.

The contribution table to be filled for each traceability contributor has the form seen in Table 1.

Table 1. The contributor table.

Information / data	Type / value / equation	Notes / description
Name of effect		
Contribution identifier		
Measurement equation parameter(s) subject to effect		
Contribution subject to effect (final product or sub-tree intermediate product)		
Time correlation extent & form		
Other (non-time) correlation extent & form		
Uncertainty PDF shape		
Uncertainty & units		
Sensitivity coefficient		
Correlation(s) between affected parameters		
Element/step common for all sites/users?		
Traceable to ...		
Validation		

Name of effect – The name of the contribution. Should be clear, unique and match the description in the traceability diagram.

Contribution identifier - Unique identifier to allow reference in the traceability chains.

Measurement equation parameter(s) subject to effect – The part of the measurement equation influenced by this contribution. Ideally, the equation into which the element contributes.

Contribution subject to effect – The top level measurement contribution affected by this contribution. This can be the main product (if on the main chain), or potentially the root of a side branch contribution. It will depend on how the chain has been sub-divided.

Time correlation extent & form – The form & extent of any correlation this contribution has in time.

Other (non-time) correlation extent & form – The form & extent of any correlation this contribution has in a non-time domain. For example, spatial or spectral.

Uncertainty PDF shape – The probability distribution shape of the contribution, Gaussian/Normal Rectangular, U-shaped, log-normal or other. If the form is not known, a written description is sufficient.

Uncertainty & units – The uncertainty value, including units and confidence interval. This can be a simple equation, but should contain typical values.

Sensitivity coefficient – Coefficient multiplied by the uncertainty when applied to the measurement equation.

Correlation(s) between affected parameters – Any correlation between the parameters affected by this specific contribution. If this element links to the main chain by multiple paths within the traceability chain, it should be described here. For instance, SZA or surface pressure may be used separately in a number of models & correction terms that are applied to the product at different points in the processing.

Element/step common for all sites/users – Is there any site-to-site/user-to-user variation in the application of this contribution?

Traceable to – Describe any traceability back towards a primary/community reference.

Validation – Any validation activities that have been performed for this element?

2 Introduction

This document presents the Product Traceability and Uncertainty (PTU) information for the Microwave Radiometer (MWR) temperature profile product. The aim of this document is to provide supporting information for the users of this product within the GAIA-CLIM VO.

Using the convention in Figure 1, the main chain of the MWR instrument is pictured in Figure 2. The red boxes indicates the two main processes:

A) Calibration: the conversion from raw voltages corresponding to the received atmospheric radiance into calibrated brightness temperature (T_B);

B) Inversion: the inversion of calibrated T_B with the combination of some a priori knowledge to

estimate the atmospheric products (retrievals).

Thus, MWR uncertainties are divided in two groups: those affecting the MWR calibration (i.e. from atmospheric radiance to calibrated T_B) and those affecting the retrieval method (from calibrated T_B to MWR retrievals). The parent document (GAIA-CLIM PTU document for MWR brightness temperature product) treats the calibration process (A) and the contributions to the T_B uncertainty. This document treats the inversion process (B) and how the T_B uncertainty combine with other uncertainty sources to contribute to the uncertainty of the retrieved temperature profile.

MWR measurement: Main Chain

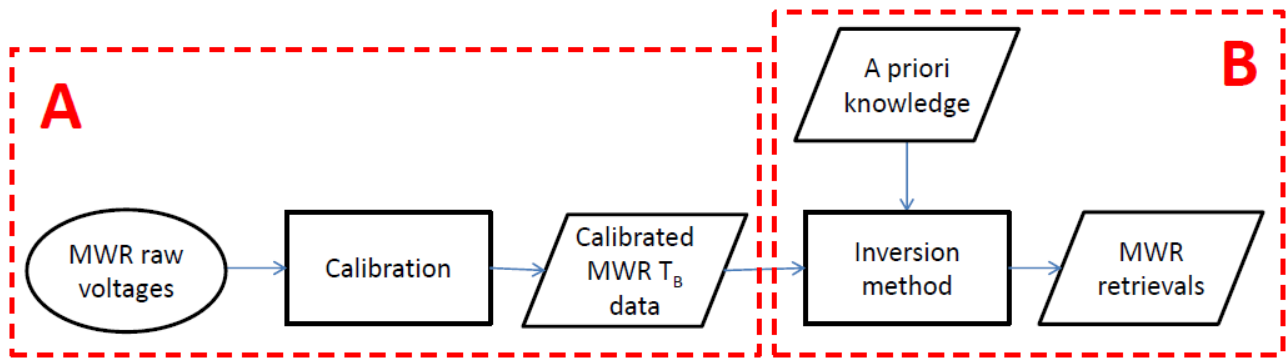


Figure 2. The main chain of the MWR instrument model diagram. The main chain displays the process of producing a geophysical product from the MWR instrument measurements. The process A (from raw voltages to calibrated brightness temperature T_B) is treated in the parent document. The process B is treated in three children documents, of which this is one.

3 Instrument description

Ground-based microwave radiometers (MWR) are instruments calibrated to measure the natural down-welling thermal emission from the atmosphere. The quantity measured by a MWR is atmospheric radiance [$W/(m^2 \cdot sr \cdot Hz)$], which is typically converted into brightness temperature (T_B , [K]) to adopt more familiar units.

Atmospheric temperature and humidity profiles, as well as column-integrated Total Water Vapour Content (TWVC) and Total Liquid Water Content (TLWC), can be inferred from ground-based MWR T_B observations.

Review articles on MWR measurements are given by Westwater et al., 2004 & 2005. Common MWR commercial units operate several channels in the 20-60 GHz frequency range. The 20-30 GHz range is referred to as K-band, while the 50-60 GHz range is called V-band.

Figure 3 provides details of the MWR measurement metrological model chain for the inversion process (B). It describes the flow diagram from the a priori knowledge and the calibrated T_B , including uncertainty sources (highlighted in red), to the retrieved atmospheric temperature product.

The uncertainty of the inverse method, that is the analysis algorithm to transform the calibrated T_B into the atmospheric products, contributes to the total uncertainty affecting the MWR atmospheric products. A variety of methods are currently used to solve the inverse problem, with somewhat different implementations, and their performances have been compared to some degree (Solheim et al. 1998; Cimini et al., 2006). Statistical algorithms, including multivariate statistical regression and neural networks, are usually exploited as they are suitable to be applied in real time. Conversely, physical retrieval methods, such as optimal estimation methods (OEM), are computationally more expensive as they solve the inverse problem in a physically consistent way. OEM optimally couples MWR observations with a priori background knowledge, accounting for uncertainty from both the

observations and background and propagating uncertainty to the final product. An estimate of the uncertainty on the retrieved profiles can be derived by assuming the errors are normally distributed about the solution and that the problem is only moderately non-linear (Rodgers, 2000).

The OEM retrieval method is affected by instrumental uncertainty (detailed in the parent document GAIA-CLIM PTU document for MWR brightness temperature product) as well as other sources of uncertainty, such as a priori, absorption model, spectral response function, profile discretization, smoothing and representativeness errors (Hewison, 2006; Cimini et al., 2010; Stähli et al., 2013).

For the OEM, we adopt the following notation:

- y** the measurement vector
- y₀** the mean measurement vector
- x** the atmospheric state vector (in this case, the temperature profile)
- x_b** the background (a priori) atmospheric state vector
- \hat{x}** the estimated atmospheric state vector
- K** the Jacobian matrix of the observation vector with respect to the state vector
- B** the background (a priori) uncertainty covariance matrix
- R** the measurement uncertainty covariance matrix
- u(\hat{x})** the estimated retrieval uncertainty affecting **\hat{x}**

Thus, the OEM provides the following iterative solution (Rodgers, 2000):

$$\hat{x}_{i+1} = \hat{x}_i + [\mathbf{B}^{-1} + \mathbf{K}_i^T \mathbf{R}^{-1} \mathbf{K}_i]^{-1} \cdot [\mathbf{K}_i^T \mathbf{R}^{-1} (\mathbf{y} - F(\hat{x}_i)) - \mathbf{B}^{-1} (\hat{x}_i - \mathbf{x}_b)]$$

While the estimated retrieval uncertainty is given by the diagonal terms of the posterior covariance matrix:

$$\mathbf{S}_i = [\mathbf{B}^{-1} + \mathbf{K}_i^T \mathbf{R}^{-1} \mathbf{K}_i]^{-1}$$

$$u(\hat{x}) = \mathbf{diag}(\mathbf{S}_i)$$

Inaccurate estimates of **R** and **B** would cause the OEM to produce results that are not strictly optimal. Given the relative larger uncertainty associated with the estimation of the background error covariances, this is likely to be the dominant source of non-optimality (Hewison, 2006).

4 Product Traceability Chain

MWR temperature profile product

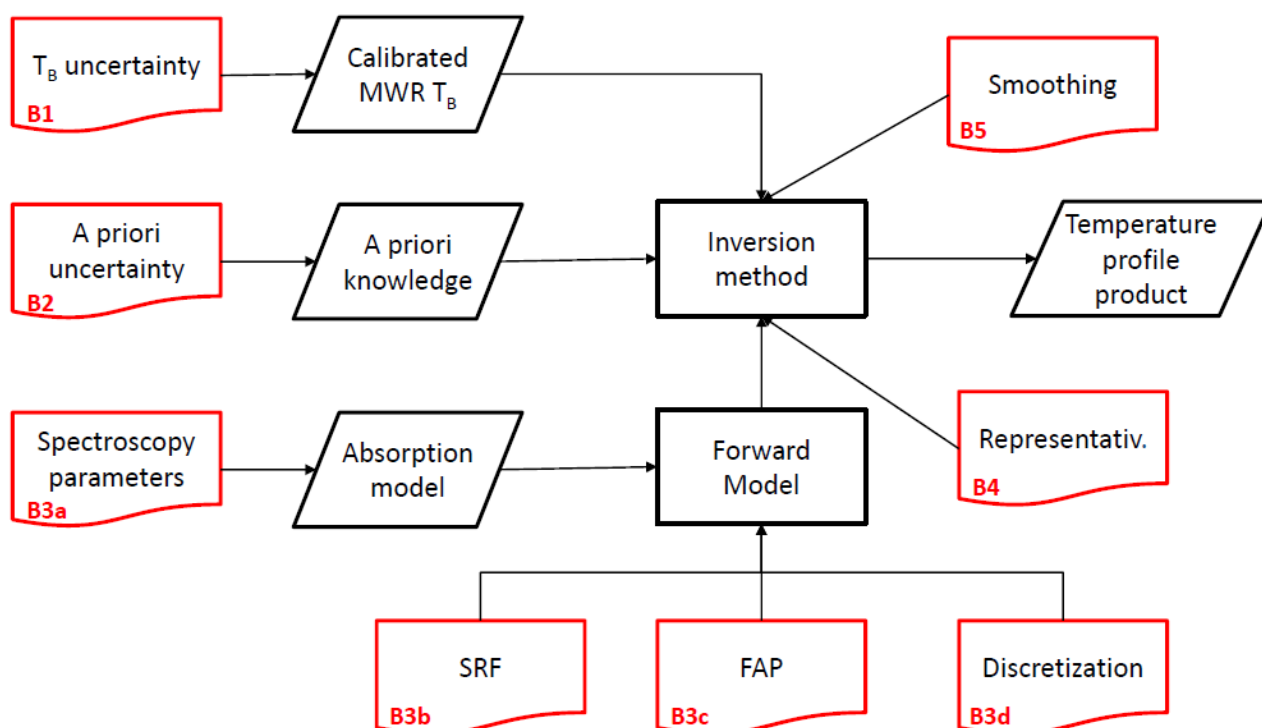


Figure 3. The metrological model chain of the MWR temperature profile product. It describes the flow diagram of the measurement, from the a priori knowledge and the calibrated TB, including uncertainty sources (highlighted in red), to the retrieved atmospheric temperature product.

All uncertainties quoted here are in the point-to-point profile temperature product at vertical spacing of the retrievals (~20-350 m within 0-5 km; 350-700 m within 5-10 km).

5 Element contributions

5.1 Brightness temperature uncertainty (B1)

The primary measurand of a MWR is brightness temperature (T_B). The estimated uncertainty for the measured T_B are detailed in the parent document GAIA-CLIM PTU document for MWR brightness temperature product. The T_B uncertainty are then propagated through the OEM formalism to estimate the uncertainty of the retrieved temperature profile. As shown in Figure 4 (right), the typical T_B uncertainty of 0.3-1.1 K maps to typical uncertainty contributions of 0.2-0.3 K within the lowest 2 km and with less than 0.2 K above 2 km.

Information / data	Type / value / equation	Notes / description
Name of effect	T_B uncertainty	
Contribution identifier	B1	
Measurement equation parameter(s) subject to effect	R	
Contribution subject to effect (final product or sub-tree intermediate product)	$\hat{x} \pm u(\hat{x})$	Estimated temperature profile and uncertainty
Time correlation extent & form	None	Random
Other (non-time) correlation extent & form	None	Random
Uncertainty PDF shape	Normal	
Uncertainty & units	<0.3 K (1σ) below 2 km <0.2 K (1σ) above 2 km	Point to point uncertainties at retrieval vertical resolution
Sensitivity coefficient	1	
Correlation(s) between affected parameters	None	
Element/step common for all sites/users?	Yes	
Traceable to ...	None	
Validation	Field experiments	Maschwitz et al., 2013

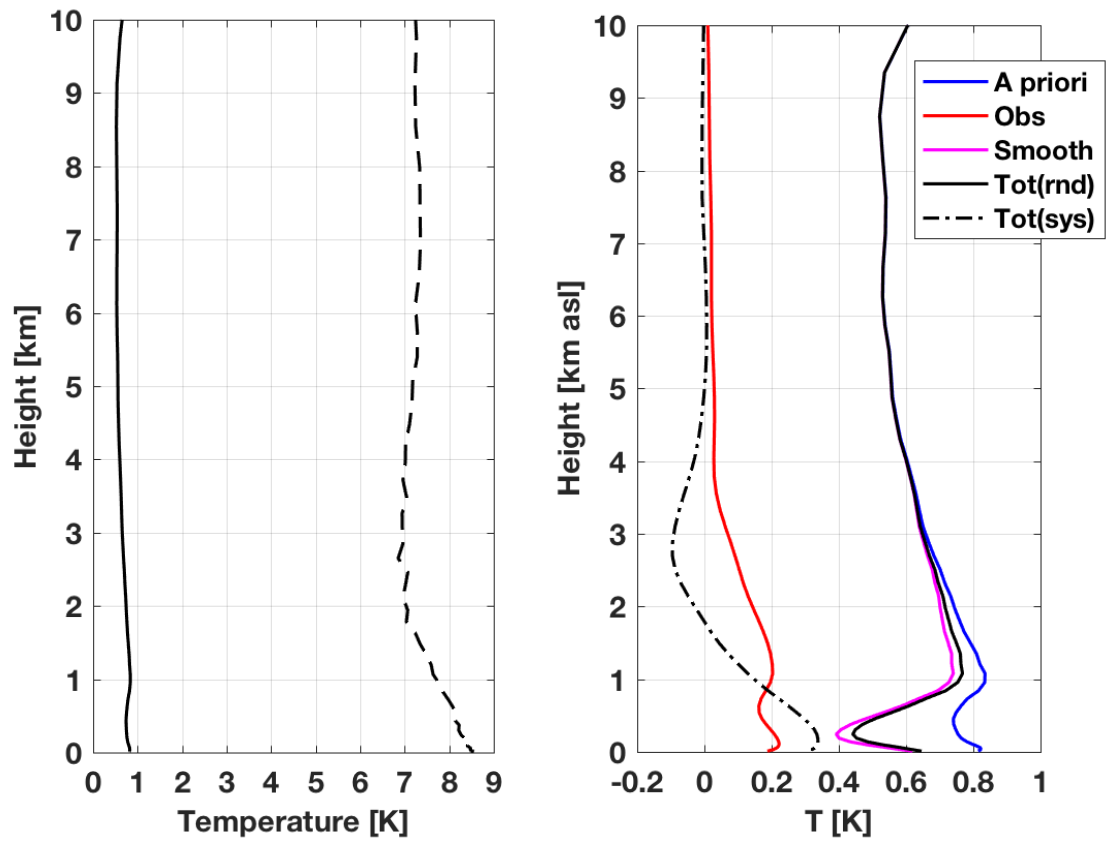


Figure 4. Left: Typical uncertainty for the a priori background from NWP (solid) and climatology (dashed). NWP data from Martinet et al, 2015. Climatology data courtesy of DWD (computed from radiosonde launched from Lindenberg in 2003-2004). Right: Contribution from a priori NWP (blue), observation (red), smoothing (magenta) uncertainties to the total uncertainty (black solid). The systematic uncertainty estimated for MWR calibration is shown in black dash-dotted line.

5.2 A priori uncertainty (B2)

When the Optimal Estimation Method is used, MWR observations are optimally coupled with a priori background knowledge, accounting for the uncertainty from both the observations and the background. Thus, an estimate of the a priori background uncertainty is needed, in the form of the background error covariance matrix **B**. A priori information may come from different sources, usually climatology (e.g. a set of historic radiosonde profiles) or the output of a numerical weather prediction (NWP) model. In case of climatology, **B** is estimated as the covariance matrix with respect to the mean value. In case of NWP model output, **B** is estimated from an ensemble of perturbed assimilation cycles (Martinet et al., 2015), similar to / the same as that used operationally for data assimilation purposes. Figure 4 shows examples of two such a priori uncertainties. However, the operational **B** matrix was found to significantly underestimate the NWP error for planetary boundary layer temperature above complex terrain (Martinet et al., 2017) and polar regions (Cimini et al. 2010). Thus, in those cases the diagonal terms of the temperature **B** matrix were modified below 2 km altitude considering the variance of typical radiosonde minus NWP differences. This correction resulted in a multiplicative factor of ~2-3 in std.

Information / data	Type / value / equation	Notes / description
Name of effect	A priori uncertainty	
Contribution identifier	B2	
Measurement equation parameter(s) subject to effect	B	
Contribution subject to effect (final product or sub-tree intermediate product)	$\hat{x} \pm u(\hat{x})$	Estimated temperature profile and uncertainty
Time correlation extent & form	None	Random
Other (non-time) correlation extent & form	None	
Uncertainty PDF shape	Normal	
Uncertainty & units (1σ)	0.4-0.7 K (1σ)	Martinet et al., 2015
Sensitivity coefficient	1	
Correlation(s) between affected parameters	None	
Element/step common for all sites/users?	Yes	
Traceable to ...	None	
Validation	Field experiment	Martinet et al., 2017

5.3 Forward Model (B3)

Any inversion method relying on Forward Model (FM) calculations, such as OEM, is affected by the uncertainty of the assumed model. The FM uncertainty includes uncertainty related to the atmospheric absorption model spectroscopy, the fast model parametrization, and the profile representation in the radiative transfer model. The contributions of these terms to the overall forward model error covariance have been evaluated by Hewison (2006), showing it is dominated by the uncertainties in the spectroscopy, which are the most difficult to estimate accurately.

Information / data	Type / value / equation	Notes / description
Name of effect	Profile discretization	
Contribution identifier	B3	
Measurement equation parameter(s) subject to effect		
Contribution subject to effect (final product or sub-tree intermediate product)	$\hat{x} \pm u(\hat{x})$	
Time correlation extent & form	None	
Other (non-time) correlation extent & form	None	
Uncertainty PDF shape	Normal	
Uncertainty & units (1σ)	<0.2 K (1σ) below 3 km <0.1 K (1σ) above 3 km	Based on Hewison, 2006
Sensitivity coefficient	1	
Correlation(s) between affected parameters	None	
Element/step common for all sites/users?	Yes	
Traceable to ...	None	
Validation	None	On-going

5.4 Spectroscopic parameters (B3a)

The radiative transfer model (RTM) calculations are affected by the uncertainty of the assumed atmospheric absorption model. This relates to the uncertainty affecting the values of the spectroscopic parameters used within the model. This contribution is often estimated as the difference in zenith T_B calculated by two or more different absorption models (Hewison, 2006; Cimini et al., 2010). Estimates for a global average are reported in the table below (after Hewison, 2006; Table 2-1). These values map onto an uncertainty for the temperature profile of the order of 0.1-0.2 K in the first 3 km and below 0.1 K above that.

ν [GHz]	22.235	23.035	23.835	26.235	30.00	51.250	52.280	53.850	54.940	56.660	57.290	58.800
σT_B [K]	1.01	1.01	0.94	0.74	0.69	1.20	0.88	0.23	0.03	0.01	0.01	0.01

Another approach consists in quantifying the spectroscopic uncertainty impact by perturbing the atmospheric profile by an amount that is reasonably attributable to the spectroscopic uncertainty (Stähli et al., 2013). However, a rigorous approach requires propagating uncertainties in line parameters to uncertainty in absorption, as suggested by Boukabara et al. 2005. Such a rigorous approach is currently being investigated within GAIA-CLIM (Cimini, 2017).

Information / data	Type / value / equation	Notes / description
Name of effect	Spectroscopic parameters	
Contribution identifier	B3a	
Measurement equation parameter(s) subject to effect	S_i	
Contribution subject to effect (final product or sub-tree intermediate product)	B3	
Time correlation extent & form	None	
Other (non-time) correlation extent & form	None	
Uncertainty PDF shape	Normal	
Uncertainty & units (1σ)	<0.2 K (1σ) below 3 km <0.1 K (1σ) above 3 km	Based on Hewison, 2006
Sensitivity coefficient	1	
Correlation(s) between affected parameters	None	
Element/step common for all sites/users?	Yes	
Traceable to ...	None	
Validation	None	On-going

5.5 Spectral Response Function (B3b)

RTM calculations require the knowledge of the channel spectral response function (SRF), which characterizes the finite bandwidth for each MWR channel (Löhnert and Maier, 2012). Band-averaged T_B can be obtained by convolving the SRF with high-resolution RTM calculations. Band-averaged T_B may significantly differ from monochromatic T_B evaluated at the channel's center frequency, as the atmospheric absorption may change non-linearly across the bandwidth of each channel. To avoid the need for expensive multiple RTM computations, it is often assumed to be approximated by an equivalent monochromatic frequency (EMF) for each channel (Cimini et al., 2010). The EMF is determined as the monochromatic frequency that minimizes the difference with the band-averaged T_B for a representative data set of atmospheric profiles. The EMF does not always correspond to the nominal central frequency. Once the EMF is accurately determined, the impact on T_B is negligible (i.e. < 0.05 K, Cimini et al., 2006; Hewison, 2006).

Information / data	Type / value / equation	Notes / description
Name of effect	Spectral Response Function (SRF)	
Contribution identifier	B3b	
Measurement equation parameter(s) subject to effect	S_i	
Contribution subject to effect (final product or sub-tree intermediate product)	B3	
Time correlation extent & form	None	
Other (non-time) correlation extent & form	None	
Uncertainty PDF shape	Normal	
Uncertainty & units (1σ)	< 0.1 K (1σ)	
Sensitivity coefficient	1	
Correlation(s) between affected parameters	None	
Element/step common for all sites/users?	Yes	
Traceable to ...	None	
Validation	Field experiments	Cimini et al., 2006 Hewison et al., 2006

5.6 Fast Absorption Predictor (B3c)

The OEM solution introduced in Section 3 requires iterative calculations. Thus, a fast RTM is mostly convenient, using a Fast Absorption Predictor (FAP) model to calculate the atmospheric absorption as a function of thermodynamical predictors (Hewison, 2006). One such fast RTM is RTTOV-gb, developed specifically for ground-based MWR observations (De Angelis, 2016). RTTOV-gb has been tested against reference RTM, showing residual errors smaller than typical MWR T_B uncertainties (<0.05 K for K-band channels, 0.01-0.2 K for V-band channels; 1σ at 19° - 90° elevation). These values are a factor ~ 2 -3 smaller than those reported by Hewison, 2006 (Table 2-3). This is probably due to the choice of better-suited predictors, which in RTTOV-gb follows the ones carefully developed for satellite RTM calculations.

Information / data	Type / value / equation	Notes / description
Name of effect	Fast Absorption Predictor (FAP)	
Contribution identifier	B3c	
Measurement equation parameter(s) subject to effect	S_i	
Contribution subject to effect (final product or sub-tree intermediate product)	B3	
Time correlation extent & form	None	
Other (non-time) correlation extent & form	None	
Uncertainty PDF shape	Normal	
Uncertainty & units (1σ)	<0.1 K (1σ)	
Sensitivity coefficient	1	
Correlation(s) between affected parameters	None	
Element/step common for all sites/users?	Yes	
Traceable to ...	None	
Validation	Numerical validation	De Angelis et al., 2016

5.7 Discretization (B3d)

The discretization of the background profiles introduces uncertainty in T_B calculated by the RTM. This contribution has been evaluated using a set of high-resolution radiosondes to compute T_B through a RTM and comparing with T_B calculated using the same profiles reduced by a discretization method, as that used for NWP models (Hewison, 2006; Table 2-4). Large impact is found when using WMO standard levels (0.4-1.7 K), which reduces substantially when significant levels are added (0.03-0.21 K). Using the levels designed for RTTOV-gb (De Angelis et al., 2016), the impact on T_B becomes negligible (<0.05 K).

Information / data	Type / value / equation	Notes / description
Name of effect	Discretization	
Contribution identifier	B3d	
Measurement equation parameter(s) subject to effect	S_i	
Contribution subject to effect (final product or sub-tree intermediate product)	B3	
Time correlation extent & form	None	
Other (non-time) correlation extent & form	None	
Uncertainty PDF shape	Normal	
Uncertainty & units (1σ)	<0.1 K (1σ)	
Sensitivity coefficient	1	
Correlation(s) between affected parameters	None	
Element/step common for all sites/users?	Yes	
Traceable to ...	None	
Validation		Using standard atmosphere and RTTOV-gb levels (De Angelis et al., 2016)

5.8 Representativeness (B4)

The representativeness error accounts for the instrument sensitivity to fluctuations on smaller scales than can be represented by the background. To compensate for this, it is usual to add the representativeness errors to the instrumental error to get a larger observational error. The representativeness error has been estimated by studying the fluctuations in the MWR signal on typical time scales within a 6-day period of clear and cloudy conditions (Hewison, 2006). It was found that the representativeness term evaluated in this way dominates the observation error of those channels most sensitive to cloud. These values map onto an uncertainty for the temperature profile of the order of 0.1-0.3 K in the first 3 km and below 0.1 K above that. Ideally, the representativeness error shall be evaluated dynamically, e.g. based on time series of observations within 1 hour window of each observation. This would allow the errors to be reduced in periods of atmospheric stability, when MWR observations are more representative of the background state. Inclusion of observations of meteorological covariates would help better quantify this uncertainty, although this is not currently performed.

Information / data	Type / value / equation	Notes / description
Name of effect	Representativeness error	
Contribution identifier	B4	
Measurement equation parameter(s) subject to effect	R	
Contribution subject to effect (final product or sub-tree intermediate product)	$\hat{x} \pm u(\hat{x})$	
Time correlation extent & form	diurnal/seasonal	Depends on atmospheric conditions, and thus may be correlated with diurnal/seasonal cycle
Other (non-time) correlation extent & form	None	
Uncertainty PDF shape	Normal	
Uncertainty & units (1σ)	<0.3 K (1 σ) below 3 km <0.1 K (1 σ) above 3 km	Based on Hewison, 2006
Sensitivity coefficient	1	
Correlation(s) between affected parameters	None	
Element/step common for all sites/users?	Yes	
Traceable to ...	None	
Validation	None	

5.9 Smoothing error (B5)

The smoothing error is part of the total uncertainty estimated with the OEM. It is related to the vertical resolution of MWR temperature profiles, which is limited due to the passive approach. A quantitative definition of the vertical resolution builds on the averaging kernel matrix concept. The averaging kernel defines the sensitivity of the retrieved quantities to the true atmospheric state. The broadness of the averaging kernels gives information on the vertical resolution; e.g. a perfect vertical resolution corresponds to averaging kernels in the form of delta functions. Using the same notation as in Section 3, the averaging kernel matrix is defined as (Rodgers, 2000):

$$\mathbf{A}_i = [\mathbf{B}^{-1} + \mathbf{K}_i^T \mathbf{R}^{-1} \mathbf{K}_i]^{-1} \mathbf{K}_i^T \mathbf{R}^{-1} \mathbf{K}_i$$

The smoothing error is defined as $(\mathbf{A} - \mathbf{I})(\mathbf{x} - \mathbf{x}_b)$ whose covariance is $\mathbf{S}_S = (\mathbf{A} - \mathbf{I})\mathbf{B}(\mathbf{A} - \mathbf{I})^T$. As shown in Figure 4 (right), the smoothing error is dominating the total uncertainty.

Information / data	Type / value / equation	Notes / description
Name of effect	Smoothing error	
Contribution identifier	B5	
Measurement equation parameter(s) subject to effect	\mathbf{S}_i	
Contribution subject to effect (final product or sub-tree intermediate product)	$\hat{\mathbf{x}} \pm u(\hat{\mathbf{x}})$	
Time correlation extent & form	None	
Other (non-time) correlation extent & form	Vertical	The averaging kernels indicate the correlation of the retrievals at different vertical levels.
Uncertainty PDF shape	Normal	
Uncertainty & units (1σ)	0.4-0.8 K (1σ) from 0-10 km	
Sensitivity coefficient	1	
Correlation(s) between affected parameters	None	
Element/step common for all sites/users?	Yes	
Traceable to ...	OEM formalism	Traceable linked to that of B and R
Validation	Field experiments	Löhnert and Maier, 2012

6 Uncertainty Summary

Element identifier	Contribution name	Uncertainty contribution form	Typical value	Traceability level (L/M/H)	random, structured random, quasi-systematic or systematic?	Correlated to? (Use element identifier)
B1	T _B uncertainty	Normal	0.3 K	M	random	None
B2	A priori	Normal	0.4-0.7 K	M	random	None
B3	Forward model	Normal	0.2 K	M	random	None
B3a	Spectroscopy	Normal	0.2 K	L	random	None
B3b	SRF	Normal	<0.1 K	H	systematic	None
B3c	FAP	Normal	<0.1 K	H	random	None
B3d	Discretization	Normal	<0.1 K	H	systematic	None
B4	Representativeness	Normal	0.1-0.3 K	L	random	None
B5	Smoothing	Normal	0.4-0.8 K	H	random	None

The estimated uncertainties are combined following the OEM formalism (Rodgers, 2000). Using the same notation as in Section 3, the random uncertainty of the estimated temperature profile $\hat{\mathbf{x}}_i$ is given by the diagonal terms of the posterior covariance matrix:

$$u_{rnd}(\hat{\mathbf{x}}_i) = \mathbf{diag}(\mathbf{S}_i) = \mathbf{diag}([\mathbf{B}^{-1} + \mathbf{K}_i^T \mathbf{R}^{-1} \mathbf{K}_i]^{-1})$$

The background uncertainty covariance matrix (\mathbf{B}) and the measurement uncertainty covariance matrix (\mathbf{R}) are related to the Uncertainty Summary Table above as follows. \mathbf{B} is given by the a priori uncertainty (B2). \mathbf{R} is usually split in three contributions $\mathbf{R} = \mathbf{E} + \mathbf{F} + \mathbf{M}$ (Hewison, 2006), where the instrument noise (\mathbf{E}) corresponds to T_B uncertainty (B1); \mathbf{F} corresponds to the forward model uncertainty (B3); and \mathbf{M} corresponds to the representativeness uncertainty (B4). The smoothing uncertainty (B5) is given by the combined contributions of \mathbf{B} , \mathbf{R} , and \mathbf{K}_i as explained in Section 5.9. The relative contributions of \mathbf{B} , \mathbf{R} , and smoothing to the total random uncertainty are depicted in Figure 4.

Introducing the gain matrix $\mathbf{G} = \mathbf{S}_i \mathbf{K}_i^T \mathbf{R}^{-1}$ (Rodgers, 2000), the systematic uncertainty of the retrieved temperature profile is estimated in the assumption of a linear retrieval as:

$$u_{sys}(\hat{\mathbf{x}}_i) = \mathbf{G} * u_{sys}(\mathbf{y})$$

where $u_{sys}(\mathbf{y})$ includes the T_B systematic uncertainty affecting the MWR calibration (see the parent GAIA-CLIM PTU document for MWR brightness temperature product). Typical values of the estimated systematic uncertainty are shown in Figure 4. Finally, Figure 5 shows an example of a MWR retrieved temperature profile with the associated random and systematic uncertainties.

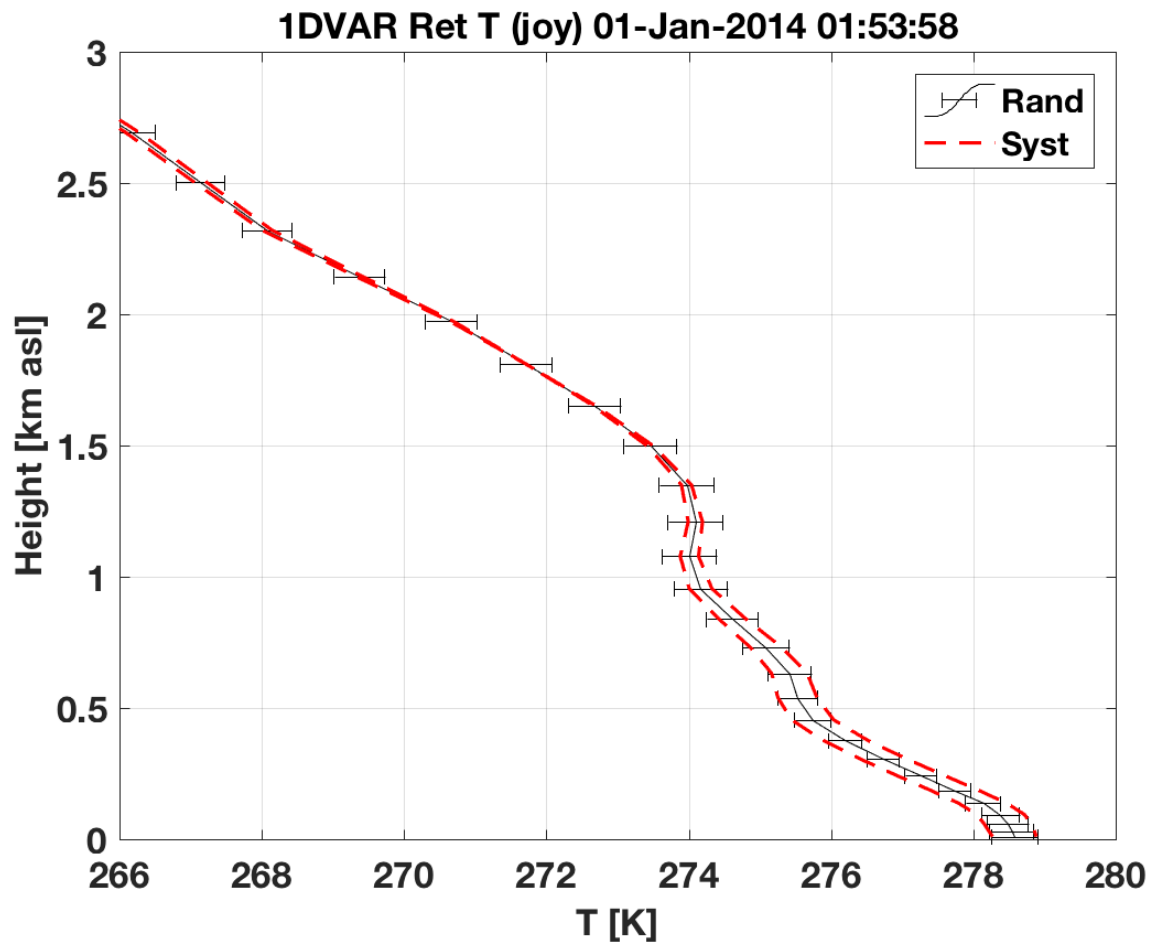


Figure 5. An example of temperature profile retrieval at the Joyce site (Juelich, Germany) on January 1st 2014, 01:53 UTC. The associated random (errorbars) and systematic (red dashed lines) uncertainties are also shown.

7 Traceability uncertainty analysis

Traceability level definition is given in Table 2.

Table 2. Traceability level definition table

Traceability Level	Descriptor	Multiplier
High	SI traceable or globally recognised community standard	1
Medium	Developmental community standard or peer-reviewed uncertainty assessment	3
Low	Approximate estimation	10

Analysis of the summary table would suggest the following contributions, shown in Table 3, should be considered further to improve the overall uncertainty of the MWR temperature profile product. The entries are given in an estimated priority order.

Table 3. Traceability level definition further action table.

Element identifier	Contribution name	Uncertainty contribution form	Typical value	Traceability level (L/M/H)	random, structured random, quasi-systematic or systematic?	Correlated to? (Use element identifier)
B3a	Spectroscopy	Normal	0.2 K	L	random	None
B2	A priori	Normal	0.4-0.7 K	M	random	None
B4	Representativeness	Normal	0.1-0.3 K	L	random	None

7.1 Recommendations

Suggestions for improving the assessment of the T_B calibration uncertainty (B1) are given in the parent document GAIA-CLIM PTU document for MWR brightness temperature product.

In addition, the top priority is to quantify rigorously the spectroscopic parameter contribution (B3a), which may be significantly underestimated. This is ongoing within GAIA-CLIM (Cimini, 2017).

Another priority is to better characterise the a priori uncertainty (B2), especially when the a priori information is from a NWP model. There is emerging evidence that this contribution may be underestimated for sites with strong surface temperature inversions (Cimini et al., 2010; Martinet et al., 2017).

Finally, the representativeness error (B4) shall be characterised for each site and MWR instrument. Inclusion of observations of meteorological covariates would help better quantify this uncertainty. Ideally, this could be evaluated dynamically to make this contribution flow-dependent.

8 Conclusion

The MWR temperature profile product has been assessed against the GAIA CLIM traceability and uncertainty criteria.

References

- Boukabara S. A., S. A. Clough, J.-L. Moncet, A. F. Krupnov, M. Yu. Tretyakov, and V. V. Parshin (2005), Uncertainties in the Temperature Dependence of the Line-Coupling Parameters of the Microwave Oxygen Band: Impact Study, *IEEE Trans. Geosci. Rem. Sens.*, 43, 5, doi: 10.1109/TGRS.2004.839654.
- Cimini, D., T. J. Hewison, L. Martin (2006), Comparison of brightness temperatures observed from ground-based microwave radiometers during TUC, *Meteorologische Zeitschrift*, Vol.15, No.1, 2006, pp.19-25.
- Cimini, D., T. J. Hewison, L. Martin, J. Güldner, C. Gaffard and F. S. Marzano (2006), Temperature and humidity profile retrievals from ground-based microwave radiometers during TUC, *Met. Zeitschrift*, Vol. 15, No. 1, 45-56.
- Cimini D., E. R. Westwater, and A. J. Gasiewski (2010), Temperature and humidity profiling in the Arctic using millimeter-wave radiometry and 1DVAR, *IEEE Transactions on Geoscience and Remote Sensing*, Vol. 48, 3, 1381-1388, 10.1109/TGRS.2009.2030500.
- Cimini D. (2017), Report on G2.14: Missing uncertainty associated with MW absorption models, GAIA-CLIM 2nd General Assembly, ECMWF, Reading, Feb. 8-9, 2017.
- De Angelis, F., Cimini, D., Hocking, J., Martinet, P., and Kneifel, S. (2016), RTTOV-gb – adapting the fast radiative transfer model RTTOV for the assimilation of ground-based microwave radiometer observations, *Geosci. Model Dev.*, 9, 2721-2739, doi:10.5194/gmd-9-2721-2016, Online: <http://www.geosci-model-dev.net/9/2721/2016/>
- De Angelis, F., Cimini, D., Löhnert, U., Caumont, O., Haeferle, A., Pospichal, B., Martinet, P., Navas-Guzmán, F., Klein-Baltink, H., Dupont, J.-C., and Hocking, J. (2017), Long term Observations minus Background monitoring of ground-based microwave radiometer network. Part 1: Brightness Temperatures, *Atmos. Meas. Tech. Discuss.*, doi:10.5194/amt-2017-112, in review.
- GAIA-CLIM Product Traceability and Uncertainty (PTU) document for the Microwave Radiometer (MWR) brightness temperature product (2017), *PTU_MWR_Brightness_Temperature_V1.0.pdf*
- Hewison T. (2006), *Profiling Temperature and Humidity by Ground-based Microwave Radiometers*, PhD Thesis, Department of Meteorology, University of Reading.
- Löhnert, U. and Maier, O. (2012), Operational profiling of temperature using ground-based microwave radiometry at Payerne: prospects and challenges, *Atmos. Meas. Tech.*, 5, 1121-1134, doi:10.5194/amt-5-1121-2012.
- Martinet, P., Dabas, A., Donier, J. M., Douffet, T., Garrouste, O., and Guillot, R. (2015), 1D-Var temperature retrievals from microwave radiometer and convective scale model, *Tellus A*, 67, 2015. Doi: 10.3402/tellusa.v67.27925.
- Martinet, P., Cimini, D., De Angelis, F., Canut, G., Unger, V., Guillot, R., Tzanos, D., and Paci, A.: Combining ground-based microwave radiometer and the AROME convective scale model through 1DVAR retrievals in complex terrain: an Alpine Valley case study, *Atmos. Meas. Tech. Discuss.*, <https://doi.org/10.5194/amt-2017-144>, in review, 2017.
- Rodgers, C. D.: *Inverse methods for atmospheric sounding: theory and practice*, vol. 2, World scientific, 2000.
- Solheim F., J. Godwin, E. Westwater, Y. Han, S. Keihm, K. Marsh, R. Ware (1998), Radiometric Profiling of Temperature, Water Vapor, and Liquid Water using Various Inversion Methods, *Radio Science*, 33, pp. 393-404, DOI: 10.1029/97RS03656.
- Stähli, O., Murk, A., Kämpfer, N., Mätzler, C., and Eriksson, P. (2013), Microwave radiometer to

retrieve temperature profiles from the surface to the stratopause, *Atmos. Meas. Tech.*, 6, 2477-2494, doi:10.5194/amt-6-2477-2013.

Westwater E.R., S. Crewell, C. Mätzler: A Review of Surface-Based Microwave and Millimeter Wave Radiometric Remote Sensing of the Troposphere, *URSI Radio Science Bulletin*, No. 310, 59-80, 2004. Online:

<https://pdfs.semanticscholar.org/09ae/6c38f5d28fdd6c62703327c01a36d0d8af16.pdf>

Westwater E. R., S. Crewell, C. Mätzler, D. Cimini: Principles of surface-based microwave and millimeter wave radiometric remote sensing of the troposphere *Quaderni della Società Italiana di Elettromagnetismo* Vol.: 1, No.3, 50-90, 2005. Online:

http://radiometrics.com/data/uploads/2012/12/Westwater_QSIE_2005.pdf



Product Traceability and Uncertainty for the Microwave Radiometer (MWR) total water vapor content product

Version 1.0

*GAIA-CLIM
Gap Analysis for Integrated
Atmospheric ECV Climate Monitoring
Mar 2015 - Feb 2018*

A Horizon 2020 project; Grant agreement: 640276

Date: 21 December 2017

Dissemination level: PU

Work Package 2; Task 2.1.2; Compiled by Domenico Cimini (CNR)

Table of Contents

1	Product overview	4
1.1	Guidance notes	4
2	Introduction.....	4
3	Instrument description.....	4
4	Product Traceability Chain	5
5	Element contributions	5
6	Uncertainty Summary	5
7	Traceability uncertainty analysis	6
7.1	Recommendations	6
8	Conclusion	6
	References.....	7

Version history

Version	Principal updates	Owner	Date
0.1 draft	First draft – after Webex meeting on Oct 9 th 2017	CNR	17.11.2017
1.0	First issue – after feedback from NPL and Project Scientific Lead	CNR	21.12.2017

1 Product overview

Product name: MWR total water vapor content product

Product technique: Total water vapor content estimated from humidity profile retrievals from multichannel brightness temperature measurements and a priori knowledge

Product measurand: Total water vapor content [kg/m²]

Product form/range: Total column-integrated water vapor content.

Product dataset: TOPROF data set

Site/Sites/Network location:

SITE	LAT	LON	HEIGHT(m)	MWR	LOCATION	COUNTRY
JOYCE	50.91	6.41	111	HATPRO G2	Juelich	DE
LACROS	51.35	12.43	125	HATPRO G2	Liepzig	DE
Payerne	46.82	6.95	491	HATPRO G1	Payerne	CH
SIRTA	48.80	2.36	156	HATPRO G2	Paris	FR
CESAR	51.97	4.93	-0.7	HATPRO G1	Cabauw	NL
RAO	52.21	14.12	125	MP3000A	Lindenberg	DE

Product time period: Jan 1, 2015 – Feb 27, 2016

Data provider: TOPROF

Instrument provider: Site management

Product assessor: Domenico Cimini, CNR

Assessor contact email: domenico.cimini@imaa.cnr.it

1.1 Guidance notes

This document is meant to be an annex to GAIA-CLIM Product Traceability and Uncertainty (PTU) document for the Microwave Radiometer (MWR) humidity profile product (PTU_MWR_Humidity_profile_V1.0.pdf). The reader should refer to that PTU document for the details about the humidity profile uncertainty used here to estimate the total water vapor content (TWVC) uncertainty.

2 Introduction

This document presents the Product Traceability and Uncertainty (PTU) information for the Microwave Radiometer (MWR) total water vapor content (TWVC) product. The TWVC and its uncertainty are derived from the MWR humidity profile product and relative uncertainties. The reader shall refer to the MWR humidity profile PTU document for details on the estimated uncertainty (PTU_MWR_Humidity_profile_V1.0.pdf).

3 Instrument description

The instrument description is given in the GAIA-CLIM PTU document for the MWR humidity profile product (PTU_MWR_Humidity_profile_V1.0.pdf).

4 Product Traceability Chain

The product traceability chain is given in the GAIA-CLIM PTU document for the MWR humidity profile product (PTU_MWR_Humidity_profile_V1.0.pdf).

5 Element contributions

The element contributions are given in the GAIA-CLIM PTU document for the MWR humidity profile product (PTU_MWR_Humidity_profile_V1.0.pdf).

6 Uncertainty Summary

The uncertainty summary is given in the GAIA-CLIM PTU document for the MWR humidity profile product (PTU_MWR_Humidity_profile_V1.0.pdf). Here we adopt the same notation (see Section 3), in particular:

- z the vertical coordinate (e.g., the altitude above ground)
- $\hat{\mathbf{x}}$ the estimated atmospheric state vector (i.e. the humidity profile)
- $u_{rnd}(\hat{\mathbf{x}})$ the estimated random uncertainty affecting $\hat{\mathbf{x}}$
- $u_{sys}(\hat{\mathbf{x}})$ the estimated systematic uncertainty affecting $\hat{\mathbf{x}}$

Thus, TWVC and the associated uncertainties are derived from the retrieved humidity profile and the relative uncertainties by:

$$TWVC = \int_0^{TOA} \hat{\mathbf{x}} \cdot d\mathbf{z}$$
$$u_{rnd}(TWVC) = \sqrt{\sum_{l=1}^{N_l} u_{rnd}(\hat{\mathbf{x}}_l)^2 \cdot \Delta z_l^2}$$
$$u_{sys}(TWVC) = \int_0^{TOA} u_{sys}(\hat{\mathbf{x}}) \cdot d\mathbf{z}$$

Note that the smoothing error is removed by the vertical averaging, thus only the observation uncertainty is included in $u_{rnd}(\hat{\mathbf{x}})$, which includes the random noise, a priori, forward model, and representativeness uncertainties. Figure 1 shows a time series of MWR retrieved TWVC products with the associated random and systematic uncertainties.

7 Traceability uncertainty analysis

The traceability uncertainty analysis is given in the GAIA-CLIM PTU document for the MWR humidity profile product (PTU_MWR_Humidity_profile_V1.0.pdf).

7.1 Recommendations

The recommendations are given in the GAIA-CLIM PTU document for the MWR humidity profile product (PTU_MWR_Humidity_profile_V1.0.pdf).

8 Conclusion

The MWR total water vapor content (TWVC) product has been assessed against the GAIA CLIM traceability and uncertainty criteria.

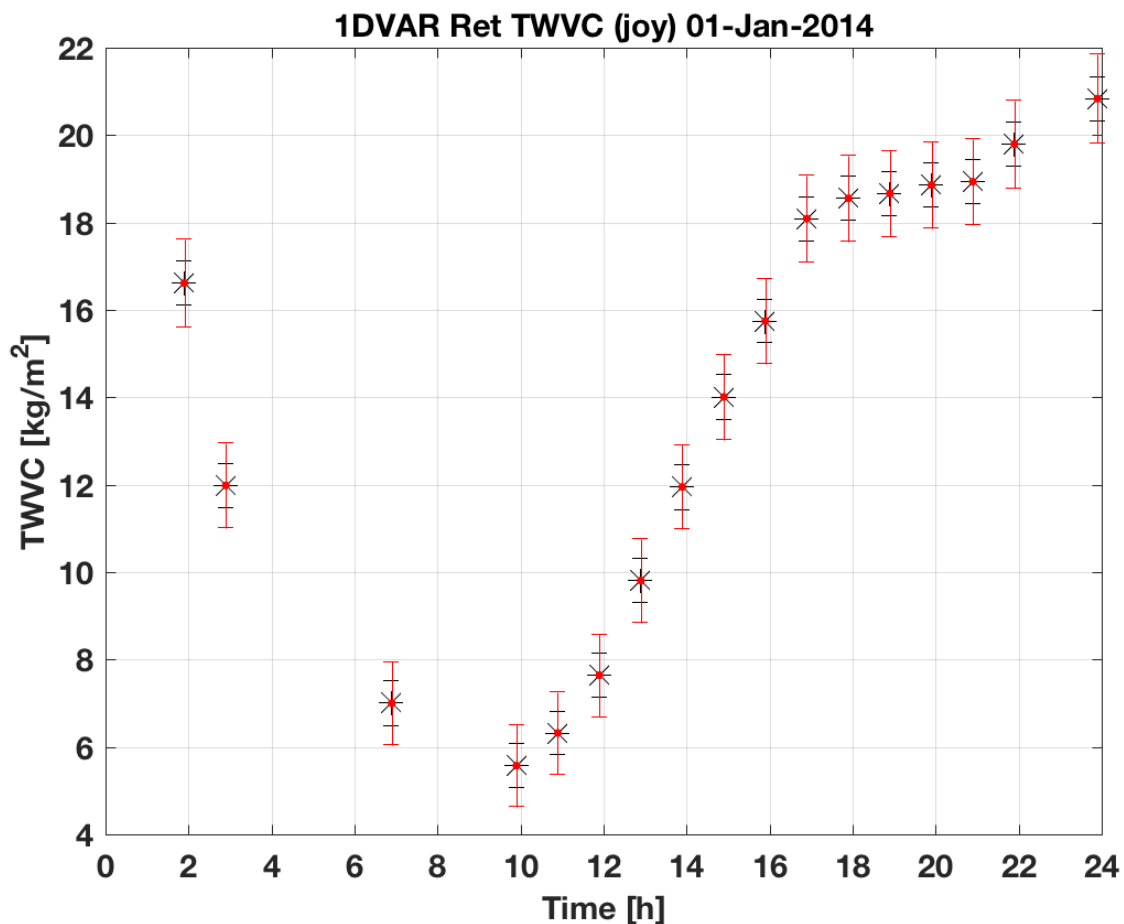


Figure 1. An example of TWVC time series retrieval at the Joyce site (Juelich, Germany) on January 1st 2014. The associated random and systematic uncertainties are shown in black and red errorbars, respectively.

References

GAIA-CLIM Product Traceability and Uncertainty (PTU) document for the Microwave Radiometer (MWR) humidity profile product (2017), PTU_MWR_Humidity_profile_V1.0.pdf



Product Traceability and Uncertainty for the Microwave Radiometer (MWR) humidity profile product

Version 1.0

*GAIA-CLIM
Gap Analysis for Integrated
Atmospheric ECV Climate Monitoring
Mar 2015 - Feb 2018*

A Horizon 2020 project; Grant agreement: 640276

Date: 19 December 2017

Dissemination level: PU

Work Package 2; Task 2.1.2; Compiled by Domenico Cimini (CNR)

Table of Contents

1	Product overview	4
1.1	Guidance notes	4
2	Introduction.....	6
3	Instrument description.....	7
4	Product Traceability Chain	9
5	Element contributions	10
5.1	Brightness temperature uncertainty (B1)	10
5.2	A priori uncertainty (B2).....	11
5.3	Forward Model (B3).....	13
5.4	Spectroscopic parameters (B3a).....	14
5.5	Spectral Response Function (B3b).....	15
5.6	Fast Absorption Predictor (B3c).....	16
5.7	Discretization (B3d)	17
5.8	Representativeness (B4).....	18
5.9	Smoothing error (B5)	19
6	Uncertainty Summary	20
7	Traceability uncertainty analysis	22
7.1	Recommendations	22
8	Conclusion	22
	References.....	23

Version history

Version	Principal updates	Owner	Date
0.1 draft	First draft – adapted existing text to the template provided by NPL	CNR	8.11.2017
0.2 draft	Second draft – after Webex meeting on Oct 9 th 2017	CNR	15.11.2017
1.0	First issue – after feedback from NPL and Project Scientific Lead	CNR	19.12.2017

1 Product overview

Product name: MWR humidity profile product

Product technique: Humidity profile retrieval from multichannel brightness temperature measurements and a priori knowledge

Product measurand: Absolute Humidity [kg/m^3]

Product form/range: Profile

Product dataset: TOPROF data set

Site/Sites/Network location:

SITE	LAT	LON	HEIGHT(m)	MWR	LOCATION	COUNTRY
JOYCE	50.91	6.41	111	HATPRO G2	Juelich	DE
LACROS	51.35	12.43	125	HATPRO G2	Liepzig	DE
Payerne	46.82	6.95	491	HATPRO G1	Payerne	CH
SIRTA	48.80	2.36	156	HATPRO G2	Paris	FR
CESAR	51.97	4.93	-0.7	HATPRO G1	Cabauw	NL
RAO	52.21	14.12	125	MP3000A	Lindenberg	DE

Product time period: Jan 1, 2015 – Feb 27, 2016

Data provider: TOPROF

Instrument provider: Site management

Product assessor: Domenico Cimini, CNR

Assessor contact email: domenico.cimini@imaa.cnr.it

1.1 Guidance notes

For general guidance see the Guide to Uncertainty in Measurement & its Nomenclature, published as part of the GAIA-CLIM project.

This document is a measurement product technical document which should be stand-alone i.e. intelligible in isolation. Reference to external sources (mostly peer-reviewed) and documentation from previous studies is given, but the content provided here shall not require the reading of all these reference documents to gain a clear understanding of the GAIA CLIM product and associated uncertainties entered into the Virtual Observatory (VO).

In developing this guidance, we adopted the convention proposed by the QA4ECV project (<http://www.qa4ecv.eu/>) through the Traceability and Uncertainty Propagation Tool (TUPT). This convention is summarized in Figure 1.

QA4ECV TUPT convention

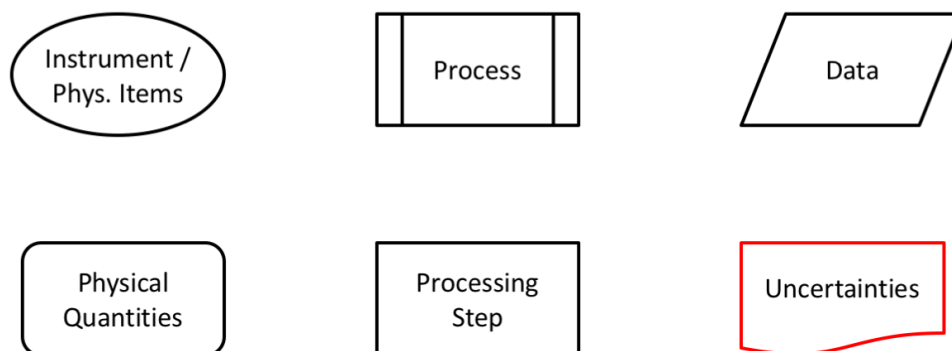


Figure 1. The convention proposed by the QA4ECV project (<http://www.qa4ecv.eu/>) through the Traceability and Uncertainty Propagation Tool (TUPT). This convention is adopted hereafter to draw the MWR model diagram.

The contribution table to be filled for each traceability contributor has the form seen in Table 1.

Table 1. The contributor table.

Information / data	Type / value / equation	Notes / description
Name of effect		
Contribution identifier		
Measurement equation parameter(s) subject to effect		
Contribution subject to effect (final product or sub-tree intermediate product)		
Time correlation extent & form		
Other (non-time) correlation extent & form		
Uncertainty PDF shape		
Uncertainty & units		
Sensitivity coefficient		
Correlation(s) between affected parameters		
Element/step common for all sites/users?		
Traceable to ...		
Validation		

Name of effect – The name of the contribution. Should be clear, unique and match the description in the traceability diagram.

Contribution identifier - Unique identifier to allow reference in the traceability chains.

Measurement equation parameter(s) subject to effect – The part of the measurement equation influenced by this contribution. Ideally, the equation into which the element contributes.

Contribution subject to effect – The top level measurement contribution affected by this contribution. This can be the main product (if on the main chain), or potentially the root of a side branch contribution. It will depend on how the chain has been sub-divided.

Time correlation extent & form – The form & extent of any correlation this contribution has in time.

Other (non-time) correlation extent & form – The form & extent of any correlation this contribution has in a non-time domain. For example, spatial or spectral.

Uncertainty PDF shape – The probability distribution shape of the contribution, Gaussian/Normal Rectangular, U-shaped, log-normal or other. If the form is not known, a written description is sufficient.

Uncertainty & units – The uncertainty value, including units and confidence interval. This can be a simple equation, but should contain typical values.

Sensitivity coefficient – Coefficient multiplied by the uncertainty when applied to the measurement equation.

Correlation(s) between affected parameters – Any correlation between the parameters affected by this specific contribution. If this element links to the main chain by multiple paths within the traceability chain, it should be described here. For instance, SZA or surface pressure may be used separately in a number of models & correction terms that are applied to the product at different points in the processing.

Element/step common for all sites/users – Is there any site-to-site/user-to-user variation in the application of this contribution?

Traceable to – Describe any traceability back towards a primary/community reference.

Validation – Any validation activities that have been performed for this element?

2 Introduction

This document presents the Product Traceability and Uncertainty (PTU) information for the Microwave Radiometer (MWR) humidity profile product. The aim of this document is to provide supporting information for the users of this product within the GAIA-CLIM VO.

Using the convention in Figure 1, the main chain of the MWR instrument is pictured in Figure 2. The red boxes indicate the two main processes:

A) Calibration: the conversion from raw voltages corresponding to the received atmospheric radiance into calibrated brightness temperature (T_B);

B) Inversion: the inversion of calibrated T_B with the combination of some a priori knowledge to

estimate the atmospheric products (retrievals).

Thus, MWR uncertainties are divided in two groups: those affecting the MWR calibration (i.e. from atmospheric radiance to calibrated T_B) and those affecting the retrieval method (from calibrated T_B to MWR retrievals). The parent document (GAIA-CLIM PTU document for MWR brightness temperature product) treats the calibration process (A) and the contributions to the T_B uncertainty. This document treats the inversion process (B) and how the T_B uncertainty combines with other uncertainty sources to contribute to the uncertainty of the retrieved humidity profile.

MWR measurement: Main Chain

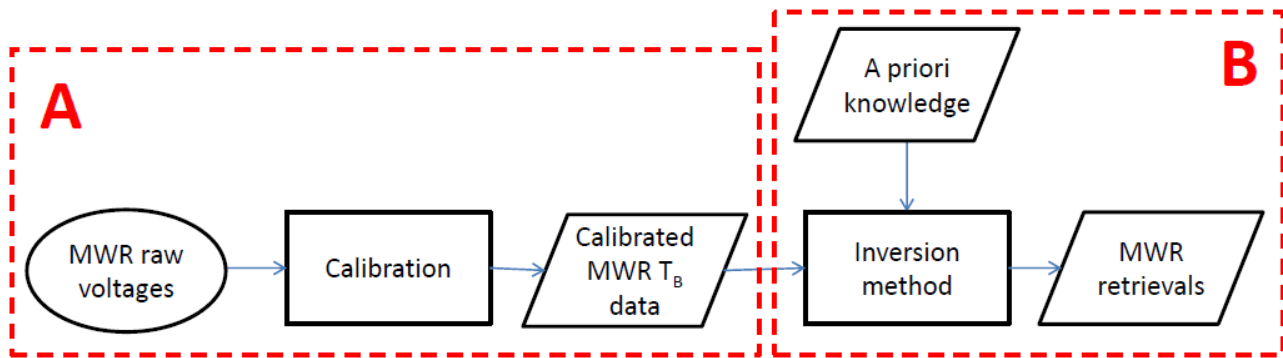


Figure 2. The main chain of the MWR instrument model diagram. The main chain displays the process of producing a geophysical product from the MWR instrument measurements. The process A (from raw voltages to calibrated brightness temperature T_B) is treated in the parent document. The process B is treated in three children documents, of which this is one.

3 Instrument description

Ground-based microwave radiometers (MWR) are instruments calibrated to measure the natural down-welling thermal emission from the atmosphere. The quantity measured by a MWR is atmospheric radiance [$W/(m^2 \cdot sr \cdot Hz)$], which is typically converted into brightness temperature (T_B , [K]) to adopt more familiar units.

Atmospheric temperature and humidity profiles, as well as column-integrated Total Water Vapour Content (TWVC) and Total Liquid Water Content (TLWC), can be inferred from ground-based MWR T_B observations.

Review articles on MWR measurements are given by Westwater et al., 2004 & 2005. Common MWR commercial units operate several channels in the 20-60 GHz frequency range. The 20-30 GHz range is referred to as K-band, while the 50-60 GHz range is called V-band.

Figure 3 provides details of the MWR measurement metrological model chain for the inversion process (B). It describes the flow diagram from the a priori knowledge and the calibrated T_B , including uncertainty sources (highlighted in red), to the retrieved atmospheric temperature product.

The uncertainty of the inverse method, that is the analysis algorithm to transform the calibrated T_B into the atmospheric products, contributes to the total uncertainty affecting the MWR atmospheric products. A variety of methods are currently used to solve the inverse problem, with somewhat different implementations, and their performances have been compared to some degree (Solheim et al. 1998; Cimini et al., 2006). Statistical algorithms, including multivariate statistical regression and neural networks, are usually exploited as they are suitable to be applied in real time. Conversely, physical retrieval methods, such as optimal estimation methods (OEM), are computationally more expensive as they solve the inverse problem in a physically consistent way. OEM optimally couples MWR observations with a priori background knowledge, accounting for uncertainty from both the observations and background and propagating uncertainty to the final product. An estimate of the uncertainty on the retrieved profiles can be derived by assuming the errors are normally distributed

about the solution and that the problem is only moderately non-linear (Rodgers, 2000).

The OEM retrieval method is affected by instrumental uncertainty (detailed in the parent document GAIA-CLIM PTU document for MWR brightness temperature product) as well as other sources of uncertainty, such as a priori, absorption model, spectral response function, profile discretization, smoothing and representativeness errors (Hewison, 2006; Cimini et al., 2010; Stähli et al., 2013).

For the OEM, we adopt the following notation:

- y** the measurement vector
- y₀** the mean measurement vector
- x** the atmospheric state vector (in this case, the humidity profile)
- x_b** the background (a priori) atmospheric state vector
- $\hat{\mathbf{x}}$** the estimated atmospheric state vector
- K** the Jacobian matrix of the observation vector with respect to the state vector
- B** the background (a priori) uncertainty covariance matrix
- R** the measurement uncertainty covariance matrix
- u($\hat{\mathbf{x}}$)** the estimated retrieval uncertainty affecting **$\hat{\mathbf{x}}$**

Thus, the OEM provides the following iterative solution (Rodgers, 2000):

$$\hat{\mathbf{x}}_{i+1} = \hat{\mathbf{x}}_i + [\mathbf{B}^{-1} + \mathbf{K}_i^T \mathbf{R}^{-1} \mathbf{K}_i]^{-1} \cdot [\mathbf{K}_i^T \mathbf{R}^{-1} (\mathbf{y} - F(\hat{\mathbf{x}}_i)) - \mathbf{B}^{-1} (\hat{\mathbf{x}}_i - \mathbf{x}_b)]$$

While the estimated retrieval uncertainty is given by the diagonal terms of the posterior covariance matrix:

$$\mathbf{S}_i = [\mathbf{B}^{-1} + \mathbf{K}_i^T \mathbf{R}^{-1} \mathbf{K}_i]^{-1}$$

$$u(\hat{\mathbf{x}}) = \mathbf{diag}(\mathbf{S}_i)$$

Inaccurate estimates of **R** and **B** would cause the OEM to produce results that are not strictly optimal. Given the relative larger uncertainty associated with the estimation of the background error covariances, this is likely to be the dominant source of non-optimality (Hewison, 2006).

4 Product Traceability Chain

MWR humidity profile product

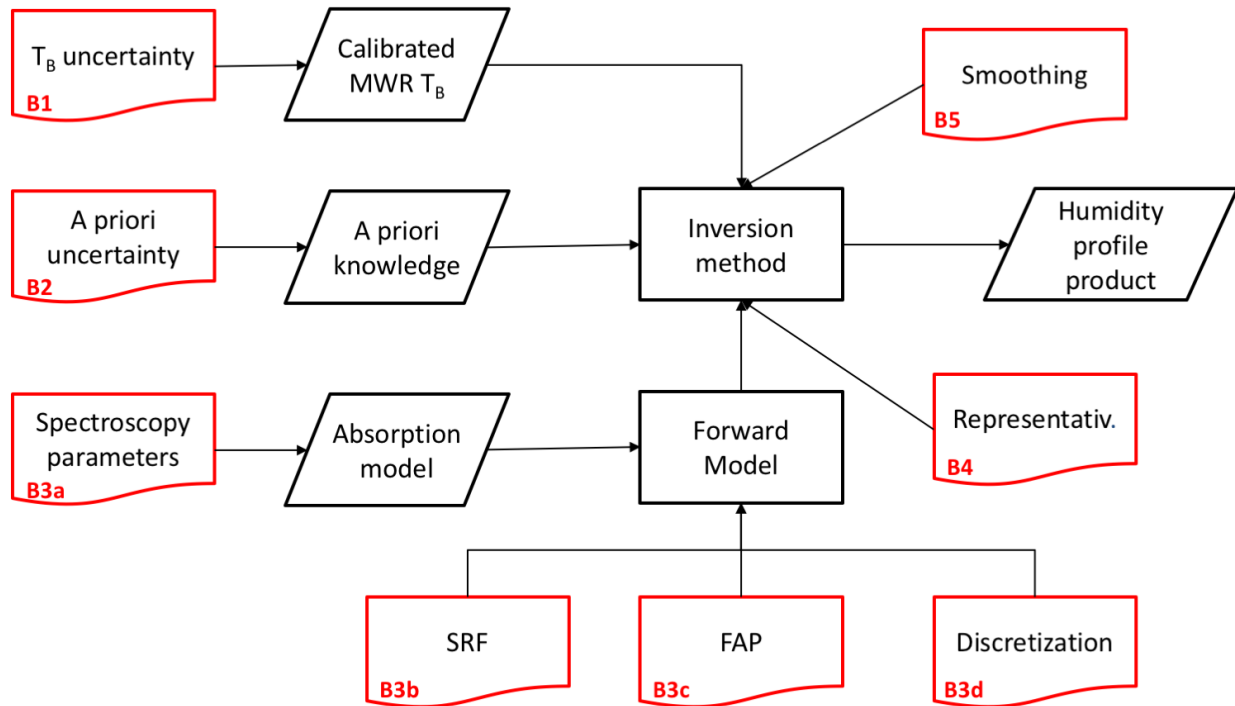


Figure 3. The metrological model chain of the MWR humidity profile product. It describes the flow diagram of the measurement, from the a priori knowledge and the calibrated TB, including uncertainty sources (highlighted in red), to the retrieved atmospheric humidity product.

All uncertainties quoted here are in the point-to-point profile humidity product at vertical spacing of the retrievals (~20-350 m within 0-5 km; 350-700 m within 5-10 km). However, it must be noted that the uncertainty does depend upon atmospheric conditions, particularly on water vapor content. The values given here are typical of midlatitude winter conditions. The uncertainty values change dynamically according to the atmospheric conditions through the Jacobian \mathbf{K}_i .

5 Element contributions

5.1 Brightness temperature uncertainty (B1)

The primary measurand of a MWR is brightness temperature (T_B). The estimated uncertainty for the measured T_B are detailed in the parent document GAIA-CLIM PTU document for MWR brightness temperature product. The T_B uncertainty are then propagated through the OEM formalism to estimate the uncertainty of the retrieved humidity profile. As shown in Figure 4 (right), the typical T_B uncertainty of 0.3-1.1 K maps to typical uncertainty contributions of 0.1-0.2 g/m³ within the lowest 2 km and with less than 0.1 g/m³ above 2 km.

Information / data	Type / value / equation	Notes / description
Name of effect	T_B uncertainty	
Contribution identifier	B1	
Measurement equation parameter(s) subject to effect	R	
Contribution subject to effect (final product or sub-tree intermediate product)	$\hat{x} \pm u(\hat{x})$	Estimated humidity profile and uncertainty
Time correlation extent & form	None	Random
Other (non-time) correlation extent & form	None	Random
Uncertainty PDF shape	Normal	
Uncertainty & units	<0.2 g/m ³ (1 σ) below 2 km <0.1 g/m ³ (1 σ) above 2 km	Point to point uncertainties at retrieval vertical resolution
Sensitivity coefficient	1	
Correlation(s) between affected parameters	None	
Element/step common for all sites/users?	Yes	
Traceable to ...	None	
Validation		

5.2 A priori uncertainty (B2)

When Optimal Estimation Method is used, MWR observations are optimally coupled with a priori background knowledge, accounting for the uncertainty from both the observations and the background. Thus, an estimate of the a priori background uncertainty is needed, in the form of the background error covariance matrix **B**. A priori information may come from different sources, usually climatology (e.g. a set of historic radiosonde profiles) or the output of a numerical weather prediction (NWP) model. In case of climatology, **B** is estimated as the covariance matrix with respect to the mean value. In case of NWP model output, **B** is estimated from an ensemble of perturbed assimilation cycles (Martinet et al., 2015), similar to those used operationally for data assimilation purposes. Figure 4 shows examples of two such a priori uncertainties. Typical values go from 1 to 3 g/m³ near the surface, decreasing with height above 1-2 km.

Information / data	Type / value / equation	Notes / description
Name of effect	A priori uncertainty	
Contribution identifier	B2	
Measurement equation parameter(s) subject to effect	B	
Contribution subject to effect (final product or sub-tree intermediate product)	$\hat{x} \pm u(\hat{x})$	Estimated humidity profile and uncertainty
Time correlation extent & form	None	Random
Other (non-time) correlation extent & form	None	
Uncertainty PDF shape	Normal	
Uncertainty & units (1σ)	0.1-1.0 g/m ³ (1 σ)	
Sensitivity coefficient	1	
Correlation(s) between affected parameters	None	
Element/step common for all sites/users?	Yes	
Traceable to ...	None	
Validation		

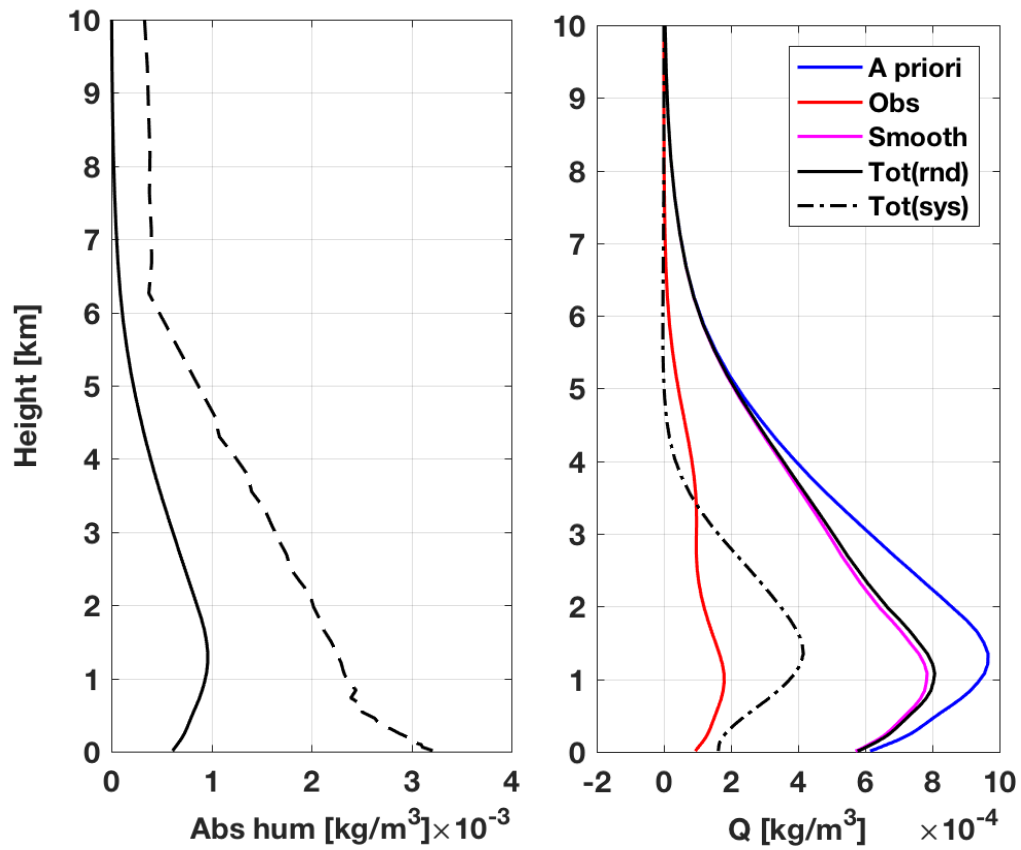


Figure 4. Left: Typical uncertainty for the a priori background from NWP (solid) and climatology (dashed). NWP data from Martinet et al, 2015. Climatology data courtesy of DWD (computed from radiosonde launched from Lindenberg in 2003-2004). Right: Contribution from a priori NWP (blue), observation (red), smoothing (magenta) uncertainties to the total uncertainty (black solid). The systematic uncertainty estimated for MWR calibration is shown in black dash-dotted line. The values given here are typical for midlatitude winter conditions.

5.3 Forward Model (B3)

Any inversion method relying on Forward Model (FM) calculations, such as OEM, is affected by the uncertainty of the assumed model. The FM uncertainty includes uncertainty related to the atmospheric absorption model spectroscopy, the fast model parametrization, and the profile representation in the radiative transfer model. The contributions of these terms to the overall forward model error covariance have been evaluated by Hewison (2006), showing it is dominated by the uncertainties in the spectroscopy, which are the most difficult to estimate accurately. This gap has been identified in the GAIA-CLIM Gaps Assessment and Impacts Document (GAID, [gap 2.37](#): Poorly quantified uncertainties in spectroscopic information) and it also contributes to one of the [high-level project's recommendations](#).

Information / data	Type / value / equation	Notes / description
Name of effect	Profile discretization	
Contribution identifier	B3	
Measurement equation parameter(s) subject to effect		
Contribution subject to effect (final product or sub-tree intermediate product)	$\hat{x} \pm u(\hat{x})$	
Time correlation extent & form	None	
Other (non-time) correlation extent & form	None	
Uncertainty PDF shape	Normal	
Uncertainty & units (1σ)	<0.2 g/m ³ (1σ) below 3 km <0.1 g/m ³ (1σ) above 3 km	Based on Hewison, 2006
Sensitivity coefficient	1	
Correlation(s) between affected parameters	None	
Element/step common for all sites/users?	Yes	
Traceable to ...	None	
Validation	None	On-going

5.4 Spectroscopic parameters (B3a)

The radiative transfer model (RTM) calculations are affected by the uncertainty of the assumed atmospheric absorption model. This relates to the uncertainty affecting the values of the spectroscopic parameters used within the model. This contribution is often estimated as the difference in zenith T_B calculated by two or more different absorption models (Hewison, 2006; Cimini et al., 2010). Estimates for a global average are reported in the table below (after Hewison, 2006; Table 2-1). These values map onto an uncertainty for the humidity profile of the order of 0.1-0.2 g/m³ in the first 3 km and below 0.1 g/m³ above that.

ν [GHz]	22.235	23.035	23.835	26.235	30.00	51.250	52.280	53.850	54.940	56.660	57.290	58.800
σT_B [K]	1.01	1.01	0.94	0.74	0.69	1.20	0.88	0.23	0.03	0.01	0.01	0.01

Another approach consists of quantifying the spectroscopic uncertainty impact by perturbing the atmospheric profile by an amount that is reasonably attributable to the spectroscopic uncertainty (Stähli et al., 2013). However, a rigorous approach requires propagating uncertainties in line parameters to uncertainty in absorption, as suggested by Boukabara et al. 2005. Such a rigorous approach is currently being investigated within GAIA-CLIM (Cimini, 2017).

Information / data	Type / value / equation	Notes / description
Name of effect	Spectroscopic parameters	
Contribution identifier	B3a	
Measurement equation parameter(s) subject to effect	S_i	
Contribution subject to effect (final product or sub-tree intermediate product)	B3	
Time correlation extent & form	None	
Other (non-time) correlation extent & form	None	
Uncertainty PDF shape	Normal	
Uncertainty & units (1σ)	<0.2 g/m ³ (1σ) below 3 km <0.1 g/m ³ (1σ) above 3 km	Based on Hewison, 2006
Sensitivity coefficient	1	
Correlation(s) between affected parameters	None	
Element/step common for all sites/users?	Yes	
Traceable to ...	None	
Validation	None	On-going

5.5 Spectral Response Function (B3b)

RTM calculations require the knowledge of the channel spectral response function (SRF), which characterizes the finite bandwidth for each MWR channel (Löhnert and Maier, 2012). Band-averaged T_B can be obtained by convolving the SRF with high-resolution RTM calculations. Band-averaged T_B may significantly differ from monochromatic T_B evaluated at the channel's center frequency, as the atmospheric absorption may change non-linearly across the bandwidth of each channel. To avoid recourse to expensive multiple RTM computations, frequently an equivalent monochromatic frequency (EMF) for each channel (Cimini et al., 2010) is utilised instead. The EMF is determined as the monochromatic frequency that minimizes the difference with the band-averaged T_B for a representative data set of atmospheric profiles. The EMF does not always correspond to the nominal central frequency. Once the EMF is accurately determined, the impact on T_B is negligible (i.e. < 0.05 K, Cimini et al., 2006; Hewison, 2006).

Information / data	Type / value / equation	Notes / description
Name of effect	Spectral Response Function (SRF)	
Contribution identifier	B3b	
Measurement equation parameter(s) subject to effect	$F(\hat{x}_i)$	The forward modelled T_B
Contribution subject to effect (final product or sub-tree intermediate product)	B3	
Time correlation extent & form	None	
Other (non-time) correlation extent & form	None	
Uncertainty PDF shape	Normal	
Uncertainty & units (1σ)	< 0.1 K (1σ)	
Sensitivity coefficient	K_i	The forward model Jacobian
Correlation(s) between affected parameters	None	
Element/step common for all sites/users?	Yes	
Traceable to ...	None	
Validation	Field experiments	Cimini et al., 2006 Hewison et al., 2006

5.6 Fast Absorption Predictor (B3c)

The OEM solution introduced in Section 3 requires iterative calculations. Thus, a fast RTM is most convenient, using a Fast Absorption Predictor (FAP) model to calculate the atmospheric absorption as a function of thermodynamical predictors (Hewison, 2006). One such fast RTM is RTTOV-gb, developed specifically for ground-based MWR observations (De Angelis, 2016). RTTOV-gb has been tested against reference RTM, showing residual errors smaller than typical MWR T_B uncertainties (<0.05 K for K-band channels, 0.01-0.2 K for V-band channels; 1σ at 19° - 90° elevation). These values are a factor ~ 2 -3 smaller than those reported by Hewison, 2006 (Table 2-3). This is probably due to the choice of better-suited predictors, which in RTTOV-gb follows those carefully developed for satellite RTM calculations.

Information / data	Type / value / equation	Notes / description
Name of effect	Fast Absorption Predictor (FAP)	
Contribution identifier	B3c	
Measurement equation parameter(s) subject to effect	$F(\hat{\mathbf{x}}_i)$	The forward modelled T_B
Contribution subject to effect (final product or sub-tree intermediate product)	B3	
Time correlation extent & form	None	
Other (non-time) correlation extent & form	None	
Uncertainty PDF shape	Normal	
Uncertainty & units (1σ)	<0.1 K (1σ)	
Sensitivity coefficient	K_i	The forward model Jacobian
Correlation(s) between affected parameters	None	
Element/step common for all sites/users?	Yes	
Traceable to ...	None	
Validation	Numerical validation	De Angelis et al., 2016

5.7 Discretization (B3d)

The discretization of the background profiles introduces uncertainty in T_B calculated by the RTM. This contribution has been evaluated using a set of high-resolution radiosondes to compute T_B through a RTM and comparing with T_B calculated using the same profiles reduced by a discretization method, similar to that used for NWP models (Hewison, 2006; Table 2-4). A large impact is found when using WMO standard levels (0.4-1.7 K), which reduces substantially when significant levels are added (0.03-0.21 K). Using the levels designed for RTTOV-gb (De Angelis et al., 2016), the impact on T_B becomes negligible (<0.05 K).

Information / data	Type / value / equation	Notes / description
Name of effect		
Contribution identifier	B3d	
Measurement equation parameter(s) subject to effect	$F(\hat{x}_i)$	The forward modelled T_B
Contribution subject to effect (final product or sub-tree intermediate product)	B3	
Time correlation extent & form	None	
Other (non-time) correlation extent & form	None	
Uncertainty PDF shape	Normal	
Uncertainty & units (1σ)	<0.1 K (1σ)	
Sensitivity coefficient	K_i	The forward model Jacobian
Correlation(s) between affected parameters	None	
Element/step common for all sites/users?	Yes	
Traceable to ...	None	
Validation		Using standard atmosphere and RTTOV-gb levels (De Angelis et al., 2016)

5.8 Representativeness (B4)

The representativeness error accounts for the instrument sensitivity to fluctuations on smaller scales than can be represented by the background. To compensate for this, it is usual to add the representativeness errors to the instrumental error to get a larger observational error. The representativeness error has been estimated by studying the fluctuations in the MWR signal on typical time scales within a 6-day period of clear and cloudy conditions (Hewison, 2006). It was found that the representativeness term evaluated in this way dominates the observation error of those channels most sensitive to cloud. These values map into an uncertainty for the humidity profile of the order of 0.1-0.2 g/m³ in the first 3 km and below 0.1 g/m³ above that. Ideally, the representativeness error shall be evaluated dynamically, e.g. based on time series of observations within 1 hour window of each observation. This would allow the errors to be reduced in periods of atmospheric stability, when MWR observations are more representative of the background state.

Information / data	Type / value / equation	Notes / description
Name of effect	Representativeness error	
Contribution identifier	B4	
Measurement equation parameter(s) subject to effect	R	
Contribution subject to effect (final product or sub-tree intermediate product)	$\hat{x} \pm u(\hat{x})$	
Time correlation extent & form	diurnal/seasonal	Depends on atmospheric conditions, and thus may be correlated with diurnal/seasonal cycle
Other (non-time) correlation extent & form	None	
Uncertainty PDF shape	Normal	
Uncertainty & units (1σ)	<0.2 g/m ³ (1 σ) below 3 km <0.1 g/m ³ (1 σ) above 3 km	Based on Hewison, 2006
Sensitivity coefficient	1	
Correlation(s) between affected parameters	None	
Element/step common for all sites/users?	Yes	
Traceable to ...	None	
Validation	None	

5.9 Smoothing error (B5)

The smoothing error is part of the total uncertainty estimated with the OEM. It is related to the vertical resolution of MWR humidity profiles, which is limited due to the passive approach. A quantitative definition of the vertical resolution builds on the averaging kernel matrix concept. The averaging kernel defines the sensitivity of the retrieved quantities to the true atmospheric state. The broadness of the averaging kernels gives information on the vertical resolution; e.g. a perfect vertical resolution corresponds to averaging kernels in the form of delta functions. Using the same notation as in Section 3, the averaging kernel matrix is defined as (Rodgers, 2000):

$$\mathbf{A}_i = [\mathbf{B}^{-1} + \mathbf{K}_i^T \mathbf{R}^{-1} \mathbf{K}_i]^{-1} \mathbf{K}_i^T \mathbf{R}^{-1} \mathbf{K}_i$$

The smoothing error is defined as $(\mathbf{A} - \mathbf{I})(\mathbf{x} - \mathbf{x}_b)$ whose covariance is $\mathbf{S}_S = (\mathbf{A} - \mathbf{I})\mathbf{B}(\mathbf{A} - \mathbf{I})^T$. As shown in Figure 4 (right), the smoothing error dominates the total uncertainty.

Information / data	Type / value / equation	Notes / description
Name of effect	Smoothing error	
Contribution identifier	B5	
Measurement equation parameter(s) subject to effect	\mathbf{S}_i	
Contribution subject to effect (final product or sub-tree intermediate product)	$\hat{\mathbf{x}} \pm u(\hat{\mathbf{x}})$	
Time correlation extent & form	None	
Other (non-time) correlation extent & form	Vertical	The averaging kernels indicate the correlation of the retrievals at different vertical levels.
Uncertainty PDF shape	Normal	
Uncertainty & units (1σ)	0.5-0.8 g/m ³ (1σ) below 3km <0.5 g/m ³ (1σ) above 3 km	
Sensitivity coefficient	1	
Correlation(s) between affected parameters	None	
Element/step common for all sites/users?	Yes	
Traceable to ...	OEM formalism	Traceable linked to that of B and R
Validation		

6 Uncertainty Summary

Element identifier	Contribution name	Uncertainty contribution form	Typical value	Traceability level (L/M/H)	random, structured random, quasi-systematic or systematic?	Correlated to? (Use element identifier)
B1	T _B uncertainty	Normal	0.1-0.2 g/m ³	M	random	none
B2	A priori	Normal	0.1-1.0 g/m ³	M	random	none
B3	Forward model	Normal	0.1-0.2 g/m ³	M	random	none
B3a	Spectroscopy	Normal	0.1-0.2 g/m ³	L	random	none
B3b	SRF	Normal	<0.1 g/m ³	H	systematic	none
B3c	FAP	Normal	<0.1 g/m ³	H	random	none
B3d	Discretization	Normal	<0.1 g/m ³	H	systematic	none
B4	Representativeness	Normal	0.1-0.2 g/m ³	L	random	none
B5	Smoothing	Normal	0.1-0.8 g/m ³	H	random	none

The estimated uncertainties are combined following the OEM formalism (Rodgers, 2000). Using the same notation as in Section 3, the random uncertainty of the estimated temperature profile $\hat{\mathbf{x}}_i$ is given by the diagonal terms of the posterior covariance matrix:

$$u_{rnd}(\hat{\mathbf{x}}_i) = \mathbf{diag}(\mathbf{S}_i) = \mathbf{diag}([\mathbf{B}^{-1} + \mathbf{K}_i^T \mathbf{R}^{-1} \mathbf{K}_i]^{-1})$$

The background uncertainty covariance matrix (\mathbf{B}) and the measurement uncertainty covariance matrix (\mathbf{R}) are related to the Uncertainty Summary Table above as follows. \mathbf{B} is given by the a priori uncertainty (B2). \mathbf{R} is usually split in three contributions $\mathbf{R} = \mathbf{E} + \mathbf{F} + \mathbf{M}$ (Hewison, 2006), where the instrument noise (\mathbf{E}) corresponds to T_B uncertainty (B1); \mathbf{F} corresponds to the forward model uncertainty (B3); and \mathbf{M} corresponds to the representativeness uncertainty (B4). The smoothing uncertainty (B5) is given by the combined contributions of \mathbf{B} , \mathbf{R} , and \mathbf{K}_i as explained in Section 5.9. The relative contributions of \mathbf{B} , \mathbf{R} , and smoothing to the total random uncertainty are depicted in Figure 4.

Introducing the gain matrix $\mathbf{G} = \mathbf{S}_i \mathbf{K}_i^T \mathbf{R}^{-1}$ (Rodgers, 2000), the systematic uncertainty of the retrieved humidity profile is estimated under the assumption of a linear retrieval as:

$$u_{sys}(\hat{\mathbf{x}}_i) = \mathbf{G} * u_{sys}(\mathbf{y})$$

where $u_{sys}(\mathbf{y})$ includes the T_B systematic uncertainty affecting the MWR calibration (see the parent GAIA-CLIM PTU document for MWR brightness temperature product). Typical values of the estimated systematic uncertainty are shown in Figure 4. Finally, Figure 5 shows an example of a MWR retrieved humidity profile with the associated random and systematic uncertainties.

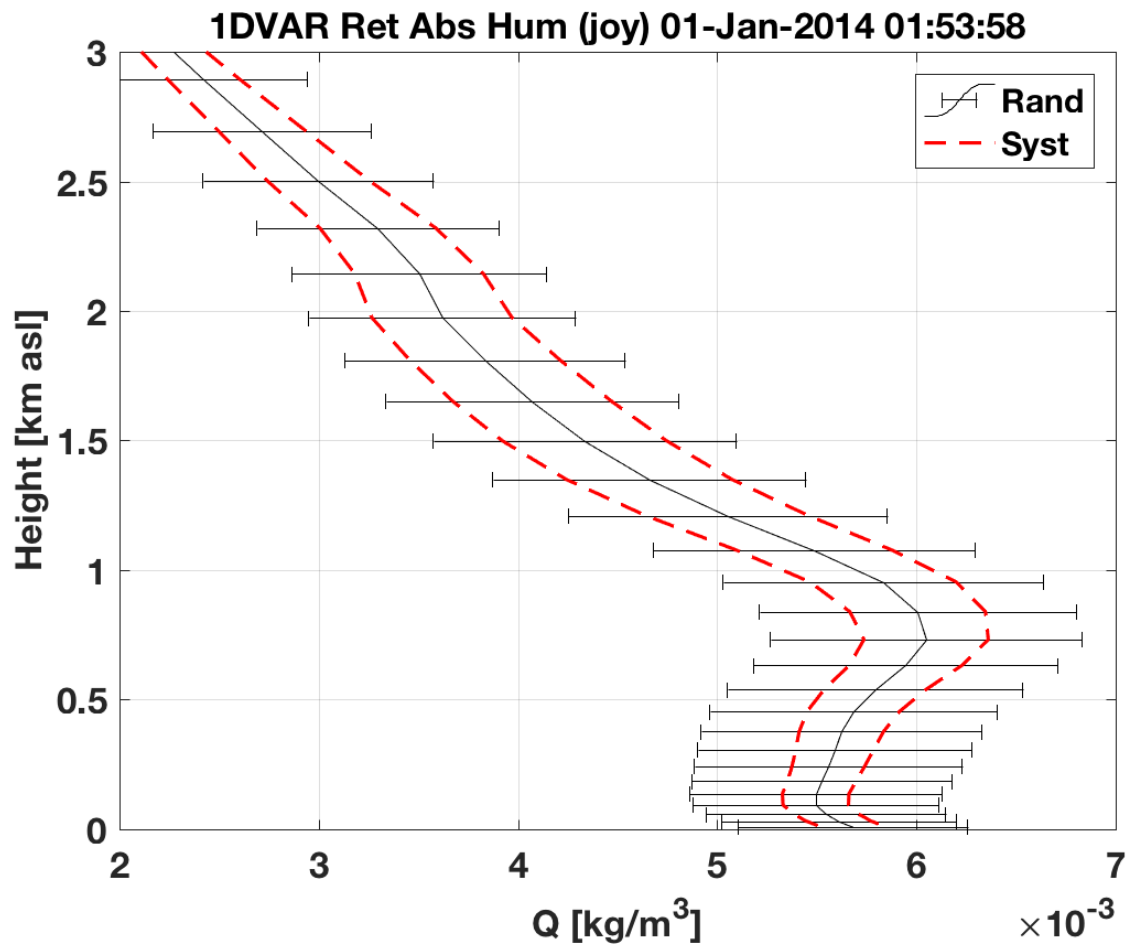


Figure 5. An example of humidity profile retrieval at the Joyce site (Juelich, Germany) on January 1st 2014, 01:53 UTC. The associated random (errorbars) and systematic (red dashed lines) uncertainties are also shown.

7 Traceability uncertainty analysis

Traceability level definition is given in Table 2.

Table 2. Traceability level definition table

Traceability Level	Descriptor	Multiplier
High	SI traceable or globally recognised community standard	1
Medium	Developmental community standard or peer-reviewed uncertainty assessment	3
Low	Approximate estimation	10

Analysis of the summary table would suggest the following contributions, shown in Table 3, should be considered further to improve the overall uncertainty of the MWR humidity profile product. The entries are given in an estimated priority order.

Table 3. Traceability level definition further action table.

Element identifier	Contribution name	Uncertainty contribution form	Typical value	Traceability level (L/M/H)	random, structured random, quasi-systematic or systematic?	Correlated to? (Use element identifier)
B3a	Spectroscopy	Normal	0.1-0.2 g/m ³	L	random	none
B2	A priori	Normal	0.1-1.0 g/m ³	M	random	none
B4	Representativeness	Normal	0.1-0.2 g/m ³	L	random	none

7.1 Recommendations

Suggestions for improving the assessment of the T_B calibration uncertainty (B1) are given in the parent document GAIA-CLIM PTU document for MWR brightness temperature product.

In addition, the top priority is to quantify rigorously the spectroscopic parameter contribution (B3a), which may be significantly underestimated. This is ongoing within GAIA-CLIM (Cimini, 2017).

Another priority is to better characterise the a priori uncertainty (B2), specially when the a priori information is from a NWP model. There have been evidences that this contribution may be underestimated (Cimini et al., 2010; Martinet et al., 2017).

Finally, the representativeness error (B4) shall be characterised for each MWR type and site climatology. This contribution may be significantly underestimated during dynamical weather. Ideally, this could be evaluated dynamically to make this contribution flow-dependent.

8 Conclusion

The MWR humidity profile product has been assessed against the GAIA CLIM traceability and uncertainty criteria.

References

- Boukabara S. A., S. A. Clough, J.-L. Moncet, A. F. Krupnov, M. Yu. Tretyakov, and V. V. Parshin (2005), Uncertainties in the Temperature Dependence of the Line-Coupling Parameters of the Microwave Oxygen Band: Impact Study, *IEEE Trans. Geosci. Rem. Sens.*, 43, 5, doi: 10.1109/TGRS.2004.839654.
- Cimini, D., T. J. Hewison, L. Martin (2006), Comparison of brightness temperatures observed from ground-based microwave radiometers during TUC, *Meteorologische Zeitschrift*, Vol.15, No.1, 2006, pp.19-25.
- Cimini, D., T. J. Hewison, L. Martin, J. Güldner, C. Gaffard and F. S. Marzano (2006), Temperature and humidity profile retrievals from ground-based microwave radiometers during TUC, *Met. Zeitschrift*, Vol. 15, No. 1, 45-56.
- Cimini D., E. R. Westwater, and A. J. Gasiewski (2010), Temperature and humidity profiling in the Arctic using millimeter-wave radiometry and 1DVAR, *IEEE Transactions on Geoscience and Remote Sensing*, Vol. 48, 3, 1381-1388, 10.1109/TGRS.2009.2030500.
- Cimini D. (2017), Report on G2.14: Missing uncertainty associated with MW absorption models, GAIA-CLIM 2nd General Assembly, ECMWF, Reading, Feb. 8-9, 2017.
- De Angelis, F., Cimini, D., Hocking, J., Martinet, P., and Kneifel, S. (2016), RTTOV-gb – adapting the fast radiative transfer model RTTOV for the assimilation of ground-based microwave radiometer observations, *Geosci. Model Dev.*, 9, 2721-2739, doi:10.5194/gmd-9-2721-2016, Online: <http://www.geosci-model-dev.net/9/2721/2016/>
- De Angelis, F., Cimini, D., Löhnert, U., Caumont, O., Haeferle, A., Pospichal, B., Martinet, P., Navas-Guzmán, F., Klein-Baltink, H., Dupont, J.-C., and Hocking, J. (2017), Long term Observations minus Background monitoring of ground-based microwave radiometer network. Part 1: Brightness Temperatures, *Atmos. Meas. Tech. Discuss.*, doi:10.5194/amt-2017-112, in review.
- GAIA-CLIM Product Traceability and Uncertainty (PTU) document for the Microwave Radiometer (MWR) brightness temperature product (2017), *PTU_MWR_Brightness_Temperature_V1.0.pdf*
- Hewison T. (2006), *Profiling Temperature and Humidity by Ground-based Microwave Radiometers*, PhD Thesis, Department of Meteorology, University of Reading.
- Löhnert, U. and Maier, O. (2012), Operational profiling of temperature using ground-based microwave radiometry at Payerne: prospects and challenges, *Atmos. Meas. Tech.*, 5, 1121-1134, doi:10.5194/amt-5-1121-2012.
- Martinet, P., Dabas, A., Donier, J. M., Douffet, T., Garrouste, O., and Guillot, R. (2015), 1D-Var temperature retrievals from microwave radiometer and convective scale model, *Tellus A*, 67, 2015. Doi: 10.3402/tellusa.v67.27925.
- Martinet, P., Cimini, D., De Angelis, F., Canut, G., Unger, V., Guillot, R., Tzanos, D., and Paci, A.: Combining ground-based microwave radiometer and the AROME convective scale model through 1DVAR retrievals in complex terrain: an Alpine Valley case study, *Atmos. Meas. Tech. Discuss.*, <https://doi.org/10.5194/amt-2017-144>, in review, 2017.
- Rodgers, C. D.: *Inverse methods for atmospheric sounding: theory and practice*, vol. 2, World scientific, 2000.
- Solheim F., J. Godwin, E. Westwater, Y. Han, S. Keihm, K. Marsh, R. Ware (1998), Radiometric Profiling of Temperature, Water Vapor, and Liquid Water using Various Inversion Methods, *Radio Science*, 33, pp. 393-404, DOI: 10.1029/97RS03656.
- Stähli, O., Murk, A., Kämpfer, N., Mätzler, C., and Eriksson, P. (2013), Microwave radiometer to

retrieve temperature profiles from the surface to the stratopause, *Atmos. Meas. Tech.*, 6, 2477-2494, doi:10.5194/amt-6-2477-2013.

Westwater E.R., S. Crewell, C. Mätzler: A Review of Surface-Based Microwave and Millimeter Wave Radiometric Remote Sensing of the Troposphere, *URSI Radio Science Bulletin*, No. 310, 59-80, 2004. Online:

<https://pdfs.semanticscholar.org/09ae/6c38f5d28fdd6c62703327c01a36d0d8af16.pdf>

Westwater E. R., S. Crewell, C. Mätzler, D. Cimini: Principles of surface-based microwave and millimeter wave radiometric remote sensing of the troposphere *Quaderni della Società Italiana di Elettromagnetismo* Vol.: 1, No.3, 50-90, 2005. Online:

http://radiometrics.com/data/uploads/2012/12/Westwater_QSIE_2005.pdf



Product Traceability and Uncertainty for the EARLINET LIDAR aerosol extinction coefficient product

Version 0.4

*GAIA-CLIM
Gap Analysis for Integrated
Atmospheric ECV Climate Monitoring
Mar 2015 - Feb 2018*

A Horizon 2020 project; Grant agreement: 640276

Date: 23 January 2018

Dissemination level: PU

*Work Package 2; Compiled by Marco Rosoldi &
Fabio Madonna (CNR-IMAA)*



Table of Contents

Table of Contents	2
1 Product overview	3
2 Introduction.....	3
3 Instrument description	4
4 Product Traceability Chain	7
5 Element contributions	8
5.1 Transmission system (1).....	8
5.2 Receiving system (2)	9
5.3 Receiver optical parameters (2a)	9
5.4 Alignment of the lidar system (2b).....	11
5.5 Detectors (3)	12
5.6 Acquisition (4).....	13
5.7 Raw Raman signals (5).....	14
5.8 Pre-processing of Raman signals (6)	15
5.9 Dead Time correction (6a)	16
5.10 Dark subtraction (6b)	18
5.11 First range bin/Trigger delay (6c).....	19
5.12 Background subtraction (6d)	21
5.13 Vertical integration (binning) (6e).....	22
5.14 Temporal integration (6f)	23
5.15 Signal gluing (6g)	24
5.16 Overlap Correction (6h).....	26
5.17 Processing of Raman signals (7).....	27
5.18 Molecular density and extinction profiles (7a).....	29
5.19 Angstrom exponent assumption (7b).....	31
5.20 Multiple scattering correction (7c)	32
5.21 Retrieval of aerosol extinction coefficient profile (7d)	33
6 Uncertainty Summary	35
7 Traceability uncertainty analysis	37
7.1 Recommendations	39
8 Conclusion	39
9 References.....	40

1 Product overview

Product name: EARLINET LIDAR aerosol extinction coefficient

Product technique: LIDAR

Product measurand: Aerosol extinction coefficient

Product form/range: profile/from full overlap altitude (250-500 m above the ground, depending on the instrument) to 12 km

Product dataset: EARLINET Database

Site/Sites/Network location:

- Evora, Portugal, 38.568 °N, 7.912 °W, 293 m
- Granada, Spain, 37.164 °N, 3.605 °W, 680 m
- Leipzig, Germany, 51.353 °N, 12.435 °E, 90 m
- Napoli, Italy, 40.8380 °N, 14.1830 °E, 118 m
- Potenza, Italy, 40.601 °N, 15.724 °E, 760 m

Product time period: June 1, 2006 – December 31, 2010

Data provider: CNR-IMAA

Instrument provider: EARLINET lidar stations

Product assessor: Fabio Madonna, CNR-IMAA

Assessor contact email: fabio.madonna@imaa.cnr.it

2 Introduction

This document presents the Product Traceability and Uncertainty (PTU) information for the EARLINET LIDAR aerosol extinction coefficient product. The aim of this document is to provide supporting information for the users of this product within the GAIA-CLIM VO. The uncertainty and traceability information contained in this document is based on the references reported at the end of the document.

The advanced network of ground-based lidar stations EARLINET (European Aerosol Research Lidar NETwork) has been operating for more than 15 years and currently consists of 31 measuring stations located in Europe, running different lidar systems and processing algorithms [1]. The EARLINET community has developed over the years robust lidar data processing algorithms to retrieve the vertical profiles of aerosol extinction coefficient in the troposphere and lower stratosphere, with a sampling time ranging from a few tens of minutes to a few hours and a vertical resolution ranging from a few hundreds of meters to many hundreds of meters, depending on the observed atmospheric scenario and the lidar system. Currently, the network is developing a rigorous quality assurance program addressing both instrument performance and evaluation of the algorithms to ensure instrument standardization and consistent lidar retrievals within the network using a common data format. For the full harmonization of data analysis and data traceability, the EARLINET Single Calculus Chain (SCC) [2,3], a tool for the automatic quality assured analysis of lidar measurements, has been developed.

The major part of the measurements is performed according to a fixed schedule three times a week: two measurements after sunset, on Monday and Thursday, and one measurement around noon (local time) on Monday. This permits an unbiased statistically significant data set. Additional measurements are performed to address specific events that are localized either in space or time (e.g., forest fires, volcanic eruptions, desert dust outbreaks). Since June 2006, EARLINET stations

have been performing measurements during the overpasses of the NASA CALIPSO satellite, launched in April 2006, in order to validate and calibrate the satellite lidar products [4].

EARLINET algorithms include the estimation of the random uncertainty and a separate estimation of the systematic uncertainties due to the retrieval assumptions, background models, and corrections implemented in a typical lidar data processing chain. For the retrieval of aerosol extinction coefficient at 532 nm, available only from night time measurements, random uncertainty estimates are typically less than 10% for values higher than $2 \times 10^{-5} \text{ m}^{-1}$ and greater for lower extinction coefficient values (see sub-section 5.21). On the other hand, the estimates of systematic uncertainty due to each contribution are less than 10%, resulting in a total maximum systematic uncertainty less than 15% for extinction coefficient values higher than $2 \times 10^{-5} \text{ m}^{-1}$ and for all the altitude levels above the full overlap altitude of the lidar system (see sub-section 5.1 and following sub-sections).

A comprehensive strategy for campaign setup and data evaluation has been established at the European level [5]. Eleven systems from nine EARLINET stations participated in the EARLINET Lidar Intercomparison 2009 (EARLI09) measurement campaign. In this campaign, three reference systems were qualified to serve as travelling standards thereafter. Eleven EARLINET systems from ten other stations have been compared against these reference systems since 2009; afterwards these systems have calibrated other instruments moving from their own station to the other sites in the various countries.

Currently, a strategy for ensuring the lidar system comparability at a global scale is missing. GALION (GAW Lidar Observation Network) is the global federation of lidar networks operating globally: the network implementation is challenging and its collective operation is limited to special events like volcanic eruptions [6]. Nevertheless, the lidar calibration facility (LICAL), undertaken by the ACTRIS-2 H2020 research infrastructure project, offers to calibrate all lidar system types from outside the ACTRIS community with a special focus on GALION federated networks. In future LICAL could become the calibration centre for the global lidar network.

3 Instrument description

The basic setup of a lidar system is shown in figure 1. Lidar technique, acronym for "light detection and ranging", is based on the transmission into the atmosphere of short light pulses, with duration ranging from a few to several hundreds of nanoseconds, by a laser transmitter, directly or by means of transmission optics (e.g. beam expander), depending on the lidar system. In any point of the atmospheric volume crossed by the laser beam, a portion of the incident light is backscattered towards the transmitter by atmospheric constituents. This light backscattered by the atmosphere at different distances from the transmitter is collected by a telescope and passes through an optical system, consisting of various elements (lenses, mirrors, filters etc.), which selects specific wavelengths or polarization states of the light collected by the telescope and whose configuration depends on the particular lidar system. The light from the optical system is forwarded to detectors, typically photomultiplier tubes, which convert it into electrical signals.

An electronic circuit (trigger) allows to synchronize the acquisition start with the emission of each laser pulse so that the electrical signals are acquired as a function of elapsed time with respect to the emission of each laser pulse. As this is the time that the light pulse takes to travel from the transmitter to the backscatter point and vice versa, then, due to the constant speed of light, it is possible to calculate the distance between the transmitter and the backscatter point and convert electrical signals acquired as a function of time into signals as a function of that distance. These are

the lidar signals, measuring the intensity of the light backscattered by the atmosphere as a function of the distance from the lidar.

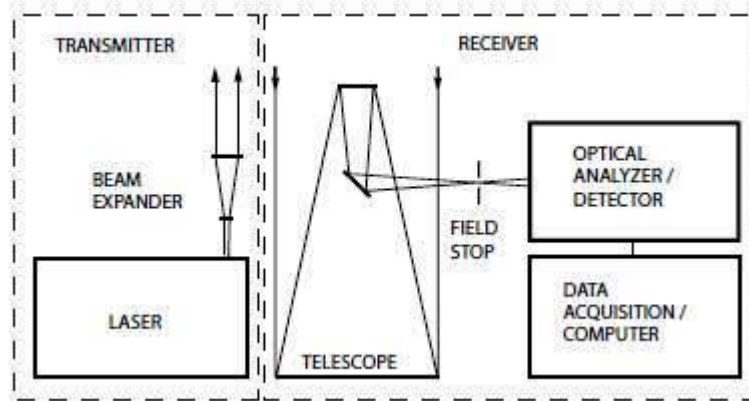


Figure 1: Principle setup of a lidar system

More specifically, the basic equation for the analysis of lidar signals (the lidar equation) describes the intensity of the measured signals depending on the distance from the lidar, several instrumental parameters and atmospheric properties. In order to retrieve the atmospheric parameters, the lidar equation needs to be inverted in the approximation of single and independent scattering. This means that a photon is scattered only once by the atmospheric constituents and that the scatterers are well separated and randomly moving. Thus, the contributions to the total scattered energy by many targets have no phase relation and the total intensity is simply the sum of the intensities scattered from each target. In this approximation, the lidar equation, in a general form, can be written as:

$$P(\lambda_L, \lambda_S, z) = P_L \frac{c \tau_d}{2} \frac{A}{z^2} \Psi(\lambda_S, \lambda_L) O(z) \beta(\lambda_S, \lambda_L, z) T(\lambda_L, z) T(\lambda_S, z) + P_B \quad (1)$$

where:

- $P(\lambda_L, \lambda_S, z)$ is the received optical power from the distance z at a specific polarization and wavelength λ_S , due to the backscattering of the laser wavelength λ_L . P_L is the mean power of a single laser pulse. $c \tau_d / 2$ represents the lidar vertical resolution, where c and τ_d are respectively the light speed and the dwell time, that is the time resolution or the sampling time of the acquisition system, whose minimum value is the duration of a laser pulse. A/z^2 is the acceptance solid angle of the telescope for light scattered at distance z , which represents the probability that a photon scattered at the distance z is collected by the receiving telescope of area A .
- $\Psi(\lambda_S, \lambda_L) = \xi(\lambda_L, \lambda_S) \eta(\lambda_S)$ is the overall system efficiency, where $\xi(\lambda_L, \lambda_S)$ is the optical efficiency, including the reflectivity and transmissivity of all the optics encountered both by the transmitted and the received light (lenses, mirrors, filters etc.), while $\eta(\lambda_S)$ is the quantum efficiency of the detector. $O(z)$ is the lidar overlap function, depending on the lidar geometry, that describes the incomplete overlap between the emitted laser beam and the receiver field of view close to the lidar. $O(z)$ ranges between 0, for $z = 0$, and 1, above a certain height z_{ovl} , called full overlap height, where the laser beam is completely imaged onto the detector and the overlap is complete.
- $\beta(\lambda_S, \lambda_L, z)$ is the atmospheric backscatter coefficient at the wavelength λ_S and distance z ; for elastic lidar signals, due to the elastic backscattering of laser pulses ($\lambda_S = \lambda_L$) by

atmospheric molecules and particles (aerosol and clouds), the backscatter coefficient is the sum of two contributions, the molecular and particle backscatter coefficients; for Raman lidar signals, due to the Raman inelastic backscattering of laser pulses ($\lambda_s \neq \lambda_L$) by atmospheric molecules (due to the transitions of roto-vibrational or purely rotational Raman spectra of these molecules), the backscatter coefficient has only the molecular contribution.

- $T(\lambda_L, z)$ and $T(\lambda_s, z)$ are the atmospheric transmissivities for the laser light at wavelength λ_L on the way from the laser source to the distance z and for the backscattered light at wavelength λ_s on the way from the distance z to the receiver; these terms can be expressed as:

$$T(\lambda_L, z) = \exp\left(-\int_0^z \alpha_{\lambda_L}(z')dz'\right) \quad \text{and} \quad T(\lambda_s, z) = \exp\left(-\int_0^z \alpha_{\lambda_s}(z')dz'\right) \quad (2)$$

where $\alpha_{\lambda_L}(z)$ and $\alpha_{\lambda_s}(z)$ are the atmospheric extinction coefficients at wavelengths λ_L and λ_s at distance z . As extinction can occur because of scattering and absorption of light by molecules and particles, the above extinction coefficients can be expressed as the sum of four components, the scattering and absorption coefficients of molecules and the scattering and absorption coefficients of particles (aerosol and clouds).

- P_B is the background contribution to the received power of the lidar signal, in addition to the contribution due to the portion of the laser beam backscattered by the atmosphere. The background signal is generated by the detector noise and, at daytime, by direct or scattered sunlight, at nighttime, by the moon, the stars as well as artificial light sources.

Typically, EARLINET lidars transmit light pulses at 355, 532 and 1064 nm and receive the elastically backscattered light from the atmosphere at the same wavelengths and the Raman inelastically backscattered light from atmospheric nitrogen molecules at 387 and 607 nm. The atmospheric profiles of aerosol extinction coefficient at 532 (355) nm are retrieved by EARLINET algorithms, using the nitrogen Raman signals at 607 (387) nm. These signals are not affected by the aerosol backscattering, as only a specific molecular species can backscatter inelastically at the corresponding Raman wavelength. As a consequence, the contribution of the aerosol in the Raman signals is confined only in the transmissivity terms, where both molecular and aerosol extinction coefficients play a role. Therefore, if backscatter and extinction coefficients of molecules are known, it is possible to solve the lidar equation (1) to retrieve the aerosol extinction coefficient.

The profile of aerosol extinction coefficient at $\lambda_L = 532\text{nm}$ is directly derived from the pre-processed Raman signals at $\lambda_s = 607\text{nm}$ by the following equation [23,24]:

$$\alpha_{\lambda_L}^{par}(z) = \frac{\frac{d}{dz}\left\{\ln\left[N(z)/P_{\lambda_s}(z)z^2\right]\right\} - \alpha_{\lambda_L}^{mol}(z) - \alpha_{\lambda_s}^{mol}(z)}{1 + (\lambda_L/\lambda_s)^{\tilde{a}}} \quad (3)$$

where: $\alpha_{\lambda_L}^{par}(z)$ is the particle extinction coefficient at the wavelength λ_L and range z ; $P_{\lambda_s}(z)$ is the power of the pre-processed Raman signal at wavelength λ_s and range z ; $N(z)$ is the number density of atmospheric nitrogen molecules at range z ; $\alpha_{\lambda_L}^{mol}(z)$ and $\alpha_{\lambda_s}^{mol}(z)$ are the molecular extinction coefficients at wavelengths λ_L and λ_s , respectively; \tilde{a} is the Ångström exponent, that describes the wavelength dependence of particle extinction coefficient. It is defined by the following relation:

$$\frac{\alpha_{\lambda_L}^{par}(z)}{\alpha_{\lambda_S}^{par}(z)} = \left(\frac{\lambda_S}{\lambda_L}\right)^{\hat{a}} \quad (4)$$

4 Product Traceability Chain

Figure 2 shows the traceability chain for atmospheric profile of aerosol extinction coefficient retrieved with Raman lidar technique within EARLINET network. The chain has been developed following the approach outlined in the Guide to Uncertainty in Measurement & its Nomenclature, published as part of the GAIA-CLIM project.

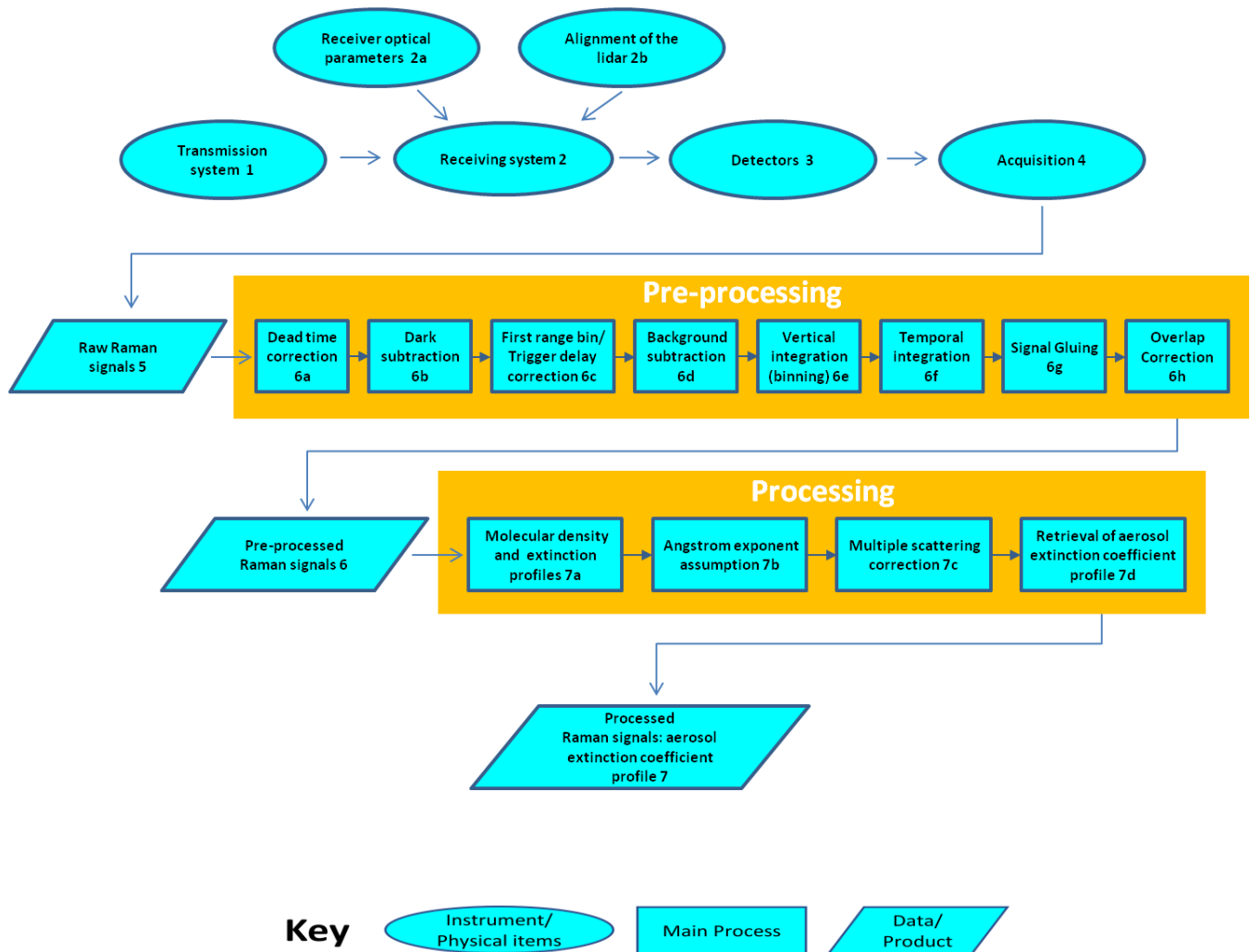


Figure 2: Traceability chain for atmospheric profile of aerosol extinction coefficient retrieved with Raman lidar technique within EARLINET network

5 Element contributions

5.1 Transmission system (1)

Light pulses at wavelength $\lambda_L = 532nm$ are sent out into the atmosphere by a laser transmitter, directly or by means of transmission optics (e.g.: beam expander, mirrors etc.) depending on the lidar system. The parameters of the laser transmitter (pulse duration, energy and repetition rate, beam diameter and divergence) as well as of the transmission optics change depending on the lidar system. Additionally, such parameters may also change for a given lidar system due to their time and temperature instability or to the replacement of one or more components of the transmission system. These variations affect the optical power transmitted in the atmosphere and therefore both the power and the random uncertainty of the Raman signals at $\lambda_S = 607nm$ used in the algorithms for the retrieval of aerosol extinction coefficient profile. However, at EARLINET lidar stations these variations are monitored and minimized (e.g., pulse energy is measured before each measurement session, lidars usually operate in air-conditioned environments), so that their contribution to the retrieval and uncertainty of aerosol extinction coefficient profile is assumed to be negligible.

Information / data	Type / value / equation	Notes / description
Name of effect	Transmission system	Contribution of variations in all the parameters related to the laser beam transmission to the atmosphere.
Contribution identifier	1	
Measurement equation parameter(s) subject to effect	P_L and $\xi(\lambda_L, \lambda_S)$ in lidar equation of Raman signals at $\lambda_S = 607nm$	
Contribution subject to effect (final product or sub-tree intermediate product)	Aerosol extinction coefficient profile $\alpha(z)$	
Time correlation extent & form	Various time scales	Extent & form not quantified
Other (non-time) correlation extent & form	1) Possible correlation with vertical range (if pulse duration increases so as to exceed the dwell time); 2) Possible correlation with the temperature of laser and transmission optics during measurements	Extent & form not quantified
Uncertainty PDF shape	N/A	Systematic effect
Uncertainty & units	0% (relative uncertainty)	(Assumed to be negligible)
Sensitivity coefficient	< 1	(Assumed to be negligible)
Correlation(s) between affected parameters	None	
Element/step common for all sites/users?	Yes	
Traceable to ...	N/A	
Validation	N/A	

5.2 Receiving system (2)

The portion of the laser radiation backscattered by the atmosphere at different altitude ranges is collected by a telescope. Two or more telescopes with different optical properties can be used to optimize lidar performances in different atmospheric regions (near range, far range). The radiation collected by the telescope passes through an optical system (consisting of lenses, mirrors, filters, beam splitters and interference filters) where it is spectrally filtered, so as only the Raman backscattered light from atmospheric nitrogen molecules at wavelength $\lambda_S = 607nm$ is transmitted to the detection system. The uncertainty contribution of the receiving system is the combination of contributions related to the receiver optical parameters (2a) and the alignment of the lidar system (2b), whose uncertainties and correlation effects are described in the corresponding sub-level sections.

Information / data	Type / value / equation	Notes / description
Name of effect	Receiving system	Combined contribution of the receiver optical parameters (2a) and alignment of the lidar system (2b)
Contribution identifier	2	
Measurement equation parameter(s) subject to effect	$O(z)$ and $\xi(\lambda_L, \lambda_S)$ in lidar equation of Raman signals at $\lambda_S = 607nm$	
Contribution subject to effect (final product or sub-tree intermediate product)	Aerosol extinction coefficient profile $\alpha(z)$	
Time correlation extent & form	Various time scales	Extent & form not quantified
Other (non-time) correlation extent & form	May affect vertical correlation	
Uncertainty PDF shape	N/A	Systematic effect
Uncertainty & units	0% (relative uncertainty) combination of 2a and 2b	Assumed to be negligible
Sensitivity coefficient	1	
Correlation(s) between affected parameters	None	
Element/step common for all sites/users?	Yes	
Traceable to ...	N/A	
Validation	N/A	

5.3 Receiver optical parameters (2a)

The optical properties of the elements forming the receiver, consisting of the telescope and the following optical filtering system, change depending on the lidar system, but they may also change for a given lidar system due to their time and temperature instability, contamination, or to the

replacement of one or more components of the receiving system. These variations in the parameters of the receiving system affect the optical power transmitted by the receiver to the detectors and therefore both the power and the random uncertainty of the Raman signals at $\lambda_S = 607nm$ used in the algorithms for the retrieval of aerosol extinction coefficient profile. However, at EARLINET lidar stations these variations are monitored and minimized (e.g., the optics are regularly cleaned, lidars usually operate in air-conditioned environments), so that their contribution to the retrieval and uncertainty of aerosol extinction coefficient profile is assumed to be negligible.

Information / data	Type / value / equation	Notes / description
Name of effect	Receiver optical parameters	Contribution of variations in all the optical parameters of the receiving system
Contribution identifier	2 a	
Measurement equation parameter(s) subject to effect	$\xi(\lambda_L, \lambda_S)$ in lidar equation of Raman signals at $\lambda_S = 607nm$	
Contribution subject to effect (final product or sub-tree intermediate product)	Aerosol extinction coefficient profile $\alpha(z)$	
Time correlation extent & form	Various time scales	Extent & form not quantified
Other (non-time) correlation extent & form	1) Possible correlation with vertical range due to the correlation of the optical efficiency of the receiving system with the incident angle of backscattered light and, consequently, with the vertical range; 2) Possible correlation with the temperature of the receiver components during measurements	Extent & form not quantified
Uncertainty PDF shape	N/A	Systematic effect
Uncertainty & units	0% (relative uncertainty)	(Assumed to be negligible)
Sensitivity coefficient	< 1	(Assumed to be negligible)
Correlation(s) between affected parameters	None	
Element/step common for all sites/users?	Yes	
Traceable to ...	N/A	
Validation	N/A	

5.4 Alignment of the lidar system (2b)

The correct alignment of the lidar system, that is the alignment of the laser beam with the receiving system and of the telescope with the optics of filtering system, is ensured by specific tests developed by the EARLINET quality assurance program. In particular, the telecover test and the Rayleigh fit test are performed to check and correct the alignment of the lidar system in the near range (planetary boundary layer) and in the far range (free troposphere or above), respectively. A detailed description of these tests can be found in [7].

For each lidar system there is a certain degree of misalignment between the laser beam and the receiving system due to residual uncertainties in the telecover and Rayleigh fit tests or possible mechanical/thermal instabilities of the optical and mechanical components forming both transmission and receiving systems. The misalignment of a lidar system changes the incident angle on the receiver of the backscattered light at each altitude level, which affects both the overlap function and the optical power transmitted by the receiver to the detectors and, definitively, the power of the Raman signals at $\lambda_S = 607nm$ used in the algorithms for the retrieval of aerosol extinction coefficient profile. At EARLINET stations the above quality assurance tests for the correct alignment of the lidar system are regularly performed, so that the contribution of the lidar misalignment to the uncertainty of aerosol extinction coefficient profile is assumed negligible.

Information / data	Type / value / equation	Notes / description
Name of effect	Alignment of the lidar system	Contribution of lidar misalignment
Contribution identifier	2b	
Measurement equation parameter(s) subject to effect	$O(z)$ and $\xi(\lambda_L, \lambda_S)$ in lidar equation of Raman signals at $\lambda_S = 607nm$	
Contribution subject to effect (final product or sub-tree intermediate product)	Aerosol extinction coefficient profile $\alpha(z)$	
Time correlation extent & form	Various time scales	Extent & form not quantified
Other (non-time) correlation extent & form	1) Possible correlation with vertical range due to the correlation of $O(z)$ and optical efficiency of the receiving system with the vertical range; 2) Possible correlation with the temperature of components forming both transmission and receiving systems during measurements	Extent & form not quantified
Uncertainty PDF shape	N/A	Systematic effect
Uncertainty & units	0% (relative uncertainty)	Assumed to be negligible
Sensitivity coefficient	1	
Correlation(s) between affected parameters	None	

Element/step common for all sites/users?	Yes	
Traceable to ...	No	
Validation	No	

5.5 Detectors (3)

The Raman backscattered light at $\lambda_S = 607\text{nm}$ from the filtering optical system is forwarded to detectors, consisting of photomultiplier tubes (PMTs), where it is converted to electrical signals. The main uncertainty contribution of the detectors is related to the spatial inhomogeneities of their photocathode, that is the variation of its sensitivity with the position of incident light on it. This can cause range dependent artifacts in Raman signals at $\lambda_S = 607\text{nm}$, because the backscattered light at different altitude levels is projected by the receiving system onto different areas of the photocathode characterized by different sensitivities. Therefore, the power of the Raman signals at $\lambda_S = 607\text{nm}$ at different altitudes may change not only because of vertical distribution of atmospheric parameters, but also because of the variability with the altitude of detector quantum efficiency. The effects of PMT spatial inhomogeneities on lidar signals have been simulated in Simeonov et al. [8] and Freudenthaler [9], where optical configurations to minimize these effects are also described. With conventional optical configurations (direct illumination of the PMT), lidar signal deviations up to 90% have been calculated, which can result in very large systematic uncertainty in the retrieved aerosol extinction coefficient. This uncertainty, depending on the exact location of the lidar spots on the PMT, usually unknown, is unpredictable. With suitable optical setups before the PMT, consisting of field lens, optical diffusers, mirror tubes and optical fibers used alone or in combination, maximum deviations of lidar signals can be strongly reduced, ranging between 30% and 1%, depending on the optical setup used to image the telescope primary mirror on a small area of the PMT photocathode.

Another uncertainty contribution of the detectors is related to the variations of their quantum efficiency due to their ageing. These variations also affect the power of the Raman signals at $\lambda_S = 607\text{nm}$.

For EARLINET lidars, equipped with suitable optical setups minimizing the effects of PMTs spatial inhomogeneities, the contribution of the detectors to the uncertainty of aerosol extinction coefficient profile is assumed negligible. In particular, the telecover test, regularly performed for the correct alignment of the lidar in the near range and described in [7], also allows to identify possible deviations in lidar signals due to the PMT inhomogeneities. In this case, the optical system before the PMT is optimized so as to minimize these deviations.

Information / data	Type / value / equation	Notes / description
Name of effect	Detectors	Contribution related to the efficiency of detectors
Contribution identifier	3	
Measurement equation parameter(s) subject to effect	$\eta(\lambda_S)$ in lidar equation of Raman signals at $\lambda_S = 607\text{nm}$	
Contribution subject to effect (final product or sub-tree intermediate product)	Aerosol extinction coefficient profile $\alpha(z)$	
Time correlation extent & form	Various time scales	Extent & form not quantified

Other (non-time) correlation extent & form	Correlation with vertical range due to the correlation with vertical range of the intensity distribution of the lidar spot on the PMT photocathode	Extent & form (depending on the particular lidar system) not quantified
Uncertainty PDF shape	N/A	Systematic effect
Uncertainty & units	0% (relative uncertainty)	Assumed to be negligible
Sensitivity coefficient	<1	Assumed to be negligible
Correlation(s) between affected parameters	None	May be linked to the chosen backscattering Raman cross-section
Element/step common for all sites/users?	Yes	The different sites use different optical configurations to reduce the effects of spatial inhomogeneities of the detector photocathode
Traceable to ...	No	
Validation	[8,9]	

5.6 Acquisition (4)

A trigger circuit synchronizes the acquisition of the electric signal from the detector with the emission of each laser pulse in order to measure the intensity of the Raman backscattered light from the atmosphere at different distances from the transmitter. This is the Raman lidar signal. Usually, the acquisition of this signal is performed both in analog and photon counting mode, in order to increase the detectable dynamic range of lidar signals: for analog acquisition, an Analog to Digital Converter (ADC) is used to sample the average voltage produced by the incident photons on the detector, at regular time intervals τ_d (time resolution or sampling time of the acquisition system) after the emission of each laser pulse; for photon counting acquisition, a counting system (a discriminator plus a fast counter) is used to measure the number of incident photons on the detector at regular time intervals τ_d after the emission of each laser pulse. For both analog and photon counting Raman signals the vertical resolution, determined by the time resolution of the acquisition system, typically ranges from a few meters up to a few tens of meters.

The uncertainty contributions of the acquisition system are related to the background contribution P_B of lidar signals, the response time of the acquisition system in photon counting mode and any asynchrony between the emission of laser pulses and signal acquisition. These cause biases and distortions in both analog and photon counting Raman signals, which result in biases and distortions in the retrieved aerosol extinction coefficient profile. In EARLINET algorithms, lidar signals are corrected for all these effects in the pre-processing phase (see section 6), where the uncertainty and correlation effects of each contribution are described in the corresponding sub-level section. After these corrections, all the contributions of the acquisition system to the uncertainty of aerosol extinction coefficient profile are assumed negligible.

Information / data	Type / value / equation	Notes / description
Name of effect	Acquisition	Contribution related to conversion of the electric signal from the detector to a

		lidar signal (both in analog and photon counting mode)
Contribution identifier	4	
Measurement equation parameter(s) subject to effect	P_B and z in lidar equation of Raman signals at $\lambda_S = 607nm$	
Contribution subject to effect (final product or sub-tree intermediate product)	Aerosol extinction coefficient profile $\alpha(z)$	
Time correlation extent & form	See sub-levels 6a,6b,6c,6d	
Other (non-time) correlation extent & form	See sub-levels 6a,6b,6c,6d	
Uncertainty PDF shape	N/A	Systematic effect
Uncertainty & units	0% (relative uncertainty) combination of 6a,6b,6c,6d	Assumed to be negligible
Sensitivity coefficient	1	
Correlation(s) between affected parameters	See sub-levels 6a,6b,6c,6d	
Element/step common for all sites/users?	Yes	
Traceable to ...	See sub-levels 6a,6b,6c,6d	
Validation	See sub-levels 6a,6b,6c,6d	

5.7 Raw Raman signals (5)

Both analog and photon counting Raman signals produced by single laser pulses are integrated over a fixed time interval, that is over a fixed number of laser shots, depending on the pulse repetition rate of the lidar. This is done for two main reasons: firstly, the lidar technique is commonly used to study atmospheric processes with a dynamic which is usually much slower than the time characteristic of the single shot lidar profiles; secondly, the electronic setup allowing to store single shot lidar profiles is quite demanding. Typically, the raw lidar signals used in EARLINET algorithms have a time resolution ranging from 10 to 60 s and a vertical resolution from a few meters up to a few tens of meters.

Raw Raman signals are provided with their random uncertainty, which is the standard deviation of the Poisson distribution of counts (square root of the counts) for photon counting signals. For analog signals the random uncertainty, which is the standard deviation of the normal distribution of voltages is usually not provided. The random uncertainty of raw Raman signals produces a random uncertainty in the aerosol extinction profile, depending on the following processing of raw Raman signals, which in turn depends on aerosol load and specifications of each instrument. As raw Raman signals are not directly used in the retrieval algorithm of aerosol extinction profile, the random uncertainty that they produce in such direct retrieval is not provided.

Information / data	Type / value / equation	Notes / description
Name of effect	Raw Raman signals	Contribution of random uncertainty of raw Raman signals
Contribution identifier	5	
Measurement equation parameter(s) subject to effect	Lidar equation of Raman signals at $\lambda_s = 607nm$	
Contribution subject to effect (final product or sub-tree intermediate product)	Aerosol extinction coefficient profile $\alpha(z)$	
Time correlation extent & form	N/A	
Other (non-time) correlation extent & form	N/A	
Uncertainty PDF shape	Poisson/normal distribution for photon counting/analog signals;	Statistical uncertainty
Uncertainty & units	N/A	Depending on the following processing of raw Raman signals.
Sensitivity coefficient	1	
Correlation(s) between affected parameters	N/A	
Element/step common for all sites/users?	Yes	Changes according to the system experimental setup
Traceable to ...	N/A	
Validation	No	

5.8 Pre-processing of Raman signals (6)

The raw Raman signals are pre-processed to apply instrumental corrections and, optionally, a vertical smoothing or temporal averaging. This stage is commonly known as “pre-processing” of lidar signals and represents a necessary step to apply the aerosol extinction profile retrieval algorithm. The pre-processing procedure contains the following steps: dead time correction (6a), dark subtraction (6b), trigger delay/first range bin correction (6c), background subtraction (6d), vertical integration or binning (6e), temporal integration (6f), signal gluing (6g) and overlap correction (6h).

The pre-processed Raman signals have time and vertical resolutions depending, respectively, on temporal and vertical integration performed by the pre-processing module. Typically, time and vertical resolutions range from a few tens of minutes to a few hours and from 30 to 60 m, respectively.

The uncertainty residual contributions in aerosol extinction profile due to systematic effects are assumed negligible due to the instrumental corrections (6a, 6b, 6c, 6d, 6h) applied to the signals.

The random or statistical uncertainties of raw Raman signals are propagated at each step of the pre-processing, from the beginning to the end of the pre-processing chain, using the standard formula of statistical uncertainty propagation. For example, for the lidar station of Potenza, Italy, the random

uncertainty of the pre-processed Raman signals is typically less than 10% through the entire troposphere and possibly higher, between 10% and 20%, in the vertical range from 10 to 12 km, with a vertical resolution of 60 m and a time resolution between 1 and 2 hours.

The resulting random uncertainty of the pre-processed Raman signals produces a random uncertainty in the aerosol extinction profile. As this random uncertainty depends on the following processing applied on the pre-processed signals, it is not provided at this step.

The uncertainty contribution to the aerosol extinction profile due to the pre-processing is the combination of contributions of several steps, whose uncertainties and correlations are described in the corresponding sub-level sections.

Information / data	Type / value / equation	Notes / description
Name of effect	Pre-processing	Combined contribution of all the pre-processing steps 6a, 6b, ...6h applied to the raw signals
Contribution identifier	6	
Measurement equation parameter(s) subject to effect	Lidar equation of Raman signals at $\lambda_s = 607nm$	
Contribution subject to effect (final product or sub-tree intermediate product)	Aerosol extinction coefficient profile $\alpha(z)$	
Time correlation extent & form	Different correlation scales	See inside the different pre-processing steps
Other (non-time) correlation extent & form	Different correlation scales	See inside the different pre-processing steps
Uncertainty PDF shape	Poisson/normal distribution for photon counting/analog signals	Statistical uncertainty
Uncertainty & units	N/A combination of 6a,6b,6c,6d, 6e, 6f, 6g, 6h	Depending on the following processing of pre-processed Raman signals.
Sensitivity coefficient	1	
Correlation(s) between affected parameters	N/A	
Element/step common for all sites/users?	Yes	Changes according to the system experimental setup.
Traceable to ...	N/A	
Validation	See inside the different pre-processing steps	

5.9 Dead Time correction (6a)

Each acquisition system in photon counting mode is characterized by a dead time, or response time, a time interval during which the system is unable to count incident photons. As a result, the acquisition is characterized by a maximum count rate above which the observed count rate is no

longer proportional to the number of incident photons, but depends instead on the dead time duration. Therefore, for high count rates, typically occurring in the near range, raw Raman signals in photon counting mode are affected by distortions which result in artifacts in the retrieved aerosol extinction coefficient profile. These signals can be corrected using two different ideal models describing a photon counting system: a paralyzable model and a not paralyzable one. A paralyzable system is unable to record a second output pulse unless there is a time interval of at least the dead time τ between two successive input pulses. If an additional pulse arrives during the response time, the dead time of the system is further extended by τ . For high count rates, the system is not able to respond and it remains completely paralyzed, by providing a zero count rate. By using Poisson probability distribution, a paralyzable system is described by the following formula [10]:

$$N_m = N_r \exp(-\tau N_r)$$

where N_m and N_r are the measured count rate and the real count rate, respectively. In a not paralyzable system the dead time τ is independent of the arrival of additional counts. For high count rates, the system will asymptotically approach a maximum count rate, N_{max} , which is the inverse of the dead time. A not paralyzable system is described by the following formula [10]:

$$N_m = \frac{N_r}{1 + \tau N_r}$$

The correction for dead time is performed by inverting one of the two previous equations with respect to the real count rate N_r , given the known value of dead time. Concerning the equation to be used, it is necessary to specify that real systems are never completely paralyzable or not paralyzable, but their behavior is somewhat intermediate between these two ideal models. Therefore, neither of the two previous equations describes a real photon counting system accurately. However, for count rates not too high, typically $< 10\text{--}30$ MHz depending on the value of τ , the two models produce very similar results and the choice between the two models becomes irrelevant [2]. The dead time value can be accurately measured as described in Johnson et al. [11, 12] or is provided by the PMT manufacturer. In EARLINET algorithms, the raw Raman signals in photon counting mode are always corrected for dead time (wherever it is possible) and particular care is addressed to the optimization of lidar channel in order to not have too high count rates. Under these conditions, the uncertainty of aerosol extinction coefficient profile due to the dead time correction is assumed negligible.

Information / data	Type / value / equation	Notes / description
Name of effect	Dead time correction	Contribution due to the response time of photon counting acquisition system
Contribution identifier	6a	
Measurement equation parameter(s) subject to effect	Lidar equation of raw Raman signals at $\lambda_s = 607\text{nm}$ in photon counting mode	
Contribution subject to effect (final product or sub-tree intermediate product)	Aerosol extinction coefficient profile $\alpha(z)$	
Time correlation extent & form	Possible long term	Extent & form not quantified

	correlation (the dead time is not necessarily constant and should be measured regularly)	
Other (non-time) correlation extent & form	Correlation with vertical range because only the lower part of extinction profile is affected	Extent & form not quantified
Uncertainty PDF shape	N/A	Systematic effect
Uncertainty & units	0% (relative uncertainty)	Assumed to be negligible (the dead time measured or provided by the manufacturer as well as correction formula are very accurate)
Sensitivity coefficient	1	
Correlation(s) between affected parameters	N/A	
Element/step common for all sites/users?	Yes	Two different correction models are applied: paralyzable and non-paralyzable
Traceable to ...	No	Manufacturer specifications or measurements performed at each lidar station
Validation	[2 ,10, 11, 12]	

5.10 Dark subtraction (6b)

Raw Raman signals acquired in analog mode can be affected by electronic distortions not related to the Raman backscattered light from the atmosphere and mainly caused by the laser power circuits, the detector dark current (temperature dependent) and the amplification circuits of the analog acquisition system. These electronic distortions result in distortions in the aerosol extinction coefficient profile, which depend on both the lidar system and the particular measurement session. Analog raw Raman signals are corrected for electronic distortions by performing the dark subtraction, typically consisting in the following procedure:

- 1) N raw signals are acquired with the telescope completely obstructed, before or after the acquisition of the ordinary raw signals of each measurement session. These dark signals are not affected by any light backscattered from the atmosphere and may contain only the electronic distortions.
- 2) The N dark signals are averaged for each range bin; the random uncertainty of the average dark signal can also be calculated as the standard deviation of the dark signals (voltages) for each range bin.
- 3) From each raw Raman signal the average dark signal obtained in the previous step is subtracted to obtain the raw Raman signal corrected for electronic distortions. The random uncertainty of this signal can be calculated by combining in quadrature the uncertainties of the uncorrected raw Raman signal and of the average dark signal.

In EARLINET algorithms, where raw Raman signals in analog mode are dark subtracted, the residual contribution to the uncertainty of aerosol extinction coefficient profile due to electronic distortions is assumed negligible, assuming that electronic distortions remain stable in the time interval between dark and ordinary signals acquisition.

Information / data	Type / value / equation	Notes / description
Name of effect	Dark subtraction	Contribution of electronic distortions in analog signals
Contribution identifier	6b	
Measurement equation parameter(s) subject to effect	P_B in lidar equation of raw Raman signals at $\lambda_S = 607nm$ in analog mode	
Contribution subject to effect (final product or sub-tree intermediate product)	Aerosol extinction coefficient profile $\alpha(z)$	
Time correlation extent & form	Various time scales	Extent & form not quantified (dark signals are acquired for each measurement session)
Other (non-time) correlation extent & form	Possible correlation with the temperature of detector	Extent & form not quantified
Uncertainty PDF shape	N/A	Systematic effect
Uncertainty & units	0% (relative uncertainty)	Assumed to be negligible due to dark subtraction from analog raw Raman signals
Sensitivity coefficient	1	
Correlation(s) between affected parameters	N/A	
Element/step common for all sites/users?	Yes	The number of dark signals and their averaging time can change for the different stations
Traceable to ...	N/A	
Validation	No	

5.11 First range bin/Trigger delay (6c)

The electronics of both the acquisition system and the trigger, which provides the logic signals for the start of the acquisition, can cause a discrepancy between the instant of emission of a laser pulse and the start of the acquisition related to that laser pulse. Two different situations may occur. In the first, the start of the acquisition is delayed compared to the instant of emission of the laser pulse and the discrepancy dt , called *trigger delay*, results in an underestimation dz of the altitudes in Raman signals. Alternatively, the start of the acquisition is in advance compared to the instant of emission of the laser pulse and the discrepancy dt , called *first range bin*, results in an overestimation dz of the altitudes in Raman signals. The above discrepancy, trigger delay or first range bin, affects both analog and photon counting acquisition, is generally different for each channel and leads to errors

not only in the determination of the altitudes in Raman signals, but also in the retrieval of aerosol extinction coefficient profile, especially in the near range.

The measurement of trigger delay or first range bin and the calculus of absolute error in aerosol extinction coefficient profile due to this discrepancy are described in [7,13]. Raw Raman signals both in analog and photon counting mode are corrected by interpolating them to the correct time or range bins [2]. Consider, for example, a lidar channel with vertical resolution of 15m, corresponding to a dwell time of 100ns. Suppose also that the same channel is affected by a trigger delay/first range bin of dt . The raw uncorrected lidar signal of the channel is $S_{\text{raw}}=\{(t_1,s_1), (t_2,s_2),\dots,(t_n,s_n)\}$, where the instants t_i are 50, 150, 250,...ns, corresponding, in the range domain, to 7.5, 22.5, 37.5,...m. Because the channel is affected by a trigger delay/first range bin of dt , the measured intensities s_1, s_2,\dots,s_n refer to the instants $t_1+dt, t_2+dt,\dots,t_n+dt$ and not to the instants t_1,t_2,\dots,t_n . As a consequence, the correct association between measured intensities and times-range bins should be $S_{\text{corr}}=\{(t_1+dt,s_1), (t_2+dt,s_2),\dots,(t_n+dt,s_n)\}$.

In EARLINET algorithms, where raw Raman signals are corrected for trigger delay/first range bin, the residual contribution to the uncertainty of aerosol extinction coefficient profile due to the trigger delay/first range bin correction is assumed negligible.

Information / data	Type / value / equation	Notes / description
Name of effect	First range bin/Trigger delay correction	Contribution due to asynchrony between the emission of laser pulses and the start of signal acquisition in both analog and photon counting channels
Contribution identifier	6c	
Measurement equation parameter(s) subject to effect	Altitude z in lidar equation of raw Raman signals at $\lambda_s = 607\text{nm}$ in both analog and photon counting mode	
Contribution subject to effect (final product or sub-tree intermediate product)	Aerosol extinction coefficient profile $\alpha(z)$	
Time correlation extent & form	Possible long term correlation due to long term instability of trigger delay/first range bin	Extent & form not quantified
Other (non-time) correlation extent & form	1) Correlation with vertical range: the lower part of extinction profile is mostly affected; 2) Possible correlation with vertical range if the value of trigger delay/first range bin is not a multiple of the time resolution of the acquisition system	1) Extent & form quantified in [7] 2) Extent & form not quantified
Uncertainty PDF shape	N/A	Systematic effect
Uncertainty & units	0% (relative uncertainty)	Assumed to be negligible due

		to the first range bin/trigger delay correction of raw Raman signals
Sensitivity coefficient	1	
Correlation(s) between affected parameters	N/A	
Element/step common for all sites/users?	Yes	Measurement techniques and values of trigger delay/first range bin can change for the different lidar stations
Traceable to ...	No	Trigger delay/first range bin measurements performed at each lidar station with accuracy within the time resolution of the acquisition system
Validation	[2, 7, 13]	

5.12 Background subtraction (6d)

Raw Raman signals measured both in analog and photon counting mode consist of two contributions: the contribution of Raman backscattered light from the atmosphere and the background contribution, generated by direct or scattered sunlight in day time, or by the moon, stars and artificial light sources at night time. The background signal, range independent, is an uncertainty source for Raman signals and, consequently, for the retrieved aerosol extinction coefficient profile. Therefore, it is necessary to subtract from each raw Raman signal its background contribution, in order to consider only the signal due to the Raman backscattered light from the atmosphere. Because this signal decreases with increasing range, the background contribution of a raw Raman signal is usually obtained by averaging it in the far range, above 20km, where the signal due to the backscattering from the atmosphere is neglectable with respect to the background signal. The random uncertainty of the background signal is calculated as the standard deviation of the values of the raw Raman signal within the selected averaging range in the far range [14].

From each raw Raman signal, both in analog and photon counting mode, the corresponding background signal is subtracted. The random uncertainty of this background subtracted raw Raman signal is calculated by combining in quadrature the uncertainties of the raw Raman signal and of the background signal [14].

Note that for an ideal lidar system the background signal includes also the range independent dark contribution which, therefore, should not be subtracted from the raw analog signals. However, in real systems, with range dependent electronic distortions in analog raw signals, the dark signal needs to be separately subtracted from analog raw signals in order to remove these distortions.

In EARLINET algorithms, where raw Raman signals, both in analog and photon counting mode, are background subtracted, the residual contribution to the uncertainty of aerosol extinction coefficient profile due to the background signals is assumed negligible.

Information / data	Type / value / equation	Notes / description
--------------------	-------------------------	---------------------

Name of effect	Background subtraction	Contribution of background in analog and photon counting signals
Contribution identifier	6d	
Measurement equation parameter(s) subject to effect	P_B in lidar equation of raw Raman signals at $\lambda_S = 607nm$ in both analog and photon counting mode	
Contribution subject to effect (final product or sub-tree intermediate product)	Aerosol extinction coefficient profile $\alpha(z)$	
Time correlation extent & form	Possible correlation with the time of measurement session	Extent & form not quantified
Other (non-time) correlation extent & form	Possible correlation with background light, bandwidth of $607nm$ interference filter and field of view of the receiver	Extent & form not quantified
Uncertainty PDF shape	N/A	Systematic effect
Uncertainty & units	0% (relative uncertainty)	Assumed to be negligible due to background subtraction from raw Raman signals
Sensitivity coefficient	1	
Correlation(s) between affected parameters	N/A	
Element/step common for all sites/users?	Yes	
Traceable to ...	N/A	
Validation	[14]	

5.13 Vertical integration (binning) (6e)

Raw Raman signals are usually vertically integrated or smoothed (binning), in order to increase their signal to noise ratio (SNR) or, equivalently, to reduce their relative random uncertainty. In binned signals each point is obtained by summing (photon counting) or averaging (analog) the acquired signals (counts or voltages) in a certain number of range bins and associating as height the mean of the height range relative to the binned range points. The random uncertainty of each point is then calculated by combining in quadrature the random uncertainties (standard deviations) of signals in the binned ranges [14]. The binning reduces the vertical resolution of raw Raman signals to values typically ranging from 30 to 60m. The random uncertainty of the binned raw Raman signals produces a random uncertainty in the aerosol extinction profile which depends on the following processing of these signals. As binned raw Raman signals are not directly used in the retrieval algorithm of aerosol extinction profile, the random uncertainty that they produce in such direct retrieval is not provided.

Information / data	Type / value / equation	Notes / description
Name of effect	Vertical integration (binning)	Contribution of vertical integration of raw Raman signals
Contribution identifier	6e	
Measurement equation parameter(s) subject to effect	Lidar equation of Raman signals at $\lambda_s = 607nm$	
Contribution subject to effect (final product or sub-tree intermediate product)	Aerosol extinction coefficient profile $\alpha(z)$	
Time correlation extent & form	N/A	
Other (non-time) correlation extent & form	Possible correlation with the binning range (i.e. the number of range bins)	Extent & form not quantified
Uncertainty PDF shape	Poisson/normal distribution for photon counting/analog signals;	Statistical uncertainty
Uncertainty & units	N/A	Depending on the following processing of binned raw Raman signals.
Sensitivity coefficient	1	
Correlation(s) between affected parameters	N/A	
Element/step common for all sites/users?	Yes	The number of binned points, the vertical resolution and random uncertainty of binned raw Raman signals can change for the different stations
Traceable to ...	N/A	
Validation	[14]	

5.14 Temporal integration (6f)

In order to further increase their SNR, binned raw Raman signals are temporally integrated, by summing (photon counting) or averaging (analog) them over a time interval from a few tens of minutes to a few hours, depending on the observed atmospheric scenario. The random uncertainty of the resulting time integrated signals is obtained, for each range bin, by combining in quadrature the random uncertainties (standard deviations) of single signals that are integrated. The uncertainty of time integrated Raman signals affects the random uncertainty of the aerosol extinction profile which depends on the following processing of these signals. The integration time of raw Raman signals is carefully selected so that during this time the atmosphere is stable and the uncertainty contribution to the aerosol extinction profile due to the atmospheric variability can be considered negligible.

As time integrated Raman signals are not directly used in the retrieval algorithm of aerosol extinction profiles, the random uncertainty that they produce in such direct retrieval is not provided.

Information / data	Type / value / equation	Notes / description
Name of effect	Temporal integration	Contribution of temporal integration of raw Raman signals
Contribution identifier	6f	
Measurement equation parameter(s) subject to effect	Lidar equation of Raman signals at $\lambda_s = 607nm$	
Contribution subject to effect (final product or sub-tree intermediate product)	Aerosol extinction coefficient profile $\alpha(z)$	
Time correlation extent & form	Various time scales	Extent & form not quantified (the integration time changes for each measurement session)
Other (non-time) correlation extent & form	N/A	
Uncertainty PDF shape	Poisson/normal distribution for photon counting/analog signals	Statistical uncertainty
Uncertainty & units	N/A	Depending on the following processing of time integrated Raman signals.
Sensitivity coefficient	1	
Correlation(s) between affected parameters	N/A	
Element/step common for all sites/users?	Yes	The integration time and random uncertainty of time integrated Raman signals can change for the different stations according to the system experimental setup.
Traceable to ...	N/A	
Validation	No	

5.15 Signal gluing (6g)

The dynamic range of tropospheric lidar signals is very high (at least 4 orders of magnitude). In the near range the signal is extremely high, while in the far range it is extremely weak. In both of these extreme conditions, a good signal to noise ratio and linearity between light intensity and measured signal are required. Lidar signals acquired in analog mode have a high signal to noise ratio in the near range, but a low signal to noise ratio and possible distortions in the far range. On the other hand, lidar signals acquired in photon counting mode show a very good signal to noise ratio in the far range, but they are problematic for high count rates, that occurs in the near range. In these conditions, the signals in photon counting mode lose their linearity due to the dead time and the greater the count rate, the more difficult it is to correct for this effect. Given the complementarity

between analog and photon counting signals, it is possible to extend the detectable dynamic range of lidar, by appropriately combining the analog and photon counting signals resulting from the previous pre-processing steps.

In particular, it is assumed that the “main” signal is the signal in photon counting mode and the corresponding analog signal is considered just an extension of the signal in photon counting mode in the near range. Generally, this operation is called gluing between analog and photon counting signals. This gluing is usually performed by the following steps [2]:

- 1) Identifying a minimum range z_{\min} above which non linear effects in the photon counting signal, due to the dead time, are absent or corrected in reliable way. Typically, z_{\min} corresponds to a count rate of about 10-30MHz in the photon counting signal [15, 16, 17]
- 2) Identifying a maximum range z_{\max} below which distortions in the analog signal are neglectable. This maximum range corresponds to a value of the analog signal of V_{fs}/K , where V_{fs} is the maximum acquisition value and K is a factor depending on the quality of the ADC. (Typically K ranges from 5000 to 20000).
- 3) z_{\max} and z_{\min} are selected so that z_{\max} is higher than z_{\min} and analog and photon counting signals can be glued; if this is not possible, the gluing is not performed and the following processing steps are generally applied only to the photon counting signal above z_{\min} .
- 4) A linear fit of photon counting signal and of analog signal is performed in the interval $[z_{\min}, z_{\max} - dz]$, with $dz = 0$.
- 5) If the coefficients of linear fits in the previous step are consistent, the procedure goes to the next step; otherwise, it returns to the step 4) with $dz = z$, where z is a multiple of the vertical resolution of lidar signals resulting from the previous pre-processing steps (typically ranging from 30 to 60m).
- 6) The analog signal is scaled on the photon counting signal by a linear fit in the interval $[z_{\min}, z_{\max} - dz]$. The gluing factor a is calculated by minimizing the following quantity:

$$\sum_i [S_{PC}(z_i) - a S_{analog}(z_i)]^2$$

where S_{PC} and S_{analog} are photon counting and analog signals resulting from the previous pre-processing steps in the gluing range.

- 7) The gluing point is identified in the interval $[z_{\min}, z_{\max} - dz]$ as the point for which the squared difference between the analog signal and photon counting signal is minimum.
- 8) Finally, the glued signal is formed by the scaled analog signal, for ranges below the gluing point, and by the photon counting signal for ranges above the gluing point.

The random uncertainty of the glued signal is the random uncertainty of the scaled analog signal (obtained by uncertainty propagation formula) and of photon counting signal, respectively below and above the gluing point. This uncertainty produces the random uncertainty of the aerosol extinction profile. As this random uncertainty depends on the following processing of glued Raman signals, it is not provided at this step.

Information / data	Type / value / equation	Notes / description
--------------------	-------------------------	---------------------

Name of effect	Signal gluing	Contribution due to the combination of analog and photon counting signals
Contribution identifier	6g	
Measurement equation parameter(s) subject to effect	Lidar equation of Raman signals at $\lambda_s = 607nm$	
Contribution subject to effect (final product or sub-tree intermediate product)	Aerosol extinction coefficient profile $\alpha(z)$	
Time correlation extent & form	N/A	
Other (non-time) correlation extent & form	Possible correlation with the gluing range	Extent & form not quantified
Uncertainty PDF shape	Normal/Poisson distribution below/above the gluing point	Statistical uncertainty
Uncertainty & units	N/A	Depending on the following processing of glued Raman signals
Sensitivity coefficient	1	
Correlation(s) between affected parameters	N/A	
Element/step common for all sites/users?	Yes	Similar methods for the different stations
Traceable to ...	N/A	
Validation	[2, 15, 16, 17]	

5.16 Overlap Correction (6h)

The glued Raman signal, resulting from the previous pre-processing steps, can be corrected for incomplete overlap by using a suitable overlap function, depending on the lidar geometry, that is the combination of all geometric factors, including the laser beam diameter, shape, divergence and tilt, the telescope focal ratio, the receiver field of view and the location of emitter and receiver optical axes relative to each other (coaxial or biaxial configuration). The overlap function $O(z)$ and the full overlap height z_{ovl} can be determined both theoretically and experimentally. Theoretical determination can be performed by raytracing simulations or by the methods described in Kuze et al. [18], Measures [19], and Chourdakis et al. [20]. Experimental determination can be performed by measurements at different zenith angles under homogeneous and stationary atmospheric conditions, or by the methods described in Wandinger and Ansmann [21] and Freudenthaler [22].

If the Raman signal is not corrected with an overlap function, the resulting uncertainty in the aerosol extinction profile at heights below z_{ovl} can reach 50% [21]; in this case, the provided extinction profile is cut below z_{ovl} , typically ranging from 250 to 500 m above the ground, depending on the lidar system, and above z_{ovl} the systematic uncertainty in the extinction profile due to the overlap function is assumed negligible.

If the Raman signal is corrected for overlap, the extinction profile is provided starting from a minimum height $z_0 < z_{ovl}$ above which the profile is considered trustworthy and the residual uncertainty due to the overlap function is assumed negligible. In EARLINET stations, lidar signals are usually not corrected for overlap and extinction profiles are provided starting from z_{ovl} .

Information / data	Type / value / equation	Notes / description
Name of effect	Overlap correction	Contribution due to the correction with overlap function
Contribution identifier	6h	
Measurement equation parameter(s) subject to effect	$O(z)$ in lidar equation of Raman signals at $\lambda_S = 607nm$	
Contribution subject to effect (final product or sub-tree intermediate product)	Aerosol extinction coefficient profile $\alpha(z)$	
Time correlation extent & form	Possible long term correlation ($O(z)$ is not necessarily constant and should be determined regularly)	Extent & form not quantified
Other (non-time) correlation extent & form	Correlation with vertical range (only the lower part of extinction profile from ground to z_{ovl}/z_0 is affected)	Extent & form not quantified
Uncertainty PDF shape	N/A	Systematic effect
Uncertainty & units	0% for $z > z_{ovl}/z_0$ up to 50% for $z < z_{ovl}/z_0$	Assumed to be negligible due to the cut of the extinction profile below z_{ovl} or $z_0 < z_{ovl}$
Sensitivity coefficient	1	
Correlation(s) between affected parameters	N/A	
Element/step common for all sites/users?	Yes	Usually, overlap correction is not applied in EARLINET lidar stations
Traceable to ...	N/A	
Validation	[18, 19, 20, 21, 22]	

5.17 Processing of Raman signals (7)

The processing of Raman signals to retrieve the aerosol extinction coefficient profile comprises several steps. First, an estimation of molecular density profile and the corresponding molecular extinction profile (7a) is needed. In particular, the atmospheric nitrogen number density profile and the molecular extinction coefficient profiles at wavelengths λ_L and λ_S are required. Secondly, an assumption of aerosol Ångström exponent (7b) and, optionally, the correction for multiple

scattering (7c) are required. Finally, suitable and stable numerical methods are needed to calculate the derivative present in the equation (3) for the retrieval of aerosol extinction coefficient profile.

The profile of aerosol extinction coefficient has a time sampling which is the integration time used in pre-processing of Raman signals, ranging from a few tens of minutes to a few hours. The effective vertical resolution of aerosol extinction profile ranges from a few hundreds of meters to many hundreds of meters, depending on the vertical integration (binning) performed in pre-processing of Raman signals and on method and vertical smoothing used to calculate the derivative in equation (3) [25].

The uncertainty contributions for the retrieval of aerosol extinction profile are systematic, associated to assumptions and corrections described above, and statistical, due to the propagation of random uncertainty of pre-processed Raman signal.

Total maximum systematic uncertainty, calculated by combining all systematic contributions less than 10% (7a, 7b, 7c), is less than 15% for extinction coefficient values higher than $2 \times 10^{-5} \text{ m}^{-1}$ and greater for lower extinction coefficient values. On the other hand, random uncertainty estimates are typically less than 10% for extinction coefficient values higher than $2 \times 10^{-5} \text{ m}^{-1}$ and greater for lower extinction coefficient values (7d).

The total uncertainty of aerosol extinction profile due to the processing is the combination of contributions of each step, whose uncertainties and correlation effects are described in the corresponding sub-level sections.

Information / data	Type / value / equation	Notes / description
Name of effect	Processing of Raman signals	Combined contribution of all the processing steps 7a,7b,7c, 7d applied to the pre-processed Raman signals
Contribution identifier	7	
Measurement equation parameter(s) subject to effect	Raman equation (3) for the retrieval of aerosol extinction coefficient profile	Include additional correction related to spectral dependence and multiple scattering as well as assumptions on molecular density and extinction coefficient profiles
Contribution subject to effect (final product or sub-tree intermediate product)	Aerosol extinction coefficient profile $\alpha(z)$	
Time correlation extent & form	Different correlation scales	See inside the different processing steps
Other (non-time) correlation extent & form	Different correlation scales	See inside the different processing steps
Uncertainty PDF shape	N/A	Combination of propagated random and estimated systematic uncertainties
Uncertainty & units	Random: <10% (1σ) for $\alpha(z) > 2 \times 10^{-5} \text{ m}^{-1}$	Combination of propagated random and estimated systematic uncertainties

	$>10\%(1\sigma)$ for $\alpha(z) < 2 \times 10^{-5} \text{ m}^{-1}$ Systematic: $< 15\%$ for $\alpha(z) > 2 \times 10^{-5} \text{ m}^{-1}$ $> 15\%$ for $\alpha(z) < 2 \times 10^{-5} \text{ m}^{-1}$ Combination of 7a, 7b, 7c, 7d	
Sensitivity coefficient	1	
Correlation(s) between affected parameters	N/A	
Element/step common for all sites/users?	Yes	Possible changes according to the different processing procedures at different lidar stations
Traceable to ...	N/A	
Validation	See inside the different processing steps	

5.18 Molecular density and extinction profiles (7a)

The number density profile of atmospheric nitrogen molecules $N(z)$ is calculated from air density profile, which is obtained from atmospheric pressure and temperature profiles. These can be obtained by using standard atmospheric models, provided by climatological models or measured by co-located and simultaneous radio-soundings. In EARLINET algorithms, models are typically used as co-located and simultaneous radio-soundings are not available due to their high cost. The profiles of molecular extinction coefficient $\alpha_{\lambda_L}^{\text{mol}}(z)$ and $\alpha_{\lambda_S}^{\text{mol}}(z)$ are calculated by using the Rayleigh scattering theory [26,27], and air density profile obtained from atmospheric pressure and temperature profiles. The uncertainty contribution to the aerosol extinction profile due to the assumption on molecular scattering cross sections, considered constant with the vertical range, is assumed negligible. On the other hand, temperature and pressure profiles used for the retrieval of molecular density profile may differ from the real profiles and these differences are a source of uncertainty in the retrieval of aerosol extinction profile. In particular, the difference between the temperature gradient $dT/dz = -6.5\text{K/km}$ assumed in standard temperature profiles and real temperature gradients results in the most significant uncertainty contribution in the aerosol extinction coefficient profile. This uncertainty contribution can be considerable in presence of strong temperature inversions, typically occurring in the lower troposphere. For example, it has been estimated that a temperature gradient of 13 K/km in the altitude range between 1.8 and 2 km can produce an uncertainty in the aerosol extinction coefficient at the same range higher than 30% [28]. However, the uncertainty due to differences between assumed and real temperature gradients decreases with increasing vertical smoothing window length, that usually increases with increasing the vertical range.

Sensitivity studies, based on temperature and pressure profiles measured with radio-soundings, show that, without strong temperature inversions, so that differences between assumed and real (measured) temperature gradients are not too large, the systematic uncertainty contribution associated to the assumption of temperature and pressure profiles is typically less than 10%, but can also increase up to 30% for values of extinction coefficient lower than $2 \times 10^{-5} \text{ m}^{-1}$ [28,29].

Lower or negligible uncertainty contributions can be obtained by using pressure and temperature profiles measured with co-located and simultaneous radio-soundings, if available, or provided by NWP re-analysis. To this end, in the future the EARLINET network will also provide non-NRT products obtained by reprocessing the lidar measurements with these pressure and temperature profiles.

Information / data	Type / value / equation	Notes / description
Name of effect	Molecular density and extinction profile	Contributions due to the assumption of molecular density and extinction profiles
Contribution identifier	7a	
Measurement equation parameter(s) subject to effect	$N(z)$, $\alpha_{\lambda_L}^{\text{mol}}(z)$ and $\alpha_{\lambda_S}^{\text{mol}}(z)$ in Raman equation (3) for the retrieval of aerosol extinction coefficient profile	
Contribution subject to effect (final product or sub-tree intermediate product)	Aerosol extinction coefficient profile $\alpha(z)$	
Time correlation extent & form	Possible long term correlation across multiple measurement sessions	Extent & form not quantified
Other (non-time) correlation extent & form	Possible correlation with vertical range due to different lengths of vertical smoothing window at different altitude ranges	Extent & form not quantified
Uncertainty PDF shape	N/A	Systematic effect
Uncertainty & units	$< 10\%$ for $\alpha(z) > 2 \times 10^{-5} \text{ m}^{-1}$ between 10% and 30% for $\alpha(z) < 2 \times 10^{-5} \text{ m}^{-1}$	Without strong temperature inversions
Sensitivity coefficient	1	
Correlation(s) between affected parameters	N/A	
Element/step common for all sites/users?	Yes	Different methods may be applied for obtaining the molecular density profile
Traceable to ...	N/A	
Validation	[26,27,28,29]	

5.19 Angstrom exponent assumption (7b)

The Ångström exponent \mathring{a} , as defined in equation (4), is an unknown dimensionless quantity that needs to be estimated. Typical values are in the range from 0 to 2. Fixed values are generally used. For ice particles of cirrus clouds the value of $\mathring{a} = 0$ is used, while for aerosols most lidar stations, such as Potenza, use the value of $\mathring{a} = 1$, other stations use the value of $\mathring{a} = 1.5$ or variable user-defined values according to actual meteorological conditions. Alternatively, values measured with sun photometers or derived from multi-wavelength simultaneous measurements of extinction coefficient are used.

The assumed value of Ångström exponent may differ from its real value, depending on specific microphysical properties of aerosol particles. Therefore, the assumption of Ångström exponent is a source of systematic uncertainty in the retrieval of the aerosol extinction profile. Sensitivity studies of aerosol extinction profile to the Ångström exponent show that a variation of the assumed value of 0.5 or 1 causes deviations of aerosol extinction profile less than 5% [28,30]. These deviations can be considered as a reasonable estimate of the uncertainty contribution to the aerosol extinction profile due to the Angstrom exponent assumption.

Information / data	Type / value / equation	Notes / description
Name of effect	Ångström exponent assumption	Contributions due to the assumption of Angstrom exponent
Contribution identifier	7b	
Measurement equation parameter(s) subject to effect	Ångström exponent \mathring{a} defined by equation (4): $\frac{\alpha_{\lambda_L}^{par}(z)}{\alpha_{\lambda_S}^{par}(z)} = \left(\frac{\lambda_S}{\lambda_L}\right)^{\mathring{a}}$	
Contribution subject to effect (final product or sub-tree intermediate product)	Aerosol extinction coefficient profile $\alpha(z)$	
Time correlation extent & form	Possible long term correlation across multiple measurement sessions	Extent & form not quantified
Other (non-time) correlation extent & form	N/A	
Uncertainty PDF shape	N/A	Systematic effect
Uncertainty & units	<5% (relative uncertainty)	
Sensitivity coefficient	1	
Correlation(s) between affected parameters	N/A	
Element/step common for all sites/users?	Yes	Different methods may be applied to estimate the Ångström exponent
Traceable to ...	N/A	
Validation	[28, 30]	

5.20 Multiple scattering correction (7c)

When the lidar laser beam goes through an optically dense medium, such as fog or clouds, not only the singly backscattered photons, but also photons undergoing multiple scattering processes may remain in the lidar receiver field of view and are forwarded to the receiving system. Under these conditions, lidar equations (1) and (3), valid only in single scattering approximation, are not valid anymore. This affects the extinction coefficient retrieval. The major effect of multiple scattering is to make lidar signals higher and extinction coefficient lower than those measured in single scattering conditions. The extinction coefficient profile can be corrected for multiple scattering, by introducing in lidar equations correction factors [31]. These are estimated from multiple scattering models that calculate multiple scattering intensities for lidar returns, considering the scattering characteristics of the scattering medium and the lidar system specifications, that is the receiver field of view, the laser beam divergence and the distance between the laser transmitter and the scattering volume [32].

In EARLINET algorithms, the correction of the extinction coefficient profile for multiple scattering is not performed. The uncertainty contribution in extinction coefficient profile without correction for multiple scattering is negligible in cloud-free atmosphere, 12% and 4% at the base and top of cirrus clouds, 10% and less than 3% at the base and inside cumulus clouds [28].

Information / data	Type / value / equation	Notes / description
Name of effect	Multiple scattering correction	Contribution due to the multiple scattering
Contribution identifier	7c	
Measurement equation parameter(s) subject to effect	Lidar equations (1) and (3) for the retrieval of aerosol extinction coefficient profile	
Contribution subject to effect (final product or sub-tree intermediate product)	Aerosol extinction coefficient profile $\alpha(z)$	
Time correlation extent & form	Possible long term correlation depending on change in both the applied correction method and lidar system	Extent & form not quantified
Other (non-time) correlation extent & form	Possible correlation with vertical range	For clouds: uncertainty at the base is greater than at the top; for aerosols: extent & form not quantified
Uncertainty PDF shape	N/A	Systematic effect
Uncertainty & units	0% (relative uncertainty)	Correction for multiple scattering is not performed; uncertainty contribution assumed to be negligible for aerosols
Sensitivity coefficient	1	
Correlation(s) between affected parameters	N/A	
Element/step common for all	Yes	Different models or corrections

sites/users?		may be applied at different lidar stations
Traceable to ...	N/A	
Validation	[28,31,32]	

5.21 Retrieval of aerosol extinction coefficient profile (7d)

The processing algorithm requires the calculation of the derivative with respect to the range of the logarithm of the ratio between the number density profile of atmospheric nitrogen molecules and the range corrected pre-processed Raman signal. There are several methods to calculate the derivative in a stable way.

The most common methods use linear fit or digital filters, such as Savitzky-Golay filter [33]. The result of the derivative fluctuates substantially with vertical range so that a vertical smoothing must be applied. This implies a reduction of vertical resolution and statistical uncertainty with respect to the pre-processed Raman signal. The wider the smoothing window, the lower the effective vertical resolution and the statistical uncertainty. The methods to determine the relation between the length of the smoothing window and the resulting effective vertical resolution are described in [24,25]. Usually, as the statistical uncertainty increases with increasing the vertical range, different smoothing window lengths, increasing with the vertical range, are used, resulting in effective vertical resolution that decreases with increasing the vertical range. The effective vertical resolution of aerosol extinction profiles at 532nm provided by EARLINET database ranges from a few hundreds of meters to many hundreds of meters.

The statistical uncertainty of the pre-processed Raman signal propagates through the processing algorithm, resulting in the statistical uncertainty of the aerosol extinction coefficient profile. This can be estimated numerically, with the Monte Carlo method, or analytically, by means of error propagation theory applied to equation (3).

The Monte Carlo method is based on the random generation of new lidar signals. Each range bin of these signals is considered as a sample element of a probability distribution with a mean value and standard deviation that corresponds to the value and uncertainty of the pre-processed signal. The probability distribution is assumed to be Normal for the analog signal and Poissonian for the photo counting signal. The extracted lidar signals are then processed with the same algorithm used for the pre-processed signal, to produce a set of solutions in addition to that obtained from the pre-processed signal. The standard deviation of these solutions is finally used as the statistical uncertainty profile of the aerosol extinction profile obtained from the original pre-processed signal.

The statistical uncertainty of the aerosol extinction coefficient profile depends on the method by which the derivative is calculated, the applied smoothing and the method used to estimate the uncertainty itself. For the retrieval of aerosol extinction coefficient at 532 nm, random uncertainty estimates are typically less than 10% for values higher than $2 \times 10^{-5} \text{ m}^{-1}$ and greater for lower extinction coefficient values. This typical value of random uncertainty has been evaluated as the median value of random uncertainties of aerosol extinction coefficient values greater than $2 \times 10^{-5} \text{ m}^{-1}$ on the whole EARLINET quality assured database, involving measurements of 28 stations over Europe since 2000. From the same database, the typical detection limit for aerosol extinction coefficient of $1 \times 10^{-6} \text{ m}^{-1}$ has been estimated as the value below which 95% of the values have a random uncertainty higher than 100%.

Information / data	Type / value / equation	Notes / description
Name of effect	Retrieval of aerosol extinction coefficient profile	Contribution due to the propagation of statistical uncertainty through the processing algorithm
Contribution identifier	7d	
Measurement equation parameter(s) subject to effect	Power of the pre-processed Raman signal $P_{\lambda_S}(z)$ at wavelength $\lambda_S = 607\text{nm}$ in Raman equation (3) for the retrieval of aerosol extinction coefficient profile	
Contribution subject to effect (final product or sub-tree intermediate product)	Aerosol extinction coefficient profile $\alpha(z)$	
Time correlation extent & form	N/A	
Other (non-time) correlation extent & form	Correlation with vertical range due to the smoothing	Extent & form not quantified (Depending on the method to calculate the derivative, the applied vertical smoothing and the method to calculate uncertainty)
Uncertainty PDF shape	Normal/Poisson distribution below/above the gluing point	Statistical uncertainty
Uncertainty & units	$< 10\% (1\sigma)$ for $\alpha(z) > 2 \times 10^{-5} \text{ m}^{-1}$ $> 10\% (1\sigma)$ for $\alpha(z) < 2 \times 10^{-5} \text{ m}^{-1}$ Detection limit: $\alpha(z) = 1 \times 10^{-6} \text{ m}^{-1}$	Depends on the method to calculate the derivative, the applied vertical smoothing and the method to calculate uncertainty. Typical values are provided
Sensitivity coefficient	1	
Correlation(s) between affected parameters	N/A	
Element/step common for all sites/users?	Yes	Different smoothing and methods to calculate derivative and uncertainty may be applied.
Traceable to ...	N/A	
Validation	[25,33]	Validation by means of test functions like step function and Gaussian profile.

6 Uncertainty Summary

Element identifier	Contribution name	Uncertainty contribution form	Typical value	Traceability level (L/M/H)	random, structured random, quasi-systematic or systematic?	Correlated to? (Use element identifier)
1	Transmission system	N/A	0 %	M	systematic	none
2a	Receiver optical parameters	N/A	0 %	M	systematic	none
2b	Alignment of the lidar system	N/A	0 %	M	systematic	none
2	Receiving system	N/A	0 % combination of 2a & 2b	M	systematic	2a & 2b
3	Detectors	N/A	0 %	M	systematic	none
4	Acquisition	N/A	0 % combination of 6a, 6b, 6c & 6d	M	systematic	6a, 6b, 6c & 6d
5	Raw Raman signals	Poiss/norm distribution	N/A	M	random	6b, 6d, 6e, 6f, 6g & 7d
6a	Dead time correction	N/A	0 %	M	systematic	4
6b	Dark subtraction	N/A	0 %	M	systematic	4
6c	First range bin/Trigger delay correction	N/A	0 %	M	systematic	4
6d	Background subtraction	N/A	0 %	M	systematic	4
6e	Vertical integration (binning)	Poiss/norm distribution	N/A	M	random	5, 6b, 6d, 6f, 6g & 7d
6f	Temporal integration	Poiss/norm distribution	N/A	M	random	5, 6b, 6d, 6e, 6g & 7d
6g	Signal gluing	Poiss/norm distribution	N/A	M	random	5, 6b, 6d, 6e, 6f & 7d
6h	Overlap correction	N/A	0% for $z > z_{ovl}/z_0$ up to 50% for $z < z_{ovl}/z_0$ 0 %	M	systematic	none

6	Pre-processing	Poiss/norm distribution	N/A combination of 6a, 6b, 6c, 6d, 6e, 6f, 6g, 6h	M	random	5, 6a, 6b, 6c, 6d, 6e, 6f, 6g, 6h & 7d
7a	Molecular density and extinction profile	equation (3) for the retrieval of aerosol extinction coefficient profile	< 10% for $\alpha(z) > 2 \times 10^{-5} \text{ m}^{-1}$ > 10% for $\alpha(z) < 2 \times 10^{-5} \text{ m}^{-1}$	M	systematic	none
7b	Ångström exponent assumption	equation (3) for the retrieval of aerosol extinction coefficient profile	< 5%	M	systematic	none
7c	Multiple scattering correction	N/A	0 %	M	systematic	none
7d	Retrieval of aerosol extinction coefficient profile	Poiss/norm distribution	<10% (1 σ) for $\alpha(z) > 2 \times 10^{-5} \text{ m}^{-1}$ >10%(1 σ) for $\alpha(z) < 2 \times 10^{-5} \text{ m}^{-1}$	M	random	5, 6b, 6d, 6e, 6f & 6g
7	Processing of Raman signals	N/A	Random: <10% (1 σ) for $\alpha(z) > 2 \times 10^{-5} \text{ m}^{-1}$ >10%(1 σ) for $\alpha(z) < 2 \times 10^{-5} \text{ m}^{-1}$ Systematic: < 15% for $\alpha(z) > 2 \times 10^{-5} \text{ m}^{-1}$ > 15% for $\alpha(z) < 2 \times 10^{-5} \text{ m}^{-1}$ combination of 7a, 7b, 7c, 7d	M	Random and systematic	5, 6b, 6d, 6e, 6f, 6g, 7a, 7b, 7c, 7d

Summarizing, the contributions of the main sources of uncertainty are as follows:

- Total statistical uncertainty U_{stat} , calculated starting from random uncertainties of raw lidar signals, by using the uncertainty propagation rules or Monte Carlo simulation for all applied signal handling procedures both in pre-processing and processing stages: dark subtraction, background subtraction, binning, temporal integration, signal gluing and the calculus of aerosol extinction coefficient $\alpha(z)$ by equation (3), including a vertical smoothing.
 U_{stat} : < 10% for $\alpha(z) > 2 \times 10^{-5} \text{ m}^{-1}$; > 10% for $\alpha(z) < 2 \times 10^{-5} \text{ m}^{-1}$. Typical values are provided, with coverage factor $k=1$, corresponding to one standard deviation 1σ .
- Systematic uncertainty associated to the estimation of molecular density/extinction profile $U_{\text{p,T}}$.
 $U_{\text{p,T}}$: < 10% for $\alpha(z) > 2 \times 10^{-5} \text{ m}^{-1}$; > 10% for $\alpha(z) < 2 \times 10^{-5} \text{ m}^{-1}$. Uncertainty values based on the sensitivity of the extinction coefficient retrieval at 532 nm to the air density profile, considering as a reference the air density profile obtained from temperature and pressure profiles measured with radiosoundings [28,29].
- Systematic uncertainty associated to the Ångström exponent assumption $U_{\text{Å}}$
 $U_{\text{Å}}$: < 5%. Uncertainty value based on the sensitivity of the extinction coefficient retrieval at 532 nm to the Ångström exponent assumption [28,30].
- Total maximum systematic uncertainty $U_{\text{syst}}^{\text{max}} = U_{\text{p,T}} + U_{\text{Å}}$: < 15% for $\alpha(z) > 2 \times 10^{-5} \text{ m}^{-1}$; > 15% for $\alpha(z) < 2 \times 10^{-5} \text{ m}^{-1}$

Assuming the total maximum systematic uncertainty $U_{\text{syst}}^{\text{max}}$ as a normal random uncertainty with coverage factor $k = 3$ (3σ), the total uncertainty for $k = 2$ (2σ), resulting from the combination of $U_{\text{syst}}^{\text{max}}$ and U_{stat} , is given by:

$U_{\text{tot}} = [(2/3U_{\text{syst}}^{\text{max}})^2 + (2U_{\text{stat}})^2]^{1/2}$, giving typical uncertainties less than 23% for $\alpha(z) > 2 \times 10^{-5} \text{ m}^{-1}$ and higher than 23% for $\alpha(z) < 2 \times 10^{-5} \text{ m}^{-1}$.

7 Traceability uncertainty analysis

Traceability level definition is given in Table 1.

Table 1. Traceability level definition table

Traceability Level	Descriptor	Multiplier
High	SI traceable or globally recognised community standard	1
Medium	Developmental community standard or peer-reviewed uncertainty assessment	3
Low	Approximate estimation	10

Analysis of the summary table would suggest the following contributions, shown in Table 2, should be considered further to improve the overall uncertainty of the EARLINET aerosol extinction coefficient product. The entries are given in an estimated priority order.

Table 2. Traceability level definition further action table.

Element identifier	Contribution name	Uncertainty contribution form	Typical value	Traceability level (L/M/H)	random, structured random, quasi-systematic or systematic?	Correlated to? (Use element identifier)
7a	Molecular density and extinction profile	equation (3) for the retrieval of aerosol extinction coefficient profile	$< 10\%$ for $\alpha(z) > 2 \times 10^{-5} \text{ m}^{-1}$ $> 10\%$ for $\alpha(z) < 2 \times 10^{-5} \text{ m}^{-1}$	M	systematic	none
7b	Ångström exponent assumption	equation (3) for the retrieval of aerosol extinction coefficient profile	$< 5\%$	M	systematic	none
3	Detectors	N/A	0 %	M	systematic	none
6h	Overlap correction	N/A	0% for $z > z_{\text{ovl}}/z_0$ up to 50% for $z < z_{\text{ovl}}/z_0$	M	systematic	none
7d	Retrieval of aerosol extinction coefficient profile	Poiss/norm distribution	$< 10\% (1\sigma)$ for $\alpha(z) > 2 \times 10^{-5} \text{ m}^{-1}$ $> 10\% (1\sigma)$ for $\alpha(z) < 2 \times 10^{-5} \text{ m}^{-1}$	M	random	5, 6b, 6d, 6e, 6f & 6g
1	Transmission system	N/A	0 %	M	systematic	none
2a	Receiver optical parameters	N/A	0 %	M	systematic	none
2b	Alignment of the lidar system	N/A	0 %	M	systematic	none
6a	Dead time correction	N/A	0 %	M	systematic	4
6b	Dark subtraction	N/A	0 %	M	systematic	4
6c	First range bin/Trigger delay correction	N/A	0 %	M	systematic	4

6d	Background subtraction	N/A	0 %	M	systematic	4
7c	Multiple scattering correction	N/A	0 %	M	systematic	none

7.1 Recommendations

- ✓ The systematic uncertainty associated to the estimation of molecular density/extinction profile (7a) can be reduced by using pressure and temperature profiles measured with co-located and simultaneous radio-soundings, if available, or provided by NWP re-analysis.
- ✓ Both uncertainty contributions (7a) and (7b), based on sensitivity studies performed on specific measurement sessions and lidar systems, could potentially be improved by extending the sensitivity studies to multiple measurements and lidar systems and by making uniform the methodologies to estimate both the molecular density profile and the Ångström exponent.
- ✓ An assessment of the uncertainty of the detector efficiency (3), due to the spatial inhomogeneities of its photocathode and to the variations of its quantum efficiency, should be evaluated.
- ✓ The experimental determination of overlap function for all the systems in the network can improve the uncertainty contribution of overlap correction (6h) below z_{ovl}/z_0 .
- ✓ The random uncertainty (7d) could potentially be improved by making uniform all applied signal handling procedures both in pre-processing and processing stages: dark subtraction, background subtraction, binning, temporal integration, signal gluing and the calculus of aerosol extinction coefficient $\alpha(z)$ by equation (3), including a vertical smoothing.
- ✓ Finally, there are eight contributions that do not have an assigned uncertainty. Some analysis to determine the magnitude of these potential contributions would better constrain the uncertainty budget.

8 Conclusion

The EARLINET lidar aerosol extinction coefficient product has been assessed against the GAIA CLIM traceability and uncertainty criteria.

9 References

1. G. Pappalardo, A. Amodeo, A. Apituley, A. Comeron, V. Freudenthaler, H. Linné, A. Ansmann, J. Bösenberg, G. D'Amico, I. Mattis, L. Mona, U. Wandinger, V. Amiridis, L. Alados-Arboledas, D. Nicolae, and M. Wiegner: EARLINET: towards an advanced sustainable European aerosol lidar network, *Atmos. Meas. Tech.*, 7, 2389–2409, <https://doi.org/10.5194/amt-7-2389-2014>, 2014.
2. D'Amico, G., Amodeo, A., Mattis, I., Freudenthaler, V., and Pappalardo, G.: EARLINET Single Calculus Chain – technical – Part 1: Pre-processing of raw lidar data, *Atmos. Meas. Tech.*, 9, 491–507, doi:10.5194/amt-9-491-2016, 2016.
3. Mattis, I., D'Amico, G., Baars, H., Amodeo, A., Madonna, F., and Iarlori, M.: EARLINET Single Calculus Chain – technical – Part 2: Calculation of optical products, *Atmos. Meas. Tech.*, 9, 3009–3029, doi:10.5194/amt-9-3009-2016, 2016.
4. N. Papagiannopoulos, L. Mona, L. Alados-Arboledas, V. Amiridis, H. Baars, I. Biniotoglou, D. Bortoli, G. D'Amico, A. Giunta, J. L. Guerrero-Rascado, A. Schwarz, S. Pereira, N. Spinelli, U. Wandinger, X. Wang, and G. Pappalardo: CALIPSO climatological products: evaluation and suggestions from EARLINET, *Atmos. Chem. Phys.*, 16, 2341–2357, doi:10.5194/acp-16-2341-2016, 2016.
5. Wandinger, U., Freudenthaler, V., Baars, H., Amodeo, A., Engelmann, R., Mattis, I., Groß, S., Pappalardo, G., Giunta, A., D'Amico, G., Chaikovsky, A., Osipenko, F., Slesar, A., Nicolae, D., Belegante, L., Talianu, C., Serikov, I., Linné, H., Jansen, F., Apituley, A., Wilson, K. M., de Graaf, M., Trickl, T., Giehl, H., Adam, M., Comerón, A., Muñoz-Porcar, C., Rocadenbosch, F., Sicard, M., Tomás, S., Lange, D., Kumar, D., Pujadas, M., Molero, F., Fernández, A. J., Alados-Arboledas, L., Bravo-Aranda, J. A., Navas-Guzmán, F., Guerrero-Rascado, J. L., Granados-Muñoz, M. J., Preißler, J., Wagner, F., Gausa, M., Grigorov, I., Stoyanov, D., Iarlori, M., Rizi, V., Spinelli, N., Boselli, A., Wang, X., Lo Feudo, T., Perrone, M. R., De Tomasi, F., and Burlizzi, P.: EARLINET instrument intercomparison campaigns: overview on strategy and results, *Atmos. Meas. Tech.*, 9, 1001–1023, doi:10.5194/amt-9-1001-2016, 2016.
6. P. Sawamura, J. P. Vernier, J. E. Barnes, T. A. Berkoff, E. J. Welton, L. Alados-Arboledas, F. Navas-Guzman, G. Pappalardo, L. Mona, F. Madonna, D. Lange, M. Sicard, S. Godin-Beekmann, G. Payen, Z. Wang, S. Hu, S. N. Tripathi, C. Cordoba-Jabonero and R. M. Hoff: Stratospheric AOD after the 2011 eruption of Nabro volcano measured by lidars over the Northern Hemisphere, *Environ. Res. Lett.*, 7, 034013, doi:10.1088/1748-9326/7/3/034013, 2012.
7. EARLINET ASOS NA3 Quality Assurance webpage at https://www.meteo.physik.uni-muenchen.de/~stlidar/earlinet_asos/EARLINET-ASOS-NA3-QA.html.
8. V. Simeonov, G. Larcheveque, P. Quaglia, H. Van Den Bergh, and B. Calpini: Influence of the Photomultiplier Tube Spatial Uniformity on Lidar Signals, *Appl. Opt.* 38, 5186–5190, 1999.
9. Freudenthaler, V., Effects of spatially inhomogeneous photomultiplier sensitivity on lidar signals and remedies, *Proceedings of the 22nd International Laser Radar Conference (ILRC 2004)*, Matera, Italy, 12–16 July, ESA Publications Division, SP-561, 37–40, 2004.

10. Evans, R. D.: The Atomic Nucleus, McGraw-Hill, New York, chapter 28, 785–794, 1955.
11. F. A. Johnson, R. Jones, T. P. McLean, and E. R. Pike: Dead-time corrections to photon counting distributions, *Phys. Rev. Lett.*, 16, N. 13, pp. 589-592, 1966.
12. Whiteman, D. N., Melfi, S. H., and Ferrare, R. A.: Raman lidar system for the measurement of water vapor and aerosols in the Earth's atmosphere, *Appl. Opt.*, 31, 3068–3082, 1992.
13. Freudenthaler, V., Linné, H., Chaikovsky, A., Groß, S., and Rabus, D.: Internal quality assurance tools, *Atmos. Meas. Tech. Discuss.*, in preparation, 2016.
14. Amodeo, A., Statistical error evaluation in aerosol optical properties retrieval, 5th EARLINET-ASOS workshop -Training course, Thessaloniki, 25 – 26 February 2008, available at <https://www.earlinet.org/index.php?id=66>
15. Whiteman, D. N., Demoz, B., Rush, K., Schwemmer, G., Gentry, B., Di Girolamo, P., Comer, J., Veselovskii, I., Evans, K., Melfi, S. H., Wang, Z., Cadirola, M., Mielke, B., Venable, D., and Van Hove, T.: Raman Lidar Measurements during the International H2O Project. Part I: Instrumentation and Analysis Techniques, *J. Atmos. Oceanic Tech.*, 23, 157–169, 2006.
16. Newsom, R. K., Turner, D. D., Mielke, B., Clayton, M., Ferrare, R., and Sivaraman, C.: Simultaneous analog and photon counting detection for Raman lidar, *Appl. Opt.*, 48, 3903–3914, 2009.
17. Walker, M., Venable, D., and Whiteman, D. N.: Gluing for Raman lidar systems using the lamp mapping technique, *Appl. Opt.*, 53, 8535–8543, 2014.
18. Kuze, H., H. Kinjo, Y. Sakurada, and N. Takeuchi, Field-of-view dependence of lidar signals by use of Newtonian and Cassegrainian telescopes, *Appl. Opt.*, 37, 3128–3132, 1998.
19. Measures, R. M., *Laser remote sensing: fundamentals and applications*, 2 ed., 510 pp., Krieger Publishing Company, Malabar, Florida, 1992.
20. Chourdakis, G., A. Papayannis, and J. Porteneuve, Analysis of the receiver response for a noncoaxial lidar system with fiber-optic output, *Appl. Opt.*, 41, 2715–2723, 2002.
21. Wandinger, U., and A. Ansmann, “Experimental determination of the lidar overlap profile with Raman lidar”, *Appl. Opt.*, 41, 511–514, 2002.
22. Freudenthaler, V., *Handbook of instruments*, Tech. rep., EARLINET ASOS, 2007.
23. Ansmann, A., M. Riebesell, and C. Weitkamp, “Measurements of atmospheric aerosol extinction profiles with Raman lidar”, *Optics Letters* 15, 746-748, 1990.
24. Pappalardo G., A. Amodeo, M. Pandolfi, U. Wandinger, A. Ansmann, J. Bosenberg, V. Matthias, V. Amiridis, F. De Tomasi, M. Frioud, M. Iarlori, L. Komguem, A. Papayannis, F. Rocadenbosch, and X. Wang, “Aerosol lidar intercomparison in the framework of the EARLINET, project. 3. Raman lidar algorithm for aerosol extinction, backscatter and lidar ratio”, *Appl. Opt.*, 43(28), 5370–5385, 2004.

25. Iarlori, M., Madonna, F., Rizi, V., Trickl, T., and Amodeo, A.: Effective resolution concepts for lidar observations, *Atmos. 20 Meas. Tech.*, 8, 5157-5176, doi:10.5194/amt-8-5157-2015, 2015.
26. A. Bucholtz, Rayleigh-scattering calculations for the terrestrial atmosphere, *Appl. Opt.* Vol. 34, N. 15, pp. 2765-2773 (1995).
27. R. Miles et al, Laser Rayleigh scattering, *Meas. Sci. Technol.* , 12, R33-R51 (2001).
28. Ansmann, A., U. Wandinger, M. Riebesell, C. Weitkamp, and W. Michaelis, Independent measurement of extinction and backscatter profiles in cirrus clouds by using a combined Raman elastic-backscatter lidar, *Appl. Opt.*, 31, 7113–7131, 1992.
29. Mattis, I., Retrieval of aerosol optical properties, 5th EARLINET-ASOS workshop -Training course, Thessaloniki, 25 – 26 February 2008, available at <https://www.earlinet.org/index.php?id=66>
30. Ansmann, A. and Müller, D., “Lidar and atmospheric aerosol particles”, in: *LIDAR – Range-resolved optical remote sensing of the atmosphere*, edited by: Weitkamp, C., Springer, New York, USA, 105–141, 2005.
31. Wandinger, U., “Multiple-scattering influence on extinction and backscatter coefficient measurements with Raman and high-spectral resolution lidars”, *Applied Optics*, Vol.37, N.3, 417 - 427, 1998.
32. Eloranta, E.E., “Practical model for the calculation of multiply scattered lidar returns”, *Applied Optics*, Vol.37, N.12, 2464 – 2472, 1998.
33. I. Mattis, A. Chaikovsky, A. Amodeo, G. D’Amico, and G. Pappalardo: Assessment report of existing calculus subsystems used within EARLINET-ASOS, available at <http://wiki.tropos.de/images/7/7a/Subsystems.pdf>, April 1, 2007.



Product Traceability and Uncertainty for the Ozone Profile Differential Absorption Lidar Product

Version 0.1.10

*GAIA-CLIM
Gap Analysis for Integrated
Atmospheric ECV Climate Monitoring
Mar 2015 - Feb 2018*

A Horizon 2020 project; Grant agreement: 640276

Date: 20 January 2018

Dissemination level: Final

*Work Package 2; Compiled by
Arnoud Apituley, Anne van Gijzel (KNMI)*



Royal Netherlands
Meteorological Institute
Ministry of Infrastructure
and Water Management

Table of Contents

1	Version history	3
2	Product overview	4
2.1	Guidance notes	5
3	Introduction	9
4	Instrument description.....	10
5	Product Traceability Chain	15
6	Element contributions	17
6.1	Emission sub-system (1)	17
6.2	Receiving sub-system (2)	18
6.3	Receiver optical parameters (2a)	19
6.4	Alignment (2b)	20
6.5	Pre-processing (3).....	22
6.5.1	Detection noise (3a)	22
6.5.2	Saturation (pulse pile-up) correction (3b)	23
6.5.3	Background noise extraction (3c)	24
6.6	External inputs (4).....	27
6.6.1	Ozone absorption cross section differential (4a).....	27
6.6.2	Rayleigh extinction cross section differential (4b)	29
6.6.3	Interfering gases' cross section differential (4c).....	30
6.6.4	Oxygen absorption cross section differential (4d)	32
6.6.5	Interfering gases' atmospheric profiles (4e)	33
6.6.6	Uncertainty owing to air number density, temperature and pressure profiles (4f)	34
6.7	Spatiotemporal integration (5).....	38
6.7.1	Propagation of uncertainty when combining two intensity ranges (5a).....	38
7	Uncertainty summary	40
8	Traceability uncertainty analysis	46
8.1	Recommendations	47
9	Conclusion	50
	References	51

1 Version history

Version	Principal updates	Owner	Date
0.1 draft	First draft	KNMI	12.12.2017
0.1.10	Final draft	KNMI	20.01.2018

2 Product overview

Product name: Ozone concentration profile

Product technique: Differential Absorption Lidar

Product measurand: Ozone (O₃)

Product form/range: profile (ground to 50 km, 1-2 hours averaged)

Product dataset: Ozone concentration profile

Site/Sites/Network location:

- Table Mountain, Wrightwood CA, USA (Tropospheric)
- Mauna Loa, Hawaii, USA (Stratospheric)
- Lauder, New Zealand (Stratospheric)

Product time period: Jan 1 – Dec 31, 2014

Data provider: NDACC

Instrument provider: Various

Product assessor: Arnoud Apituley, KNMI

Assessor contact email: apituley@knmi.nl

2.1 Guidance notes

For general guidance see the Guide to Uncertainty in Measurement & its Nomenclature, published as part of the GAIA-CLIM project.

This document is a measurement product technical document which should be stand-alone i.e. intelligible in isolation. Reference to external sources (preferably peer-reviewed) and documentation from previous studies is clearly expected and welcomed, but with sufficient explanatory content in the GAIA CLIM document not to necessitate the reading of all these reference documents to gain a clear understanding of the GAIA CLIM product and associated uncertainties entered into the Virtual Observatory (VO).

In developing this guidance, we have created a convention for the traceability identifier numbering as shown in Figure 1. The ‘main chain’ from raw measurand to final product forms the axis of the diagram, with top level identifiers (i.e. 1, 2, 3 etc.). Side branch processes add sub-level components to the top level identifier (for example, by adding alternate letters & numbers, or 1.3.2 style nomenclature).

The key purpose of this sub-level system is that all the uncertainty from a sub-level are summed in the next level up.

For instance, using Figure 1, contributors 2a1, 2a2 and 2a3 are all assessed as separate components to the overall traceability chain (have a contribution table). The contribution table for (and uncertainty associated with) 2a, should combine all the sub-level uncertainties (and any additional uncertainty intrinsic to step 2a). In turn, the contribution table for contributor 2, should include all uncertainties in its sub-levels.

Therefore, only the top level identifiers (1, 2, 3, etc.) shown in bold in the summary table need be combined to produce the overall product uncertainty. The branches can therefore be considered in isolation, for the more complex traceability chains, with the top level contribution table transferred to the main chain. For instance, see Figure 2 & Figure 3 as an example of how the chain can be divided into a number of diagrams for clearer representation.

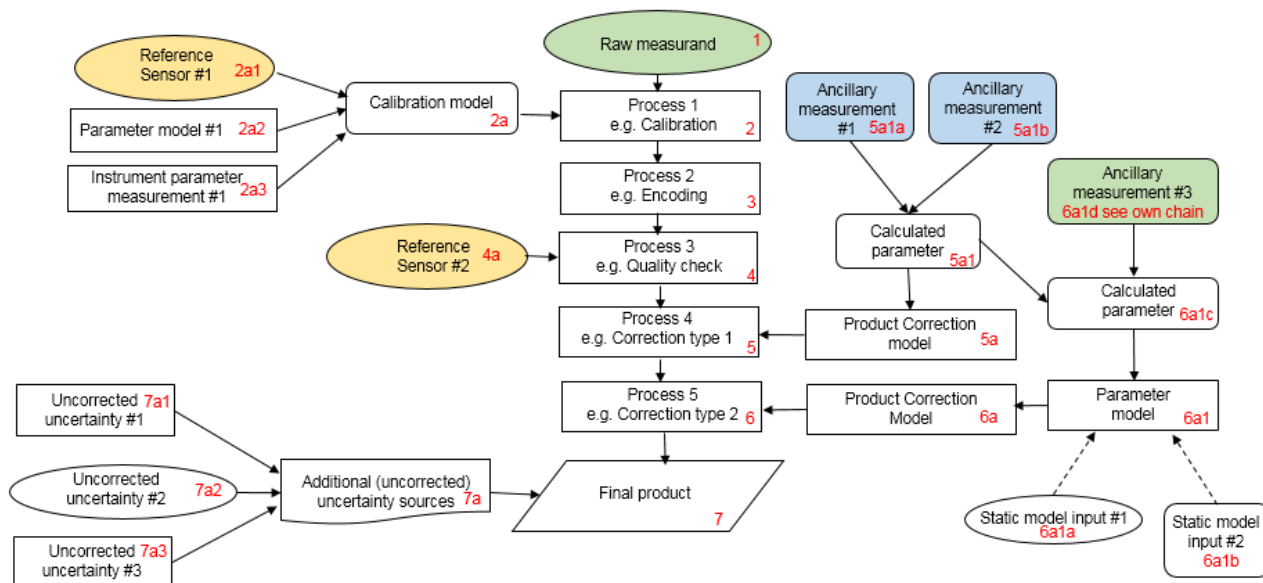


Figure 1. Example traceability chain. Green represents a key measurand or ancillary measurand recorded at the same time with the product raw measurand. Yellow represents a source of traceability. Blue represents a static ancillary measurement

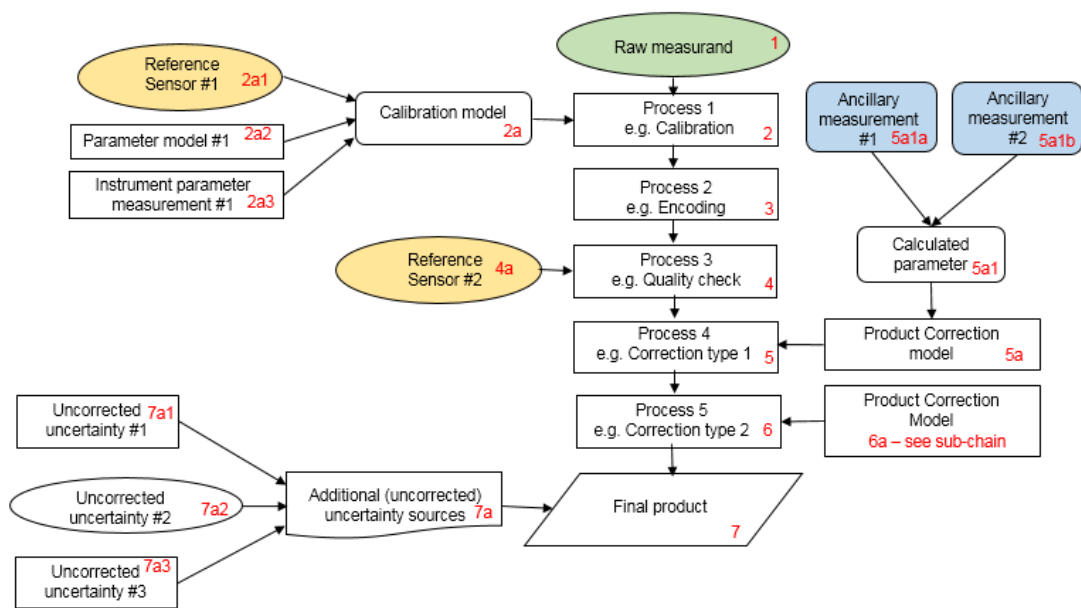


Figure 2. Example chain as sub-divided chain. Green represents a key measurand or ancillary measurand recorded at the same time with the product raw measurand. Yellow represents a source of traceability. Blue represents a static ancillary measurement

When deciding where to create an additional sub-level, the most appropriate points to combine the uncertainties of sub-contributions should be considered, with additional sub-levels used to illustrate where their contributions are currently combined in the described process.

A short note on colour coding. Colour coding can/should be used to aid understanding of the key contributors, but we are not suggesting a rigid framework at this time. In Figure 1, green represents a key measurand or ancillary or complementary measurand recorded at the same time with the raw measurand; yellow represents a primary source of traceability & blue represents a static ancillary measurement (site location, for instance). Any colour coding convention you use, should be clearly described.

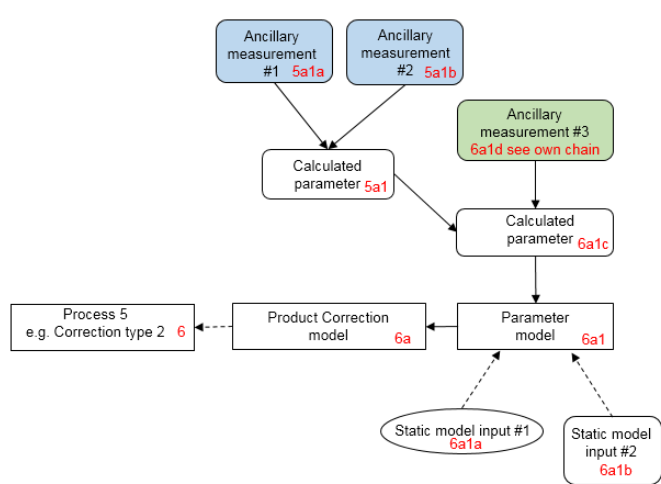


Figure 3. Example chain contribution 6a sub-chain. Green represents a key measurand or ancillary measurand recorded at the same time with the product raw measurand. Blue represents a static ancillary measurement

The contribution table to be filled for each traceability contributor has the form seen in Table 1.

Table 1. The contributor table.

Information / data	Type / value / equation	Notes / description
Name of effect		
Contribution identifier		
Measurement equation parameter(s) subject to effect		
Contribution subject to effect (final product or sub-tree intermediate product)		
Time correlation extent & form		
Other (non-time) correlation extent & form		
Uncertainty PDF shape		
Uncertainty & units		
Sensitivity coefficient		
Correlation(s) between affected parameters		
Element/step common for all sites/users?		
Traceable to ...		
Validation		

Name of effect – The name of the contribution. Should be clear, unique and match the description in the traceability diagram.

Contribution identifier - Unique identifier to allow reference in the traceability chains.

Measurement equation parameter(s) subject to effect – The part of the measurement equation influenced by this contribution. Ideally, the equation into which the element contributes.

Contribution subject to effect – The top level measurement contribution affected by this contribution. This can be the main product (if on the main chain), or potentially the root of a side branch contribution. It will depend on how the chain has been sub-divided.

Time correlation extent & form – The form & extent of any correlation this contribution has in time.

Other (non-time) correlation extent & form – The form & extent of any correlation this contribution has in a non-time domain. For example, spatial or spectral.

Uncertainty PDF shape – The probability distribution shape of the contribution, Gaussian/Normal Rectangular, U-shaped, log-normal or other. If the form is not known, a written description is sufficient.

Uncertainty & units – The uncertainty value, including units and confidence interval. This can be

a simple equation, but should contain typical values.

Sensitivity coefficient – Coefficient multiplied by the uncertainty when applied to the measurement equation.

Correlation(s) between affected parameters – Any correlation between the parameters affected by this specific contribution. If this element links to the main chain by multiple paths within the traceability chain, it should be described here. For instance, SZA or surface pressure may be used separately in a number of models & correction terms that are applied to the product at different points in the processing. See Figure 1, contribution 5a1, for an example.

Element/step common for all sites/users – Is there any site-to-site/user-to-user variation in the application of this contribution?

Traceable to – Describe any traceability back towards a primary/community reference.

Validation – Any validation activities that have been performed for this element?

3 Introduction

This document presents the Product Traceability and Uncertainty (PTU) information for the ozone profile differential absorption lidar product. The aim of this document is to provide supporting information for the users of this product within the GAIA-CLIM VO. The uncertainty and traceability information contained in this document is based on the details given in LeBlanc et al. (2016b).

LeBlanc et al. (2016b) describe an approach for the definition, propagation, and reporting of uncertainty in the ozone differential absorption lidar data products contributing to the Network for the Detection of Atmospheric Composition Change (NDACC) database. One essential aspect of the proposed approach is the propagation in parallel of all independent uncertainty components through the data processing chain before they are combined together to form the ozone combined standard uncertainty.

The independent uncertainty components contributing to the overall budget include random noise associated with signal detection, uncertainty due to saturation correction, background noise extraction, the absorption cross sections of O_3 , NO_2 , SO_2 , and O_2 , the molecular extinction cross sections, and the number densities of the air, NO_2 , and SO_2 . The expression of the individual uncertainty components and their step-by-step propagation through the ozone differential absorption lidar (DIAL) processing chain are thoroughly estimated. All sources of uncertainty except detection noise imply correlated terms in the vertical dimension, which requires knowledge of the covariance matrix when the lidar signal is vertically filtered. In addition, the covariance terms must be taken into account if the same detection hardware is shared by the lidar receiver channels at the absorbed and non-absorbed wavelengths.

The ozone uncertainty budget is presented as much as possible in a generic form (i.e., as a function of instrument performance and wavelength) so that all NDACC ozone DIAL investigators across the network can estimate, for their own instrument and in a straightforward manner, the expected impact of each reviewed uncertainty component.

In the example of a stratospheric ozone DIAL after optimal combination of three DIAL wavelength pairs, the ozone number density standard uncertainty results mainly from three components: Rayleigh extinction cross section differential at the bottom of the profile, ozone absorption cross section differential in the middle of the profile, and detection noise at the top of the profile. For the derived ozone mixing ratio, the uncertainty component associated with the *a priori* use of ancillary air pressure can become abruptly important above 30 km as a result of the transition between the *a priori* use of radiosonde measurement ($z < 30$ km) and the *a priori* use of the NCEP analysis ($z > 30$ km). The dominant source of ozone mixing ratio uncertainty above 45 km is detection noise

4 Instrument description

The basic setup of a lidar system is shown in Fig.4. The lidar technique, acronym for ‘light detection and ranging’, is based on the transmission into the atmosphere of short light pulses, with duration ranging from a few to several hundreds of nanoseconds, by a laser transmitter, directly or by means of transmission optics. In any point of the atmospheric volume crossed by the laser beam, a portion of the incident light is backscattered by atmospheric constituents. This backscattered light is collected by a receiving telescope. The light received from the atmosphere passes through an optical system, consisting of various elements (lenses, mirrors, filters, etc.), which selects specific wavelengths of the light collected by the telescope. The light from the optical system is forwarded to detectors, typically photomultipliers that convert the light into electrical signals. An electronic trigger circuit synchronizes the data acquisition to start with the emission of each laser pulse so that atmospheric signals are acquired as a function of elapsed time with respect to the emission of each laser pulse, from which distance can be inferred unambiguously. These signals are the lidar signals, measuring the intensity of the light backscattered by the atmosphere as a function of the distance from the lidar.

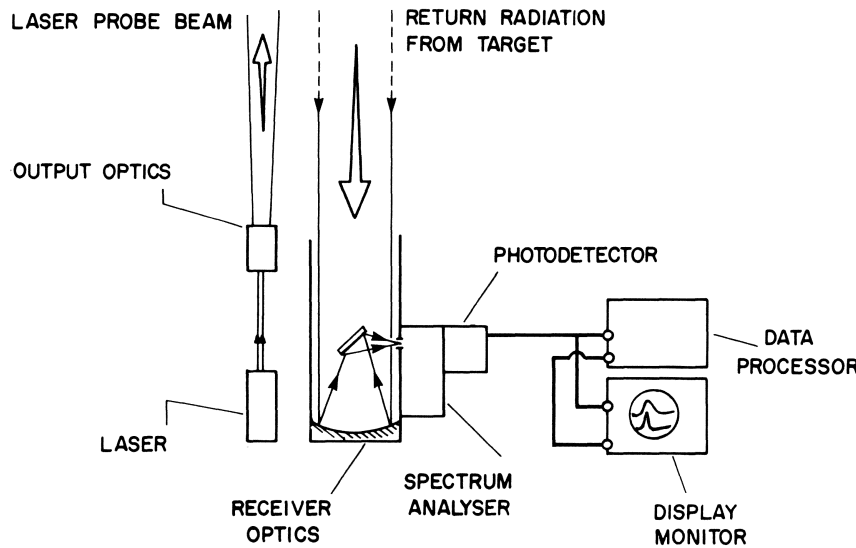


Fig. 4 Schematic of a basic vertically pointing lidar system (Measures, 1984)

To retrieve an ozone profile in the troposphere or stratosphere using the DIAL technique, we start from the Lidar Equation (e.g., Hinkley, 1976; Weitkamp, 2005). This equation in its most compressed form describes the emission of light by a laser source, its backscatter at altitude z , its extinction and scattering along its path up and back, and its collection back on a detector:

$$P(z, \lambda_E, \lambda_R) = P_L(\lambda_E) \frac{\xi(z, \lambda_R) \delta z}{(z - z_L)^2} \tau_{UP}(z, \lambda_E) \beta(z, \lambda_E, \lambda_R) \tau_{DOWN}(z, \lambda_R) \quad (1)$$

- λ_E is the laser emission wavelength and λ_R is the receiver detection wavelength. Note that this subscript may change to indicate different wavelengths later on in the document;
- P is the total number of photons collected at wavelength λ_R on the lidar detector surface;
- δz is the thickness of the backscattering layer sounded during the time interval δt ($\delta z = c\delta t/2$, where c is the speed of light);
- P_L is the number of photons emitted at the emission wavelength λ_E ;
- ξ is the optical efficiency of the receiving channel, including optical and spectral transmittance

and geometric obstruction;

- z is the altitude of the backscattering layer;
- z_L is the altitude of the lidar (laser and receiver assumed to be at the same altitude);
- β is the total backscatter coefficient (including particulate β_P and molecular β_M backscatter);
- τ_{UP} is the optical thickness integrated along the outgoing beam path between the lidar and the scattering altitude z , and is defined as

$$\tau_{UP}(z) = \exp \left[- \int_{z_L}^z \left(\sigma_M(\lambda_E) N_a(z') + \alpha_P(z', \lambda_E) + \sum_i \sigma_i(z', \lambda_E) N_i(z') \right) dz' \right] \quad (2)$$

- τ_{DOWN} is the optical thickness integrated along the returning beam path between the scattering altitude z and the lidar receiver, and is defined as

$$\tau_{DOWN}(z) = \exp \left[- \int_{z_L}^z \left(\sigma_M(\lambda_R) N_a(z') + \alpha_P(z', \lambda_R) + \sum_i \sigma_i(z', \lambda_R) N_i(z') \right) dz' \right] \quad (3)$$

where σ_M is the molecular extinction cross section due to Rayleigh scattering (Strutt, 1899) (hereafter called “Rayleigh cross section” for brevity), N_a is the air number density, α_P is the particulate extinction coefficient, σ_i is the absorption cross section of absorbing constituent i , and N_i is the number density of absorbing constituent i . For the altitude range of interest of the ozone DIAL measurements, the Rayleigh cross sections can be considered constant with altitude, and therefore depend only on wavelength. The absorption cross sections, however, are in most cases temperature-dependent, and should be taken as a function of both altitude and wavelength. In the DIAL technique we consider the lidar signals measured at two different wavelengths, the light at one wavelength being more absorbed by the target species (here, ozone) than the light at the other wavelength (Mégie et al., 1977). Using the notation ON for the most absorbed wavelength, and OFF for the least absorbed wavelength, Eq. (1) can be re-written for each of the emitted wavelength:

$$P_{ON}(z) = P_L(\lambda_1) \frac{\xi_{ON}(z) \delta z}{(z - z_L)^2} \tau_{UP}(z, \lambda_1) \beta(z, \lambda_1, \lambda_2) \tau_{DOWN}(z, \lambda_2) \quad (4)$$

$$P_{OFF}(z) = P_L(\lambda_3) \frac{\xi_{OFF}(z) \delta z}{(z - z_L)^2} \tau_{UP}(z, \lambda_3) \beta(z, \lambda_3, \lambda_4) \tau_{DOWN}(z, \lambda_4) \quad (5)$$

The emitted and received wavelength subscripts have been modified as follows:

λ_1 and λ_2 are the emitted and received “ON” wavelengths respectively

λ_3 and λ_4 are the emitted and received “OFF” wavelengths respectively

To obtain ozone number density N_{O_3} , Eqs. (4)–(5) are rearranged and subsequently the vertical derivative of the logarithm of the ratio of the lidar signals measured at the ON and OFF wavelengths (Mégie et al., 1977):

$$N_{O_3}(z) = \frac{1}{\Delta \sigma_{O_3}(z)} \left[\frac{\partial}{\partial z} \left(\ln \frac{P_{OFF}(z)}{P_{ON}(z)} \right) - \Delta \sigma_M N_a(z) - \left(\sum_{ig} \Delta \sigma_{ig}(z) N_{ig}(z) \right) - \Delta \alpha_P(z) + \Lambda \eta(z) + \Lambda \beta(z) \right] \quad (6)$$

The ozone DIAL measurement model depends on the choice of the theoretical equations used as well as their implementation to the real world, i.e., after considering all the caveats associated with the design, setup, and operation of an actual lidar instrument. Equation (6) relates to the expected number of photons reaching the lidar detectors (P_{ON} and P_{OFF}), not the actual raw lidar signals

recorded in the data files by a real instrument. Its practical implementation for the retrieval of ozone therefore requires, on one hand the addition of several signal correction procedures and numerical transformations that depend on the instrumentation, and on the other hand, the development of approximations and/or the adoption of assumptions aimed to reduce the complexity of the measurement model.

In this context, uncertainty components associated with particulate extinction and backscatter (α_p and β terms in Eq. 6) will not be considered here. Their contribution is negligible in a cloud-free, “clean” atmosphere, which is mostly true for altitudes above 35 km (e.g., Godin-Beekmann et al., 2003), and in most cases of clear-sky, free-tropospheric ozone DIAL measurements for which the wavelength differential is small (Papayannis et al., 1990; McDermid et al., 2002). When present and non-negligible, the contribution of particulate extinction and backscatter is highly variable from site to site, time to time, and highly dependent on the nature and quantity of the particulate matter at the time of measurement. A number of rather different assessment methods exist (for a review, see e.g., Eisele and Trickl, 2005). Proposing a meaningful standardized treatment of this uncertainty component is therefore complex and beyond the scope of the present work.

Similarly, uncertainty due to incomplete beam-telescope overlap correction (η term in Eq. 6) is instrument-dependent and often time-dependent for the same instrument. Therefore, no standardized formulation is provided here. However an example of treatment is provided in the ISSI team report (Leblanc et al., 2016c).

The detectors quantum efficiencies and the effects of the data recorders (e.g., sky and electronic background noise, signal saturation) must be taken into account. Due to the diversity of lidar instrumentation, it is not possible to provide a single expression for the parametrization of these effects and obtain a unique, real-world version of Eq. (6) applicable to all systems. However, we use standardized expressions that characterize the most commonly found cases, with the idea that the proposed approach for the propagation of uncertainty can be similarly applied to other cases. Specifically, to transition from a theoretical to a real ozone DIAL measurement model, we apply the following transformations.

- For each lidar receiver channel, the actual raw signal R recorded in the data files is represented by a vector of discretized values rather than a continuous function of altitude range:
 $z \rightarrow z(k)$ and $R(z) \rightarrow R(k)$ for $k = 1, nk$.
- The actual raw signal recorded in the data files is a combination of laser light backscattered in the atmosphere, sky background light that can be parametrized by a constant offset, and noise generated within the electronics (dark current and possibly signal-induced noise) that can be parametrized by a linear or nonlinear function of time, i.e., altitude range.
- Only channels operating in photon-counting mode are considered hereafter. For analog channels, uncertainty due to analog-to-digital signal conversion needs to be estimated. This estimation is highly instrument-dependent, and no meaningful standardized recommendations can therefore be provided.
- In photon-counting detection mode, the recorded signals result from nonlinear transfer of the detected signals due to the inability of the counting electronics to temporally discriminate a very large number of photon-counts reaching the detector (“pulse pile-up” effect resulting in signal saturation) (e.g., Müller, 1973; Donovan et al., 1993). In the present work, we consider the most frequent case of non-paralyzable photon-counting systems (i.e., using “non-extended dead time”, Müller, 1973), which allows for an analytical correction of the pulse pile-up effect.
- The ozone DIAL measurement includes detection noise, and it is desirable to filter this noise whenever it is expected to impact the retrieved product. The filtering process impacts the propagation of uncertainties, and therefore should be included in the measurement model.

For each individual altitude $z(k)$, the filtering process consists of convolving a set of filter coefficients c_p with an unsmoothed signal s_u to obtain a smoothed signal s_m .

Given the above numerical signal transformations, a discretized version of Eq. (6) can now be formulated as follows:

$$N_{O_3}(k) = \frac{1}{\Delta\sigma_{O_3}(k)} \left[S(k) - \Delta\sigma_M N_a(k) - \left(\sum_{ig} \Delta\sigma_{ig}(k) N_{ig}(k) \right) \right] \quad (7)$$

A product commonly derived from the lidar-measured ozone number density is ozone mixing ratio q_{O_3} . The transformation simply consists of dividing the lidar-measured ozone number density by the “best available” ancillary air number density:

$$q_{O_3}(k) = \frac{1}{\Delta\sigma_{O_3}(k)} \left[\frac{S(k)}{N_a(k)} - \Delta\sigma_M - \left(\sum_{ig} \Delta\sigma_{ig}(k) q_{ig}(k) \right) \right] \quad (8)$$

The instrumentation-related input quantities to consider in the ozone uncertainty budget, described here, based on the NDACC-lidar standardized proposed approach, are the following:

1. detection noise inherent to photon-counting signal detection;
2. saturation (pulse pile-up) correction parameters (typically, photon counters’ dead time τ);
3. background noise extraction parameters (typically, fitting parameters for function B).

Based on Eqs. (7)–(8), the additional external input quantities to consider in the ozone uncertainty budget are the following:

4. ozone absorption cross sections differential σ_{O_3} ;
5. Rayleigh extinction cross sections differential σ_M ;
6. ancillary air number density profile N_a (or temperature T_a and pressure p_a profiles);
7. absorption cross sections differential for the interfering gases σ_{ig} ;
8. Number density profiles N_{ig} (or mixing ratio profile q_{ig}) of the interfering species.

The interfering gases (ig) to consider in practice are NO_2 , SO_2 , and O_2 . Because of either very low concentrations or very low values of their absorption cross section differentials for the ON and OFF wavelengths typically used for stratospheric and tropospheric ozone DIAL, no other atmospheric gases or molecules are expected to interfere with the ozone DIAL retrieval. In addition, NO_2 and SO_2 absorption is usually negligible in the stratospheric ozone retrieval (0.1–1 % ozone uncertainty or less if neglected), as well as most cases of tropospheric ozone retrieval. However it is included here to account for the potentially non-negligible effect of a heavily polluted boundary layer, or potentially heavy volcanic aerosols loading conditions (Godin-Beekmann et al., 2003). The absorption by O_2 should be considered only if any of the detection wavelengths is shorter than 294 nm as the interfering absorption relates to the Herzberg continuum, Herzberg and Wulf bands (Jenouvrier et al., 1999; Fally et al., 2000; Merienne et al., 2001). As already mentioned, the O_2 number density N_{O_2} is assumed to be directly proportional to air number density N_a (constant mixing ratio), and therefore should not be considered as an input quantity.

In order to limit the complexity of the standardization process, the contribution of uncertainty associated with the fundamental physical constants is treated differently from that of the other input quantities. We refer here to an internationally recognized and traceable standard for our recommendations on the use of physical constants, namely the International Council for Science (ICSU) Committee on Data for Science and Technology (CODATA, <http://www.codata.org/>), endorsed by the BIPM (Mohr et al., 2008). Within the CODATA, the Task Group on Fundamental

Constants (TGFC) provides the scientific and technological communities a self-consistent set of internationally recommended values of the basic constants and conversion factors of physics and chemistry that can be found here: <http://physics.nist.gov/cuu/Constants/index.html>.

Our proposed approach ensures that there is indeed no propagation of uncertainty for fundamental physical constants. To do so, we truncate the CODATA reported values to the decimal level where the CODATA reported uncertainty no longer affects rounding.

5 Product Traceability Chain

The PTU is given below for ozone profile retrievals in the stratosphere and troposphere with DIAL. The PTU is divided into two sections: the physical model is presented in Figure 5 and the processing model in Figure 6. The numbered boxes in these figures indicate the key elements in the PTU chain that are the main contributors to the overall measurement uncertainty. Each of these elements is discussed in Section 6.

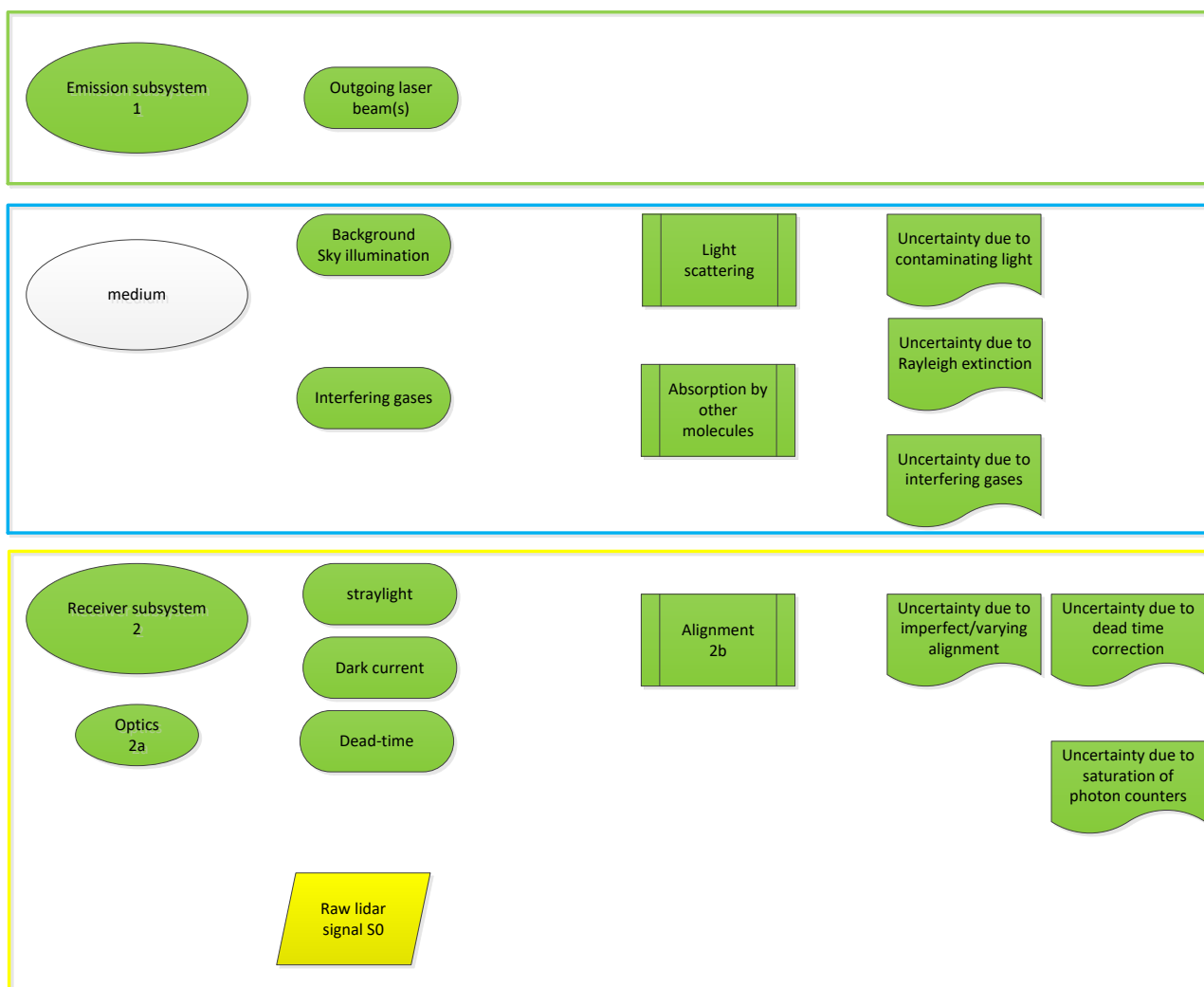


Figure 5. Four elements are shown in the physical part of the PTU chain: the emitter box (outlined by the green rectangle), the medium corresponding to the atmosphere (blue rectangle), the receiver box with e.g. the optics and detectors (yellow rectangle) and the processing software (orange rectangle on the following page). Processes and uncertainties that are considered in this document are shown as filled green shapes. Other sources of uncertainty have been listed, but are either, considered negligible, highly variable and therefore very hard to quantify, or avoidable (by proper technical design of the instrument).

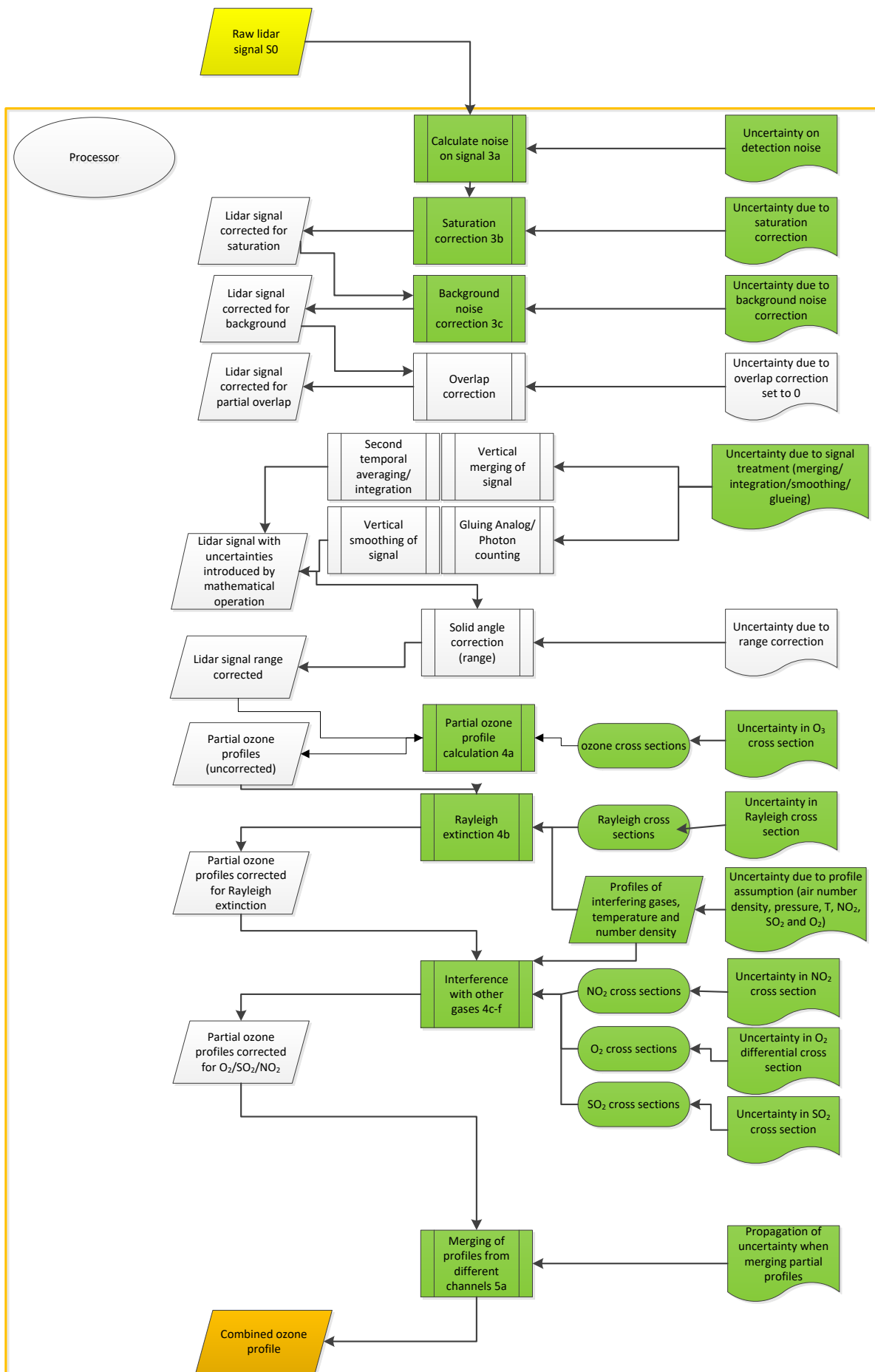


Figure 6. Flow chart of the data processing part of the PTU chain. The input originates from the lidar instrument for which the flow chart is depicted in Fig. 5.

6 Element contributions

6.1 Emission sub-system (1)

Light pulses at wavelengths $\lambda_L = 308$ and $353/355$ nm for stratospheric ozone DIAL and 266, 277, 287, 289, 291, 299, 313 and/or 316 nm for tropospheric ozone are sent out into the atmosphere by a laser transmitter directly or by means of transmission optics (mirrors, beam expander, etc.), and, if necessary, after Raman shifting to obtain another wavelength than the one produced by the laser. The parameters of the laser transmitter (pulse duration, energy and repetition rate, beam diameter and divergence) as well as of the transmission optics change are distinct for each lidar system. For this PTU, the distinction is that the stratospheric DIAL systems use larger telescopes (in the order of 1 m diameter) (McDermid, 1995), while the tropospheric lidars has a telescope with a diameter of about 90 cm and has several additional small receivers to cover the lowest ranges (McDermid, 2002). Changes over time due to aging and replacement of components, as well as responses to temperature changes may cause these parameters to change. These variations affect the optical power transmitted into the atmosphere.

Information / data	Type / value / equation	Notes / description
Name of effect	Transmission system	Contribution of variations in all the parameters related to the laser beam transmission to the atmosphere.
Contribution identifier	1	
Measurement equation parameter(s) subject to effect	P_L and $\xi(\lambda_{ON}, \lambda_{OFF})$ in lidar equation	
Contribution subject to effect (final product or sub-tree intermediate product)	Lidar signal	
Time correlation extent & form	Various time scales	Extent & form not quantified
Other (non-time) correlation extent & form	1) Possible correlation with vertical range (if pulse duration increases so as to exceed the dwell time); 2) Possible correlation with the temperature of laser and transmission optics during measurements	Extent & form not quantified
Uncertainty PDF shape	N/A	Systematic effect
Uncertainty & units	0% (relative uncertainty)	(Assumed to be negligible)
Sensitivity coefficient	< 1	(Assumed to be negligible)
Correlation(s) between affected parameters	None	
Element/step common for all sites/users?	Yes	
Traceable to ...	N/A	
Validation	N/A	

6.2 Receiving sub-system (2)

The portion of the laser radiation backscattered by the atmosphere at different altitude ranges is collected by a telescope. For tropospheric ozone DIAL the best suitable wavelengths to be used are below 300 nm. For stratospheric ozone DIAL, wavelengths longer than 300 nm are used. Two or more telescopes with different collecting apertures are usually employed to optimally cover the signal dynamic range (near range, far range). The radiation collected by the telescope passes through an optical system (consisting of lenses, mirrors, filters, beam splitters and interference filters) where it is spectrally filtered, so only backscattered light at the ON and OFF wavelengths are transmitted to the detection system. The uncertainty contribution of the receiving system is the combination of contributions related to the receiver optical parameters (2a) and the alignment of the lidar system (2b), whose uncertainties and correlation effects are described in the corresponding sub-level sections.

Information / data	Type / value / equation	Notes / description
Name of effect	Receiving system	Combined contribution of the receiver optical parameters (2a) and alignment of the lidar system (2b)
Contribution identifier	2	
Measurement equation parameter(s) subject to effect	$\xi(\lambda_L, \lambda_S)$ in lidar equation	
Contribution subject to effect (final product or sub-tree intermediate product)	Ozone profile $N_{O_3}(z)$	
Time correlation extent & form	Various time scales	Extent & form not quantified
Other (non-time) correlation extent & form	May affect vertical correlation	
Uncertainty PDF shape	N/A	Systematic effect
Uncertainty & units	0% (relative uncertainty) combination of 2a and 2b	Assumed to be negligible
Sensitivity coefficient	1	
Correlation(s) between affected parameters	None	
Element/step common for all sites/users?	Yes	
Traceable to ...	N/A	
Validation	N/A	

6.3 Receiver optical parameters (2a)

The optical properties of the elements forming the receiver, consisting of the telescope and the following optical filtering system, change depending on the lidar system, but they may also change for a given lidar system due to their time and temperature instability, contamination, or to the replacement of one or more components of the receiving system. These variations in the parameters of the receiving system affect the optical power transmitted by the receiver to the detectors and therefore both the power and the random uncertainty of the signals used for the retrieval of ozone profiles. However, for well maintained instruments, quality assurance procedures are implemented (particularly in networks such as NDACC) and these variations are monitored and minimized (e.g., the optics are regularly cleaned, lidars usually operate in air-conditioned environments), so that their contribution to the retrieval and uncertainty of aerosol extinction coefficient profile is assumed to be negligible.

Information / data	Type / value / equation	Notes / description
Name of effect	Receiver optical parameters	Contribution of variations in all the optical parameters of the receiving system
Contribution identifier	2a	
Measurement equation parameter(s) subject to effect	$\xi(\lambda_{ON}, \lambda_{OFF})$	
Contribution subject to effect (final product or sub-tree intermediate product)	Lidar signals P_{ON} and P_{OFF}	
Time correlation extent & form	Various time scales	Extent & form not quantified
Other (non-time) correlation extent & form	1) Possible correlation with vertical range due to the correlation of the optical efficiency of the receiving system with the incident angle of backscattered light and, consequently, with the vertical range; 2) Possible correlation with the temperature of the receiver components during measurements	Extent & form not quantified
Uncertainty PDF shape	N/A	Systematic effect
Uncertainty & units	0% (relative uncertainty)	(Assumed to be negligible)
Sensitivity coefficient	< 1	Assumed that only data not effected is reported
Correlation(s) between affected parameters	None	
Element/step common for all sites/users?	Yes	
Traceable to ...	N/A	
Validation	N/A	

6.4 Alignment (2b)

The correct alignment of the lidar system, that is the alignment of the laser beam with the receiving system and of the telescope with the optics of filtering system, is ensured by specific tests, as for instance developed in the frame of EARLINET quality assurance program. In particular, the so-called telecover test and the Rayleigh fit test are performed to check and correct the alignment of the lidar system in the near range (planetary boundary layer) and in the far range (free troposphere or above), respectively – see Freudenthaler (AMTD, 2018).

For each lidar system there is a certain degree of misalignment between the laser beam and the receiving system due to residual uncertainties in the telecover and Rayleigh fit tests or possible mechanical/thermal instabilities of the optical and mechanical components forming both transmission and receiving systems. The misalignment of a lidar system changes the angle on the receiver of the backscattered light at each altitude level, which affects the overlap function. For the DIAL application, there may be configurations that use multiple (two or more) outgoing laser beams that have to be co-aligned with one or more receivers. This gives rise to multiple overlap functions: one overlap function for each laser beam and associated detection channel. This implies a minimum overlap height for each of these overlap functions. For the DIAL technique to be reliably applied, only the data points originating from above the overlap function with the maximum overlap range should be applied. For the application of the DIAL technique, technical provisions should be in place to determine proper alignment, so that the minimum distance for data analysis can be determined. The minimum distance amounts to less than 10 km for stratospheric ozone lidars and less than 3 km for tropospheric ozone lidar.

Information / data	Type / value / equation	Notes / description
Name of effect	Alignment	
Contribution identifier	2b	
Measurement equation parameter(s) subject to effect	$\xi(\lambda_{ON}, \lambda_{OFF})$	
Contribution subject to effect (final product or sub-tree intermediate product)	Lidar signals P_{ON} and P_{OFF}	
Time correlation extent & form	Various time scales	Extent & form not quantified
Other (non-time) correlation extent & form	1) Possible correlation with vertical range due to the correlation of $O(z)$ and optical efficiency of the receiving system with the vertical range; 2) Possible correlation with the temperature of components forming both transmission and receiving systems during measurements	Extent & form not quantified
Uncertainty PDF shape	N/A	Systematic effect
Uncertainty & units	0% (relative uncertainty)	Assumed to be negligible
Sensitivity coefficient	<1	Assumed that only data not effected is reported

Correlation(s) between affected parameters	None	
Element/step common for all sites/users?	Yes	
Traceable to ...	No	
Validation	No	

6.5 Pre-processing (3)

6.5.1 Detection noise (3a)

Random noise is inherently present in any physical system performing an actual measurement. In the case of the ozone DIAL measurement, it is introduced at the detection level, where the signal is recorded in the data files (raw signal R). The associated detection noise uncertainty is derived from Poisson statistics associated with the probability of detection of a repeated random event (Type A uncertainty estimation) (e.g., Measures, 1984). Using the subscript (DET) for detection noise, the uncertainty in the raw signal R owing to detection noise can be expressed independently for each altitude bin k and for each of the ON and OFF receiver channels by the square root of the raw signal assuming shot noise limited detector performance.

This uncertainty component reflects purely random effects, and therefore implies no correlation between any of the samples considered. We do not consider the case of instruments that (partially) share the same detection electronics, which would require formulating propagation of correlated uncertainties. In the latter case of correlated uncertainties, identical behavior for the ON and OFF channels would have to be assumed. The uncertainty is therefore propagated to ozone number density by consistently adding in quadrature the uncertainties of the individual samples used in the signal transformations. If we assume a non-paralyzable photon-counting hardware, it is propagated to the saturation and background noise corrected signal without covariance terms (LeBlanc, 2016b):

$$u_{PON(DET)}(k) = \left(\frac{P_{ON}(k)}{R_{ON}(k)} \right)^2 \sqrt{R_{ON}(k)} \quad (9)$$

$$u_{POFF(DET)}(k) = \left(\frac{P_{OFF}(k)}{R_{OFF}(k)} \right)^2 \sqrt{R_{OFF}(k)} \quad (10)$$

It is finally propagated to the retrieved ozone number density N_{O_3} and mixing ratio q_{O_3} without covariance terms:

$$u_{NO_3(DET)}(k) = \frac{1}{|\Delta\sigma_{O_3}(k)|\delta z} \sqrt{\sum_{p=-n}^n c_p^2(k) \left(\left(\frac{u_{PON(DET)}(k+p)}{P_{ON}(k+p)} \right)^2 + \left(\frac{u_{POFF(DET)}(k+p)}{P_{OFF}(k+p)} \right)^2 \right)} \quad (11)$$

$$u_{qO_3(DET)}(k) = \frac{1}{N_a(k)|\Delta\sigma_{O_3}(k)|\delta z} \sqrt{\sum_{p=-n}^n c_p^2(k) \left(\left(\frac{u_{PON(DET)}(k+p)}{P_{ON}(k+p)} \right)^2 + \left(\frac{u_{POFF(DET)}(k+p)}{P_{OFF}(k+p)} \right)^2 \right)} \quad (12)$$

Information / data	Type / value / equation	Notes / description
Name of effect	Detection noise	
Contribution identifier	3a	
Measurement equation parameter(s) subject to effect	S	Eq. 7, 8
Contribution subject to effect (final product or sub-tree intermediate product)	N_{O_3} , q_{O_3}	Eq. 7, 8
Time correlation extent & form	Various time scales	Will change with each measurement session due to varying experimental conditions

Other (non-time) correlation extent & form	Vertical smoothing/spatial resolution	
Uncertainty PDF shape	Poisson/normal	
Uncertainty & units	0.1-100%	From near surface to maximum altitude, depending on vertical smoothing and spatial resolution
Sensitivity coefficient	1	
Correlation(s) between affected parameters	N/A	
Element/step common for all sites/users?	Yes	
Traceable to ...	Leblanc et al., 2016c	
Validation	Simeonov et al., 1999	

6.5.2 Saturation (pulse pile-up) correction (3b)

This uncertainty component is introduced only for channels operating in photon-counting mode. If we consider a non-paralyzable counting hardware, the only input quantity to introduce is the hardware's dead time (sometimes called resolving time), which characterizes the speed of the counting electronics. The dead time τ and its uncertainty u_τ are generally among the technical specifications provided by the hardware manufacturer (Type-B estimation).

The photon-counting hardware of the ON and OFF channels is different, so the channels can be considered independent and the saturation correction uncertainty can be propagated to the retrieved ozone number density and mixing ratio through the differentiation equation (Eqs.7-8), assuming no correlation between samples measured in the ON and OFF channels (no covariance terms), thus resulting in the following expressions:

$$u_{NO3(SAT)}(k) = \frac{1}{|\Delta\sigma_{O3}(k)|\delta z} \sum_{p=-n}^n c_p(k) \sqrt{\left(\frac{u_{PON(SAT)}(k+p)}{P_{ON}(k+p)} \right)^2 + \left(\frac{u_{POFF(SAT)}(k+p)}{P_{OFF}(k+p)} \right)^2} \quad (13)$$

$$u_{qO3(SAT)}(k) = \frac{1}{N_a(k)|\Delta\sigma_{O3}(k)|\delta z} \sum_{p=-n}^n c_p(k) \sqrt{\left(\frac{u_{PON(SAT)}(k+p)}{P_{ON}(k+p)} \right)^2 + \left(\frac{u_{POFF(SAT)}(k+p)}{P_{OFF}(k+p)} \right)^2} \quad (14)$$

Information / data	Type / value / equation	Notes / description
Name of effect	Saturation correction	
Contribution identifier	3b	
Measurement equation parameter(s) subject to effect	S	Eq. 7, 8
Contribution subject to effect (final product or sub-tree intermediate product)	N _{O3} , q _{O3}	Eq. 7, 8
Time correlation extent & form	Various time scales	Will change with each measurement session due to varying experimental conditions

Other (non-time) correlation extent & form	N/A	
Uncertainty PDF shape	Poisson/normal	
Uncertainty & units	Tropospheric ozone: 20% near the surface, nonlinearly decreasing with altitude to near 0, when switching to other channel jumping to a smaller peak, followed by the nonlinear decrease with altitude For stratospheric ozone it works similarly, except that the maximum is about 1%	From near surface to maximum altitude
Sensitivity coefficient	1	
Correlation(s) between affected parameters	N/A	
Element/step common for all sites/users?	Yes	
Traceable to ...	Leblanc et al., 2016c	
Validation	Donovan et al, 2003 Bristow, 1998	

6.5.3 Background noise extraction (3c)

At far range (over 100 km range), the backscattered signal is too weak to be detected and any non-zero signal reflects the presence of undesired skylight or electronic background noise. This noise is typically subtracted from the total signal by fitting the uppermost part of the lidar signal with a linear or non-linear function of altitude B . A new uncertainty component associated with the noise fitting procedure must therefore be introduced. Here we provide a detailed treatment for the simple case of a linear fit. It can be easily generalized to many other fitting functions. The linear fitting function takes the form:

$$B(k) = b_0 + b_1 z(k) \quad (15)$$

For many well-known fitting methods (e.g., least-squares), the fitting coefficients b_i can be calculated analytically together with their uncertainty u_{b_i} and their correlation coefficient r_{b_i, b_j} (Type-A estimation) (Press et al., 1986). Using the subscript “(BKG)” for “background noise”, the background noise correction uncertainty is expressed independently for the ON and OFF channels we obtain:

$$u_{PON(BKG)}(k) = \sqrt{u_{b0_ON}^2 + u_{b1_ON}^2 z^2(k) + 2z(k)u_{b0_ON}u_{b1_ON}r_{b0, b1_ON}} \quad (16)$$

$$u_{POFF(BKG)}(k) = \sqrt{u_{b0_OFF}^2 + u_{b1_OFF}^2 z^2(k) + 2z(k)u_{b0_OFF}u_{b1_OFF}r_{b0, b1_OFF}} \quad (17)$$

The above two equations can be derived analytically for any fitting function for which the fitting method allows for the proper estimation of the fitting parameters’ covariance matrix (e.g., least-squares and singular value decomposition).

Because of the nature of the background noise correction (parameters b_i are independent of altitude), the approach used for the propagation of saturation correction uncertainty can also be used for the propagation of background noise correction uncertainty. In other words since the data

acquisition hardware of the ON and OFF channels are different, the background noise correction uncertainty can be propagated assuming no correlation between the ON and OFF channels (no covariance terms):

$$u_{NO3(BKG)}(k) = \frac{1}{|\Delta\sigma_{O3}(k)|\delta z} \sum_{p=-n}^n c_p(k) \sqrt{\left(\frac{u_{PON(BKG)}(k+p)}{P_{ON}(k+p)}\right)^2 + \left(\frac{u_{POFF(BKG)}(k+p)}{P_{OFF}(k+p)}\right)^2} \quad (18)$$

$$u_{qO3(BKG)}(k) = \frac{1}{N_a(k)|\Delta\sigma_{O3}(k)|\delta z} \sum_{p=-n}^n c_p(k) \sqrt{\left(\frac{u_{PON(BKG)}(k+p)}{P_{ON}(k+p)}\right)^2 + \left(\frac{u_{POFF(BKG)}(k+p)}{P_{OFF}(k+p)}\right)^2} \quad (19)$$

The order of magnitude of the propagated ozone uncertainty due to background noise correction depends on many factors, including the relative magnitude of the ON and OFF signals with respect to noise being subtracted, and the slope of the signal-induced noise if signal-induced noise is present.

Having a constant noise and the case of noise having a well-known, small constant slope are the simplest cases to deal with, for which the only uncertainty component to consider is that due to the fitting parameters. In the presence of non-negligible signal-induced noise, the slope of the noise is no longer constant with altitude, and the background correction becomes much more uncertain. The uncertainty associated with non-linear fits is typically larger than that associated with a linear fit, but most importantly, the actual altitude dependence of the signal-induced noise is usually unknown, and an additional uncertainty component that cannot be quantified accurately should be introduced. For this reason, it is strongly recommended to design lidar receivers in such a way that no signal—induced noise is present at all. For the systems under consideration, this is assumed to be the case.

Information / data	Type / value / equation	Notes / description
Name of effect	Background Noise Extraction	
Contribution identifier	3c	
Measurement equation parameter(s) subject to effect	S	Eq. 7, 8
Contribution subject to effect (final product or sub-tree intermediate product)	NO ₃ , qO ₃	Eq. 7, 8
Time correlation extent & form	Various time scales	Will change with each measurement session due to varying experimental conditions, e.g. sky brightness (sun, moon, stars)
Other (non-time) correlation extent & form	N/A	
Uncertainty PDF shape	Poisson/normal	
Uncertainty & units	Tropospheric ozone: 1% at top of partial profiles, decreasing with signal strength to <0.1% For stratospheric ozone 1% near top of profile and decreasing below, negligible in the troposphere	From near surface to maximum altitude

Sensitivity coefficient	1	
Correlation(s) between affected parameters	N/A	
Element/step common for all sites/users?	Yes	
Traceable to ...	Leblanc et al., 2016c	
Validation	McDermid et al., 1990; McGee et al., 1995	

6.6 External inputs (4)

6.6.1 Ozone absorption cross section differential (4a)

When the uncertainty due to the ozone absorption cross-section differential is computed, the actual magnitude of this uncertainty can be very different depending on the type of backscatter (Rayleigh or Raman), and depending on the source of ozone absorption cross-section used. Temperature-dependent ozone absorption cross-sections values originate from various published works by spectroscopy groups around the world (e.g., Serdyuchenko et al., 2014; Bass and Paur, 1984; Bogumil et al., 2003; Chehade et al., 2013; Daumont et al., 1992; Brion et al., 1998; Burrows et al., 1999). These groups usually provide at least one type of uncertainty estimates associated with the cross-section values. Occasionally, they provide separate components due to systematic and random effects. If present, these two components are not introduced and propagated similarly. To account for this distinction, the subscripts “*R*” (for “random”) and “*S*” (for “systematic”) will be used hereafter whenever needed. Expressions for the ozone uncertainty due to the absorption cross-section differential are now provided for four common cases that are relevant to the suggested data sets.

6.6.1.1 Random component

In this case, the random component of the cross-sections uncertainty $u_{\sigma O_3}$ is used to derive the random component of the cross-section differential uncertainty (no covariance terms).

- Applied to the DIAL equation (**Eq. (7)**) assuming no covariance terms from the cross-section differential. For Rayleigh backscatter DIAL systems, the corresponding component is propagated to ozone number density and mixing ratio using:

$$u_{NO_3(\Delta\sigma O_3 R)}(k) = \frac{2N_{O_3}(k)}{|\Delta\sigma_{O_3}(k)|} \sqrt{u_{\sigma O_3-1(R)}^2(k) + u_{\sigma O_3-3(R)}^2(k)} \quad (20)$$

$$u_{qO_3(\Delta\sigma O_3 R)}(k) = \frac{2q_{O_3}(k)}{|\Delta\sigma_{O_3}(k)|} \sqrt{u_{\sigma O_3-1(R)}^2(k) + u_{\sigma O_3-3(R)}^2(k)} \quad (21)$$

- For Raman backscatter DIAL systems, this uncertainty component is propagated to ozone number density and mixing ratio using:

$$u_{NO_3(\Delta\sigma O_3 R)}(k) = \frac{N_{O_3}(k)}{|\Delta\sigma_{O_3}(k)|} \sqrt{u_{\sigma O_3-1(R)}^2(k) + u_{\sigma O_3-2(R)}^2(k) + u_{\sigma O_3-3(R)}^2(k) + u_{\sigma O_3-4(R)}^2(k)} \quad (22)$$

$$u_{qO_3(\Delta\sigma O_3 R)}(k) = \frac{q_{O_3}(k)}{|\Delta\sigma_{O_3}(k)|} \sqrt{u_{\sigma O_3-1(R)}^2(k) + u_{\sigma O_3-2(R)}^2(k) + u_{\sigma O_3-3(R)}^2(k) + u_{\sigma O_3-4(R)}^2(k)} \quad (23)$$

6.6.1.2 Systematic component

The cross-sections uncertainty component due to systematic effects is not always present or reported. It is most often estimated by comparing several cross-section datasets and observing biases between those datasets. The expression for the propagation of this component depends on the degree of correlation between the datasets used. Here we consider only two cases: when a unique source of cross-section is used for all wavelengths (i.e., dataset originating from a single set of laboratory measurements), and when two independent cross-section datasets are used for the ON and OFF wavelengths.

- In the first case, applicable to the selected case study instruments, it is assumed that the same dataset is used for the absorption cross-sections at all wavelengths. The systematic component of the cross-sections uncertainty $u_{\sigma O_3(S)}$ is used to derive a systematic component of the cross-section differential's uncertainty $u_{\Delta\sigma O_3(S)}$ assuming full correlation between all wavelengths. In this case the same expression holds for both Rayleigh and Raman backscatter channels:

$$u_{NO3(\Delta\sigma O3S)}(k) = \frac{N_{O3}(k)}{|\Delta\sigma_{O3}(k)|} \left| u_{\sigma O3_1(S)}(k) + u_{\sigma O3_2(S)}(k) - u_{\sigma O3_3(S)}(k) - u_{\sigma O3_4(S)}(k) \right| \quad (24)$$

$$u_{qO3(\Delta\sigma O3S)}(k) = \frac{q_{O3}(k)}{|\Delta\sigma_{O3}(k)|} \left| u_{\sigma O3_1(S)}(k) + u_{\sigma O3_2(S)}(k) - u_{\sigma O3_3(S)}(k) - u_{\sigma O3_4(S)}(k) \right| \quad (25)$$

- In the second case, it is assumed that two independent datasets are used for the cross-sections at the ON and OFF wavelengths. Though usually not the case, this situation can occur because laboratory studies often focus on specific spectral regions, not necessarily covering all the wavelengths in use by a particular DIAL system. With the assumption of two independent cross-section datasets, the systematic component of the cross-sections uncertainty reported by both datasets is assumed randomized (Type-B estimation). Therefore the uncertainty component due to systematic effects should be propagated assuming that 1) the cross-section values used within the same dataset are fully correlated, and 2) none of cross-section values of one dataset is correlated with a cross-section value of the other dataset. The resulting ozone uncertainty component can then be written for both Rayleigh and Raman backscatter channels:

$$u_{NO3(\Delta\sigma O3S)}(k) = \frac{N_{O3}(k)}{|\Delta\sigma_{O3}(k)|} \sqrt{\left(u_{\sigma O3_1(S)}(k) + u_{\sigma O3_2(S)}(k) \right)^2 + \left(u_{\sigma O3_3(S)}(k) + u_{\sigma O3_4(S)}(k) \right)^2} \quad (26)$$

$$u_{qO3(\Delta\sigma O3S)}(k) = \frac{q_{O3}(k)}{|\Delta\sigma_{O3}(k)|} \sqrt{\left(u_{\sigma O3_1(S)}(k) + u_{\sigma O3_2(S)}(k) \right)^2 + \left(u_{\sigma O3_3(S)}(k) + u_{\sigma O3_4(S)}(k) \right)^2} \quad (27)$$

In **Eqs. (24)-(27)**, the Rayleigh backscatter case simply consists of replacing subscripts “3” and “4” by “1” and “2” respectively.

Equations (20)-(27) show that the relative uncertainty in the retrieved ozone is directly proportional to the relative uncertainty in the ozone absorption cross-section, which makes this latter factor the main source of uncertainty in the nominal measurement region of the ozone DIAL method (Godin-Beekmann and Nair, 2012). For stratospheric ozone DIAL pairs (308/355 and 332/387), the absorption cross-section at the “ON” wavelength is much larger than that at the “OFF” wavelength, resulting in an ozone relative uncertainty mostly dominated by the absorption cross-section uncertainty at the “ON” wavelength, and therefore leading to approximate 1-to-1 relationship between the ozone number density relative uncertainty and the absorption cross-section relative uncertainty. For tropospheric ozone DIAL pairs (299/316, 289/299, 266/289, and 287/294), the absorption cross-sections at the “ON” and “OFF” wavelengths are closer to each other. As a result, the curves depart slightly from the 1-1 relation observed for the stratospheric pairs. A 1-to-1 relationship is also observed for the all-systematic case as a result of the linear combination of **Eqs. (26)-(27)**.

Information / data	Type / value / equation	Notes / description
Name of effect	Ozone absorption cross section differential	
Contribution identifier	4a	
Measurement equation parameter(s) subject to effect	$\Delta\sigma_{O3}$	Eq. 7, 8
Contribution subject to effect (final product or sub-tree intermediate product)	N_{O3}, q_{O3}	Eq. 7, 8
Time correlation extent & form	None	

Other (non-time) correlation extent & form	None	
Uncertainty PDF shape	Unknown	Random and Systematic
Uncertainty & units	2% for stratospheric ozone, 4-6% for tropospheric ozone depending on wavelengths used	Constant with altitude for number density and wavelength pair
Sensitivity coefficient	1	
Correlation(s) between affected parameters	N/A	
Element/step common for all sites/users?	No	No community consensus about consistent use of cross sections.
Traceable to ...	Leblanc et al., 2016c	
Validation	Godin-Beekmann and Nair, 2012	

6.6.2 Rayleigh extinction cross section differential (4b)

An approach similar to that used for the ozone absorption cross-section differential uncertainty can be used for the Rayleigh extinction cross-section differential uncertainty. Analytical expressions of Rayleigh scattering based on atmospheric composition usually provide better cross-section estimates than laboratory studies, e.g., Bates (1984); Eberhard (2010); Bucholtz, (1995). Using an analytical expression to compute Rayleigh extinction cross-sections is equivalent to considering the case of a single-source component (namely, the analytical function), therefore implying full correlation between all values. Under this assumption, the Rayleigh extinction cross-section differential uncertainty propagated to ozone number density and mixing ratio can be written for Rayleigh and Raman backscatter channels:

$$u_{NO3(\Delta\sigma MS)}(k) = N_a(k) \left| \frac{u_{\sigma M-1(S)}(k) + u_{\sigma M-2(S)}(k) - u_{\sigma M-3(S)}(k) - u_{\sigma M-4(S)}(k)}{\Delta\sigma_{O3}(k)} \right| \quad (28)$$

$$u_{qO3(\Delta\sigma MS)}(k) = \left| \frac{u_{\sigma M-1(S)}(k) + u_{\sigma M-2(S)}(k) - u_{\sigma M-3(S)}(k) - u_{\sigma M-4(S)}(k)}{\Delta\sigma_{O3}(k)} \right| \quad (29)$$

When cross-section uncertainties due to random effects only are used and for Rayleigh backscatter channels, the Rayleigh extinction cross-section differential uncertainty $u_{NO3(\Delta\sigma MR)}$ propagated to ozone number density and mixing ratio can be written:

$$u_{NO3(\Delta\sigma MR)}(k) = \frac{2N_a(k)}{|\Delta\sigma_{O3}(k)|} \sqrt{u_{\sigma M-1(R)}^2(k) + u_{\sigma M-3(R)}^2(k)} \quad (30)$$

$$u_{qO3(\Delta\sigma MR)}(k) = \frac{2\sqrt{u_{\sigma M-1(R)}^2(k) + u_{\sigma M-3(R)}^2(k)}}{|\Delta\sigma_{O3}(k)|} \quad (31)$$

For Raman backscatter channels, this uncertainty component can be written:

$$u_{NO3(\Delta\sigma MR)}(k) = \frac{N_a(k)}{|\Delta\sigma_{O3}(k)|} \sqrt{u_{\sigma M-1(R)}^2(k) + u_{\sigma M-2(R)}^2(k) + u_{\sigma M-3(R)}^2(k) + u_{\sigma M-4(R)}^2(k)} \quad (32)$$

$$u_{qO3(\Delta\sigma MR)}(k) = \frac{\sqrt{u_{\sigma M-1(R)}^2(k) + u_{\sigma M-2(R)}^2(k) + u_{\sigma M-3(R)}^2(k) + u_{\sigma M-4(R)}^2(k)}}{|\Delta\sigma_{O3}(k)|} \quad (33)$$

Equations (29), (31) and (33) show that for a specific DIAL pair, the lidar-retrieved mixing ratio

uncertainty is directly proportional to the relative uncertainty in the Rayleigh cross-section. For a particular value of Rayleigh cross-section relative uncertainty, the DIAL pairs with longer wavelengths (e.g., 299/316 for tropospheric systems, and the Raman pair for stratospheric systems) yield larger ozone mixing ratio uncertainties.

Information / data	Type / value / equation	Notes / description
Name of effect	Rayleigh extinction cross section differential	
Contribution identifier	4b	
Measurement equation parameter(s) subject to effect	$\Delta\sigma_M$	Eq. 7, 8
Contribution subject to effect (final product or sub-tree intermediate product)	N_{O_3} , q_{O_3}	Eq. 7, 8
Time correlation extent & form	None	
Other (non-time) correlation extent & form	None	
Uncertainty PDF shape	Unknown	
Uncertainty & units	10-0.1%	From near surface to half maximum altitude. See Figs. 7 and 8.
Sensitivity coefficient	1	
Correlation(s) between affected parameters	N/A	
Element/step common for all sites/users?	Yes	
Traceable to ...	Leblanc et al., 2016c	
Validation	Sullivan et al., 2015 Brinksma et al., 2000	

6.6.3 Interfering gases' cross section differential (4c)

Once again, an approach similar to that used for the ozone absorption and Rayleigh cross-section differentials can be used for the absorption cross-section differential of the interfering gases. The resulting uncertainty components due to random and systematic effects and propagated to ozone number density and mixing ratio can be written for NO_2 and SO_2 ($ig=NO_2, SO_2$). The particular case of absorption by O_2 in the Herzberg and Wulf bands (applied to case study instruments) region is presented below.

Random effects, Rayleigh backscatter case:

$$u_{NO_3(\Delta\sigma_{igR})}(k) = \frac{2N_{ig}(k)}{|\Delta\sigma_{O_3}(k)|} \sqrt{u_{\sigma_{ig-1(R)}}^2(k) + u_{\sigma_{ig-3(R)}}^2(k)} \quad (34)$$

$$u_{qO_3(\Delta\sigma_{igR})}(k) = \frac{2q_{ig}(k)}{|\Delta\sigma_{O_3}(k)|} \sqrt{u_{\sigma_{ig-1(R)}}^2(k) + u_{\sigma_{ig-3(R)}}^2(k)} \quad (35)$$

Random effects, Raman backscatter case:

$$u_{NO_3(\Delta\sigma_{igR})}(k) = \frac{N_{ig}(k)}{|\Delta\sigma_{O_3}(k)|} \sqrt{u_{\sigma_{ig-1(R)}}^2(k) + u_{\sigma_{ig-2(R)}}^2(k) + u_{\sigma_{ig-3(R)}}^2(k) + u_{\sigma_{ig-4(R)}}^2(k)} \quad (36)$$

$$u_{qO3(\Delta\sigma_{igR})}(k) = \frac{q_{ig}(k)}{|\Delta\sigma_{O3}(k)|} \sqrt{u_{\sigma_{ig-1}(R)}^2(k) + u_{\sigma_{ig-2}(R)}^2(k) + u_{\sigma_{ig-3}(R)}^2(k) + u_{\sigma_{ig-4}(R)}^2(k)} \quad (37)$$

Systematic effects, single dataset, both Rayleigh and Raman backscatter:

$$u_{NO3(\Delta\sigma_{igS})}(k) = \frac{N_{ig}(k)}{|\Delta\sigma_{O3}(k)|} |u_{\sigma_{ig-1}(S)}(k) + u_{\sigma_{ig-2}(S)}(k) - u_{\sigma_{ig-3}(S)}(k) - u_{\sigma_{ig-4}(S)}(k)| \quad (38)$$

$$u_{qO3(\Delta\sigma_{igS})}(k) = \frac{q_{ig}(k)}{|\Delta\sigma_{O3}(k)|} |u_{\sigma_{ig-1}(S)}(k) + u_{\sigma_{ig-2}(S)}(k) - u_{\sigma_{ig-3}(S)}(k) - u_{\sigma_{ig-4}(S)}(k)| \quad (39)$$

Systematic effects, two different datasets for ON and OFF wavelengths, both Rayleigh and Raman backscatter:

$$u_{NO3(\Delta\sigma_{igS})}(k) = \frac{N_{ig}(k)}{|\Delta\sigma_{O3}(k)|} \sqrt{(u_{\sigma_{ig-1}(S)}(k) + u_{\sigma_{ig-2}(S)}(k))^2 + (u_{\sigma_{ig-3}(S)}(k) + u_{\sigma_{ig-4}(S)}(k))^2} \quad (40)$$

$$u_{qO3(\Delta\sigma_{igS})}(k) = \frac{q_{ig}(k)}{|\Delta\sigma_{O3}(k)|} \sqrt{(u_{\sigma_{ig-1}(S)}(k) + u_{\sigma_{ig-2}(S)}(k))^2 + (u_{\sigma_{ig-3}(S)}(k) + u_{\sigma_{ig-4}(S)}(k))^2} \quad (41)$$

This time the ozone mixing ratio uncertainty is proportional to the relative uncertainty in the interfering gas' cross-section and to the interfering gas' mixing ratio. DIAL pairs with longer wavelengths yield a larger ozone mixing ratio uncertainty due to the large NO₂ cross-section values in the UV region. In “normal” NO₂ background conditions, the relative impact of NO₂ absorption on retrieved ozone remains very small for both tropospheric and stratospheric ozone systems. The ozone mixing ratio uncertainty due to SO₂ cross-section uncertainty is almost negligible for stratospheric DIAL pairs (Higgins band) because of the weak SO₂ absorption in this region compared to that of ozone. The impact of SO₂ absorption on retrieved ozone is therefore negligible except in the case of heavy SO₂ loads (i.e., 100 ppbv or above).

Information / data	Type / value / equation	Notes / description
Name of effect	Interfering gases' cross section differential	
Contribution identifier	4c	
Measurement equation parameter(s) subject to effect	$\Delta\sigma_{ig}$	Eq. 7, 8
Contribution subject to effect (final product or sub-tree intermediate product)	NO ₃ , qO ₃	Eq. 7, 8
Time correlation extent & form	None	
Other (non-time) correlation extent & form	None	
Uncertainty PDF shape	N/A	
Uncertainty & units	Variable, <10%	Depending on interfering gas species. For illustration, see Figs.7 and 8.
Sensitivity coefficient	1	
Correlation(s) between affected parameters	N/A	

Element/step common for all sites/users?	Yes	
Traceable to ...	Leblanc et al., 2016c	
Validation	Papayannis et al., 1990	

6.6.4 Oxygen absorption cross section differential (4d)

An approach similar to that used for the other cross-section differentials can be used for the O₂ absorption in the region of the Herzberg and Wulf bands (Fally et al., 2000). This interfering absorption only impacts DIAL measurements using wavelengths shorter than 294 nm, i.e. the tropospheric ozone DIAL system in the case selection. In addition, the impact depends on the position of the laser line with respect to the position of the individual Herzberg lines. When the lines are coincident and the resulting absorption non-negligible, the expression of uncertainty for this component due to random and systematic effects and propagated to ozone number density and mixing ratio can be formulated in the same manner as the other interfering gases, with the exception that the O₂ mixing ratio q_{O_2} is a well-known constant ($q_{O_2} \sim 0.209$):

- Random effects, Rayleigh backscatter case:

$$u_{NO3(\Delta\sigma_{O_2R})}(k) = \frac{2q_{O_2}N_a(k)}{|\Delta\sigma_{O_3}(k)|} \sqrt{u_{\sigma_{O_2-1(R)}}^2(k) + u_{\sigma_{O_2-3(R)}}^2(k)} \quad (42)$$

$$u_{qO3(\Delta\sigma_{O_2R})}(k) = \frac{2q_{O_2}}{|\Delta\sigma_{O_3}(k)|} \sqrt{u_{\sigma_{O_2-1(R)}}^2(k) + u_{\sigma_{O_2-3(R)}}^2(k)} \quad (43)$$

- Random effects, Raman backscatter case:

$$u_{NO3(\Delta\sigma_{O_2R})}(k) = \frac{q_{O_2}N_a(k)}{|\Delta\sigma_{O_3}(k)|} \sqrt{u_{\sigma_{O_2-1(R)}}^2(k) + u_{\sigma_{O_2-2(R)}}^2(k) + u_{\sigma_{O_2-3(R)}}^2(k) + u_{\sigma_{O_2-4(R)}}^2(k)} \quad (44)$$

$$u_{qO3(\Delta\sigma_{O_2R})}(k) = \frac{q_{O_2}}{|\Delta\sigma_{O_3}(k)|} \sqrt{u_{\sigma_{O_2-1(R)}}^2(k) + u_{\sigma_{O_2-2(R)}}^2(k) + u_{\sigma_{O_2-3(R)}}^2(k) + u_{\sigma_{O_2-4(R)}}^2(k)} \quad (45)$$

- Systematic effects, single dataset, both Rayleigh and Raman backscatter:

$$u_{NO3(\Delta\sigma_{O_2S})}(k) = \frac{q_{O_2}N_a(k)}{|\Delta\sigma_{O_3}(k)|} |u_{\sigma_{O_2-1(S)}}(k) + u_{\sigma_{O_2-2(S)}}(k) - u_{\sigma_{O_2-3(S)}}(k) - u_{\sigma_{O_2-4(S)}}(k)| \quad (46)$$

$$u_{qO3(\Delta\sigma_{O_2S})}(k) = \frac{q_{O_2}}{|\Delta\sigma_{O_3}(k)|} |u_{\sigma_{O_2-1(S)}}(k) + u_{\sigma_{O_2-2(S)}}(k) - u_{\sigma_{O_2-3(S)}}(k) - u_{\sigma_{O_2-4(S)}}(k)| \quad (47)$$

- Systematic effects, two different datasets for ON and OFF wavelengths, both Rayleigh and Raman backscatter:

$$u_{NO3(\Delta\sigma_{O_2S})}(k) = \frac{q_{O_2}N_a(k)}{|\Delta\sigma_{O_3}(k)|} \sqrt{(u_{\sigma_{O_2-1(S)}}(k) + u_{\sigma_{O_2-2(S)}}(k))^2 + (u_{\sigma_{O_2-3(S)}}(k) + u_{\sigma_{O_2-4(S)}}(k))^2} \quad (48)$$

$$u_{qO3(\Delta\sigma_{O_2S})}(k) = \frac{q_{O_2}}{|\Delta\sigma_{O_3}(k)|} \sqrt{(u_{\sigma_{O_2-1(S)}}(k) + u_{\sigma_{O_2-2(S)}}(k))^2 + (u_{\sigma_{O_2-3(S)}}(k) + u_{\sigma_{O_2-4(S)}}(k))^2} \quad (49)$$

Equations (42)-(49) show that the ozone mixing ratio uncertainty due to O₂ absorption is directly proportional to the relative uncertainty in the O₂ cross-section.

Information / data	Type / value / equation	Notes / description
Name of effect	Oxygen absorption cross section differential	

Contribution identifier	4d	
Measurement equation parameter(s) subject to effect	$\Delta\sigma_{ig}$	Eq. 7, 8
Contribution subject to effect (final product or sub-tree intermediate product)	N_{O_3}, q_{O_3}	Eq. 7, 8
Time correlation extent & form	None	
Other (non-time) correlation extent & form	None	
Uncertainty PDF shape		
Uncertainty & units	<2%	Only important for measurement wavelengths shorter than 294 nm
Sensitivity coefficient	1	
Correlation(s) between affected parameters	N/A	
Element/step common for all sites/users?	Yes	
Traceable to ...	Leblanc et al., 2016c	
Validation	N/A	

6.6.5 Interfering gases' atmospheric profiles (4e)

Another source of uncertainty introduced in **Eq. (7)** is the *a priori* use of ancillary NO_2 and SO_2 number density or mixing ratio profiles. The term “*a priori*” here does not mean that the ozone DIAL retrieval uses a variational/optimal estimation method (it does not), but simply means that the information comes from ancillary (i.e., non-lidar) measurements or models, and is input as “truth” in the ozone DIAL processing chain. The input quantities in this case can be of a different nature, namely mixing ratio or number density (e.g., Ahmad et al., 2007; Bauer et al., 2012; Bracher et al., 2005; Brohede et al., 2007; Brühl et al., 2013; Cao et al., 2006; Hopfner et al., 2013; He et al., 2014; McLinden et al., 2014). In order to ensure self-consistency in our measurement model, input quantities independent of air number density should be chosen:

- When the input quantity independent of air number density is the interfering gas' number density N_{ig} (with uncertainty u_{Nig}), the propagated ozone number density and mixing ratio uncertainties should be written:

$$u_{NO_3(Nig)}(k) = \left| \frac{\Delta\sigma_{ig}(k)}{\Delta\sigma_{O_3}(k)} \right| u_{Nig}(k) \text{ with } ig = NO_2, SO_2 \quad (50)$$

$$u_{qO_3(Nig)}(k) = \frac{1}{N_a(k)} \left| \frac{\Delta\sigma_{ig}(k)}{\Delta\sigma_{O_3}(k)} \right| u_{Nig}(k) \text{ with } ig = NO_2, SO_2 \quad (51)$$

- When the input quantity independent of air number density is the interfering gas' mixing ratio q_{ig} (with uncertainty u_{qig}), the propagated ozone number density and mixing ratio uncertainties should be written:

$$u_{NO_3(qig)}(k) = N_a(k) \left| \frac{\Delta\sigma_{Nig}(k)}{\Delta\sigma_{O_3}(k)} \right| u_{qig}(k) \text{ with } ig = NO_2, SO_2 \quad (52)$$

$$u_{qO_3(qig)}(k) = \left| \frac{\Delta\sigma_{Nig}(k)}{\Delta\sigma_{O_3}(k)} \right| u_{qig}(k) \text{ with } ig = NO_2, SO_2 \quad (53)$$

Equation (53) shows that the lidar-retrieved ozone mixing ratio uncertainty due to the interfering gases is directly proportional to the gases' mixing ratio uncertainty. The NO₂ mixing ratio uncertainty component remains very small in most cases. One exception is for highly-polluted boundary layer conditions where NO₂ mixing ratio can reach 10 to 100 ppbv, resulting in ozone mixing ratio uncertainty of 0.5 to 5 ppbv for the most-commonly used DIAL wavelengths. Tropospheric ozone DIAL pairs are more affected in polluted conditions case due to the larger SO₂ absorption cross-section differential at the wavelengths used for tropospheric ozone DIAL.

Information / data	Type / value / equation	Notes / description
Name of effect	Interfering gases' atmospheric profiles	
Contribution identifier	4e	
Measurement equation parameter(s) subject to effect	N_{ig}, q_{ig}	Eq. 7, 8
Contribution subject to effect (final product or sub-tree intermediate product)	NO ₃ , qO ₃	Eq. 7, 8
Time correlation extent & form	Various time scales	Will change with each measurement session due to varying experimental conditions in terms of atmospheric composition
Other (non-time) correlation extent & form	None	
Uncertainty PDF shape	Poisson/normal	
Uncertainty & units	NO ₂ : 0.01-10% tropospheric DIAL 0.001-0.1% stratospheric DIAL SO ₂ : 0.01-100% tropospheric DIAL 0.001-0.1% stratospheric DIAL	Uncertainty depends on wavelengths used for the measurement (tropospheric or stratospheric DIAL)
Sensitivity coefficient	1	
Correlation(s) between affected parameters	None	
Element/step common for all sites/users?	Yes	
Traceable to ...	Leblanc et al., 2016c	
Validation	None	

6.6.6 Uncertainty owing to air number density, temperature and pressure profiles (4f)

The last input quantity to consider in our ozone DIAL measurement model is ancillary air number density. Air density is generally not estimated directly, but rather derived from air temperature and pressure. Here we provide expressions for the propagation of this uncertainty component for both cases, i.e., when air number density is considered the input quantity, and when temperature and pressure are considered the input quantities.

6.6.6.1 Estimation from air number density profile

If the air number density N_a is not derived from air temperature and pressure, then its uncertainty

u_{Na} can be propagated directly to ozone number density and mixing ratio. The result however will be different whether mixing ratio or number density is used as input quantity for the interfering gases' profiles:

- If number density is used as input quantity for the interfering gases' profiles:

$$u_{NO3(Na)}(k) = \left| \frac{\Delta\sigma_M + q_{O2}\Delta\sigma_{O2}(k)}{\Delta\sigma_{O3}(k)} \right| u_{Na}(k) \quad (54)$$

$$u_{qO3(Na)}(k) = \left| q_{O3} + \frac{\Delta\sigma_M + q_{O2}\Delta\sigma_{O2}(k)}{\Delta\sigma_{O3}(k)} \right| \frac{u_{Na}(k)}{N_a(k)} \quad (55)$$

- If mixing ratio is used as input quantity for the interfering gases' profiles:

$$u_{NO3(Na)}(k) = \left| \frac{\Delta\sigma_M + \Delta\sigma_{NO2}(k)q_{NO2}(k) + \Delta\sigma_{SO2}(k)q_{SO2}(k) + q_{O2}\Delta\sigma_{O2}(k)}{\Delta\sigma_{O3}(k)} \right| u_{Na}(k) \quad (56)$$

$$u_{qO3(Na)}(k) = \left| q_{O3} + \frac{\Delta\sigma_M + \Delta\sigma_{NO2}(k)q_{NO2}(k) + \Delta\sigma_{SO2}(k)q_{SO2}(k) + q_{O2}\Delta\sigma_{O2}(k)}{\Delta\sigma_{O3}(k)} \right| \frac{u_{Na}(k)}{N_a(k)} \quad (57)$$

In **Eqs. (54)-(57)**, the effect of absorption by O_2 in the Herzberg and Wulf bands region is included. This term can be neglected if the ON and OFF wavelengths are longer than 294 nm. In **Eq. (57)**, it is again assumed that the interfering gases' mixing ratio profiles are independent from the air number density profile (no covariance terms involved).

6.6.6.2 Estimation from air temperature and pressure profile

When using radiosonde measurements, meteorological analysis, or assimilation models, the air number density is typically derived from air temperature T_a and pressure p_a following the ideal gas law (with k_B being the Boltzmann constant):

$$N_a(k) = \frac{p_a(k)}{k_B T_a(k)} \quad (58)$$

In this case, air number density is no longer the input quantity, but air temperature and pressure are. The propagation of uncertainty due to the use of an *a priori* temperature and pressure profile now depends on the degree of correlation between pressure and temperature.

- If temperature and pressure are measured or computed independently, with uncertainty estimates u_{Ta} and u_{pa} respectively, and if number density is used as input quantity for the interfering gases, the air number density uncertainty propagated to ozone number density and mixing ratio will be:

$$u_{NO3(Na)}(k) = \left| \frac{\Delta\sigma_M + q_{O2}\Delta\sigma_{O2}(k)}{\Delta\sigma_{O3}(k)} \right| N_a(k) \sqrt{\frac{u_{pa}^2(k)}{p_a^2(k)} + \frac{u_{Ta}^2(k)}{T_a^2(k)}} \quad (59)$$

$$u_{qO3(Na)}(k) = \left| \frac{\Delta\sigma_M + q_{O2}\Delta\sigma_{O2}(k)}{\Delta\sigma_{O3}(k)} \right| \sqrt{\frac{u_{pa}^2(k)}{p_a^2(k)} + \frac{u_{Ta}^2(k)}{T_a^2(k)}} \quad (60)$$

- If temperature and pressure are measured or computed independently, with uncertainty estimates u_{Ta} and u_{pa} respectively, and if mixing ratio is used as input quantity for the interfering gases, the air number density uncertainty propagated to ozone number density will be:

$$u_{NO3(Na)}(k) = \left| \frac{\Delta\sigma_M + q_{NO2}\Delta\sigma_{NO2}(k) + q_{SO2}\Delta\sigma_{SO2}(k) + q_{O2}\Delta\sigma_{O2}(k)}{\Delta\sigma_{O3}(k)} \right| N_a(k) \sqrt{\frac{u_{pa}^2(k)}{p_a^2(k)} + \frac{u_{Ta}^2(k)}{T_a^2(k)}} \quad (61)$$

- If temperature and pressure are known to be fully correlated, and if number density is used as input quantity for the interfering gases, the ozone number density uncertainty due to air number density will be written:

$$u_{NO3(Na)}(k) = \left| \frac{\Delta\sigma_M + q_{O2}\Delta\sigma_{O2}(k)}{\Delta\sigma_{O3}(k)} \right| N_a(k) \left| \frac{u_{pa}(k)}{p_a(k)} - \frac{u_{Ta}(k)}{T_a(k)} \right| \quad (62)$$

- If temperature and pressure are known to be fully correlated, and if mixing ratio is used as input quantity for the interfering gases, the ozone number density uncertainty due to air number density will be written:

$$u_{NO3(Na)}(k) = \left| \frac{\Delta\sigma_M + q_{NO2}\Delta\sigma_{NO2}(k) + q_{SO2}\Delta\sigma_{SO2}(k) + q_{O2}\Delta\sigma_{O2}(k)}{\Delta\sigma_{O3}(k)} \right| N_a(k) \left| \frac{u_{pa}(k)}{p_a(k)} - \frac{u_{Ta}(k)}{T_a(k)} \right| \quad (63)$$

Because the ozone and interfering gases' absorption cross-sections depend on temperature, the covariance terms of the cross-section differentials and the air number density covariance matrix are not strictly zero. However the correlation coefficients are expected to be very small and the assumption of two "independent" input quantities still holds.

The largest ozone uncertainty in the upper stratosphere is that due to pressure. DIAL pairs using longer wavelengths (e.g., 299/316 nm) are more impacted than pairs using shorter wavelengths, in particular the tropospheric ozone DIAL. Note that with current pressure-temperature measurement capabilities (typically 0.5 K and 0.1 hPa uncertainties), the lidar-retrieved ozone uncertainty due to temperature is about 10 times larger than that due to pressure uncertainty.

Information / data	Type / value / equation	Notes / description
Name of effect	External air number density, temperature and pressure profiles	This table corresponds to both 6.6.6.1 and 6.6.6.2
Contribution identifier	4f	
Measurement equation parameter(s) subject to effect	N_a	Eq. 7
Contribution subject to effect (final product or sub-tree intermediate product)	N_{O3} , q_{O3}	Eq. 7, 8
Time correlation extent & form	Various time scales	Will change with each measurement session due to varying experimental conditions in terms of atmospheric state
Other (non-time) correlation extent & form	None	
Uncertainty PDF shape	Poisson/normal	
Uncertainty & units	<1% for stratospheric ozone, <0.1% for tropospheric ozone. When using VMR, the uncertainty associated with this item can be substantial; linked to the uncertainty of the source information	
Sensitivity coefficient	1	
Correlation(s) between affected parameters	None	
Element/step common for all sites/users?	Yes	

Traceable to ...	Leblanc et al., 2016c	
Validation	Godin-Beekmann et al., 2003 Brinksma et al., 2000	

6.7 Spatiotemporal integration (5)

6.7.1 Propagation of uncertainty when combining two intensity ranges (5a)

Ozone DIAL instruments are most often designed with multiple signal intensity ranges in order to maximize the overall altitude range of the profile. Reduced signal intensity is achieved using neutral density filters or other optical systems attenuating the Rayleigh-backscattered signals, or using Raman backscatter channels which typically are 750 times weaker than Rayleigh backscatter channels. Until now, our ozone DIAL measurement model referred to a single intensity range. We now provide a formulation for the propagation of uncertainty when at least two intensity ranges are combined to form a single profile. Combining individual intensity ranges into a single profile can occur either during lidar signal processing or after the ozone number density is calculated individually for each intensity range. Here we present the case of combining ozone number density after it was calculated for individual intensity ranges. The case of combining the lidar signals is presented in **Leblanc et al., 2016a** and is applied in the selected cases for GaiaClim. The principles governing the propagation of uncertainty are the same in both cases.

A single profile covering the entire useful range of the instrument is typically obtained by combining the most accurate overlapping sections of the profiles retrieved from individual ranges. The thickness of the transition region typically varies from a few meters to a few kilometres, depending on the instrument and on the intensity ranges considered. Assuming that the transition region's bottom altitude is $z(k_1)$ and its top altitude is $z(k_2)$, the combined ozone profile between a low range i_L and a high range i_H , is typically obtained by computing a weighted average of the ozone values retrieved for each range:

$$N_{O_3}(k) = w(k)N_{O_3}(k, i_L) + (1 - w(k))N_{O_3}(k, i_H) \quad k_1 < k < k_2 \text{ and } 0 < w(k) < 1 \quad (64)$$

$$q_{O_3}(k) = w(k)q_{O_3}(k, i_L) + (1 - w(k))q_{O_3}(k, i_H) \quad k_1 < k < k_2 \text{ and } 0 < w(k) < 1 \quad (65)$$

Using this formulation, all uncertainty components associated with atmospheric extinction corrections are propagated without change as they do not depend on the intensity range considered:

$$u_{NO_3(X)}(k) = u_{NO_3(X)}(k, i_L) = u_{NO_3(X)}(k, i_H) \text{ for all } k \quad (66)$$

$$u_{qO_3(X)}(k) = u_{qO_3(X)}(k, i_L) = u_{qO_3(X)}(k, i_H) \text{ for all } k \quad (67)$$

With $X = \Delta\sigma_{O_3}, \Delta\sigma_M, Na, \Delta\sigma_{ig}, Nig, \Delta\sigma_{O_2}$ and $ig = NO_2, SO_2$.

Because of its random nature, ozone uncertainty due to detection noise for the combined profile is obtained by adding in quadrature (no covariance terms) the detection noise uncertainties of the individual ranges:

$$u_{NO_3(DET)}(k) = \sqrt{(w(k)u_{NO_3(DET)}(k, i_L))^2 + ((1 - w(k))u_{NO_3(DET)}(k, i_H))^2} \quad k_1 < k < k_2 \quad (68)$$

$$u_{qO_3(DET)}(k) = \sqrt{(w(k)u_{qO_3(DET)}(k, i_L))^2 + ((1 - w(k))u_{qO_3(DET)}(k, i_H))^2} \quad k_1 < k < k_2 \quad (69)$$

Assuming that the saturation correction and the background noise extraction have been applied consistently for all intensity ranges within the same data processing algorithm, the associated uncertainty components can be propagated to the combined profile assuming full correlation between the intensity ranges:

$$u_{NO_3(X)}(k) = |w(k)u_{NO_3(X)}(k, i_L) + (1 - w(k))u_{NO_3(X)}(k, i_H)| \quad k_1 < k < k_2 \quad (70)$$

$$u_{qO_3(X)}(k) = |w(k)u_{qO_3(X)}(k, i_L) + (1 - w(k))u_{qO_3(X)}(k, i_H)| \quad k_1 < k < k_2 \quad (71)$$

with $X = SAT, BKG$.

Information / data	Type / value / equation	Notes / description
Name of effect	Combining two intensity ranges	
Contribution identifier	5	
Measurement equation parameter(s) subject to effect	$\text{NO}_3, q_{\text{O}_3}$	Eq. 7, 8
Contribution subject to effect (final product or sub-tree intermediate product)	$\text{NO}_3, q_{\text{O}_3}$	Eq. 7, 8
Time correlation extent & form	Same as underlying profile	See text
Other (non-time) correlation extent & form	None	
Uncertainty PDF shape	Same as underlying profile	See text
Uncertainty & units	Same as underlying profile	See text
Sensitivity coefficient	1	
Correlation(s) between affected parameters	Yes	1-4
Element/step common for all sites/users?	Yes	
Traceable to ...	Leblanc et al., 2016c	
Validation	Kuang et al., 2011	

7 Uncertainty summary

Having reviewed and propagated all the independent uncertainty components considered in our ozone DIAL measurement model, we can combine them into a single total uncertainty estimate:

- If number density is used as input quantity for the interfering gases, the combined standard uncertainty of retrieved ozone number density and mixing ratio can be written:

$$u_{NO_3}(k) = \sqrt{u_{NO_3(DET)}^2(k) + u_{NO_3(SAT)}^2(k) + u_{NO_3(BKG)}^2(k) + u_{NO_3(Na)}^2(k) + u_{NO_3(NNO_2)}^2(k) + u_{NO_3(NSO_2)}^2(k) + u_{NO_3(\Delta\sigma O_3R)}^2(k) + u_{NO_3(\Delta\sigma NO_2R)}^2(k) + u_{NO_3(\Delta\sigma SO_2R)}^2(k) + u_{NO_3(\Delta\sigma O_2R)}^2(k) + u_{NO_3(\Delta\sigma O_3S)}^2(k) + u_{NO_3(\Delta\sigma NO_2S)}^2(k) + u_{NO_3(\Delta\sigma SO_2S)}^2(k) + u_{NO_3(\Delta\sigma O_2S)}^2(k) + u_{NO_3(\Delta\sigma M)}^2(k)} \quad (72)$$

$$u_{qO_3}(k) = \sqrt{u_{qO_3(DET)}^2(k) + u_{qO_3(SAT)}^2(k) + u_{qO_3(BKG)}^2(k) + u_{qO_3(Na)}^2(k) + u_{qO_3(NNO_2)}^2(k) + u_{qO_3(NSO_2)}^2(k) + u_{qO_3(\Delta\sigma O_3R)}^2(k) + u_{qO_3(\Delta\sigma NO_2R)}^2(k) + u_{qO_3(\Delta\sigma SO_2R)}^2(k) + u_{qO_3(\Delta\sigma O_2R)}^2(k) + u_{qO_3(\Delta\sigma O_3S)}^2(k) + u_{qO_3(\Delta\sigma NO_2S)}^2(k) + u_{qO_3(\Delta\sigma SO_2S)}^2(k) + u_{qO_3(\Delta\sigma O_2S)}^2(k) + u_{qO_3(\Delta\sigma M)}^2(k)} \quad (73)$$

- If mixing ratio is used as input quantity for the interfering gases, the combined standard uncertainty of retrieved ozone number density and mixing ratio can be written:

$$u_{NO_3}(k) = \sqrt{u_{NO_3(DET)}^2(k) + u_{NO_3(SAT)}^2(k) + u_{NO_3(BKG)}^2(k) + u_{NO_3(Na)}^2(k) + u_{NO_3(qNO_2)}^2(k) + u_{NO_3(qSO_2)}^2(k) + u_{NO_3(\Delta\sigma O_3R)}^2(k) + u_{NO_3(\Delta\sigma NO_2R)}^2(k) + u_{NO_3(\Delta\sigma SO_2R)}^2(k) + u_{NO_3(\Delta\sigma O_2R)}^2(k) + u_{NO_3(\Delta\sigma O_3S)}^2(k) + u_{NO_3(\Delta\sigma NO_2S)}^2(k) + u_{NO_3(\Delta\sigma SO_2S)}^2(k) + u_{NO_3(\Delta\sigma O_2S)}^2(k) + u_{NO_3(\Delta\sigma M)}^2(k)} \quad (74)$$

$$u_{qO_3}(k) = \sqrt{u_{qO_3(DET)}^2(k) + u_{qO_3(SAT)}^2(k) + u_{qO_3(BKG)}^2(k) + u_{qO_3(Na)}^2(k) + u_{qO_3(qNO_2)}^2(k) + u_{qO_3(qSO_2)}^2(k) + u_{qO_3(\Delta\sigma O_3R)}^2(k) + u_{qO_3(\Delta\sigma NO_2R)}^2(k) + u_{qO_3(\Delta\sigma SO_2R)}^2(k) + u_{qO_3(\Delta\sigma O_2R)}^2(k) + u_{qO_3(\Delta\sigma O_3S)}^2(k) + u_{qO_3(\Delta\sigma NO_2S)}^2(k) + u_{qO_3(\Delta\sigma SO_2S)}^2(k) + u_{qO_3(\Delta\sigma O_2S)}^2(k) + u_{qO_3(\Delta\sigma M)}^2(k)} \quad (75)$$

Though **Eqs. (72)-(73)** are exclusive of **Eqs. (74)-(75)**, the resulting combined uncertainty is quantitatively identical in both formulations if we assume identical input quantity uncertainty values. The only difference between the two sets of equations is a re-distribution of the contribution of the components due to the ancillary number densities or mixing ratios. Because of the correlated terms, the ozone combined standard uncertainty should not be computed for individual intensity ranges and then merged into a single profile. Instead, the individual uncertainty components should first be propagated to the merged profile (**Eqs. (64)-(71)**) and then added in quadrature to obtain the combined standard uncertainty (**Eqs. (72)-(75)**).

Similarly, the total combined ozone density (or mixing ratio) uncertainty can be used to characterize a single profile, but should not be used for the combination of “dependent” profiles (for example a climatology computed from multiple profiles measured by the same instrument). Instead, uncertainty components due to systematic effects in altitude and/or time must be separated from components due to random effects. Typically, uncertainty due to detection noise will always be added in quadrature, while for other components, knowledge (type-A or type-B estimation) of the covariance matrix in the time and/or altitude dimension(s) will be needed. For this reason, it is recommended to always keep a trace of each individual component together with the combined standard uncertainty.

For stratospheric ozone lidar observations with the lidar located above the boundary layer, the ozone number density standard uncertainty results mainly from three components, namely, Rayleigh extinction cross section differential at the bottom of the profile, ozone absorption cross section differential in the middle of the profile, and detection noise at the top of the profile. For the derived ozone mixing ratio, the uncertainty component associated with the *a priori* use of ancillary

air pressure is largely dependent on the uncertainty of the used source profile, which when combining for instance a radio sounding with a reanalysis product, may introduce a large change in uncertainty at the switch between sources. For ozone number density and ozone mixing ratio uncertainty alike, the dominant source above 40-45 km is detection noise, depending on the site altitude and laser strength. For lidars located at lower altitudes, local air pollution may play a role and (interfering gases) should be considered when pollution conditions occur. An example of the magnitude and vertical distribution of the error contributions is illustrated in Fig. 7, which applies to one specific lidar, but -although with caution, may be taken as representative for similar stratospheric ozone lidars. In addition the error contributions due to variable atmospheric conditions may be location specific.

For tropospheric ozone lidar observations with the lidar located above the boundary layer, the combined ozone number density standard uncertainty results mainly from the ozone absorption cross section differential uncertainty. Below 12 km, the uncertainty owing to Rayleigh extinction cross section differential and detection noise are the other important components. Uncertainty owing to detection noise dominates in the upper part of the profile (above 22 km). For lidars located at lower altitudes inside the boundary layer, interfering gases may play a substantial role, depending on local circumstances and the time of observation. The total uncertainty will thus depend on location (altitude and air composition) and the chosen lidar setup (laser strength, wavelengths, etc.). An example of the magnitude and vertical distribution of the error contributions is illustrated in Fig. 8.

Uncertainty summary for stratospheric ozone:

Element identifier	Contribution name	Uncertainty contribution form	Typical value	Traceability level (L/M/H)	random, structured random, quasi-systematic or systematic?	Correlated to? (Use element identifier)
1	Emission sub-system	N/A	Negligible	M	Systematic	None
2	Receiving sub-system					
2a	Optical parameters	N/A	Negligible for well designed and maintained systems	M	Systematic	1
2b	Alignment	N/A	Negligible in most cases	M	Systematic	1
3	Pre-processing					
3a	Detection noise	Poiss/norm distribution	Large (10-100%) at top of profile, increasing with a factor 20 every 10 km above the ozone maximum where it is 0.3-5%)	H	Random	3b, 3c
3b	Saturation	N/A	Largest at	H	Systematic	3a, 3c

	correction		bottom of partial profile (~1%), rapidly decreasing with altitude			
3c	Background noise	Poiss/norm distribution	1% near top of profile, negligible 12 km below	H	Random	3a, 3b
4	External inputs					
4a	Ozone absorption cross section differential	N/A	2%	H	Random and systematic	None
4b	Rayleigh extinction cross section differential	N/A	Largest in lower part of profile (<10%), below 1% above 20 km	H	Systematic	None
4c1	NO ₂ cross section differential	N/A	Variable in space and time, often negligible	H	Systematic	None
4c2	SO ₂ cross section differential	N/A	Variable in space and time, often negligible	H	Systematic	None
4d	O ₂ cross section differential	N/A	0 (only affects wavelength shorter than 294 nm)	H	Systematic	None
4e	Profiles of interfering gases	N/A	Often negligible except in highly polluted areas	L	Random and Systematic	4c1, 4c2
4f	Number density, temperature and pressure	N/A	<1% for ozone in number density, large contribution in mixing ratio, depending on uncertainty of source	M	Random and Systematic	4a, 4b, 4c1, 4c2, 4d, 4e
5	Spatiotemporal integration					
5a	Combining two intensity ranges	N/A	Negligible	M	Random	None

Uncertainty summary for tropospheric ozone (lidar located above boundary layer):

Element identifier	Contribution name	Uncertainty contribution form	Typical value	Traceability level (L/M/H)	random, structured random, quasi-systematic or systematic?	Correlated to? (Use element identifier)
1	Emission sub-system		Negligible			
2	Receiving sub-system		Negligible			
2a	Optical parameters	N/A	Negligible for well designed and maintained systems	M	Systematic	1
2b	Alignment	N/A	Negligible in most cases	M	Systematic	1
3	Pre-processing					
3a	Detection noise	Poiss/norm distribution	Large (20%) at top of profile (25 km), lowest near bottom (1-2% at 3 km)	H	Random	3b, 3c
3b	Saturation correction	N/A	Largest near bottom of partial profile (>10%), rapidly decreases with altitude	H	Systematic	3a, 3c
3c	Background noise	Poiss/norm distribution	1% at top of partial profiles, decreasing with signal strength to <0.1%	H	Random	3a, 3b
4	External inputs					
4a	Ozone absorption cross section differential	N/A	4-6% depending on wavelength	H	Random and systematic	None
4b	Rayleigh extinction cross section differential	N/A	<10% at bottom of profile, decreasing with altitude	H	Systematic	None
4c1	NO ₂ cross section differential	N/A	variable in space (NO ₂ concentration) and time, often negligible	H	Systematic	None
4c2	SO ₂ cross section	N/A	variable in	H	Systematic	None

	differential		space and time, often negligible			
4e	O ₂ cross section differential	N/A	Effect depends on laser beam characteristics, typically <0.3% at bottom of profile and decreasing with altitude	H	Systematic	None
4f	Profiles of interfering gases	N/A	Often negligible except in polluted areas	L	Random and Systematic	4c1, 4c2
4g	Number density, temperature and pressure	N/A	<0.1%	M	Random and Systematic	4a, 4b, 4c1, 4c2, 4d, 4e
5	Spatiotemporal integration		Negligible			
5a	Combining two intensity ranges	N/A	Negligible	M	Random	None

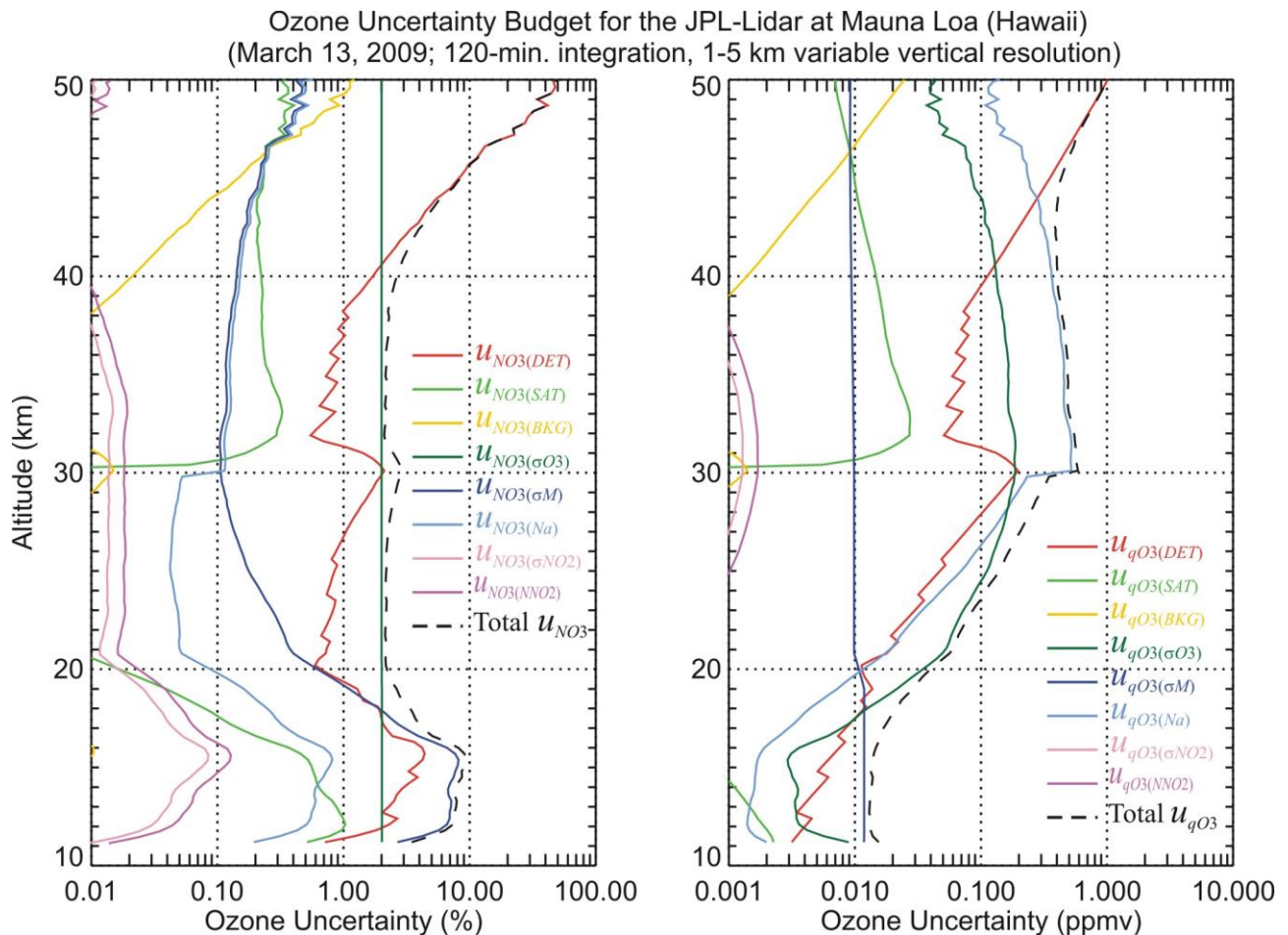


Figure 7. From Leblanc et al. (2016b, their Fig. 16). Example of ozone relative uncertainty (left) and mixing ratio uncertainty (right) budgets computed for the JPL stratospheric ozone DIAL located at Mauna Loa Observatory (Hawaii) for a nighttime observation.

Ozone Uncertainty Budget for the tropospheric ozone lidar at JPL-Table Mountain (California)
(November 18, 2009; 120-min. integration, 0.5-1.5 km variable vertical resolution)

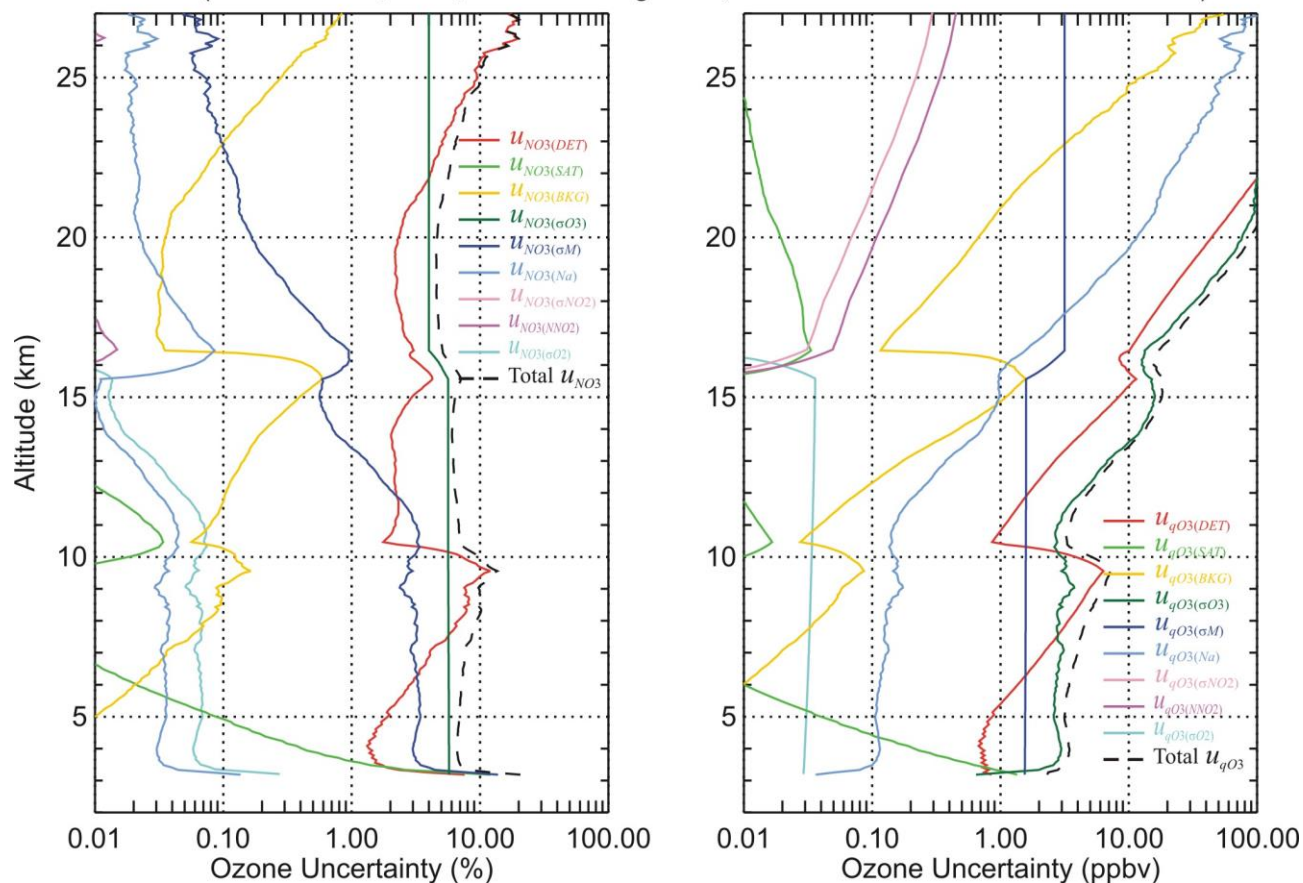


Figure 8. From Leblanc et al. (2016b, their Fig. 17). Example of ozone uncertainty budgets for the JPL tropospheric ozone lidar at Table Mountain (California) for number density (left) and mixing ratio (right) for a nighttime observation.

8 Traceability uncertainty analysis

Traceability level definition is given in Table 2.

Table 2. Traceability level definition table

Traceability Level	Descriptor	Multiplier
High	SI traceable or globally recognised community standard	1
Medium	Developmental community standard or peer-reviewed uncertainty assessment	3
Low	Approximate estimation	10

Analysis of the uncertainty summaries would suggest the following contributions, shown in Table 3, should be considered further to improve the overall uncertainty of the DIAL ozone profile product. The entires are given in an estimated priority order.

Table 3. Traceability level definition further action table.

Element identifier	Contribution name	Uncertainty contribution form	Typical value	Traceability level (L/M/H)	random, structured random, quasi-systematic or systematic?	Correlated to? (Use element identifier)
4f	Profiles of interfering gases	N/A	Often negligible except in polluted areas	L	Random and Systematic	4c1, 4c2
4g	Number density, temperature and pressure	N/A	<0.1%	M	Random and Systematic	4a, 4b, 4c1, 4c2, 4d, 4e

8.1 Recommendations

For the benefit of increasing the usability of ozone profile data originating from Differential Absorption Lidar instruments the recommendations are:

1. Application of the uncertainty propagation as outlined above and in more detailed form in Leblanc et al. (2016b, 2016c) is recommended for all ozone lidar systems, in particular those linked up in networks.
2. It should be technically feasible to set-up and operate a centralised data processing facility for ozone lidar data, which would have the obvious benefit of homogeneous data processing and therefore uncertainty budget estimation
3. Various variable uncertainty sources have been identified that are hard to quantify or highly variable in space/time or instrument-specific. These are listed as uncertainty boxes that are not filled green in Figures 8 and 9 which are expansions of those in section 5 (Figures 5 and 6). Further research into these items, and consideration of these items for individual systems when determining their PTU, is recommended.
4. In the current uncertainty analysis, use of only photon counting is assumed. It is recommended to include analysis for analog detection as well as the hybrid analog and photon counting detection modes. This may be of particular interest for the application for tropospheric ozone DIAL.

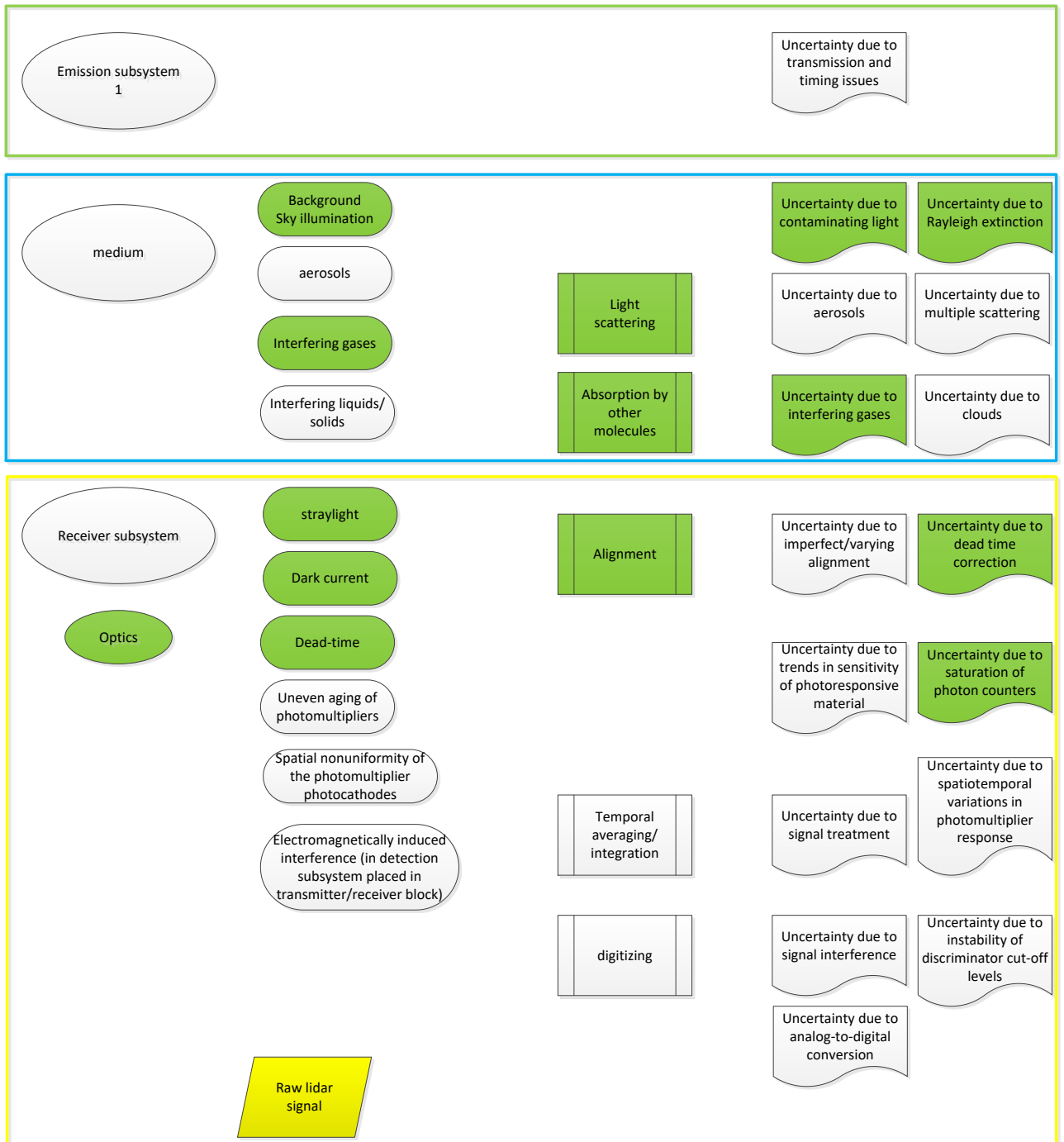


Figure 9. Expansion of flow chart in Fig. 5. Various variable uncertainty sources have been identified that are hard to quantify or highly variable in space/time or instrument-specific. These are listed as uncertainty boxes that are not filled green in the flowchart below which is an expansion of the one in section 5.

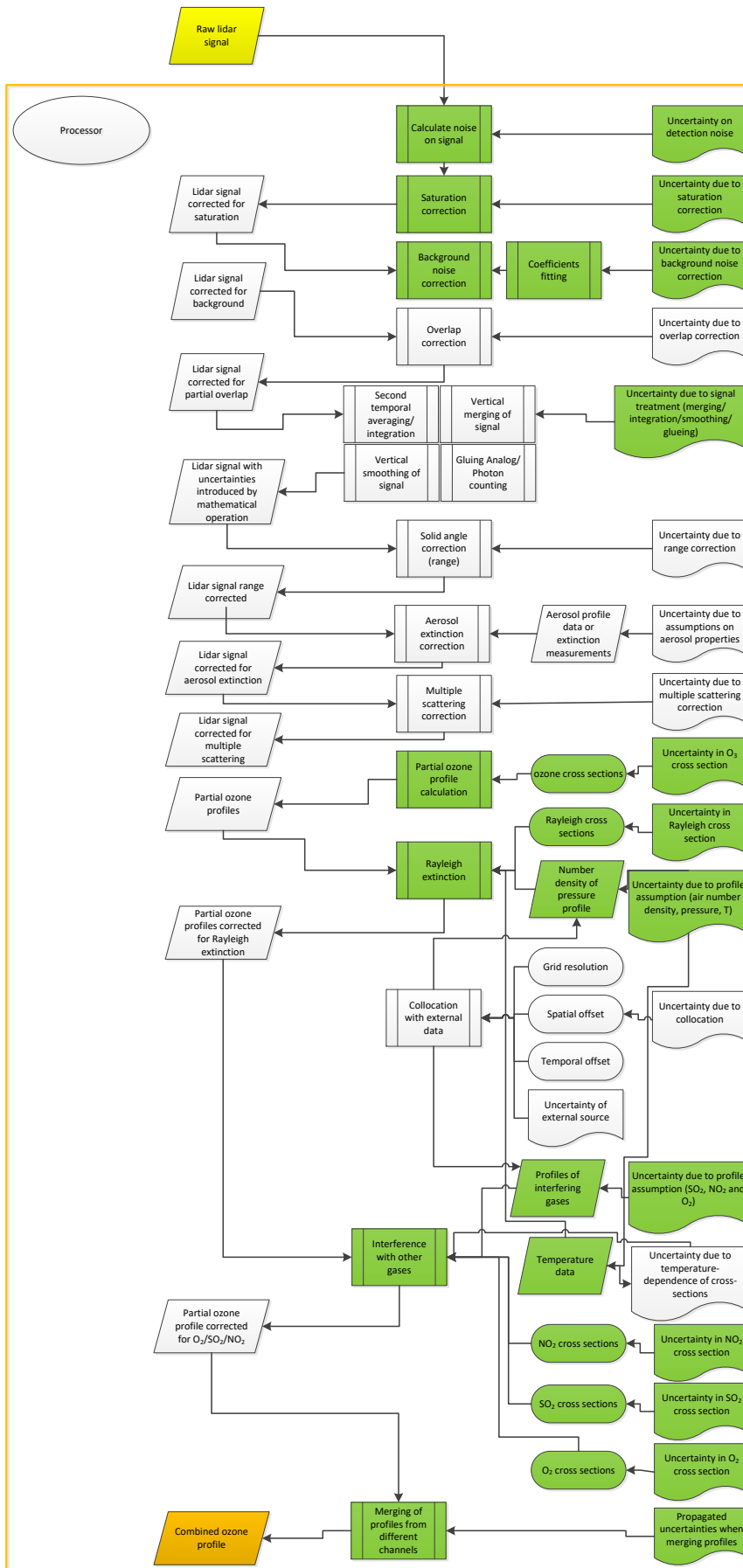


Figure 10. Expansion of flow chart in Fig. 6. Various variable uncertainty sources have been identified that are hard to quantify or highly variable in space/time or instrument-specific. These are listed as uncertainty boxes that are not filled green in the flowchart below which is an expansion of the one in section 5.

9 Conclusion

The ozone profile differential absorption lidar product has been assessed against the GAIA CLIM traceability and uncertainty criteria.

References

1. Ahmad, Z., McClain, C. R., Herman, J. R., Franz, B. A., Kwiatkowska, E. J., Robinson, W. D., Bucsela, E. J., and Tzortziou, M.: Atmospheric correction for NO₂ absorption in retrieving water-leaving reflectances from the SeaWiFS and MODIS measurements, *Appl. Opt.*, 46(26), 6504-6512, 2007.
2. Bass, A. M., and Paur, R. J.: The Ultraviolet Cross-sections of Ozone: I. The Measurements, *Proc. Quadriennial Ozone Symp.*, Halkidiki, Greece, 606-616, 1984.
3. Bates, D. R.: Rayleigh-scattering by air, *Planet Space Sci.*, 32, 785-790, 10.1016/0032-0633(84)90102-8, 1984.
4. Bauer, R., Rozanov, A., McLinden, C. A., Gordley, L. L., Lotz, W., Russell, J. M., Walker, K. A., Zawodny, J. M., Ladstätter-Weissenmayer, A., Bovensmann, H., and Burrows, J. P.: Validation of SCIAMACHY limb NO₂ profiles using solar occultation measurements, *Atmos. Meas. Tech.*, 5, 1059-1084, 10.5194/amt-5-1059-2012, 2012.
5. Bogumil, K., Orphal, J., Homann, T., Voigt, S., Spietz, P., Fleischmann, O. C., Vogel, A., Hartmann, M., Kromminga, H., Bovensmann, H., Frerick, J., and Burrows, J. P.: Measurements of molecular absorption spectra with the SCIAMACHY pre-flight model: instrument characterization and reference data for atmospheric remote-sensing in the 230-2380 nm region, *J. Photochem. Photobiol. A*, 157, 167-184, 10.1016/s1010-6030(03)00062-5, 2003.
6. Bracher, A., Sinnhuber, M., Rozanov, A., and Burrows, J. P.: Using a photochemical model for the validation of NO₂ satellite measurements at different solar zenith angles, *Atmos. Chem. Phys.*, 5, 393-408, 10.5194/acp-5-393-2005, 2005.
7. Brinksma, E.J., Bergwerff, J.B., Bodeker, G.E., Boersma, K.F., Boyd, I.S., Connor, B.J., de Haan, J.F., Hogervorst, W., Hovenier, J.W., Parrish, A., Tsou, J.J., Zawodny, J.M., and Swart, D.P.J.: Validation of 3 years of ozone measurements over Network for the Detection of Stratospheric Change station Lauder, New Zealand, *J. Geophys. Res.*, 105(D13), 17291-17306, doi:10.1029/2000JD900143, 2000.
8. Brion, J., Chakir, A., Charbonnier, J., Daumont, D., Parrisé, C., and Malicet, J.: Absorption Spectra Measurements for the Ozone Molecule in the 350-830 nm Region, *J. Atmos. Chem.*, 30, 291-299, 10.1023/a:1006036924364, 1998.
9. Bristow, M.P.: Lidar-signal compression by photomultiplier gain modulation: influence of detector nonlinearity, *Appl. Opt.* 37, 6468-6479, 1998.
10. Brohede, S., McLinden, C. A., Berthet, G., Haley, C. S., Murtagh, D., and Sioris, C. E.: A stratospheric NO₂ climatology from Odin/OSIRIS limb-scatter measurements, *Can. J. Phys.*, 85, 1253-1274, 10.1139/p07-141, 2007.
11. Brühl, C., Lelieveld, J., Höpfner, M., and Tost, H.: Stratospheric SO₂ and sulphate aerosol, model simulations and satellite observations, *Atmos. Chem. Phys. Discuss.*, 13, 11395-11425, 10.5194/acpd-13-11395-2013, 2013.
12. Burrows, J. P., Richter, A., Dehn, A., Deters, B., Himmelmann, S., and Orphal, J.: Atmospheric remote-sensing reference data from GOME - 2. Temperature-dependent absorption cross-sections of O-3 in the 231-794 nm range, *J. Quant. Spectr. Rad. Trans.*, 61, 509-517, 10.1016/s0022-4073(98)00037-5, 1999.
13. Bucholtz, A.: Rayleigh-scattering calculations for the terrestrial atmosphere, *Appl. Opt.*, 34(15), 2765-2773, 1995.
14. Cao, N., Fukuchi, T., Fujii, T., Collins, R. L., Li, S., Wang, Z., and Chen, Z.: Error analysis for NO₂ DIAL measurement in the troposphere, *Appl. Phys. B: Lasers and Optics*, 82, 141-148, 10.1007/s00340-005-2050-8, 2006.
15. Chehade, W., Gorshelev, V., Serdyuchenko, A., Burrows, J. P., and Weber, M.: Revised temperature-dependent ozone absorption cross-section spectra (Bogumil et al.) measured with the SCIAMACHY satellite spectrometer, *Atmos. Meas. Tech.*, 6, 3055-3065,

- doi:10.5194/amt-6-3055-2013, 2013.
16. Daumont, D., Brion, J., Charbonnier, J., and Malicet, J.: Ozone UV Spectroscopy I: Absorption Cross-Sections at Room Temperature, *J. Atmos Chem.*, 15, 145-155, 10.1007/bf00053756, 1992.
 17. Donovan, D. P., Whiteway, J. A., and Carswell, A. I.: Correction for nonlinear photon-counting effects in lidar systems, *Appl. Opt.*, 32(33), 6742-6753, 1993.
 18. Eberhard, W. L.: Correct equations and common approximations for calculating Rayleigh scatter in pure gases and mixtures and evaluation of differences, *Appl. Opt.*, 49(7), 1116-1130, 2010.
 19. Eisele, H. and Trickl, T.: Improvements of the aerosol algorithm in ozone lidar data processing by use of evolutionary strategies, *Appl. Opt.*, 44, 2638–2651, 2005.
 20. Fally, S., Vandaele, A. C., Carleer, M., Hermans, C., Jenouvrier, A., Merienne, M. F., Coquart, B., and Colin, R.: Fourier transform spectroscopy of the O-2 Herzberg bands. III. Absorption cross-sections of the collision-induced bands and of the Herzberg continuum, *J. Mol. Spectrosc.*, 204, 10-20, 10.1006/jmsp.2000.8204, 2000.
 21. Freudenthaler, V., Linné, H., Chaikovski, A., Rabus, D., and Groß, S.: EARLINET lidar quality assurance tools, *Atmos. Meas. Tech. Discuss.*, <https://doi.org/10.5194/amt-2017-395>, in review, 2018.
 22. Godin-Beekmann, S., Porteneuve, J., and Garnier, A.: Systematic DIAL lidar monitoring of the stratospheric ozone vertical distribution at Observatoire de Haute-Provence (43.92 degrees N, 5.71 degrees E), *J. Environ. Monit.*, 5, 57-67, 10.1039/b205880d, 2003.
 23. Godin-Beekmann, S., and Nair, P. J.: Sensitivity of stratospheric ozone lidar measurements to a change in ozone absorption cross-sections, *J. Quant. Spectr. Rad. Trans.*, 113, 1317-1321, 10.1016/j.jqsrt.2012.03.002, 2012.
 24. He, H., Loughner, C. P., Stehr, J. W., Arkinson, H. L., Brent, L. C., Follette-Cook, M. B., Tzortziou, M. A., Pickering, K. E., Thompson, A. M., Martins, D. K., Diskin, G. S., Anderson, B. E., Crawford, J. H., Weinheimer, A. J., Lee, P., Hains, J. C., and Dickerson, R. R.: An elevated reservoir of air pollutants over the Mid-Atlantic States during the 2011 DISCOVER-AQ campaign: Airborne measurements and numerical simulations, *Atmos. Env.*, 85, 18-30, 10.1016/j.atmosenv.2013.11.039, 2014.
 25. Hinkley, E. D.: Laser monitoring of the atmosphere, *Topics in applied physics*, 14, Springer-Verlag, New York, 380 pp., 1976.
 26. Hopfner, M., Glatthor, N., Grabowski, U., Kellmann, S., Kiefer, M., Linden, A., Orphal, J., Stiller, G., von Clarmann, T., Funke, B., and Boone, C. D.: Sulfur dioxide (SO₂) as observed by MIPAS/Envisat: temporal development and spatial distribution at 15-45 km altitude, *Atmos. Chem. Phys.*, 13, 10405-10423, 10.5194/acp-13-10405-2013, 2013.
 27. Jenouvrier, A., Merienne, M. F., Coquart, B., Carleer, M., Fally, S., Vandaele, A. C., Hermans, C., and Colin, R.: Fourier transform spectroscopy of the O-2 Herzberg bands - I. Rotational analysis, *J. Mol. Spectrosc.*, 198, 136-162, 10.1006/jmsp.1999.7950, 1999.
 28. Kuang, S., Burris, J.F., Newchurch, M.J., Johnson, S. and Long, S.: Differential absorption lidar to measure sub-hourly variation of tropospheric ozone profiles, *IEEE Trans. on GeoSc. and Rem. Sens.*, 49(1), 557-571, 2011.
 29. Leblanc, T., Sica, R. J., van Gijssel, J. A. E., Godin-Beekmann, S., Haefele, A., Trickl, T., Payen, G., and Gabarrot, F.: Proposed standardized definitions for vertical resolution and uncertainty in the NDACC lidar ozone and temperature algorithms – Part 1: Vertical resolution, *Atmos. Meas. Tech.*, 9, 4029-4049, <https://doi.org/10.5194/amt-9-4029-2016>, 2016a.
 30. Leblanc, T., Sica, R. J., van Gijssel, J. A. E., Godin-Beekmann, S., Haefele, A., Trickl, T., Payen, G., and Liberti, G.: Proposed standardized definitions for vertical resolution and uncertainty in the NDACC lidar ozone and temperature algorithms – Part 2: Ozone DIAL uncertainty budget, *Atmos. Meas. Tech.*, 9, 4051-4078, <https://doi.org/10.5194/amt-9-4051-2016>, 2016b.

31. Leblanc, T., Sica R., van Gijsel, A., Godin-Beekmann, S., Haefele, A., Trickl, T., Payen, G., and Liberti, G.: Standardized definition and reporting of vertical resolution and uncertainty in the NDACC lidar ozone and temperature algorithms, ISSI Team on NDACC Lidar Algorithms Report, available for download at: http://www.issibern.ch/teams/ndacc/ISSI_Team_Report.htm, 2016c.
32. McDermid, I. S., Godin, S. M., and Lindquist L. O.: Ground-based laser DIAL system for long-term measurements of stratospheric ozone, *Appl. Opt.*, 29, 3603–3612, 1990.
33. McDermid, I. S., Beyerle, G., Haner, D. A., and Leblanc, T.: Redesign and improved performance of the tropospheric ozone lidar at the Jet Propulsion Laboratory Table Mountain Facility, *Appl. Opt.*, 41, 7550–7555, 2002.
34. McGee, T. J., Gross, M. R., Singh, U. N., Butler, J. J., and Kimvilakani, P. E.: Improved stratospheric ozone lidar, *Opt. Eng.*, 34, 1421–1430, 1995.
35. McLinden, C. A., Fioletov, V., Boersma, K. F., Kharol, S. K., Krotkov, N., Lamsal, L., Makar, P. A., Martin, R. V., Veefkind, J. P., and Yang, K.: Improved satellite retrievals of NO₂ and SO₂ over the Canadian oil sands and comparisons with surface measurements, *Atmos. Chem. Phys.*, 14, 3637–3656, 10.5194/acp-14-3637-2014, 2014.
36. Measures, R. M.: *Laser remote sensing: fundamentals and applications*, Wiley, 510 pp., 1984.
37. Mégie, G., Allain, J. Y., Chanin, M. L., and Blamont, J. E.: Vertical Profile of Stratospheric Ozone by Lidar Sounding from Ground, *Nature*, 270, 32–9–331, 1977.
38. Merienne, M. F., Jenouvrier, A., Coquart, B., Carleer, M., Fally, S., Colin, R., Vandaele, A. C., and Hermans, C.: Improved data set for the Herzberg band systems of O-16(2), *J. Mol. Spectrosc.*, 207, 120–120, 10.1006/jmsp.2001.8314, 2001.
39. Mohr, P. J., Taylor, B. N., and Newell, D. B.: CODATA recommended values of the fundamental physical constants: 2006, *Rev. Mod. Phys.*, 80, 633–730, 10.1103/RevModPhys.80.633, 2008.
40. Müller, J. W.: Dead-time problems, *Nucl. Instr. and Meth.*, 112, 47–57, 10.1016/0029-554x(73)90773-8, 1973.
41. Papayannis, A., Ancellet, G., Pelon, J., and Megie, G.: Multiwavelength lidar for ozone measurements in the troposphere and the lower stratosphere, *Appl. Opt.*, 29, 467–476, 1990.
42. Press, W. H.; Flannery, B. P., Teukolsky, S. A., and Vetterling W. T.: *Numerical Recipes: The Art of Scientific Computing* (1st ed.), New York, Cambridge University Press. ISBN 978-0-521-88068-8, 1986.
43. Serdyuchenko, A., Gorshchev, V., Weber, M., Chehade, W., and Burrows, J. P.: High spectral resolution ozone absorption cross-sections - Part 2: Temperature dependence, *Atmos. Meas. Tech.*, 7, 625–636, 10.5194/amt-7-625-2014, 2014.
44. Simeonov, V., Larcheveque, G., Quaglia, P., van den Bergh, H. and Calpini, V.: Influence of the photomultiplier tube spatial uniformity on lidar signals, *Appl. Opt.* 38, 5186–5190, 1999.
45. Strutt, J. W. (Lord Rayleigh): XXXIV. On the transmission of light through an atmosphere containing small particles in suspension, and on the origin of the blue of the sky, *Philos. Mag.*, 47, 375–384, 10.1080/14786449908621276, 1899.
46. Sullivan, J. T., McGee, T. J., Leblanc, T., Sumnicht, G. K., and Twigg, L. W.: Optimization of the GSFC TROPOZ DIAL retrieval using synthetic lidar returns and ozonesondes – Part 1: Algorithm validation, *Atmos. Meas. Tech.*, 8, 4133–4143, 10.5194/amt-8-4133-2015, 2015.
47. Weitkamp, C.: *Lidar: Range-Resolved Optical Remote Sensing of the Atmosphere*, Springer Series in Optical Sciences, 102, Springer, 460 pp., 2005.



Product Traceability and Uncertainty for the temperature profile lidar product

Version 0.4

*GAIA-CLIM
Gap Analysis for Integrated
Atmospheric ECV Climate Monitoring
Mar 2015 - Feb 2018*

A Horizon 2020 project; Grant agreement: 640276

Date: 19 January 2018

Dissemination level: Final

*Work Package 2; Compiled by
Arnoud Apituley, Anne van Gijzel (KNMI)*



Royal Netherlands
Meteorological Institute
Ministry of Infrastructure
and Water Management

Table of Contents

1	Product overview	4
1.1	Guidance notes	4
2	Introduction.....	7
3	Instrument description.....	8
3.1	Retrieval methodology	9
4	Product Traceability Chain	16
5	Element contributions	18
5.1	Alignment (1)	18
5.2	Pre-processing (2).....	20
5.2.1	Detection noise (2a)	20
5.2.2	Saturation (pulse pile-up) correction (2b).....	22
5.2.3	Background noise extraction (2c)	24
5.3	External inputs (3).....	26
5.3.1	Rayleigh extinction cross section (3a)	26
5.3.2	Uncertainty owing to air number density, temperature and pressure profiles (3b).....	28
5.3.4	Interfering gases' cross sections (3c)	30
5.3.5	Interfering gases' atmospheric profiles (3d)	32
5.3.6	Acceleration of gravity (3e)	34
5.3.7	Molecular mass of air (3f).....	36
5.3.8	External temperature for tie-on at the top of the profile (3g).....	37
5.4	Spatio-temporal integration (4)	38
5.4.1	Propagation of uncertainty when vertically filtering (smoothing) the lidar signal or temperature profile (4a)	38
5.4.2	Propagation of uncertainty when merging multiple channels together (4b).....	40
6	Uncertainty summary	42
7	Traceability uncertainty analysis	45
7.1	Recommendations	46
8	Conclusion	48
	References.....	49

Version history

Version	Principal updates	Owner	Date
0.3 draft	First draft	KNMI	12.12.2017
0.4 draft	Advanced draft	KNMI	11.01.2018
0.4e	Incorporating TG's comments	KNMI	15.01.2018
0.4f	Final draft	KNMI	16.01.2018
0.4g	Final version	KNMI	02.02.2018

1 Product overview

Product name: Temperature profile

Product technique: Rayleigh/Mie, Raman Lidar

Product measurand: Temperature (T)

Product form/range: profile (ground to 110 km, 15/30 to 70 km, 1-8 hours averaged)

Product dataset: Temperature profile

Site/Sites/Network location:

- Table Mountain, Wrightwood CA, USA
- Mauna Loa, Hawaii, USA
- Purple Crow Lidar, Ontario, Canada

Product time period: Jan 1 – Dec 31, 2014

Data provider: NDACC

Instrument provider: Various

Product assessor: Arnoud Apituley, KNMI

Assessor contact email: apituley@knmi.nl

1.1 Guidance notes

For general guidance see the Guide to Uncertainty in Measurement & its Nomenclature, published as part of the GAIA-CLIM project.

This document is a measurement product technical document which should be stand-alone i.e. intelligible in isolation. Reference to external sources (preferably peer-reviewed) and documentation from previous studies is clearly expected and welcomed, but with sufficient explanatory content in the GAIA CLIM document not to necessitate the reading of all these reference documents to gain a clear understanding of the GAIA CLIM product and associated uncertainties entered into the Virtual Observatory (VO).

In developing this guidance, we have created a convention for the traceability identifier numbering as shown in Figure 1. The ‘main chain’ from raw measurand to final product forms the axis of the diagram, with top level identifiers (i.e. 1, 2, 3 etc.). Side branch processes add sub-level components to the top level identifier (for example, by adding alternate letters & numbers, or 1.3.2 style nomenclature).

The key purpose of this sub-level system is that all the uncertainty from a sub-level are summed in the next level up.

For instance, using Figure 1, contributors 2a1, 2a2 and 2a3 are all assessed as separate components to the overall traceability chain (have a contribution table). The contribution table for (and uncertainty associated with) 2a, should combine all the sub-level uncertainties (and any additional uncertainty intrinsic to step 2a). In turn, the contribution table for contributor 2, should include all uncertainties in its sub-levels.

Therefore, only the top level identifiers (1, 2, 3, etc.) shown in bold in the summary table need be combined to produce the overall product uncertainty. The branches can therefore be considered in isolation, for the more complex traceability chains, with the top level contribution table transferred to the main chain. For instance, see Figure 2 & Figure 3 as an example of how the chain can be divided into a number of diagrams for clearer representation.

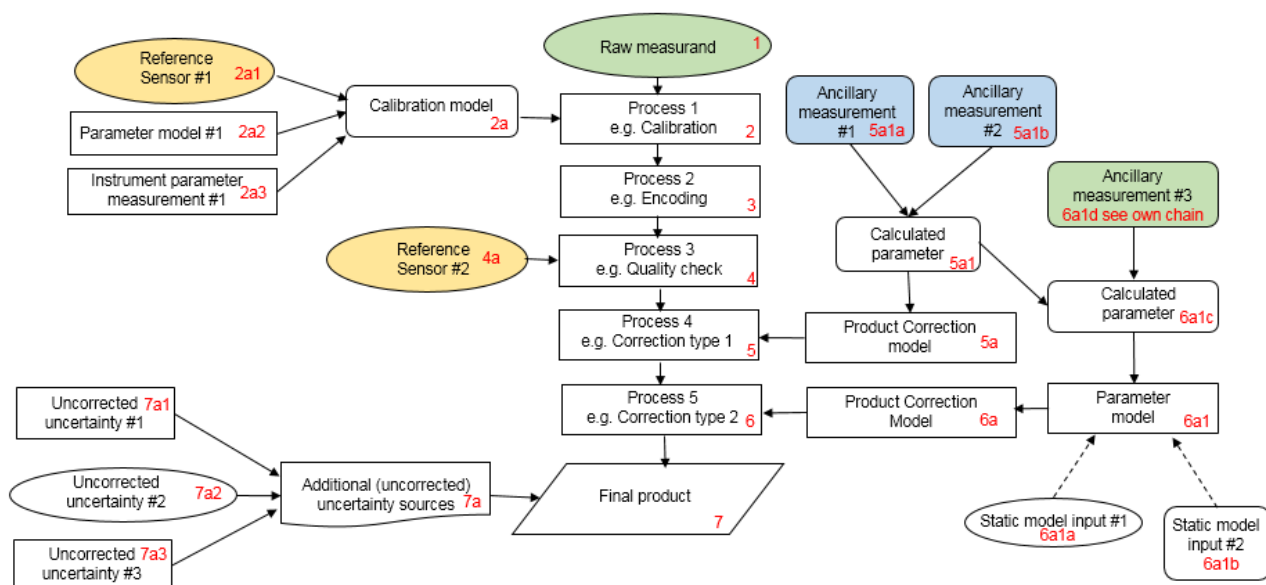


Figure 1. Example traceability chain. Green represents a key measurand or ancillary measurand recorded at the same time with the product raw measurand. Yellow represents a source of traceability. Blue represents a static ancillary measurement

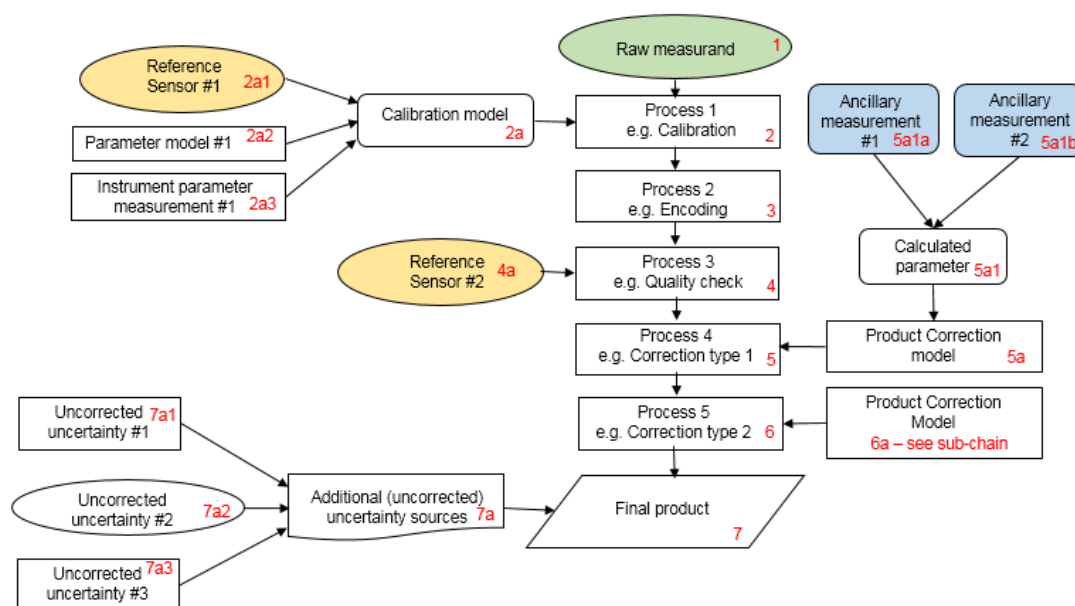


Figure 2. Example chain as sub-divided chain. Green represents a key measurand or ancillary measurand recorded at the same time with the product raw measurand. Yellow represents a source of traceability. Blue represents a static ancillary measurement

When deciding where to create an additional sub-level, the most appropriate points to combine the uncertainties of sub-contributions should be considered, with additional sub-levels used to illustrate where their contributions are currently combined in the described process.

A short note on colour coding. Colour coding can/should be used to aid understanding of the key contributors, but we are not suggesting a rigid framework at this time. In Figure 1, green represents a key measurand or ancillary or complementary measurand recorded at the same time with the raw measurand; yellow represents a primary source of traceability & blue represents a static ancillary measurement (site location, for instance). Any colour coding convention you use, should be clearly described.

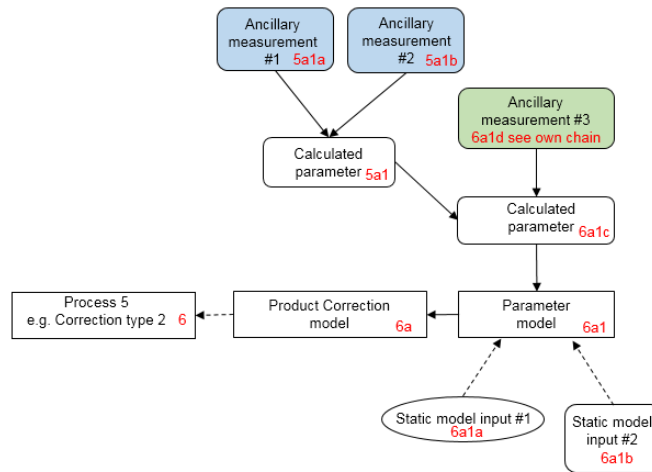


Figure 3. Example chain contribution 6a sub-chain. Green represents a key measurand or ancillary measurand recorded at the same time with the product raw measurand. Blue represents a static ancillary measurement

The contribution table to be filled for each traceability contributor has the form seen in Table 1.

Table 1. The contributor table.

Information / data	Type / value / equation	Notes / description
Name of effect		
Contribution identifier		
Measurement equation parameter(s) subject to effect		
Contribution subject to effect (final product or sub-tree intermediate product)		
Time correlation extent & form		
Other (non-time) correlation extent & form		
Uncertainty PDF shape		
Uncertainty & units		
Sensitivity coefficient		
Correlation(s) between affected parameters		
Element/step common for all sites/users?		
Traceable to ...		
Validation		

Name of effect – The name of the contribution. Should be clear, unique and match the description in the traceability diagram.

Contribution identifier - Unique identifier to allow reference in the traceability chains.

Measurement equation parameter(s) subject to effect – The part of the measurement equation influenced by this contribution. Ideally, the equation into which the element contributes.

Contribution subject to effect – The top level measurement contribution affected by this contribution. This can be the main product (if on the main chain), or potentially the root of a side branch contribution. It will depend on how the chain has been sub-divided.

Time correlation extent & form – The form & extent of any correlation this contribution has in time.

Other (non-time) correlation extent & form – The form & extent of any correlation this contribution has in a non-time domain. For example, spatial or spectral.

Uncertainty PDF shape – The probability distribution shape of the contribution, Gaussian/Normal Rectangular, U-shaped, log-normal or other. If the form is not known, a written description is sufficient.

Uncertainty & units – The uncertainty value, including units and confidence interval. This can be a simple equation, but should contain typical values.

Sensitivity coefficient – Coefficient multiplied by the uncertainty when applied to the measurement equation.

Correlation(s) between affected parameters – Any correlation between the parameters affected by this specific contribution. If this element links to the main chain by multiple paths within the traceability chain, it should be described here. For instance, SZA or surface pressure may be used separately in a number of models & correction terms that are applied to the product at different points in the processing. See Figure 1, contribution 5a1, for an example.

Element/step common for all sites/users – Is there any site-to-site/user-to-user variation in the application of this contribution?

Traceable to – Describe any traceability back towards a primary/community reference.

Validation – Any validation activities that have been performed for this element?

2 Introduction

This document presents the Product Traceability and Uncertainty (PTU) information for temperature profiles retrieved with Rayleigh/Mie and Raman lidars. It does not cover measurements made with the pure rotational Raman, DIAL, Brillouin-Doppler nor optimal estimation techniques, and not for resonance fluorescence lidar observations. Specifically, we will focus on discussing the uncertainties associated with the temperature retrieval using the density integration technique. The aim of this document is to provide supporting information for the users of this product within the GAIA-CLIM VO. The uncertainty and traceability information contained in this document is based on the details given in Leblanc et al. (2016c, 2016d).

Leblanc et al. (2016c) describe an approach for the definition, propagation, and reporting of uncertainty in the temperature profile lidar data products contributing to the Network for the Detection of Atmospheric Composition Change (NDACC) database. One essential aspect of the proposed approach is the propagation in parallel of all independent uncertainty components through

the data processing chain before they are combined together to form the temperature combined standard uncertainty.

The independent uncertainty components contributing to the overall budget cover signal detection, saturation correction, background noise extraction, and temperature to tie-on at the top of the profile, as well as minor components such as absorption cross-sections of ozone and NO₂, the molecular extinction cross-sections, the use of ancillary air, ozone, and NO₂ number densities, the acceleration of gravity, and the molecular mass of air. The expression of the individual uncertainty components and their step-by-step propagation through the temperature profile processing chain are thoroughly estimated. All sources of uncertainty except detection noise imply correlated terms in the vertical dimension, which requires knowledge of the covariance matrix when the lidar signal is integrated from the top of the profile.

The temperature uncertainty budget is presented as much as possible in a generic form (i.e., as a function of instrument performance and wavelength) so that investigators can calculate uncertainty estimates for their own instrument in a straightforward manner and assess the expected impact. The approach and recommendations described here apply to the density integration technique (Hauchecorne and Chanin, 1980), but not to the Optimal Estimation Method (OEM; Sica and Haefele, 2015), for which vertical resolution and uncertainties are computed implicitly by the OEM.

3 Instrument description

The basic setup of a typical, vertically pointing lidar system is shown in Figure 4. The lidar technique, acronym for "light detection and ranging", is based on the transmission into the atmosphere of short light pulses, with duration ranging from a few to several hundreds of nanoseconds, by a laser transmitter, directly or by means of transmission optics. In any point of the atmospheric volume crossed by the laser beam, a portion of the incident light is backscattered by atmospheric constituents. This backscattered light is collected by a receiving telescope. The light received from the atmosphere passes through an optical system, consisting of various elements (lenses, mirrors, filters, etc.), which selects specific wavelengths of the light collected by the telescope. The light from the optical system is forwarded to detectors, typically photomultipliers that convert the light into electrical signals.

An electronic trigger circuit synchronizes the data acquisition to start with the emission of each laser pulse so that atmospheric signals are acquired as a function of elapsed time with respect to the emission of each laser pulse, from which distance can be inferred unambiguously. These signals are the lidar signals, measuring the intensity of the light backscattered by the atmosphere as a function of the distance from the lidar.

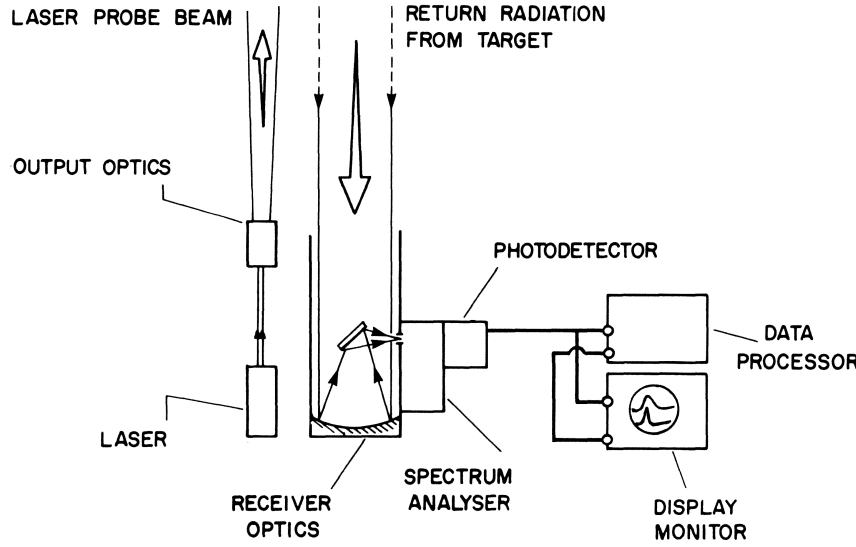


Figure 4. Schematic of a basic vertically pointing lidar system (Measures, 1984)

Temperature profiles in the middle atmosphere (15-80 km) have been measured by lidar since the 1980s using the density integration technique (e.g., Hauchecorne and Chanin, 1980; Keckhut et al., 1993, 2011). In the articles describing these measurements, the uncertainty is often limited to statistical noise (e.g., Hauchecorne and Chanin, 1980), and it is less common to include other components such as saturation (e.g., Leblanc et al., 1998), ozone absorption correction (Sica et al., 2001) or the initialization of temperature with an external data source at the top of the profile (Argall, 2007). Leblanc et al. (1998) provide a review of the most common error sources made in the lidar temperature retrievals which were assessed with synthetic lidar signals. NDACC intercomparison campaigns have also contributed to assessing lidar measurement uncertainties (Keckhut et al., 2004).

3.1 Retrieval methodology

To retrieve a temperature profile in the stratosphere or mesosphere using the density integration technique, we start from the Lidar Equation (e.g., Hinkley, 1976; Weitkamp, 2005). This equation in its most compressed form describes the emission of light by a laser source, its backscatter at altitude z , its extinction and scattering along its path up and back, and its collection back on a detector:

$$P(z, \lambda_E, \lambda_R) = P_L(\lambda_E) \frac{\eta(z, \lambda_R) \delta z}{(z - z_L)^2} \tau_{UP}(z, \lambda_E) \beta(z, \lambda_E, \lambda_R) \tau_{DOWN}(z, \lambda_R) \quad (1)$$

- λ_E is the laser emission wavelength and λ_R is the receiver detection wavelength;
- P is the total number of photons collected at wavelength λ_R on the lidar detector surface;
- δz is the thickness of the backscattering layer sounded during the time interval δt ($\delta z = c \delta t / 2$, where c is the speed of light);
- P_L is the number of photons emitted at the emission wavelength λ_E ;
- η is the optical efficiency of the receiving channel, including optical and spectral transmittance and geometric obstruction;
- z is the altitude of the backscattering layer;
- z_L is the altitude of the lidar (laser and receiver assumed to be at the same altitude);
- β is the total backscatter coefficient (including particulate β_P and molecular β_M backscatter);
- τ_{UP} is the optical thickness integrated along the outgoing beam path between the lidar and the scattering altitude z , and is defined as

$$\tau_{UP}(z) = \exp \left[- \int_{z_L}^z \left(\sigma_M(\lambda_E) N_a(z') + \alpha_P(z', \lambda_E) + \sum_i \sigma_i(z', \lambda_E) N_i(z') \right) dz' \right] \quad (2)$$

$-\tau_{DOWN}$ is the optical thickness integrated along the returning beam path between the scattering altitude z and the lidar receiver, and is defined as

$$\tau_{DOWN}(z) = \exp \left[- \int_{z_L}^z \left(\sigma_M(\lambda_R) N_a(z') + \alpha_P(z', \lambda_R) + \sum_i \sigma_i(z', \lambda_R) N_i(z') \right) dz' \right] \quad (3)$$

where σ_M is the molecular extinction cross section due to Rayleigh scattering (Strutt, 1899) (hereafter called “Rayleigh cross section” for brevity), N_a is the air number density, α_P is the particulate extinction coefficient, σ_i is the absorption cross section of absorbing constituent i , and N_i is the number density of absorbing constituent i . For altitudes between the ground and 90 km, the Rayleigh cross-sections can be considered constant with altitude, and therefore depend only on wavelength. The absorption cross-sections however are in most cases temperature-dependent, and should be taken as a function of both altitude and wavelength. Temperature is retrieved by inverting Eq. (1) with respect to the backscatter term β .

If there are no aerosols present, the backscatter coefficient β and, thus, the lidar signal collected on the detector are proportional to the air number density. Temperature can then be computed by vertically integrating the air number density under the assumptions that there is a hydrostatic balance and that the air is an ideal gas (Hauchecorne and Chanin, 1980). This inversion technique works for both elastic scattering (Rayleigh backscatter by the air molecules) and inelastic scattering (vibrational Raman backscatter by the nitrogen molecules) (Strauch et al., 1971; Gross et al., 1997). The backscatter coefficient can generically be written as a function of air number density N_a :

$$\beta(z) = \sigma_\beta N_a(z) \quad (4)$$

For Rayleigh backscatter, the effective cross-section σ_β is the molecular (Rayleigh) scattering cross-section at the emission wavelength λ_E :

$$\sigma_\beta = \sigma_M(\lambda_E) \quad (5)$$

For Raman backscatter, the effective cross-section σ_β is the vibrational Raman scattering cross-section of a well-mixed gas (typically nitrogen) at the Raman-shifted wavelength λ_R , multiplied by the mixing ratio of the well-mixed gas (e.g., 0.781 for nitrogen):

$$\sigma_\beta = 0.781 \sigma_{N_2}(\lambda_E, \lambda_R) \quad (6)$$

Substituting into the lidar equation Eq. (1), we obtain an expression of air number density as a function of the backscatter lidar signal:

$$N_a(z) = \frac{P(z, \lambda_E, \lambda_R) (z - z_L)^2}{\sigma_\beta \eta(z, \lambda_E, \lambda_R) \delta z P_L(\lambda_E) \tau_{UP}(z, \lambda_E) \tau_{DOWN}(z, \lambda_R)} \quad (7)$$

A temperature profile is then calculated assuming hydrostatic balance and assuming that the air is an ideal gas with a constant mean molecular mass:

$$T(z - \delta z) = \frac{N_a(z)}{N_a(z - \delta z)} T(z) + \frac{M_a}{R_a N_a(z - \delta z)} \overline{N_a(z)} \overline{g(z)} \delta z \quad (8)$$

T is the retrieved temperature, M_a is the molecular mass of dry air, R_a is the ideal gas constant, and g is the acceleration of gravity. The horizontal bar above N_a and g represents the average value of N_a and g between z and $z - \delta z$. An essential aspect of the method is that all altitude-independent terms (e.g., Rayleigh cross-section, lidar receiver efficiency) cancel out when computing the ratio of air

number density at altitudes z and $z-\delta z$.

In this PTU, we will not treat uncertainties originating from aerosols (particulate extinction and particulate backscatter), or clouds (causing multiple scattering), as these factors are usually avoided by taking observations in clear air. For instance, temperature profiles from Rayleigh channels start above 25 to 30 km, where air can be considered free from aerosols - unless there is a very large volcanic eruption inserting a substantial number of particles high into the stratosphere which has not been the case for many years. When present, the contribution of particulate extinction and backscatter and multiple scattering is highly variable and it is not feasible to propose a standardised treatment here, but we refer to the work done by Earlinet (Mattis et al., 2016). As most temperature profiles are reported starting at higher altitudes, uncertainty due to correcting for incomplete beam-telescope overlap (which applies only at altitudes in the lower free troposphere) is not treated here either.

To transform the theoretical to a real temperature measurement model, we will consider the following conditions.

1. For each lidar receiver channel, the actual raw signal R recorded in the data files is represented by a vector of discretized values rather than a continuous function of altitude range: $z \rightarrow z(k)$ and $R(z) \rightarrow R(k)$ for $k = 1, nk$.
2. Only channels operating in photon-counting mode are considered in this measurement model. The estimation of the uncertainty due to analog-to-digital signal conversion is highly instrument-dependent, and therefore no meaningful standardized recommendations can be made.
3. Only channels operating in photon-counting mode are considered hereafter. For analog channels, uncertainty due to analog-to-digital signal conversion needs to be estimated. This estimation is highly instrument-dependent, and no meaningful standardized recommendations can therefore be provided.
4. In photon-counting detection mode, the recorded signals result from nonlinear transfer of the detected signals due to the inability of the counting electronics to temporally discriminate a very large number of photon-counts reaching the detector ("pulse pile-up" effect resulting in signal saturation) (e.g., Müller, 1973; Donovan et al., 1993). In the present work, we consider the most frequent case of non-paralyzable photon-counting systems (i.e., using "non-extended dead time", Müller, 1973), which allows for an analytical correction of the pulse pile-up effect.

Given the above four conditions, the photon counts P reaching the detector of a given channel can be expressed as a function of the discretized raw signal R recorded in the data files at altitude $z(k)$:

$$P(k) = \frac{R(k)}{1 - \tau \frac{c}{2\delta z L} R(k)} - B(k) \quad (9)$$

B is the sum of sky and electronic background noise, τ is the photon-counting hardware dead-time characterizing the pulse pile-up effect (sometimes called resolving time), c the speed of light, and L the number of laser pulses for which the signal was actually recorded in the data files.

5. The signal is then corrected for all known altitude-dependent factors according to Eq. (7). For a given channel operating at the emission wavelength λ_E and detection wavelength λ_R (λ_E and λ_R are identical for Rayleigh backscatter channels), N is then defined as the lidar-measured relative number density that can be written as a function of the saturation-background-corrected signal P :

$$N(k) = \frac{(z(k) - z_L)^2}{\eta(k)} P(k) \exp \left(\sum_{k'=0}^k \left((\sigma_{M-E} + \sigma_{M-R}) N_a(k') + \sum_{ig} (\sigma_{ig-E}(k') + \sigma_{ig-R}(k')) N_{ig}(k') \right) \delta z \right) \quad (10)$$

Here, the efficiency factor η does not have to be known in an absolute manner, but only its variation

with altitude range is of importance. Furthermore, if the observation can be considered to be with full overlap between the beam and the telescope field-of-view, η is constant with altitude and does not need to be included at all. The subscript “ M ” refers to the Rayleigh cross-sections and “ ig ” to the absorption cross-sections of the interfering gases. The subscripts extensions E and R refer to the emitted (λ_E) and received wavelengths (λ_R) respectively.

With the assumption of full overlap, the lidar-measured relative number density differs from the air number density only by a constant multiplication factor, and therefore does not need to include any of the constant terms with altitude found in the lidar equation as these terms cancel out in the temperature integration process (which implies the ratio of density at two consecutive altitudes).

6. The temperature profile is initialised at the the top of the profile $z(k_{TOP})$ using an external temperature measurement $T_a(k_{TOP})$ in a procedure called the “temperature tie-on”. Integrating the relative number density obtained from the lidar measurement, the temperature profile can be calculated downward. Eq. (8) then becomes:

$$T(k) = \frac{N(k_{TOP})}{N(k)} T_a(k_{TOP}) + \frac{M_a \delta z}{R_a N(k)} S(k) \quad (11)$$

where $S(k)$ is the discretized version of the summation term in Eq. (7):

$$S(k) = \sum_{k'=k}^{k_{TOP}-1} \overline{N(k')} \overline{g(k')} \quad (12)$$

The horizontal bar above N and g denotes the mean value of N and g in the vertical layer comprised between $z(k')$ and $z(k'+1)$. The lidar-derived relative density N can be approximated by an exponential function of altitude range, and the layer-averaged density is computed using its geometric mean:

$$\overline{N(k')} = \sqrt{N(k') N(k'+1)} \quad (13)$$

The Earth’s gravity field is three-dimensional but its variation with longitude is so small that it can be approximated by a function of latitude and altitude only. For small vertical increments, the variation of g with height is nearly linear, and its layer-averaged value can be expressed as a function of the height h above the reference ellipsoid averaged between $z(k')$ and $z(k'+1)$:

$$\overline{g(k')} = g_0 \left(1 + g_1 \overline{h(k')} + g_2 \overline{h^2(k')} \right) \quad (14)$$

The height above the reference ellipsoid averaged between $z(k')$ and $z(k'+1)$ takes the form:

$$\overline{h(k')} = \frac{1}{2} (h(k') + h(k'+1)) \quad (15)$$

The constants g_0 , g_1 and g_2 in Eq. (14) relate to the Earth’s geometry and to the geodetic latitude of the lidar site. The derivation of the constants g_0 , g_1 and g_2 following the World Geodetic System (NIMA-WGS, 1984) is provided in Leblanc et al. (2016d, section 3.5).

7. Optional smoothing: As in any real physical measurement, detection noise induces undesired high-frequency noise in the raw lidar signals. This noise can be reduced by digitally filtering the signals and/or the retrieved temperature profiles. The filtering process impacts the propagation of uncertainties and therefore should be included in the measurement model. When filtering is applied to the lidar signal (i.e., before temperature is computed), the signal’s exponential decrease with altitude must be taken into account. For a given altitude $z(k)$, the filtering process in this case therefore consists of convolving a set of filter coefficients c_p with the logarithm of the unsmoothed signal s_u ($s_u=R$ or $s_u=P$ or $s_u=N$) to obtain a smoothed signal s_m following:

$$s_m(k) = \exp \left(\sum_{p=-n}^n c_p(k) \log(s_u(k+p)) \right) \quad (16)$$

When vertical filtering is applied to the retrieved temperature profile, the filtering process at each

individual altitude $z(k)$ consists of convolving the filter coefficients c_p with the unsmoothed temperature T to obtain a smoothed temperature T_m following the expression:

$$T_m(k) = \sum_{p=-n}^n c_p(k) T(k+p) \quad (17)$$

In Eqs. (16)-(17), the filter coefficients should be symmetric ($c_p=c_{-p}$ for all p) to achieve proper smoothing. Their number and values determine which noise frequencies will be reduced most. A review of digital filtering and recommendations for the use of standardized vertical resolution definitions are provided in (Leblanc et al., 2016a).

8. Optional merging: Temperature lidar instruments are usually designed with multiple channels of varying signal intensity to maximize the overall altitude range of the profile. Here, the propagation of uncertainty is considered for two channels being merged to form a single profile. This profile covering the entire useful range of the instrument is typically obtained by combining the most accurate overlapping sections of the profiles retrieved from individual channels. Merging individual intensity channels into a single profile can be done either during lidar signal processing or after the temperature is calculated for each individual channel. The thickness of the transition region can vary from a few meters to a few kilometers, depending on the instrument and on the intensity of the channels considered.

When the merging procedure is applied before the temperature profile is computed, it can be done on the raw signals ($s=R$), the saturation-background corrected signals ($s=P$), or the lidar-derived relative density ($s=N$). The signals of the channels to combine are of different magnitude, and signal normalization of one channel with respect to the other is necessary before combining the channels (κ being the scaling factor). Since the signals decrease with altitude is nearly exponential, the merging procedure should be done on the logarithm of the signal rather than the signal itself. Considering a low-intensity channel i_L and a high-intensity channel i_H , and assuming that the transition region's bottom and top altitudes are $z(k_1)$ and $z(k_2)$ respectively, the merged signal s_M at any altitude bin k comprised between k_1 and k_2 is typically obtained by computing a weighted average of the log-signal values s_m (or s if unsmoothed) for each range and at the same altitude bin:

$$s_M(k) = \exp(w(k) \log(s(k, i_L)) + (1-w(k)) \log(\kappa s(k, i_H))) \quad k_1 \leq k \leq k_2 \text{ and } 0 \leq w(k) \leq 1 \quad (18)$$

When the merging procedure is applied to the retrieved temperature profiles, the merged temperature T_M at any altitude bin k comprised between k_1 and k_2 is typically obtained by computing a weighted average of the temperature values T_m (or T if unsmoothed) retrieved for each range at the same altitude bin:

$$T_M(k) = w(k) T_m(k, i_L) + (1-w(k)) T_m(k, i_H) \quad k_1 \leq k \leq k_2 \text{ and } 0 \leq w(k) \leq 1 \quad (19)$$

With this set of equations, the input quantities' standard uncertainty must be introduced, propagated through the temperature measurement model, and then combined to produce a temperature combined standard uncertainty profile.

The instrumentation-related input quantities to consider in the temperature uncertainty budget are:

1. Alignment
2. Detection noise inherent to photon-counting signal detection
3. Saturation (pulse pile-up) correction parameters (typically, photon-counters' dead-time τ)
4. Background noise extraction parameters (typically, fitting parameters for function B)

The last three will be grouped together as pre-processing steps.

Based on Eqs. (10)-(14), the additional input quantities to consider in the NDACC-lidar standardized temperature uncertainty budget are:

5. Rayleigh extinction cross-sections σ_M
6. Ancillary air number density profile N_a (or temperature T_a and pressure p_a profiles)

7. Absorption cross-sections of the interfering gases σ_{ig}
8. Number density profiles N_{ig} (or mixing ratio profile q_{ig}) of the interfering species
9. Acceleration of gravity g
10. The molecular mass of air M_a
11. External (a priori) air temperature for tie-on at the top of the profile $T_a(k_{TOP})$

Besides these eleven factors, uncertainties due to vertical filtering of the lidar signal or the retrieved temperature profile will also be discussed next to the treatment of uncertainties originating from merging signals or retrieved temperature profiles from multiple channels.

The above input quantities are not listed in order of significance, but instead, in the order they are introduced into the lidar temperature model. Quantitatively, the most significant uncertainty components are typically detection noise (1) and temperature tie-on (10) at the top of the profile, and saturation correction (2) and molecular extinction (4 and 5) at the bottom of the profile. The interfering gases “*ig*” to consider in practice are ozone and NO₂. Because of either very low concentrations or very low values of their absorption cross-sections, no other atmospheric gases or molecules are known to interfere with the temperature retrieval. The impact of absorption by ozone on the temperature retrieval is very small (<0.1 K) if working at wavelengths near the ozone minimum absorption region (e.g., 355 nm, 387 nm), but can account for up to 1 K error if neglected when working in the Chappuis band (e.g., 532 nm and 607 nm). Conversely, absorption by NO₂ is very small for temperature retrievals in the Chappuis band, but can account for up to a 0.2 K error if neglected at 355 nm and 387 nm.

The uncertainty contribution of the acceleration of gravity is very small (<0.1 K) provided given an altitude-dependent formulation of gravity (e.g., Eq. (14)) (Lemoine et al., 1998). In the upper mesosphere, the change in the air major species’ mixing ratio induces a change with altitude of the air molecular mass and Rayleigh scattering cross-sections. However the induced changes remain below 0.1 K below 90 km, which is much less than the expected uncertainty arising due to remaining sources such as detection noise and tie-on temperature uncertainty (Argall, 2007). For temperature profiles reaching 100 km or higher, the change of the molecular mass of air with altitude should be taken into account.

When the receiver field-of-view and the laser beam are known to not fully overlap, an additional “instrumentation-related” uncertainty component must be introduced to take into account the overlap correction (altitude-dependent term η in Eq. (10)). Also, if the lidar receiver uses very narrow filters (typically narrower than 0.7 nm), another “instrumentation-related” uncertainty component must be introduced to take this into account: the temperature dependence of the Raman backscatter cross-sections (causing again the term η in Eq. (10) to be altitude-dependent). Because the overlap function and the filter width and position are strongly instrument-dependent, a standardized approach for the treatment of those uncertainty components cannot be proposed here. In the rest of this work, we will therefore assume full overlap and wide-enough filters to prevent an altitude dependence of the lidar transmission function which is valid for the specific subset of lidars being characterised here. As stated above, and for consistency with the ozone and aerosol extinction PTUs, we will nevertheless briefly discuss alignment. The receiver optical parameters and the transmission system will not be treated as these factors are deemed to be of less importance for temperature retrievals.

The exact altitude of each data bin k can be determined experimentally, for example by tracking the exact position in the data stream of the laser beam backscattering off the laser room hatch (assuming that the receiver and the transmission of the laser beam in the atmosphere are located in the same room). The time (i.e., altitude) resolution of today’s state-of-the-art lidar data acquisition hardware is very high (of the order of nanoseconds, i.e., a few meters). The exact altitude of the lidar instrument can also be determined to a precision better than a meter using the current standard

geo-positioning methods. For well-designed and well-validated lidar instruments, there is therefore no uncertainty associated with the determination of altitude, and hence no uncertainty associated with the range correction (z^2) term in Eq. (10).

Uncertainties associated with fundamental physical constants will not be considered here, but we do recommend to use the values reported by the International Council for Science (ICSU) Committee on Data for Science and Technology (CODATA, <http://www.codata.org/>), endorsed by the BIPM (Mohr et al., 2008). Note that if the uncertainty of a fundamental constant is of similar order of magnitude as that of some other uncertainty components already identified, then this constant must be included among the input quantities and its uncertainty should be taken into account and propagated just like all other input quantities.

4 Product Traceability Chain

The PTU is given below for temperature profile retrievals in the mesosphere, stratosphere and upper troposphere with lidar. The PTU is divided into two sections: the physical model is presented in Figure 5 and the processing model in Figure 6. The numbered boxes in these figures indicate the key elements in the PTU chain that are the main contributors to the overall measurement uncertainty. Each of these elements is discussed in Section 5. It is currently assumed that the contributions of the other (unnumbered) elements are negligible. There would be a clear benefit to evaluating these additional elements in future.

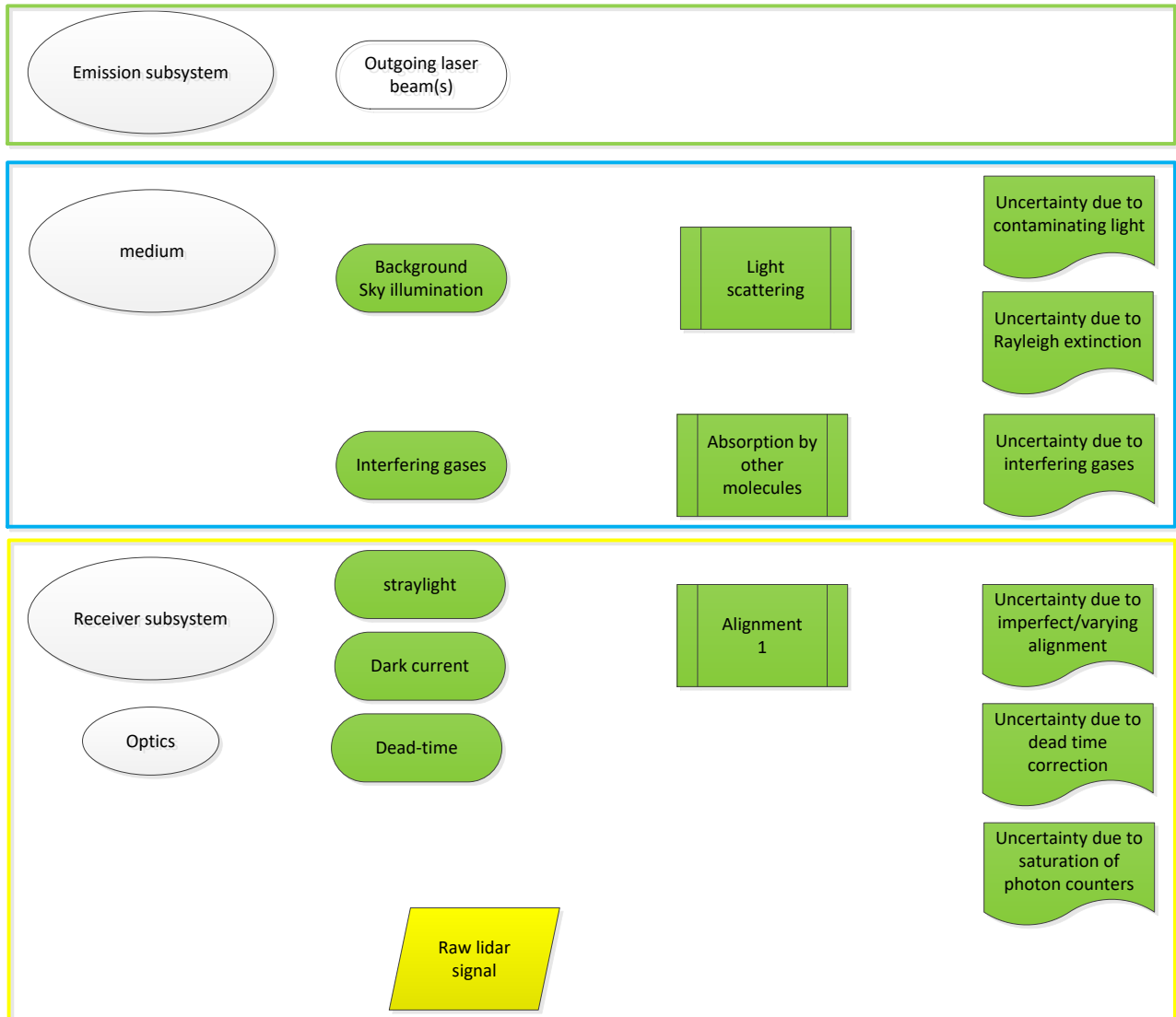


Figure 5. Three elements are shown in the physical part of the PTU chain: the emitter box (outlined by the green rectangle), the medium corresponding to the atmosphere (blue rectangle), the receiver box with e.g. the optics and detectors (yellow rectangle). The processing software part is shown in Figure 6. Processes, components and uncertainties that are dealt with are printed as filled green shapes. Items that are numbered following the discussion in the Element contribution section (5).

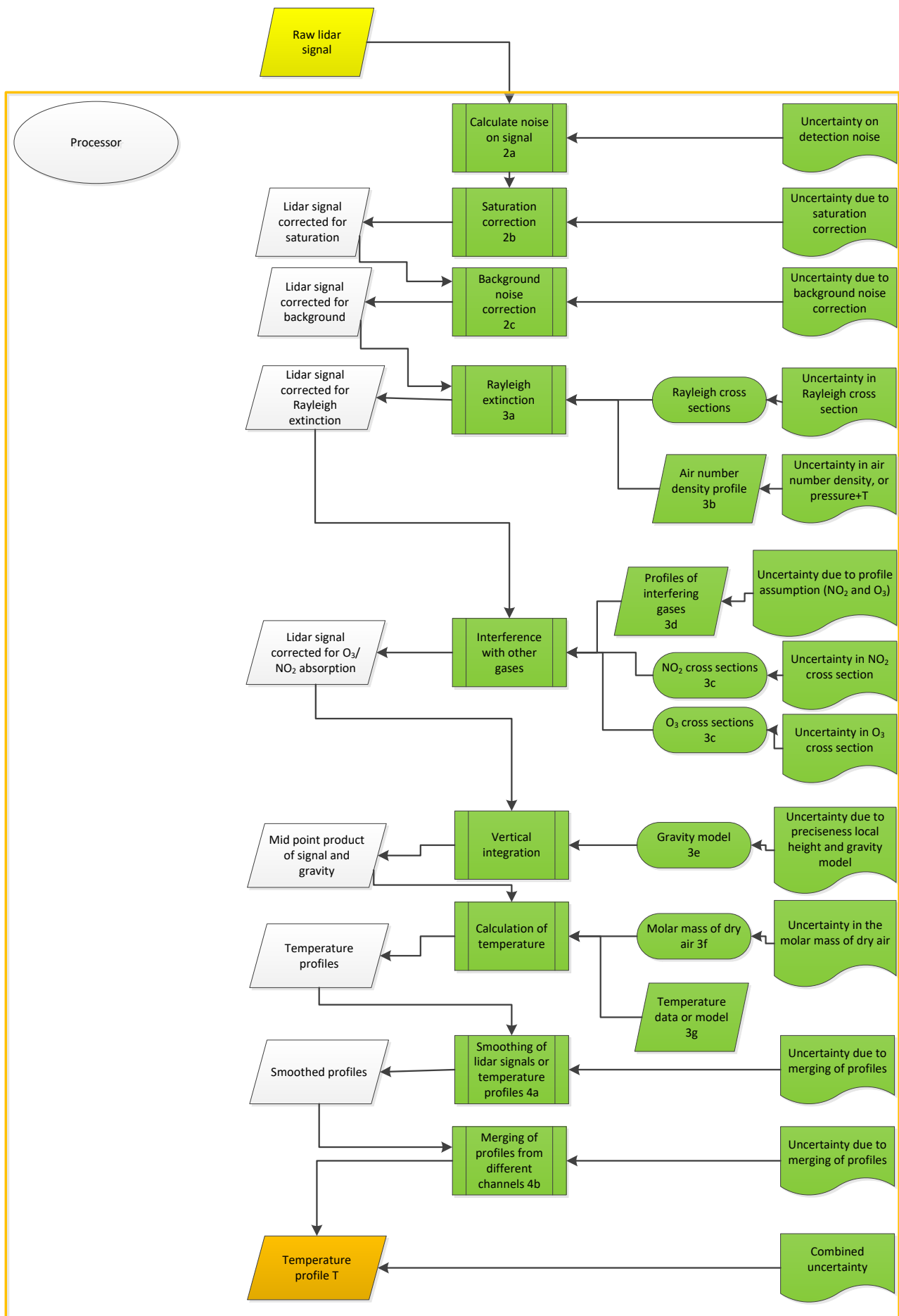


Figure 6. Continuation of Figure 5 with the processing software steps.

5 Element contributions

5.1 Alignment (1)

The correct alignment of the lidar system, that is the alignment of the laser beam with the receiving system and of the telescope with the optics of filtering system, is ensured by specific tests, as for instance developed in the framework of the EARLINET quality assurance program. In particular, the telecover test and the Rayleigh fit test are performed to check and correct the alignment of the lidar system in the near range (planetary boundary layer) and in the far range (free troposphere or above), respectively – see Freudenthaler et al. (2018).

For each lidar system there is a certain degree of misalignment between the laser beam and the receiving system due to residual uncertainties in the telecover and Rayleigh fit tests or possible mechanical/thermal instabilities of the optical and mechanical components forming both transmission and receiving systems. The misalignment of a lidar system changes the angle on the receiver of the backscattered light at each altitude level, which affects the overlap function. Most temperature lidar systems start at relatively high altitudes and then there is usually a full overlap.

Information / data	Type / value / equation	Notes / description
Name of effect	Alignment	
Contribution identifier	1	
Measurement equation parameter(s) subject to effect	η	In Eq. 1
Contribution subject to effect (final product or sub-tree intermediate product)	Lidar signal P	Eq. 1
Time correlation extent & form	Various time scales	Extent & form not quantified
Other (non-time) correlation extent & form	1) Possible correlation with vertical range 2) Possible correlation with the temperature of components forming both transmission and receiving systems during measurements	Extent & form not quantified
Uncertainty PDF shape	N/A	Systematic effect
Uncertainty & units	0% (relative uncertainty)	Assumed to be negligible for a well maintained system
Sensitivity coefficient	<1	Assumed that only data not effected is reported
Correlation(s) between affected parameters	None	
Element/step common for all sites/users?	Yes	
Traceable to ...	No	
Validation	Keckhut et al., 1993	

5.2 Pre-processing (2)

5.2.1 Detection noise (2a)

Random noise is inherently present in any physical system performing an actual measurement. Signal detection uncertainty is introduced at the detection level, where the signal is recorded in the data files (raw signal R). It is derived from Poisson statistics associated with the probability of detection of a repeated random event (Type-A uncertainty estimation). Using the subscript “(DET)” for “detection noise”, the uncertainty in the raw (summed) signal R due to detection noise expressed for each altitude bin k and for a single temperature channel is written:

$$u_{R(DET)}(k) = \sqrt{R(k)} \quad (20)$$

There is no correlation between any of the samples considered as this uncertainty component is due to purely random effects (signal detection). It is propagated to the retrieved temperature profile by systematically assigning the individual input quantities covariance matrix's non-diagonal terms to zero. Assuming a non-paralyzable photon-counting hardware, this uncertainty component is therefore propagated to the saturation and background noise-corrected signal P by converting Eq. (9):

$$u_{P(DET)}(k) = \left(\frac{P(k)}{R(k)} \right)^2 \sqrt{R(k)} \quad (21)$$

This uncertainty component is then propagated to the lidar-derived relative density N by:

$$u_{N(DET)}(k) = \frac{N(k)}{P(k)} u_{P(DET)}(k) \quad (22)$$

Next, it is propagated through Eq. (11) assuming that the signals are uncorrelated between two consecutive altitudes:

$$u_{N(DET)}^-(k') = \frac{1}{2} \sqrt{\frac{N(k'+1)}{N(k')} u_{N(DET)}^2(k') + \frac{N(k')}{N(k'+1)} u_{N(DET)}^2(k'+1)} \quad (23)$$

The detection noise uncertainty then needs to be propagated to the sum S defined in Eq. (12). This sum involves correlated terms as two consecutive terms contain two occurrences of the same values (k' and $k'+1$ first level, then $k'+1$ and $k'+2$ next level, etc.).

$$u_{S(DET)}(k) = \sqrt{\sum_{k'=k}^{k_{TOP}-1} g^2(k') u_{N(DET)}^2(k') + 2 \sum_{k'=k}^{k_{TOP}-2} \sum_{k''=k'+1}^{k_{TOP}-1} g(k') g(k'') u_{N(DET)}^-(k') u_{N(DET)}^-(k'') r_{k'k''}} \quad (24)$$

The correlation coefficients $r_{k'k''}$ between the terms $\bar{N}(k')$ and $\bar{N}(k'')$ are not strictly known. However, with the realistic assumption that the values of two consecutive terms are almost equal (i.e., N values, g values and $u_{N(DET)}$ values), the equation above can be simplified to:

$$u_{S(DET)}(k) = \sqrt{2 \sum_{k'=k}^{k_{TOP}-1} g^2(k') u_{N(DET)}^2(k')} \quad (25)$$

This expression is different from an expression assuming that all terms are independent (it is a factor of $\sqrt{2}$ larger), and it is also different from an expression assuming that all the terms are fully correlated (the weighed sum of all individual uncertainties).

Finally, the temperature uncertainty due to detection noise $u_{T(DET)}$ is computed for the density integration:

$$u_{T(DET)}(k) = \frac{1}{N(k)T(k)} \sqrt{T^2(k) u_{N(DET)}^2(k) + T_a^2(k_{TOP}) u_{N(DET)}^2(k_{TOP}) + \left(\frac{M_a \delta z}{R_a} \right)^2 u_{S(DET)}^2(k)} \quad (26)$$

The temperature uncertainty due to detection noise can be of any order of magnitude, depending on altitude and lidar performance and/or specification such as signal magnitude, emission wavelength, vertical sampling, and the duration of temporal integration. In general, the temperature uncertainty increases with an e-folding rate (of about 14 km) as a function of signal magnitude and of altitude.

Information / data	Type / value / equation	Notes / description
Name of effect	Detection noise	
Contribution identifier	2a	
Measurement equation parameter(s) subject to effect	R	Eq. 9
Contribution subject to effect (final product or sub-tree intermediate product)	T	Eq.19
Time correlation extent & form	Various time scales (structured random)	Will change with each measurement session due to varying experimental conditions
Other (non-time) correlation extent & form	Vertical smoothing/spatial resolution	
Uncertainty PDF shape	Poisson/normal	
Uncertainty & units	Large (>1 K) at the top of profile, decreasing downwards to a minimal uncertainty at the bottom of the profile	
Sensitivity coefficient	1	
Correlation(s) between affected parameters	Not applicable	
Element/step common for all sites/users?	Yes	
Traceable to ...	Leblanc et al., 2016d	
Validation	Simoneov et al., 1999	

5.2.2 Saturation (pulse pile-up) correction (2b)

This uncertainty component is introduced only for channels operating in photon-counting mode. If we consider a non-paralyzable counting hardware, the only input quantity to introduce is the hardware's dead time (sometimes called resolving time), which characterizes the speed of the counting electronics. The dead time τ and its uncertainty u_τ are generally among the technical specifications provided by the hardware manufacturer (Type-B estimation).

This uncertainty component is introduced where the signal is recorded in the data files (raw signal R). Using the subscript “(SAT)” for “saturation”, the saturation correction uncertainty propagated to the saturation and background noise-corrected signal P is obtained:

$$u_{P(SAT)}(k) = \frac{2\delta z}{cL} P^2(k) u_\tau \quad (27)$$

Just like the detection noise component, the saturation correction uncertainty component is propagated to the lidar-derived relative density N :

$$u_{N(SAT)}(k) = \frac{N(k)}{P(k)} u_{P(SAT)}(k) \quad (28)$$

The saturation correction is applied to the lidar signals consistently at all altitudes. Its uncertainty is therefore propagated assuming full correlation between two consecutive altitudes $z(k')$ and $z(k'+1)$.

$$u_{\bar{N}(SAT)}(k') = \frac{\bar{N}(k')}{2} \left(\frac{u_{N(SAT)}(k')}{N(k')} + \frac{u_{N(SAT)}(k'+1)}{N(k'+1)} \right) \quad (29)$$

The saturation correction uncertainty then propagates to the sum S defined in Eq. (12) assuming again full correlation between altitude bins:

$$u_{S(SAT)}(k) = \sum_{k'=k}^{k_{TOP}-1} g(k') u_{\bar{N}(SAT)}(k') \quad (30)$$

Finally, the temperature uncertainty due to saturation correction $u_{T(SAT)}$ is for the density integration with the same full correlation assumptions:

$$u_{T(SAT)}(k) = \frac{1}{N(k)} \left| T(k) u_{N(SAT)}(k) - T_a(k_{TOP}) u_{N(SAT)}(k_{TOP}) - \frac{M_a \delta z}{R_a} u_{S(SAT)}(k) \right| \quad (31)$$

Information / data	Type / value / equation	Notes / description
Name of effect	Saturation correction	
Contribution identifier	2b	
Measurement equation parameter(s) subject to effect	P	Eq.9
Contribution subject to effect (final product or sub-tree intermediate product)	T	Eq.19
Time correlation extent & form	Various time scales (structured random)	Will change with each measurement session due to varying experimental conditions
Other (non-time) correlation extent & form	N/A	
Uncertainty PDF shape	Poisson/normal	
Uncertainty & units	Can be large (~1 K) at bottom of profile, rapidly decreasing with decreasing signal strength	Depends on the used setup, photon counters and signal intensity

Sensitivity coefficient	1	
Correlation(s) between affected parameters	Not applicable	
Element/step common for all sites/users?	yes	
Traceable to ...	Leblanc et al., 2016d	
Validation	Donovan et al, 2003 Bristow, 1998	

5.2.3 Background noise extraction (2c)

At far range, the backscattered signal is too weak to be detected and any non-zero signal reflects the presence of undesired skylight or electronic background noise. This background noise is typically subtracted from the total signal by fitting the uppermost part of the lidar signal with a linear or non-linear function of altitude B . A new uncertainty component associated with the noise fitting procedure must therefore be introduced. Here we provide a detailed treatment for the simple case of a linear fit. It can be easily generalized to many other fitting functions. The linear fitting function takes the form:

$$B(k) = b_0 + b_1 z(k) \quad (32)$$

For many well-known fitting methods (e.g., least-squares), the fitting coefficients b_i can be calculated analytically together with their uncertainty u_{b_i} and their correlation coefficient rb_i, b_j (Type-A estimation) (Press et al., 1986). Using the subscript “(BKG)” for “background noise”, the background noise correction uncertainty can then be introduced by

$$u_{P(BKG)}(k) = \sqrt{u_{b_0}^2 + u_{b_1}^2 z^2(k) + 2z(k) \text{cov}(b_0, b_1)} \quad (33)$$

The above expression can be expanded and/or modified based on the actual form of the fitting function, and taking into account the fitting coefficients’ covariance matrix returned by the fitting routine. Just like the saturation correction uncertainty, the uncertainty component due to the background noise extraction can be propagated through the temperature retrieval assuming full correlation in altitude:

$$u_{N(BKG)}(k) = \frac{N(k)}{P(k)} u_{P(BKG)}(k) \quad (34)$$

$$u_{\bar{N}(BKG)}(k') = \frac{\bar{N}(k')}{2} \left(\frac{u_{N(BKG)}(k')}{N(k')} + \frac{u_{N(BKG)}(k'+1)}{N(k'+1)} \right) \quad (35)$$

$$u_{S(BKG)}(k) = \sum_{k'=k}^{k_{TOP}-1} g(k') u_{\bar{N}(BKG)}(k') \quad (36)$$

$$u_{T(BKG)}(k) = \frac{1}{N(k)} \left| T(k) u_{N(BKG)}(k) - T_a(k_{TOP}) u_{N(BKG)}(k_{TOP}) - \frac{M_a \delta z}{R_a} u_{S(BKG)}(k) \right| \quad (37)$$

The order of magnitude of this uncertainty component depends on the magnitude of the background noise, and if signal-induced noise is present, on the slope of this noise with respect to the signal slope. In general, a systematic pattern which consists of a rapid increase in the first 3-4 km below the tie-on altitude as density is integrated downward can be seen, followed by a decrease as we get further and further from the tie-on altitude. The e-folding rate is about 7 km for the entire family of curves, which reflects the main influence of the $1/N$ term in Eq. (37). The temperature uncertainty maximum is larger when the magnitude of the noise is larger.

Information / data	Type / value / equation	Notes / description
Name of effect	Background noise correction	
Contribution identifier	2c	
Measurement equation parameter(s) subject to effect	B(k)	Eq. 9
Contribution subject to effect (final product or sub-tree intermediate product)	T	

Time correlation extent & form	Various time scales (structured random)	Will change with each measurement session due to varying experimental conditions, e.g. sky brightness, dark current
Other (non-time) correlation extent & form	Not applicable	
Uncertainty PDF shape	Poisson/normal	
Uncertainty & units	<0.3 K	
Sensitivity coefficient	1	
Correlation(s) between affected parameters	Not applicable	
Element/step common for all sites/users?	Yes	
Traceable to ...	Leblanc et al., 2016d	
Validation	Keckhut et al., 1993 Leblanc et al., 1998	

5.3 External inputs (3)

5.3.1 Rayleigh extinction cross section (3a)

All lidar-derived relative density uncertainty components due to the atmospheric extinction are computed starting from Eq. (10). The Rayleigh extinction cross-sections at the emitted and received wavelengths are among the input quantities. Their values typically originate from theoretical calculations assuming a given atmospheric composition (see for example Bates, 1984; Eberhard, 2010), and can be assumed constant with altitude (well-mixed atmosphere). A review of the different calculations and the associated uncertainties can be found in Leblanc et al. (2016d, Appendix D and section 3.5 therein). The uncertainty, as reported in the literature, is either due to random or systematic effects, or both. These two types of uncertainty are not introduced and propagated identically in the lidar temperature measurement model. The subscripts suffix “*Rand*” (for “random”) and “*Sys*” (for “systematic”) are used hereafter to make this distinction.

5.3.1.1 Relative density uncertainty for Rayleigh backscatter channels

For Rayleigh backscatter channels, the received wavelength (λ_R) is identical to the emitted wavelength (λ_E), and the cross-section uncertainty due to random and systematic effects is introduced and propagated identically throughout the temperature retrieval. Using the subscript “(σ_M)” for “molecular extinction cross-section” uncertainty component, and the suffixes “*Rand*” and “*Sys*” for random and “systematic” components respectively, the Rayleigh extinction cross-section uncertainty due to random and systematic effects can be propagated to the lidar-derived relative density N :

$$u_{N(\sigma MX)}(k) = 2N(k)\delta z \sum_{k'=0}^k N_a(k') u_{\sigma M_E_X} \text{ with } X=Rand, Sys \quad (38)$$

5.3.1.2 Relative density uncertainty for Raman backscatter channels

For Raman backscatter channels (Strauch et al., 1971), the received and emitted wavelengths are different, and the cross-section uncertainty due to random and systematic effects are introduced and propagated differently. The uncertainty component due to random effect is computed as:

$$u_{N(\sigma MR)}(k) = N(k)\delta z \sum_{k'=0}^k N_a(k') \sqrt{u_{\sigma M_E_Rand}^2 + u_{\sigma M_R_Rand}^2} \quad (39)$$

The uncertainty component due to systematic effects is computed as:

$$u_{N(\sigma MS)}(k) = N(k)\delta z \sum_{k'=0}^k N_a(k') (u_{\sigma M_E_Sys} + u_{\sigma M_R_Sys}) \quad (40)$$

5.3.1.3 Propagation to temperature

For both Rayleigh and Raman backscatter, both random and systematic components of the lidar-derived relative density uncertainty due to Rayleigh extinction cross-sections are propagated to temperature similarly to the saturation and background uncertainty components:

$$u_{\bar{N}(\sigma MX)}(k') = \frac{\bar{N}(k')}{2} \left(\frac{u_{N(\sigma MX)}(k')}{N(k')} + \frac{u_{N(\sigma MX)}(k'+1)}{N(k'+1)} \right) \text{ with } X=Rand, Sys \quad (41)$$

$$u_{S(\sigma MX)}(k) = \sum_{k'=k}^{k_{TOP}-1} g(k') u_{\bar{N}(\sigma MX)}(k') \text{ with } X=Rand, Sys \quad (42)$$

$$u_{T(\sigma MX)}(k) = \frac{1}{N(k)} \left| T(k) u_{N(\sigma MX)}(k) - T_a(k_{TOP}) u_{N(\sigma MX)}(k_{TOP}) - \frac{M_a \delta z}{R_a} u_{S(\sigma MX)}(k) \right| \text{ with } X=Rand, Sys \quad (43)$$

Information / data	Type / value / equation	Notes / description
Name of effect	Rayleigh extinction cross sections	
Contribution identifier	3a	
Measurement equation parameter(s) subject to effect	$\Delta\sigma_M$	Eq. 10
Contribution subject to effect (final product or sub-tree intermediate product)	T	Eq. 11
Time correlation extent & form	None	
Other (non-time) correlation extent & form	None	
Uncertainty PDF shape	Unknown	
Uncertainty & units	Large (~1 K) at bottom of profile	See line numbered 4 in Figure 8 for an example of how it changes with altitude
Sensitivity coefficient	1	
Correlation(s) between affected parameters	Not applicable	
Element/step common for all sites/users?	Yes	
Traceable to ...	Leblanc et al., 2016d	
Validation	She et al., 1992	

5.3.2 Uncertainty owing to air number density, temperature and pressure profiles (3b)

An external, a priori profile of air number density (N_a) is needed to correct for Rayleigh extinction as formulated in Eq. (10). Air number density is generally not estimated directly, but rather derived from air temperature and pressure. Below we discuss the propagation of uncertainty for both ways of obtaining air number density.

5.3.2.1 Estimation from an air number density profile

Here, it is assumed that the air density profile N_a is made of fully-correlated values in altitude. If air number density is not derived from air temperature and pressure, its uncertainty u_{Na} is propagated to the lidar-derived relative density by:

$$u_{N(Na)}(k) = N(k) \delta z (\sigma_{M_E} + \sigma_{M_R}) \sum_{k'=0}^k u_{Na}(k') \quad (44)$$

This component is then propagated to temperature using the same approach as for saturation and background noise correction uncertainties.

5.3.2.2 Estimation from an air temperature and pressure profile

When the ancillary number density is computed from an ancillary temperature T_a and pressure p_a source (e.g., radiosonde measurements or meteorological models), the uncertainties u_{Ta} and u_{pa} must be introduced and the degree of correlation between temperature and pressure must be estimated. If temperature and pressure are measured or computed independently, then the complete covariance matrix in the vertical dimension needs to be estimated. This is the most complex case to consider because of the interplay between the lack of correlation between T_a and p_a at any given altitude, and the high correlation between the temperature values at two consecutive altitudes, or between the pressure values at two consecutive altitudes. However, a good approximation consists of considering the propagation linearly, i.e., first combining the uncertainties at one fixed level assuming no correlation, and then propagating the combined uncertainty assuming full correlation between two consecutive altitudes. In this case, the lidar-derived relative density uncertainty due to the ancillary air number density can be written:

$$u_{N(Na)}(k) = N(k) \delta z \sum_{k'=0}^k (\sigma_{M_E} + \sigma_{M_R}) N_a(k') \sqrt{\frac{u_{pa}^2(k')}{p_a^2(k')} + \frac{u_{Ta}^2(k')}{T_a^2(k')}} \quad (45)$$

If temperature and pressure are known to be fully correlated, then, the lidar-derived relative density uncertainty due to the ancillary air number density becomes:

$$u_{N(Na)}(k) = N(k) \delta z \sum_{k'=0}^k (\sigma_{M_E} + \sigma_{M_R}) N_a(k') \left| \frac{u_{pa}(k')}{p_a(k')} - \frac{u_{Ta}(k')}{T_a(k')} \right| \quad (46)$$

5.3.2.3 Propagation to the temperature profile

The lidar-derived number density uncertainty due to ancillary air number density is propagated to temperature assuming full correlation in altitude:

$$u_{\bar{N}(Na)}(k') = \frac{\bar{N}(k')}{2} \left(\frac{u_{N(Na)}(k')}{N(k')} + \frac{u_{N(Na)}(k'+1)}{N(k'+1)} \right) \quad (47)$$

$$u_{S(Na)}(k) = \sum_{k'=k}^{k_{TOP}-1} g(k') u_{\bar{N}(Na)}(k') \quad (48)$$

$$u_{T(Na)}(k) = \frac{1}{N(k)} \left| T(k) u_{N(Na)}(k) - T_a(k_{TOP}) u_{N(Na)}(k_{TOP}) - \frac{M_a \delta z}{R_a} u_{S(Na)}(k) \right| \quad (49)$$

Information / data	Type / value / equation	Notes / description
Name of effect	External air number density, temperature and pressure profiles	This table corresponds to the entire section 5.3.2
Contribution identifier	3b	
Measurement equation parameter(s) subject to effect	N	Eq. 10
Contribution subject to effect (final product or sub-tree intermediate product)	T	Eq. 11
Time correlation extent & form	Various time scales (structured random)	Will change with each measurement session due to varying experimental conditions
Other (non-time) correlation extent & form	altitude	
Uncertainty PDF shape		
Uncertainty & units	Largest (<0.2 K) at bottom of profile	See line numbered 5 in Figure 8
Sensitivity coefficient	1	
Correlation(s) between affected parameters		
Element/step common for all sites/users?	yes	
Traceable to ...	Leblanc et al., 2016d	
Validation	Leblanc et al., 1998	

5.3.4 Interfering gases' cross sections (3c)

Temperature-dependent ozone and NO₂ absorption cross-section values typically can be found in published works originating from spectroscopy groups around the world (e.g., Brion et al., 1998; Bogumil et al., 2003; Chehade et al., 2013; Gorshelev et al., 2014; Burkholder and Talukdar, 1994; Burrows et al., 1999; Vandaele et al., 1998). The random component of the cross-section uncertainty is normally provided in these works. Occasionally, one or more components due to systematic effects are also provided. For the ozone absorption cross-section, a review and assessment of the available datasets is summarized Leblanc et al. (2016d). Just like for Rayleigh extinction cross-sections, these two types of components are not introduced and propagated identically in the lidar temperature measurement model. The formulation of their propagation is identical to that just presented for Rayleigh extinction cross-sections, except that the air number density is replaced by the interfering gas number density, and the cross-section uncertainty is now a function of temperature, i.e., altitude.

For Rayleigh backscatter channels:

$$u_{N(\sigma_{igX})}(k) = 2N(k)\delta z \sum_{k'=0}^k N_{O_3}(k') u_{\sigma_{ig_1X}}(k') \quad \text{with } ig = O_3, NO_2 \text{ and } X=Rand, Sys \quad (50)$$

For Raman backscatter channels:

$$u_{N(\sigma_{igRand})}(k) = N(k)\delta z \sqrt{\sum_{k'=0}^k N_{ig}^2(k') (u_{\sigma_{ig_E_Rand}}^2(k') + u_{\sigma_{ig_R_Rand}}^2(k'))} \quad \text{with } ig = O_3, NO_2 \quad (51)$$

$$u_{N(\sigma_{igS})_{ys}}(k) = N(k)\delta z \sum_{k'=0}^k N_a(k') (u_{\sigma_{ig_E_Sys}}(k') + u_{\sigma_{ig_R_Sys}}(k')) \quad \text{with } ig = O_3, NO_2 \quad (52)$$

Their propagation to temperature can then be written:

$$u_{\bar{N}(\sigma_{igX})}(k') = \frac{\bar{N}(k')}{2} \left(\frac{u_{N(\sigma_{igX})}(k')}{N(k')} + \frac{u_{N(\sigma_{igX})}(k'+1)}{N(k'+1)} \right) \quad \text{with } ig = O_3, NO_2 \text{ and } X=Rand, Sys \quad (53)$$

$$u_{S(\sigma_{igX})}(k) = \sum_{k'=k}^{k_{TOP}-1} g(k') u_{\bar{N}(\sigma_{igX})}(k') \quad \text{with } ig = O_3, NO_2 \text{ and } X=Rand, Sys \quad (54)$$

$$u_{T(\sigma_{igX})}(k) = \frac{1}{N(k)} \left| T(k) u_{N(\sigma_{igX})}(k) - T_a(k_{TOP}) u_{N(\sigma_{igX})}(k_{TOP}) - \frac{M_a \delta z}{R_a} u_{S(\sigma_{igX})}(k) \right| \quad ig = O_3, NO_2; X=Rand, Sys \quad (55)$$

The contribution of ozone absorption to uncertainty in the temperature profiles is larger in the visible (532 nm and 607 nm which are both in the Chappuis band) than in the ultraviolet (355 nm and 387 nm). Conversely, the contribution of NO₂ absorption is larger for ultraviolet wavelengths than for wavelengths in the visible domain.

Information / data	Type / value / equation	Notes / description
Name of effect	Interfering gases' cross section differential	
Contribution identifier	3c	
Measurement equation parameter(s) subject to effect	$\Delta\sigma_{ig}$	Eq. 11
Contribution subject to effect (final product or sub-tree intermediate product)	N	Eq. 11
Time correlation extent & form	None	
Other (non-time) correlation extent & form		

Uncertainty PDF shape		
Uncertainty & units	For ozone: up to 1 K error if neglected when working in the Chappuis band (e.g., 532 nm and 607 nm) For NO ₂ : up to a 0.2 K error if neglected at 355 nm and 387 nm	Depends on the quantity and profile of the interfering gas and wavelength used for retrieval.
Sensitivity coefficient	1	
Correlation(s) between affected parameters		
Element/step common for all sites/users?	yes	
Traceable to ...	Leblanc et al., 2016d	
Validation	Sica et al., 2001	for ozone retrievals with the 532 and 589 nm wavelengths (contribution of ozone is negligible around 350 nm) At this moment NO ₂ is not yet corrected for, although it is recommended.

5.3.5 Interfering gases' atmospheric profiles (3d)

The ozone and NO₂ absorption terms in Eq. (10) form the sum of a priori ozone and NO₂ number densities taken at all altitudes from the ground to the altitude considered $z(k)$. Depending on the data source, these ancillary profiles may be mixing ratio or number density (Ahmad et al., 1987; Bauer et al., 2012; Bracher et al., 2005; Brohede et al., 2007) Assuming that all values within the same ancillary profile are fully correlated, uncertainty components due to the ancillary ozone and NO₂ profiles can be propagated to temperature similarly to the uncertainty component due to air number density:

$$u_{N(Nig)}(k) = N(k) \sum_{k'=0}^k (\sigma_{ig_E}(k') + \sigma_{ig_R}(k')) u_{Nig}(k') \text{ with } ig = O_3, NO_2 \quad (56)$$

$$u_{\bar{N}(Nig)}(k') = \frac{\bar{N}(k')}{2} \left(\frac{u_{N(Nig)}(k')}{N(k')} + \frac{u_{N(Nig)}(k'+1)}{N(k'+1)} \right) \quad (57)$$

$$u_{S(Nig)}(k) = \sum_{k'=k}^{k_{TOP}-1} g(k') u_{\bar{N}(Nig)}(k') \quad (58)$$

$$u_{T(Nig)}(k) = \frac{1}{N(k)} \left| T(k) u_{N(Nig)}(k) - T_a(k_{TOP}) u_{N(Nig)}(k_{TOP}) - \frac{M_a \delta z}{R_a} u_{S(Nig)}(k) \right| \quad (59)$$

The contribution of ozone is larger for visible wavelengths than in the UV, and the contribution of NO₂ is larger for ultraviolet wavelengths than in the visible.

Information / data	Type / value / equation	Notes / description
Name of effect	Interfering gases' atmospheric profiles	
Contribution identifier	3d	
Measurement equation parameter(s) subject to effect	N_{ig}	Eq. 10
Contribution subject to effect (final product or sub-tree intermediate product)	N	
Time correlation extent & form	Various time scales	Will change with each measurement session due to varying experimental conditions in terms of atmospheric composition
Other (non-time) correlation extent & form	None	
Uncertainty PDF shape	Poisson/normal	
Uncertainty & units	For ozone: up to 1 K error if neglected when working in the Chappuis band (e.g., 532 nm and 607 nm) For NO ₂ : depending on NO ₂ density, but up to a 0.2 K error if neglected at 355 nm and 387 nm	
Sensitivity coefficient	1	
Correlation(s) between affected parameters	None	

Element/step common for all sites/users?	Yes	
Traceable to ...	Leblanc et al., 2016d Faduilha et al., 2005	
Validation	-	For ozone The NO ₂ -correction is recommended but not yet implemented in the current lidar products.

5.3.6 Acceleration of gravity (3e)

The acceleration of gravity is an input quantity introduced in Eq. (12). The constants g_0 , g_1 and g_2 relate to the Earth's geometry and to the geodetic latitude of the lidar site. If a value of the local ellipsoid height at the lidar site $h(0)$ is not known, we can approximate it to the site's altitude above mean sea level $z(0)$. For all altitude-dependent and latitude-dependent formulations of the acceleration of gravity, the difference between $h(0)$ and $z(0)$ is by far the largest source of error in the computation of the acceleration of gravity. We therefore can define a new uncertainty component u_h associated with the approximation of h . The values of h at neighboring altitudes are fully correlated, and their standard uncertainty can be deduced directly from Eq. (15):

$$u_{\bar{h}}(k') = \frac{1}{2}(u_h(k') + u_h(k'+1)) \quad (62)$$

The height uncertainty is then propagated to temperature:

$$u_{T(g)}(k) = \frac{1}{N(k)} \frac{M_a \delta z}{R_a} g_0 \sum_{k'=k}^{k_{TOP}-1} N(k') (g_1 + 2g_2 \bar{h}(k')) u_{\bar{h}}(k') \quad (63)$$

The relative uncertainty in the temperature profiles is therewith directly related to the relative uncertainty in gravity. An example is given in Figure 7 below, where the altitude-dependence of gravity is considered, but latitude not. Deviations in the temperature profiles depend on the assumed and true latitude as well as on altitude, and can reach up to 0.7 K. Similar simulations have been carried out for the case where gravity is treated as a constant (both altitude-dependence and latitude-dependence neglected). There up to 6 K deviations are found.

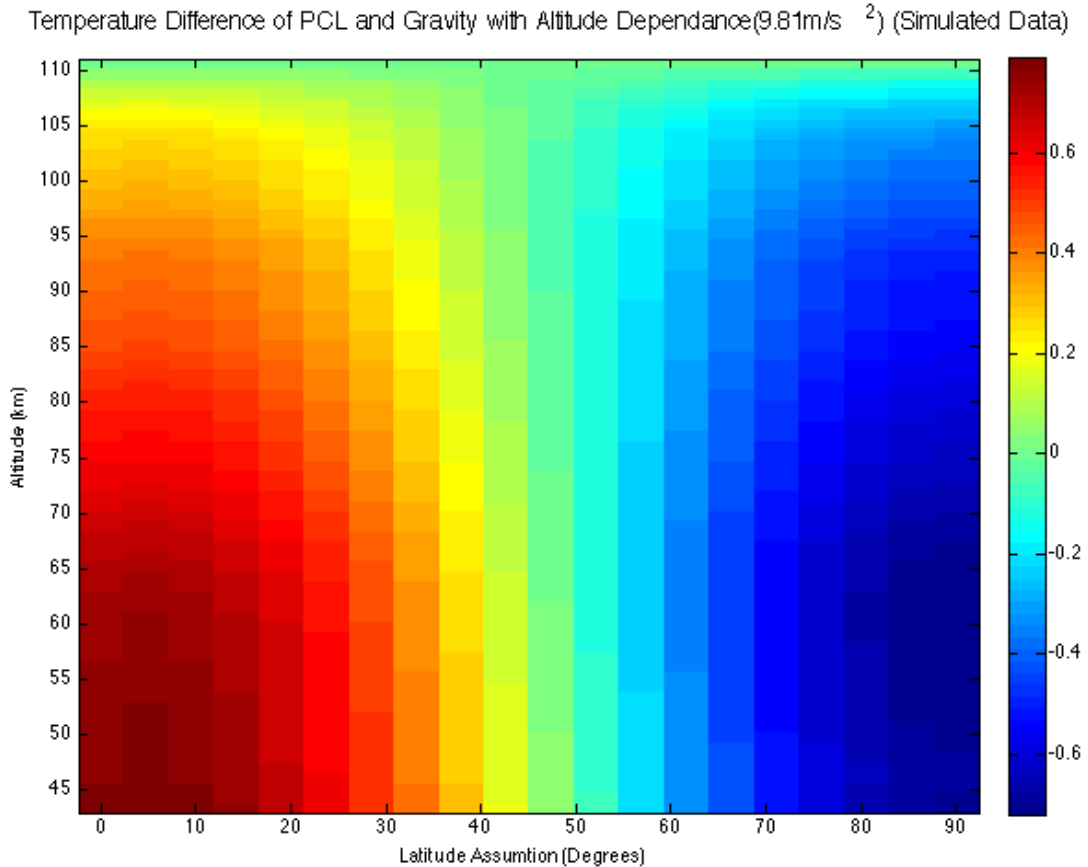


Figure 7. Effect of disregarding the contribution of latitude to gravity taking the altitude-dependence of gravity into account. The gravity is simulated here for a latitude of 45 degrees. The offset in temperature then depends on the latitude of the site (horizontal axis) and the altitude (vertical axis). Simulations and figure prepared by professor R. Sica, PI of the Purple Crow lidar (Western university, Ontario, Canada).

Information / data	Type / value / equation	Notes / description
Name of effect	Acceleration of gravity	
Contribution identifier	3e	
Measurement equation parameter(s) subject to effect	G	Eq. 12
Contribution subject to effect (final product or sub-tree intermediate product)	S	Eq.12
Time correlation extent & form	None	
Other (non-time) correlation extent & form	Geolocation of instrument	
Uncertainty PDF shape	N/A	
Uncertainty & units	<0.2 K if altitude- and latitude-dependent gravity is used which is the case for the systems described.	
Sensitivity coefficient	1	
Correlation(s) between affected parameters		
Element/step common for all sites/users?	yes	
Traceable to ...	Leblanc et al., 2016d	
Validation	Sica and Haefele., 2015	

5.3.7 Molecular mass of air (3f)

The molecular mass of dry air M_a is introduced in Eq. (11). Its uncertainty u_{Ma} , can be propagated to temperature using:

$$u_{T(Ma)}(k) = \frac{\delta z}{R_a} \frac{S(k)}{N(k)} u_{Ma} \quad (60)$$

The uncertainty introduced by this component remains negligible below 90 km, which is above the highest altitude reported by most lidar systems, and it has a variation with altitude similar to that due to acceleration of gravity. According to Keckhut et al. (1993), the dissociation of oxygen should lead to a 2% correction at 100 km and 7% correction at 110 km. The lidar systems used here do not report temperatures at these altitudes.

Information / data	Type / value / equation	Notes / description
Name of effect	Molecular mass of air	
Contribution identifier	3f	
Measurement equation parameter(s) subject to effect	M_a	Eq. 11
Contribution subject to effect (final product or sub-tree intermediate product)	T	Eq.11
Time correlation extent & form	Various time scales	
Other (non-time) correlation extent & form	None	
Uncertainty PDF shape	N/A	
Uncertainty & units	<0.1 K when altitude is below 90 km. Increasingly important with altitude above	
Sensitivity coefficient	1	
Correlation(s) between affected parameters		
Element/step common for all sites/users?	Yes	
Traceable to ...	Leblanc et al., 2016d	
Validation	Keckhut et al., 1993 Argall, 2007	

5.3.8 External temperature for tie-on at the top of the profile (3g)

An external or ancillary temperature value T_a at altitude $z(k_{TOP})$ is needed to initialize the profile at the top. Using the subscript “(TIE)” for “tie-on”, the ancillary temperature uncertainty $u_{Ta(k_{TOP})}$ is propagated to the retrieved temperature profile):

$$u_{T(TIE)}(k) = \frac{N(k_{TOP})}{N(k)} u_{Ta}(k_{TOP}) \quad (61)$$

The uncertainty due to ancillary temperature is reduced downward with altitude with an approximate e-folding rate of 7 km due to the term $1/N$ in the equation above.

Information / data	Type / value / equation	Notes / description
Name of effect	Tie-on temperature	
Contribution identifier	3g	
Measurement equation parameter(s) subject to effect	$T_a(k_{TOP})$	Eq. 11
Contribution subject to effect (final product or sub-tree intermediate product)	T	Eq. 11
Time correlation extent & form	Various time scales (structured random)	Will change with each measurement session due to varying experimental conditions.
Other (non-time) correlation extent & form		
Uncertainty PDF shape	N/A	
Uncertainty & units	Negligible from 20 km below tie-on altitude	Depends on uncertainty of the external temperature and whether data are reported up to tie-on temperature.
Sensitivity coefficient	1	
Correlation(s) between affected parameters	None	
Element/step common for all sites/users?	Yes	When using the density integration technique
Traceable to ...	Leblanc et al., 2016d	
Validation	Leblanc et al., 1998	

5.4 Spatio-temporal integration (4)

5.4.1 Propagation of uncertainty when vertically filtering (smoothing) the lidar signal or temperature profile (4a)

The smoothing procedure was introduced as an optional step in the measurement model and is applied either to the lidar signal or to the retrieved temperature profile for the instruments targeted for GaiaClim.

5.4.1.1 Smoothing the lidar signal before the temperature profile is computed

From Eq. (16) and using the same notations, the uncertainty component due to detection noise is propagated to the smoothed signal profile assuming no correlation between the neighbouring points:

$$u_{sm(DET)}(k) = s_m(k) \sqrt{\sum_{p=-n}^n c_p^2(k) \frac{u_{s(DET)}^2(k+p)}{s^2(k+p)}} \quad (62)$$

For all other uncertainty components except temperature tie-on, acceleration of gravity, and the molecular mass of air, full correlation is assumed between the neighbouring points, and the uncertainty in the smoothed signal can be written:

$$u_{sm(X)}(k) = s_m(k) \sum_{p=-n}^n c_p(k) \frac{u_{s(X)}(k+p)}{s(k+p)} \quad (63)$$

with $X = SAT, BKG, \sigma_{MR}, \sigma_{MS}, N_a, \sigma_{igR}, \sigma_{igS}, N_{ig}$.

The uncertainty components due to temperature tie-on, acceleration of gravity, and the molecular mass of air are not included in the above expression because they are introduced later in the data processing. In this case, the respective equations in sections 5.3.6 to 5.3.8 apply directly to the temperature profile retrieved from the smoothed lidar-derived number density.

5.4.1.2 Smoothing the retrieved temperature profile

The temperature uncertainty components due to detection noise are propagated to the smoothed temperature profile assuming no correlation between neighbouring points:

$$u_{Tm(DET)}(k) = \sqrt{\sum_{p=-n}^n c_p^2(k) u_{T(DET)}^2(k+p)} \quad (64)$$

For all other uncertainty components, full correlation is assumed between the two channels:

$$u_{Tm(X)}(k) = \sum_{p=-n}^n c_p(k) u_{T(X)}(k+p) \quad (65)$$

with $X = SAT, BKG, \sigma_{MR}, \sigma_{MS}, N_a, \sigma_{igR}, \sigma_{igS}, N_{ig}, g, TTOP, Ma$.

Information / data	Type / value / equation	Notes / description
Name of effect	Vertical filtering	
Contribution identifier	4a	
Measurement equation parameter(s) subject to effect	P or T	Eq.9 or Eq. 11
Contribution subject to effect (final product or sub-tree intermediate product)	T _m	Eq. 17
Time correlation extent & form	None	

Other (non-time) correlation extent & form		
Uncertainty PDF shape		
Uncertainty & units	Up to 2 K	Depending on the filter type used, the number of altitude bins used and the shape of the profile
Sensitivity coefficient	1	
Correlation(s) between affected parameters		
Element/step common for all sites/users?	Yes, but optional	
Traceable to ...	Leblanc et al., 2016d	
Validation	Leblanc et al., 1998	

5.4.2 Propagation of uncertainty when merging multiple channels together (4b)

The merging procedure was again introduced as an optional step in the measurement model. If present it can be applied either to the lidar signals or the temperature profiles. For the chosen sites, merging is applied.

5.4.2.1 Merging lidar signals before computing the temperature profile

The uncertainty components of the low and high channels due to detection noise are propagated to the merged signal profile assuming no correlation between the two channels:

$$u_{sM(SDET)}(k) = s_M(k) \sqrt{\left(w(k) \frac{u_{sm(DET)}(k, i_L)}{s_m(k, i_L)} \right)^2 + \left((1-w(k)) \frac{u_{sm(DET)}(k, i_H)}{s_m(k, i_H)} \right)^2} \quad k_1 \leq k \leq k_2 \text{ and } 0 \leq w(k) \leq 1 \quad (66)$$

If the signal to be merged is the lidar-derived relative density ($s=N$), all uncertainty components due to atmospheric extinction propagate to the merge density using:

$$u_{sM(X)}(k) = s_M(k) \left(w(k) \frac{u_{sm(X)}(k, i_L)}{s_m(k, i_L)} + (1-w(k)) \frac{u_{sm(X)}(k, i_H)}{s_m(k, i_H)} \right) \quad k_1 \leq k \leq k_2 \text{ and } 0 \leq w(k) \leq 1 \quad (67)$$

with $X = \sigma MR, \sigma MS, Na, \sigma igR, \sigma igS, Nig$.

For the uncertainty components of instrumental origin (namely, the saturation correction and background noise extraction), the degree of correlation between the channels hardware needs to be estimated before we can use a specific formulation for the propagation of the uncertainty components of instrumental origin. If the two channels use different hardware, they can be assumed independent and the merged signal uncertainties due to saturation correction and background noise extraction can be written

$$u_{sM(SX)}(k) = s_M(k) \sqrt{\left(w(k) \frac{u_{sm(X)}(k, i_L)}{s_m(k, i_L)} \right)^2 + \left((1-w(k)) \frac{u_{sm(X)}(k, i_H)}{s_m(k, i_H)} \right)^2} \quad k_1 \leq k \leq k_2 \text{ and } 0 \leq w(k) \leq 1 \quad (68)$$

with $X = SAT, BKG$.

If the two channels share the same hardware and if the saturation and background noise corrections have been applied consistently for both channels within the same data processing algorithm, the associated uncertainty components can be propagated to the combined profile assuming full correlation:

$$u_{sM(X)}(k) = s_M(k) \left(w(k) \frac{u_{sm(X)}(k, i_L)}{s_m(k, i_L)} + (1-w(k)) \frac{u_{sm(X)}(k, i_H)}{s_m(k, i_H)} \right) \quad k_1 \leq k \leq k_2 \text{ and } 0 \leq w(k) \leq 1 \quad (69)$$

with $X = SAT, BKG$.

The uncertainty components owing to temperature tie-on, acceleration of gravity, and the molecular mass of air are not included in the above expressions because they are introduced later in the data processing. In this case, the respective equations from sections 5.3.6 to 5.3.8 apply directly to the temperature profile retrieved from the merged lidar-derived number density.

5.4.2.2 Merging the temperature profiles retrieved for individual channels

The temperature uncertainty components of the low and high channels due to detection noise are propagated to the merged temperature profile assuming no correlation between the two channels:

$$u_{TM(DET)}(k) = \sqrt{\left(w(k) u_{Tm(DET)}(k, i_L) \right)^2 + \left((1-w(k)) u_{Tm(DET)}(k, i_H) \right)^2} \quad k_1 \leq k \leq k_2 \text{ and } 0 \leq w(k) \leq 1 \quad (70)$$

For all uncertainty components that are not of instrumental origin, full correlation is assumed between the two channels:

$$u_{TM(X)}(k) = w(k) u_{Tm(X)}(k, i_L) + (1-w(k)) u_{Tm(X)}(k, i_H) \quad \text{with } k_1 \leq k \leq k_2 \text{ and } 0 \leq w(k) \leq 1 \quad (71)$$

and $X = \sigma MR, \sigma MS, Na, \sigma igR, \sigma igS, Nig, g, TTOP, Ma$.

Just like in the case of merging the signals, for all uncertainty components of instrumental origin (namely, the saturation correction and background noise extraction) the degree of correlation between the channels hardware needs to be estimated. If the two channels use different hardware, they can be assumed independent and the temperature uncertainties due to saturation correction and background noise extraction can be written:

$$u_{TM(X)}(k) = \sqrt{\left(w(k)u_{Tm(X)}(k, i_L)\right)^2 + \left((1-w(k))u_{Tm(X)}(k, i_H)\right)^2} \quad k_1 \leq k \leq k_2 \text{ and } 0 \leq w(k) \leq 1 \quad (72)$$

with $X = SAT, BKG$

If the two channels share the same hardware and if the saturation and background noise corrections have been applied consistently for both channels within the same data processing algorithm, the associated uncertainty components can be propagated to the combined profile assuming full correlation:

$$u_{TM(X)}(k) = w(k)u_{Tm(X)}(k, i_L) + (1-w(k))u_{Tm(X)}(k, i_H) \quad k_1 \leq k \leq k_2 \text{ and } 0 \leq w(k) \leq 1 \quad (73)$$

with $X = SAT, BKG$.

Information / data	Type / value / equation	Notes / description
Name of effect	Merging of data from multiple channels	
Contribution identifier	4b	
Measurement equation parameter(s) subject to effect	P or T	Eq.9 or Eq.11
Contribution subject to effect (final product or sub-tree intermediate product)	T_M	Eq. 19
Time correlation extent & form	None	
Other (non-time) correlation extent & form	None	
Uncertainty PDF shape	N/A	
Uncertainty & units	Usually negligible	Depends on other corrections. For instance if uncertainty on the dead-time correction is large, the difference introduced in the merged profile is not negligible
Sensitivity coefficient	1	
Correlation(s) between affected parameters	Yes	1-3
Element/step common for all sites/users?	When multiple channels are available	
Traceable to ...	Leblanc et al., 2016d	
Validation	Jalali et al., 2016	

6 Uncertainty summary

Having reviewed and propagated all the independent uncertainty components considered in our lidar temperature measurement model, we can combine them into a unique temperature combined standard uncertainty:

$$u_T(k) = \sqrt{u_{T(DET)}^2(k) + u_{T(SAT)}^2(k) + u_{T(BKG)}^2(k) + u_{T(TTOP)}^2(k) + u_{T(\sigma MRand)}^2(k) + u_{T(\sigma MRSys)}^2(k) + u_{T(NA)}^2(k) + u_{T(g)}^2(k) + u_{T(Ma)}^2(k) + u_{T(\sigma O3Rand)}^2(k) + u_{T(\sigma O3Sys)}^2(k) + u_{T(NO3)}^2(k) + u_{T(\sigma NO2Rand)}^2(k) + u_{T(\sigma NO2Sys)}^2(k) + u_{T(NNO2)}^2(k)} \quad (74)$$

All uncertainty components should be set to zero at the tie-on altitude $z(k_{TOP})$, except for the uncertainty due to the ancillary temperature $u_{T(TTOP)}$. Also, when using multiple channels, the temperature combined standard uncertainty should not be computed for individual intensity channels and then merged into a single profile. Instead, the individual uncertainty components should first be propagated to the merged temperature profile and then added in quadrature to obtain the combined standard uncertainty.

When combining multiple profiles measured by the same instrument, for example to compute a climatology, uncertainty components due to systematic effects in altitude and/or time must remain separated from components due to random effects. Uncertainty due to detection noise is always added in quadrature, but for other components, knowledge of the covariance matrix in the time and/or altitude dimension(s) is required (type-A or type-B estimation).

Element identifier	Contribution name	Uncertainty contribution form	Typical value	Traceability level (L/M/H)	random, structured random, quasi-systematic or systematic?	Correlated to? (Use element identifier)
1	Alignment	N/A	negligible	M	Systematic	
2	Pre-processing					
2a	Detection noise	Poisson/normal distribution	Large (>1 K) at the top of profile	H	random	
2b	Saturation correction	N/A	Large (~1 K) at low range of profile	H	systematic	
2c	Background noise correction	Poisson/normal distribution	<0.3 K	H	random	
3	External inputs					
3a	Rayleigh extinction cross section	N/A	Large (~1 K) at low range of profile	H	Systematic	3b
3b	Air number density	N/A	Largest (<0.2 K) at low range of profile	M	Random and systematic	3a, 3f
3c1	Ozone cross section	N/A	up to 1 K error if neglected when working in the Chappuis band (e.g., 532	H	Random and systematic	3d1

			nm and 607 nm)			
3c2	NO ₂ cross section	N/A	up to a 0.2 K error if neglected at 355 nm and 387 nm	H	systematic	3d2
3d1	Ozone profile	N/A	up to 1 K error if neglected when working in the Chappuis band (e.g., 532 nm and 607 nm)	M	Random and systematic	3c1
3d2	NO ₂ profile	N/A	Depending on NO ₂ density, but up to a 0.2 K error if neglected at 355 nm and 387 nm	L	Random and systematic	3c2
3e	Gravity	N/A	<0.2 K if altitude-/latitude-dependent gravity is used	H	systematic	
3f	Molecular mass of air	N/A	<0.1 K when altitude is below 90 km. Relevant when above 100 km.	H	systematic	
3g	External temperature at top	N/A	Large at top of profile	L/M	Random and systematic	
4	Spatiotemporal integration					
4a	Vertical filtering	N/A	Variable, Up to 2 K	H	systematic	
4b	Merging of multiple channels	N/A	Negligible	M	random	

An example uncertainty budget for the lidar at Mauna Loa is presented in Figure 8, where the individual contributions are given for the three channels covering the altitude domain and for the final merged product.

Temperature uncertainty budget for the JPL-Lidar at Mauna Loa (Hawaii)
(13 March 2009; 120 min. integration, 0.3–5 km variable vertical resolution)

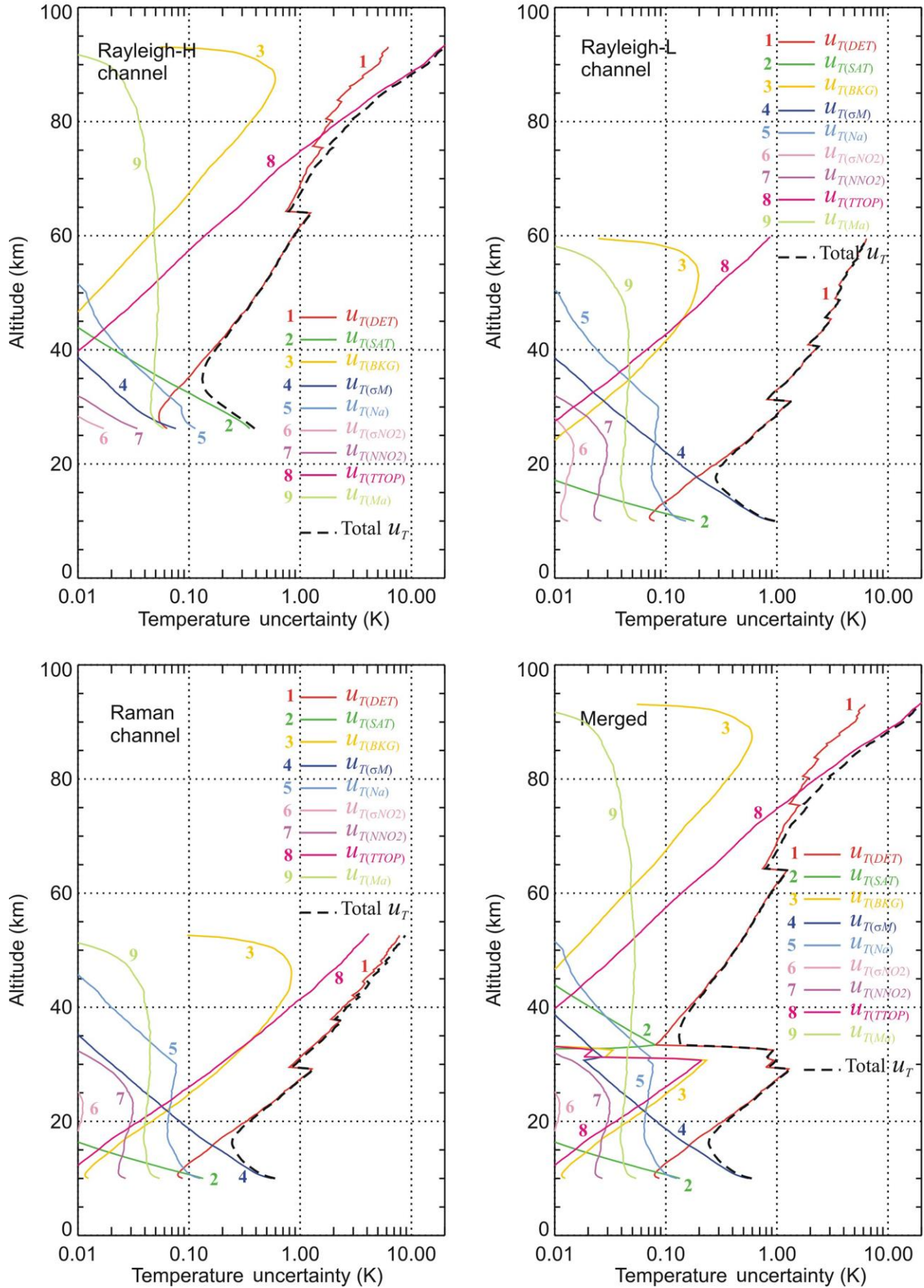


Figure 8. Example of uncertainty budget for the temperature retrievals done with the lidar at Mauna Loa for the high intensity Rayleigh channel (upper left), low intensity Rayleigh channel (upper right), the Raman channel (lower left) and the final profile combining these three channels. Figure reproduced from Leblanc et al., 2016c, their figure 10.

7 Traceability uncertainty analysis

The traceability level definition is given in Table 2.

Table 2. Traceability level definition table

Traceability Level	Descriptor	Multiplier
High	SI traceable or globally recognised community standard	1
Medium	Developmental community standard or peer-reviewed uncertainty assessment	3
Low	Approximate estimation	10

Analysis of the summary table would suggest the following contributions, shown in Table 3, should be considered further to improve the overall uncertainty of the NDACC temperature product. The entires are given in an estimated priority order.

Table 3. Traceability level definition further action table.

Element identifier	Contribution name	Uncertainty contribution form	Typical value	Traceability level (L/M/H)	random, structured random, quasi-systematic or systematic?	Correlated to? (Use element identifier)
3b	Profiles of number density or pressure and temperature	N/A	Largest (<0.2 K) at bottom of profile	M	Random and Systematic	3a
3d2	Profiles of interfering gases: NO ₂	N/A	Depending on NO ₂ density, but up to a 0.2 K error if neglected at 355 nm and 387 nm	L	Random and Systematic	3c
3g	External temperature at tie-on altitude	N/A	Large at top of profile, variable in value depending on closeness model/data	L/M	Random and Systematic	
4a	Vertical filtering	N/A	Variable, Up to 2 K	M	Random and Systematic	

7.1 Recommendations

It is recommended to further research the uncertainty sources that may be involved in the temperature profile retrievals with lidar. The two figures below provide an overview of identified (possible) sources/contributors of uncertainty for the instrumental part (Figure 9) and the processing software part (Figure 10).

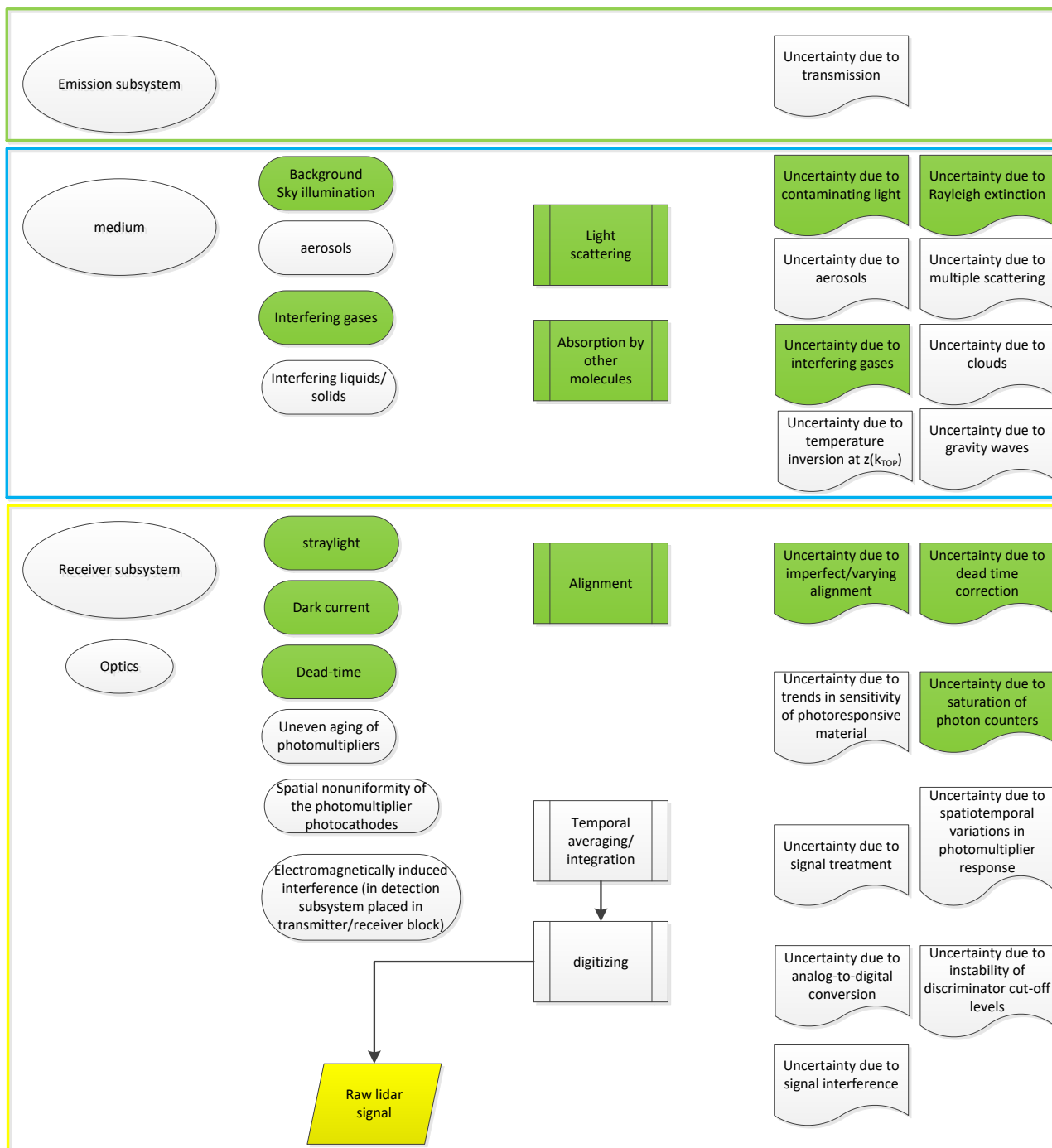


Figure 9. Additional possible sources of uncertainty in the instrumental part of the temperature profile retrieval. Green filled shapes have been discussed in this PTU, unfilled shapes have been identified as possible sources, but are considered negligible in many cases, highly variable, avoidable or complicated to determine.

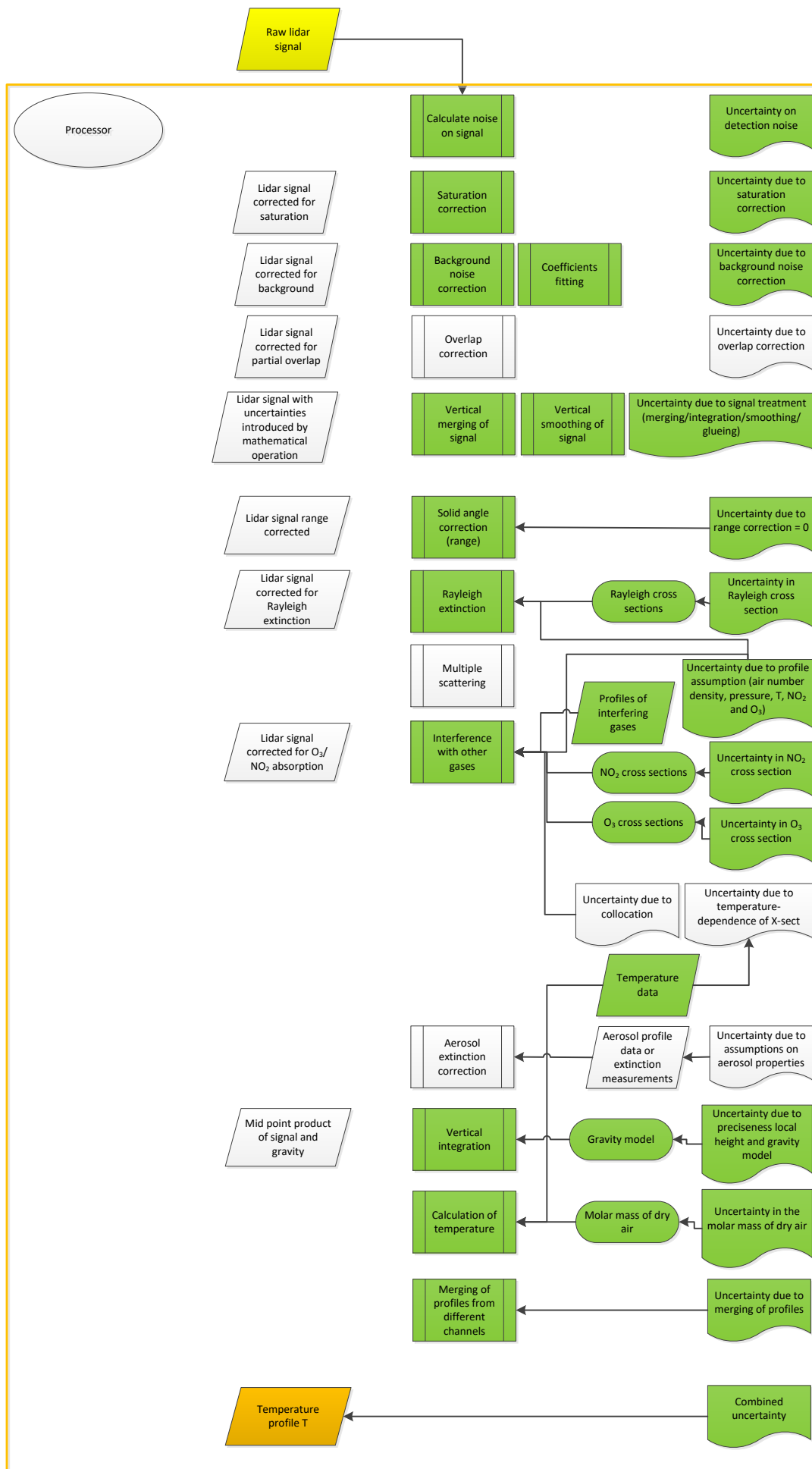


Figure 10. Continuation of Figure 9 with the processing software part.

8 Conclusion

The lidar temperature profile product has been assessed against the GAIA CLIM traceability and uncertainty criteria.

References

1. Ahmad, Z., McClain, C. R., Herman, J. R., Franz, B. A., Kwiatkowska, E. J., Robinson, W. D., Bucsela, E. J., and Tzortziou, M.: Atmospheric correction for NO₂ absorption in retrieving water-leaving reflectances from the SeaWiFS and MODIS measurements, *Appl. Opt.*, 46(26), 6504-6512, 2007.
2. Argall, P. S.: Upper altitude limit for Rayleigh lidar, *Ann. Geophys.*, 25, 19-25, 10.5194/angeo-25-19-2007, 2007.
3. Bates, D. R.: Rayleigh-scattering by air, *Planet Space Sci.*, 32, 785-790, 10.1016/0032-0633(84)90102-8, 1984.
4. Bauer, R., Rozanov, A., McLinden, C. A., Gordley, L. L., Lotz, W., Russell, J. M., Walker, K. A., Zawodny, J. M., Ladstätter-Weissenmayer, A., Bovensmann, H., and Burrows, J. P.: Validation of SCIAMACHY limb NO₂ profiles using solar occultation measurements, *Atmos. Meas. Tech.*, 5, 1059-1084, 10.5194/amt-5-1059-2012, 2012.
5. Bogumil, K., Orphal, J., Homann, T., Voigt, S., Spietz, P., Fleischmann, O. C., Vogel, A., Hartmann, M., Kromminga, H., Bovensmann, H., Frerick, J., and Burrows, J. P.: Measurements of molecular absorption spectra with the SCIAMACHY pre-flight model: instrument characterization and reference data for atmospheric remote-sensing in the 230-2380 nm region, *J. Photochem. Photobiol. A*, 157, 167-184, 10.1016/s1010-6030(03)00062-5, 2003.
6. Bracher, A., Sinnhuber, M., Rozanov, A., and Burrows, J. P.: Using a photochemical model for the validation of NO₂ satellite measurements at different solar zenith angles, *Atmos. Chem. Phys.*, 5, 393-408, 10.5194/acp-5-393-2005, 2005.
7. Brion, J., Chakir, A., Charbonnier, J., Daumont, D., Parisse, C., and Malicet, J.: Absorption Spectra Measurements for the Ozone Molecule in the 350–830 nm Region, *J. Atmos. Chem.*, 30, 291-299, 10.1023/a:1006036924364, 1998.
8. Bristow, M.P.: Lidar-signal compression by photomultiplier gain modulation: influence of detector nonlinearity, *Appl. Opt.* 37, 6468-6479, 1998.
9. Brohede, S., McLinden, C. A., Berthet, G., Haley, C. S., Murtagh, D., and Sioris, C. E.: A stratospheric NO₂ climatology from Odin/OSIRIS limb-scatter measurements, *Can. J. Phys.*, 85, 1253-1274, 10.1139/p07-141, 2007.
10. Burkholder, J. B., and Talukdar, R. K.: Temperature dependence of the ozone absorption spectrum over the wavelength range 410 to 760 nm, *Geophysical Research Letters*, 21, 581-584, 10.1029/93gl02311, 1994.
11. Burrows, J. P., Richter, A., Dehn, A., Deters, B., Himmelmann, S., and Orphal, J.: Atmospheric remote-sensing reference data from GOME - 2. Temperature-dependent absorption cross-sections of O₃ in the 231-794 nm range, *J. Quant. Spectr. Rad. Trans.*, 61, 509-517, 10.1016/s0022-4073(98)00037-5, 1999.
12. Chehade, W., Gorshelev, V., Serdyuchenko, A., Burrows, J. P., and Weber, M.: Revised temperature-dependent ozone absorption cross-section spectra (Bogumil et al.) measured with the SCIAMACHY satellite spectrometer, *Atmos. Meas. Tech.*, 6, 3055-3065, doi:10.5194/amt-6-3055-2013, 2013.
13. Donovan, D. P., Whiteway, J. A., and Carswell, A. I.: Correction for nonlinear photon-counting effects in lidar systems, *Appl. Opt.*, 32(33), 6742-6753, 1993.
14. Eberhard, W. L.: Correct equations and common approximations for calculating Rayleigh scatter in pure gases and mixtures and evaluation of differences, *Appl. Opt.*, 49(7), 1116-1130, 2010.
15. Faduilhe, D., Keckhut P., Bencherif H., Robert L., Baldy S.: Stratospheric temperature monitoring using a vibrational Raman lidar. Part 1: Aerosols and ozone interferences, *J. Environ. Monit.*, 7(4), 357-364, 2005.
16. Freudenthaler, V., Linné, H., Chaikovski, A., Rabus, D., and Groß, S.: EARLINET lidar quality assurance tools, *Atmos. Meas. Tech. Discuss.*, doi:10.5194/amt-2017-395, in review,

- 2018.
17. Gorshchev, V., Serdyuchenko, A., Weber, M., Chehade, W., and Burrows, J. P.: High spectral resolution ozone absorption cross-sections - Part 1: Measurements, data analysis and comparison with previous measurements around 293 K, *Atmos. Meas. Tech.*, 7, 609-624, 10.5194/amt-7-609-2014, 2014.
 18. Gross, M. R., McGee, T. J., Ferrare, R. A., Singh, U. N., and Kimvilakani, P.: Temperature measurements made with a combined Rayleigh-Mie and Raman lidar, *Appl. Opt.*, 36, 5987-5995, 1997.
 19. Hauchecorne, A., and Chanin, M. L.: Density and temperature profiles obtained by lidar between 35-km and 70-km, *Geophys. Res. Lett.*, 7, 565-568, 1980.
 20. Hinkley, E. D.: Laser monitoring of the atmosphere, *Topics in applied physics*, 14, Springer-Verlag, New York, 380 pp., 1976.
 21. Jalali, A, Sica, R.J. and Argall, P.S.: Extending and Merging the Purple Crow Lidar Temperature Climatologies Using the Inversion Method, *ILRC27, EPJ Web of Conferences*, 119, doi:10.1051/epjconf/201611917005, 2016.
 22. Keckhut, P., Hauchecorne, A., and Chanin, M. L.: A critical-review of the database acquired for the long-term surveillance of the middle atmosphere by the French Rayleigh lidars, *Journal of Atmospheric and Oceanic Technology*, 10, 850-867, 10.1175/1520-0426(1993)010<0850:acrot>2.0.co;2, 1993.
 23. Keckhut, P., McDermid, S., Swart, D., McGee, T., Godin-Beekmann, S., Adriani, A., Barnes, J., Baray, J. L., Bencherif, H., Claude, H., di Sarra, A. G., Fiocco, G., Hansen, G., Hauchecorne, A., Leblanc, T., Lee, C. H., Pal, S., Megie, G., Nakane, H., Neuber, R., Steinbrecht, W., and Thayer, J.: Review of ozone and temperature lidar validations performed within the framework of the Network for the Detection of Stratospheric Change, *J. Environ. Monit.*, 6, 721–733, doi:10.1039/b404256e, 2004.
 24. Keckhut, P., Randel, W. J., Claud, C., Leblanc, T., Steinbrecht, W., Funatsu, B. M., Bencherif, H., McDermid, I. S., Hauchecorne, A., Long, C., Lin, R., and Baumgarten, G.: An evaluation of uncertainties in monitoring middle atmosphere temperatures with the ground-based lidar network in support of space observations, *J. Atmos. Sol.-Terr. Phys.*, 73, 627–642, doi:10.1016/j.jastp.2011.01.003, 2011.
 25. Leblanc, T., McDermid, I. S., Hauchecorne, A., and Keckhut, P.: Evaluation of optimization of lidar temperature analysis algorithms using simulated data, *J. Geophys. Res.*, 103, 6177-6187, 1998.
 26. Leblanc, T., Sica, R. J., van Gijsel, J. A. E., Godin-Beekmann, S., Haefele, A., Trickl, T., Payen, G., and Gabarrot, F.: Proposed standardized definitions for vertical resolution and uncertainty in the NDACC lidar ozone and temperature algorithms – Part 1: Vertical resolution, *Atmos. Meas. Tech.*, 9, 4029-4049, <https://doi.org/10.5194/amt-9-4029-2016>, 2016a.
 27. Leblanc, T., Sica, R. J., van Gijsel, J. A. E., Godin-Beekmann, S., Haefele, A., Trickl, T., Payen, G., and Liberti, G.: Proposed standardized definitions for vertical resolution and uncertainty in the NDACC lidar ozone and temperature algorithms – Part 2: Ozone DIAL uncertainty budget, *Atmos. Meas. Tech.*, 9, 4051-4078, <https://doi.org/10.5194/amt-9-4051-2016>, 2016b.
 28. Leblanc, T., Sica, R. J., van Gijsel, J. A. E., Haefele, A., Payen, G., and Liberti, G.: Proposed standardized definitions for vertical resolution and uncertainty in the NDACC lidar ozone and temperature algorithms – Part 3: Temperature uncertainty budget, *Atmos. Meas. Tech.*, 9, 4079–4101, doi:10.5194/amt-9-4079-2016, 2016c.
 29. Leblanc, T., Sica R., van Gijsel, J. A. E., Godin-Beekmann, S., Haefele, A., Trickl, T., Payen, G., and Liberti, G.: Standardized definition and reporting of vertical resolution and uncertainty in the NDACC lidar ozone and temperature algorithms, *ISSI Team on NDACC Lidar Algorithms Report*, available for download at: http://www.issibern.ch/teams/ndacc/ISSI_Team_Report.htm, 2016d.

30. Lemoine, F. C., Kenyon, S. C., Factor, J. K., Trimmer, R. G., Pavlis, N. K., Chinn, D. S., Cox, C. M., Klosko, S. M., Luthcke, S. B., Torrence, M. H., Wang, Y. M., Williamson, R. G., Pavlis, E. C., Rapp, R. H., and Olson, T. R.: The Development of the Joint NASA GSFC and the National Imagery and Mapping Agency (NIMA) Geopotential Model EGM96, Tech. Rep., 1998.
31. Mattis, I., D'Amico, G., Baars, H., Amodeo, A., Madonna, F., and Iarlori, M.: EARLINET Single Calculus Chain – technical – Part 2: Calculation of optical products, *Atmos. Meas. Tech.*, 9, 3009–3029, doi:10.5194/amt-9-3009-2016, 2016.
32. Measures, R. M.: *Laser remote sensing: fundamentals and applications*, Wiley, 510 pp., 1984.
33. Mohr, P. J., Taylor, B. N., and Newell, D. B.: CODATA recommended values of the fundamental physical constants: 2006, *Rev. Mod. Phys.*, 80, 633-730, 10.1103/RevModPhys.80.633, 2008.
34. Müller, J. W.: Dead-time problems, *Nucl. Instr. and Meth.*, 112, 47-57, 10.1016/0029-554x(73)90773-8, 1973.
35. NIMA: Department of Defense World Geodetic System 1984, Tech. Rep., 3rd Edition, 175 pp available at: earth-info.nga.mil/GandG/publications/tr8350.2/wgs84fin.pdf, 2000.
36. Press, W. H.; Flannery, B. P., Teukolsky, S. A., and Vetterling W. T.: *Numerical Recipes: The Art of Scientific Computing* (1st ed.), New York, Cambridge University Press. ISBN 978-0-521-88068-8, 1986.
37. She, C.Y., Alvarez, R.J., Caldwell, L.M. and Krueger, D.A.: High-spectral-resolution rayleigh-mie lidar measurement of vertical aerosol and atmospheric profiles, *Appl. Phys. B*, 55(22), 154-158, doi: 10.1007/BF00324067, 1992.
38. Sica, R. J., Zylawy, Z. A., and Argall, P. S.: Ozone Corrections for Rayleigh-Scatter Temperature Determinations in the Middle Atmosphere, *J. Atmos. Ocean. Tech.*, 18, 1223-1228, doi:10.1175/1520-0426(2001)018<1223:OCFRST>2.0.CO;2, 2001.
39. Sica, R. J., and Haeefe, A.: Retrieval of temperature from a multiple-channel Rayleigh-scatter lidar using an optimal estimation method, *Appl. Opt.*, 54, 1872-1889, 10.1364/ao.54.001872, 2015.
40. Simeonov, V., Larcheveque, G., Quaglia, P., van den Bergh, H. and Calpini, V.: Influence of the photomultiplier tube spatial uniformity on lidar signals, *Appl. Opt.* 38, 5186-5190, 1999.
41. Strauch, R. G., Derr, V. E., and Cupp, R. E.: Atmospheric temperature measurement using raman backscatter, *Appl. Opt.*, 10, 2665-&, 10.1364/ao.10.002665, 1971.
42. Strutt, J. W. (Lord Rayleigh): XXXIV. On the transmission of light through an atmosphere containing small particles in suspension, and on the origin of the blue of the sky, *Philos. Mag.*, 47, 375-384, 10.1080/14786449908621276, 1899.
43. Vandaele, A. C., Hermans, C., Simon, P. C., Carleer, M., Colin, R., Fally, S., Merienne, M. F., Jenouvrier, A., and Coquart, B.: Measurements of the NO₂ absorption cross-section from 42 000 cm⁻¹ to 10 000 cm⁻¹ (238-1000 nm) at 220 K and 294 K, *J. Quant. Spectr. Rad. Trans.*, 59, 171-184, 10.1016/s0022-4073(97)00168-4, 1998.
44. Weitkamp, C.: *Lidar: Range-Resolved Optical Remote Sensing of the Atmosphere*, Springer Series in Optical Sciences, 102, Springer, 460 pp., 2005.



Product Traceability and Uncertainty for the NDACC UV-visible spectroscopy total column ozone product

Version 0.6

*GAIA-CLIM
Gap Analysis for Integrated
Atmospheric ECV Climate Monitoring
Mar 2015 - Feb 2018*

A Horizon 2020 project; Grant agreement: 640276

Date: 22 January 2018

Dissemination level: PU



Work Package 2 - Compiled by Karin Kreher (BKS), François Hendrick (BIRA), Caroline Fayt (BIRA), Christian Hermans (BIRA) and Michel Van Roozendaal (BIRA)

Table of Contents

1	Product overview	5
1.1	Guidance notes	5
2	Introduction.....	9
3	Instrument description.....	9
4	Total O ₃ column algorithm	11
5	Product Traceability Chain	12
6	Element contributions	16
6.1	Raw radiance spectra (1)	16
6.2	Offset and dark signal correction (2).....	17
6.3	Wavelength calibration (3).....	18
6.4	High resolution solar Fraunhofer atlas (3a).....	19
6.5	Instrument slit function (3b).....	20
6.6	Wavelength calibrated radiance spectra (4)	22
6.7	DOAS spectral fit (5)	23
6.8	Retrieval strategy (5a)	24
6.9	Cross-sections at instrument resolution (5b)	25
6.10	Calibrated wavelength grid (5b1)	27
6.11	Laboratory absorption cross-sections (5b2).....	28
6.12	Ring effect cross-sections (5b3)	29
6.13	Differential Slant Column Densities (DSCDs) (6)	30
6.14	Residual amount in reference spectrum – Langley plot approach (7)	31
6.15	Extracted AMFs (7a)	32
6.16	AMF, AVK, ozone profile, and effective airmass location extraction (7a1)	34
6.17	Latitude & longitude of the instrument (7a2)	35
6.18	Altitude of station (7a3).....	36
6.19	AMF & AVK look-up tables, horizontal displacement & TOMS climatology (7a4)	37
6.20	Decimal day number (7a5)	38
6.21	Solar Zenith Angle (SZA) (7a6)	39
6.22	Surface albedo climatology (7a7).....	40
6.23	Absolute slant column densities (SCDs) (8).....	41
6.24	Conversion of SCDs into vertical column densities (VCDs) (9).....	42
6.25	VCDs quality screening (10)	43
6.26	Quality controlled total O ₃ VCDs (11)	43
6.27	GEOMS HDF creation routine (12)	44
6.28	Extracted AVKs, ozone profiles, and effective airmass location (12a).....	45
6.29	GEOMS UV-vis total O ₃ data file (13).....	46

7	Uncertainty Summary	48
8	Traceability uncertainty analysis	50
8.1	Recommendations	52
9	Conclusion	52
	References	53

Version history

Version	Principal updates	Owner	Date
0.1 draft	First draft	BKS	29/07/2017
0.2 draft	Second draft	BKS, NPL	29/11/2017
0.3 draft	Third draft	BKS, BIRA	12/12/2017
0.4 draft	Fourth draft	BKS, BIRA	14/12/2017
0.5 draft	Fifth draft	BKS, BIRA	18/12/2017
0.6 draft	Sixth draft	BKS, BIRA, NPL	26/01/2018
1.0	Final issue	BKS, NPL	1/2/2018

1 Product overview

Product name: Total Column Ozone VCD (Vertical Column Density)

Product technique: DOAS (Differential Optical Absorption Spectroscopy)

Product measurand: Ozone in Dobson Units

Product form/range: Total column integrated along a slant column path

Product dataset: NDACC

Site/Sites/Network location:

- Harestua, Norway, 60.2 °N, 10.8 °E, 596 m asl
- Jungfraujoch, Switzerland, 46.55 °N, 7.98 °E, 3580 m asl

Product time period: 2000 - 2014

Data provider: BIRA-IASB

Instrument provider: BIRA-IASB

Product assessor: Francois Hendrick

Assessor contact email: Francois.Hendrick@aeronomie.be

1.1 Guidance notes

For general guidance see the Guide to Uncertainty in Measurement & its Nomenclature, published as part of the GAIA-CLIM project.

This document is a measurement product technical document which should be stand-alone i.e. intelligible in isolation. Reference to external sources (preferably peer-reviewed) and documentation from previous studies is clearly expected and welcomed, but with sufficient explanatory content in the GAIA-CLIM document not to necessitate the reading of all these reference documents to gain a clear understanding of the GAIA-CLIM product and associated uncertainties entered into the Virtual Observatory (VO).

In developing this guidance, we have created a convention for the traceability identifier numbering as shown in Figure 1. The ‘main chain’ from raw measurand to final product forms the axis of the diagram, with top level identifiers (i.e. 1, 2, 3 etc.). Side branch processes add sub-levels components to the top level identifier (for example, by adding alternate letters & numbers, or 1.3.2 style nomenclature).

The key purpose of this sub-level system is that all the uncertainties from a sub-level are summed in the next level up.

For instance, using Figure 1 contributors 2a1, 2a2 and 2a3 are all assessed as separate components to the overall traceability chain (have a contribution table). The contribution table for (and uncertainty associated with) 2a, should combine all the sub-level uncertainties (and any additional uncertainty intrinsic to step 2a). In turn, the contribution table for contributor 2, should include all uncertainties in its sub-levels.

Therefore, only the top level identifiers (1, 2, 3, etc.) shown in bold in the summary table need be combined to produce the overall product uncertainty. The branches can therefore be considered in isolation, for the more complex traceability chains, with the top level contribution table transferred to the main chain. For instance, Figure 2 & Figure 3 as an example of how the chain can be divided into a number of diagrams for clearer representation.

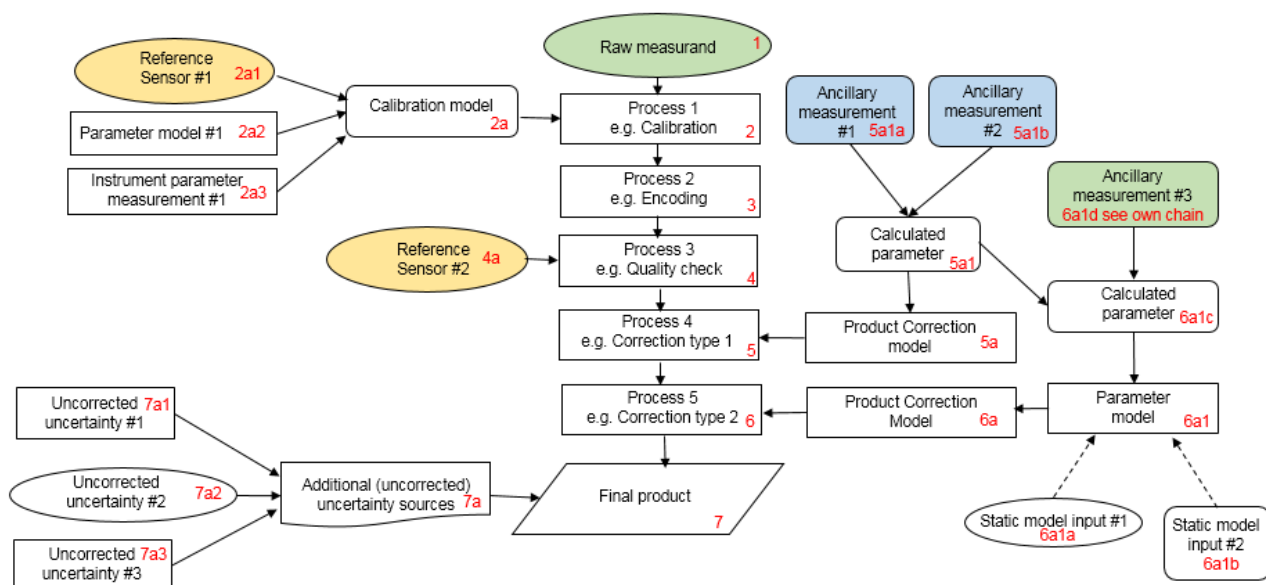


Figure 1. Example traceability chain. Green represents a key measurand or ancillary measurand recorded at the same time with the product raw measurand. Yellow represents a source of traceability. Blue represents a static ancillary measurement

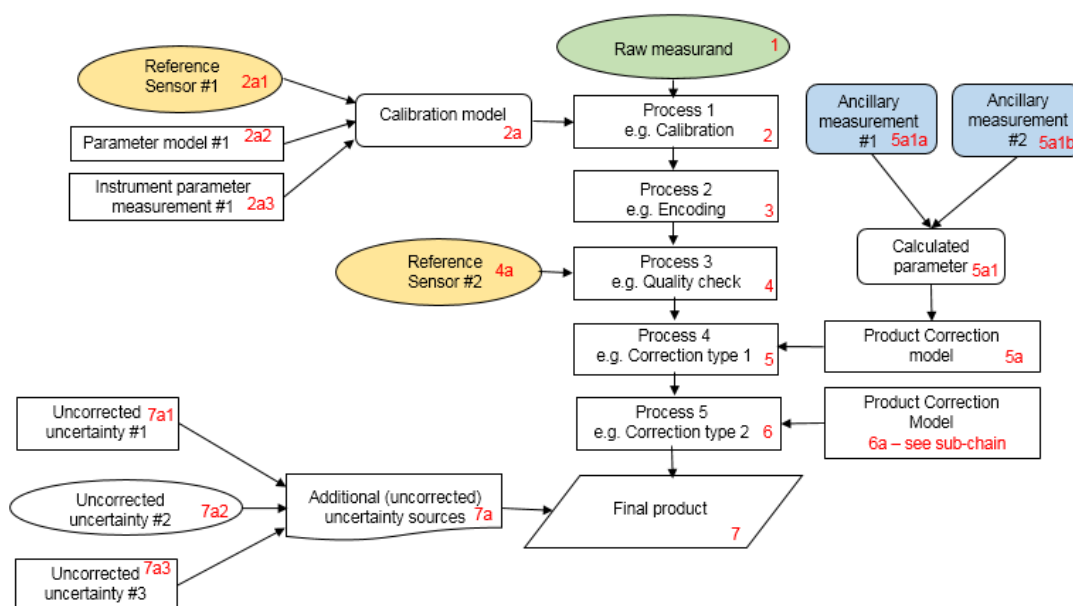


Figure 2. Example chain as sub-divided chain. Green represents a key measurand or ancillary measurand recorded at the same time with the product raw measurand. Yellow represents a source of traceability. Blue represents a static ancillary measurement

When deciding where to create an additional sub-level, the most appropriate points to combine the uncertainties of sub-contributions should be considered, with additional sub-levels used to illustrate where their contributions are currently combined in the described process.

A short note on colour coding. Colour coding can/should be used to aid understanding of the key contributors, but we are not suggesting a rigid framework at this time. In Figure 1, green represents a key measurand or ancillary or complementary measurand recorded at the same time with the raw measurand; yellow represents a primary source of traceability & blue represents a static ancillary measurement (site location, for instance). Any colour coding convention you use, should be clearly described.

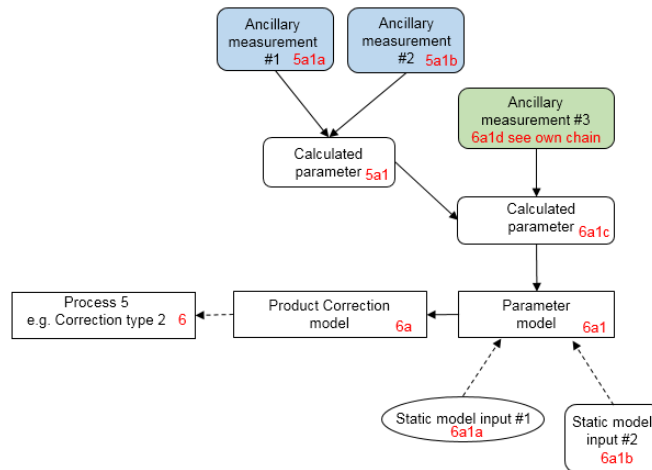


Figure 3. Example chain contribution 6a sub-chain. Green represents a key measurand or ancillary measurand recorded at the same time with the product raw measurand. Blue represents a static ancillary measurement

The contribution table to be filled for each traceability contributor has the form seen in Table 1.

Table 1. The contributor table.

Information / data	Type / value / equation	Notes / description
Name of effect		
Contribution identifier		
Measurement equation parameter(s) subject to effect		
Contribution subject to effect (final product or sub-tree intermediate product)		
Time correlation extent & form		
Other (non-time) correlation extent & form		
Uncertainty PDF shape		
Uncertainty & units		
Sensitivity coefficient		
Correlation(s) between affected parameters		
Element/step common for all sites/users?		
Traceable to ...		
Validation		

Name of effect – The name of the contribution. Should be clear, unique and match the description in the traceability diagram.

Contribution identifier - Unique identifier to allow reference in the traceability chains.

Measurement equation parameter(s) subject to effect – The part of the measurement equation influenced by this contribution. Ideally, the equation into which the element contributes.

Contribution subject to effect – The top level measurement contribution affected by this contribution. This can be the main product (if on the main chain), or potentially the root of a side branch contribution. It will depend on how the chain has been sub-divided.

Time correlation extent & form – The form & extent of any correlation this contribution has in time.

Other (non-time) correlation extent & form – The form & extent of any correlation this contribution has in a non-time domain. For example, spatial or spectral.

Uncertainty PDF shape – The probability distribution shape of the contribution, Gaussian/Normal Rectangular, U-shaped, log-normal or other. If the form is not known, a written description is sufficient.

Uncertainty & units – The uncertainty value, including units and confidence interval. This can be a simple equation, but should contain typical values.

Sensitivity coefficient – Coefficient multiplied by the uncertainty when applied to the measurement equation.

Correlation(s) between affected parameters – Any correlation between the parameters affected by this specific contribution. If this element links to the main chain by multiple paths within the traceability chain, it should be described here. For instance, SZA or surface pressure may be used separately in a number of models & correction terms that are applied to the product at different points in the processing. See Figure 1, contribution 5a1, for an example.

Element/step common for all sites/users – Is there any site-to-site/user-to-user variation in the application of this contribution?

Traceable to – Describe any traceability back towards a primary/community reference.

Validation – Any validation activities that have been performed for this element?

The summary table, explanatory notes and referenced material in the traceability chain should occupy <= 1 page for each element entry. Once the summary tables have been completed for the full end-to-end process, the uncertainties can be combined, allowing assessment of the combined uncertainty, relative importance of the contributors and correlation scales both temporally and spatially. The unified form of this technical document should then allow easy comparison of techniques and methods.

2 Introduction

This document presents the Product Traceability and Uncertainty (PTU) information for the NDACC UV-visible spectroscopy total column ozone product, and in particular for the BIRA measurements made at Harestua and Jungfraujoch. The aim of this document is to assess the current status of the traceability and uncertainty information and to provide supporting information for the users of this product within the GAIA-CLIM VO. The uncertainty and traceability information contained in this document is based on the details given in Hendrick et al, 2011 and the NORS report. (http://nors.aeronomie.be/projectdir/PDF/NORS_D4.3_UB.pdf)

The Network for the Detection of Atmospheric Composition Change (NDACC) consists of a set of globally distributed research stations providing consistent, standardized, long-term measurements of atmospheric trace gases, such as ozone. The aim of the network is to 1) detect changes and trends in atmospheric composition and understanding their impact on the stratosphere and troposphere, 2) to establish scientific links and feedbacks between climate change and atmospheric composition, 3) to validate atmospheric measurements from satellites, 4) to support process-focused scientific field campaigns, and to test and improve theoretical models of the atmosphere.

Within NDACC, the UV-vis Working Group includes more than 35 certified UV-visible spectrometers which are deployed worldwide from pole to pole. With an emphasis on the long-term evolution of the ozone layer, these instruments have provided more than two decades of regular measurements of total column amounts of O₃ but also NO₂, BrO and OCIO retrieved from zenith scattered sunlight DOAS (Differential Optical Absorption Spectroscopy) observations.

DOAS is a measurement technique used to determine the amount of atmospheric trace gas species, such as ozone, by analysing zenith-sky spectra at large solar zenith angles (SZAs). For the analysis of total column ozone, the absorption features of ozone and other relevant trace gases are fitted in the Chappuis bands within a wavelength window of 450-550 nm using a nonlinear least-squares fitting algorithm. This wavelength range avoids contamination by the strongest water vapour (H₂O) and oxygen dimer (O₄) absorption bands while allowing for a good ozone retrieval. Because the light source is the sun and the sun is low on the horizon at large SZA, this allows for a long light path through the atmosphere and the depth of the absorption of the trace gas of interest is used to determine the amount of trace gas measured along the slant paths the sunlight travels through the atmosphere before arriving at the detector. Hence, the product of the spectral analysis are the slant column densities (SCDs), which are then converted into vertical column densities (VCDs) using so-called air mass factors (AMFs) derived by radiative transfer (RT) calculations from locally measured or climatological ozone and air density profiles (see traceability chain in Figure 2 for a more explicit overview).

Hendrick et al. (2011) conclude that the precision in the total column ozone measurements is 4.7% at 1 σ level to which the largest contribution is coming from the AMF and from the uncertainty in the SCD estimated to be 3% (1 σ) at twilight (including the impact of unknown instrumental and systematic misfit effects) and that the total accuracy, important for comparison with other instruments, is 5.9 %.

3 Instrument description

Although there is quite a variety of individual designs for DOAS instruments (see e.g. Figure 3 in PETERS et al. 2012), in general, DOAS instruments consist of: (1) the receiving optics (telescope) to collect the light and guide it into the spectrometer, (2) a grating spectrometer to separate the radiation

into the different wavelengths and to re-image them onto a detector, and (3) a detector to convert the spectrum into a signal which is then read out and transferred to the control computer.

At the Jungfraujoch station, the BIRA-IASB SAOZ (Système d'Analyse par Observation Zénithale) instrument has been operated by BIRA-IASB at the Jungfraujoch station from early 1990's to 2014 (see Figure 4, left). It is a broad-band (300-600 nm), medium resolution (~ 1 nm) diode-array UV-vis spectrometer that measures zenith scattered sunlight (Pommereau and Goutail, 1988). Between 1990 and 2009 two different versions of the SAOZ instrument were used. The first (NMOS) described in Van Roozendaal et al. (1994) is based on a Jobin-Yvon spectrometer (model CP200) coupled to a 512 diode Hamamatsu NMOS detector. In December 1998, the system was upgraded to a 1024 diode Hamamatsu detector. This second version (SAM) provides low sun spectra with a better resolution and a higher signal to noise ratio than the NMOS version. The equipment is operated outside, placed in a dust-and-water proof container. The zenith-sky light is collected through a quartz window with a total field of view of 10° . Measurements are performed from sunrise to sunset up to a SZA of 94° .

Since July 2010, a research-grade MAX-DOAS spectrometer has been operated by BIRA-IASB in parallel to the SAOZ instrument, at the Jungfraujoch station (see Figure 4, right). In brief, it is a dual-channel system composed of two grating spectrometers covering the UV (300 – 390 nm) and visible (400 – 580 nm) wavelength ranges and connected to cooled CCD detectors. The instrumental function is close to a Gaussian with a full width at half maximum (FWHM) of 0.4 nm and 0.5 nm in the UV and visible, respectively. The optical head is mounted on a commercial sun tracker (INTRA, Brusag) and is linked to the spectrometers through optical fibres. The instrument is pointing towards the city of Berne (northwest direction) and a full MAX-DOAS scan consists of the following elevation angles: -10° , -8° , -6° , -4° , -2° , 0° , 1° , 3° , 4° , 5° , 8° , 10° , 15° , 30° , and 90° (zenith). For the retrieval of total O_3 columns, only the twilight zenith-sky observations are used.



Figure 4: Pictures of the SAOZ (left) and research-grade MAX-DOAS spectrometers.

The Harestua instrument consists of two commercial grating spectrometers (ORIEL MultiSpec, 12 cm focal length) mounted together outdoor inside a protection case thermally regulated and continuously flushed with dry nitrogen (see Figure 5). Light from the zenith sky is collected through hemispherical quartz domes and directed towards the entrance of each spectrometer using a depolarising quartz-fibre bundle, which also serves as entrance slit (200 micron width). Spectra are recorded using 1024 pixels cooled diode-array detectors covering respectively the region from 400 to 560 nm with a resolution of 1.2 nm (Spectrometer 1), and the region from 320 to 395 nm with a resolution of 0.7 nm (Spectrometer 2). Two computers (PC) control the acquisition of the spectra. Measurements are performed from sunrise to sunset up to a SZA of 96° . This instrument was continuously operated from January 1998 to April 2013. In November 2012, a new generation instrument based on a similar design was installed to take over from the old one.



Figure 5: Picture of the Harestua instrument currently in operation.

4 Total O₃ column algorithm

Total O₃ VCDs are retrieved from twilight zenith-sky UV-visible spectroscopy observations using the standard NDACC approach described in Hendrick et al., 2011 (see also <http://ndacc-uvvis-wg.aeronomie.be/tools.php>). This method is based on the following expression:

$$VCD(\theta) = \frac{DSCD(\theta) + RCD}{AMF(\theta)} \quad (1)$$

where $VCD(\theta)$ is the O₃ VCD at solar zenith angle (SZA) θ , $DSCD(\theta)$ is the O₃ differential slant column density (DSCD) at SZA θ , RCD is the residual O₃ amount in the reference measurement (a fixed spectrum usually recorded at high sun around local noon), and $AMF(\theta)$ the so-called air mass factor at SZA θ .

First, zenith radiance spectra are analyzed using the DOAS (Differential Optical Absorption Spectroscopy) technique (Platt and Stutz, 2008). The O₃ DSCD, which is the primary product of the DOAS analysis, is retrieved in the 450-550 nm wavelength range, taking into account the spectral signatures of NO₂, H₂O, O₄, and the filling-in of the solar Fraunhofer bands by the Ring effect (Grainger and Ring, 1962). The O₃ absorption cross-sections at 223 K are from Bogumil et al. (2003). A third- to fifth-order polynomial is used to fit the low frequency spectral structure due to molecular and Mie scattering.

In a second step, the absolute O₃ SCD at SZA θ is calculated by adding the RCD to the $DSCD(\theta)$, the RCD being determined using the Langley plot method based on Vaughan et al. (1997). The $VCD(\theta)$ is then derived by dividing the absolute O₃ SCD at SZA θ by an appropriate $AMF(\theta)$. For the selection

of the SZA range representative of twilight conditions, the best compromise between accuracy and precision is achieved in the 86-91° SZA range. The recommended approach is to apply a linear fit on VCDs in the above SZA range and then derive the column value at an effective SZA, which is usually fixed at 90°.

The standard O₃ AMF climatology used in the NDACC total O₃ retrieval is based on the TOMS version 8 (TV8) ozone and temperature profile climatology (Bhartia et al., 2004). It consists of 18 LUTs generated using the UVSPEC/DISORT RTM initialised with TV8, each of these LUT corresponding to one TV8 latitude (10° latitude bands between 90°S and 90°N) (Hendrick et al., 2011). The other entry parameters are: wavelength, ground albedo, altitude of the station, day of the year, and SZA. The extraction of appropriate O₃ AMFs for a given station is done by using the dedicated interpolation routine developed in the framework of the NDACC UV-vis WG (see <http://ndacc-uvvis-wg.aeronomie.be/tools.php>).

5 Product Traceability Chain

The product traceability chain (Figures 6a and 6b) describes each processing step from the raw data (raw radiance spectra) via an intermediate product (differential slant column density - DSCDs) to the final product (quality-controlled total ozone vertical column density - VCD). This chain includes all the calibration and quality control procedures applied within the processing routine.

The complete traceability chain has been divided in 2 parts to be more legible with Figure 6a displaying the first part of the processing chain up to the DSCDs which also includes the physical chain. Elements (A) – (E) in Figure 6a display the steps of the physical chain with solar radiation (A) as input and symbols (B) – (D) representing the main instrumental parts of the DOAS instrument culminating into the measurand which is the raw radiance spectrum (E) and the starting point for the processing chain. As already described under Section 3, the DOAS instruments considered here have two separate units, one containing the telescope and calibration unit (B), and the other one consisting of spectrometer, detector and computer, discussed further under (C) and (D).

(B) Entrance optics

The entrance optics consists of a telescope and a fibre bundle which feeds the light into the spectrometer. This set-up has several advantages:

- 1 As fibre bundles have low light losses, they can be quite long (many meters), resulting in flexible set-up options.
- 2 If the individual fibres within a bundle have a small enough diameter, a fibre bundle can be configured to have a circular aperture at the telescope side and a rectangular shape at the spectrometer slit. This reduces light losses at the slit side of the fibre and minimises the field-of-view of the instrument for the same throughput at the other side, since the latter depends on the fibre bundle total diameter.
- 3 If long enough, quartz fibres are depolarising, minimizing effects from the polarisation dependency of most grating spectrometers in combination with the polarised nature of Rayleigh scattered light.
- 4 If long enough, quartz fibres cause mode mixing leading to a more homogenous illumination of the spectrometer. Mode mixing can be enhanced by using additional treatment of the fibres, e.g. by increasing the bending angles of the fibres.

Any instrumental effects arising from the type of entrance optics used will be dealt with in the processing chain with element identifiers 3, 4 and 5 (including the respective sub-chains).

(C) Grating Spectrometer

The most important parameters for characterising the spectral properties of a DOAS instrument are its spectral range, the spectral resolution, the spectral sampling and the stability of the spectral recording. The spectral range needs to be large enough to cover the spectral window of interest, and it is usually advisable to have a slightly wider range than actually needed to avoid having to use the edge of the detector. The required spectral resolution depends on species and is usually between 0.2 and 1.0 nm. In general, better spectral resolution improves the information content of the measurements but it also reduces the overall throughput and thus the signal to noise ratio. The optimum choice therefore depends on instrument and species. Spectral sampling needs to be large enough to allow good interpolation of the spectra. Spectral stability is vital for good DOAS fits and one should aim at having stability better than at least $1/10^{\text{th}}$ of a detector pixel by temperature stabilising the spectrometer.

Spectrometer straylight can be an issue for measurements particularly in the UV as it decreases apparent absorptions of atmospheric trace gases. Spectral straylight (photons detected in the incorrect spectrometer wavelength channel) is present in all instruments. Accurate characterisation of straylight is best performed with a powerful monochromatic light source (tunable laser) operated at different wavelengths. Alternatively, for a more qualitative analysis, optical cut-off filters can be applied which are opaque for wavelengths below a certain threshold in combination with a broadband or monochromatic light source. However, in DOAS analyses usually a measured spectrum is analysed against a Fraunhofer reference spectrum, which is typically affected by a similar straylight level, often the fitted additional offset is found to be small, while the actual straylight level of the individual spectra might be much larger.

Polarisation sensitivity: The efficiency of both gratings and mirrors is polarisation dependent, and therefore most spectrometers used in DOAS instruments have pronounced polarisation dependency. As atmospheric light is polarised by both Rayleigh and aerosol scattering effects, with their magnitude depending on the relative position of sun and viewing direction, this can create problems in the data analysis. Therefore, most instruments employ fibre optics which are depolarising which is also the case for the instruments discussed here (see also discussion of entrance optics above).

Slit function or instrument transfer function describes the response of the instrument to a monochromatic input. As a result of a finite slit width, spectrometer resolving power and aberrations, and detector pixel size, even a single wavelength input will result in a broadened and blurred line on the detector. Section 6.5 describes in more detail how the slit function is characterised and used within the data processing.

These effects are all dealt with as part of the data processing and are covered in the processing chain under element identifiers 3, 4 and 5 (including the respective sub-chains).

(D) Detector (CCD, PDA)

Several sources contribute to the spectral or instrumental noise. These include photon noise, readout noise and dark current noise. Instrumental noise can be determined by calculating the root mean square of the ratio of two subsequent spectra from a smooth light source (e.g., a halogen lamp). Since the observed signal follows Poisson statistics, the noise level should decrease with the square root of the signal. It is recommended to determine the noise level by calculating the ratio of many spectra at short integration time using a constant light source. A log-log plot of the resulting noise as a function of number of added spectra should yield a straight line with a slope of -0.5. Deviations from this behaviour are an indicator for additional noise sources other than photon noise.

Dark signal is composed of two components – an electronic offset which is artificially added to the signal independent of exposure time and a second term which increases with exposure time. Both terms depend on temperature and can therefore change during operations. Two different approaches can be used to characterise the dark signal: Either, only a limited set of exposure times is used during measurements and dark measurements for each of these exposure times are then subtracted during data calibration. Alternatively, the two components of the dark signal can be determined independently of each other by using very short exposure times for the offset and one or several long exposure times for the dark current. The latter approach allows computation of the dark signal for arbitrary exposure times and is used for the instruments and data analysis discussed here. To characterise changes of dark signal over time, dark measurements should be repeated on a regular basis. The dark signal and its treatment is further discussed under section 6.2

Detector linearity: Good linearity of the detector is a prerequisite for accurate DOAS retrievals as otherwise the large dynamic range of individual spectra introduced by the Fraunhofer lines would result in artefacts at the positions of Fraunhofer lines. Often, detectors deviate from strictly linear behaviour at very low and very large signals, with decreasing efficiency when nearing saturation. For instruments having detectors with non-linear behaviour, the range of good linearity should be determined in the lab and the exposure times during measurements should be selected to result in signals within the linear range. Deviations from linearity can also be characterised and corrected to some degree on the measurements. Nonlinearities can originate from the pixels of the detector or from the electronics processing the signal of the detector and are therefore either pixel specific or common to all pixels. In most instruments, the latter effect dominates.

Detector pixel-to-pixel variability: Both CCD and Photo Diode Array (PDA) detectors have small variations in sensitivity from pixel to pixel. This will cancel when taking the ratio between two measurements taken with the same instrument, but only if the spectral calibration is completely stable. If this is not the case, pixel-to-pixel variability will introduce high frequency structures in the residuals.

Pixel-to-pixel variability can be characterised by taking a measurement with a broadband light source and applying a high pass filter on the result, for example by subtracting a version of the image / spectrum which has been smoothed over 5 pixels. Dividing all measurements pixel wise by this correction will cancel most of the detector variability. As pixel-to-pixel variability is a detector property which usually does not change over time, it is sufficient to characterize it once.

Temperature dependence: Temperature changes of the instrument can influence the operation of instrument in several ways. In particular, for instruments not having a temperature stabilisation, the spectral calibration of the instrument (conversion of pixel number to wavelength) will change with temperature as result of mechanical changes of the instrument. This necessitates application of shift and stretch spectral corrections in the DOAS analysis. In addition, defocusing due to mechanical changes can lead to changes in slit function which impact on the residual and the absolute accuracy of the absorption measurements. This can be at least partly compensated by fitting the slit function in the DOAS retrieval but is limited by parametrisation of the shape of the slit function and computation time. Characterisation of the temperature dependence of the instrument can be done by systematically changing the instrument temperature by heaters or coolers over a temperature range covering all expected instrument temperatures while taking measurements of a spectral line lamp.

These effects are all dealt with as part of the data processing and are covered in the processing chain under element identifiers 2 and 5 (including the respective sub-chains).

NDACC UV-visible total O₃ processing chain – Part A: DOAS retrieval

BIRA-IASB, Belgium

BKScientific GmbH, Germany

v2 - 20/01/2018

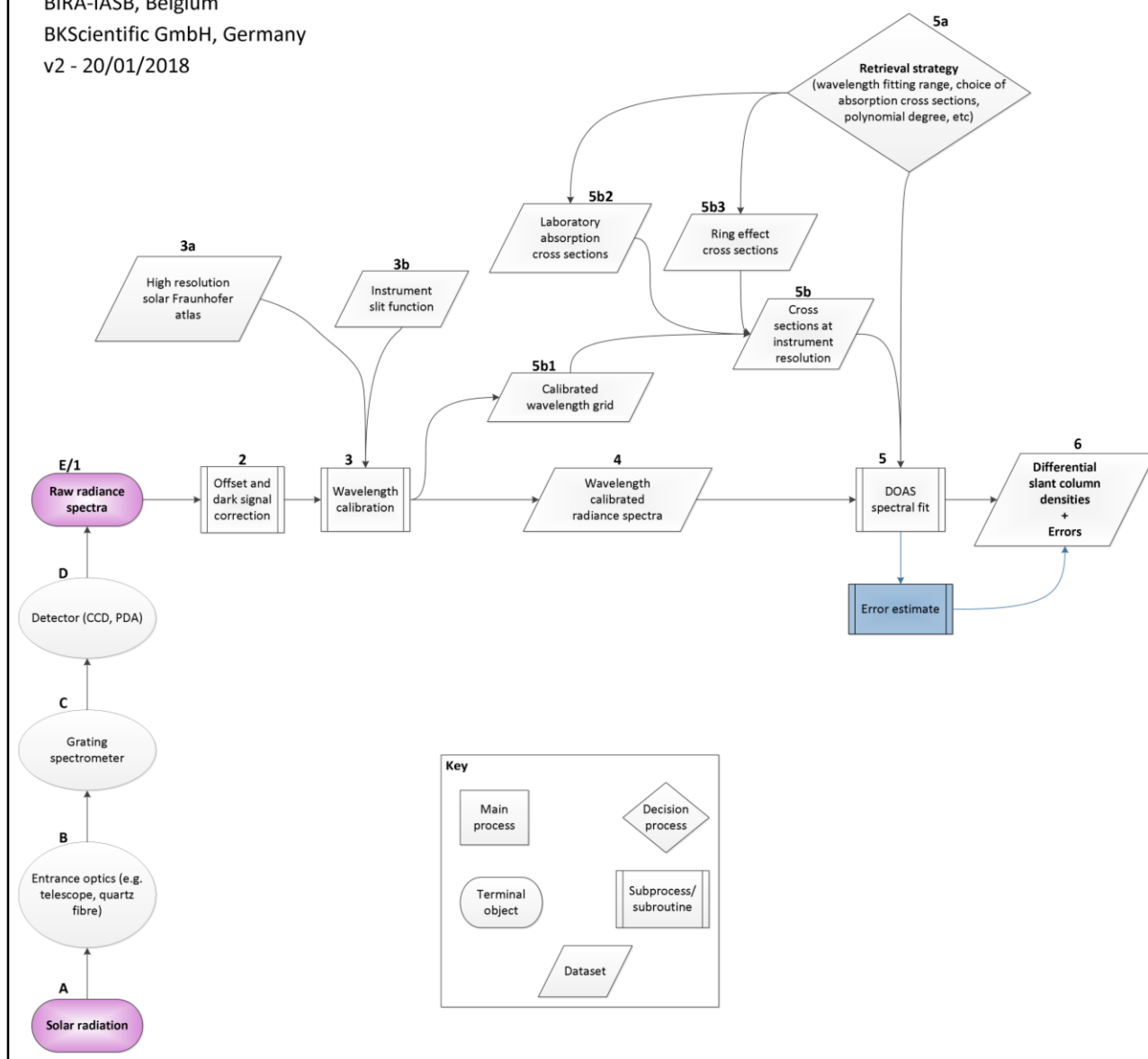


Figure 6a: Traceability chain for UV-visible spectroscopic measurements of total column O₃. The first part shows the chain from the initial raw radiance spectra (1) to the differential slant column densities (6) including all side chain elements. The key lists all the shapes used within the processing chain. This diagram also shows the physical chain (A) – (E) with the oval shape marking important instrumental parts.

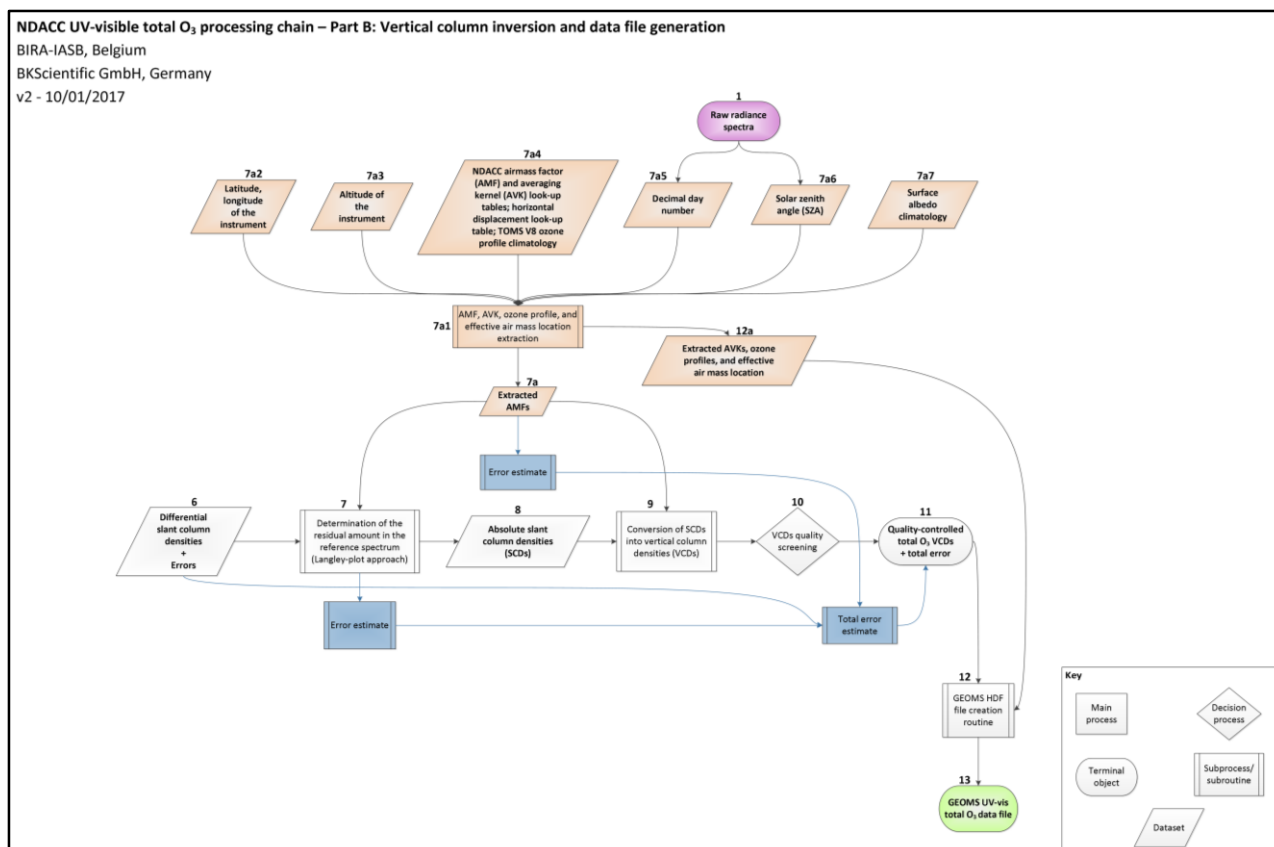


Figure 6b: Traceability chain for UV-visible spectroscopic measurements of total column O₃. The second part shows the chain from the differential slant column densities (6) to the final UV-vis total column ozone data product (13) including all side chain elements.

6 Element contributions

6.1 Raw radiance spectra (1)

As described in more detail in Section 3, the MAX-DOAS instrument at Jungfraujoch is making MAX-DOAS measurements (as in acquiring raw radiance spectra) during most of the day but is looking up in the zenith during twilight. For the retrieval of total O₃ columns, only these twilight zenith-sky observations (86-91° SZA) are used. The same is also true for the measurements made at Harestua. At both stations, the integration time is about 2 minutes around 90° SZA and this corresponds to the accumulation of one single scan.

Photon noise results from the inherent statistical variation in the arrival rate of photons incident on the CCD or PDA. Photoelectrons generated within the semiconductor device constitute the signal, the magnitude of which fluctuates randomly with photon incidence at each measuring location (pixel) on the CCD. The interval between photon arrivals is governed by Poisson statistics, and therefore, the photon noise is equivalent to the square-root of the signal.

Information / data	Type / value / equation	Notes / description
Name of effect	Raw radiance spectra	Light intensity measured in counts per pixel/diode
Contribution identifier	(1)	
Measurement equation parameter(s) subject to effect	$L_{\text{raw}} = L_{\text{raw}}$	No measurement equation, the uncertainty considered

		here is photon noise, other contributions are considered further down the chain
Contribution subject to effect (final product or sub-tree intermediate product)	Wavelength calibrated radiance spectra	
Time correlation extent & form	None	
Other (non-time) correlation extent & form	None	
Uncertainty PDF shape	Normal	
Uncertainty & units	$L_{\text{raw noise}} = \sqrt{\text{signal}}$ Photon noise in photoelectron S/N ratio typically between 1000 and 10000	Square-root of the signal in photoelectrons. Photon noise can be easily estimated by ratioing spectra acquired under same illumination. DOAS systems typically achieve S/N ratios of a few thousands
Sensitivity coefficient	1	
Correlation(s) between affected parameters	None	
Element/step common for all sites/users?	Yes	
Traceable to ...	N/A	statistical
Validation	N/A	

6.2 Offset and dark signal correction (2)

All raw radiance spectra are corrected for their **offset and dark current contribution** (for more details, see Section 5).

Brief description of dark current & offset: The electronic offset is artificially added to the signal independent of exposure time while the dark current increases with exposure time. As both, the dark signal and electronic offset, depend on temperature, it is useful to stabilise the temperature of the CCD or PDA and associated electronic parts to ± 1 K or preferably better accuracy even if it is not cooled.

The BIRA spectrometers at Harestua and Jungfraujoch are kept around 235 K by means of a thermoelectric Pelletier cooling system (accuracy: ± 0.1 K (1σ)). In addition, the whole setup, excluding the CCD, is mounted inside a box thermally regulated using a second Pelletier system (accuracy: ± 1 K (1σ)). In order to minimize thermal stress on mechanical and optical parts. The correction of daytime spectra for dark current is performed using night time dark current measurements (filter wheel in close position).

Information / data	Type / value / equation	Notes / description
Name of effect	Offset and dark current correction	Platt & Stutz, 2008

Contribution identifier	(2)	
Measurement equation parameter(s) subject to effect	$L_{offset_cor} = L_{raw} - (L_{dc} + L_{offset})$	
Contribution subject to effect (final product or sub-tree intermediate product)	Wavelength calibrated radiance spectra	
Time correlation extent & form	24 hours	In the case of Harestua and Jungfraujoch instruments, dark current is measured every night using the filter wheel in the close position. A time correlation is therefore not expected.
Other (non-time) correlation extent & form	None	
Uncertainty PDF shape	Normal	The uncertainty in the offset and dark current correction is very small; night to night differences minimal
Uncertainty & units (1σ)	Square-root of number of thermal electrons per second Noise _{dark} = $\sqrt{\text{dark signal}}$ Around 0.1%	Dark current level is typically around 600cts out of 30000cts; The uncertainty on the combined dark current + offset is around 25cts
Sensitivity coefficient	1	
Correlation(s) between affected parameters	None	
Element/step common for all sites/users?	Yes	
Traceable to ...	Community agreed procedure	
Validation	N/A	

6.3 Wavelength calibration (3)

The **wavelength calibration** (e.g. see Platt and Stutz, 2008) of the reference spectrum is firstly determined using a lamp spectrum (e.g. Hg calibration lamp) and secondly, and more importantly, using a procedure based on the alignment of the Fraunhofer structures of the reference spectrum (I_0) with those of an accurately calibrated high-resolution solar reference atlas, degraded to the resolution of the instrument, i.e. convolved with the instrumental slit function (3b). The solar Fraunhofer atlas used for this purpose is the Chance and Kurucz (2010) spectrum.

For the Jungfraujoch and Harestua data sets, calibration lamp spectra are measured once a year. The Fraunhofer calibration is performed for each spectrum as part of the data analysis.

Information / data	Type / value / equation	Notes / description
Name of effect	Wavelength calibration	2 step process: 1. lamp measurement with distinct lines (e.g. Hg) for wavelength calibration, 2. Fraunhofer ref spectrum
Contribution identifier	(3)	
Measurement equation parameter(s) subject to effect	DSCD(θ)	Shift and stretch applied in each analysis sub-regions, to correct the wavelength alignment
Contribution subject to effect (final product or sub-tree intermediate product)	Wavelength calibrated radiance spectra	
Time correlation extent & form	lamp calibration annually, Fraunhofer – spectrum interval.	
Other (non-time) correlation extent & form	None	
Uncertainty PDF shape	Normal	
Uncertainty & units (1σ)	<0.1 nm (1σ)	Note that any residual shift uncertainty, however, is dealt with in the DOAS fit
Sensitivity coefficient	Non-linear	Any shift residual is re-accessed in the DOAS fit.
Correlation(s) between affected parameters	None	
Element/step common for all sites/users?	Yes	
Traceable to ...	NIST Atomic Spectra Database (ver 5.5.2), 2018 & Fraunhofer lines traceable to Chance and Kurucz (2010)	
Validation	Sensitivity tests	

6.4 High resolution solar Fraunhofer atlas (3a)

The high resolution solar Fraunhofer atlas spectrum used here within the analysis is the Chance and Kurucz spectrum (2010).

Information / data	Type / value / equation	Notes / description
Name of effect	High resolution solar Fraunhofer atlas	Chance and Kurucz (2010)
Contribution identifier	(3a)	

Measurement equation parameter(s) subject to effect	DSCD(θ)	
Contribution subject to effect (final product or sub-tree intermediate product)	Wavelength calibrated radiance spectra	
Time correlation extent & form	Systematic - one list used for full data record.	
Other (non-time) correlation extent & form	None	
Uncertainty PDF shape	Normal	
Uncertainty & units (1σ)	3.5% – 4% (1σ)	Absolute accuracy of 3.5–4% over the relevant wavelength range addressed. The absolute vacuum wavelength accuracy is $\leq 3.2 \times 10^4$ nm above 305 nm. Chance and Kurucz (2010)
Sensitivity coefficient	1 to wavelength – co-efficient product of DOAS fit.	
Correlation(s) between affected parameters	Wavelength calibration.	
Element/step common for all sites/users?	Yes	
Traceable to ...	Traceable back to the wavelength calibration using Chance and Kurucz (2010).	
Validation	N/A	

6.5 Instrument slit function (3b)

The **instrument slit function** or instrument transfer function describes the response of the instrument to a monochromatic input. As a result of a finite slit width, spectrometer resolution and aberrations and detector pixel size, a single monochromatic wavelength input will result in a broadened and blurred line on the detector. As the solar spectrum is highly structured by Fraunhofer lines, accurate knowledge of the instrument function is important for passive DOAS retrievals to correct for filling-in of Fraunhofer lines by inelastic scattering (Ring effect) (Grainger and Ring, 1962). The instrument slit function is essential to convolute the absorption cross-sections of atmospheric gases. Depending on the instrument type, the slit function can be wavelength dependent. In many instruments it also depends on the temperature of the spectrometer and may change over time.

Therefore, slit function characterisation is a task that needs to be repeated regularly in order to identify and characterize changes in the instrument. Instrumental slit functions are generally characterized in the lab using a spectral line lamp (e.g. HgCd). Temporal changes of the slit function are monitored by taking regular measurements with a spectral line lamp placed in front of the telescope or fiber. For a good representation of the slit function, a full and homogenous illumination of the instrument needs to be ensured (e.g. by using a diffusor). To minimize spectrometer non-linearity effects on the slit function spectra, the emission peaks which are used for the analysis are recorded at a similar saturation as the MAX-DOAS measurement spectra.

A good knowledge of the instrumental slit function and its potential wavelength variation is important to avoid systematic errors in the retrieved slant columns due to spectral shape mismatch between the reference and atmospheric spectra.

In the case of the BIRA spectrometers at Harestua and Jungfraujoch, the corresponding instrument slit functions are characterized using HgCd lamp measurements at the time of installation and maintenance of the systems. In addition, slit functions are automatically adjusted using the DOAS spectral fitting software QDOAS making use of the solar Fraunhofer lines.

Information / data	Type / value / equation	Notes / description
Name of effect	Instrument slit function	
Contribution identifier	(3b)	
Measurement equation parameter(s) subject to effect	$y^*(\lambda) = \int_{-\infty}^{\infty} F(\lambda') y(\lambda - \lambda') d\lambda'$	The instrument slit function is firstly applied to the solar reference spectrum - and further down the chain, secondly to the high-res absorption cross-sections
Contribution subject to effect (final product or sub-tree intermediate product)	Wavelength calibrated radiance spectra	
Time correlation extent & form	Yearly	Annual calibration
Other (non-time) correlation extent & form	None	Instrument temperature is stabilised, if any, just very small temperature fluctuations. Slit width has a thermal dependence, however, if this causes changes in the slit width, this will be taken care of in DOAS analysis accordingly, as the line width is a DOAS fit variable.
Uncertainty PDF shape	Normal	
Uncertainty & units (1σ)	<0.1%	The uncertainty on the broad Chappuis ozone cross-section due to ISRF errors is very small (<0.1%), however the error on fitted ozone SCD due to possible misfits introduce by ISRF errors on the Ring effect, or water vapour absorption at 510 nm is larger and can possibly reach the percent level.
Sensitivity coefficient	1	

Correlation(s) between affected parameters	None	
Element/step common for all sites/users?	Yes	
Traceable to ...	The slit function is generally recorded in an ASCII file associated to the spectra files.	Community agreed procedure
Validation	Intercomparisons campaigns	e.g. Piters et al., 2012; Roscoe et al, 2010, Vandaele et al., 2005

6.6 Wavelength calibrated radiance spectra (4)

Given the importance of the wavelength registration for DOAS evaluations in general, the measured spectra have to be aligned with the highest accuracy. This is achieved by correlating the measured spectra with an accurately calibrated high-resolution solar reference spectrum (Chance and Kurucz, 2010) degraded to the resolution of the instrument, i.e. convolved with the instrumental slit function. Least-squares techniques as implemented in the QDOAS software suite (http://uv-vis.aeronomie.be/software/QDOAS/QDOAS_manual.pdf) are used to align the spectra accurately with the Fraunhofer reference.

Wavelength scale shift and stretch are taken into account in the wavelength calibration scheme. To this end, the spectral interval is divided into a number of equally spaced sub-intervals. The fitting algorithm used for the DOAS retrieval is then applied in each sub-interval to fit the measured intensities to those of the high-resolution solar spectrum, according to the equation

$$I_0(\lambda) = I_S(\lambda - \Delta_i) \exp\left(-\sum_{j=1}^m S^j c_j\right)$$

where I_S is the solar spectrum convolved at the resolution of the instrument assuming symmetric (Harestua) or asymmetric (Jungfraujoch) Gaussian line shapes, Δ_i is a fitted constant shift in sub-interval i , and the c_j are optional absorber coefficients accounting for possible light absorption in the reference spectrum I_0 . A value of the shift Δ_i is calculated in each sub-interval i and a polynomial is fitted through the individual points in order to reconstruct an accurate wavelength calibration $\Delta(\lambda)$ for the complete analysis interval.

Information / data	Type / value / equation	Notes / description
Name of effect	Wavelength calibrated radiance spectra	This is a product, not a processing step
Contribution identifier	(4)	
Measurement equation parameter(s) subject to effect	$I_0(\lambda) = I_S(\lambda - \Delta_i) \exp\left(-\sum_{j=1}^m S^j c_j\right)$	
Contribution subject to effect (final product or sub-tree intermediate product)	Differential slant column of ozone	
Time correlation extent & form	None	

Other (non-time) correlation extent & form	None	
Uncertainty PDF shape	Normal	Assumed
Uncertainty & units (1σ)	Uncertainty in wavelength shift in nm, same as in (3) but not to be added up into the summary	
Sensitivity coefficient	1	For small shift values, DSCD errors will scale linearly with shift errors. This can easily be shown by linearizing shift and stretch terms in the DOAS equation.
Correlation(s) between affected parameters	None	
Element/step common for all sites/users?	Yes, but actual numbers are instrument specific	
Traceable to ...	Fraunhofer lines traceable back to the wavelength calibration using Chance and Kurucz (2010).	
Validation	N/A	

6.7 DOAS spectral fit (5)

Each “to-be-analysed” spectrum is ratioed with a so-called “reference” spectrum to remove the dominating Fraunhofer bands and, if relevant, some instrumental artefacts. This “ratio” spectrum is then fitted with the absorption convolved cross-sections of the absorbers relevant for the wavelength range chosen for the analysis. Before the ratio is taken, as part of the fitting procedure, it is essential to properly align the analysed spectrum with respect to the reference using shift and stretch, before taking the ratio. This optimisation is performed as part of the DOAS retrieval procedure using a non-linear iterative least-squares scheme (Marquardt-Levenberg).

For total column retrievals of O₃ from zenith-sky UV-visible spectra the recommended wavelength range is 450-550 nm and absorption cross-sections for O₃, NO₂, H₂O and O₄ are used as well as a Ring cross-section to correct for the filling in of the Fraunhofer bands (Ring effect), a polynomial term to filter out broadband atmospheric attenuation and an offset term to deal with straylight in the spectrometer.

Errors associated to the least-squares fit are due to detector noise, instrumental imperfections (small wavelength scale and resolution changes, etaloning and non-linearities of the detector, stray-light, polarisation effects, etc.) as well as errors or unknowns in the signal modelling (Ring effect, unknown absorbers, wavelength dependence of the AMF, etc). To some extent, such errors are pseudo-random in nature and, as such, can be estimated statistically from the least-squares fitting procedure. Fitting errors derived from the least-squares analysis typically give uncertainties of the order 5 DU for O₃ DSCDs around 90° SZA.

Information / data	Type / value / equation	Notes / description
Name of effect	DOAS spectral fit	Adjustable variables within the fitting procedure are:

		shift and stretch, resolution, absorber concentrations. Aim is to minimise residuals; User judgement involved when fine-tuning the analysis procedure, i.e. we are looking for a residual below a certain threshold
Contribution identifier	(5)	
Measurement equation parameter(s) subject to effect	Differential slant column of ozone	
Contribution subject to effect (final product or sub-tree intermediate product)	Quality controlled total column O ₃ VCD	
Time correlation extent & form	Variable – mainly systematic from assumptions & calibration cycle	
Other (non-time) correlation extent & form	None	
Uncertainty PDF shape	normal	
Uncertainty & units (1σ)	13.45x10 ¹⁹ molec./cm ² (5 Dobson unit)	This is the typical uncertainty in slant column densities resulting from all effects already combined
Sensitivity coefficient	1	
Correlation(s) between affected parameters	None	
Element/step common for all sites/users?	Yes	
Traceable to ...	Community agreed procedure	e.g. Hendrick et al. (2011)
Validation	Intercomparison campaigns	e.g. Piters et al., 2012; Roscoe et al, 2010, Vandaele et al., 2005

6.8 Retrieval strategy (5a)

This step combines all selected constraints and choices for the fitting routine such as wavelength fitting range, choice of absorption cross-sections, polynomial degree, etc. The following settings have been used for the total column O₃ retrieval:

- Fitting interval: 450–550 nm
- Wavelength calibration: based on reference solar atlas (Chance and Kurucz, 2010)
- Cross-sections:
 - O₃ Bogumil et al. (2003), 223° K
 - NO₂ Vandaele et al. (1997), 220° K
 - H₂O Hitran 2010 (Rothman et al., 2010)
 - O₄ Hermans (<http://spectrolab.aeronomie.be/o2.htm>)

- Ring effect Chance and Spurr (1997)
- Molecular and aerosol scattering: Polynomial of order 3, or equivalent non-polynomial high-pass filtering
- Determination of the residual amount in the reference spectrum: Langley-plot approach.
- SZA range: 86-91°SZA; the VCD is derived using a linear fit of VCD versus SZA in this range and taking the corresponding value at 90°SZA.

This is a decision making process and hence not associated with its own uncertainties.

Information / data	Type / value / equation	Notes / description
Name of effect	Retrieval strategy	Hendrick et al. (2011); http://ndacc-uvvis-wg.aeronomie.be/tools/NDACC_UVVIS-WG_O3settings_v2.pdf
Contribution identifier	(5a)	
Measurement equation parameter(s) subject to effect	Differential slant column of ozone	
Contribution subject to effect (final product or sub-tree intermediate product)	Quality controlled total column O ₃ VCD	
Time correlation extent & form	None	
Other (non-time) correlation extent & form	None	
Uncertainty PDF shape	N/A	
Uncertainty & units (1σ)	N/A	
Sensitivity coefficient	1	
Correlation(s) between affected parameters	N/A	
Element/step common for all sites/users?	N/A	
Traceable to ...	N/A	
Validation	Intercomparison campaigns	e.g. Piders et al., 2012; Roscoe et al, 2010, Vandaele et al., 2005

6.9 Cross-sections at instrument resolution (5b)

To account for the generally lower resolution of the spectrometer used for the actual measurements as compared to high-resolution literature cross-sections, the absorption cross-sections listed above in Section 6.8 are convolved with the instrumental slit function (3b) described in Section 6.5 and interpolated on the I_0 wavelength grid. Cross-sections can be pre-convolved and interpolated on an appropriate wavelength grid prior to the analysis. However, the direct use of high-resolution cross-

sections which can be convolved in real-time with a predefined slit function or with the slit function determined by the wavelength calibration procedure, is more flexible and allows to account for a possible day-to-day variability in the slit function. This latter approach is the baseline used for retrievals in Harestua and Jungfraujoch.

Information / data	Type / value / equation	Notes / description
Name of effect	Cross-sections at instrument resolution	http://ndacc-uvvis-wg.aeronomie.be/tools.php
Contribution identifier	(5b)	
Measurement equation parameter(s) subject to effect	$y^*(\lambda) = \int_{-\infty}^{\infty} F(\lambda') y(\lambda - \lambda') d\lambda'$	Equation used for folding high-res absorption cross-section y with instrument slit function F to get the same spectral resolution as the measurements
Contribution subject to effect (final product or sub-tree intermediate product)	Differential slant column of ozone	
Time correlation extent & form	Possible, e.g. if the XSs are only convolved once but the slit function changes with time	Any such time correlation is strongly minimized owing to the instrumental design, which includes active stabilisation of spectrometers and detectors. In addition, possible fluctuations at the scale of days will be efficiently compensated by the dynamical slit function adjustment performed as part of the wavelength calibration procedure.
Other (non-time) correlation extent & form	None	
Uncertainty PDF shape	Normal	
Uncertainty & units (1σ)	<0.1%	The uncertainty due to the ozone cross-section convolution process is small (<0.1%) and related to the uncertainty on the determination of the slit function.
Sensitivity coefficient	1	
Correlation(s) between affected parameters	None	
Element/step common for all sites/users?	Yes	
Traceable to ...	N/A	

Validation	Intercomparison campaigns	e.g. Piders et al., 2012; Roscoe et al, 2010, Vandaele et al., 2005
-------------------	---------------------------	---

6.10 Calibrated wavelength grid (5b1)

The wavelength grid used here is the wavelength grid of the reference spectrum I_0 , calibrated with respect to the high resolution solar Fraunhofer spectrum. Shift and stretch is taken into account in the wavelength calibration scheme. To this end, the spectral interval is divided into a number of equally spaced sub-intervals. The fitting algorithm used for the DOAS retrieval (QDOAS) is then applied in each sub-interval to fit the measured intensities to those of the high-resolution solar spectrum.

Information / data	Type / value / equation	Notes / description
Name of effect	Calibrated wavelengths grid	Shift and stretch applied in equally spaced sub-intervals determine by the user
Contribution identifier	(5b1)	
Measurement equation parameter(s) subject to effect	Differential slant column of ozone	
Contribution subject to effect (final product or sub-tree intermediate product)	Quality controlled total column O ₃ VCD	
Time correlation extent & form	Systematic	
Other (non-time) correlation extent & form	None	
Uncertainty PDF shape	Normal	
Uncertainty & units (1σ)	± 0 nm	Unquantified
Sensitivity coefficient	1	
Correlation(s) between affected parameters	The same calibration is used for the noon reference spectrum and the twilight spectra	
Element/step common for all sites/users?	Yes	
Traceable to ...	Community agreed procedure	Wavelength calibration procedure is available at http://uv-vis.aeronomie.be/software/QDOAS/QDOAS_manual.pdf .
Validation	N/A since specific for each instrument	

6.11 Laboratory absorption cross-sections (5b2)

Comparison studies (e.g. Orphal, 2003) showed that differences of up to 4% in the ozone values depending on the cross-section sources can occur in the region of the Chappuis bands, and even more in the Huggins bands. Therefore the recommendation is the use of a common ozone cross-section data set to avoid systematic differences (Hendrick et al. 2011). From test evaluations, the O₃ cross-section of Bogumil et al. (2003) is recommended since it gives the smallest variance in the residuals as well as good consistency with the ozone retrieval in the UV Huggins bands. Vandaele et al. (1997) at 220 K is generally used for stratospheric NO₂ retrievals and therefore adequate for NO₂ removal in the O₃ fitting range (Hendrick et al., 2011).

Information / data	Type / value / equation	Notes / description
Name of effect	Laboratory absorption cross-sections	O ₃ - Bogumil et al. (2003), 223K NO ₂ - Vandaele et al. (1997), 220K H ₂ O - Hitran 2010 (Rothman et al., 2010) O ₄ - Hermans (http://spectrolab.aeronomie.be/o2.htm)
Contribution identifier	(5b2)	
Measurement equation parameter(s) subject to effect	Differential slant column of ozone	
Contribution subject to effect (final product or sub-tree intermediate product)	Quality controlled total column O ₃ VCD	
Time correlation extent & form	Systematic – across data set in VO	
Other (non-time) correlation extent & form	None	
Uncertainty PDF shape	Normal	
Uncertainty & units (1σ)	Units are cm ² /molec. O ₃ XS specifically introduces an uncertainty of 3% (systematic)	The uncertainty on the O ₃ XS is the main contributor compared to the other species (NO ₂ , H ₂ O, etc.)
Sensitivity coefficient	1	O ₃ uncertainties due to the indirect impact of uncertainties on other cross-section are related to cross-correlation effects. Largest interferences are due to water vapour and O ₄ absorption bands which occasionally can lead to significant interference with ozone. On extreme cases (very humid or heavy cloud contamination), errors of several percent can occur. To minimise the impact of such effects, spectra contaminated by strong H ₂ O or O ₄ absorptions are flagged or excluded

		from the retrieval.
Correlation(s) between affected parameters	Possible	Yes, there can be correlations between the overlapping XSs, hence wavelengths intervals are carefully chosen to minimize that effect.
Element/step common for all sites/users?	Yes	
Traceable to ...	Cross-sections databases (e.g. HITRAN).	
Validation	Cross-sections comparison exercises.	

6.12 Ring effect cross-sections (5b3)

In short: For the correction of the Ring effect “filling-in” solar Fraunhofer lines, the approach published in Chance and Spurr (1997) is still recommended. The ozone differential absorption features are broad enough in the Chappuis bands to ensure that their filling-in by the Ring effect is quite small. However, due to its impact on the Fraunhofer lines, the Ring effect cannot be neglected and is usually treated as a “pseudo” absorber.

More detailed background: Because of Rotational Raman Scattering (RRS), a small fraction of the incident photons undergo a wavelength change of a few nanometres, i.e. a part of the scattering is inelastic. This causes an intensity loss at their incident wavelength and a gain at the neighbouring wavelengths to which they are redistributed. RRS causes the so-called “filling-in” of Fraunhofer lines, which have a slightly different shape in the “earthshine” radiance than in the direct solar light. This effect was first discovered by Grainger and Ring (ref) and is referred to as the Ring effect.

The atmospheric absorption lines are also broadened by RRS events occurring after absorption (molecular Ring effect). Although RRS accounts for only a few percent of the measured intensity, it significantly affects DOAS measurements of scattered radiation since typical trace gas absorptions are of the order of a percent or less. If not properly corrected, the Ring effect can produce strongly structured residuals in the differential optical density, due to the fact that Fraunhofer lines do not cancel perfectly between I and I_0 .

Usually the Ring effect is taken into account by including an additional absorber in the DOAS fit. Ring cross sections S_{Ring} can be measured (Solomon et al., 1987) or calculated (Chance and Spurr, 1997). The Ring effect can then be approximated using the following development for an optically thin atmosphere (Van Roozendaal et al., 2002; Wagner, 1999) and the QDOAS tool calculates a Ring cross-section according to the approach discussed in Wagner, 1999. The Ring effect is generally a major contributor to the differential absorption spectrum, since rotational Raman scattered light typically represents a few percent of the total scattered light. It is therefore critical to include a correction for the Ring effect. Neglecting this effects leads to substantial systematic residual features that may bias ozone DSCDs by several percent due to cross-correlation effect.

Information / data	Type / value / equation	Notes / description
Name of effect	Ring effect cross-sections	http://uv-vis.aeronomie.be/software/QDOAS/QDOAS_manual.pdf
Contribution identifier	(5b3)	

Measurement equation parameter(s) subject to effect	Differential slant column of ozone	
Contribution subject to effect (final product or sub-tree intermediate product)	Quality controlled total column O ₃ VCD	
Time correlation extent & form	Method uncertainties are systematic	
Other (non-time) correlation extent & form	None	
Uncertainty PDF shape	Normal	
Uncertainty & units (1σ)	Units are cm ² /molec. As the other cross-sections	This Ring cross-section is fitted together with all other absorption cross-sections, and the resulting uncertainty in that fit is included the general uncertainty of the DOAS fit.
Sensitivity coefficient	1	
Correlation(s) between affected parameters	None	
Element/step common for all sites/users?	Yes	
Traceable to ...	Community agreed procedure	
Validation	Informal exercises within intercomparison campaigns	e.g. Piders et al., 2012; Roscoe et al, 2010, Vandaele et al., 2005

6.13 Differential Slant Column Densities (DSCDs) (6)

Molecular absorption cross-sections are fitted to the logarithm of the ratio spectrum (5) – the ratio of the measured spectrum and the reference spectrum (i.e. a spectrum measured around local noon when the light path is at a minimum for ground-based measurements). The resulting fit coefficients are the integrated number of molecules per unit area along the atmospheric light path for each trace gas, the **differential slant column densities (SCDs)** which are the direct product of the DOAS analysis.

Information / data	Type / value / equation	Notes / description
Name of effect	Differential Slant Column Densities (DSCDs)	This is not a processing step but describes an important interim product in the processing chain including uncertainties Hendrick et al. (2011)
Contribution identifier	(6)	
Measurement	DSCD, RCD	

equation parameter(s) subject to effect		
Contribution subject to effect (final product or sub-tree intermediate product)	Quality controlled total column O ₃ VCD	
Time correlation extent & form	Systematic	
Other (non-time) correlation extent & form	None	
Uncertainty PDF shape	normal	
Uncertainty & units (1σ)	13.45x10 ¹⁹ ; Uncertainty in molec./cm ² In general, 3% uncertainty in the ozone DSCDs	
Sensitivity coefficient	1	
Correlation(s) between affected parameters	None	
Element/step common for all sites/users?	Yes	
Traceable to ...	Community agreed procedure	
Validation	Intercomparison campaigns	e.g. Piders et al., 2012; Roscoe et al, 2010, Vandaele et al., 2005

6.14 Residual amount in reference spectrum – Langley plot approach (7)

The amount of O₃ present in the optical light path to the instrument minus the amount present in a reference measurement (RCD), is the direct product of the DOAS analysis (see Sect. 4). The RCD is derived using the so-called **Langley plot method**, which consists in rearranging Eq. (1) in Sect. 4 and plotting DSCD(θ) as a function of AMF(θ), the intercept at AMF=0 giving the RCD (Roscoe et al., 1994; Vaughan et al., 1997).

Information / data	Type / value / equation	Notes / description
Name of effect	Langley plot approach	To determine the residual amount in the reference spectrum (RCD) using the Langley plot approach. Van Roozendael et al. (1998), Also: https://en.wikipedia.org/wiki/Langley_extrapolation

Contribution identifier	(7)	
Measurement equation parameter(s) subject to effect	Absolute SCD: DSCD+RCD	
Contribution subject to effect (final product or sub-tree intermediate product)	Quality controlled total column O ₃ VCD	
Time correlation extent & form	Systematic over reference spectrum measurement cycle.	At Harestua and Jungfraujoch, the DOAS analysis is done using daily noon reference spectra, so the Langley plot approach is applied on a daily basis.
Other (non-time) correlation extent & form	Langley plot can only be done on clear mornings or evenings so have a synoptic correlation.	
Uncertainty PDF shape	Normal	
Uncertainty & units (1σ)	~3%; absolute numbers expressed in molec./cm ² Approx. 2% of the total error budget.	
Sensitivity coefficient	1	
Correlation(s) between affected parameters	No	
Element/step common for all sites/users?	Yes	
Traceable to ...	Community agreed procedure and standard	
Validation	Intercomparison campaigns	Informal validation

6.15 Extracted AMFs (7a)

So far, NDACC UV-visible groups commonly use their own DOAS settings and ozone AMFs calculated with different RTMs and sets of ozone, pressure and temperature profiles, with or without latitudinal and seasonal variations. Differences between AMFs are causing the largest discrepancies between the NDACC ozone data sets. The NDACC UV-visible WG provides recommendations to reduce these discrepancies through the use of standardized DOAS settings and O₃ AMF look-up tables (LUTs) calculated using the TOMS version 8 (TV8) O₃ profile climatology that account for the latitudinal and seasonal dependencies of the O₃ vertical profile (Hendrick et al., 2011; see also Sect. 4).

AMFs are extracted for any given station using an interpolation routine in Fortran fed by the LUTs and input values for location (latitude, longitude, altitude) of the station, time of the measurements, wavelength, surface albedo, solar zenith angle (SZA; θ in the table below) .

Information / data	Type / value / equation	Notes / description
Name of effect	Extracted AMFs	Ozone AMFs extracted for time, location and surface albedo
Contribution identifier	(7a)	
Measurement equation parameter(s) subject to effect	RCD, VCD	
Contribution subject to effect (final product or sub-tree intermediate product)	Quality-controlled total column O ₃ VCD	
Time correlation extent & form	Systematic – given site methodology	
Other (non-time) correlation extent & form	None	
Uncertainty PDF shape	Normal	
Uncertainty & units (1σ)	mean uncertainty on AMF: 3.6% (1 σ); no unit. 3.6% corresponds to 3.2e17 molec/cm ² (12 Dobson unit) for a VCD value of 8.9e18 molec/cm ² (330 Dobson Unit), which is a typical yearly mean value for O ₃ VCD at 90°SZA at Harestua. Similar values are found at Jungfraujoch where the yearly mean O ₃ VCD at 90°SZA is about 8.3e18 molec/cm ² (310 Dobson Unit)	Derived by adding in quadrature the uncertainties related to the choice of the O ₃ profile climatology, clouds, aerosols, albedo, and choice of the radiative transfer model for calculating AMFs.
Sensitivity coefficient	1	
Correlation(s) between affected parameters	None	
Element/step common for all sites/users?	LUTs and extraction routine are common for all stations.	
Traceable to ...	Community approved procedure	Hendrick et al. (2011)
Validation	AMF LUTs have been validated by comparison to AMFs calculated from O ₃ sonde and lidar profiles at a selection of stations.	Hendrick et al. (2011)

6.16 AMF, AVK, ozone profile, and effective airmass location extraction (7a1)

The AMF is a key element in the VCD retrieval and its extraction is described in 6.15. AVK, ozone profile, and effective air mass location are provided as ancillary information in the final GEOMS HDF files but are not part of the VCD retrieval itself (ozone profiles are indirectly involved in the retrieval since they are used to generate AMF LUT; see Sect. 6.15). They are all extracted from ad-hoc LUTs (see Hendrick et al., 2011; http://nors.aeronomie.be/projectdir/PDF/D4.4_NORS_SR.pdf). Effective air mass location (expressed in latitude, longitude) are derived using a LUT of horizontal displacement depending on the SZA and altitude. The interpolated horizontal displacement vertical profile is then converted into a latitude, longitude profile based on the solar azimuth angle at the measurement time.

Information / data	Type / value / equation	Notes / description
Name of effect	AMF, AVK, ozone profile, effective airmass location extraction	
Contribution identifier	(7a1)	
Measurement equation parameter(s) subject to effect	RCD and AMF	In contrast to AMF (see 7a), AVK, ozone profiles, and air mass location do not affect any measurement equation parameter.
Contribution subject to effect (final product or sub-tree intermediate product)	Quality controlled total ozone VCDs for AMF	AVK, ozone profiles, and effective air mass location are used to characterize the retrieved O ₃ VCD but are not part of its retrieval. Ancillary data only & not effecting the measurement equation parameters
Time correlation extent & form	Systematic - presumably over full dataset time period.	
Other (non-time) correlation extent & form	None	
Uncertainty PDF shape	Normal	
Uncertainty & units (1σ)	0 (no units)	The uncertainties of these ancillary datasets are not included since they are not part of the data retrieval – purely there as additional information if found helpful for the interpretation of the results
Sensitivity coefficient	1	
Correlation(s) between affected parameters	N/A	
Element/step common for all sites/users?	Yes, within the BIRA sites	Other site operators have different protocols.
Traceable to ...	Community approved procedure	Hendrick et al. (2011) for AMF, AVK, and ozone profiles; for

		effective air mass location, see http://nors.aeronomie.be/projectdiar/PDF/D4.4_NORS_SR.pdf
Validation	AMF LUTs have been validated through comparison to AMFs calculated from O ₃ sonde and lidar profiles at a selection of 9 stations (Hendrick et al., 2011). O ₃ profiles from the TOMS version 8 have been validated through comparison to O ₃ sonde profiles at about 40 stations located all around the world (McPeters et al., 2007). AVK and effective air mass location have not been validated so far.	

6.17 Latitude & longitude of the instrument (7a2)

Latitude and longitude of the instrument are used to extract AMF and ancillary parameters (AVK, effective air mass location). They are taken from the list of NDACC stations (<http://www.ndsc.ncep.noaa.gov/sites/>).

Information / data	Type / value / equation	Notes / description
Name of effect	Latitude and longitude of the instrument	
Contribution identifier	(7a2)	
Measurement equation parameter(s) subject to effect	AMF and RCD calculations	AVK and effective air mass location are ancillary parameters only and do not affect measurement equation parameters.
Contribution subject to effect (final product or sub-tree intermediate product)	Quality controlled total column O ₃ VCD	
Time correlation extent & form	Systematic – list updates.	
Other (non-time) correlation extent & form	None	
Uncertainty PDF shape	Normal	
Uncertainty & units (1σ)	Uncertainty is in 0°.	The uncertainty on the position of the instruments has not been estimated so far. Sensitivity tests show that a difference of 0.1° on the latitude or longitude of the

		instrument has an impact of less than 0.02% on the AMF, and therefore on the RCD determination.
Sensitivity coefficient	Not estimated.	
Correlation(s) between affected parameters	SZA, AMF	
Element/step common for all sites/users?	Yes	
Traceable to ...	Location logged with GPS	http://www.ndsc.ncep.noaa.gov/sites/
Validation	No validation of the latitude and longitude of the instrument done so far.	

6.18 Altitude of station (7a3)

The altitude of an instrument is used to extract AMF and ancillary parameters (AVK, effective air mass location). It is taken from the list of NDACC stations (<http://www.ndsc.ncep.noaa.gov/sites/>).

Information / data	Type / value / equation	Notes / description
Name of effect	Altitude	Altitude of the instrument
Contribution identifier	(7a3)	
Measurement equation parameter(s) subject to effect	AMF and RCD	
Contribution subject to effect (final product or sub-tree intermediate product)	Quality controlled total column O ₃ VCD	
Time correlation extent & form	Systematic over dataset time period.	
Other (non-time) correlation extent & form	None	
Uncertainty PDF shape	Normal	
Uncertainty & units (1σ)	A few meters.	Looking at the NDACC AMF LUTs, the impact on AMF of taking a site altitude of 4km instead of 0km is 5%. Therefore, an uncertainty of a few meters on the altitude of the station has a negligible impact on the AMF and on the VCD.
Sensitivity coefficient	1	

Correlation(s) between affected parameters	None	
Element/step common for all sites/users?	Yes	
Traceable to ...	Altitude logged with GPS	http://www.ndsc.ncep.noaa.gov/sites/
Validation	No validation of the altitude of the instrument is done.	

6.19 AMF & AVK look-up tables, horizontal displacement & TOMS climatology (7a4)

O₃ AMFs and AVK are extracted from LUTs calculated using the TOMS version 8 (TV8) O₃ profile climatology, from which the O₃ vertical profiles reported in the GEOMS files are also extracted. The horizontal displacement LUT has been created by simple ray tracing calculation using the standard AFGL 1976 atmosphere (http://nors.aeronomie.be/projectdir/PDF/D4.4_NORS_SR.pdf). Only the AMFs are used in the retrieval of O₃ VCDs, the other parameters being provided as ancillary information in the GEOMS HDF files.

Information / data	Type / value / equation	Notes / description
Name of effect	AMF and AVK LUTs, horizontal displacement LUT, TOMS V8 ozone profile climatology	See table (6.16)
Contribution identifier	(7a4)	
Measurement equation parameter(s) subject to effect	AMF LUTs and TOMS version 8 climatology affect AMF and RCD	AVK and horizontal displacement (effective air mass location) are ancillary parameters only and do not affect measurement equation parameters.
Contribution subject to effect (final product or sub-tree intermediate product)	Quality controlled total column O ₃ VCD	
Time correlation extent & form	Systematic	
Other (non-time) correlation extent & form	Assumed 1976 profiles – presumably changed since.	
Uncertainty PDF shape	Normal	
Uncertainty & units (1σ)	AMF is unitless. – contributes to 3.6% on the O ₃ VCD total uncertainty, which corresponds to 3.2e17 molec/cm ² (12 Dobson Unit) for a VCD value of 8.9e18 molec/cm ² (330 Dobson Unit), which is a typical yearly mean	See table 6.16

	value for O ₃ VCD at 90°SZA at Harestua. Similar values are found at Jungfraujoch where the yearly mean O ₃ VCD at 90°SZA is about 8.3e18 molec/cm ² (310 Dobson Unit)	
Sensitivity coefficient	1	
Correlation(s) between affected parameters	None	
Element/step common for all sites/users?	Yes	
Traceable to ...	Hendrick et al. (2011) for AMF and AVK; McPeters et al. (2007) for TOMS version 8 climatology, and http://nors.aeronomie.be/projectdir/PDF/D4.4_NORS_SR.pdf for effective air mass location.	
Validation	AMF LUTs have been validated through comparison to AMFs calculated from O ₃ sonde and lidar profiles at a selection of 9 stations (Hendrick et al., 2011). O ₃ profiles from the TOMS version 8 climatology have been validated through comparison to O ₃ sonde profiles at about 40 stations located all around the world (McPeters et al., 2007). AVK and effective air mass location have not been validated so far.	

6.20 Decimal day number (7a5)

The decimal day number corresponding to each measurement is determined using the computer clock. Since the latter is generally updated online to a time server (e.g. NTP), the uncertainty introduced this way should be minimal.

Information / data	Type / value / equation	Notes / description
Name of effect	Decimal day number	
Contribution identifier	(7a5)	
Measurement equation parameter(s) subject to effect	AMF calculation	
Contribution subject to effect (final product or sub-tree intermediate product)	Quality controlled total column O ₃ VCD	

Time correlation extent & form	Computers controlling the instruments are synchronised in time once per day with server like NTP.	
Other (non-time) correlation extent & form	None	
Uncertainty PDF shape	Normal	
Uncertainty & units (1σ)	Assumed negligible compared to other contributions	
Sensitivity coefficient	1	
Correlation(s) between affected parameters	SZA	The deviation of the computer clock with respect to the time server over 24h is about 5s at maximum. Therefore the impact on the SZA is expected to be small, even at high SZA.
Element/step common for all sites/users?	Yes	
Traceable to ...	N/A	
Validation	Validation of the internal clock to time server like NTP.	

6.21 Solar Zenith Angle (SZA) (7a6)

As knowledge of the solar zenith angle (SZA) is crucial for the computation of air mass factors, in particular for stratospheric applications, accurate time has to be saved with the observations. The exact time is usually provided by a GPS sensor or – in case of separated instruments situated indoors – via network time synchronisation. The Solar Zenith Angle (SZA) is directly calculated from the time stamp of the measured raw spectrum, generally using the Meeus (1998) algorithm.

Information / data	Type / value / equation	Notes / description
Name of effect	Solar Zenith Angle (SZA)	
Contribution identifier	(7a6)	
Measurement equation parameter(s) subject to effect	AMF and RCD dependent on the SZA	
Contribution subject to effect (final product or sub-tree intermediate product)	Quality controlled total column O ₃ VCD	
Time correlation extent & form	Systematic	
Other (non-time) correlation extent & form	None	

Uncertainty PDF shape	Normal	
Uncertainty & units (1σ)	0.01 in degree	Assumed, to be confirmed by sensitivity study
Sensitivity coefficient	cos(SZA)	True until high SZA (to be determined)
Correlation(s) between affected parameters	time (7a5)	
Element/step common for all sites/users?	Yes	For sites other than those on VO, uncertainty can be different
Traceable to ...	Meeus, J. "Astronomical Algorithms". Second edition 1998, Willmann-Bell, Inc., Richmond, Virginia, USA	
Validation	Through intercomparison campaign such as CINDI & CINDI-2	Piters et al., 2012; Roscoe et al., 2010, Vandaele et al., 2005

6.22 Surface albedo climatology (7a7)

A global monthly mean climatology of the surface albedo derived from satellite data at 494 nm (Koelemeijer et al., 2003) is coupled to the interpolation routine, so the latter can be initialized with realistic albedo values in a transparent way (Hendrick et al., 2011). The interpolation routine, O₃ AMF LUTs, albedo climatology as well as DOAS settings are publicly available at <http://uv-vis.aeronomie.be/groundbased>.

Information / data	Type / value / equation	Notes / description
Name of effect	Surface albedo climatology	
Contribution identifier	(7a7)	
Measurement equation parameter(s) subject to effect	AMF; AVK depends also on surface albedo but it does not play any role (only ancillary information) in the O ₃ VCD retrieval	
Contribution subject to effect (final product or sub-tree intermediate product)	Quality controlled total column O ₃ VCD	
Time correlation extent & form	None	
Other (non-time) correlation extent & form	None	
Uncertainty PDF shape	Normal	
Uncertainty & units (1σ)	~0.02 at 335nm; Albedo has no units	Koelemeijer et al. (2003) Note: the topography is taken

	Assumed negligible	into account in the climatology through the use of a surface pressure database
Sensitivity coefficient	Not determined but given the zenith viewing geometry, the impact of albedo on AMF is very small (<0.7% when going from an albedo value of 0.04 (ice free sea) to 1 (fresh snow); see Hendrick et al., 2011).	
Correlation(s) between affected parameters	None	
Element/step common for all sites/users?	Yes	
Traceable to ...	Koelemeijer et al. (2003)	
Validation	Comparison of Koelemeijer et al. (2003) surface albedo database to TOMS measurements showed satisfactory agreement.	

6.23 Absolute slant column densities (SCDs) (8)

The obtention of absolute slant column densities (SCDs) is the end product of the first step of the O₃ VCD retrieval (the second step being the conversion of these SCDs into VCDs using the AMFs).

Information / data	Type / value / equation	Notes / description
Name of effect	Quality controlled SCDs	
Contribution identifier	(8)	
Measurement equation parameter(s) subject to effect	VCD	
Contribution subject to effect (final product or sub-tree intermediate product)	Quality controlled total column O ₃ VCD	
Time correlation extent & form	Systematic	
Other (non-time) correlation extent & form	None	
Uncertainty PDF shape	Normal	
Uncertainty & units (1σ)	Overall uncertainty of ~5%; , which corresponds to 7.5e18 molec/cm ² for an absolute SCD value of 1.5e20 molec/cm ² , which is a typical yearly mean value for O ₃	

	SCD at 90°SZA at Harestua. Similar values are found at Jungfraujoch where the yearly mean O ₃ SCD at 90°SZA is about 1.4e18 molec/cm ²	
Sensitivity coefficient	1	
Correlation(s) between affected parameters	None	
Element/step common for all sites/users?	Yes	
Traceable to ...	Community approved process	e.g. Hendrick et al. (2011)
Validation	N/A	

6.24 Conversion of SCDs into vertical column densities (VCDs) (9)

The conversion of SCDs into vertical column densities (VCDs) is the second and last step of the O₃ VCD retrieval. It consists in dividing the SCDs by appropriate AMFs to get VCDs.

Information / data	Type / value / equation	Notes / description
Name of effect	Conversion of SCDs into VCDs	
Contribution identifier	(9)	
Measurement equation parameter(s) subject to effect	$VCD(\theta) = \frac{SCD(\theta)}{AMF(\theta)}$	
Contribution subject to effect (final product or sub-tree intermediate product)	Quality controlled total column O ₃ VCD	
Time correlation extent & form	Systematic – a linearised assumption?	
Other (non-time) correlation extent & form	None	
Uncertainty PDF shape	N/A	
Uncertainty & units (1σ)	N/A	
Sensitivity coefficient	1	
Correlation(s) between affected parameters	N/A	
Element/step common for all sites/users?	Yes	
Traceable to ...	N/A	
Validation	N/A	

6.25 VCDs quality screening (10)

Each group has its own quality screening procedure for VCDs. In the case of the BIRA spectrometers at Harestua and Jungfraujoch, it is done through the removal of data with large fit residuals and the visual inspection of the O₃ VCD time-series (plots of VCDs versus time and comparison between neighbourhood data point values).

Information / data	Type / value / equation	Notes / description
Name of effect	VCDs quality screening	
Contribution identifier	(10)	
Measurement equation parameter(s) subject to effect	$VCD' = VCD$	
Contribution subject to effect (final product or sub-tree intermediate product)	Quality controlled total column O ₃ VCD	
Time correlation extent & form	Systematic	
Other (non-time) correlation extent & form	N/A	
Uncertainty PDF shape	Screening process can change the overall distribution of the uncertainty since the number of higher uncertainty will decrease after the screening.	
Uncertainty & units (1σ)	N/A	
Sensitivity coefficient	1	
Correlation(s) between affected parameters	No	
Element/step common for all sites/users?	No; each group has its own quality screening criteria.	
Traceable to ...	N/A	
Validation	N/A	

6.26 Quality controlled total O₃ VCDs (11)

Quality controlled total O₃ VCDs are the end product resulting from the VCDs quality screening.

Information / data	Type / value / equation	Notes / description
Name of effect	Quality controlled	Hendrick et al. (2011)

Contribution identifier	(11)	
Measurement equation parameter(s) subject to effect	N/A	
Contribution subject to effect (final product or sub-tree intermediate product)	Quality controlled total column O ₃ VCD	
Time correlation extent & form	None	
Other (non-time) correlation extent & form	None	
Uncertainty PDF shape	Normal	
Uncertainty & units (1σ)	Overall uncertainty of ~6%; , which corresponds to 5.3e17 molec/cm ² (19.8 Dobson Unit) for a VCD value of 8.9e18 molec/cm ² (330 Dobson Unit), which is a typical yearly mean value for O ₃ VCD at 90°SZA at Harestua. Similar values are found at Jungfraujoch where the yearly mean O ₃ VCD at 90°SZA is about 8.3e18 molec/cm ² (310 Dobson Unit)	
Sensitivity coefficient	1	
Correlation(s) between affected parameters	N/A	
Element/step common for all sites/users?	Yes	
Traceable to ...	N/A	
Validation	Intercomparison campaigns.	e.g. Piders et al., 2012; Roscoe et al, 2010, Vandaele et al., 2005

6.27 GEOMS HDF creation routine (12)

O₃ VCDs and ancillary information (AVKs, O₃ vertical profiles, and effective air mass location) are converted from their native ascii format to the GEOMS HDF4 format using the GEOMS UVVIS DOAS templates and conversion routines available at <https://avdc.gsfc.nasa.gov/index.php?site=1876901039>.

There is no new uncertainty in this process.

Information / data	Type / value / equation	Notes / description
--------------------	-------------------------	---------------------

Name of effect	GEOMS HDF creation routine	https://avdc.gsfc.nasa.gov/index.php?site=1876901039
Contribution identifier	(12)	
Measurement equation parameter(s) subject to effect	N/A	
Contribution subject to effect (final product or sub-tree intermediate product)	Quality controlled total column O ₃ VCD	
Time correlation extent & form	None	
Other (non-time) correlation extent & form	None	
Uncertainty PDF shape	N/A	
Uncertainty & units (1σ)	N/A	
Sensitivity coefficient	N/A	
Correlation(s) between affected parameters	N/A	
Element/step common for all sites/users?	Yes, except that data providers can also use their own ASCII to GEOMS conversion routines.	
Traceable to ...	N/A	
Validation	No validation required; GEOMS HDf files can be tested again the GEOMS QA/QC checker available at https://avdc.gsfc.nasa.gov/index.php?site=1829327959 .	

6.28 Extracted AVKs, ozone profiles, and effective airmass location (12a)

Extracted AVKs, ozone profiles and effective air mass location are provided as ancillary information to the O₃ VCDs reported in the GEOMS HDF files. They do not affect any measurement equation parameter and are a specific subset of (7a1).

Information / data	Type / value / equation	Notes / description
Name of effect	Extracted AVKs, ozone profiles, and effective airmass location	
Contribution identifier	(12a)	
Measurement equation parameter(s) subject to effect	Extracted AVKs, ozone profiles, and effective	

	airmass location are provided as ancillary information and do not affect any measurement equation parameter.	
Contribution subject to effect (final product or sub-tree intermediate product)	Quality controlled total column O ₃ VCD	
Time correlation extent & form	None	
Other (non-time) correlation extent & form	None	
Uncertainty PDF shape	Normal	
Uncertainty & units (1σ)	N/A	
Sensitivity coefficient	1	
Correlation(s) between affected parameters	N/A	
Element/step common for all sites/users?	Yes	
Traceable to ...	http://ndacc-uvvis-wg.aeronomie.be/tools.php	
Validation	O ₃ profiles extracted from the TOMS version 8 climatology have been validated through comparison to O ₃ sonde profiles at about 40 stations located all around the world (McPeters et al., 2007). AVK and effective air mass location have not been validated so far.	

6.29 GEOMS UV-vis total O₃ data file (13)

The GEOMS UV-vis total O₃ file is the total O₃ column retrieval end product which is made available to users.

Information / data	Type / value / equation	Notes / description
Name of effect	GEOMS UV-vis total O ₃ data file	This is the final product
Contribution identifier	(13)	
Measurement equation parameter(s) subject to effect	N/A	

Contribution subject to effect (final product or sub-tree intermediate product)	N/A	
Time correlation extent & form	None	
Other (non-time) correlation extent & form	None	
Uncertainty PDF shape	N/A	
Uncertainty & units (1σ)	N/A	
Sensitivity coefficient	N/A	
Correlation(s) between affected parameters	N/A	
Element/step common for all sites/users?	Yes	
Traceable to ...	NDACC database (http://www.ndacc.org)	
Validation	No validation required; GEOMS HDF files can be tested again the GEOMS QA/QC checker available at https://avdc.gsfc.nasa.gov/index.php?site=1829327959 .	

7 Uncertainty Summary

Element identifier	Contribution name	Uncertainty contribution form	Typical value	Traceability level (L/M/H)	random, structured random, quasi-systematic or systematic?	Correlated to? (Use element identifier)
1	Raw radiance spectra	$L_{\text{raw noise}} = \sqrt{\text{signal}}$ (Photon noise in counts)	0.01-0.1% (negligible compared to other uncertainties)	N/A	random	4
2	Offset and dark signal correction	$\text{DarkNoise} = \sqrt{\text{DarkSignal}}$	Around 0.1%	M	random & systematic	none
3	Wavelength calibration	wavelength shift & stretch	<0.1 nm	H	systematic	none
3a	High resolution solar Fraunhofer atlas	wavelength accuracy	3.5-4%	H	systematic	none
3b	Instrument slit function	shape of slit function	<0.1%	M	random	none
4	Wavelength calibrated radiance spectra	wavelength accuracy	<0.1nm, based on (3)	M	random & systematic	1
5	DOAS spectral fit	fitting uncertainty	13.45×10^{19} molec./cm ²	M	random & systematic	none
5a	Retrieval strategy	N/A	N/A	N/A	N/A	N/A
5b	Cross-sections at instrument resolution	XS shape & wavelength calibration	<0.1%	M	random & systematic	5b2
5b1	Calibrated wavelength grid	wavelength accuracy	<0.1 nm	M	random & systematic	3,4
5b2	Laboratory absorption cross-section	XS shape & wavelength calibration	3% for ozone	M	random & systematic	5b
5b3	Ring effect cross-sections	Ring XS calculations	estimated roughly 5%	L	random & systematic	none
6	Differential Slant Column Densities (DSCDs)	Combined uncertainty in DSCDs	13.45×10^{19} molec./cm ² or 3%	M	random & systematic	none
7	Residual amount in reference spectrum – Langley plot	Langley extrapolation	~3%	M	random & systematic	7a

	approach					
7a	Extracted AMFs	Differences in AMF calculation approaches	3.6% mean uncertainty	M	random	7a1, 7a4, 12a
7a1	AMF, AVK, ozone profile, and effective airmass location extraction	not effecting the data product uncertainty	N/A	N/A	N/A	7a
7a2	Latitude & longitude of the instrument	exact location	assumed negligible	M	random	none
7a3	Altitude of station	exact altitude	assumed negligible	M	random	none
7a4	AMF & AVK look-up tables, horizontal displacement & TOMS climatology	TOMS climatology	3.6% on O ₃ VCD	M	random & systematic	7a
7a5	Decimal day number	accuracy of date & time	assumed negligible	H	random	7a6
7a6	Solar Zenith Angle (SZA)	accuracy of time	0.01°	H	random	7a5
7a7	Surface albedo climatology	accuracy of surface albedo values	assumed negligible	M	random	none
8	Quality controlled absolute slant column densities (SCDs)	combined uncertainty in calculated SCDs	~5%	M	random & systematic	6, 11
9	Conversion of SCDs into vertical column densities (VCDs)	N/A	N/A	N/A	N/A	N/A
10	VCDs quality screening	N/A	N/A	N/A	N/A	N/A
11	Quality controlled total O₃ VCDs	combined uncertainty in calculated VCDs	~6% corresponds to 5.3e ¹⁷ molec./cm ² or 19.8 DU	H	random & systematic	8
12	GEOMS HDF creation routine	N/A	N/A	N/A	N/A	N/A
12a	Extracted AVKs, ozone profiles,	N/A	N/A	N/A	N/A	N/A

	and effective airmass location					
13	GEOMS UV-vis total O₃ data file	Same as (11)	~6%	H	Systematic + random	11

The element components of the main chain are shown in bold.

Table 2 shows the uncertainty budget from Hendrick et al. 2011, that, although it contains a different set of contributions, results in a similar overall uncertainty estimate of 6% (1 σ). The uncertainty contributions are assumed independent & randomly distributed, so combined in quadrature.

Table 2. Uncertainty summary table from Hendrick et al 2011, table 4 with the corresponding element contribution numbers alongside. Items with an asterisk indicate this is part of an element contribution in this PTU document.

Table 4. Error budget of zenith-sky total O₃ columns measurements in the visible (%).

Error source	Error (%)	
(a) Random		
Slant column spectral fit, including interference effects	3	(7)
O ₃ AMF		
TV8 climatology	1.0	(7a4)*
Clouds	3.3	(7a4)*
Aerosols	0.6	(7a4)*
Albedo	0.7	(7a7)
RTM	0.7	
Precision	4.7	
(b) Systematic		
O ₃ cross sections	3.0	(5b2)
Residual column	2.0	(7)
Total Accuracy	5.9	(11 & 13)

8 Traceability uncertainty analysis

Traceability level definition is given in Table 3.

Table 3. Traceability level definition table

Traceability Level	Descriptor	Multiplier
High	SI traceable or globally recognised community standard	1
Medium	Developmental community standard or peer-reviewed uncertainty assessment	3
Low	Approximate estimation	10

Analysis of the summary table would suggest the following contributions, shown in Table 4, should be considered further to improve the overall uncertainty of the NDACC temperature product.

Table 4. Traceability level definition further action table.

Element identifier	Contribution name	Uncertainty contribution form	Typical value	Traceability level (L/M/H)	random, structured random, quasi-systematic or systematic?	Correlated to? (Use element identifier)
2	Offset and dark signal correction	DarkNoise= $\sqrt{\text{DarkSignal}}$	Around 0.1%	M	random & systematic	none
3b	Instrument slit function	shape of slit function	<0.1%	M	random	none
4	Wavelength calibrated radiance spectra	wavelength accuracy	<0.1nm, based on (3)	M	random & systematic	1
5	DOAS spectral fit	fitting uncertainty	13.45×10^{19} molec./cm ²	M	random & systematic	none
5b	Cross-sections at instrument resolution	XS shape & wavelength calibration	<0.1%	M	random & systematic	5b2
5b1	Calibrated wavelength grid	wavelength accuracy	<0.1 nm	M	random & systematic	3,4
5b2	Laboratory absorption cross-section	XS shape & wavelength calibration	3% for ozone	M	random & systematic	5b
5b3	Ring effect cross-sections	Ring XS calculations	estimated roughly 5%	L	random & systematic	none
6	Differential Slant Column Densities (DSCDs)	Combined uncertainty in DSCDs	13.45×10^{19} molec./cm ² or 3%	M	random & systematic	none
7	Residual amount in reference spectrum – Langley plot approach	Langley extrapolation	~3%	M	random & systematic	7a
7a	Extracted AMFs	Differences in AMF calculation approaches	3.6% mean uncertainty	M	random	7a1, 7a4, 12a
7a2	Latitude & longitude of the instrument	exact location	assumed negligible	M	random	none
7a3	Altitude of station	exact altitude	assumed negligible	M	random	none
7a4	AMF & AVK look-up tables, horizontal displacement &	TOMS climatology	3.6% on O ₃ VCD	M	random & systematic	7a

	TOMS climatology					
8	Quality controlled absolute slant column densities (SCDs)	combined uncertainty in calculated SCDs	~5%	M	random & systematic	6, 11

8.1 Recommendations

There are 15 contributions, see Table 4, that are not SI traceable or do not have a globally recognised community standard. Or, to be more precise, it is actually not so much that these contributions are not necessarily globally recognised or documented as part of reports but rather not as well represented in the peer-reviewed literature as prudent to acknowledge full traceability. One example is that differences in the exact method how to calculate AMFs still causes the largest discrepancies between different data sets. Further analysis and sensitivity studies to quantify and determine the magnitude of these potential contributions would better constrain the uncertainty budget and provide further confidence in traceability.

The contributions given in Table 4 can be divided into some general categories.

Contributions related to wavelength calibration (3, 4 & 5b1) although strictly not SI traceable, are referenced to line calibration lamps, a community standard across many spectroscopy disciplines. In as much, the additional (and onerous step) to SI traceability is unlikely to be necessary, and could be argued that is vicariously SI traceable through the literature wavelength values provided by NMIs such as NIST. The remaining issue for this product is a sensitivity assessment of the impact of the wavelength uncertainty on the retrieved product uncertainty.

Many contributions have ascribed uncertainty assessments in their native units, (cross-section uncertainty) that would not be independently verified by the product suppliers. As such, these uncertainties can be taken at face value. The remaining issue for this product is a sensitivity assessment of the impact of these uncertainty on the retrieved product uncertainty.

Contributions where no assessment of the element uncertainty (e.g. site location & altitude and time stamp uncertainty) has been undertaken, should be addressed. In many cases these are assumed negligible, however, some analysis to evidence this assumption would progress the uncertainty budget towards reference status.

The majority of contributions in Table 4 could be advanced towards reference status with sensitivity studies to understand how these uncertainties propagate to the retrieved product uncertainty.

The validation of the component uncertainty contributions could be made piece-wise, rather than in the cumulative uncertainty to add evidence to the assessment robustness.

9 Conclusion

The UV-visible total column ozone product has been assessed against the GAIA CLIM traceability and uncertainty criteria.

References

- Bhartia, P. K., Wellemeyer, C. G., Taylor, S. L., Nath, N., and Gopalan, A., Solar Backscatter (SBUV) Version 8 profile algorithm, in: Proceedings of the Quadrennial Ozone Symposium 2004, Athens, Greece, edited by C. Zerefos, ISBN 960-630-103-6, pp. 295-296, 2004.
- Bogumil, K., Orphal, J., Homann, T., Voigt, S., Spietz, P., Fleischmann, O. C., Vogel, A., Hartmann, M., Bovensmann, H., Frerik, J., and Burrows, J. P., Measurements of molecular absorption spectra with the SCIAMACHY Pre-Flight Model: Instrument characterization and reference spectra for atmospheric remote sensing in the 230-2380 nm region, *J. Photochem. Photobiol. A*, 157, 167–184, 2003.
- Chance, K. and Spurr, R. J. D., Ring effect studies: Rayleigh scattering including molecular parameters for rotational Raman scattering, and the Fraunhofer spectrum, *Applied Optics*, 36, 5224-5230, 1997.
- Chance, K. and Kurucz, R. L., An improved high-resolution solar reference spectrum for earth's atmosphere measurements in the ultraviolet, visible, and near infrared. *Journal of Quantitative Spectroscopy and Radiative Transfer*, 111(9):1289-1295, 2010.
- Hendrick, F., Pommereau, J.-P., Goutail, F., Evans, R.D., Ionov, D., Pazmino, A., Kyrö, E., Held, G., Eriksen, P., Dorokhov, V., Gil, M., and Van Roozendaal, M., NDACC/SAOZ UV-visible total ozone measurements: improved retrieval and comparison with correlative ground-based and satellite Observations, *Atmos. Chem. Phys.*, 11, 5975–5995, doi:10.5194/acp-11-5975-2011, 2011.
- Grainger, J. and Ring, J.: Anomalous Fraunhofer line profiles, *Nature*, 193, p. 762, 1962.
- Koelemeijer, R. B. A., de Haan, J. F., and Stammes, P.: A database of spectral surface reflectivity in the range 335-772 nm derived from 5.5 years of GOME observations, *J. Geophys. Res.*, 108(D2), 4070, doi:10.1029/2002JD002429, 2003.
- McPeters, R. D., Labow, G. J., and Logan, J. A., Ozone climatological profiles for satellite retrieval algorithms, *J. Geophys. Res.*, 112, D05308, doi:10.1029/2005JD006823, 2007.
- NIST Atomic Spectra Database, [https://physics.nist.gov/PhysRefData/ ASD/lines_form.html](https://physics.nist.gov/PhysRefData/ASD/lines_form.html) [2018, January 15]. National Institute of Standards and Technology, Gaithersburg, MD.
- Orphal, J.: A critical review of the absorption cross-sections of O₃ and NO₂ in the 240-790 nm region, *J. of Photochem. and Photobiol. A: Chemistry*, 157, 185-209, 2003.
- Peters, A.J.M., Boersma, K.F., Kroon, M., Hains, J.C., Van Roozendaal, M., Wittrock, F., Abuhassan, N., Adams, C., Akrami, M., Allaart, M.A.F., Apituley, A., Bergwerff, J.B., Berkhout, A.J.C., Brunner, D., Cede, A., Chong, J., Clémer, K., Fayt, C., Frieß, U., Gast, L.F.L., Gil-Ojeda, M., Goutail, F., Graves, R., Griesfeller, A., Großmann, K., Hemerijckx, G., Hendrick, F., Henzing, B., Herman, J., Hermans, C., Hoexum, M., van der Hoff, G.R., Irie, H., Johnston, P.V., Kanaya, Y., Kim, Y.J., Klein Baltink, H., Kreher, K., et al., The Cabauw Intercomparison campaign for Nitrogen Dioxide measuring Instruments (CINDI): design, execution, and early results, *Atmospheric Measurement Techniques Discussions*, 4, 5935-6005, 2012.
- Platt, U. and Stutz, J.: Differential Optical Absorption Spectroscopy: Principles and Applications. *Physics of Earth and Space Environments*. Springer, Berlin, 2008.
- Roscoe, H. K., Squires, J. A. C., Oldham, D. J., Sarkissian, A., Pommereau, J.-P., and Goutail, F.: Improvements to the accuracy of zenith-sky measurements of total ozone by visible spectrometers, *J. Quant. Spectrosc. Radiat. Transfer*, 52(5), 639-648, 1994.
- Roscoe, H. K., Van Roozendaal, M., Fayt, C., du Piesanie, A., Abuhassan, N., Adams, C., Akrami, M., Cede, A., Chong, J., Clémer, K., Friess, U., Gil Ojeda, M., Goutail, F., Graves, R.,

- Griesfeller, A., Grossmann, K., Hemerijckx, G., Hendrick, F., Herman, J., Hermans, C., Irie, H., Johnston, P. V., Kanaya, Y., Kreher, K., Leigh, R., Merlaud, A., Mount, G. H., Navarro, M., Oetjen, H., Pazmino, A., Perez-Camacho, M., Peters, E., Pinardi, G., Puertedura, O., Richter, A., Schönhardt, A., Shaiganfar, R., Spinei, E., Strong, K., Takashima, H., Vlemmix, T., Vrekoussis, M., Wagner, T., Wittrock, F., Yela, M., Yilmaz, S., Boersma, F., Hains, J., Kroon, M., Peters, A., and Kim, Y. J.: Intercomparison of slant column measurements of NO₂ and O₄ by MAX-DOAS and zenith-sky UV and visible spectrometers, *Atmos. Meas. Tech.*, 3, 1629–1646, doi:10.5194/amt-3-1629-2010, 2010.
- Rothman, L. S., I.E. Gordon, R.J. Barber, H. Dothe, R.R. Gamache, A. Goldman, V.I. Perevalov, S.A. Tashkun, and J. Tennyson, HITEMP, the high-temperature molecular spectroscopic database, *J. Quant. Spectroscopy Radiat. Transfer*, 111, 2139–2150, 2010.
- Solomon, S., Schmeltekopf, A. L., and Sanders, R. W., On the interpretation of zenith sky absorption measurements. *Journal of Geophysical Research*, 92(D7):8311–8319, 1987.
- Vandaele, A. C., Hermans, C., Simon, P. C., Carleer, M., Colin, R., Fally, S., Mérienne, M.-F., Jenouvrier, A., and Coquart, B.: Measurements of the NO₂ absorption cross section from 42 000 cm⁻¹ to 10 000 cm⁻¹ (238–1000 nm) at 220 K and 294 K, *J. Quant. Spectrosc. Ra.*, 59, 171–184, 1997.
- Vandaele, A. C., Fayt, C., Hendrick, F., Hermans, C., Humbled, F., Van Roozendael, M., Gil, M., Navarro, M., Puertedura, O., Yela, M., Braathen, G., Stebel, K., Tørnkqvist, K., Johnston, P., Kreher, K., Goutail, F., Mieville, A., Pommereau, J.-P., Khaikine, S., Richter, A., Oetjen, H., Wittrock, F., Bugarski, S., Frieß, U., Pfeilsticker, K., Sinreich, R., Wagner, T., Corlett, G., and Leigh, R.: An intercomparison campaign of ground-based UV-visible measurements of NO₂, BrO, and OClO slant columns: Methods of analysis and results for NO₂, *J. Geophys. Res.*, 110, D08305, doi:10.1029/2004JD005423, 2005.
- Van Roozendael, M., M. De Maziere, and P.C. Simon, Ground-based visible measurements at the Jungfraujoch station since 1990, *J. Quant. Spectrosc. Radiat. Transfer*, 52, 231–240, 1994.
- Van Roozendael, M., Peters, P., Roscoe, H. K., De Backer, H., Jones, A. E., Bartlett, L., Vaughan, G., Goutail, F., Pommereau, J.-P., Kyrö, E., Wahlstrom, C., Braathen, G., and Simon, P. C., Validation of ground-based visible measurements of total ozone by comparison with Dobson and Brewer spectrophotometers, *J. Atmos. Chem.*, 29, 55–83, 1998.
- Van Roozendael, M., Soebijanta, V., Fayt, C., and Lambert, J., Investigation of DOAS issues affecting the accuracy of the GDP version 3.0 total ozone product. In *ERS-2 GOME GDP 3.0 Implementation and Delta Validation*, 2002.
- Vaughan, G., Roscoe, H. K., Bartlett, L. M., O'Connor, F., Sarkissian, A., Van Roozendael, M., Lambert, J.-C., Simon, P. C., Karlsen, K., Kaestad Hoiskar, B. A., Fish, D. J., Jones, R. L., Freshwater, R., Pommereau, J.-P., Goutail, F., Andersen, S. B., Drew, D. G., Hughes, P. A., Moore, D., Mellqvist, J., Hegels, E., Klupfel, T., Erle, F., Pfeilsticker, K., and Platt, U.: An intercomparison of ground-based UV-visible sensors of ozone and NO₂, *J. Geophys. Res.*, 102, 1411–1422, 1997.
- Wagner, T., Satellite Observations of Atmospheric HalogenOxides. PhD thesis, University of Heidelberg, 1999.



Product Traceability and Uncertainty for the GNSS IPW Product

Version 1.0

*GAIA-CLIM
Gap Analysis for Integrated
Atmospheric ECV Climate Monitoring
Mar 2015 - Feb 2018*

A Horizon 2020 project; Grant agreement: 640276

Date: 02 February 2017

Dissemination level: PU

Work Package 2; Compiled by Kalev Rannat & Jonathan Jones

Table of Contents

1	Product overview	5
1.1	Guidance notes	5
2	Introduction.....	9
2.1	Instruments	9
2.1.1	Instruments for GNSS data acquisition.....	9
2.1.2	Instruments for surface meteorological data acquisition	11
2.2	Methods	12
2.2.1	Network solution (DD)	12
2.2.2	Precise Point Positioning (PPP)	12
2.2.3	PPP or DD?	12
2.3	Software.....	12
2.3.1	Software for GNSS data processing.....	12
2.3.2	Software for GNSS IPW derivation.....	13
3	Product Traceability Chain	15
4	Element contributions	16
4.1	Satellite orbits (1)	16
4.2	Satellite clocks (2)	18
4.3	GNSS observations (3).....	19
4.3.1	Additional uncertainty sources (3a)	20
4.4	Forward Model (GNSS-data processing) (4)	26
4.5	Model and software-specific constraints set by data analyst (4a)	28
4.6	Atmospheric load (4b).....	29
4.7	Ocean tidal load (4c)	30
4.8	Mapping functions (4d).....	31
4.9	Zenith Total Delay (5).....	32
4.10	Site Ts (Surface temperature) (6)	33
4.11	Site Surface Pressure Ps (7).....	34
4.12	Mean temperature of the atmosphere Tm (8)	35
4.13	Site latitude and height above the mean sea level (9).....	36
	Physical constants (10).....	37
4.14	37
4.15	GNSS-IPW Processor and Uncertainty Estimator (11)	38
5	Uncertainty Summary	42
6	Traceability uncertainty analysis	45
6.1	Summary	46
6.2	Recommendations	46

7 Conclusion46

References.....48

Version history

Version	Principal updates	Owner	Date
0.1 draft	First circulated draft	TUT	11.10.2017
0.3 draft	Third draft	TUT	26.10.2017
0.4 draft	Fourth draft	TUT	04.12.2017
0.5 draft	Fifth draft	TUT	12.12.2017
0.6 draft	Sixth draft	TUT	04.01.2018
0.7 draft	Seventh draft	TUT	09.01.2018
1.0	Issued as part of D2.8	TUT	02.02.2018

1 Product overview

Product name: GNSS IPW (Global Navigation Satellite System Integrated Precipitable Water)

Product technique: Total Column Water Vapour (also known and hereafter named as Integrated Precipitable Water) derived from GNSS signal delays and ground-based meteorological data

Product measurand: IPW in kg/m^2

Product form/range: IPW time series

Product dataset: E-GVAP

Site/Sites

- GRUAN <https://www.gruan.org/network/sites/>

Other networks having sites with high-quality GNSS-data, but not (yet) implementing GRUAN-like uncertainty analysis which could be included in future:

- IGS Network (<http://www.igs.org/>)
- EUREF Network (<http://www.epncb.oma.be/>)
- Various National Geodetic Agencies (e.g. Ordnance Survey GB, <https://www.ordnancesurvey.co.uk/>)
- Various National Meteorological and Hydrological Agencies (e.g. Met Office, <https://www.metoffice.gov.uk/>)
- Various Commercial Agencies (e.g. Leica, <http://www.smartnet-eu.com/>)

Product time period: Depends on site and available in delayed-mode for GRUAN GNSS-product public access.

Data provider: GRUAN

Instrument provider: not identified, but the instrumentation and installations must follow the Current IGS Site Guidelines (<https://kb.igs.org/hc/en-us/articles/202011433-Current-IGS-Site-Guidelines>), sections 2.1.9 and 2.1.11).

Product assessor (for GRUAN): Kalev Rannat & Galina Dick

Assessor contact email (for GRUAN): kalev.rannat@gmail.com or galina.dick@gfz-potsdam.de

1.1 Guidance notes

For general guidance see the Guide to Uncertainty in Measurement & its Nomenclature, published as part of the GAIA-CLIM project.

This document is a measurement product technical document which should be stand-alone i.e. intelligible in isolation. Reference to external sources (preferably peer-reviewed) and documentation from previous studies is clearly expected and welcomed, but with sufficient explanatory content in the GAIA-CLIM document not to necessitate the reading of all these reference documents to gain a clear understanding of the GAIA-CLIM product and associated uncertainties entered into the Virtual Observatory (VO).

In developing this guidance, we have created a convention for the traceability identifier numbering as shown in Figure 1. The ‘main chain’ from raw measurand to final product forms the axis of the diagram, with top level identifiers (i.e. 1, 2, 3 etc.). Side branch processes add sub-levels components to the top level identifier (for example, by adding alternate letters & numbers, or 1.3.2

style nomenclature).

The key purpose of this sub-level system is that all the uncertainties from a sub-level are summed in the next level up.

For instance, using Figure 1, contributors 2a1, 2a2 and 2a3 are all assessed as separate components to the overall traceability chain (have a contribution table). The contribution table for (and uncertainty associated with) 2a, should combine all the sub-level uncertainties (and any additional uncertainty intrinsic to step 2a). In turn, the contribution table for contributor 2, should include all uncertainties in its sub-levels.

Therefore, only the top level identifiers (1, 2, 3, etc.) shown in bold in the summary table need be combined to produce the overall product uncertainty. The branches can therefore be considered in isolation, for the more complex traceability chains, with the top level contribution table transferred to the main chain. For instance, see Figure 2 & Figure 3 as an example of how the chain can be divided into a number of diagrams for clearer representation.

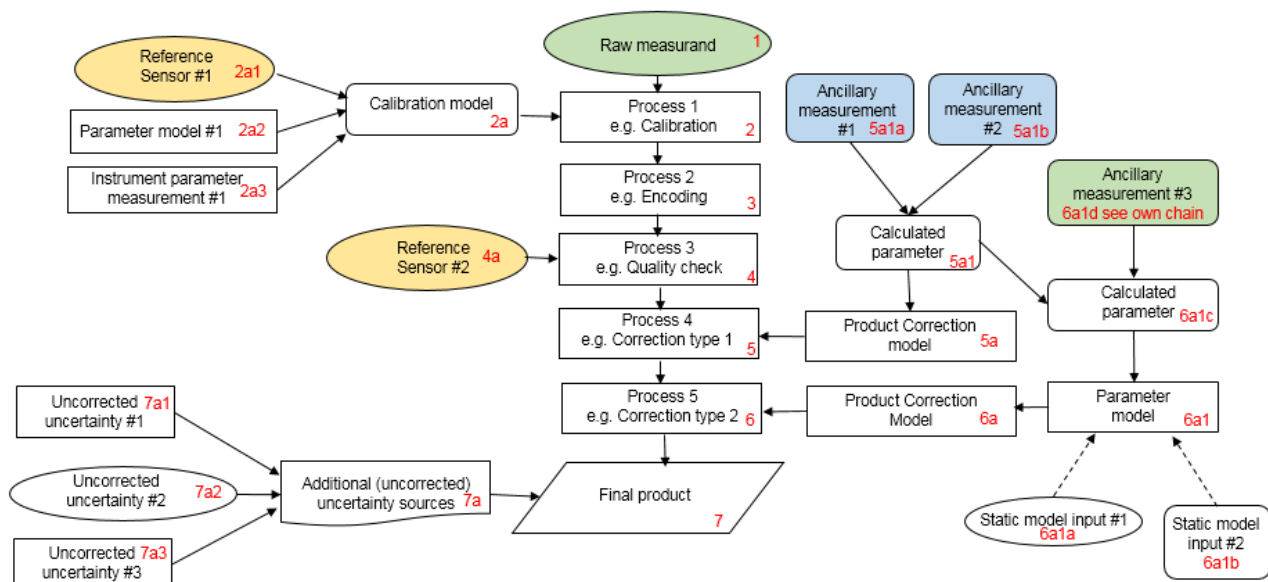


Figure 1. Example traceability chain. Green represents a key measurand or ancillary measurand recorded at the same time with the product raw measurand. Yellow represents a source of traceability. Blue represents a static ancillary measurement

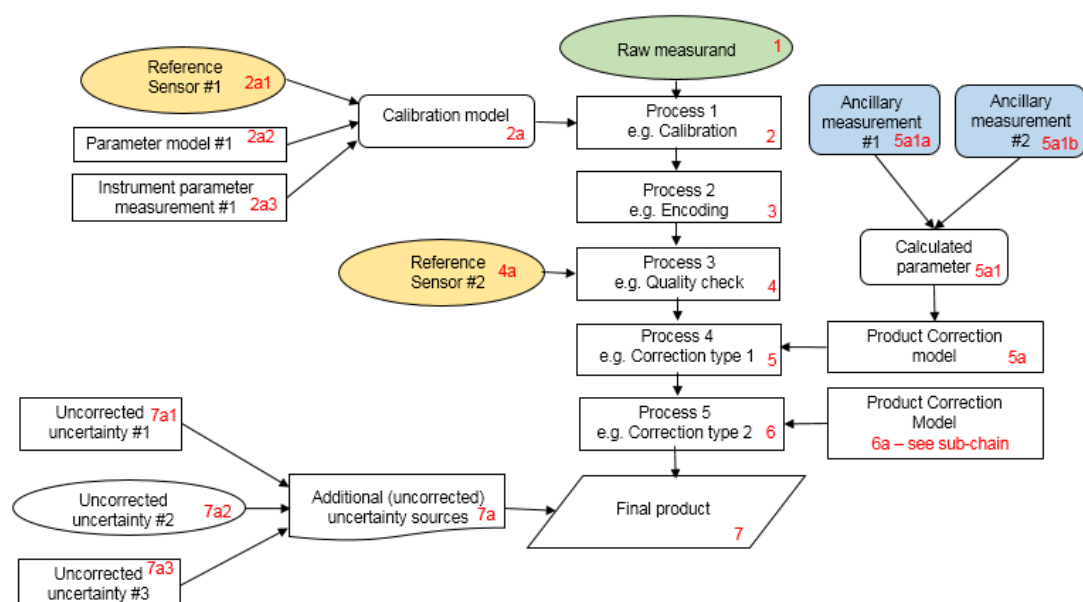


Figure 2. Example chain as sub-divided chain. Green represents a key measurand or ancillary measurand recorded at the same time with the product raw measurand. Yellow represents a source of traceability. Blue represents a static ancillary measurement

When deciding where to create an additional sub-level, the most appropriate points to combine the uncertainties of sub-contributions should be considered, with additional sub-levels used to illustrate where their contributions are currently combined in the described process.

A short note on colour coding. Colour coding can/should be used to aid understanding of the key contributors, but we are not suggesting a rigid framework at this time. In Figure 2, green represents a key measurand or ancillary or complementary measurand recorded at the same time with the raw measurand; yellow represents a primary source of traceability & blue represents a static ancillary measurement (site location, for instance). Any colour coding convention you use, should be clearly described.

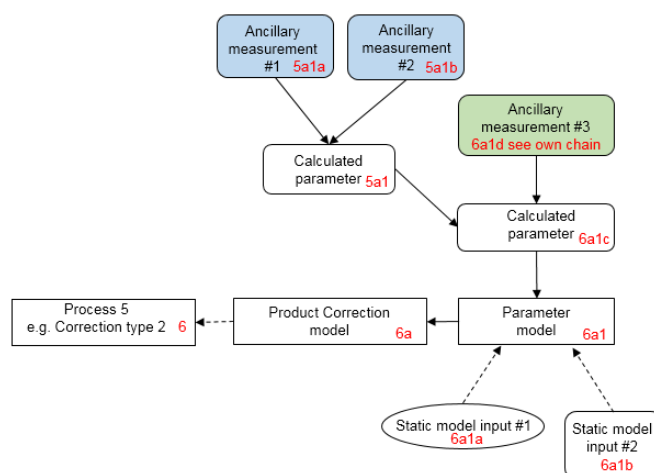


Figure 3. Example chain contribution 6a sub-chain. Green represents a key measurand or ancillary measurand recorded at the same time with the product raw measurand. Blue represents a static ancillary measurement

The contribution table to be filled for each traceability contributor has the form seen in Table 1.

Table 1. The contributor table.

Information / data	Type / value / equation	Notes / description
Name of effect		
Contribution identifier		
Measurement equation parameter(s) subject to effect		
Contribution subject to effect (final product or sub-tree intermediate product)		
Time correlation extent & form		
Other (non-time) correlation extent & form		
Uncertainty PDF shape		
Uncertainty & units		
Sensitivity coefficient		
Correlation(s) between affected parameters		
Element/step common for all sites/users?		
Traceable to ...		
Validation		

Name of effect – The name of the contribution. Should be clear, unique and match the description in the traceability diagram.

Contribution identifier - Unique identifier to allow reference in the traceability chains.

Measurement equation parameter(s) subject to effect – The part of the measurement equation influenced by this contribution. Ideally, the equation into which the element contributes.

Contribution subject to effect – The top level measurement contribution affected by this contribution. This can be the main product (if on the main chain), or potentially the root of a side branch contribution. It will depend on how the chain has been sub-divided.

Time correlation extent & form – The form & extent of any correlation this contribution has in time.

Other (non-time) correlation extent & form – The form & extent of any correlation this contribution has in a non-time domain. For example, spatial or spectral.

Uncertainty PDF shape – The probability distribution shape of the contribution, Gaussian/Normal Rectangular, U-shaped, log-normal or other. If the form is not known, a written description is sufficient.

Uncertainty & units – The uncertainty value, including units and confidence interval. This can be

a simple equation, but should contain typical values.

Sensitivity coefficient – Coefficient multiplied by the uncertainty when applied to the measurement equation.

Correlation(s) between affected parameters – Any correlation between the parameters affected by this specific contribution. If this element links to the main chain by multiple paths within the traceability chain, it should be described here. For instance, SZA or surface pressure may be used separately in a number of models & correction terms that are applied to the product at different points in the processing. Figure 1, contribution 5a1, for an example.

Element/step common for all sites/users – Is there any site-to-site/user-to-user variation in the application of this contribution?

Traceable to – Describe any traceability back towards a primary/community reference.

Validation – Any validation activities that have been performed for this element?

The summary table, explanatory notes and referenced material in the traceability chain should occupy ≤ 1 page for each element entry. Once the summary tables have been completed for the full end-to-end process, the uncertainties can be combined, allowing assessment of the combined uncertainty, relative importance of the contributors and correlation scales both temporally and spatially. The unified form of this technical document should then allow easy comparison of techniques and methods.

2 Introduction

This document presents the Product Traceability and Uncertainty (PTU) information for the GNSS IPW product. The aim of this document is to provide supporting information for the users of this product within the GAIA-CLIM VO.

2.1 Instruments

2.1.1 Instruments for GNSS data acquisition

Unique receivers and antennas are not encouraged at stations. Only previously known brands and models as described in the IGS rcvr_ant.tab and IGS08.atx file are accepted with full standing within the IGS network <ftp://igs.org/pub/station/general/>.

2.1.1.1 Receivers

A number of GNSS receiver types may be used. The majority consist of a stand-alone receiver connected to the internet (either directly or by way of a PC). Alternatively, a GNSS receiver may be a PC-card type, e.g. <https://www.novatel.com/products/gnss-receivers/oem-receiver-boards/oemv-receivers/oemv-2/>



Figure 4 Leica GR10 reference GNSS receiver



Figure 5 PC-card type GNSS receiver

2.1.1.2 Antenna

A number of manufacturers produce reference-quality choke-ring GNSS antenna; however, not all sites use them operationally. Some GNSS sites use lower quality non-choke ring type antennas.

The station's GNSS antenna absolute calibration must be available in an igs08.atx table (See: <ftp://igs.org/pub/station/general/igs08.atx>).

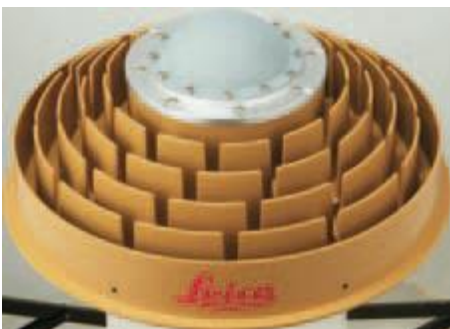


Figure 6 Leica AR25 choke-ring reference GNSS antenna



Figure 7 Leica non-choke-ring antenna

Manufacturer Links

Leica: <http://leica-geosystems.com/en-gb/products/gnss-systems>

Trimble: <http://www.trimble.com/positioning-services/>

Javad: <https://www.javad.com/>

Novotel: <https://www.novatel.com/#latestNews>

Ashtech: <https://www.navtechgps.com/receivers/>

2.1.2 Instruments for surface meteorological data acquisition

Ideally, reference quality meteorological sensors should be installed at the GNSS site, as close to the same position and height as the GNSS antenna as possible. In practice, meteorological parameters used for ZTD to PWV conversion can come from a variety of sources depending upon availability (in order of preference):

- Collocated reference quality meteorological instruments
- Collocated lower-quality meteorological instruments e.g. collocated AWS (Vaisala, Paroscientific etc.)
- Using the nearest/next-nearest available meteorological site data, adjusting meteorological pressure to the height of the GNSS antenna
- Using triangulated/interpolated data from three nearby meteorological surface sites, adjusting meteorological pressure to the height of the GNSS antenna
- From NWP data

Longer distances (between GNSS sensor & meteorological instruments) make it difficult to reliably approximate surface meteorological data to the GNSS antenna's geodetic position which introduces additional uncertainty. The uncertainty associated with the surface meteorological data must be quantified and accounted for.

Example combined PTU sensors include e.g. Vaisala (<https://store.vaisala.com/eu/ptu301-combined-pressure-humidity-and-temperature-transmitter/PTU30011801G1BCPB1A0F1FAB0B0A/dp>)

2.2 Methods

2.2.1 Network solution (DD)

Using Double Differences (DD), the clock errors of both the satellite and receiver are eliminated (Hoffmann-Wellenhof, et al., 1992). A large network is necessary to obtain absolute estimates. Observations of a network of receivers, gathered over a certain time window (e.g. 12 hours) are necessary to determine the position of a receiver accurately. The determination is performed using GNSS processing software, which estimates the position of the receivers in the network and, simultaneously, the atmospheric correction or atmospheric delay.

2.2.2 Precise Point Positioning (PPP)

For this method, the orbits and satellite clocks are estimated using a separate scheme and then used as *a priori* information to estimate the position of the receiver and atmospheric term (J. Zumberge et al., 1997). This method requires very accurate and stable satellite information but has the advantage of being completely scalable with respect to the number of GNSS sites in the processing scheme.

2.2.3 PPP or DD?

Both methods should give similar quality results if everything is done in a correct and consistent way. The results (in GNSS IPW context the Zenith Total Delay and its 1σ errors) cannot be classified as “worse” or “better” based on information about the data processing method. However, it may be useful for the data analyst to know which method was used and with which method-specific constraints. The GRUAN GNSS product is processed solely by PPP method.

2.3 Software

2.3.1 Software for GNSS data processing

A very brief summary about geodetic software (as available at October 2017):

BERNESE (<http://www.bernese.unibe.ch/>)

GAMIT/GLOBK (<http://www.gpsg.mit.edu/~simon/gtgk/>)

GIPSY/OASIS (<https://gipsy-oasis.jpl.nasa.gov/>)

These three are the most widely used geodetic software in scientific communities. But there are far more applications doing the same or similar processing. For example:

- RTKlib - An Open Source Program Package for GNSS Positioning (www.rtklib.com), by Univ. Tokio

On-line post-processing facilities like:

- AUSPOS (<http://www.ga.gov.au/bin/gps.pl>)
- Canadian Geodetic Survey CSRS-PPP on-line service (<https://webapp.geod.nrcan.gc.ca/geod/tools-outils/ppp.php>).

Or, in-house developed solutions, non-commercial, but not open, for example:

- EPOS (<http://www.gfz-potsdam.de/en/section/global-geomonitoring-and-gravity-field/topics/earth-system-parameters-and-orbit-dynamics/epos/>) used by Helmholtz-Zentrum Potsdam Deutsches GeoForschungsZentrum GFZ.

GRUAN processing:

GRUAN GNSS data processing at the GFZ is based on GFZ EPOS8 software which is based on least squares adjustment using a sliding window approach and makes use of the IERS standards. Operational GPS data processing at the GFZ is performed in PPP mode and provides all tropospheric products: the zenith total delays (ZTD), the integrated water vapour (IWV), the slant total delays (STD) and tropospheric gradients in near-real time and in post-processing.

Using PPP strategy:

The main idea of the PPP strategy is the processing of each site separately, fixing the high quality GPS orbits and clocks. Thus the Near Real Time (NRT) processing is split into two steps:

- 1) **"Base cluster" analysis:** estimation of high quality GPS orbits and clocks from a global network (using about 100 IGS sites), where an orbit relaxation starting with the Ultra Rapid GFZ predictions is performed. Among the estimated parameters for the "base cluster" step are (1) GPS orbits with predicted Ultra Rapid orbits from GFZ used as initials, (2) Satellite clocks, and (3) ZTDs for 4-hour intervals.
- 2) **PPP analysis:** estimation of ZTDs/IWV/STDs using parallel processing of stations in clusters with PPP based on fixed orbits and clocks from the first step, adjusting for (1) the ZTDs with resolution of 15 minutes, and (2) tropospheric east and north gradients with hourly resolution.

The main characteristics of GFZ EPOS8 software processing include:

- 1) Use of a sliding 24-hour data window
- 2) Elevation cut-off angle: 7 degrees
- 3) Sampling rate of GPS data 2.5 minutes
- 4) Reference frame:
 - Earth rotation parameters: GFZ GPS solution/prediction
 - The station coordinates are held fixed, once determined with sufficient accuracy within ITRF

2.3.2 Software for GNSS IPW derivation

No “off the shelf” software exists for this processing. Each agency (or data analyst) uses their own implementation, based on well-documented algorithms and best practices published. The general processing always follows the measurement main chain (and accounts for the effects) shown in Figure 8.

GNSS IPW Measurement: Main Chain

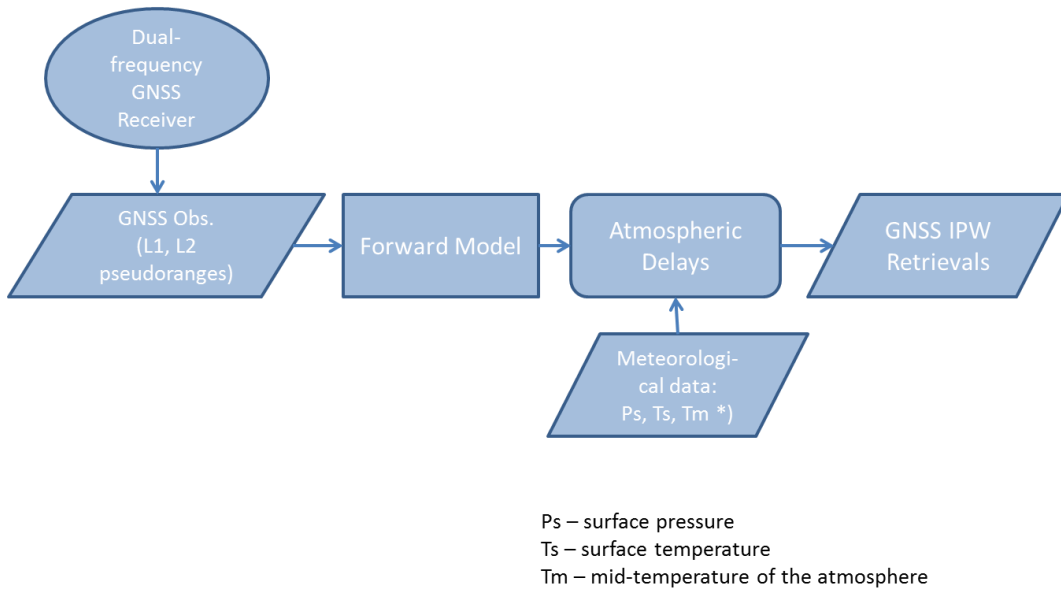


Figure 8 Main processing chain for GNSS-PW technique

The three principal techniques (Section 2.3.1) are implemented as follows:

The users of Bernese software package get ZTDs from the final (tropospheric) solution of GNSS data processing. The hydrostatic component of ZTD – the Zenith Hydrostatic Delay (ZHD) can be calculated with Saastamoinen model (J. Saastamoinen 1972) by using the site latitude and height above the mean sea level as parameters. The Zenith Wet Delay (ZWD) is the remaining component of the ZTD (i.e., $ZWD = ZTD - ZHD$) and is converted into IPW if surface temperature is known (mean atmospheric temperature (T_m) calculated). This is the approach used for GRUAN.

The GAMIT package includes a meteorological utility (GAMIT *metutil*) that can be used for IPW derivation. However, it is possible to use any self-developed software by using GAMIT-calculated ZTD and its formal error.

GIPSY has limited outputs – IPW can be calculated by two parameters extracted from its final solution (Zenith Wet Delay and its formal error, what in fact is a formal error of Zenith Total Delay). Zenith Total Delay can be calculated after additionally finding the Zenith Hydrostatic Delay ZHD) by using Saastamoinen model with the GNSS site's latitude and height above the mean sea level (AMSL).

All three processes are black-box processes whereby the uncertainty cannot be independently verified.

3 Product Traceability Chain

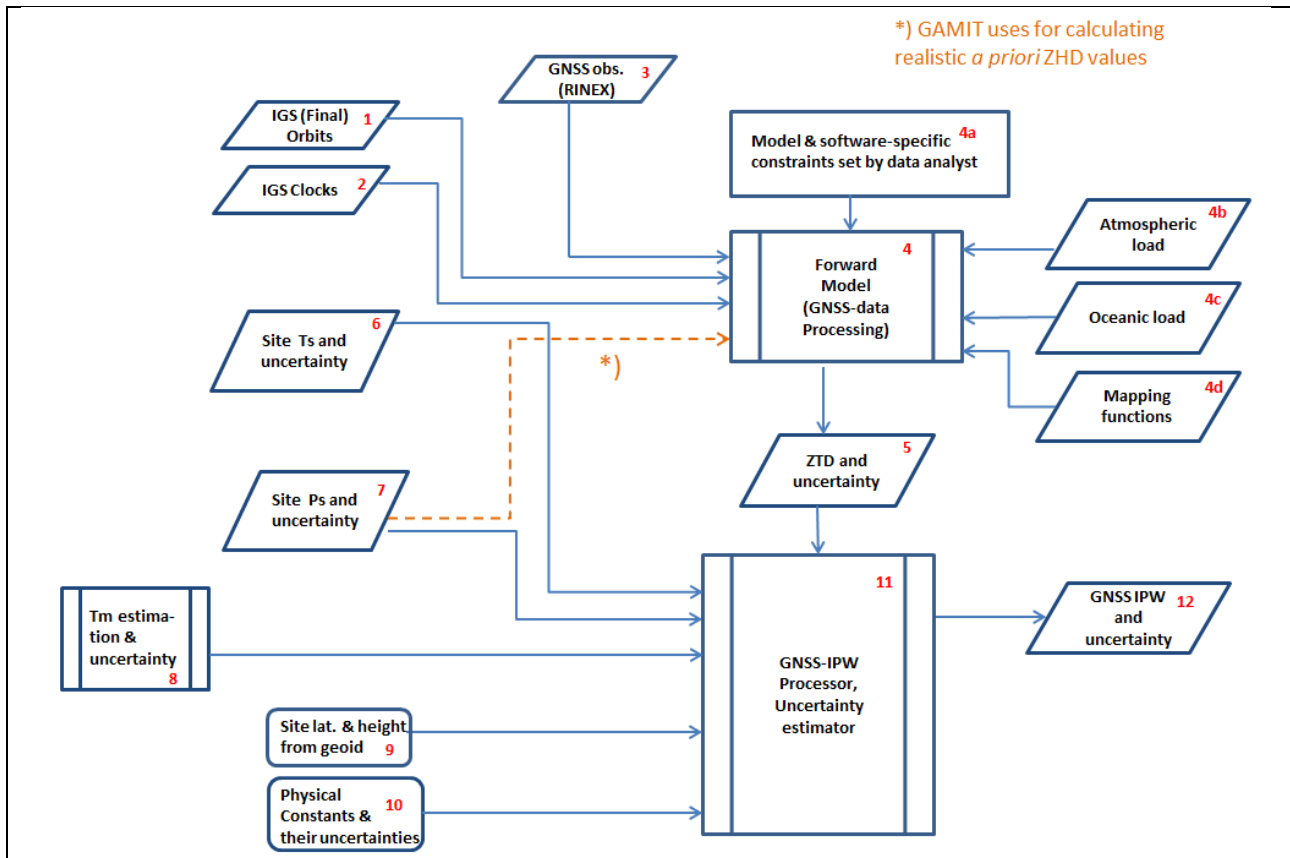


Figure 9 Product traceability chain for GNSS-IPW technique

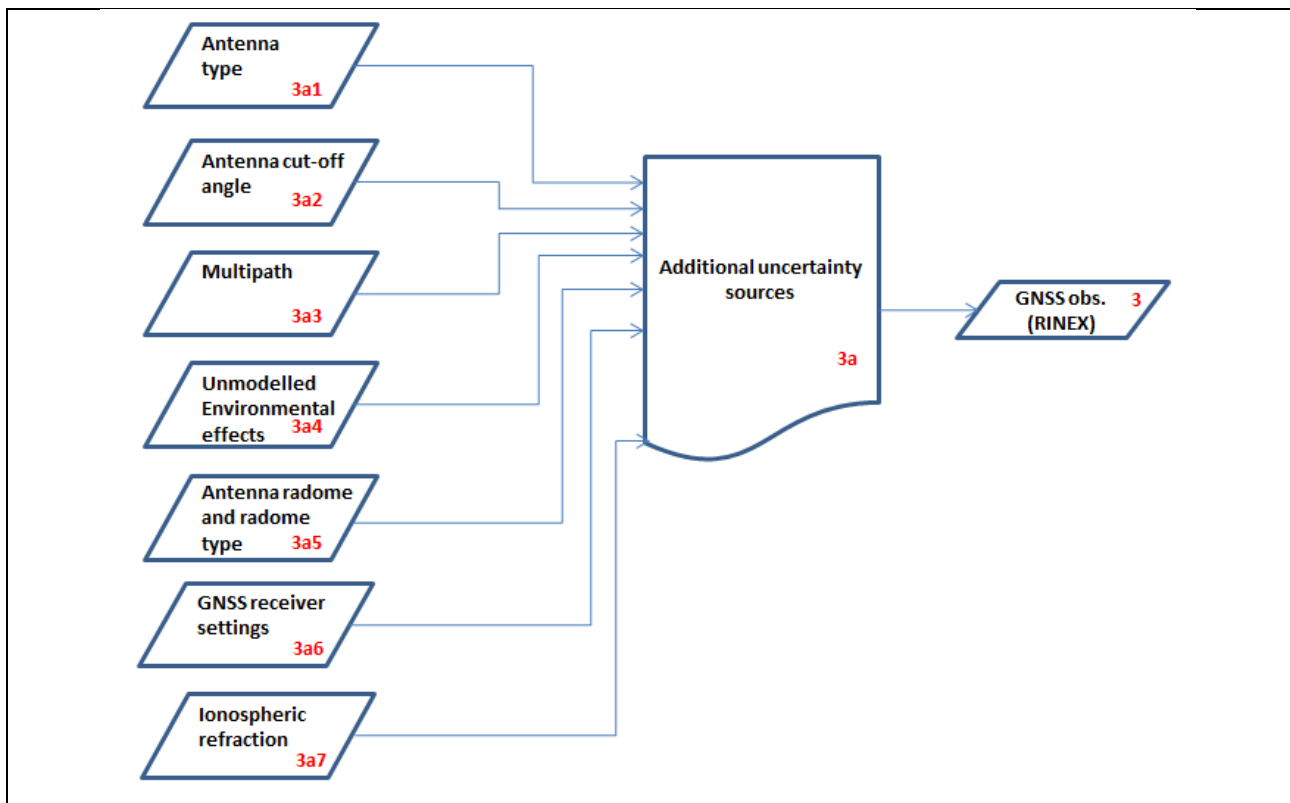


Figure 10 Additional detail on the GNSS obs term in the product traceability chain

As shown in Figure 9, ZTD and its uncertainty are products of the Forward Model (GNSS-data processing software). All uncertainties contributing to the ZTD and its formal uncertainty have their own specific contributions. At the GNSS-data processing phase, many of these effects can be either corrected or ignored (for example, by using or not using the oceanic and atmospheric load).

For GNSS-IPW uncertainty quantification it is possible to use analytics given by Ning et al., (2016) to quantify all effects except for ZTD and its uncertainty (term 5 in Figure 9). We have combined effects of all contributors, analysed, weighted and scaled by the GNSS-processing software. There can be made only numeric experiments to quantify some effects for each site or a site in the fixed network of sites, meaning that the results cannot necessarily be generalised and applied more broadly.

For GRUAN GNSS data processing by GFZ (and EPOS8 software) the Figure 9 would look a little different. For the Forward Model, the items 1 (IGS orbits) and 2 (IGS clocks) can be considered as EPOS8 own products, not external (GFZ is one of the IGS data analysis centres). This serves to reduce, to a small degree to which the GRUAN processing contains black-box processes.

4 Element contributions

4.1 Satellite orbits (1)

All GNSS Analysis Centres (ACs) must use GNSS orbits and clocks in their processing to estimate the satellite position and any clock offsets (between satellite and receiver). However, this is not done in a consistent manner by all ACs. Most ACs using a DD approach will rely on the IGS products, and which product is determined by the latency requirement, e.g. the majority of the ACs using a DD approach in E-GVAP use the predicted half ¹ of the IGS Ultra rapid products. However, some ACs may estimate the equivalent orbits and clocks themselves (e.g. CODE). If an AC employs a PPP processing strategy, they will calculate their own orbits and clocks, generally to a higher accuracy than those provided by the IGS products; as this is necessary to account for clock offsets (which are eliminated by DD processing). ACs (including GFZ for GRUAN) processing data for climate applications normally use the IGS final products.

Note 1: Orbit accuracies are 1D mean RMS values over the three XYZ geocentric components. IGS accuracy limits, except for predicted orbits, are based on comparisons with independent laser ranging results and discontinuities between consecutive days. The precision is better.

Information / data	Type / value / equation	Notes / description
Name of effect	IGS Final Products orbit	
Contribution identifier	1	
Measurement equation parameter(s) subject to effect	$\Delta ZTD = P_{\text{sat}}(x,y,z)$ $u_{ZTD} = u_{P_{\text{sat}}(x,y,z)}$	
Contribution subject to effect (final product or sub-tree)	ZTD	

¹ There are 2 categories of Ultra Rapid Products (the so-called “Predicted Half” and “Observed”. The first is delivered every 15 min in real-time and the second with time latency 3-9 hrs, also with 15 min intervals, but based on results of laser ranging. The “first option” is almost present in real-time, but the “second option” is more accurate. AC’s interested in meteorological applications need results as fast as possible using the “predicted half”

intermediate product)		
Time correlation extent & form	Between 15 mins & 1 day depending on application	
Other (non-time) correlation extent & form	orbital timescales	GPS satellite to satellite
Uncertainty PDF shape	Normal	
Uncertainty & units	Typically, ± 2.5 cm (1σ)	Orbits accurate to ~ 2.5 cm See Table 2. GRUAN GNSS product is calculated by using IGS Final Products
Sensitivity coefficient	c (speed of light)	
Correlation(s) between affected parameters	None	
Element/step common for all sites/users?	Yes	
Traceable to ...		
Validation	Inter-comparison studies.	

Table 2. Orbit uncertainty contributions. Taken from <http://www.igs.org/products#GPS>

Type		Accuracy	Latency	Updates	Sample Interval
Broadcast	orbits	~ 100 cm	real time	--	Daily
	Sat. clocks	~ 5 ns RMS ~ 2.5 ns SDev			
Ultra-Rapid (predicted half)	orbits	~ 5 cm	real time	at 03, 09, 15, 21 UTC	15 min
	Sat. clocks	~ 3 ns RMS ~ 1.5 ns SDev			
Ultra-Rapid (observed half)	orbits	~ 3 cm	3 - 9 hours	at 03, 09, 15, 21 UTC	15 min
	Sat. clocks	~ 150 ps RMS ~ 50 ps SDev			
Rapid	orbits	~ 2.5 cm	17 - 41 hours	at 17 UTC daily	15 min
	Sat. & Stn. clocks	~ 75 ps RMS ~ 25 ps SDev			5 min
Final	orbits	~ 2.5 cm	12 - 18 days	every Thursday	15 min
	Sat. & Stn. clocks	~ 75 ps RMS ~ 20 ps SDev			Sat.: 30s Stn.: 5 min

The effect of orbit errors on ZTD estimates are complicated by the dependence on the ground network geometry, especially when a network strategy is used as opposed to a point-positioning strategy (Zumberge et al., 1997). A complete error analysis is therefore difficult to perform analytically but can be performed numerically for a given network (Ge, et al., 2000).

Ge, et al., (2000), using a network strategy, have investigated the accuracy of near real-time ZTD estimates and their sensitivity to GPS satellite orbit errors and shown that ZTD errors are dominated by biases in the orbital semi-major axis and its eccentricity. Therefore, although the major orbit error for GPS satellites is in the along-track direction, the radial orbit errors have a larger effect on ZTD estimates. For instance, a 1 m bias in the semimajor axis can cause 10 to 20 mm ZTD errors.

In (T.Ning et al., 2016) it is demonstrated by practical tests (using PPP strategy), that the simulated ZTD error due to orbit errors (additional radial and tangential components) for 3 GRUAN sites ishas been around 1.5 to 3 mm. These error components are implemented only for GRUAN GNSS data analysis (by GFZ).

4.2 Satellite clocks (2)

All GNSS Analysis Centres (ACs) must use GNSS orbits and clocks in their processing to estimate the satellite position and any clock offsets (between satellite and receiver), however this is not done in a consistent manner by all ACs. Most ACs using a DD approach will rely on the IGS products, and which product is determined by the latency requirement. e.g. the majority of the ACs using a DD approach in E-GVAP use the predicted half of the IGS Ultra rapid products. However, some ACs may estimate the equivalent orbits and clocks themselves (e.g. CODE). If an AC employs a PPP processing strategy, then they will calculate their own orbits and clocks, generally to a higher accuracy than those provided by the IGS products as this is necessary for accounting for clock offsets (which are eliminated by DD processing). ACs processing for climate applications (including GRUAN GNSS data processing) use the IGS Final products.

Note 2: The accuracy (neglecting any contributions from internal instrumental delays, which must be calibrated separately) of all clocks is expressed relative to the IGS timescale, which is linearly aligned to GPS time in one-day segments. The standard deviation (SDev) values are computed by removing a separate bias for each satellite and station clock, whereas this is not done for the RMS values.

Information / data	Type / value / equation	Notes / description
Name of effect	IGS Final Products clock error	
Contribution identifier	2	
Measurement equation parameter(s) subject to effect	$\Delta ZTD = t_{\text{clock}}/c$ $u_{ZTD} = u_{\text{Psat}(x,y,z)}$	
Contribution subject to effect (final product or sub-tree intermediate product)	ZTD	Note that the satellite and receiver clock errors get canceled out while using Double Differenced strategy in GNSS data processing (Bernese, GAMIT).
Time correlation extent & form	Between 15 mins & 1 day	

	depending on application	
Other (non-time) correlation extent & form	None	
Uncertainty PDF shape	Normal	
Uncertainty & units	Typically, clocks accurate to ~75 ps (1 σ) RMS (~20 ps SDev)	See Table 2 GRUAN GNSS product is processed with IGS Final Products
Sensitivity coefficient	c^{-1} (speed of light)	
Correlation(s) between affected parameters	None	
Element/step common for all sites/users?	Yes	
Traceable to ...		
Validation	Inter-comparison studies.	

4.3 GNSS observations (3)

The GNSS-receiver must track both code and phase on L1 and L2 under non-AS (anti-spoofing), as well as, AS conditions (Hofmann-Wellenhof et al. 1992). The required observables are L1, L2, P2, and at least one of C1 or P1. The L1 and L2 correspond to the carrier phase data in cycles, P1 and P2 are L1/L2 pseudoranges using P-code in metres, C1 is the C/A code pseudorange on L1 in metres (the user may be referred to Hoffmann-Wellenhof, et al., chapter 5). A 2-frequency receiver is needed to enable elimination of ionospheric refraction by linear combinations described in Hofmann-Wellenhof, et al., (chapters 6.2.1, 6.3.2). GNSS-PW processing uses phase observations only, due to precision issues (definitions for code- and phase observations can be found from Hofmann-Wellenhof et al, chapter 6.1). Alternatively, the reader can find several helpful books and publications about the principles of GNSS and GNSS measurements. For example, Teunissen and Montenbruck (2017).

First of all, the usable GNSS-observations must be made with the apparatus matching the technical requirements (i.e., it must exist in regularly updated tables in IGS database, used by data processing software). These apparatus-level choices are the GNSS-receiver and antenna (and radome) types:

ftp://igs.org/pub/station/general/rcvr_ant.tab

Correct choices for the technical basis is a must – if these are not met the data will be unusable and without any options for correcting afterwards.

The observational data is taken “as is”. The quality depends mostly on the apparatus and installation (how well it is situated, serviced and tuned). Installation following the technical requirements and best practices keeps the unwanted effects to a minimum. The data user should determine whether the apparatus and installation is good enough for their specific purpose. For evaluating the quality of the observational data, some free analytic software, like UNAVCO’s TEQC (<https://www.unavco.org/software/data-processing/teqc/teqc.html>) or Anubis from Geodetic observatory Pecny (<http://www.pecny.cz/gop/index.php/gnss/sw/anubis>) can be used.

The data recording interval is often chosen to be 30 s for meteorological purposes. The data is usually

recorded into the receiver's memory and automatically transferred to the closest server of the relevant GNSS network. In common practice, the data is recorded in the manufacture's native binaries and often converted into RINEX and compressed to reduce archived data volumes.

4.3.1 Additional uncertainty sources (3a)

4.3.1.1 Antenna type (3a1)

Geodetic grade antennas with multipath suppressing effects are recommended - choke-ring types (with the latest modifications on the market). Multipath cannot be completely avoided, but efforts must be made to keep the effect minimal by choosing a compliant antenna configuration, monumentation of the antenna and choosing and maintaining an appropriate surrounding environment for the antenna installation (clear-horizon, without reflective surfaces from buildings etc. nearby).

There is no way to give any direct estimate as to how much a certain antenna type would have impact on ZTDs (measured in mm). Rather, what is given for the antenna (by its type) is the antenna gain (the antenna gain describes how well the antenna converts radio waves arriving from a specified direction into electrical power, measured in dB).

Information / data	Type / value / equation	Notes / description
Name of effect	Antenna type	Set by network/installation
Contribution identifier	3a1	
Measurement equation parameter(s) subject to effect	$\Delta ZTD = f(\text{elevation, azimuth})$	Determines the overall quality of the measurement.
Contribution subject to effect (final product or sub-tree intermediate product)	ZTD	
Time correlation extent & form	Systematic over lifetime of sensor installation.	
Other (non-time) correlation extent & form	Systematic for siting duration.	
Uncertainty PDF shape	Normal	
Uncertainty & units	0 mm (1σ)	Unquantified. Assumed negligible for well maintained sites using state-of-the-art equipment and following best-guidance. All GRUAN sites are required to do so.
Sensitivity coefficient	1	
Correlation(s) between affected parameters	Correlated to similar antenna types within a network	Affects all observed parameters
Element/step common for all sites/users?	Yes	

Traceable to ...	None	
Validation	Comparison with independent datasets with the same receiver, but with a different antenna.	Validation issues: Ref. to Mader (1999)

4.3.1.2 *Antenna Radome and radome type (antenna/radome combinations) (3a5)*

GNSS-observations will be affected by everything that could cover the antenna (either the snow or the antenna radome if employed). A radome discourages birds from perching on the antenna, known as a common source of signal attenuation. However, if possible (e.g., in non-snow climatic conditions), no antenna radome is recommended as it attenuates and otherwise distorts signals owing to imperfections in manufacture. In areas with seasonal snowcover the usage of the radome is inevitable. The radome type must match with the antenna type (and the installations must be made according to the manufacture's/vendor's technical instructions).

Information / data	Type / value / equation	Notes / description
Name of effect	Radome effect	Typically only used where needed for precipitation reasons.
Contribution identifier	3a5	
Measurement equation parameter(s) subject to effect	$ZTD' = ZTD$	
Contribution subject to effect (final product or sub-tree intermediate product)	ZTD	
Time correlation extent & form	Systematic	Although in some cases an additional seasonal effect
Other (non-time) correlation extent & form	None	
Uncertainty PDF shape	Normal	Assumed
Uncertainty & units	1 - 5 mm	Ning et al. 2016
Sensitivity coefficient	1	
Correlation(s) between affected parameters	Antenna type (3a1)	
Element/step common for all sites/users?	No	Site specific
Traceable to ...	No	
Validation	No	

The radome effect (depending on the antenna elevation cut-off angle) goes from 1 mm up to 5 mm in vertical component of the antenna position as found by T. Ning, et al., (2011). However, this result is strictly only valid for the specific type of radome used in these experiments.

Each type of antenna has its characteristic Phase Centre Variation diagram (dependence of the phase centre from GNSS-signal transmitter's elevation and azimuth). For high-quality observations the antenna-radome pairs must be calibrated, i.e., the data processing software must have adequate tables for the antenna phase centre variation – PCV models in use. These tables are used by any GNSS-data processing software, and must be regularly updated. Antenna phase center variations can have an amplitude of several centimeters. Ignoring phase center variations can lead to serious (up to 10 cm) vertical errors (Mader 1999).

Calibrations can be done only by licensed institutions having the relevant technical capabilities. For example, NGS's (National Geodetic Survey) Antenna Calibration Program provides Global Navigation Satellite System (GNSS) antenna calibrations for specific antenna codes (antenna model + radome).

<https://www.ngs.noaa.gov/ANTCAL/>

For Trimble GNSS-antenna TRM29659.00 with radome SNOW, the calibration table would look like this:

https://www.ngs.noaa.gov/ANTCAL/LoadFile?file=TRM29659.00_SNOW.atx

Changing a radome from one type to another may cause discontinuities in the vertical component of the site position time series, as demonstrated by Emardson et al., (2000). Biases in vertical coordinate project into IPW values also, i.e., care must be taken to properly quantify this aspect of any instrumental change. It is primarily the responsibility of the site operator to find and install appropriate technical equipment. The data analyst cannot mitigate the impact of incorrect technical choices and technical setups not associated with the data processing.

The GNSS antenna retrieves the GNSS signal and transmits it to the receiver along a standard coaxial cable. The receiver then interprets the signal and the site administrator can make a number of choices (the most relevant are the sampling and data recording rate, antenna elevation cutoff angle and smoothing ON/OFF) which affect the data acquisition and usability:

4.3.1.3 *Antenna Elevation cut-off angle (3a2)*

This parameter is set according to user preferences. There is no clear rule across the global GNSS network what it should be (for older receivers it has been often set to 10-15 degrees). The lower the angle, the more vulnerable the observations are to the multi-path and data loss due to the obstructions on the horizon. However, the lower the angle, the more data could be used (possibly useful for near real time meteorological applications). The latest suggestions for geodetic networks recommend antenna cut-off angles set to 0 deg. The data analyst must later take care what to use for the data processing software (there is no sense to use 0 degrees cut-off angles while knowing that the horizon is masked by forest or other local obstructions). However, increasing cut-off angle will also increase ZTD formal error, because fewer satellites will be in view which shall serve to increase the formal error due to worse satellite constellation available to quantify the ZTD. This setting (initially set by site operator) may be over-ruled by the GNSS data processing centre, where it can be finally chosen and fixed according to the site's specifications and the intended application.

For GRUAN GNSS data product the antenna cut-off angle is chosen as 7 degrees.

Information / data	Type / value / equation	Notes / description
--------------------	-------------------------	---------------------

Name of effect	elevation cut-off angle	
Contribution identifier	3a2	
Measurement equation parameter(s) subject to effect	$\Delta ZTD = f(\text{cut-off angle}), U_{\text{cut}}$	
Contribution subject to effect (final product or sub-tree intermediate product)	ZTD	
Time correlation extent & form	None	
Other (non-time) correlation extent & form	Low angle measurement	
Uncertainty PDF shape	U-shaped	
Uncertainty & units	0	Unquantified. Assumed negligible for a well-sited station and for reasonable choices of elevation cut-off as is the case for GRUAN processing.
Sensitivity coefficient	$\Delta ZTD \propto \cos(\text{cut-off angle})$	
Correlation(s) between affected parameters	Effects on pseudoranges and Signal/Noise Ratio	
Element/step common for all sites/users?	Yes	
Traceable to ...		
Validation	Inter-comparison studies.	

Dedicated investigations have been carried out for the GNSS sites in Sweden and Finland. Ning and Elgered (2012) found that, depending on the station, the best IWV agreement were obtained at cutoff angles 10° and 15° . However, when investigating IWV trends, the study indicated an optimum elevation cut-off angle of between 20° and 25° . The standard deviation becomes larger as the elevation cutoff angle increases. When data are removed from the analysis and the geometry becomes weaker. The number of observations typically drops below 50% when the elevation cutoff angle is higher than 25 degrees, and the formal uncertainties increase approximately from 0.3 kg/m^2 for the 5° solution up to 5 kg/m^2 for the 40° solution (Ning, T and Elgered, G., 2012).

Similar investigations have been made for a broader area, covering the latitudes between 35N-67N by Keernik and Rannat (2016) and the results agree well with that presented by Ning and Elgered (2012). The smallest IWV formal uncertainty as well as RMSD values (from 1.0 to 2.1 mm) between GNSS and comparison techniques were obtained at 10° . The correlation between IWV trends derived from GNSS and comparison techniques were the highest in case of 20° .

4.3.1.4 Multipath (3a3)

Multipath effects are always present. However, the effects can be significantly reduced/suppressed by using appropriate antenna types and installations (e.g., avoiding antenna installation nearby reflective objects, following the recommendations for antenna mounting & using microwave absorbing materials below the antenna ground plane). According to empirical study by Ning, Elgered &

Johansson (2011) - significant offsets in IPW occur (~ 0.3 to 1.6 mm, depending on antenna cut-off angle) while using (or not using) the microwave absorber.

Multipath effect is site-specific and therefore needs to be quantified on a site-by-site basis empirically. It is correlated with the uncertainty arising from choice of antenna cut-off angle as the closer to the horizon, the more the received signal is vulnerable to multipath effects.

Information / data	Type / value / equation	Notes / description
Name of effect	Multipath	
Contribution identifier	3a3	
Measurement equation parameter(s) subject to effect	f(elevation, azimuth)	Determines the overall quality of the measurement.
Contribution subject to effect (final product or sub-tree intermediate product)	ZTD	
Time correlation extent & form	Systematic	
Other (non-time) correlation extent & form	None	
Uncertainty PDF shape	Normal	Assumed
Uncertainty & units	0 mm (1σ)	Unquantified. For mathematical model of multipath the reader can be referred to Hoffmann-Wellenhof, et al., chapter 6. Maximum change in range for L1 signal is about 5 cm. Will be site specific and would require empirical determination. GRUAN choice of 7 degrees cut-off should mitigate for the GRUAN processed data
Sensitivity coefficient	1	
Correlation(s) between affected parameters	Correlated to the site co-ordinates and ZTD	
Element/step common for all sites/users?	Yes	Site-specific, cannot be generalized
Traceable to ...	None	
Validation		Multipath analysis, for example with Anubis from Geodetic observatory Pecný (http://www.pecny.cz/gop/index.php/gnss/sw/anubis)

4.3.1.5 Unmodelled environmental effects (3a4)

Not all effects can be modelled. For example, temporary electromagnetic interference, the effects of trees on the horizon (especially after the rain), cleanliness of the antenna, magnetic storms etc. There exists minimal information on these effects although by their nature they are random or structured random effects that may impact individual observations. There is insufficient information presently

to build a credible effects table for such effects.

4.3.1.6 GNSS receiver settings (3a6)

The GNSS receiver manufacturer leaves a lot of settings to be configured by the site administrator. All of them have an impact on the recorded data quality, but not all have a significant impact on data processing for meteorological purposes.

Information / data	Type / value / equation	Notes / description
Name of effect	GNSS receiver settings	
Contribution identifier	3a6	
Measurement equation parameter(s) subject to effect	$ZTD' = ZTD$	
Contribution subject to effect (final product or sub-tree intermediate product)	ZTD	
Time correlation extent & form	Systematic	Settings for the duration of measurments.
Other (non-time) correlation extent & form	None	
Uncertainty PDF shape	Normal	Assumed
Uncertainty & units	0 mm	Unquantified. For GRUAN sites configurations are actively managed so effect can be assumed negligible
Sensitivity coefficient	1	
Correlation(s) between affected parameters	3a1 & 3a5	
Element/step common for all sites/users?	No	Site settings may change for according to local conditions.
Traceable to ...	No	
Validation	No	Optimised at setup

The site administrator (depending on the user needs), may also choose options for signal smoothing and the data sampling rates. Switching “smoothing” (can be named differently, for example, ”MULTIPATH REDUCTION strobe ON/OFF → OFF for JAVAD receiver) on/off is available on every GNSS receiver and can be set by the site operator. While good and reasonable for most of the engineering-related field-works, it is not recommended to do any smoothing for meteorological or climatological data acquisition. The data analyst at GNSS Data Analysis Centres need to get the data as is. This is the case for all GRUAN processed data.

For contemporary GNSS receivers the sampling rate can be set from sub-seconds to seconds and tens of seconds. For GRUAN it is required (Shoji, Y., et al., GRUAN TD6) that the receiver must track with a sampling interval of 30 seconds or smaller. We need to distinguish between the sampling rate (which is not the data recording rate, that is usually set in coarser time-slices to avoid enormous data files for archiving) at which the receiver processes observational data, and the sampling rate used

(and set by data analyst) for the GNSS-data processing software.

The native sampling rate will fix the rate of measurements the receiver processes internally for resolving navigational tasks. The sampling rate of the GNSS-data processing software has a substantial effect on formal errors numeric values estimated by the software.

4.3.1.7 Ionospheric refractions (3a7)

The Earth's ionosphere contains electrons delaying the propagation of the GNSS signal. In practice the ionospheric-free linear combination is used to remove the first order ionospheric delay, which normally accounts for ~99.9% of the total delay. The second order delay can have a significant impact on the ZTD (0.6 – 4 mm), particularly during strong solar events such as ionospheric storms (Fritsche et al. 2005). Third and higher order terms are insignificant over long time series.

Information / data	Type / value / equation	Notes / description
Name of effect	Ionospheric correction	
Contribution identifier	5b	
Measurement equation parameter(s) subject to effect	$ZTD' = ZTD$	Effect gets mostly cancelled by using linear combination of L1, L2
Contribution subject to effect (final product or sub-tree intermediate product)	ZTD	
Time correlation extent & form	Solar storm scales – 5-10 days.	
Other (non-time) correlation extent & form	None	
Uncertainty PDF shape	Normal	Assumed
Uncertainty & units	0.6 – 4 mm (3σ)	Fritsche et al. 2005. This effect is independent of processing choice.
Sensitivity coefficient	1	
Correlation(s) between affected parameters	No	
Element/step common for all sites/users?	Yes	
Traceable to ...	No	
Validation	No	

4.4 Forward Model (GNSS-data processing) (4)

Information / data	Type / value / equation	Notes / description
--------------------	-------------------------	---------------------

Name of effect	Forward model	Combination of individual contributions.
Contribution identifier	4	
Measurement equation parameter(s) subject to effect	$ZTD' = ZTD$	
Contribution subject to effect (final product or sub-tree intermediate product)	ZTD	
Time correlation extent & form	Systematic	
Other (non-time) correlation extent & form	None	
Uncertainty PDF shape	Normal	Assumed
Uncertainty & units	4 mm	IGS claims ZTD uncertainty 4 mm. T.Ning et al., 2016 have validated it by calculating additional orbital error components added to the initial formal ZTD uncertainty and reached to comparable results (~4mm). It could be concluded that ZTD uncertainty significantly below 4 mm is suspicious (unrealistic, it does not matter what software was used).
Sensitivity coefficient	1	
Correlation(s) between affected parameters	None	
Element/step common for all sites/users?	Yes	
Traceable to ...	No	
Validation	Yes	Ning et al. 2016

At this step the GNSS-data is processed by geodetic software (for example, Bernese, GAMIT/GLOBK, GIPSY/OASIS). Some bigger data processing centres have developed their own software also (for example, GFZ uses EPOS, Canadian Geodetic Survey uses its own CSRS-PPP, etc.). Meteorological applications of geodetic software have existed since the early nineties, after the publication of Bevis et.al 1992 & Bevis et al. 1994.

The forward model (hereafter geodetic software) is a specialised software developed for precise positioning. It uses GNSS satellites' data (the orbits and satellite clock errors) delivered online by IGS services and GNSS-observational data acquired by GNSS-receivers as input.

Although developed by different institutions, the software has a lot in common. The GNSS observations can be expressed as Normal Equations (NEQ), including position, ambiguities and ZTD

(ref. software user manuals – e.g., Bernese - Dach, R, et al., 2007, 2015 and GAMIT – Herring, T., et al., 2009 and Kouba, J., 2009). From NEQ the coordinates, satellite and receiver clock parameters, ZTD and phase ambiguities are estimated via least-squares adjustment (or Kalman Filter).

Using numerous physical and statistical models internally, it gives precise geographical position for the GNSS-receiver's antenna and Zenith Total Delay with its formal 1σ error == formal standard deviation (interpreted as ZTD uncertainty). These two are the most important tropospheric parameters for estimating GNSS-IPW uncertainty. The same software could be used for satellite orbit calculations & finding ionospheric parameters, for example Total Electron Content (TEC), but this is beyond the scope of this document.

The software uses numerous models of geophysical processes internally for estimating or eliminating known physical effects. However, not all effects can be modelled. As a result, whatever does not fit (or cannot be described by) the model in the GNSS-data processing step, is relegated to the residuals. By a common assumption the residuals from GNSS processing also contain unmodeled parts of the neutral, often called the non-isotropic part of the atmosphere, and should reflect local heterogeneities in the atmosphere. The atmospheric information contained in the residuals remains poorly understood.

Many errors such as multipath, clock errors or higher order ionospheric terms can be masked in the residuals and can thus be misinterpreted as tropospheric influences. Multipath can be suppressed by different techniques in data analysis. For example, a thorough analysis of postfit residuals has been attempted by Shoji et al. (2004), where the effect of multipath is removed with time-averaged postfit residuals, so-called multipath maps.

Some software does not offer ZTD directly. For example GIPSY, where Zenith Wet Delay (ZWD) is the final tropospheric product and ZTD must be calculated as a sum of ZWD and Zenith Hydrostatic Delay (ZHD). The ZHD is usually calculated via the Saastamoinen model from the site's geographical latitude and height above the mean sea level.

4.5 Model and software-specific constraints set by data analyst (4a)

The software settings have a combined effect on the results. Each operator tries to do “their best” by trying-comparing-tuning until reaching a satisfactory result. Software settings are not identical from software package to package. It is even impossible to make completely identical tests by different software – the range of settings is not common for all software. There exist always “the default settings”, but these are not applicable for each site and network configuration. Determining the appropriate settings for the application requires expertise.

The following table includes only some of the typical settings. For detailed (software-specific) information the reader would need to check the software manuals.

All software packages include the following core choices:

- Antenna cut-off angle
- Mapping functions
- Oceanic tides (including or not)
- Atmospheric load (including or not)
- Processing step (sampling rate)

Different options of initial setup make it nearly impossible to complete truly identical calculations/experiments with two different software packages even while running in the same mode (for example GAMIT and Bernese in network mode). None of these software-specific settings can be declared as “insignificant”- they have an effect on the final result that could be estimated only by a data analyst being aware about the software peculiarities.

For making the data processing really transparent and the results comparable, the GNSS-data provider should provide a description of the data processing with software-specific settings (processing defaults).

Information / data	Type / value / equation	Notes / description
Name of effect	Analyst software settings	Combination of software setting effects
Contribution identifier	4a	
Measurement equation parameter(s) subject to effect	$ZTD' = ZTD$	
Contribution subject to effect (final product or sub-tree intermediate product)	ZTD	
Time correlation extent & form	Systematic	
Other (non-time) correlation extent & form	None	
Uncertainty PDF shape	Normal	Assumed
Uncertainty & units	0 mm	Unquantified .Effect assumed zero but could be much larger and is systematic. These settins relate to general IGS-quality GNSS-processing. For GRUAN, these are the settings for proprietary software EPOS8 used by GFZ.
Sensitivity coefficient	1	
Correlation(s) between affected parameters	None	
Element/step common for all sites/users?	Yes – for GRUAN network	
Traceable to ...	No	
Validation	No	

4.6 Atmospheric load (4b)

Redistribution of air masses due to atmospheric circulation causes loading deformation of the Earth’s crust, which can be as large as 20 mm for the vertical component and 3 mm for horizontal components

(Petri and Boy, 2006). These vertical errors correspond to uncertainties in ZTD up to ~10 mm, and therefore should not be ignored in cal/val procedures. A good overview about atmospheric effects on tropospheric delays can be found in Tregoning and Watson (2009).

Information / data	Type / value / equation	Notes / description
Name of effect	Atmospheric load	
Contribution identifier	4b	
Measurement equation parameter(s) subject to effect	$ZTD' = ZTD$	
Contribution subject to effect (final product or sub-tree intermediate product)	ZTD	
Time correlation extent & form	Synoptic timescales (structured random)	
Other (non-time) correlation extent & form	None	
Uncertainty PDF shape	Normal	Assumed
Uncertainty & units	Up to 10 mm	Independent of remaining terms, applies to all GNSS-IPW products
Sensitivity coefficient	1	
Correlation(s) between affected parameters	None	
Element/step common for all sites/users?	Yes	
Traceable to ...	No	
Validation	No	

4.7 Ocean tidal load (4c)

The Ocean Tidal Loading Effects to Displacements at GNSS Sites can be of the order of ~20 mm, as presented in D. Zhao et al., (2013). Using models of ocean tides is an inevitable requirement for the coastal or near to the coast GNSS-sites. Ocean tide is not an issue for far in-land sites (or for the coastal sites with no tides).

Information / data	Type / value / equation	Notes / description
Name of effect	Ocean tidal load	
Contribution identifier	4c	
Measurement equation parameter(s) subject to effect	$ZTD' = ZTD$	
Contribution subject to effect (final product or sub-tree intermediate product)	ZTD	

Time correlation extent & form	Systematic	
Other (non-time) correlation extent & form	Geographical	Only applied near the coast.
Uncertainty PDF shape	Normal	Assumed
Uncertainty & units	Up to 20 mm if uncorrected.	Corrected in the GRUAN product, residuals are assumed to be zero
Sensitivity coefficient	1	
Correlation(s) between affected parameters	4b	
Element/step common for all sites/users?	Coastal sites only.	
Traceable to ...	No	
Validation	No	

4.8 Mapping functions (4d)

The atmospheric propagation delay is implemented in the following manner:

$$\text{AtmDelay}(e) = \text{ZHD} * \text{DryMap}(e) + \text{ZWD} * \text{WetMap}(e),$$

where e is the elevation angle of the satellite, ZHD is the Zenith Hydrostatic Delay, ZWD is the Zenith Wet Delay, *DryMap* is the mapping function for the dry (hydrostatic) delay and *WetMap* is the mapping function for the wet delay.

A mapping function is a mathematical model for the elevation dependence of the respective delays. The mapping functions (for both the dry and the wet terms) are approximately equal to the cosecant of elevation.

Usually the GNSS data processing software allows to switch between different mapping functions. For example, for meteorological studies, the Global Mapping Function (GMF) developed by Boehm et al., (2006b) from fitting numerical weather model (NWM) data over 20 years. A more accurate reconstruction of the NWM data can be obtained by interpolating hydrostatic and wet mapping function coefficients as a function of time and location from the global grid files compiled by the Vienna group (Boehm et al., 2006a), known as a Vienna Mapping Function. There exist also widely used Niell Mapping Functions (Niell, A., 1996, 2000). The choice between mapping functions is based on user considerations. GFZ, processing the GRUAN data, has chosen their own approach – GFZ-VMF1 that was evaluated and compared to others by Zus, F., et al., (2015). It was also pointed out that it is difficult to distinguish the MF-caused error from a variety of other errors presented at the low elevation angles, e.g. poor or missing antenna PCV models and multipath.

Information / data	Type / value / equation	Notes / description
Name of effect	Mapping function	
Contribution identifier	4d	

Measurement equation parameter(s) subject to effect	ZTD' = ZTD, function of satellite elevation angle	GFZ-VMF1
Contribution subject to effect (final product or sub-tree intermediate product)	ZTD	
Time correlation extent & form	Systematic	
Other (non-time) correlation extent & form	Geographical	
Uncertainty PDF shape	Normal	Assumed
Uncertainty & units	0-10 mm, depends on elevation angle	Difficult to quantify (Zus., et al., 2015)
Sensitivity coefficient	1	
Correlation(s) between affected parameters	ZWD, ZHD	
Element/step common for all sites/users?	Yes	
Traceable to ...	No	
Validation	No	

The accuracy of mapping functions depend on the elevation angle. The higher the angle, the more insignificant the errors become. The mapping function causes errors to increase significantly below an elevation angle of 10 degrees. The reader may find numeric examples from Stoew, Nilsson, Elgered and Jarlemark (2007) and T.Ning et al., (2016). In Ning et al., the mean of slant delay error for Niell hydrostatic mapping function grows from 0.0 mm at 15 degrees to 0.7 mm at 10 degrees, 3.5 mm at 7 degrees and 10.6 mm at 5 degrees. The GNSS-data processing operator can switch between different mapping functions, but the main difference in accuracy exists below 10 degrees cutoff angle. For GRUAN the cut-off is 7 degrees which may imply an uncertainty contribution of 3.5mm.

4.9 Zenith Total Delay (5)

ZTD is one of the final products of GNSS-data processing, where the actual surface meteorological parameters are usually not necessary for quantifying the delay itself and its formal (1σ) error. ZTD is an observable which is converted from the slant delays using mapping functions (section 4.8).

Uncertainty and error sources for ZTD:

- ionospheric refraction (3a7)
- satellite orbits and clocks (1,2)
- signal multipath (3a3)
- antenna Phase Centre Variations and radome effects
- mapping functions(4d)
- atmospheric and tidal loads (4b, 4c)
- + everything disturbing the measurements – electromagnetic interference, earth-quakes, etc... (3a4)
- Also, the error in *a priori* Zenith Hydrostatic Delays used by GNSS-data processing:

According to Tregoning and Herring (2006) *a priori* zenith hydrostatic delay errors project into GPS height estimates with typical sensitivities of up to 0.2 mm/hPa, depending on the elevation angle cutoff and elevation angle dependent data weighting used in the analysis. This generates height errors of up to 10 mm and seasonal variations of up to 2 mm amplitude. The errors in zenith delay estimates are about half the magnitude of the height errors.

ZTD uncertainty is understood as a formal 1σ error of the Zenith Total Delay.

The 1σ uncertainty is claimed by IGS as 4 mm in the IGS ZTD product as a lower threshold level, but it can be achieved only if:

- ionospheric refraction is completely eliminated (without 2nd and 3rd order components applied), measurements in “normal conditions” (i.e. no solar activities, thunderstorms, ...)
- IGS final products used for satellite orbits
- Both antenna Phase Centre Variation and radome calibrations implemented (it is suggested not to use a radome whenever possible)
- Signal multipath minimized by using microwave absorber below antenna or locating/installing with “free horizon” (usually not installed)
- Antenna elevation cut-off ≥ 10 deg. (often not the case)

Uncertainty of ZTD, calculated by PPP method (and EPOS8 software) for GRUAN sites, is the main contributor (ca 75%) to GNSS-IPW uncertainty (ref. table 4 in T.Ning et al., 2016).

4.10 Site Ts (Surface temperature) (6)

Site surface temperature is used for estimating the mean temperature of the atmosphere from the Bevis et al., 1992 approximation formula:

$$T_m = 70.2 + 0.72T_s,$$

where T_s denotes surface temperature at the site.

It is recommended to use regularly calibrated thermometers with temperature sensor accuracy below 0.1 K (Ref. GRUAN TD6). Often the GNSS-sites do not have co-located meteorological instruments (what is not a case for GRUAN), then the meteorological data can be obtained from the closest meteorological stations or NWP or reanalysis.

Information / data	Type / value / equation	Notes / description
Name of effect	Surface temperature	
Contribution identifier	6	
Measurement equation parameter(s) subject to effect	$T_m \propto T_s$	
Contribution subject to effect (final product or sub-tree intermediate product)	T_m	
Time correlation extent & form	Diurnal	

Other (non-time) correlation extent & form	Latitudinal	Assumed mid-atmosphere temperature.
Uncertainty PDF shape	Normal	Assumed
Uncertainty & units	0.1 K (1 σ)	For GRUAN sites the sensor is always co-located and well calibrated against primary or secondary standards
Sensitivity coefficient		
Correlation(s) between affected parameters	No	
Element/step common for all sites/users?	Yes	
Traceable to ...	No	
Validation	No	

4.11 Site Surface Pressure Ps (7)

Site surface pressure is the most important meteorological parameter in GNSS-IPW processing. Ideally it is measured nearby the GNSS-antenna and pressure-corrected by height differences.

The pressure correction due to the height differences between the GPS-antenna and pressure sensor is done by using the formula derived from hypsometric equation (Wallace and Hobbs, 2006):

$P_{GPS} = P_s \cdot e^{\frac{-g\Delta H}{R_d T}}$, where P_{GPS} denotes air pressure at GPS-antenna height (hPa), P_s is air pressure at the height of the pressure sensor, ΔH is the height difference between the sensor and antenna (m), g is gravity acceleration ($\text{m}\cdot\text{s}^{-2}$). R_d 287.053 is a gas constant of dry air ($\text{J}\cdot\text{K}^{-1}\cdot\text{kg}^{-1}$), T is the actual mean temperature of the layer between the antenna and pressure sensor (K).

It is recommended (Shoji, Y., et al., 2012) to keep the accuracy of the pressure sensor below 0.5 hPa. For GRUAN sites the data is always measured at the site and the pressure sensors are regularly calibrated.

Information / data	Type / value / equation	Notes / description
Name of effect	Surface pressure	
Contribution identifier	7	
Measurement equation parameter(s) subject to effect	hypsometric equation	
Contribution subject to effect (final product or sub-tree intermediate product)	Tm	
Time correlation extent & form	Synoptic scales	
Other (non-time) correlation extent & form	None	
Uncertainty PDF shape	Normal	Assumed

Uncertainty & units	±0.2 hPa (1σ)	Assuming regularly calibrated meteorological instruments as is the case for GRUAN processed data
Sensitivity coefficient		
Correlation(s) between affected parameters	No	
Element/step common for all sites/users?	Yes	
Traceable to ...	Site pressure instrumentation	
Validation	Yes	Local meteorological measurements.

4.12 Mean temperature of the atmosphere T_m (8)

T_m in units of [K] is the mean temperature of the atmosphere as defined in (Davis et al. 1985) as

$$T_m = \frac{\int \frac{P_v}{T} dz}{\int \frac{P_v}{T^2} dz}, \text{ where } T \text{ is the temperature and } P_v \text{ is the partial pressure of water vapor.}$$

Although not suggested for climatological applications (it is recommended to use T_m from reanalysis – ERA Interim, ERA5, ...), the Bevis et al 1992 approximation is still the main option for near real time data processing.

σT_m = 1.3 K as claimed by (J. Wang et al., 2005) as an rms difference based on global comparisons between the NECP/NCAR reanalysis and the radiosonde measurements over 6 years of data.

σT_m = 1.1 K obtained from ECMWF reanalysis, ref. (T.Ning et al., 2016)

Information / data	Type / value / equation	Notes / description
Name of effect	Mean atmosphere temperature	
Contribution identifier	8	
Measurement equation parameter(s) subject to effect	$T_m = 70.2 + 0.72T_s$ (Bevis et al., 1992) Used also in NRT products by GFZ, (GRUAN)	T _s – surface temperature T _m can be also obtained from NWP model or reanalysis, or radiosonde (if available)
Contribution subject to effect (final product or sub-tree intermediate product)	ZTD	
Time correlation extent & form	Synoptic scales	
Other (non-time) correlation		

extent & form		
Uncertainty PDF shape	Normal	Assumed
Uncertainty & units	1.1-1.3 K (1 σ)	Given values reflect the suggestions given by T.Ning et al, 2016 - use reanalysis.
Sensitivity coefficient		
Correlation(s) between affected parameters	No	
Element/step common for all sites/users?	Yes	
Traceable to ...	No	
Validation	No	

4.13 Site latitude and height above the mean sea level (9)

Site latitude λ and height above the mean sea level H is needed for estimating Zenith Hydrostatic Delay by knowing surface pressure P_0 at the site (by Saastamoinen 1972):

$ZHD = (2.2767 + 0.0015) * P_0 / f(\lambda, H)$, where

$f(\lambda, H) = 1 - 2.66 * 10^{-3} * \cos(2\lambda) - 2.8 * 10^{-7} * H$

describes height and latitude approximation of the mean gravity acceleration, and ZHD is measured in millimeters; P_0 is the total ground pressure in hPa; λ and H are the site latitude in degrees and the height above the mean sea level in meters.

Information / data	Type / value / equation	Notes / description
Name of effect	Latitude & site altitude	
Contribution identifier	9	
Measurement equation parameter(s) subject to effect	ZHD, ZTD	
Contribution subject to effect (final product or sub-tree intermediate product)	ZHD, ZTD	
Time correlation extent & form	Systematic	
Other (non-time) correlation extent & form	None	
Uncertainty PDF shape	Normal	Assumed
Uncertainty & units	0 deg / 0 m	Unquantified, the uncertainty in height and latitude has negligible effect on calculating ZHD

Sensitivity coefficient	See text	
Correlation(s) between affected parameters	None	
Element/step common for all sites/users?	Yes	
Traceable to ...	No	
Validation	No	

Site altitude should be known within 1 m for allowing acceptable accuracy of pressure corrections to the GNSS receiver's antenna height. By GRUAN requirements (Shoji, Y., et al., GRUAN TD6) the height difference between the surface pressure sensor and the GPS antenna must be measured with an accuracy of 1 m or better.

4.14 Physical constants (10)

The GNSS-IPW Processor and Uncertainty Estimator (11) uses state of the art formulas known in GNSS meteorology (e.g., Bevis et al., 1992) for converting ZTD (and its uncertainty) to IPW (and its uncertainty). These formulas use several physical constants, listed in the following table.

Name of parameter	Value	Notes / description
Constant used in derivation of ZHD	2.2767 ± 0.0015	Dimensionless. It gives around 10% into IPW uncertainty budget, being the 3 rd largest contributor after ZTD and surface pressure uncertainties (T.Ning et al., 2016, Table 4)
k₂'	22.1 ± 2.2 [K/hPa]	Constant and their from Table 1, Bevis et al. 1994, used for calculating the conversion factor ZWD → IPW
k₃	373900 ± 1200 [K ² /hPa]	Constant and their from Table 1, Bevis et al 1994, used for calculating the conversion factor ZWD → IPW
R_w	461.522 ± 0.008 [J/(kg*K)]	Specific gas constant for water vapour
ρ_w	1000 ± 0.002 [kg/m ³]	Density of liquid water

The constants used by T.Ning (marked with yellow and 1 mb = 1hPa):

Reference	k ₁ (K mb ⁻¹)		k ₂ (K mb ⁻¹)		k ₃ (10 ⁵ K ² mb ⁻¹)	
	Value	Error	Value	Error	Value	Error
Smith and Weintraub (1953)	77.607	0.013	71.6	8.5	3.747	0.031
Thayer (1974)	77.604	0.014	64.79	0.08	3.776	0.004
Hasagawa and Stokesbury (1975)	77.600	0.032	69.40	0.15	3.701	0.003
Bevis et al. (1994)	77.60	0.05	70.4	2.2	3.739	0.012

It is noted that the values of physical constants used have varied over time. At least in part for some subset of these parameters this relates to real changes arising from changes in atmospheric composition and climate change.

Information / data	Type / value / equation	Notes / description
Name of effect	Physical constants	
Contribution identifier	10	
Measurement equation parameter(s) subject to effect	ZTD' = ZTD	
Contribution subject to effect (final product or sub-tree intermediate product)	ZTD	
Time correlation extent & form	Systematic	
Other (non-time) correlation extent & form	None	
Uncertainty PDF shape	Normal	Assumed
Uncertainty & units	Typically 10% in IPW	By an example of T.Ning et al., 2016, given for σ_c
Sensitivity coefficient	1	
Correlation(s) between affected parameters	None	
Element/step common for all sites/users?	Yes	
Traceable to ...	No	
Validation	No	

4.15 GNSS-IPW Processor and Uncertainty Estimator (11)

The IPW processor uses processing steps described in several scientific articles and textbooks since publication of Bevis et al., 1992, 1994. IPW uncertainty estimation in GRUAN is based on T.Ning et al., 2016. The only difference between the GRUAN GNSS data product and any non-GRUAN IPW uncertainty processing is the missing component of additional errors from the GNSS-satellite's radial and tangential orbit errors (as published by J Dousa 2010 and T.Ning et al., 2016). The technical difficulty here is that calculation of these orbital error components cannot be done as post-processing or additional modelling, but initial data (like receiver clock and ambiguity errors) is needed from the

GNSS-processing steps (e.g. from the “Black Box” software) measurement by measurement.

All the rest can be undertaken as part of “standard processing” that should be made according to the best practices (i.e. using only reliable data and possibly the mean temperature of the atmosphere from the reanalysis like ERA Interim, ERA5).

Once the ZTD (product of GNSS-data processing, Traceability Diagram step 5) is found, the IPW is derived with a simple formula

IPW=ZWD/Q, where

ZWD (Zenith Wet Delay) is found from ZTD by subtracting the hydrostatic component (ZHD) from it:

ZWD=ZTD-ZHD.

Calculation of ZHD is explained in section 4.13.

Uncertainty of ZHD can be calculated as given by T.Ning et al., 2016 (Eq. 25):

$$\sigma_{\text{ZHD}} = \sqrt{\left(\frac{2.2767\sigma_{P_0}}{f(\lambda, H)}\right)^2 + \left(\frac{P_0\sigma_c}{f(\lambda, H)}\right)^2},$$

, where P_0 is surface pressure, σ_{P_0} is the uncertainty of surface pressure and σ_c is uncertainty of the constant 2,2767.

Information / data	Type / value / equation	Notes / description
Name of effect	Zenith Hydrostatic Delays	
Contribution identifier	5a	
Measurement equation parameter(s) subject to effect	ZHD	
Contribution subject to effect (final product or sub-tree intermediate product)		
Time correlation extent & form	Systematic	Assuming assumption errors are persistent.
Other (non-time) correlation extent & form	Geographic, synoptic	Some correlation with climatology
Uncertainty PDF shape	Normal	Assumed
Uncertainty & units	0 mm	Unquantified.
Sensitivity coefficient	1	
Correlation(s) between affected parameters	No	
Element/step common for all sites/users?	Yes	
Traceable to ...	No	

Validation	No	
-------------------	----	--

After knowing values for ZTD and ZHD (with uncertainties), the next step is to calculate the conversion factor Q (T.Ning, et al., 2016, Eq. 26):

$$Q = 10^{-6} \rho_w R_w \left(k'_2 + \frac{k_3}{T_m} \right)$$

where the constants are given in contribution 10, (section 4.14). The uncertainty of Q is given by (Ning et al. eq 27),

$$\sigma_Q = 10^{-6} \rho_w R_w \sqrt{\left(\frac{\sigma_{k_3}}{T_m} \right)^2 + \sigma_{k'_2}^2 + \left(k_3 \frac{\sigma_{T_m}}{T_m^2} \right)^2}.$$

where T_m is from Bevis approximation or from reanalysis like ERA Interim, ERA5, contribution 9, section 4.12.

Information / data	Type / value / equation	Notes / description
Name of effect	ZWD to IPW conversion factor, Q	
Contribution identifier	11a	
Measurement equation parameter(s) subject to effect	Q	Numeric value of Q is usually around 6.5 (T.Ning et al., 2016)
Contribution subject to effect (final product or sub-tree intermediate product)	IPW, σ_{IPW}	
Time correlation extent & form	Systematic	
Other (non-time) correlation extent & form	None	
Uncertainty PDF shape	Normal	Assumed
Uncertainty & units	0.0338 $\sigma_Q = 10^{-6} \rho_w R_w \sqrt{\left(\frac{\sigma_{k_3}}{T_m} \right)^2 + \sigma_{k'_2}^2 + \left(k_3 \frac{\sigma_{T_m}}{T_m^2} \right)^2}$	Nondimensional, depends on T_m (cannot be generalised). includes uncertainties from k_3 , k'_2 and T_m according to table by T.Ning et al 2016, for site LDB0 (Lindenberg)
Sensitivity coefficient	1	
Correlation(s) between affected parameters	None	
Element/step common for all sites/users?	Yes	
Traceable to ...	No	
Validation	No	

From surface temperature measurements Q can be estimated with an error less than 2% (Bevis et al. 1992, 1994).

The impact of the uncertainty associated with the conversion factor between the IPW and the zenith wet delay (ZWD) is proportional to the amount of water vapour and increases slightly for moist weather conditions (T.Ning et al. 2016).

Different approximation formulas can be found for the conversion factor, for example, the so-called *annual model* by Emardson and Derks (2000), not using the surface temperature, but just the site latitude and the day of the year.

GFZ has implemented modelling and calculation of additional orbital errors (radial and tangential components) not included in initial PPP solution (tropospheric product). The nature of these errors is described in Dousha (2010) and the implementation briefly in T.Ning, et al., (2016). The ZTD errors caused by the orbital errors for each time epoch are calculated and added to the corresponding formal error. With this additional procedure the GRUAN GNSS product's ZTD uncertainty estimates get realistic (in fact, this procedure makes GRUAN ZTD uncertainties comparable with IGS-defined 4 mm, as demonstrated by T.Ning, et al., 2016).

It must be noticed, that this kind of additional implementations are data processing method- and software-specific and not implemented by any AC's yet (except GFZ for GRUAN).

Information / data	Type / value / equation	Notes / description
Name of effect	GNSS-IPW Processor and Uncertainty Estimator	Combination of uncertainties.
Contribution identifier	11	
Measurement equation parameter(s) subject to effect	$IPW' = IPW$	
Contribution subject to effect (final product or sub-tree intermediate product)	IPW	
Time correlation extent & form	Systematic	
Other (non-time) correlation extent & form	None	
Uncertainty PDF shape	Normal	Assumed
Uncertainty & units	< 1 mm	A requirement for usability of GNSS IPW in meteorological application
Sensitivity coefficient	1	
Correlation(s) between affected parameters	None	
Element/step common for all sites/users?	Yes	
Traceable to ...	No	
Validation	No	

5 Uncertainty Summary

Derivation of IPW starts from obtaining the ZTDs from the final (tropospheric) solution of GNSS data processing. The hydrostatic component of ZTD – the Zenith Hydrostatic Delay (ZHD) can be calculated with Saastamoinen model (J. Saastamoinen 1972) by using the site latitude and height above the mean sea level as parameters. The Zenith Wet Delay (ZWD) is the remaining component of the ZTD (i.e., $ZWD=ZTD-ZHD$) and is converted by a conversion factor Q into IPW if surface temperature is known (mean atmospheric temperature (T_m) calculated).

ZWD (Zenith Wet Delay) is found from ZTD by subtracting the hydrostatic component (ZHD) from it:

$$ZWD=ZTD-ZHD.$$

$IPW = (ZTD-ZHD)/ Q$ (in T. Ning, et al., (2016), IPW is denoted with V)

Total uncertainty of GRUAN-processed GNSS IPW (IPW) can be expressed as (T. Ning, et al., (2016), Eq. 29)

$$\sigma_V = \sqrt{\left(\frac{\sigma_{ZTD}}{Q}\right)^2 + \left(\frac{2.2767\sigma_{P_0}}{f(\lambda, H)Q}\right)^2 + \left(\frac{P_0\sigma_c}{f(\lambda, H)Q}\right)^2 + \left(V\frac{\sigma_Q}{Q}\right)^2}.$$

where the combined uncertainties are

- σ_{ZTD} in the software derived ZTD value (section 4.9)
- σ_{P_0} in the surface pressure (section 4.11)
- σ_c in the conversion constant (section 4.14)
- σ_Q in the ZTD to IPW conversion factor, Q (**Error! Reference source not found.**)

where $f(\lambda, H)$ is used for calculating ZHD as given in section 4.9, λ denotes geographical latitude and H is the height above the mean sea level in Saastamoinen model and V denotes the value of IPW calculated as a result from GNSS-IPW Processor.

The direct uncertainties used in the final calculation are highlighted in orange in Table 3, the pink highlights in Table 3 are the contribution uncertainties directly used in their calculation. Figure 11 shows the values of these uncertainties and the variation in the calculated overall uncertainty via the different processors.

The predominant uncertainty contribution is from σ_{ZTD} and represents over 75 % of the total IPW uncertainty (according to T.Ning et al.) at approximately ~ 4 mm IPW.

The σ_{ZTD} uncertainty 4 mm is calculated by IGS and is a black-body processed number with limited understanding to date. However, the numerical values up to 10 mm can still be considered normal, but care must be taken how the values have developed within a larger time window.

The ZTD (1σ) uncertainty given as 4 mm by IGS, requires ideal observing conditions to be fulfilled and hence represents a best case scenario. This ZTD (1σ) uncertainty value of 4 mm is in good concordance with T.Ning et al. 2016 results, where the contribution of additional (radial and tangential) orbital error components added to the formal error coming from the GNSS-data processor was in order of 1-3 mm. Usually, the GNSS-processing software like Bernese or GIPSY gives 1σ uncertainty values around 2 mm as detailed below. These estimates are incomplete.

By Bernese documentation (v5.0):

In a successful run of the program, an a posteriori sigma of unit weight of the order of 1.0–1.5 mm with elevation-dependent weighting and 2.0–2.5 mm without elevation dependent weighting is expected for phase processing. The user must be aware, that these sigmas are just the numbers indicating that the data processing has ended successfully. How to use these estimates in further data processing (do they need additional monitoring and calibration) depends on data analyst and the application.

With GAMIT, using realistic sigma algorithms as described by T.Herring (2003) and a priori 10 mm error for L1 phase, the corresponding values for ZTD 1σ errors are around 3-4 mm or even higher. For reprocessing, the observations with 1σ uncertainty over 10 mm are usually filtered out as outliers and everything between 4-10 mm should not be interpreted as suspicious. It is also a common practice to remove ZTD estimates with uncertainties larger than 3σ of the mean formal uncertainty given by the GNSS-processing software. It is important to follow the behaviour of uncertainty values in a longer timeframe to notice and understand whether there are some jumps or other visible irregularities in ZTD (and its 1σ error's) time series.

With Bernese and GIPSY (using different initial constraints, as 1 mm for a priori ZTD error) resulting with final ZTD uncertainties around 1.5-2 mm, the data analyst has left “hands free” to decide how to weigh or rescale the results into realistic. The final truth comes out only from intercomparison experiments (using independent measurement techniques) and additional statistical analysis.

Table 3. Uncertainty summary table

Element identifier	Contribution name	Uncertainty contribution form	Typical value	Traceability level (L/M/H)	random, structured random, quasi-systematic or systematic?	Correlated to? (Use element identifier)
1	IGS Final Orbits	Statistical	~2.5 cm	H	systematic	Antenna pos., ZTD, σ_{ZTD}
2	IGS clocks	Statistical	75 ps	H	systematic	Antenna pos., ZTD, σ_{ZTD}
3	Uncertainty contributors to GNSS observations					
3a1	Antenna type and radome	constant	± 0 mm	L	systematic	GNSS obs., ZTD, σ_{ZTD}
3a2	Antenna cut-off	constant	± 0 mm	L	systematic	GNSS obs., ZTD, σ_{ZTD}
3a3	Multipath	constant	± 0 mm	L/M	Quasi-systematic	GNSS obs., ZTD, σ_{ZTD}
3a4	Unmodelled environmental effects	constant	± 0 mm	L	Systematic	GNSS obs., ZTD, σ_{ZTD}
4	Forward model	constant	± 13 mm	M	Quasi-	

					Systematic	
4a	Analyst software settings	constant	±0 mm	M	Systematic (site level)	
4b	Atmospheric load	constant	±10 mm	H	Systematic	
4c	Oceanic load	constant	±20 mm	H	Systematic	
5	ZTD, σ_{ZTD}	constant	± 4 mm (1σ)	M	Random	σ_{IPW}
5a	ZHD assumptions	constant	±10 mm / 2 mm	H	Systematic	
5b	Ionospheric load	constant	±0.6-4 mm	H	Quasi-systematic	
6	Uncertainty of surface temperature, T_s	constant	± 0.1 K (1σ)	H	systematic	T_m
7	Uncertainty of surface pressure, σ_{P0}	constant	± 0.2 hPa (1σ)	H	systematic	ZHD, ZTD
8	Uncertainty of T_m	constant	± 1-2 K	H	systematic	σ_Q
10	Uncertainties of physical constants					
10	σ_c - uncertainty of constant 2.2767 used in derivation of ZHD	constant	0.0015 (non-dimensional)	M	systematic	σ_{ZHD} , σ_{IPW}
10	$\sigma_{k2'}$	constant	2.2 [K/hPa]	M	systematic	Q , σ_{IPW}
10	σ_{k3}	constant	1200 [K ² /hPa]	M	systematic	Q , σ_{IPW}
10	σ_{Rw}	constant	0.008 [J/(kg*K)]	H	systematic	Q , σ_{IPW}
10	σ_{ρ_w}	constant	0.002 [kg/m ³]	H	systematic	Q , σ_{IPW}
11	GNSS-IPW Processor assumptions	constant	0 mm	M	systematic	
11a	ZWD to IPW conversion, Q	constant		H	systematic	

Input variable	LDB0	LDRZ	NYA2	Uncertainty	Corresponding IWV uncertainty								
					LDB0			LDRZ			NYA2		
					[kg m ⁻²]	[%]	[%] ^e	[kg m ⁻²]	[%]	[%] ^e	[kg m ⁻²]	[%]	[%] ^e
ZTD [mm]	2487	2376	2434	3.8, 3.7, 3.3 ^a	0.59	1.8	79.9	0.58	2.2	82.2	0.49	2.1	77.0
Ground pressure P_0 [hPa]	1000.1	968.7	1005.6	0.2 ^b	0.07	0.2	1.2	0.07	0.3	1.3	0.07	0.3	1.5
Constant ^f	2.2767	2.2767	2.2767	0.0015	0.23	0.7	12.2	0.22	0.9	11.9	0.23	1.0	17.0
Mean temperature T_m [K]	274.6	270.8	262.3	1.1 ^c	0.13	0.4	3.8	0.1	0.4	2.5	0.09	0.4	2.6
k_2' [K hPa ⁻¹]	22.1	22.1	22.1	2.2 ^d	0.05	0.2	0.6	0.04	0.2	0.5	0.03	0.2	0.3
k_3 [$10^5 \times K^2$ hPa ⁻¹]	3.739	3.739	3.739	0.012 ^d	0.10	0.3	2.3	0.08	0.3	1.6	0.07	0.3	1.6
IWV [kg m ⁻²]	33	26	23										
Conversion factor Q	6.4	6.5	6.7										
Total IWV uncertainty					0.66	2.0		0.64	2.4		0.56	2.4	

^a The values are given by the mean ZTD uncertainty calculated from 1 year of data for LDB0, LDRZ, and NYA2, respectively. ^b For GRUAN sites equipped with surface barometers which are calibrated routinely. ^c Taken from Wang et al. (2005) based on the comparison between ECMWF reanalysis and radiosonde data. ^d Taken from Table 1 in Bevis et al. (1994). ^e Percentage of the total IWV uncertainty. ^f The constant given in Eq. (23).

Figure 11. Uncertainties in the GNSS-derived IWV calculated from the uncertainties associated with input variables by T.Ning et al., 2016 (Table 4). (originating from T. Ning, et al., 2016) gives a short summary about the parameter contributions (in percentage) to the total IPW uncertainty on example of three GRUAN sites in 2014. The example data is processed using PPP strategy and the resulting ZTD and its uncertainties are averaged over the full year.

The results are characteristic – i.e., in normal conditions similar numeric values can be expected from any sites. The numeric values presented in Fig. 8 are calculated by methods described in T.Ning, et al., (2016).

Averaging over a year (or years) could be reasonable for trend calculations. In severe weather conditions (or for shorter time intervals) the ZTD uncertainties from GNSS software can differ significantly from those given in the table. The example (Figure 8) is given based on PPP data processing strategy. However, many GNSS data analysis centres use Double Differenced (DD) strategy where the results of one site can be significantly affected by corrupted data from adjacent sites or by temporary data gaps from some sites in the network. This is why it is key to know how the data was processed. Fortunately, this is the case for the GRUAN data characterised here.

6 Traceability uncertainty analysis

Traceability level definition is given in Table 4.

Table 4. Traceability level definition table

Traceability Level	Descriptor	Multiplier
High	SI traceable or globally recognised community standard	1
Medium	Developmental community standard or peer-reviewed uncertainty assessment	3
Low	Approximate estimation	10

Analysis of the summary table would suggest the following contributions, shown in Table 5, should be considered further to improve the overall uncertainty of the GRUAN IPW product. The entires are given in an estimated priority order.

Table 5. Traceability level definition further action table.

Element identifier	Contribution name	Uncertainty contribution form	Typical value	Traceability level (L/M/H)	random, structured random, quasi-systematic or systematic?	Correlated to? (Use element identifier)
5	Uncertainty of ZTD, σ_{ZTD}	random	± 4 mm (by IGS)	L	Predominantly systematic	12, (σ_{IPW})
8	Tm	constant	Tm and its uncertainty depends on source what is used	M	systematic	8, (σ_Q)
10	Uncertainties of physical constants σ_{k2} and σ_{k3}	constant	Values change as the atmosphere changes (trace gases etc)	M	systematic	12, (Q, σ_{IPW})

Attention must be paid on usage of T_m (mean temp. of the atmosphere). It must be made clear what is/was used. If using approximation formulas then they depend on latitude and may differ from site to site. NWP or Reanalyses should be used by preference.

Multipath mitigation is a generic issue, but site-specific.

Uncertainty of ZTD – no special issues, but the full GNSS data processing process must be transparent (in common practice it is not) and using calibration and rescalings if needed.

6.1 Summary

It is nearly impossible to describe all the details and to quantify the effects possibly having impact on GNSS IPW derivation. The process remains a “black-box issue” unless all the software-related details (with algorithms and constraints) are not made public (fully documented) and the data processing (from GNSS observational and meteorological data to GNSS IPW) made completely transparent. This PTU-document gives a general view about the GNSS IPW Product and how it should be derived, trying to make an accent on GRUAN data processing implemented by GFZ. The GRUAN GNSS product has still not been public during compilation of this document. GRUAN GNSS data product will be the only reference quality GNSS IPW, following the concept of full traceability and the best practices known to date.

6.2 Recommendations

It would be useful to understand the behaviour of the uncertainty of all components contributing to the final GNSS IPW uncertainty. Knowing systematic software-dependent differences it will be possible to rescale the uncertainty values used in calculating the IPW total uncertainty. For this additional intercomparison experiments should be used. No uncertainty values should be used mechanically, without knowing what are the realistic values.

If the data processing would be transparent (i.e., full traceability of the process that is still not a common practice), then a lot of additional reference quality GNSS data worldwide could be used for cal/val procedures (additionally to the GRUAN data). Transparency means also having information about the software and its settings with all metadata description used for calculating the GNSS products. Future work should address the uncertainty propagation, specifically through the ZTD generating software. In Table 3 all the contributions numbered 1-4 are combined into the ZTD uncertainty, but should be individually assessed and combined in accordance with the conditions of measurement.

7 Conclusion

There exists a lot of high-quality GNSS data from global or national geodetic networks that could be used as data with reference quality, but it needs additional information about the data processing and evaluation whether the processing is fully traceable or not. The GRUAN GNSS product should be taken as an example (using uncertainty analysis as described by T.Ning *et al* 2016) and is the specific processing choices which have been highlighted herein.

It is currently unavoidable that a subset of current GNSS-data processing software is a „black box“, but the data processing procedures must be (or should be made) transparent (i.e. how exactly a certain „black box“ was used). If everything is done by the best practices, the results can be trusted and taken as reliable. For example, while using ZTD 1σ errors processed by Bernese (or GIPSY) do not include

additional orbital error components, which contribute an additional 1-3 mm to the ZTD as demonstrated in T. Ning et al 2016. Unfortunately, calculation of these additional orbital error components (J. Dousha 2010, T.Ning et al 2016) is not implemented in any distributable GNSS-processing software yet. The first implementation is done by GFZ (Deutsches GeoForschungsZentrum GFZ) for GRUAN-data processing with their in-house EPOS software and for GRUAN sites only.

It is necessary to assign ZTD 1σ uncertainty a value of 4 mm (a value claimed by IGS) for estimating the total GNSS IPW uncertainty if using results from Bernese or GIPSY and the ZTD errors' time series looks stable (around 2 mm) and does not include obvious outliers. The 1σ uncertainties from GAMIT don't need upscaling for making them „more realistic“. However, care must be taken with uncertainty values exceeding 10 mm – in common practice they are considered as outliers and the corresponding measurements should be excluded from further analysis (regardless of choice of GNSS data processing software).

Whatever software is used (either available today or developed in the future) – the ZTD uncertainty cannot be used without additional information/analysis how it was derived (the process transparency is a must). It is key to understand its temporal behaviour within the time window of certain investigations and how well the numeric values match with those obtained from independent techniques (i.e., how realistic they are). Before responsible usage of ZTD in cal/val processes, the observables must be calibrated according to the results from independent techniques.

The data analyst must take care on these software-based differences, by not using the formal uncertainty values mechanically and doing necessary scaling of these uncertainties according to intercomparison experiments (for example, GNSS versus VLBI, MWR or radiosonde).

References

- Blewitt, G., Basics of the GPS technique, published by the Swedish Land Survey, 1997
- Boehm, J. B. Werl, and H. Schuh, Troposphere mapping functions for GPS and very long baseline interferometry from European Centre for Medium-Range Weather Forecasts operational analysis data, *J. Geophys. Res.*, 111, B02406, doi:10.1029/2005JB003629, 2006a.
- Boehm J, A Niell, P Tregoning, H Schuh (2006b) The Global Mapping Function (GMF): A new empirical mapping function based on data from numerical weather model data. *Geophysical Research Letters* 33 L07304 DOI:10.129/2005GL025546
- COST Action 716: Exploitation of Ground-Based GPS for Climate and Numerical Weather Prediction Applications, Final Report, Edited by G. Elgered, H.-P. Plag, H. van der Marel, S. Barlag, and J. Nash
- Dach, R., Hugentobler, U., Fridez, P., Meindl, M. (Editors), User manual of the Bernese GPS Software Version 5.0, AIUB, 2007
- Dach, R., Lutz, S., Walser, P., Fridez, P. (Editors), User manual of the Bernese GPS Software Version 5.2, AIUB, 2015
- Douša, J.: The impact of errors in predicted GPS orbits on zenith troposphere delay estimation, *GPS Solut.*, 14, 229–239, doi:10.1007/s10291-009-0138-z, 2010.
- Emardson, T.R. and Derks, H.J.P., On the relation between the wet delay and the integrated precipitable water vapour in the European atmosphere, *Meteorol. Appl.* 7, 61–68 (2000)
- Emardson, T.R., Johansson, J. and Elgered, G., The Systematic Behavior of Water Vapor Estimates Using Four Years of GPS Observations, *IEEE TRANSACTIONS ON GEOSCIENCE AND REMOTE SENSING*, VOL. 38, NO. 1, JANUARY 2000
- Herring, T., *GPS Solutions* (2003) 7: 194. <https://doi.org/10.1007/s10291-003-0068-0>
- Herring, T.A., King, R.W., McClusky, S.C., *GAMIT Reference Guide*, Rel. 10.3, Department of Earth, Atmospheric, and Planetary Sciences, Massachusetts Institute of Technology
- Keernik, H., Rannat, K., An analysis of 16-year long datasets of GNSS measurements: IWV trends and diurnal cycle in Europe, 4th GNSS4SWEC Workshop and WG/MC, 8th-10th of March, 2016, Reykjavík
- Kouba, J. (2009) A Guide to Using International GNSS Service (IGS) Products. <https://kb.igs.org/hc/en-us/articles/201271873-A-Guide-to-Using-the-IGS-Products> (last checked 15. January 2018)
- Mader, G.L., GPS antenna calibration at the National Geodetic Survey, *GPS Solutions* 3(1):50–58, doi: 10.1007/PL00012780, 1999
- Niell, A., Global mapping functions for the atmosphere delay at radio wavelengths, *J. Geophys. Res.*, 101, 3227–3246, 1996.
- Niell, A., Improved atmospheric mapping functions for VLBI and GPS, *Earth Planets Space*, 52, 699–702, doi:10.1029/95JB03048, 2000.
- Ning, T., Elgered, G., and Johansson, J. M.: The impact of microwave absorber and radome geometries on GNSS measurements of station coordinates and atmospheric water vapour, *Adv. Space. Res.*, 47, 186–196, doi:10.1016/j.asr.2010.06.023, 2011.
- Ning, T., Elgered, G., Trends in the Atmospheric Water Vapor Content From Ground-Based GPS: The Impact of the Elevation Cutoff Angle, *IEEE JOURNAL OF SELECTED TOPICS IN APPLIED EARTH OBSERVATIONS AND REMOTE SENSING*, VOL. 5, NO. 3, JUNE 2012
- Petrie E. J., M. A. King, P. Moore, D. A. Lavallée, Higher-order ionospheric effects on the GPS reference frame and velocities. *J Geophys Res* 115, B03417. doi:10.1029/2009jb006677, 2010.

- Petrov, L., and J.-P. Boy (2004), Study of the atmospheric pressure loading signal in very long baseline interferometry observations, *J. Geophys. Res.*, 109, B03405, doi:10.1029/2003JB002500.
- Saastamoinen, J., Atmospheric correction for the troposphere and stratosphere in radio ranging of satellites, in *The Use of Artificial Satellites for Geodesy*, Geophys. Monogr. Ser, vol. 15, edited by S. W. Henriksen et al., pp. 247–251, AGU, Washington, D. C., 1972.
- Shoji, Y., Nakamura, H., Iwabuchi, T., Aonashi, K., Seko, H., Mishima, K., Itagaki, A., Ichikawa, R., and Ohtani, R.: Tsukuba GPS Dense Net Campaign Observation: Improvement in GPS Analysis of Slant Path Delay by Stacking One-way Postfit Phase Residuals, *J. Meteor. Soc. Japan*, 82, 301–314, 2004.
- Shoji, Y., Braun, J., Wang, J., Rannat, K., Dick, G., Elgered, G., Gutman, S. and Wickert, J., GRUAN Ground-based GNSS Site Guidelines, <https://www.gruan.org/documentation/gruan/td/gruan-td-6/>
- Stoew, B., Nilsson, T., Elgered, G. And Jarlemark P.O.J, Temporal Correlations of Atmospheric Mapping Function Errors in GPS Estimation, *Journal of Geodesy*, Vol. 81, pp. 311-323, 2007
- Teunissen, P. and Montenbruck (editors), *Springer Handbook of Global Navigation Satellite Systems* (Springer Handbooks), Springer, 2017.
- Tregoning, P., and T. A. Herring (2006), Impact of a priori zenith hydrostatic delay errors on GPS estimates of station heights and zenith total delays, *Geophys. Res. Lett.*, 33, L23303, doi:10.1029/2006GL027706.
- Tregoning, P. and Watson, C., Atmospheric effects and spurious signals in GPS analyses, *JOURNAL OF GEOPHYSICAL RESEARCH*, VOL. 114, B09403, doi:10.1029/2009JB006344, 2009
- Wallace, J. M., and P. V. Hobbs, 2006: *Atmospheric Science: An Introductory Survey*. 2nd edition, Academic Press, 69-72.
- Zhao, D., Xu, X., Li, J., Duan, J., Yu, L., Ocean Tidal Loading Effects to Displacements at GNSS Sites, in J. Sun et al. (eds.), *China Satellite Navigation Conference (CSNC) 2013 Proceedings*, Lecture Notes in Electrical Engineering 245, DOI: 10.1007/978-3-642-37407-4_2, _ Springer-Verlag Berlin Heidelberg 2013
- Zumberge, J. F., M. B. Heflin, D. C. Jefferson, M. M. Watkins, F. H. Webb, *Precise point positioning for the efficient and robust analysis of GPS data from large networks*, *J. Geophys. Res.*, 102 (B3), 5005-5017, doi:10.1029/96JB03860, 1997
- Zus, F., Dick, G., Dousa, J., and Wickert, J.: Systematic errors of mapping functions which are based on the VMF1 concept, *GPS Solut.*, 19, 277–286, doi:10.1007/s10291-014-0386-4, 2015.



Product Traceability and Uncertainty for the MUSICA ground-based NDACC/FTIR tropospheric H₂O profile product

Version 3

*GAIA-CLIM
Gap Analysis for Integrated
Atmospheric ECV Climate Monitoring
Mar 2015 - Feb 2018*

A Horizon 2020 project; Grant agreement: 640276

Date: 22 Dec 2017

Dissemination level: PU

Work Package 2; Compiled by Matthias Schneider (IMK)

Table of Contents

1. Product overview	4
1.1 Guidance notes	4
2. Introduction	6
3. Instrument description	7
4. Product Traceability Chain	11
4.1 Processing chain	11
4.2 Theoretical background for the processing of FTIR spectra	11
4.3 Propagation of uncertainties	12
4.4 Trace gas ratios	13
4.5 Traceability of uncertainties	13
5. Element contributions	16
5.1 Measurement noise (A1)	16
5.2 Spectral baseline distortions (A2)	17
5.3 Line of Sight / Pointing (B1)	18
5.4 Instrumental line shape (B2)	20
5.5 Spectroscopic parameters and parameterisations (B3)	22
5.6 Solar spectroscopy (B4)	25
5.7 Atmospheric temperature profile assumptions (B5)	26
6. Uncertainty Summary	27
7. Traceability uncertainty analysis	28
7.1 Recommendations	29
8. Conclusions	29
9. References	29

Version history

Version	Principal updates	Owner	Date
0 draft	First draft	IMK	13.12.2017
1 draft	Minor changes by TG (NPL)	IMK	19.12.2017
2 draft	Minor changes by MS (IMK)	IMK	22.12.2017
3 draft	Minor changes following PT comments	IMK	11.01.2018

1. Product overview

Product name: MUSICA ground-based NDACC/FTIR tropospheric H₂O profile product

Product technique: Remote sensing based on high resolution infrared solar absorption spectrometry

Product measurand: vertical distribution of tropospheric H₂O.

Product form/range: from ground to about 8km (high latitudes) and 12km (low latitudes).

Product dataset: MUSICA ground-based NDACC/FTIR dataset

Site/Sites/Network location: see the following Table 1

Table 1. List of current MUSICA NDACC/FTIR sites (ordered from north to south) and available MUSICA data record. DOFS values report the trace of the averaging kernel matrix. Type 1 is for the tropospheric H₂O profile product considered herein, and Type 2 for the isotopologue ratio product HDO/H₂O (and the {H₂O,δD}-pair product). Adapted from Barthlott et al. (2017).

Site	Location	Altitude	Data record	DOFS (type 1)	DOFS (type 2)
Eureka, Canada	80.1° N, 86.4° W	610 m a.s.l.	2006–2014	2.9	1.7
Ny-Ålesund, Norway	78.9° N, 11.9° E	21 m a.s.l.	2005–2014	2.8	1.6
Kiruna, Sweden	67.8° N, 20.4° E	419 m a.s.l.	1996–2014	2.8	1.6
Bremen, Germany	53.1° N, 8.9° E	27 m a.s.l.	2004–2014	2.8	1.6
Karlsruhe, Germany	49.1° N, 8.4° E	110 m a.s.l.	2010–2014	2.8	1.6
Jungfraujoch, Switzerland	46.6° N, 8.0° E	3580 m a.s.l.	1996–2014	2.7	1.6
Izaña, Tenerife, Spain	28.3° N, 16.5° W	2367 m a.s.l.	1999–2014	2.9	1.7
Altzomoni, Mexico	19.1° N, 98.7° W	3985 m a.s.l.	2012–2014	2.7	1.7
Addis Ababa, Ethiopia	9.0° N, 38.8° E	2443 m a.s.l.	2009–2013	2.6	1.6
Wollongong, Australia	34.5° S, 150.9° E	30 m a.s.l.	2007–2014	2.7	1.6
Lauder, New Zealand	45.1° S, 169.7° E	370 m a.s.l.	1997–2014	2.8	1.6
Arrival Heights, Antarctica	77.8° S, 166.7° E	250 m a.s.l.	2002–2014	2.7	1.4

1.1 Guidance notes

The contribution table to be filled for each traceability contributor has the form seen in Table

Table 2. The contributor table.

Information / data	Type / value / equation	Notes / description
Name of effect		
Contribution identifier		
Measurement equation parameter(s) subject to effect		
Contribution subject to effect (final product or sub-tree intermediate product)		
Time correlation extent & form		
Other (non-time) correlation		

extent & form		
Uncertainty PDF shape		
Uncertainty & units		
Sensitivity coefficient		
Correlation(s) between affected parameters		
Element/step common for all sites/users?		
Traceable to ...		
Validation		

Name of effect – The name of the contribution. Should be clear, unique and match the description in the traceability diagram.

Contribution identifier - Unique identifier to allow reference in the traceability chains.

Measurement equation parameter(s) subject to effect – The part of the measurement equation influenced by this contribution. Ideally, the equation into which the element contributes.

Contribution subject to effect – The top level measurement contribution affected by this contribution. This can be the main product (if on the main chain), or potentially the root of a side branch contribution. It will depend on how the chain has been sub-divided.

Time correlation extent & form – The form & extent of any correlation this contribution has in time.

Other (non-time) correlation extent & form – The form & extent of any correlation this contribution has in a non-time domain. For example, spatial or spectral.

Uncertainty PDF shape – The probability distribution shape of the contribution, Gaussian/Normal Rectangular, U-shaped, log-normal or other. If the form is not known, a written description is sufficient.

Uncertainty & units – The uncertainty value, including units and confidence interval. This can be a simple equation, but should contain typical values.

Sensitivity coefficient – Coefficient multiplied by the uncertainty when applied to the measurement equation.

Correlation(s) between affected parameters – Any correlation between the parameters affected by this specific contribution. If this element links to the main chain by multiple paths within the traceability chain, it should be described here. For instance, SZA or surface pressure may be used separately in a number of models & correction terms that are applied to the product at different points in the processing.

Element/step common for all sites/users – Is there any site-to-site/user-to-user variation in the application of this contribution?

Traceable to – Describe any traceability back towards a primary/community reference.

Validation – Any validation activities that have been performed for this element?

2. Introduction

Most atmospheric molecules interact with electromagnetic radiation in the infrared spectral region, which makes infrared remote sensing an important tool for atmospheric research. High quality solar absorption spectra are measured in the framework of the international networks NDACC (Network for the Detection of Atmospheric Composition Change, <https://www2.acom.ucar.edu/irwg>) and TCCON (Total Carbon Column Observing Network, <http://www.tccon.caltech.edu>). NDACC covers the middle infrared spectral range 700 - 4200 cm^{-1} and TCCON the near infrared spectral range 3900 - 14000 cm^{-1} . The products considered herein were retrieved from NDACC spectra in the 2600 - 3100 cm^{-1} spectral range. The retrievals were performed centrally by the MUSICA NDACC/FTIR retrieval processing approach (the MUSICA activities have been funded by the European Research Council under the European Community's Seventh Framework Programme).

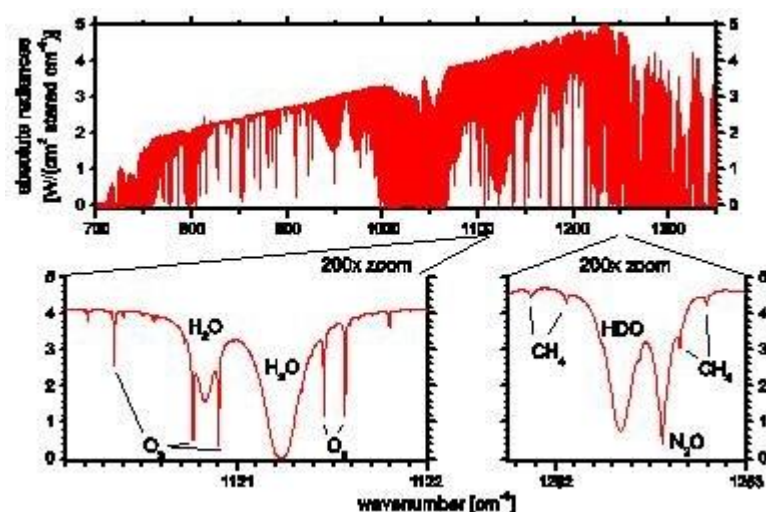


Figure 1. Upper panel: spectrum measured by an NDACC FTIR with the 700 – 1350 cm^{-1} filter setting. Bottom panels: zoomed spectral microwindows containing signatures of atmospheric molecules (here H_2O , HDO , O_3 , N_2O and CH_4).

Figure 1 shows an example of a spectrum measured in the NDACC spectral region 700 - 1350 cm^{-1} . The bottom panel gives an impression of the huge amount of information present in these high resolution spectra. It shows two spectral microwindows with the wavenumber scale being expanded by a factor of 200. Individual rotational-vibrational lines of different absorbers (O_3 , H_2O , HDO , N_2O , CH_4 , etc.) are discernable. The high spectral resolution allows measurements of the pressure-broadening effect, i.e., the line shape depends on the

pressure at which the absorption takes place (e.g., compare widths of the lines of H₂O, which absorbs mainly in the lower troposphere, with the width of the lines of O₃, which absorbs mainly in the stratosphere). The high resolution spectra disclose not only the total column amount of the absorber but also contain some information about its vertical distribution.

3. Instrument description

Figure 2 shows the two main components of a ground-based FTIR experiment: a precise solar tracker and a high resolution Fourier Transform Spectrometer (FTS). An FTS is based on a Michelson interferometer, consisting of a beamsplitter that divides the incoming radiance into two beams. One of them is reflected by a fixed mirror or retroreflector while the other one is sent to a moving mirror, causing a variable optical path. At the beamsplitter again, they recombine and interfere according to their wavelength and optical path difference. The optical path difference is measured with a monochromatic laser. The observed intensity fluctuations are an interferogram which is converted by a Fourier Transformation into a spectrum. A very detailed description of Fourier transform spectrometry can be found in the textbook of Davis, Abrams and Brault (Davis et al., 2001).

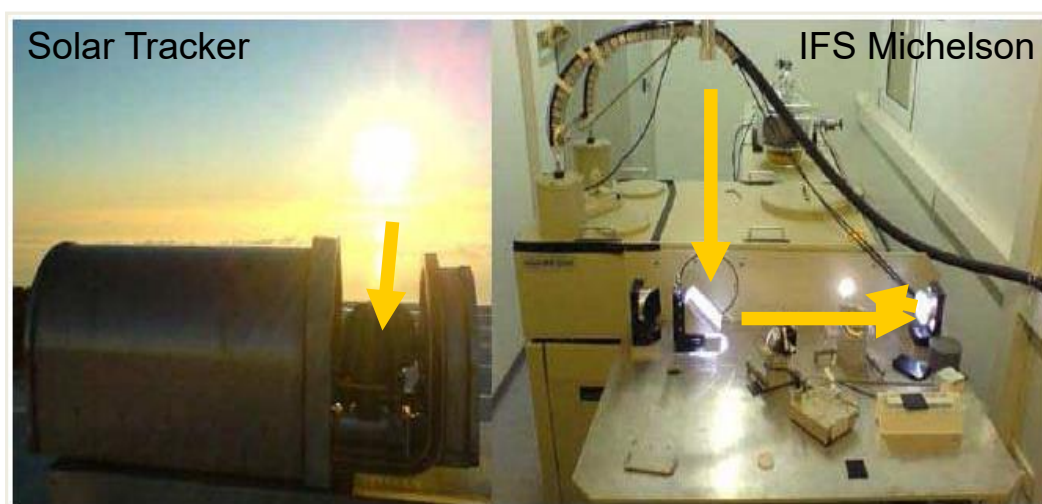


Figure 2. The ground-based FTIR experiment at the Izaña Atmospheric Research Centre. The solar tracker (left photograph) is situated at the top of the experimental housing. It collects the direct solar beam and reflects it into the housing of the FTIR spectrometer (right photograph). Then the solar beam is coupled into the spectrometer (circular light spot on the right part of the photograph).

The physical model chain of the FTIR measurement (Figure 3) displays the physical processes associated with the Fourier transform infrared spectroscopy for atmospheric solar absorption measurements (Figure 4 provides the key for the symbols used). For ground-based FTIR spectroscopy, the primary measurand is the interferogram which is the detected (solar) light intensity against the optical path difference of the moving mirror of a Michelson interferometer setup. Using a fast Fourier transformation (FFT), the interferogram is transformed into an (uncalibrated) transmittance spectrum. Cell spectra are measured in addition to atmospheric spectra. From these dedicated cell measurements, where sharp

absorption lines of the gas in the cell (e.g., HBr, N₂O or HCl, at a verified low pressure) are measured, the instrumental line shape (ILS) can be estimated.

Within NDACC, the ILS is then used as an input parameter in the retrieval process, with the purpose of mimicking the instrument's potential small misalignment in the forward model of the radiative transfer in the retrieval software.

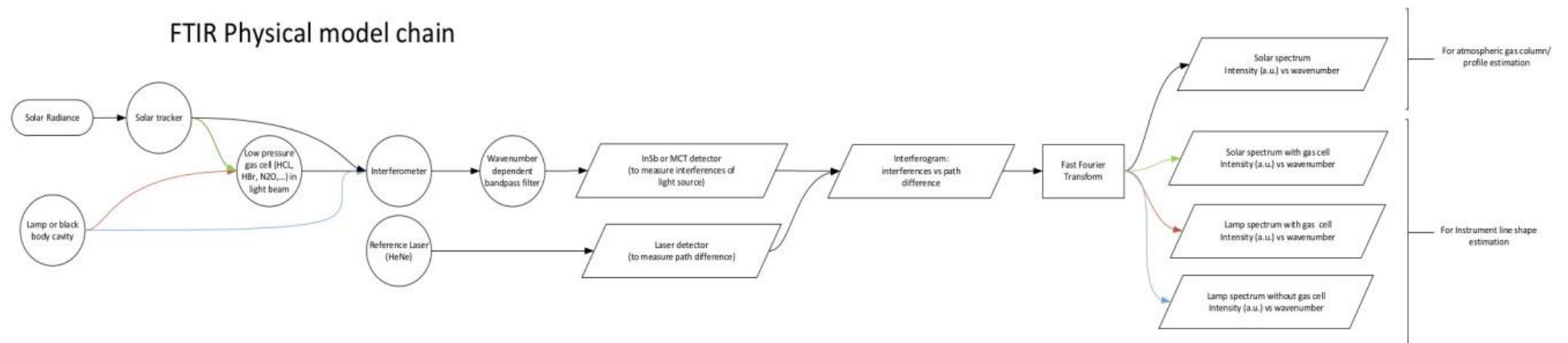


Figure 3. The physical model chain (Measurement Chain).

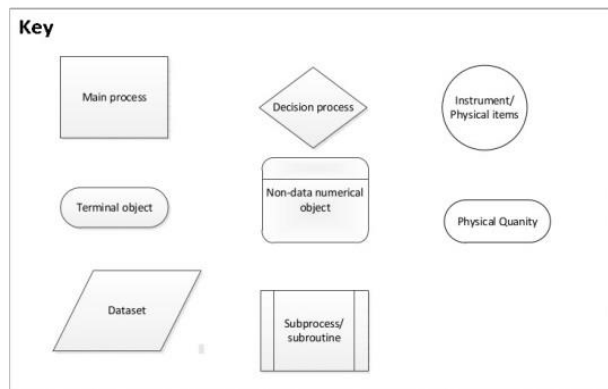


Figure 4. Meaning of the symbols used in the chain figures (Figs. 3, 5 and 6).

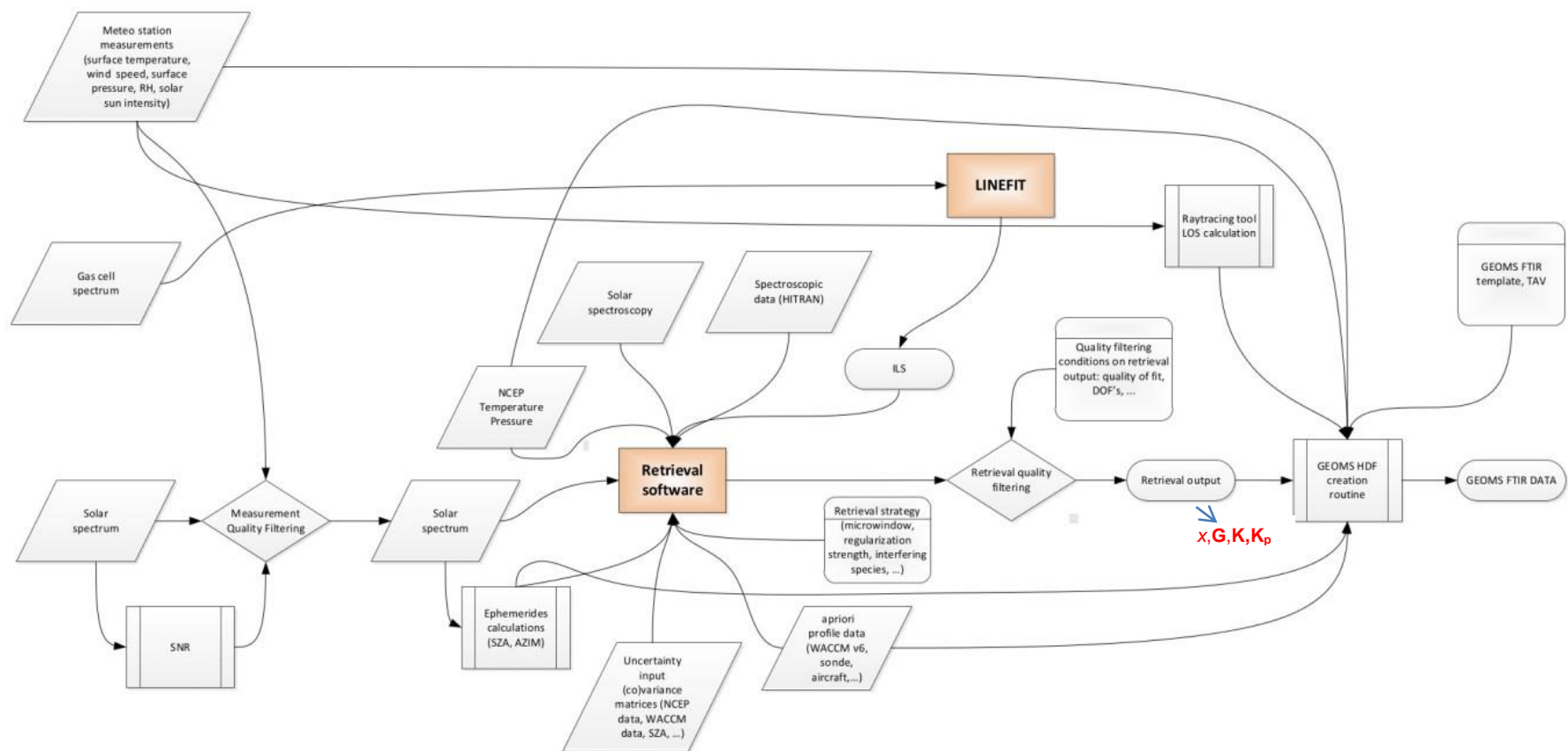


Figure 5. NDACC processing chain (the retrieval output is the trace gas product state vector x together with the gain matrix G and the Jacobians K and K_p , which enable to analytically estimate the propagation of the uncertainties into the retrieved state vector).

4. Product Traceability Chain

4.1 Processing chain

The processing chain (Figure 5) display all required *a priori* and input parameters necessary to determine a retrieval of the abundance of a target gas out of an FTIR spectrum. In the NDACC measurements the retrieval software uses optimal estimation or Tikhonov regularization to derive information about the vertical distribution of the target gas in the atmosphere.

All input parameters to the fitting algorithm are provided along with an uncertainty estimate and the retrieval software will propagate all different uncertainty contributions towards the uncertainty on the retrieved concentrations of the target gas. This uncertainty propagation is estimated according to Rodgers (2000), and is possible whenever the retrieval processor outputs the trace gas products together with the gain matrix (**G**) and the Jacobian matrices (**K** and **K_p**).

4.2 Theoretical background for the processing of FTIR spectra

In the following we give a very brief introduction into the principles of the ground-based FTIR retrieval method. It is an optimal estimation retrieval method and commonly used in atmospheric remote sensing. For more details please refer to Rodgers (2000) and for a general introduction on vector and matrix algebra dedicated textbooks are recommended.

Atmospheric remote sensing means that the atmospheric state is retrieved from the radiation measured after having interacted with the atmosphere. This interaction of radiation with the atmosphere is modelled by a radiative transfer model (also called forward model, F), which relates the measurement vector and the atmospheric state vector by:

$$y = F(x, p). \quad (1)$$

We measure y (the measurement vector, e.g. a solar absorption spectrum in the case of a ground-based FTIR) and are interested in x (the atmospheric state vector). Vector p represents auxiliary parameters (like solar elevation angle) or instrumental characteristics (like the instrumental line shape), which are not part of the retrieval state vector. However, a direct inversion of Eq. (1) is generally not possible, because there are many atmospheric states x that can explain one and the same measurement y .

For solving this ill-posed problem a cost function is set up, that combines the information provided by the measurement with *a priori* known characteristics of the atmospheric state:

$$[y - F(x, p)]^T \mathbf{S}_\epsilon^{-1} [y - F(x, p)] + [x - x_a]^T \mathbf{S}_a^{-1} [x - x_a]. \quad (2)$$

Here, the first term is a measure of the difference between the measured spectrum

(represented by y) and the spectrum simulated for a given atmospheric state (represented by x), while taking into account the actual measurement noise level (\mathbf{S}_ϵ is the measurement noise covariance matrix). The second term of the cost function (Eq. 2) constrains the atmospheric solution state (x) towards an *a priori* most likely state x_a , where the nature and strength of the constraint are defined by the *a priori* covariance matrix \mathbf{S}_a . The constrained solution is reached at the minimum of the cost function (Eq. 2). Due to the nonlinear behaviour of $F(x,p)$, the minimisation is generally achieved iteratively. For the $i+1$ th iteration it is:

$$x_{i+1} = x_a + \mathbf{G}_i[y - F(x_i, p) + \mathbf{K}_i(x_i - x_a)]. \quad (3)$$

This Eq. (3) is the main measurement equation asked for in the Contributor Table (Table 1). \mathbf{K} is the Jacobian matrix (derivatives that capture how the measurement vector y will change for changes in the atmospheric state x) and \mathbf{G} is the gain matrix (derivatives that capture how the retrieved state vector x will change for changes in the measurement vector y). \mathbf{G} can be calculated from \mathbf{K} , \mathbf{S}_ϵ and \mathbf{S}_a as:

$$\mathbf{G} = (\mathbf{K}^T \mathbf{S}_\epsilon^{-1} \mathbf{K} + \mathbf{S}_a^{-1})^{-1} \mathbf{K}^T \mathbf{S}_\epsilon^{-1}. \quad (4)$$

The averaging kernel matrix \mathbf{A} is an important component of a remote sensing retrieval and it is calculated as:

$$\mathbf{A} = \mathbf{GK}. \quad (5)$$

The averaging kernel \mathbf{A} reveals how a small change of the real atmospheric state vector x affects the retrieved atmospheric state vector \hat{x} :

$$\hat{x} - x_a = \mathbf{A}(x - x_a). \quad (6)$$

4.3 Propagation of uncertainties

The propagation of parameter uncertainties ϵ_p can be estimated analytically with the help of the parameter Jacobian matrix \mathbf{K}_p (derivatives that capture how the measurement vector will change for changes in the parameter p). According to Eq. (3), using the parameter $p+\epsilon_p$ (instead of the correct parameter p) for the forward model calculations will result in an uncertainty in the retrieved atmospheric state vector x_e of:

$$x_e = -\mathbf{GK}_p. \quad (7)$$

The respective uncertainty covariance matrix \mathbf{S}_e is:

$$\mathbf{S}_e = \mathbf{GK}_p \mathbf{S}_p \mathbf{K}_p^T \mathbf{G}^T, \quad (8)$$

where \mathbf{S}_p is the covariance matrix of the uncertainties ϵ_p .

Noise on the measured radiances also affects the retrievals. The uncertainty covariance matrix for noise can be analytically calculated as:

$$\mathbf{S}_e = \mathbf{GS}_y \mathbf{G}^T, \quad (9)$$

where \mathbf{S}_y is the covariance matrix for noise on the measured radiances y .

4.4 Trace gas ratios

The results can also be used to directly estimate the ratio of the concentration of different gases. This is particularly relevant when studying the ratios of different isotopologues of the same gas. By transferring the matrices \mathbf{G} on the logarithmic scale for the state vector x , we can perform an analytical uncertainty estimation of trace gas ratios. The uncertainty covariances for the trace gas ratios are calculated in analogy to Eqs. (8) and (9):

$$\mathbf{S}_e = \mathbf{P}\mathbf{G}_{\log}\mathbf{K}_p\mathbf{S}_p\mathbf{K}_p^T\mathbf{G}_{\log}^T\mathbf{P}^T \quad (10)$$

and

$$\mathbf{S}_e = \mathbf{P}\mathbf{G}_{\log}\mathbf{S}_y\mathbf{G}_{\log}^T\mathbf{P}^T, \quad (11)$$

where \mathbf{G}_{\log} is the gain matrix with respect to the trace gas logarithmic scale concentrations of the two trace gases (derivatives that capture how the retrieved logarithmic scale state vectors x will change for changes in the measurement vector y). The matrix \mathbf{P} is an operator that realises the transformation on a basis defined as the difference between the logarithmic scale concentrations of the two trace gases, i.e. the logarithmic scale differences between the states of the two trace gases are used as proxy for the trace gas ratios. This method enables calculation of the uncertainties on a gas ratio product, which will generally be less than those for a single gas product.

The averaging kernels for trace gas ratios can be calculated as:

$$\mathbf{P}\mathbf{A}_{\log}\mathbf{P}^{-1}, \quad (12)$$

where \mathbf{A}_{\log} is the averaging kernel for the trace gas logarithmic scale concentrations of the two trace gases.

This method for analytically documenting the averaging kernels and the uncertainties of trace gas ratio remote sensing data is used by MUSICA (<http://www.imk-asf.kit.edu/english/musica.php>) for the HDO/H₂O product. For more details please refer to Schneider et al. (2012) and Barthlott et al., (2017).

4.5 Traceability of uncertainties

The contributing uncertainties of a ground-based FTIR data product are collected in the matrices \mathbf{S}_p (for the uncertainties of the parameters p) and the matrix \mathbf{S}_y (for the noise on the measured radiances). The uncertainties affect the calculations according to Eq. (3) (the “measurement equation”), i.e. the retrieval product. The propagation of the uncertainties into the retrieval product can be calculated according to Eqs. (7) - (11).

In the next Section we present the Contributor Tables (according to Table 2), i.e. we discuss the traceability of the entries in $\mathbf{S_p}$ and $\mathbf{S_y}$. The following uncertainty contributors from the physical model/measurement chain and from the processing chain represent the major sources of uncertainty, and the contribution of each one is discussed in Section 5.

Uncertainty contributors from the measurement chain:

- A1: White noise in the measured spectral radiances (measurement noise)
- A2: Spectral baseline distortions (due to intensity fluctuations, detector non-linearities and multi-reflections on optical elements)

Uncertainty contributors from the processing chain:

- B1: Line of sight/Pointing
- B2: Instrumental line shape (modulation efficiency and phase error)
- B3: Spectroscopic parameters and parameterisations
- B4: Solar spectroscopy
- B5: Atmospheric temperature profile assumptions

Figure 6 presents a summary of the overall product traceability and uncertainty chain, which effectively combines the physical and processing chains (Figures 3 and 5 respectively), and highlights (in red) where the major uncertainty effects occur within the process. It is assumed that the uncertainty contributions from the other elements in this figure are minor relative to the seven identified above.

It should be noted that the limited vertical resolution and sensitivity of the remote sensing data is not an uncertainty contributor. These limitations are not uncertain, instead they are a fully understood characteristic of the remote sensing data product and comprehensively described by the averaging kernels (see Eqs. 5 and 6). Figure 7 shows a typical averaging kernel for the MUSICA H₂O profile product. Profiling capability is limited to the troposphere.

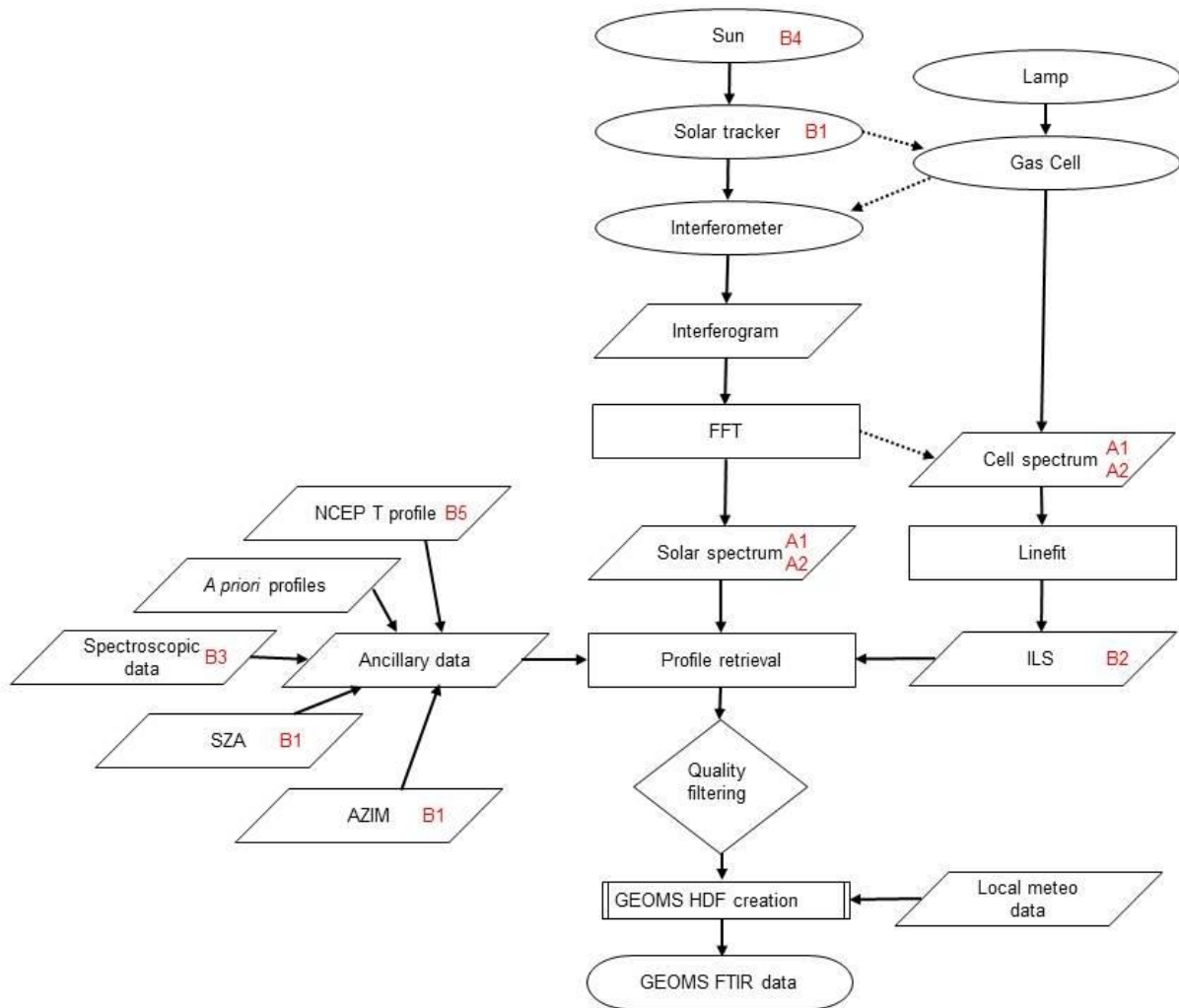


Figure 6. Overall product traceability and uncertainty chain, with key uncertainty contributors highlighted in red text

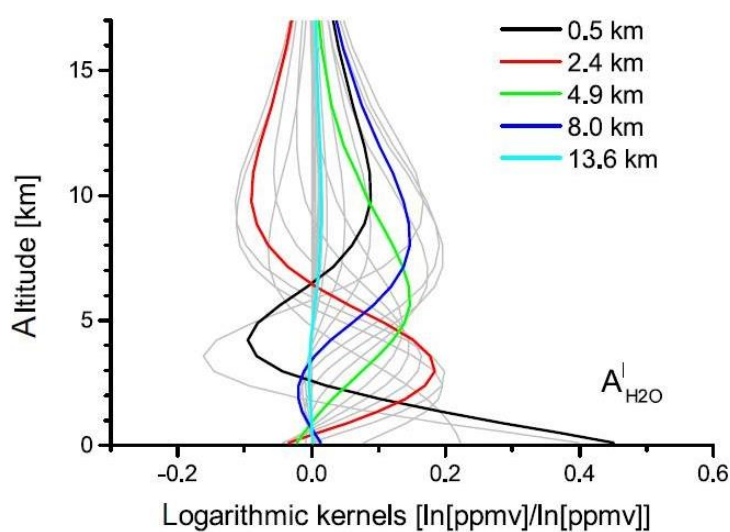


Figure 7. Logarithmic scale averaging kernel for a typical MUSICA H2O profile product (Graphic is adopted from Fig.4 of Barthlott et al., 2017). Negative values mean a negative response, e.g. for the shown example a H2O increase at 2.4 km will negatively affect the H2O concentrations retrieved at 10 km.

5. Element contributions

5.1 Measurement noise (A1)

For the measurement noise covariance matrix S_y generally a diagonal matrix is assumed. The correct entries for this matrix can be estimated by analysing the noise in a wavelength region of a measured spectrum where no significant atmospheric absorption takes place.

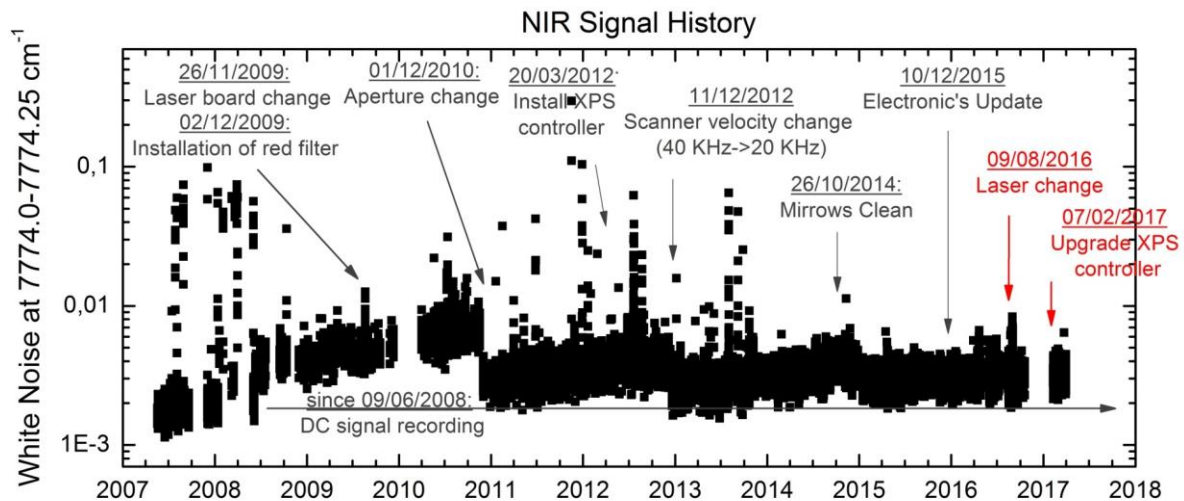


Figure 8. Evolution of the white noise (expressed as noise-to-signal ratio) in the near infrared region of the FTS at the Izaña Atmospheric Research Centre.

Figure 8 shows such analysis for a region in the near infrared. We observe that the noise depends on different instrumental settings, i.e. the entries of S_y for estimating the uncertainty contribution of measurement noise will be different for different instruments or for different time periods that shall be unique to each instrument and reflect its particular maintenance and component replacement history.

Information / data	Type / value / equation	Notes / description
Name of effect	Measurement noise	
Contribution identifier	A1	
Measurement equation parameter(s) subject to effect	Vector y in Eq. (3)	The gain matrix G , can also be affected, but only if the actual noise level is used when setting up the retrieval.
Contribution subject to effect (final product or sub-tree intermediate product)	Retrieved state vector \hat{x}	
Time correlation extent & form	None	No direct time correlation, however amplitude of noise can vary between different

		periods (e.g., by degradation of optical elements, see example of Fig. 8)
Other (non-time) correlation extent & form	None	
Uncertainty PDF shape	Normal	
Uncertainty & units	0.4%, unitless (noise-to-signal ratio)	Typical noise-to-signal ratio in the 2600 - 3100 cm^{-1} spectral range
Sensitivity coefficient	Uncertainty propagation according to Eq. (9)	
Correlation(s) between affected parameters	None	
Element/step common for all sites/users?	Yes	MUSICA processing assumes same uncertainties for all sites. These are conservative assumptions.
Traceable to ...	Traceable as shown in Fig. 8.	It is no absolute uncertainty instead it is a relative uncertainty, i.e. the noise is traceable relative to the signal.
Validation	Yes, example see Fig. 8.	

5.2 Spectral baseline distortions (A2)

Intensity fluctuations when recording the interferogram or non-linearities of the detector can cause a baseline distortion of spectrum (a frequency dependent baseline offset).

In addition multi-reflections on optical elements (solar tracker mirrors, beamsplitters, etc.) can cause an artificial channeling signal in the spectrum.

Information / data	Type / value / equation	Notes / description
Name of effect	Baseline distortions	
Contribution identifier	A2	
Measurement equation parameter(s) subject to effect	Affects vector y in Eq. (3)	If known it could be considered in $F(x,p)$. Then it would also affect the gain matrix \mathbf{G} and the Jacobian matrix \mathbf{K} in Eq. (3).
Contribution subject to effect (final product or sub-tree intermediate product)	Retrieved state vector \hat{x}	

Time correlation extent & form	Structured random	It is usually due to instrumental/hardware problems, that will remain as long as it is not corrected. This shall be instrument and time-period specific
Other (non-time) correlation extent & form		
Uncertainty PDF shape	MUSICA processing assumes 50% random (normal) and 50% systematic.	
Uncertainty & units	<0.2% (baseline-to-signal ratio), unitless	
Sensitivity coefficient	Uncertainty propagation according to Eqs. (7) and (8).	
Correlation(s) between affected parameters	None	
Element/step common for all sites/users?	Yes	MUSICA processing assumes same uncertainties for all sites. These are conservative assumptions.
Traceable to ...		It is a relative uncertainty, i.e. it is traceable relative to the signal.
Validation	Laboratory measurements, e.g. Hase (2000).	

5.3 Line of Sight / Pointing (B1)

A mis-pointing of the solar tracker generates a Doppler shift of the solar lines with respect to the telluric spectral features due to the solar rotation. The synodic rotation period of the sun is about 26.75 days, which corresponds to an observed equatorial solar velocity of about 1890ms^{-1} (Gisi et al. 2011 and references therein). A mismatch of the pointing along the solar equator of 1 arc min translates into a Doppler scaling $\Delta v/v$ of 3.9×10^{-7} . If this effect is considered in the analysis by fitting a separate shift for the solar background lines, the effects on the trace gas analysis are minor, but it gives a useful method to estimate the pointing quality at hand. Note, however, that the exact mispointing cannot be retrieved from the observed Doppler shifts, because there is no sensitivity along the direction parallel to the solar rotation axis. For this reason, we apply an additional factor of $\sqrt{2}$ for estimating the pointing error from the observed solar line scaling (we assume that the pointing uncertainty is of the same size for any direction on the solar disk).

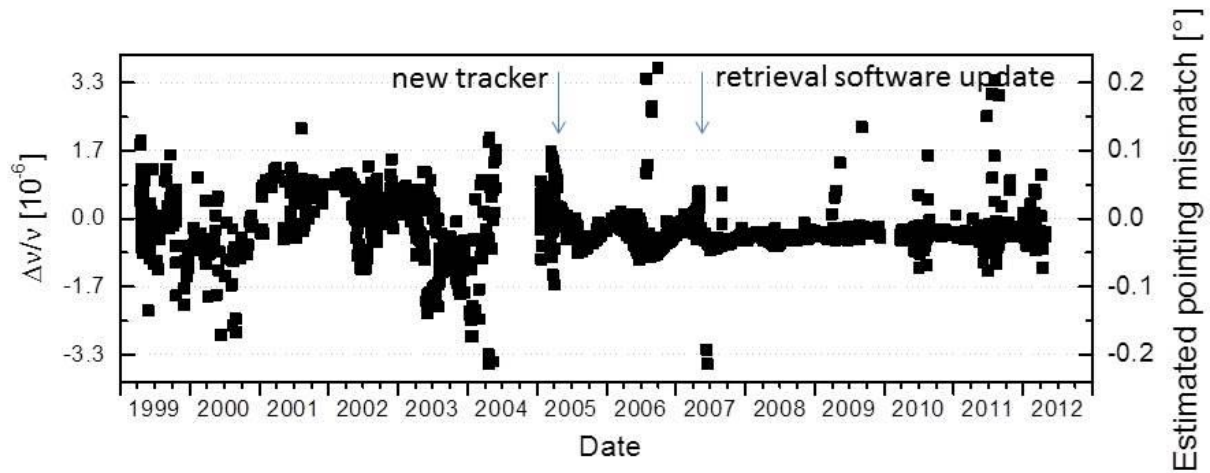


Figure 9. Evolution of solar line shifts and corresponding solar tracker pointing mismatch for the ground-based FTIR instrument of the Izaña Atmospheric Research Centre (example for 1999 - 2012).

Figure 9 shows the evolution of the solar line Doppler scaling and the respectively estimated solar tracker pointing mismatch for the ground-based FTIR experiment of the Izaña Atmospheric Research Centre. Occasionally, we observe some severe mismatch of the pointing, very likely due to the presence of clouds, which disables the camera based tracker's ability to see the sun. These outliers can easily be identified by the solar line shifts. Overall we estimate that with the latest tracker version (in operation since 2005) the pointing mismatch (1σ scatter of the mismatch) is better than 0.002° , which is less than 1% of the radius of the solar disc (the radius of the solar disc is about 0.25°). In the period from 1999 – 2004 (older tracker version), the pointing mismatch was significantly larger. Then the 1σ scatter of the mismatch was 0.04° . In summary the solar tracker pointing mismatch depends on the actual solar tracker used. It can be poorer than 0.05° or as good as about 0.002° .

Information / data	Type / value / equation	Notes / description
Name of effect	Pointing stability	
Contribution identifier	B1	
Measurement equation parameter(s) subject to effect	Affects vector function $F(x,p)$, the gain matrix \mathbf{G} and and the Jacobian matrix \mathbf{K} in Eq. (3)	
Contribution subject to effect (final product or sub-tree intermediate product)	Retrieved state vector \hat{x}	
Time correlation extent & form	Some time correlation possible (see Fig. 9).	Nature of correlation is site and time-period specific
Other (non-time) correlation extent & form	None	
Uncertainty PDF shape	MUSICA processing assumes 90% of the uncertainty to be random (normal) and the remaining 10% of the uncertainty to be	Barthlott et al. (2017)

	systematic.	
Uncertainty & units	0.1°	Barthlott et al. (2017)
Sensitivity coefficient	Uncertainty propagation according to Eqs. (7) and (8).	
Correlation(s) between affected parameters	Affect the retrieved state vector \hat{x} in the same direction over all altitudes.	Schneider et al. (2012)
Element/step common for all sites/users?	Yes	MUSICA processing assumes same uncertainties for all sites. These are conservative assumptions.
Traceable to ...	Qualitatively traceable to solar line frequency shifts (see Fig. 9)	
Validation	Possible, see example and discussion of Fig. 9.	

5.4 Instrumental line shape (B2)

The instrumental line shape (ILS) describes how the FTIR instrument will detect a monochromatic signal. It can be monitored by low pressure cell gas measurements (Hase, 2012). In NDACC this experimentally determined ILS is then used for the trace gas retrieval process.

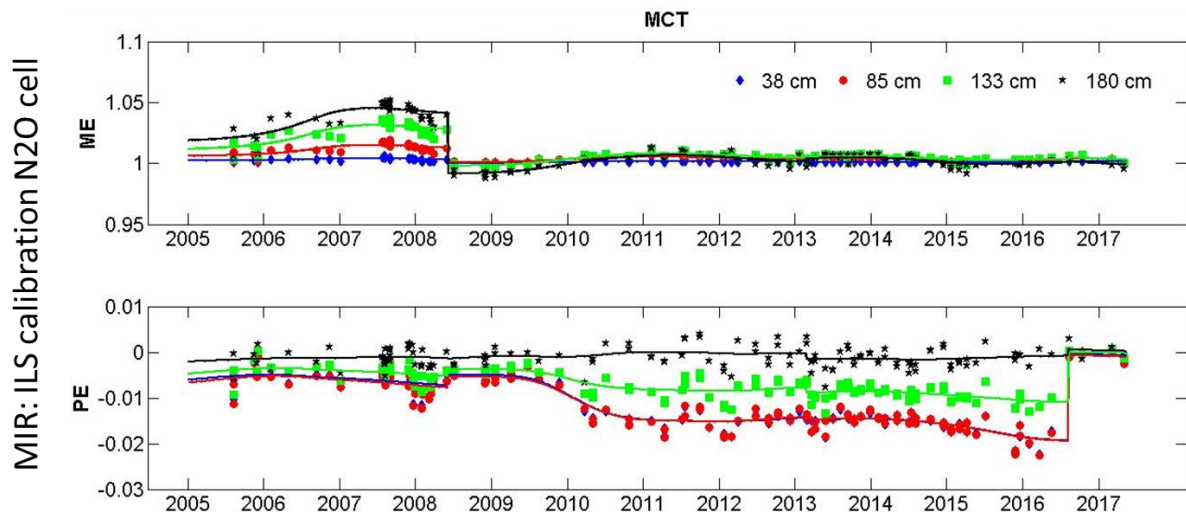


Figure 10. Evolution of the instrumental line shape of the FTS at the Izaña Atmospheric Research Centre (example for the MCT detector branch, 2005 - 2017). Upper panel: Modulation Efficiency (ME); Bottom panel: Phase Error (PE). Dots represent individual cell measurements and the lines the ILS values used when running the retrievals. The different colors represent different optical path differences (OPD): 38 cm, 85cm, 133cm and 180 cm (as given in the legend).

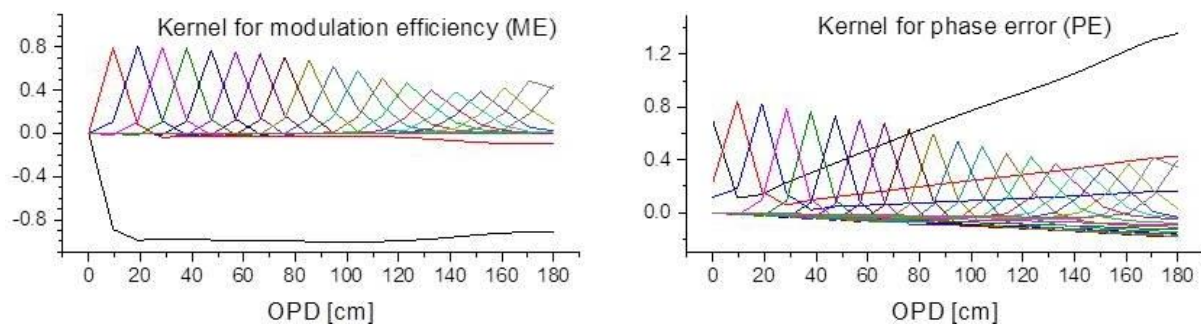


Figure 11. Example of averaging kernels for instrumental line shape retrievals using low pressure N₂O cell spectra (shown are results for the FTS at Izaña). The different colours are for 20 equidistant OPDs between 0 and 180cm. Left panel: Modulation Efficiency (ME); Right panel: Phase Error (PE).

Figure 10 shows the evolution of the ILS (modulation efficiency, ME, and phase error, PE) for the FTIR instrument at the Izaña Atmospheric Research Centre. The dots represent individual ILS measurements and the solid line is a smooth line that is fitted to the individual observations. The values given by this smooth line represent most likely the actual ILS, and are the values we use for describing the ILS during the NDACC trace gas retrievals. Thus, the difference of the values on the smooth line and the individual values can be seen as an uncertainty for the most likely ILS values. For the Izaña instrument we can estimate the ILS uncertainty to be smaller than 0.5% (concerning the modulation efficiency) and smaller than 0.003 rad (concerning the phase error). If the nominal ILS is used instead of the retrieved ILS the uncertainties will be larger, respectively.

In order to be able to rely on the ME and PE values obtained from the low pressure gas cell spectra analyses, we must consider the averaging kernels of the respective ME and PE retrievals. Examples for these kernels are shown in Fig. 11. It clearly indicates that the cell measurements allow a reliable retrieval of the ME and PE values over the whole range of OPD (optical path difference).

Information / data	Type / value / equation	Notes / description
Name of effect	Instrumental line shape (ILS)	
Contribution identifier	B2	
Measurement equation parameter(s) subject to effect	Affects vector function $F(x,p)$, the gain matrix \mathbf{G} and and the Jacobian matrix \mathbf{K} in Eq. (3)	
Contribution subject to effect (final product or sub-tree intermediate product)	Retrieved state vector \hat{x}	
Time correlation extent & form	Structured random	See example of Fig. 10. By nature these will be instrument / site specific.
Other (non-time) correlation extent & form		

Uncertainty PDF shape	MUSICA processing assumes 50% of the uncertainty to be random (normal) and the other 50% to be systematic.	Barthlott et al. (2017)
Uncertainty & units	Modulation efficiency is unitless (assumed uncertainty is 10%) and the phase error unit is rad (assumed uncertainty is 0.1 rad)	Barthlott et al. (2017)
Sensitivity coefficient	Uncertainty propagation according to Eqs. (7) and (8).	
Correlation(s) between affected parameters	Causes positive errors in the retrieved state vector \hat{x} for certain altitudes that are correlated to negative errors at other altitudes (error patterns).	Schneider et al. (2012)
Element/step common for all sites/users?	Yes	MUSICA processing assumes same uncertainties for all sites. These are conservative assumptions.
Traceable to ...	Hase (2012)	Modulation efficiency is a relative measurement, e.g. modulation efficiency at maximal optical path difference is related to the modulation efficiency at zero optical path difference.
Validation	Possible, like in Fig. 10. However, the sensitivity of these ILS retrievals has to be documented (like in Fig. 11).	

5.5 Spectroscopic parameters and parameterisations (B3)

Figure 12 depicts measured and simulated spectral microwindows in which H₂O and HDO signatures are dominant. State-of-the-art FTIR spectrometer offer spectra with a very high quality (high spectral resolution together with high signal-to-noise ratios) and small deficiencies in the theoretical description of the spectroscopic signatures can be made visible by analysing the residuals (difference between measured and simulated spectrum) obtained from a retrieval (e.g. Schneider and Hase, 2009).

The middle panel of Fig. 12 shows the residuals when using HITRAN 2008 parameters that are available for a Voigt line shape model. We see systematic residuals in the different microwindows. This strongly suggests that the absorption lines are not correctly described by the HITRAN Voigt line shape parameters. More precisely there must be an inconsistency in the errors of the line intensity parameters. If the relative error in the line intensity parameter

was the same for all lines the spectral fit will correct for this error and it would not become visible in the residuals. However, actually we observe that in some microwindows the residuals are positive and in other microwindows they are negative. This means that the relative line intensity parameter error is very likely different for the different lines. Note that similar residuals are seen across different sites confirming the underlying systematic issue with the lineshape model. Any site-to-site differences are explained by different optical paths through the atmosphere and different atmospheric compositions.

In the bottom panel of Fig. 12 we show the residuals after slightly modifying the line intensity parameters and the line pressure broadening parameters. In addition we considered a speed-dependent Voigt line shape model, i.e. an advanced line shape description model. There are some studies that show the improvement achievable by using such advanced line shape models instead of Voigt line shape models in high resolution infrared remote sensing applications (e.g. Schneider et al., 2011)

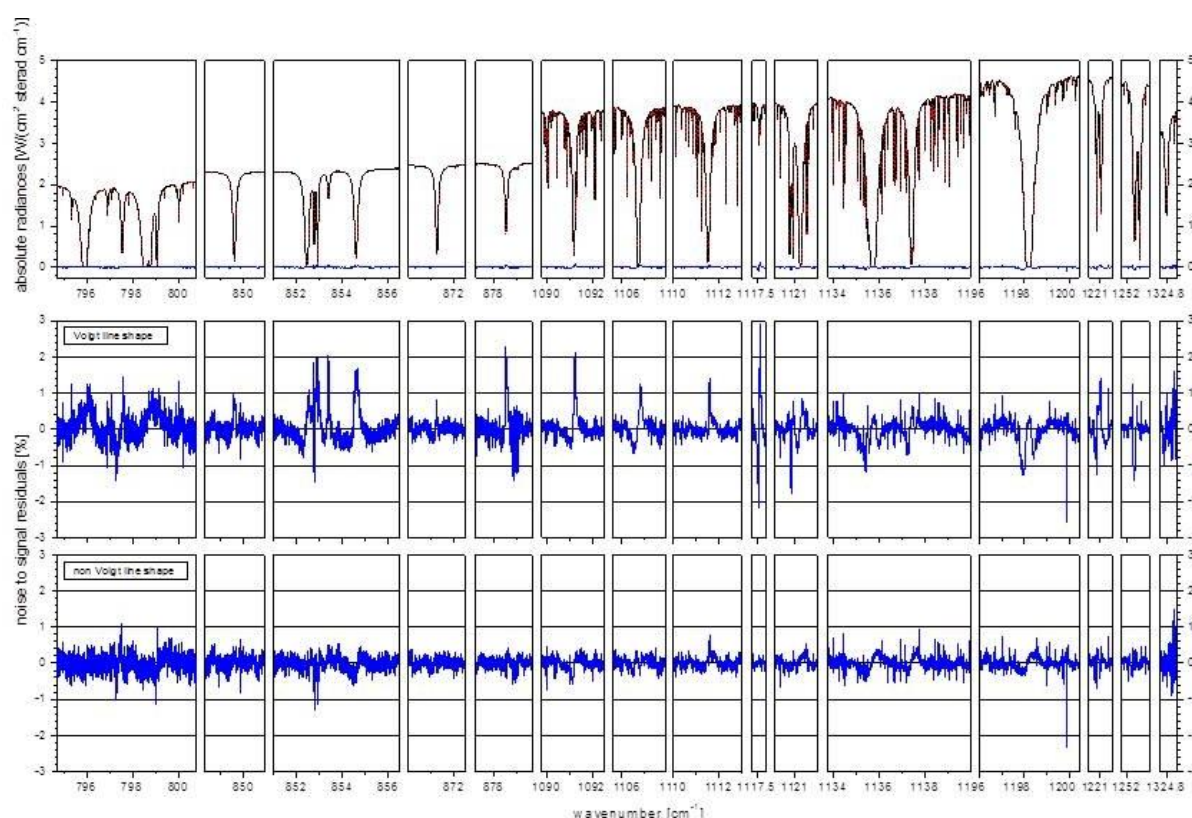


Figure 12. Example of residuals (difference between measured and simulated spectrum) for an H₂O and HDO retrieval that uses different spectral microwindows between 795 and 1325cm⁻¹ (the spectrum has been measured at the Izaña Atmospheric Research Centre). Top panel: measured and simulated spectra; Middle panel: residuals achieved when using HITRAN 2008 (Rothman et al., 2009) parameters assuming a Voigt line shape model; Bottom panel: residuals achieved when using non-Voigt line shapes.

Information / data	Type / value / equation	Notes / description
Name of effect	Spectroscopy	
Contribution identifier	B3	

Measurement equation parameter(s) subject to effect	Affects vector function $F(x,p)$, the gain matrix \mathbf{G} and and the Jacobian matrix \mathbf{K} in Eq. (3)	
Contribution subject to effect (final product or sub-tree intermediate product)	Retrieved state vector \hat{x}	
Time correlation extent & form	Systematic	It is a systematic uncertainty
Other (non-time) correlation extent & form		
Uncertainty PDF shape	Normal	
Uncertainty & units	Uncertainty of 1% for the line intensity parameter (absolute unit for line intensity parameter is $\text{cm}^{-1}/(\text{mol cm}^{-2})$: Uncertainty of 1% for the pressure broadening parameter (absolute unit for pressure broadening parameter is $\text{cm}^{-1} / \text{atm}^{-1}$)	See Barthlott et al. (2017). Furthermore, there are uncertainties by using an inadequate line shape model (see Fig. 12).
Sensitivity coefficient	Uncertainty propagation according to Eqs. (7) and (8)	
Correlation(s) between affected parameters	Causes positive errors in the retrieved state vector \hat{x} for certain altitudes that are correlated to negative errors at other altitudes (error patterns).	Schneider et al. (2012)
Element/step common for all sites/users?	Yes.	
Traceable to ...		The inconsistency between the uncertainty of line parameters or parameterisations can be visualised in the differences between simulations and measured high-resolution, high quality spectra (see Fig. 12)
Validation	It is the dominating systematic uncertainty source and can be validated by comparison to reference H ₂ O profile measurements (e.g. Schneider et al., 2016).	

5.6 Solar spectroscopy (B4)

Solar lines are also important in the infrared region. Figure 13 shows the solar transmittance between 750 and 4300 cm^{-1} as reported by Hase et al. (2010).

For high quality retrievals it is important to use a high quality atlas of solar lines. However, even then the position and also the strength of the solar line might be different in the measured spectra if compared to the atlas due to a slight mispointing to the centre of the solar disc. A shift in the position is due to a Doppler effect (see explanation in the context of Fig. 9). The solar line strengths will depend on the interaction with the solar atmosphere and will be different for observing the centre or the edge of the solar disc.

The effects of the solar line position can be well accounted for if before a trace gas retrieval the solar line position with respect to the telluric lines is estimated. This can be done by analysing the shifts between two spectral windows. A first window containing a solar line and the second window containing a well understood telluric line (see discussion in the context of Fig. 9).

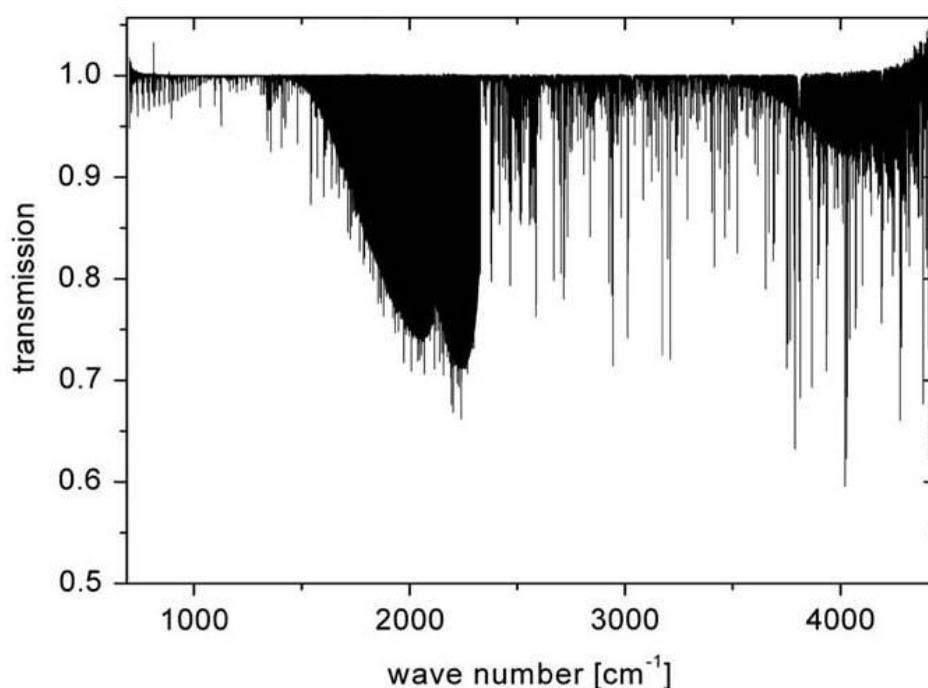


Figure 13. The final ACE-FTS solar transmission spectrum. The apparent bending of the continuum level near the low and high wavenumber ends is actually due to the envelope of increasing noise; the continuum level is constant over the whole region. Adopted from Hase et al. (2010).

Information / data	Type / value / equation	Notes / description
Name of effect	Solar lines	
Contribution identifier	B4	
Measurement equation	Affects vector function	

parameter(s) subject to effect	$F(x,p)$, the gain matrix G and the Jacobian matrix K in Eq. (3)	
Contribution subject to effect (final product or sub-tree intermediate product)	Retrieved state vector \hat{x}	
Time correlation extent & form	Structured random, similar to B1	
Other (non-time) correlation extent & form		
Uncertainty PDF shape	MUSICA processing assumes 80% random (normal) and 20% systematic.	Barthlott et al. (2017)
Uncertainty & units	Solar line intensity: 1% uncertainty. Solar line v-scale ($\Delta v/v$): 10^{-6} uncertainty	Barthlott et al. (2017)
Sensitivity coefficient	Uncertainty propagation according to Eqs. (7) and (8).	
Correlation(s) between affected parameters		
Element/step common for all sites/users?	Yes	MUSICA processing assumes same uncertainties for all sites.
Traceable to ...		
Validation	Solar line v-scale can be validated according to Fig. 9.	

5.7 Atmospheric temperature profile assumptions (B5)

The MUSICA retrievals assume the atmospheric temperature profiles as given by the NCEP (National Centre for Environmental Prediction) reanalyses. The MUSICA tropospheric water vapour retrieval assumes temperature uncertainties for three different altitude ranges (surface - 5km, 5km – 12km, 12km – top of the atmosphere), and no correlation between the uncertainties of the three altitude ranges.

Information / data	Type / value / equation	Notes / description
Name of effect	Temperature	
Contribution identifier	B5	
Measurement equation parameter(s) subject to effect	Affects vector function $F(x,p)$, the gain matrix G and the Jacobian matrix K in	

	Eq. (3)	
Contribution subject to effect (final product or sub-tree intermediate product)	Retrieved state vector \hat{x}	
Time correlation extent & form	Possible	Could occur if reanalyses data have systematic uncertainties.
Other (non-time) correlation extent & form	Possible	Correlation between different sites are possible if the reanalysis data have correlated uncertainties between different sites.
Uncertainty PDF shape	MUSICA processing assumes 70% random (normal) and 30% systematic.	Barthlott et al. (2017)
Uncertainty & units	3 K (independently for three altitude ranges: surface – 5km; 5km – 12km; 12km – top of atmosphere)	Barthlott et al. (2017)
Sensitivity coefficient	Uncertainty propagation according to Eqs. (7) and (8).	
Correlation(s) between affected parameters	Similar to B2 and B3 error patterns can occur.	
Element/step common for all sites/users?	Yes	MUSICA processing assumes same uncertainties for all sites
Traceable to ...	Barthlott et al. (2017)	
Validation	None	

6. Uncertainty Summary

Table 2. Uncertainty Summary.

Element identifier	Contribution name	Typical uncertainty value	Effect on final product (error of \hat{x}): LT: lower troposphere UT: upper troposphere	Traceability level: L/M/H	Type	Correlated to
A1	Noise	0.4%	<0.5% (LT) <1.5% (UT)	H	100% random	None
A2	Baseline	0.2%	<8% (LT)	M	50% random and	None

			<15% (UT)		50% systematic	
B1	Pointing	0.1°	<0.05%	H	90% random and 10% systematic	B4
B2	ILS	10% and 0.1 rad	0.6% (LT) 1.5% (UT)	H	50% random and 50% systematic	None
B3	Spectroscopy	1%	<2.5% (LT) <4.5% (UT)	L	100% systematic	None
B4	Solar Lines	1% and 10 ⁻⁶	<0.1%	M	80% random and 20% systematic	B1
B5	Temperature	3 K for 3 independent layers	<1% (LT) <1.5% (UT)	L	70% random and 30% systematic	None

7. Traceability uncertainty analysis

Traceability level definition is given in Table 3.

Table 3. Traceability level definition table

Traceability Level	Descriptor	Multiplier
High	SI traceable or globally recognised community standard	1
Medium	Developmental community standard or peer-reviewed uncertainty assessment	3
Low	Approximate estimation	10

Analysis of the summary table would suggest the following contributions, shown in Table 4, should be considered further to improve the overall uncertainty of the MUSICA H₂O profile product. The entries are given in an estimated priority order. In addition further work would appear warranted to properly quantify the effects currently assumed to add a negligible uncertainty contribution in Figure 6.

Table 4. Traceability level definition further action table.

Element identifier	Contribution name	Typical uncertainty value	Effect on final product (error of \hat{x}): LT: lower troposphere UT: upper troposphere	Traceability level: L/M/H	Type	Correlated to
B3	Spectroscopy	1%	<2.5% (LT) <4.5% (UT)	L	100% systematic	None
A2	Baseline	0.2%	<8% (LT)	M	50% random and	None

			<15% (UT)		50% systematic	
B5	Temperature	3 K for 3 independent layers	<1% (LT) <1.5% (UT)	L	70% random and 30% systematic	None

7.1 Recommendations

In order to further improve the traceability of the MUSICA H₂O profile products three priorities have been identified.

The top priority is to quantify rigorously the uncertainty of the simulated spectroscopic signatures (contributor B3). This work must not be limited to the investigation of line intensity and pressure broadening parameters (which are the most important parameters when using a Voigt line shape model). In the meanwhile the ground-based FTIR spectra are of such high quality that a “simple” Voigt line shape parameterisation is very likely not sufficient. It is important to investigate more advanced parameterisations (e.g. Schneider et al., 2011; Tran et al., 2017).

Another priority is to better characterise the baseline distortions for each station individually (contributor A2). This might be achieved by performing regular analyses of black body radiances by the whole observing system (solar tracker unit and FTIR spectrometer). However, such calibration measurements can hardly be automated and would need more manpower.

Finally, the atmospheric temperature uncertainty (contributor B5) should be better characterised for each individual site. This should be done in collaboration with providers of reanalyses data that are used as the atmospheric temperature in the MUSICA H₂O retrievals.

In addition to improved assessment of the key uncertainty contributors described above further work could be undertaken to quantify and assess the nature of the uncertainties from the other (assumed minor) contributors from the other elements identified in the overall product traceability and uncertainty chain (Figure 6).

8. Conclusions

The MUSICA H₂O profile product has been assessed against the GAIA CLIM traceability and uncertainty criteria.

9. References

- Barthlott et al. (2017), doi:10.5194/essd-9-15-2017.
Davis et al. (2001), ISBN 0-12-042510-6.
Gisi et al. (2011), doi:10.5194/amt-4-47-2011.
Hase (2000), Dissertation, FZK Report No. 6512, Forschungszentrum Karlsruhe, Germany.
Hase et al. (2010), doi:10.1016/j.jqsrt.2009.10.020.

Hase (2012), doi:10.5194/amt-5-603-2012
Rodgers (2000), ISBN 981-02-2740-X.
Rothman et al. (2009), doi:10.1016/j.jqsrt.2009.02.013.
Schneider and Hase (2009), doi:10.1016/j.jqsrt.2009.04.011.
Schneider et al. (2011), doi:10.1016/j.jqsrt.2010.09.008.
Schneider et al. (2012), doi:10.5194/amt-5-3007-2012.
Schneider et al. (2016), doi:10.5194/amt-9-2845-2016.
Tran et al. (2017), doi:10.1063/1.4983397.



Product Traceability and Uncertainty for the ground-based NDACC/FTIR O₃ profile product

Version 3

*GAIA-CLIM
Gap Analysis for Integrated
Atmospheric ECV Climate Monitoring
Mar 2015 - Feb 2018*

A Horizon 2020 project; Grant agreement: 640276

Date: 22 Dec 2017

Dissemination level: PU

Work Package 2; Compiled by Matthias Schneider (IMK)

Table of Contents

1. Product overview	4
1.1 Guidance notes	4
2. Introduction	4
3. Instrument description	4
4. Product Traceability Chain	4
5. Element contributions	5
5.1 Measurement noise (A1)	5
5.2 Spectral baseline distortions (A2)	7
5.3 Line of Sight (LOS) / Pointing (B1)	7
5.4 Instrumental line shape (B2)	8
5.5 Spectroscopic parameters and parameterisations (B3).....	10
5.6 Solar spectroscopy (B4)	11
5.7 Atmospheric temperature profile assumptions (B5)	12
6. Uncertainty Summary	13
7. Traceability uncertainty analysis	13
7.1 Recommendations	14
8. Conclusions	15
9. References	15

Version history

Version	Principal updates	Owner	Date
0 draft	First draft	IMK	13.12.2017
1 draft	Minor changes by TG (NPL)	IMK	19.12.2017
2 draft	Minor changes by MS (IMK)	IMK	22.12.2017
3 draft	Minor changes following PT comments	IMK	11.01.2018

1. Product overview

Product name: Ground-based NDACC/FTIR O₃ profile product

Product technique: Remote sensing based on high resolution infrared solar absorption spectrometry

Product measurand: vertical distribution of tropospheric and stratospheric O₃.

Product form/range: from ground to about 50km.

Product dataset: MUSICA ground-based NDACC/FTIR dataset

Site/Sites/Network location: Kiruna (67.8°N, 20.4°E, 420 m a.s.l.) and Izaña (28.3°N, 16.5°W, 2370 m a.s.l.).

1.1 Guidance notes

This document describes the traceability and uncertainty for ground-based FTIR profile measurements of O₃. This product closely follows that out in the PTU document for MUSICA H₂O profile measurements and should be read in conjunction with that document.

2. Introduction

See PTU document for MUSICA H₂O profiles for a general introduction.

Specific for O₃:

The O₃ retrievals are performed in 5 spectral microwindows between 991 and 1014 cm⁻¹. Please note that here we report the data product as available via the NDACC database. It should be mentioned that an O₃ product retrieved by a simultaneous temperature fit would have significantly reduced random uncertainties due to improvement in the temperature profile used in the fit and reduced uncertainties in the temperature dependence of the spectroscopic line parameters (Schneider and Hase, 2008; García et al., 2012).

3. Instrument description

See PTU document for MUSICA H₂O profiles.

4. Product Traceability Chain

The product traceability chain is the same as shown in the PTU document for MUSICA H₂O profiles (Fig. 5 in the PTU document for MUSICA H₂O profiles). The following uncertainty contributors will be considered:

Uncertainty contributors from the measurement chain:

- A1: White noise in the measured spectral radiances (measurement noise)

- A2: Spectral baseline distortions (due to intensity fluctuations, detector non-linearities and multi-reflections on optical elements)

Uncertainty contributors from the processing chain:

- B1: Line of sight/Pointing
- B2: Instrumental line shape (modulation efficiency and phase error)
- B3: Spectroscopic parameters and parameterisations
- B4: Solar spectroscopy
- B5: Atmospheric temperature profile assumptions

For details see PTU document for MUSICA H₂O profiles.

Figure 1 shows a typical averaging kernel for the ground-based FTIR O₃ profile product at Izaña.

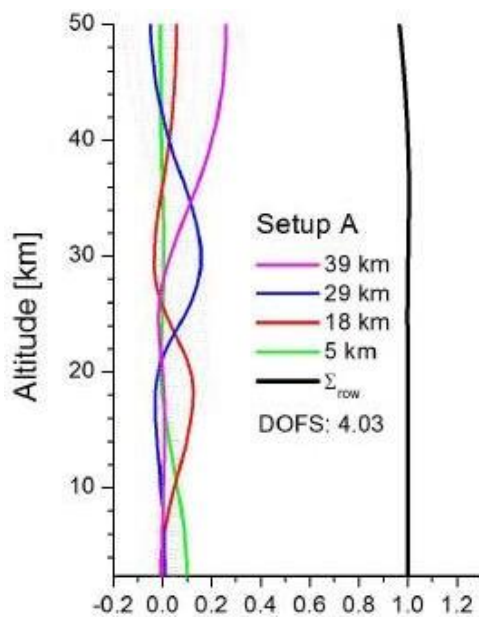


Figure 1. Logarithmic scale averaging kernel for a typical Izaña O₃ profile product (Graphic is adopted from Fig.2 of García et al., 2012). The green, red, blue and pink lines depict the response of the retrieved profile on real atmospheric O₃ increases at 5, 18, 29, and 39km altitude, respectively. The black line is the sum along the row of the kernels and represents the sensitivity of the remote sensing system.

5. Element contributions

Here only the tables are given. For more general details please see the PTU document for MUSICA H₂O profiles.

5.1 Measurement noise (A1)

The measurement noise uncertainty contribution is taken from the root-mean-square value of the spectral fit residual (difference between measured and simulated spectrum). This kind of

measurement noise includes white noise, but also systematic deficiencies in the forward simulations (error in spectroscopic parameters or parameterisations), an insufficient instrumental line shape description or spectral baseline distortions.

Information / data	Type / value / equation	Notes / description
Name of effect	Measurement noise	
Contribution identifier	A1	
Measurement equation parameter(s) subject to effect	Vector y in Eq. (3) of the PTU document for MUSICA H ₂ O profiles.	In addition the gain matrix G , because the actual noise level is for constraining the inversion process.
Contribution subject to effect (final product or sub-tree intermediate product)	Retrieved state vector \hat{x}	
Time correlation extent & form	None	No time correlation, however amplitude of noise can vary between different periods (e.g., by degradation of optical elements, see example of Fig. 8 of the PTU document for MUSICA H ₂ O profiles)
Other (non-time) correlation extent & form	None	
Uncertainty PDF shape	Normal	
Uncertainty & units	< 1%, unitless (residual-to-signal ratio)	Typical ratio for retrievals using five microwindows in the 991-1014 cm ⁻¹ spectral range.
Sensitivity coefficient	Uncertainty propagation according to Eq. (9) of the PTU document for MUSICA H ₂ O profiles	
Correlation(s) between affected parameters	None	
Element/step common for all sites/users?	Yes	
Traceable to ...	The residuals.	It is not an absolute uncertainty instead it is a relative uncertainty, i.e. the residual is traceable relative to the signal.
Validation	Yes, by analysing the residuals.	

5.2 Spectral baseline distortions (A2)

Information / data	Type / value / equation	Notes / description
Name of effect	Baseline distortions	
Contribution identifier	A2	
Measurement equation parameter(s) subject to effect	Affects vector y in Eq. (3) of the PTU document for MUSICA H ₂ O profiles.	If known it could be considered in $F(x,p)$. Then it would also affect the gain matrix \mathbf{G} and the Jacobian matrix \mathbf{K} in Eq. (3).
Contribution subject to effect (final product or sub-tree intermediate product)	Retrieved state vector \hat{x}	
Time correlation extent & form	Structured random	It is usually due to an instrumental/hardware problem, that will remain as long as it is not corrected.
Other (non-time) correlation extent & form		
Uncertainty PDF shape	The assumption is: 50% random (normal) and 50% systematic.	
Uncertainty & units	0.2% (channelling-to-signal ratio), unitless 0.3% (offset-to-signal ratio), unitless	
Sensitivity coefficient	Uncertainty propagation according to Eqs. (7) and (8) of the PTU document for MUSICA H ₂ O profiles	
Correlation(s) between affected parameters	None	
Element/step common for all sites/users?	Yes	
Traceable to ...		It is a relative uncertainty, i.e. it is traceable relative to the signal.
Validation	Laboratory measurements, e.g. Hase (2000).	

5.3 Line of Sight (LOS) / Pointing (B1)

Information / data	Type / value / equation	Notes / description
--------------------	-------------------------	---------------------

Name of effect	Pointing stability	
Contribution identifier	B1	
Measurement equation parameter(s) subject to effect	Affects vector function $F(x,p)$, the gain matrix \mathbf{G} and the Jacobian matrix \mathbf{K} in Eq. (3) of the PTU document for MUSICA H ₂ O profiles.	
Contribution subject to effect (final product or sub-tree intermediate product)	Retrieved state vector \hat{x}	
Time correlation extent & form	Some time correlation possible (see Fig. 9) of the PTU document for MUSICA H ₂ O profiles.	
Other (non-time) correlation extent & form	None	
Uncertainty PDF shape	Assumption: 90% of the uncertainty to be random (normal) and the resting 10% of the uncertainty to be systematic.	
Uncertainty & units	0.001 rad = 0.0573°	
Sensitivity coefficient	Uncertainty propagation according to Eqs. (7) and (8) of the PTU document for MUSICA H ₂ O profiles	
Correlation(s) between affected parameters	Affect the retrieved state vector \hat{x} in the same direction over all altitudes.	García et al. (2012)
Element/step common for all sites/users?	Yes	
Traceable to ...	Qualitatively traceable to solar line frequency shifts (see Fig. 9 of the PTU document for MUSICA H ₂ O profiles.)	
Validation	Possible, see example and discussion of Fig. 9 of the PTU document for MUSICA H ₂ O profiles.	

5.4 Instrumental line shape (B2)

At Kiruna and Izaña low pressure gas cell measurements are made regularly and will the determination of the modulation efficiency and the phase error within an uncertainty of

smaller than 1% and 0.01 rad (see Fig. 10 of the PTU document for MUSICA H₂O profiles).

Information / data	Type / value / equation	Notes / description
Name of effect	Instrumental line shape (ILS)	
Contribution identifier	B2	
Measurement equation parameter(s) subject to effect	Affects vector function $F(x,p)$, the gain matrix \mathbf{G} and and the Jacobian matrix \mathbf{K} in Eq. (3) of the PTU document for MUSICA H ₂ O profiles.	
Contribution subject to effect (final product or sub-tree intermediate product)	Retrieved state vector \hat{x}	
Time correlation extent & form	Likely	See example of Fig. 10 of the PTU document for MUSICA H ₂ O profiles.
Other (non-time) correlation extent & form		
Uncertainty PDF shape	Assumption: 50% of the uncertainty to be random (normal) and the other 50% to be systematic.	
Uncertainty & units	Modulation efficiency is unitless (assumed uncertainty is 0.01) and the phase error unit is rad (assumed uncertainty is 0.01 rad)	
Sensitivity coefficient	Uncertainty propagation according to Eqs. (7) and (8) of the PTU document for MUSICA H ₂ O profiles	
Correlation(s) between affected parameters	Causes positive errors in the retrieved state vector \hat{x} for certain altitudes that are correlated to negative errors at other altitudes (error patterns).	García et al. (2012)
Element/step common for all sites/users?	Yes	
Traceable to ...	Hase (2012)	Modulation efficiency is a relative measurement, e.g. modulation efficiency at maximal optical path difference is related to the modulation efficiency at zero optical path difference.
Validation	Possible, like in Fig. 10 of	

	the PTU document for MUSICA H ₂ O profiles. However, the sensitivity of these ILS retrievals has to be documented (like in Fig. 11 of the PTU document for MUSICA H ₂ O profiles.)	
--	--	--

5.5 Spectroscopic parameters and parameterisations (B3)

Information / data	Type / value / equation	Notes / description
Name of effect	Spectroscopy	
Contribution identifier	B3	
Measurement equation parameter(s) subject to effect	Affects vector function $F(x,p)$, the gain matrix \mathbf{G} and and the Jacobian matrix \mathbf{K} in Eq. (3) of the PTU document for MUSICA H ₂ O profiles.	
Contribution subject to effect (final product or sub-tree intermediate product)	Retrieved state vector \hat{x}	
Time correlation extent & form	Systematic	It is a systematic uncertainty
Other (non-time) correlation extent & form		
Uncertainty PDF shape	Normal	
Uncertainty & units	Uncertainty of 2% for the line intensity parameter (absolute unit for line intensity parameter is $\text{cm}^{-1}/(\text{mol cm}^{-2})$: Uncertainty of 5% for the pressure broadening parameter (absolute unit for pressure broadening parameter is $\text{cm}^{-1} / \text{atm}^{-1}$)	Furthermore, the might be uncertainties by using an inadequate line shape model (see Fig. 12 of the PTU document for MUSICA H ₂ O profiles).
Sensitivity coefficient	Uncertainty propagation according to Eqs. (7) and (8) of the PTU document for MUSICA H ₂ O profiles	
Correlation(s) between affected parameters	Causes positive errors in the retrieved state vector \hat{x} for certain altitudes that are correlated to negative errors at other altitudes (error	García et al. (2012)

	patterns).	
Element/step common for all sites/users?	Yes.	
Traceable to ...		The inconsistency between the uncertainty of line parameters or parameterisations can be visualised in the differences between simulations and measured high-resolution, high quality spectra (see Fig. 12 of the PTU document for MUSICA H ₂ O profiles)
Validation		

5.6 Solar spectroscopy (B4)

Information / data	Type / value / equation	Notes / description
Name of effect	Solar lines	
Contribution identifier	B4	
Measurement equation parameter(s) subject to effect	Affects vector function $F(x,p)$, the gain matrix \mathbf{G} and the Jacobian matrix \mathbf{K} in Eq. (3) of the PTU document for MUSICA H ₂ O profiles.	
Contribution subject to effect (final product or sub-tree intermediate product)	Retrieved state vector \hat{x}	
Time correlation extent & form	Structured random, similar to B1	
Other (non-time) correlation extent & form		
Uncertainty PDF shape	Assumption: 80% random (normal) and 20% systematic.	García et al. (2012)
Uncertainty & units	Solar line intensity: 1% uncertainty. Solar line v-scale ($\Delta v/v$): 10^{-6} uncertainty	García et al. (2012)
Sensitivity coefficient	Uncertainty propagation according to Eqs. (7) and (8) of the PTU document for MUSICA H ₂ O profiles	

Correlation(s) between affected parameters		
Element/step common for all sites/users?	Yes	
Traceable to ...		
Validation	Solar line v-scale can be validated according to Fig. 9 of the PTU document for MUSICA H ₂ O profiles.	

5.7 Atmospheric temperature profile assumptions (B5)

Information / data	Type / value / equation	Notes / description
Name of effect	Temperature	
Contribution identifier	B5	
Measurement equation parameter(s) subject to effect	Affects vector function $F(x,p)$, the gain matrix \mathbf{G} and the Jacobian matrix \mathbf{K} in Eq. (3) of the PTU document for MUSICA H ₂ O profiles.	
Contribution subject to effect (final product or sub-tree intermediate product)	Retrieved state vector \hat{x}	
Time correlation extent & form	Possible.	Could occur if reanalyses data have systematic uncertainties.
Other (non-time) correlation extent & form	Possible.	Correlation between different sites are possible if the reanalysis data have correlated uncertainties between different sites.
Uncertainty PDF shape	Assumption: 70% random (normal) and 30% systematic.	
Uncertainty & units	Independently for three altitude ranges: surface – 10km: 1 K 10km – 37km: 2 K 37km – top of atmosphere: 5 K	
Sensitivity coefficient	Uncertainty propagation according to Eqs. (7) and (8) of the PTU document for MUSICA H ₂ O profiles	

Correlation(s) between affected parameters	Similar to B2 and B3 error patterns can occur.	
Element/step common for all sites/users?	Yes	
Traceable to ...	None	
Validation	None	

6. Uncertainty Summary

Table 1. Uncertainty Summary.

Element identified	Contribution name	Typical uncertainty value	Effect on final product (error of \hat{x}): T: troposphere S: stratosphere	Traceability level: L/M/H	Type	Correlated to
A1	Noise	<1%	<0.5% (T) <0.2% (S)	H	100% random	A2, B2, B3
A2	Baseline	0.2% and 0.3%	<0.5% (T) <5% (S)	M	50% random and 50% systematic	A1
B1	Pointing	0.0573°	<0.03%	H	90% random and 10% systematic	B4
B2	ILS	1% and 0.01 rad	1.2% (T) 1.8% (S)	H	50% random and 50% systematic	A1
B3	Spectroscopy	2% and 5%	<10% (T) <7.5% (S)	L	100% systematic	A1
B4	Solar Lines	1% and 10^{-6}	<0.01%	M	80% random and 20% systematic	B1
B5	Temperature	1-5 K for 3 independent layers	<1% (T) <3% (S)	L	70% random and 30% systematic	None

7. Traceability uncertainty analysis

Traceability level definition is given in Table 2.

Table 2. Traceability level definition table

Traceability Level	Descriptor	Multiplier
--------------------	------------	------------

High	SI traceable or globally recognised community standard	1
Medium	Developmental community standard or peer-reviewed uncertainty assessment	3
Low	Approximate estimation	10

Analysis of the summary table would suggest the following contributions, shown in Table 3, should be considered further to improve the overall uncertainty of the O₃ profile product. The entries are given in an estimated priority order.

Table 3. Traceability level definition further action table.

Element identifier	Contribution name	Typical uncertainty value	Effect on final product (error of \hat{x}): T: troposphere S: stratosphere	Traceability level: L/M/H	Type	Correlated to
B3	Spectroscopy	2% and 5%	<10% (T) <7.5% (S)	L	100% systematic	A1
B5	Temperature	1-5 K for 3 independent layers	<1% (T) <3% (S)	L	70% random and 30% systematic	None
A2	Baseline	0.2% and 0.3%	<0.5% (T) <5% (S)	M	50% random and 50% systematic	A1

7.1 Recommendations

In order to further improve the traceability of the O₃ profile products three priorities have been identified.

Similar to the MUSICA H₂O profile product also for the O₃ profiles the top priority is to quantify rigorously the uncertainty of the simulated spectroscopic signatures (contributor B3). In the meanwhile the measured spectra are of such high quality (low noise levels, high spectral resolution) that small uncertainties in spectroscopic parameters can have a significant effect on the product quality.

Second priority is the better quantification of the atmospheric temperature uncertainty (contributor B5). This should be characterised individually for each individual site in collaboration with providers of reanalyses data that are used as the atmospheric temperature in retrievals (NCEP). However, it should also be mentioned that by a simultaneous fit of the temperature profile this uncertainty contribution would be strongly reduced (Schneider and Hase 2008; García et al., 2012).

A better characterisation of the baseline distortions for each station individually (contributor

A2) would also be recommendable. This might be achieved by performing regular analyses of black body radiances by the whole observing system (solar tracker unit and FTIR spectrometer). However, such calibration measurements can hardly be automated and would need more manpower.

In addition to improved assessment of the key uncertainty contributors described above further work could be undertaken to quantify and assess the nature of the uncertainties from the other (assumed minor) contributors from the other elements identified in the overall product traceability and uncertainty chain (see Fig.6 in MUSICA H₂O PTU document).

8. Conclusions

The ground-based NDACC/FTIR O₃ profile product for Izaña and Kiruna has been assessed against the GAIA CLIM traceability and uncertainty criteria.

9. References

- García et al. (2012), doi:10.5194/amt-5-2917-2012.
Hase (2000), Dissertation, FZK Report No. 6512, Forschungszentrum Karlsruhe, Germany.
Hase (2012), doi:10.5194/amt-5-603-2012.
Schneider and Hase (2008), doi:10.5194/acp-8-63-2008.